

# **Controlled/Living Radical Polymerization: Progress in ATRP**



ACS SYMPOSIUM SERIES **1023**

**Controlled/Living Radical  
Polymerization:  
Progress in ATRP**

**Krzysztof Matyjaszewski**, Editor  
*Carnegie Mellon University*

**Sponsored by the  
ACS Division of Polymer Chemistry, Inc.  
ACS Petroleum Research Foundation  
Arkena, Bayer, Boston Scientific, Ciba, CIP, Dionex, DSM,  
Elsevier, Evonik, General Electric, JSR, Lion,  
Mitsui Chemicals, National Starch, PPG and Sumitomo**



American Chemical Society, Washington DC



Library of Congress Cataloging-in-Publication Data

Controlled/living radical polymerization : progress in ATRP / Krzysztof Matyjaszewski, editor.

p. cm. -- (ACS symposium series; 1023)

Includes bibliographical references and index.

ISBN 978-0-8412-6995-8 (alk. paper)

1. Polymerization--Congresses. 2. Free radical reactions--Congresses. I. Matyjaszewski, K. (Krzysztof)

QD281.P6C6555 2009

547'.28--dc22

2009020531

The paper used in this publication meets the minimum requirements of American National Standard for Information Sciences—Permanence of Paper for Printed Library Materials, ANSI Z39.48–1984.

Copyright © 2009 American Chemical Society

Distributed by Oxford University Press

All Rights Reserved. Reprographic copying beyond that permitted by Sections 107 or 108 of the U.S. Copyright Act is allowed for internal use only, provided that a per-chapter fee of \$40.25 plus \$0.75 per page is paid to the Copyright Clearance Center, Inc., 222 Rosewood Drive, Danvers, MA 01923, USA. Republication or reproduction for sale of pages in this book is permitted only under license from ACS. Direct these and other permission requests to ACS Copyright Office, Publications Division, 1155 16th Street, N.W., Washington, DC 20036.

The citation of trade names and/or names of manufacturers in this publication is not to be construed as an endorsement or as approval by ACS of the commercial products or services referenced herein; nor should the mere reference herein to any drawing, specification, chemical process, or other data be regarded as a license or as a conveyance of any right or permission to the holder, reader, or any other person or corporation, to manufacture, reproduce, use, or sell any patented invention or copyrighted work that may in any way be related thereto. Registered names, trademarks, etc., used in this publication, even without specific indication thereof, are not to be considered unprotected by law.

PRINTED IN THE UNITED STATES OF AMERICA

# Foreword

The ACS Symposium Series was first published in 1974 to provide a mechanism for publishing symposia quickly in book form. The purpose of the series is to publish timely, comprehensive books developed from the ACS sponsored symposia based on current scientific research. Occasionally, books are developed from symposia sponsored by other organizations when the topic is of keen interest to the chemistry audience.

Before agreeing to publish a book, the proposed table of contents is reviewed for appropriate and comprehensive coverage and for interest to the audience. Some papers may be excluded to better focus the book; others may be added to provide comprehensiveness. When appropriate, overview or introductory chapters are added. Drafts of chapters are peer-reviewed prior to final acceptance or rejection, and manuscripts are prepared in camera-ready format.

As a rule, only original research papers and original review papers are included in the volumes. Verbatim reproductions of previous published papers are not accepted.

## ACS Books Department

# Preface

This book and an accompanying volume are addressed to chemists who are interested in radical processes and especially in controlled/living radical polymerization. They summarize the most recent accomplishments in the field.

The two volumes comprise the topical reviews and specialists' contributions presented at the American Chemical Society Symposium entitled Controlled/Living Radical Polymerization that was held in Philadelphia, Pennsylvania, August 17-21, 2008. The Philadelphia Meeting was a sequel to the previous ACS Symposia held in San Francisco, California, in 1997, in New Orleans, Louisiana, in 1999, in Boston, Massachusetts, in 2002 and in Washington, DC, in 2005. They were summarized in the ACS Symposium Series Volume 685, Controlled Radical Polymerization, Volume 768, Controlled/Living Radical Polymerization: Progress in ATRP, NMP and RAFT, Volume 854 Advances in Controlled/Living Radical Polymerization and Volume 944, Controlled/Living Radical Polymerization: From Synthesis to Materials. The Philadelphia Meeting was very successful with 90 lectures and 123 posters presented. This illustrates a continuous growth in comparison with the San Francisco Meeting (32 lectures and 35 posters), the New Orleans (50 lectures and 50 posters), the Boston Meeting (80 lectures and 79 posters) and with the Washington Meeting (77 lectures and 119 posters).

The fifty chapters submitted for publication in the ACS Symposium series could not fit into one volume and therefore we decided to split them into two volumes. In order to balance the size of each volume we did not divide the chapters into volumes related to mechanisms and materials but rather to those related to atom transfer radical polymerization (ATRP) and to other controlled/living radical polymerization methods: reversible-addition fragmentation transfer (RAFT) and other degenerative transfer techniques, as well as stable free radical polymerizations (SFRP) including nitroxide mediated polymerization (NMP) and organometallic mediated radical polymerization (OMRP).

The first chapter in this volume provides an overview of the current status of controlled/living radical polymerization (CRP) systems. The following three chapters discuss important issues relevant to all radical polymerization methods. The mechanistic and kinetic topics of ATRP are

covered in eight chapters. The macromolecular architecture, various hybrids and bio-related polymers prepared by ATRP are discussed in the next six chapters, Characterization and materials aspects of ATRP polymers are covered in six chapters, whereas the last four chapters discuss industrial applications of ATRP.

The next volume contains 10 chapters on mechanisms and kinetics of RAFT, other degenerative transfer processes, NMP and OMRP. They are followed by six chapters devoted to molecular architecture accessible by these techniques. Various materials aspects of the resulting polymers are covered in six chapters. The last two chapters present commercial application of polymers prepared by NMP and RAFT (or MADIX).

Fifty chapters published in two volumes show that CRP has made a significant progress within the last decade. New systems have been discovered; substantial progress has been achieved in understanding the mechanism and kinetics of reactions involved in all CRP systems. Significant progress has been made towards a comprehensive relationship between molecular structure and macroscopic properties. Some commercial applications of CRP were announced at the Philadelphia Meeting and it is anticipated that many new products will be soon on the market.

The financial support for the symposium from the following organizations is acknowledged: ACS Division of Polymer Chemistry, Inc., ACS Petroleum Research Foundation, Arkema, Bayer, Boston Scientific, Ciba, CIP, Dionex, DSM, Elsevier, Evonik, General Electric, JSR, Lion, Mitsui Chemicals, National Starch, PPG and Sumitomo. The excellent editorial assistance from Joyce Von Vreckin is gratefully acknowledged.

## **Krzysztof Matyjaszewski**

Department of Chemistry  
Carnegie Mellon University  
4400 Fifth Avenue  
Pittsburgh, PA 15213

## Chapter 1

# Controlled Radical Polymerization: State of the Art in 2008

Krzysztof Matyjaszewski

Center for Macromolecular Engineering, Department of Chemistry,  
Carnegie Mellon University, 4400 Fifth Avenue, Pittsburgh, PA 15213, USA

State of the art of Controlled Radical Polymerization (CRP) is presented. Stable free radical polymerization, atom transfer radical polymerization, and degenerate transfer processes, including reversible addition fragmentation transfer are discussed as the most successful CRP techniques. They provide access to new materials from many commercially available monomers under undemanding conditions. Better understanding of the structure-reactivity relationship for the various CRPs and a deeper insight into the mechanistic features can expand range of polymerizable monomers and polymer architectures. Development of a precise relationship between macromolecular structure, processing and final properties of materials will help to find new applications and accelerate commercialization of CRP products.

Controlled/living radical polymerization (CRP) is among the most rapidly developing areas of chemistry and polymer science.<sup>1-3</sup> The research on CRP encompasses very fundamental mechanistic studies, synthetic polymer chemistry, many detailed physical chemistry studies to evaluate properties of prepared materials and also search for new applications to commercialize CRP products.

During the last fifteen years an explosive increase has been observed in the number of publications on CRP, including a dramatic increase in the number of patent applications and several symposia devoted partially, or entirely, to CRP.<sup>4-7</sup>

Figure 1 illustrates results of a recent SciFinder Scholar search using the following terms: *controlled radical polymn* or *living radical polymn*



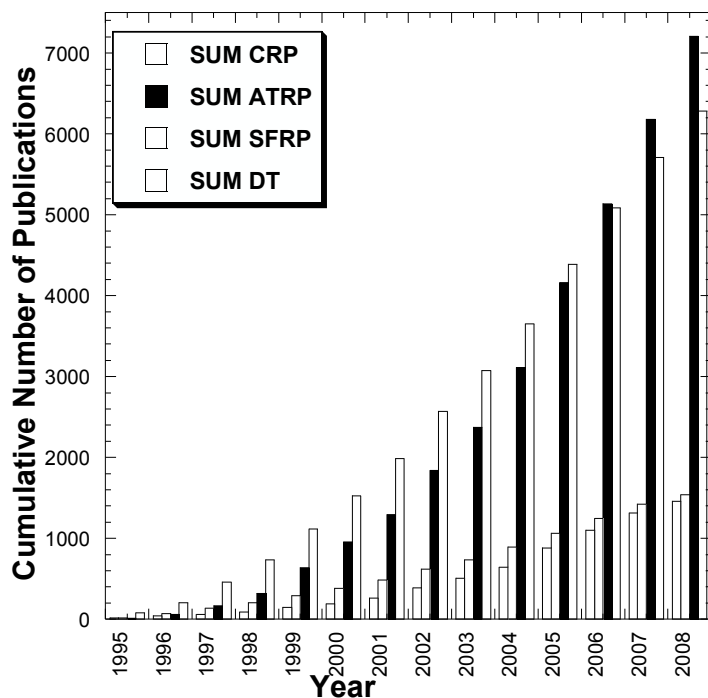


Figure 1. Results of SciFinder Search on various CRP systems as of November 15, 2008. Detail explanation of terms is provided in the text.

(“CRP&LRP” in Figure 1), *ATRP* or *atom transfer (radical) polymn* (“ATRP only”, this search does not include terms such as metal mediated or metal catalyzed (living) radical polymerization), *NMP* or *SFRP* or *nitroxide mediated polymn* or *stable free polymn* (“SFRP&NMP”) and *RAFT* or *reversible addition transfer* or *degenerative transfer* or *catalytic chain transfer* (“RAFT&DT&CT”). The latter two terms were refined with a term *radical polymn* since they coincide with other common chemical names such as *N-methylpyrrolidone* or *raft-associated proteins*. In summary, since 1995 over 12,000 papers have been published on various CRP systems and more than half of that on ATRP. During the last four years, about 3 papers per day are published daily on ATRP. There is also another trend which can be deduced from Figure 1. Progressively more papers are published on specific techniques of CRP rather than referring to a generic CRP or LRP terms.

All CRP methods rely on a dynamic equilibration between tiny amounts of propagating radicals and various types of dormant species. The essence of the process is a rapid reversible deactivation of growing radicals. Radicals always terminate and therefore CRP is never “living” in the pure sense of the living polymerization definition. Indeed, IUPAC recommends to avoid using term “living” for the radical polymerization and suggests to use the term “controlled reversible deactivation radical polymerization”.

At the same rate of polymerization (whether it is a conventional process or CRP), the same radical concentration is present and essentially the same number

(concentration) of chains terminate. However, in the conventional process, all chains are terminated (e.g.,  $10^{-3}$  M), whereas in CRP, as a result of the large total concentration of chains (e.g.,  $10^{-1}$  M of dormant and active/terminated), the fraction of terminated chains ( $10^{-3}$  M) is much smaller (typically between 1 and 10%). The remaining chains are in the dormant state, capable of reactivation, functionalization, chain extension to form block copolymers, etc. Since the proportion of terminated chains in the final product is small, they often do not affect the physical properties of the targeted materials.

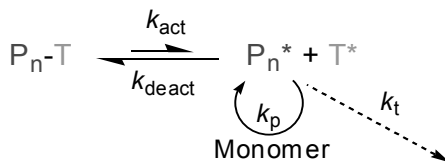
Perhaps the most important difference between conventional and CRP processes is the approach to the steady state. In a conventional radical polymerization, steady state is achieved by balancing rate of initiation and termination. In order to prepare polymers with high molecular weights ( $M_n \sim 100,000$ , i.e. with  $DP \sim 1000$ ), propagation rate must be 1000 times higher than termination rate. Consequently initiation must be also 1000 times slower than propagation. This prevents synthesis of well defined polymers. In order to prepare polymers with controlled molecular weights ( $DP_n = \Delta[M]/[I]_0$ ) and narrow molecular weight distribution, the rate of initiation should be comparable to propagation. In systems controlled by the persistent radical effect, such as ATRP and SFRP, steady state is achieved by balancing rates of activation and deactivation rather than initiation and termination. For the first time in radical polymerization, this allows decoupling the rates of initiation and termination. Termination must still be thousands times slower than propagation, but initiation can now be as fast as propagation.

The key to attaining control in CRP is the reversible deactivation of radicals (or intermittent activation of dormant species). Their interconversion should be fast, to provide a similar probability of growth for all chains and, consequently, form polymers with narrow molecular weight distribution. Fine tuning of the exchange rate offers a possibility to design molecular weight distribution and also influence polymer properties. Such polymers will preserve chain end functionalities, will be capable of cross-propagation and block copolymer formation. On the other hand, due to continuously occurring termination, polymers may lose functionality and still keep low polydispersity (especially if termination occurs at high conversion by disproportionation). Thus, a correlation between polydispersity and functionality in CRP is relatively weak.

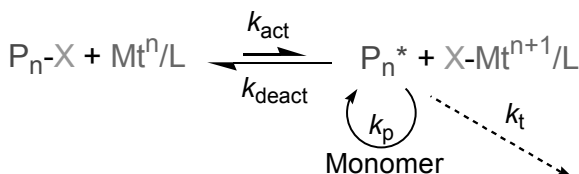
Figure 2 shows three approaches to the intermittent activation required for CRP. SFRP and ATRP employ the persistent radical effect.

SFRP (exemplified by nitroxide mediated polymerization, NMP, or organometallic radical polymerization, OMRP) relies on spontaneous homolytic cleavage of covalent species. Deactivators are typically paramagnetic species but compounds with even number of electrons could be also used (e.g. thioketone mediated polymerization, TKMP). The homolytic cleavage can be catalyzed as in ATRP. Both these processes rely on persistent radical effect (PRE). The alternative approach utilizes a degenerative transfer (DT) mechanism with alkyl iodides, dithioesters/xanthates (reversible addition fragmentation transfer, RAFT or MADIX) or organometallic species as transfer agents. DT systems do not obey PRE kinetics but follow a conventional radical polymerization with a steady state established by balancing initiation and termination rates rather than activation/deactivation.

1) SFRP: Spontaneous reversible activation of dormant species ( $T^*$  = nitroxide or metal complex)



2) ATRP: Catalyzed reversible activation of dormant species ( $X = \text{Br}, \text{Cl}; \text{Mt}^n = \text{Cu}^I, \text{Fe}^{II}, \text{Ru}^{II}$ )



3) DT: Dormant species participate in degenerative transfer with tiny amount of radicals ( $X = \text{iodide, dithioester, organometallic species, etc}$ )

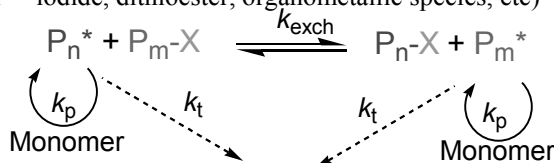


Figure 2. The three main CRP methods: SFRP, ATRP and DT

However, a clear distinction between the three classic CRP systems becomes more difficult as new CRP systems are being developed. New ATRP initiating systems such as activators re-generated by electron transfer (ARGET)<sup>8</sup> and initiators for continuous activator regeneration (ICAR)<sup>9</sup> kinetically resemble RAFT, since the rate depends on the amount of a radical initiator (AIBN, like in RAFT) and not on the reducing power or a catalyst (as in ATRP). ARGET employs reducing agents which do not generate initiating radicals, such as ascorbic acid, sugars, metal (0) (an ATRP process initiated by alkyl halides in the presence of Cu(0) and amine ligands<sup>10</sup> was recently named a single-electron-transfer living radical polymerization, SET-LRP,<sup>11</sup> although for most monomers activation occurs via atom transfer, i.e., inner sphere electron transfer but not via outer sphere electron transfer and Cu(0) predominantly serves as a reducing agent to regenerate activators as in ARGET ATRP<sup>12</sup>), amines or even some monomers themselves (DMAEMA).<sup>13,14</sup> ATRP can be carried out not only with halogens but also with pseudohalogens, including dithioesters, xanthates or dithiocarbamates.<sup>15</sup> The resulting control is due to a dual mediating system: activation/deactivation via ATRP and a degenerative exchange via RAFT. Contribution of both processes depends on monomer, structure of RAFT reagent and catalyst used. So, is it RAFT or ATRP? ATRP with alkyl iodides also has a mixed DT/ATRP element. OMRP can proceed via SFRP process but some reagents will also have DT component and some species may even participate in ATRP.

Figure 3 shows how various CRP systems inter-relate and how they conform to a classic SFRP, ATRP and DT mechanisms illustrated in Figure 2. For example, OMRP of vinyl acetate with Co derivatives proceeds with some contribution of degenerative transfer.<sup>16-18</sup> This depends on the use of additives that can promote spontaneous dissociation (SFRP) or rather favor DT process.<sup>19</sup> Some contribution of DT may also happen for acrylate polymerization. Classic dithiocarbamates as iniferters are poor transfer agents for styrene and methacrylates but are more efficient for vinyl acetate. Their activation by UV irradiation leads to homolytic bond cleavage and a predominant SFRP process with methacrylates but a concurrent DT with vinyl acetate.<sup>20</sup> In a similar way Te, Sb or Bi compounds can cleave homolytically but also can exchange with growing radicals via a degenerative process, depending on their structure and the monomers involved.<sup>21</sup>

Alkyl bromides and chlorides in ATRP cannot react directly with growing radicals and do not participate in DT process. However, alkyl iodides can.<sup>22</sup> Contribution of DT will depend on activity of catalyst and kinetics of the activation/deactivation process. ATRP deactivators are usually paramagnetic species and react fast with growing radicals. However, sometimes activators can be paramagnetic. Perhaps the most intriguing is the reversible transfer catalyzed polymerization (RTCP) with GeI<sub>4</sub>, SnI<sub>4</sub>, or PI<sub>3</sub> deactivators and GeI<sub>3</sub><sup>\*</sup>, SnI<sub>3</sub><sup>\*</sup> and PI<sub>2</sub><sup>\*</sup> activators.<sup>23,24</sup> ATRP with dithiocarbamates will predominantly occur via activation/deactivation but with xanthates and dithioesters (i.e., concurrent ATRP/RAFT or Cu-catalyzed RAFT), contribution of DT process will become progressively larger. For trithiocarbonate it can be predominantly ATRP or RAFT, depending on monomer, initiator and catalyst structure. In the presence of light, a contribution of SFRP mechanism will become possible.<sup>15,25,26</sup>

Some Mo, Os and other organometallic species show not only SFRP but also ATRP activity.<sup>27</sup> This will depend on the nature of halogen, monomer and ligands. Thus, there are many systems that show a concurrent involvement of spontaneous activation/deactivation (SFRP), a catalyzed process (ATRP) and a degenerative exchange (DT) and their contributions to the overall control depend on the structure of reagents but also reactions conditions (concentration, temperature, light, additives, etc.)

The three fundamental techniques have been constantly improved and applied to the preparation of well-defined polymers from new monomers. For example, in SFRP, recently developed nitroxides have been successfully used to polymerize acrylates, acrylamides and most recently also methacrylates in the presence of small amounts of styrene.<sup>28</sup> Cobalt porphyrines were originally used for CRP of acrylates but more recently for vinyl acetate. Both systems were successfully applied in aqueous dispersed media.

In ATRP, the range of polymerizable monomers have been extended to vinyl acetate, dienes and vinyl chloride.<sup>29,30</sup> Also, new metals (Mo, Os, Ti) and new ligands were successfully introduced. ATRP was successfully carried out in miniemulsion and microemulsion as well as in CO<sub>2</sub> or in ionic liquids. New initiating systems were developed for ATRP, such as ARGET and ICAR.<sup>8,9,31</sup> They start from oxidatively stable transition metal complexes (Cu<sup>II</sup>) and are activated in the presence of reducing agents. Reduced amount of catalyst and its

immobilization<sup>32</sup> diminishes side reactions and allows precise tuning of the polydispersities of the resulting polymers.

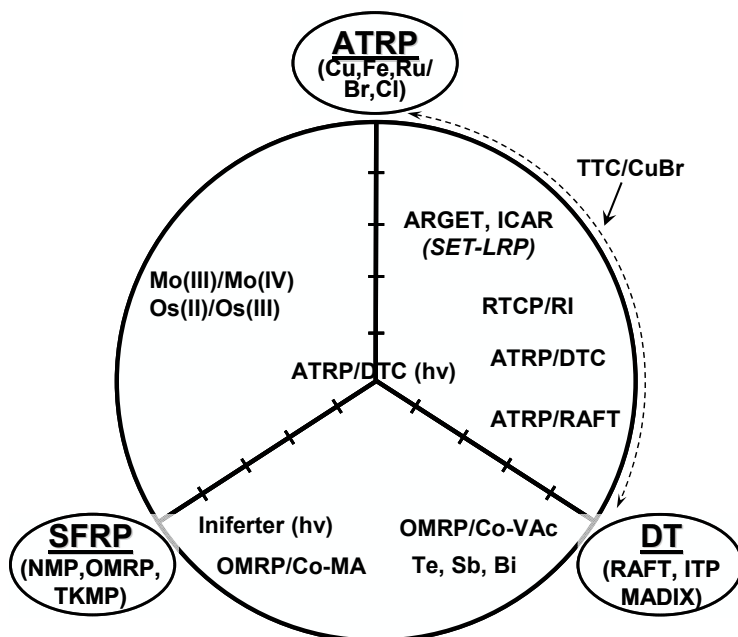


**Figure 3.** Schematic representation of various CRP systems and their relation to classic SFRP, ATRP and DT mechanisms.

RAFT and MADIX are the two most successful degenerative transfer processes but significant progress has been also demonstrated in iodine DT and in the use of Sb, Bi and other organometallic mediators.<sup>24</sup>

As mentioned before, one of the main driving forces for the rapid expansion of CRP is preparation of (co)polymers with precisely controlled architectures, composition and terminal functionality forming new materials for targeted applications.

Several chapters in this book demonstrate synthesis of new block copolymers, stars, grafts, brushes. There are new approaches for the preparation of functional polymers and their subsequent modification using e.g. “click” chemistry. New bioconjugates were prepared by either ATRP or RAFT.<sup>33</sup> Similarly, new organic-inorganic hybrids were synthesized.<sup>34,35</sup> Equally exciting is the progress in commercialization of products made by CRP. Several corporations started commercial production using SFRP, ATRP and also DT processes.

## Outlook

In introductory chapters for the proceedings volumes from the previous ACS CRP Symposia I referred to several challenges facing CRP processes:

1. How to enhance livingness of CRP systems without sacrificing the polymerization rate.
2. How to make polymers with enhanced tacticity and sequence control.

3. Comprehensive structure-reactivity correlation for various CRP systems.
4. Search for more environmentally friendly and inexpensive CRP mediating agents.
5. Fundamental structure-property correlation for new materials prepared by CRP.
6. Synthesis of advanced hybrid materials including inorganics and natural products.

These challenges have been addressed and significant progress has been made in all of these areas:

1. In all CRP systems the proportion of terminated chains increases with polymerization rate, with monomer conversion and with molecular weight. Therefore, it is possible to reduce the percentage of terminated chains at lower conversion while targeting lower molecular weight polymers. Since the proportion of terminated chains depends on the  $k_p/k_t$  ratio, it is possible to form relatively rapidly high molecular weight polyacrylates but not polystyrene or poly(methacrylates), since the former propagate  $\sim 50$  times faster but terminate with the same rate. Therefore, several approaches have been recently developed to rapidly prepare high MW polystyrene or poly(methyl methacrylate), i.e., how to increase their  $k_p/k_t$  ratio. Compartmentalization in mini/micro emulsion has been used to segregate radicals to individual droplets and reduce the probability of termination.<sup>36</sup> Conducting the reaction under high pressure significantly increases  $k_p/k_t$  ratio, due to the differences in activation volumes, and offers fast routes to high MW polymers.<sup>37</sup> It will be interesting to explore new complexing agents that could reduce bimolecular coupling by electrostatic repulsion. In a similar way, chain length dependent termination could enhance  $k_p/k_t$  ratio at higher conversion. Also, higher temperature should result at higher  $k_p/k_t$  ratio, providing transfer processes remain insignificant.

2. Sp<sup>2</sup> hybridization of radicals, and their relatively low selectivities (in comparison with active centers in ionic or coordination polymerization) prevent synthesis of highly tactic polymers and polymers with sequence control. However, Lewis acids and other complexing agents help to enhance control of sequence distribution and polymer tacticity. This led to the synthesis of the first stereo-block copolymers prepared by radical procedures, and also new copolymers with alternating sequences.<sup>38</sup> New selective complexing agents, perhaps combined with thermodynamic or kinetic control (above ceiling temperature or with neighboring group assistance) or confined space could further enhance stereo- and chemoselectivity.

3. The improvement in the first two areas has been possible because of the progress made in understanding the mechanism and kinetics of radical polymerization and the structure of radical intermediates.<sup>12,39</sup> Further advancement requires detailed structure-reactivity correlation for radicals and also for dormant species. Both experimental measurements of rate and equilibrium constants as well as computational evaluation of thermodynamic (bond dissociation, redox properties) and kinetic properties of the involved species is needed. This will help to establish order of reactivities for various species and will assist selection of the efficient initiators or sequence of monomer addition for block copolymerization.

4. The structure – reactivity correlation will also help to identify new environmentally friendly and less expensive mediating agents. This will include a range of new ATRP catalysts, to be used at ppm amounts in benign media, new alkyl (pseudo)halide initiators, nitroxides operating at lower temperatures and applicable to methacrylates, and also more environmentally friendly RAFT reagents.

5. CRP provides access to a large variety of (co)polymers with controlled MW, MWD, topology, composition and functionality. However, a full systematic evaluation of properties and potential applications of these materials is still missing. A thorough structure-property relationship for a large range of (co)polymers is very much needed. Their final properties will depend not only on their molecular structure but also on processing, since processing affects their self-assembly to complex morphologies. Experimental evaluation of “libraries” with systematically varied parameters, together with computational/simulation or theoretical treatment, will help to predict properties of new systems and suggest new applications.

6. Covalent attachment of two incompatible systems generate new hybrid materials with novel properties. These hybrids will include some amphiphilic block copolymers but also segmented copolymers with polar (acrylics) and non-polar (polyolefins) segments. These systems can act as efficient blend compatibilizers but also as surfactants and additives<sup>40</sup>. Even more exciting is the area of organic-inorganic hybrids and bioconjugates.<sup>41</sup> Dense grafting from flat, cylindrical and spherical surfaces not only prevents aggregation but leads to a new class of nanocomposites with new electronic and mechanical properties. New biomaterials and bioconjugates based on water soluble components and especially stimuli responsive organic polymers will find applications in drug delivery systems and tissue engineering.

### New Challenges

I would like to add some new challenges and indicate some new potential areas for research in the future years

1. **Controlled heterogeneity.** So far we have been obsessed with the synthesis of well-defined uniform polymer chains with low polydispersity, regular branching, pure block copolymers, stars with exact number of arms, etc. However, controlled synthesis of polymers with one or more segments displaying a distribution of chain lengths may help to generate polymers with new stable morphologies.<sup>42,43</sup> Enhanced curvature at the interphase will help prepare bicontinuous systems needed for membranes, some biorelated applications or photovoltaics. Continuous change of composition along the chain length in gradient copolymers significantly broadens glass transition and provides access to materials for vibration and noise dumping as well as more efficient surfactants. Broad distribution of branches helps processing and may also enhance properties of gels and networks. It must be stressed that we can, and need to control, such heterogeneities in order to optimize and fine tune properties rather than let them be spontaneously generated.

- 2. Cost-performance for commercial products.** Commercialization of CRP products is slower than we would like. This can be due to many factors but a simple cost-performance issue is high on the list. Less copper in ATRP will broaden MWD but can also generate new materials. Therefore controlled heterogeneity can potentially reduce the price and also enhance performance. Broader structural distributions will relax processing regimes. How important will be one or some missing arms in star polymers or brushes? How critical will be lost functionality? How do the properties of pure block copolymer compare with one containing a central tapered structure. Some answers to these questions will depend on particular applications but should be carefully studied.
- 3. Functional groups for orthogonal chemistry.** Radical polymerization, in contrast to ionic and coordination polymerization, is tolerant of many functionalities. Can we incorporate them into monomers and build polymer chains with groups capable for orthogonal and robust chemistry such as “click”, epoxy transformation, thiol-ene reaction, reversible multiple hydrogen bonding and many others?
- 4. CRP polymers for energy and environment.** As our society faces new world challenges, advanced polymers prepared by CRP can help to address some of these issues. Functional polymers prepared by CRP can be combined covalently with optoelectronically active polymers and generate bulk heterojunctions at the nanometer scale. They can be used as precursors for nanostructured graphitic carbons, and as electrode materials or membranes, both in fuel cells or water desalination. One big environmental challenge for CRP polymers is their controlled degradation (also very important for all biomedical applications). How are vinyl polymers efficiently degraded? One approach is to incorporate degradable units into the backbone by radical ring opening copolymerization. The other would be to generate stars with degradable cores or precisely controlled networks with degradable crosslinkage. These objectives and other properties can be further tuned by using stimuli responsive polymers that can respond to temperature light, pH, ionic strength, pressure, electric or magnetic field.
- 5. Computational modeling and simulation.** The increased power, enhanced precision and reduced cost of computational techniques will help in attaining a deeper insight into mechanism, analyze complex kinetic multireaction systems and predict properties of polymers with novel architectures. Computation will also help to “screen” and suggest new mediating agents for CRP and also will provide leads for synthesis of new polymers and generate materials with new morphologies and new properties.

We anticipate that these and many other issues will be studied during the next few years and will be presented at the next ACS Symposium on CRP, especially as commercial importance of CRP continuously increases.



**Acknowledgments.** Support from the National Science Foundation (CHE 07-15494) and DMR (05-49353) is gratefully acknowledged.

## References

- (1) Matyjaszewski, K.; Davis, T. P. *Handbook of Radical Polymerization*; Wiley-Interscience: Hoboken, 2002.
- (2) Matyjaszewski, K.; Spanswick, J. *Mater. Today* **2005**, 8, 26-33.
- (3) Braunecker, W. A.; Matyjaszewski, K. *Prog. Pol. Sci.* **2007**, 32, 93-146.
- (4) Matyjaszewski, K.; Editor *Controlled Radical Polymerization. (Proceedings of a Symposium at the 213th National Meeting of the American Chemical Society, held 13-17 April 1997, in San Francisco, California.) [In: ACS Symp. Ser., 1998; 685]*, 1998.
- (5) Matyjaszewski, K.; Editor *Controlled/Living Radical Polymerization. Progress in ATRP, NMP, and RAFT. (Proceedings of a Symposium on Controlled Radical Polymerization held on 22-24 August 1999, in New Orleans.) [In: ACS Symp. Ser., 2000; 768]*, 2000.
- (6) Matyjaszewski, K.; Editor *Advances in Controlled/Living Radical Polymerization. (ACS Symposium held in Boston, Massachusetts 15-18 August 2002.) [In: ACS Symp. Ser., 2003; 854]*, 2003.
- (7) Matyjaszewski, K.; Editor *Controlled/Living Radical Polymerization: From Synthesis to Materials. (ACS Symposium held in Washington, DC, 2005.) [In: ACS Symp. Ser., 2006; 944]*, 2006; Vol. 944.
- (8) Jakubowski, W.; Min, K.; Matyjaszewski, K. *Macromolecules* **2006**, 39, 39-45.
- (9) Matyjaszewski, K.; Jakubowski, W.; Min, K.; Tang, W.; Huang, J.; Braunecker, W. A.; Tsarevsky, N. V. *Proc. Natl. Acad. Sci.* **2006**, 103, 15309-15314.
- (10) Matyjaszewski, K.; Coca, S.; Gaynor, S. G.; Wei, M.; Woodworth, B. E. *Macromolecules* **1997**, 30, 7348-7350.
- (11) Percec, V.; Guliashvili, T.; Ladislaw, J. S.; Wistrand, A.; Stjerndahl, A.; Sienkowska, M. J.; Monteiro, M. J.; Sahoo, S. *J. Amer. Chem. Soc.* **2006**, 128, 14156-14165.
- (12) Lin, C. Y.; Coote, M. L.; Gennaro, A.; Matyjaszewski, K. *J. Amer. Chem. Soc.* **2008**, 130, 12762-12774.
- (13) Dong, H.; Matyjaszewski, K. *Macromolecules* **2008**, 41, 6868-6870.
- (14) Matyjaszewski, K.; Tsarevsky, N. V.; Braunecker, W. A.; Dong, H.; Huang, J.; Jakubowski, W.; Kwak, Y.; Nicolay, R.; Tang, W.; Yoon, J. A. *Macromolecules* **2007**, 40, 7795-7806.
- (15) Kwak, Y.; Nicolay, R.; Matyjaszewski, K. *Macromolecules* **2008**, 41, 6602-6604.
- (16) Debuigne, A.; Champouret, Y.; Jerome, R.; Poli, R.; Detrembleur, C. *Chem.--Eur. J.* **2008**, 14, 4046-4059.
- (17) Peng, C.-H.; Scricco, J.; Li, S.; Fryd, M.; Wayland, B. B. *Macromolecules* **2008**, 41, 2368-2373.
- (18) Debuigne, A.; Poli, R.; Jerome, C.; Jerome, R.; Detrembleur, C. *Prog. Polym. Sci.* **2009**, 34, 211-239.

- (19) Maria, B.; Kaneyoshi, H.; Matyjaszewski, K.; Poli, R. *Chem.--Eur. J.* **2007**, *13*, 2480-2492.
- (20) Otsu, T. *J. Polym. Sci., Part A: Polym. Chem.* **2000**, *38*, 2121-2136.
- (21) Kwak, Y.; Tezuka, M.; Goto, A.; Fukuda, T.; Yamago, S. *Macromolecules* **2007**, *40*, 1881-1885.
- (22) Gaynor, S. G.; Wang, J.-S.; Matyjaszewski, K. *Macromolecules* **1995**, *28*, 8051-8056.
- (23) Goto, A.; Hirai, N.; Tsujii, Y.; Fukuda, T. *Macromol. Symp.* **2008**, *261*, 18-22.
- (24) Goto, A.; Zushi, H.; Hirai, N.; Wakada, T.; Tsujii, Y.; Fukuda, T. *J. Amer. Chem. Soc.* **2007**, *129*, 13347-13354.
- (25) Kwak, Y.; Matyjaszewski, K. *Macromolecules* **2008**, *41*, 6627-6635.
- (26) Nicolay, R.; Kwak, Y.; Matyjaszewski, K. *Macromolecules* **2008**, *41*, 4585-4596.
- (27) Poli, R. *Angew. Chem., Int. Ed.* **2006**, *45*, 5058-5070.
- (28) Nicolas, J.; Dire, C.; Mueller, L.; Belleney, J.; Charleux, B.; Marque, S. R. A.; Bertin, D.; Magnet, S.; Couvreur, L. *Macromolecules* **2006**, *39*, 8274-8282.
- (29) Tang, H.; Radosz, M.; Shen, Y. *AIChE Journal* **2009**, *55*, 737-746.
- (30) Percec, V.; Popov, A. V.; Ramirez-Castillo, E.; Monteiro, M.; Barboiu, B.; Weichold, O.; Asandei, A. D.; Mitchell, C. M. *J. Amer. Chem. Soc.* **2002**, *124*, 4940-4941.
- (31) Jakubowski, W.; Matyjaszewski, K. *Angew. Chem., Int. Ed.* **2006**, *45*, 4482-4486.
- (32) Faucher, S.; Zhu, S. *J. Polym. Sci., Part A: Polym. Chem.* **2007**, *45*, 553-565.
- (33) Lutz, J.-F.; Boerner, H. G. *Prog. Pol. Sci.* **2008**, *33*, 1-39.
- (34) Tsujii, Y.; Ohno, K.; Yamamoto, S.; Goto, A.; Fukuda, T. *Adv. Polym. Sci.* **2006**, *197*, 1-45.
- (35) Chen, R.; Zhu, S.; Maclaughlin, S. *Langmuir* **2008**, *24*, 6889-6896.
- (36) Zetterlund, P. B.; Kagawa, Y.; Okubo, M. *Chem. Rev.* **2008**, *108*, 3747-3794.
- (37) Kwiatkowski, P.; Jurczak, J.; Pietrasik, J.; Jakubowski, W.; Mueller, L.; Matyjaszewski, K. *Macromolecules* **2008**, *41*, 1067-1069.
- (38) Satoh, K.; Mizutani, M.; Kamigaito, M. *Chem. Commun.* **2007**, 1260-1262.
- (39) Tang, W.; Kwak, Y.; Braunecker, W.; Tsarevsky, N. V.; Coote, M. L.; Matyjaszewski, K. *J. Amer. Chem. Soc.* **2008**, *130*, 10702-10713.
- (40) Feldman, K. E.; Kade, M. J.; de Greef, T. F. A.; Meijer, E. W.; Kramer, E. J.; Hawker, C. J. *Macromolecules* **2008**, *41*, 4694-4700.
- (41) Pressly, E. D.; Rossin, R.; Hagooley, A.; Fukukawa, K.-I.; Messmore, B. W.; Welch, M. J.; Wooley, K. L.; Lamm, M. S.; Hule, R. A.; Pochan, D. J.; Hawker, C. J. *Biomacromolecules* **2007**, *8*, 3126-3134.
- (42) Listak, J.; Jakubowski, W.; Mueller, L.; Plichta, A.; Matyjaszewski, K.; Bockstaller, M. R. *Macromolecules* **2008**, *41*, 5919-5927.
- (43) Lynd, N. A.; Meuler, A. J.; Hillmyer, M. A. *Prog. Polym. Sci.* **2008**, *33*, 875-893.

## Chapter 2

# Real and Apparent Sources of Polydispersity in Molecular Weight Distributions from Radical Polymerization

Gregory T. Russell

Department of Chemistry, University of Canterbury, Private Bag 4800,  
Christchurch, New Zealand

This paper is intended as a guide for workers in the field of radical polymerization, the aim being to assist them to understand their molecular weight distributions better. The fundamentals of molecular weight distributions are first of all summarized, then the remainder of the paper outlines some factors that perturb ideal broadness in real systems. The following phenomena are dealt with in this context: column broadening in size exclusion chromatography (SEC); SEC calibration; baseline selection in SEC; signal intensity in time-of-flight mass spectrometry (and SEC); conversion-induced broadening; chain-length-dependent termination; and chain-length-dependent propagation.

## Introduction

A Holy Grail of the macromolecular chemist is to achieve the ‘purity’ in size of micromolecular chemistry. In a real sense this quest is like that of Sisyphus in Greek mythology, who was eternally condemned to rolling a boulder uphill. The macromolecular chemist will also never reach the top of the hill, because the statistical nature of all polymerizations makes true monodispersity in size impossible to achieve by chemical means. Be that as it may, the advent of living radical polymerization (LRP) has reawakened the dream, and over the last decade there have been literally tens of thousands of papers in which workers have used this tremendous new chemical principle to

strive towards the magical polydispersity index of 1. Given this it is timely to take stock of recent and ongoing investigations into factors that influence the polydispersity of molecular weight distributions (MWDs) from RP.

## Background

When all is said and done, there are only two basic chain-growth polymerization paradigms: (1) ideal living polymerization, and (2) ‘conventional’ (or ‘classical’) chain-growth polymerization. Of course real systems show imperfections and may be a mixture of these paradigms. However this does not change the essential nature of such systems, of which it is well to be aware. Therefore the key MWD equations for each paradigm will now be summarized. In particular it will be stressed that there is a ‘natural broadening’ associated with each, a term that I use in analogy with spectroscopy, where it refers to the minimum possible linewidth of a signal.

### Ideal Living Polymerization

By ideal living polymerization is meant the situation of Figure 1.

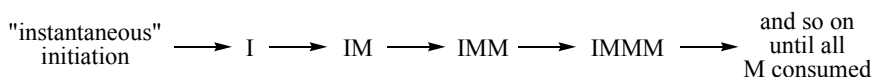


Figure 1. Schematic representation of ideal living polymerization, where I denotes initiator and M monomer.

This paradigm gives rise to a Poisson distribution of chain lengths ( $l$ ):

$$\text{number fraction of chains: } n(i) = e^{-\nu} \frac{\nu^i}{i!} \quad (1)$$

For this distribution the number-average degree of polymerization is given by

$$DP_n = \nu = \frac{x [M]_0}{[I]_0} \quad (2)$$

where  $x$  is fractional conversion, and  $[M]_0$  and  $[I]_0$  are the starting monomer and initiator concentrations respectively. The polydispersity index is  $PDI = 1 + (1/\nu)$ ; this gives the ‘natural broadening’. In all these equations, chain length refers to the number of incorporated monomer units. If one wishes to regard the initiator as contributing 1 to the chain length, then  $\nu$  remains the average number of

incorporated monomer units,  $DP_n = 1 + \nu$ , and  $i$  on the right-hand side of Equation 1 becomes  $i - 1$ .

Since Equation 1 is the very best one can achieve with a living polymerization, it is instructive to carry out sample evaluations of this equation. Such are presented in Figure 2.

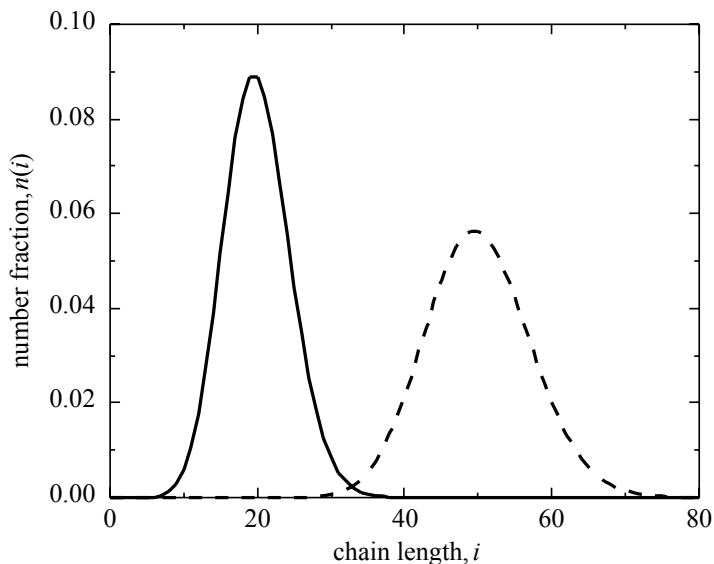


Figure 2. Poisson chain-length distributions, Equation 1, for  $\nu = 20$  (left;  $PDI = 1.05$ ) and  $\nu = 50$  (right;  $PDI = 1.02$ ).

Three important points are made by Figure 2: (1) Even though  $PDI$  is very close to 1, in terms of micromolecular idylls there is still a lot of heterogeneity in size. Yet this is the very best one can do with polymerization in terms of monodispersity. This emphasizes the point above that the stochastic nature of polymerization makes unreachable the Holy Grail of perfect monodispersity: it is simply not possible to make all growing chains march in unison. (2) Even though  $PDI$  is smaller for the case of  $DP_n = 50$ , this distribution has a greater absolute broadness. This emphasizes that  $PDI$  is only a measure of *relative* broadness. (3) One cannot independently control the *position* ( $DP_n$ ) and *broadness* ( $PDI$ ) of a Poisson distribution – they are both determined by the one parameter,  $\nu$ .

Equation 2 is well-known to hold for properly functioning LRP; although  $PDI$  is a little larger, it still has the same essential form as the equation above for ideal living polymerization (2-5).

## Conventional Chain-Growth Polymerization

By conventional chain-growth polymerization is meant the situation in Figure 3.

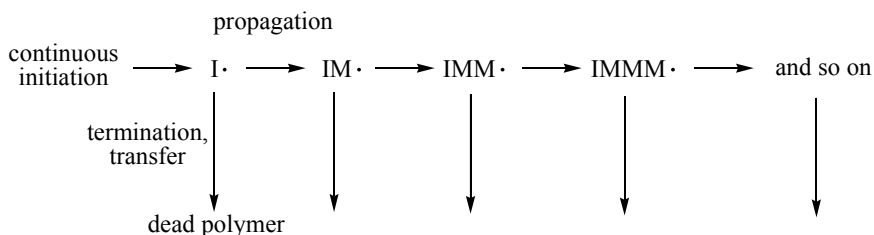


Figure 3. Schematic representation of conventional chain-growth polymerization, where a horizontal arrow denotes propagation and a vertical arrow denotes a reaction that creates a dead chain.

Assuming chain-length-independent reactivities (as signified by horizontal arrows of the same length and vertical arrows of the same length in Figure 3), this paradigm generates a Flory-Schulz (most probable) distribution (6, 7):

$$\frac{w(\log_{10} i)}{\ln 10} = F_w \left(\frac{i}{\nu}\right)^2 \exp\left(\frac{-i}{\nu}\right) + 0.5(1 - F_w) \left(\frac{i}{\nu}\right)^3 \exp\left(\frac{-i}{\nu}\right) \quad (3)$$

This is a two-parameter distribution (cf. Equation 1). For RP the values of these parameters are

$$\nu = \frac{k_p[M]}{k_{trX}[X] + 2k_t[R]} \quad (4)$$

$$F_w = \frac{k_{trX}[X] + 2k_{td}[R]}{k_{trX}[X] + 2k_{td}[R] + 2k_{tc}[R]} \quad (5)$$

These expressions feature the rate coefficients for propagation,  $k_p$ , transfer to small molecule X,  $k_{trX}$ , termination,  $k_t$ , disproportionation,  $k_{td}$  and combination,  $k_{tc}$  ( $k_t = k_{td} + k_{tc}$ ), while  $[R] = [R_i/(2k_t)]^{0.5}$  is the total radical concentration,  $R_i$  being the rate of initiation. In terms of physical meaning,  $\nu$  is the average number of propagation events that a newly formed radical (whether by initiation or transfer) undergoes before being converted into a dead chain (some people call  $\nu$  the kinetic chain length), while  $F_w$  is the *weight* fraction of dead polymer molecules formed by transfer and disproportionation.

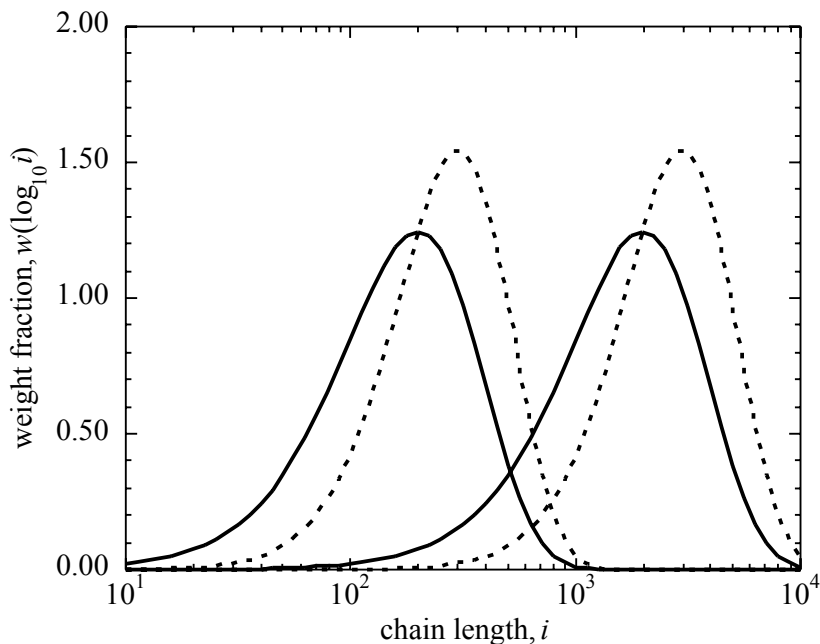


Figure 4. Flory-Schulz chain-length distributions, Equation 3, for  $\nu = 100$  (left) and  $\nu = 1\,000$  (right),  $F_w = 1$  (smaller; unbroken) and  $F_w = 0$  (taller; dashed).

Figure 4 shows some sample evaluations of Equation 3. These evaluations make clear that  $\nu$  dictates the *position* of the MWD while  $F_w$  determines its *broadness*. This one can also see from the following relations:

$$DP_n = \nu(2 - F_n) = \nu \left( 2 - \frac{2F_w}{1 + F_w} \right) \quad (6)$$

$$PDI = \frac{1}{2}(3 - F_w)(1 + F_w) \quad (7)$$

Equation 6, where  $F_n = 2F_w/(1+F_w)$  is the *number* fraction of dead chains formed by disproportionation and transfer, is just the so-called Mayo equation, which is much used because it affords control of average polymer size. Equation 7 gives a minimum value of  $PDI = 1.5$  for the case of all dead-chain formation by combination ( $F_w = 0$ ) and a maximum value of  $PDI = 2$  for the case of no combination ( $F_w = 1$ ). Thus the natural broadening of a conventional radical polymerization will be somewhere between these two  $PDI$  limits, depending on the balance between transfer/disproportionation and combination that one has.

The equations presented in this section have been known for many decades. One reason for giving them here is that they have tended to become lost in the mists of time, even though they remain highly useful, including for modeling of data. The other reason for giving them is that they establish reference points for

the broadness of MWDs. The remainder of this article will be about factors that *perturb* – either increase or decrease – this natural broadening.

## Apparent Sources of Polydispersity Perturbation

In this section I will outline some *apparent* sources of polydispersity perturbation. What I mean by the word apparent is that the MWD of the polymer is made to appear different – whether broader or narrower – to what it truly is. Such effects are obviously instrumental in origin, although one hesitates to label them as instrumental error, because in most instances it is more a case of workers not fully appreciating exactly what the instrument is delivering.

The first three subsections concern size exclusion chromatography (SEC). Although by no means a dream technique, it has many powerful virtues, and thus remains the method of choice for MWD determination of synthetic polymers. The final subsection concerns time-of-flight mass spectrometry (TOF MS), which at last is starting to emerge as a viable technique for MWD determination of relatively small macromolecules.

### Column Broadening in Size Exclusion Chromatography

Even if one succeeds in synthesizing polymer as monodisperse as in Figure 2, this will not be observed via SEC because of column broadening (8). This is the unavoidable phenomenon of molecules of identical hydrodynamic volume having a distribution of elution times. Thus for any polymer sample the *apparent* MWD delivered by SEC is always broader than the *true* MWD of the sample.

There is no routine way of deconvoluting an apparent MWD to obtain the underlying true MWD. Therefore an algorithm of Lämmel et al. (9) has been used to develop the following reverse-engineering approach (10): (1) A kinetic simulation is used to generate a MWD; (2) This MWD is divided into ‘monodisperse’ slices; (3) Each slice is subjected to an appropriate broadening function, thereby simulating what happens in SEC; (4) All the broadened slices are summed so as to obtain the simulated broadened MWD; (5) This is then compared with the experimental MWD; (6) This procedure is iterated with variation of kinetic and broadening parameters in the simulation until acceptable agreement with experiment is obtained. At this point one has parameter values that tell both about the kinetics of the polymerization and the broadening caused by the SEC instrument (10). Obviously there is some scope for ambiguity in this procedure – it may not be uniquely determined whether some broadening is due to kinetics or to the SEC columns. In our work (10) we were fortunate to know with certainty that we had a transfer-controlled system ( $PDI = 2$ , see above), and thus that all extra broadening had to be instrumental in origin.

In our work (10) we used the Gaussian function to simulate column broadening in step (3), but obviously any function could be used, for example the currently favored ‘exponentially modified Gaussian’ (8,11).



Given that low *PDI* is an explicit aim of most LRP, it can be argued that accounting for column broadening is even more important in such work.

### Size Exclusion Chromatography without Proper Calibration

Another of SEC's serious imperfections is that it relies on calibration. However there are really only a handful of polymers for which monodisperse standards are available, and all of these are common polymers. A way around this is to use universal calibration, but this firstly relies on Mark-Houwink-Kuhn-Sakurada (MHKS) parameters being known, and secondly it requires that workers are aware of the need for this procedure – many evidently are not. Further, given that the aim of much research in polymer synthesis is to make *new* polymers for which, by definition, MHKS parameters will not be available, it follows that in many cases universal calibration will not be possible anyway.

It is therefore very common (12) for workers simply to assume that calibration with one polymer holds for the different polymer that they put through a SEC instrument. This assumption has recently been investigated by Guillaneuf and Castignolles, who came to some startling conclusions (12). To illustrate these, their relatively straightforward simulation algorithm has been implemented here to generate the results of Figure 5.

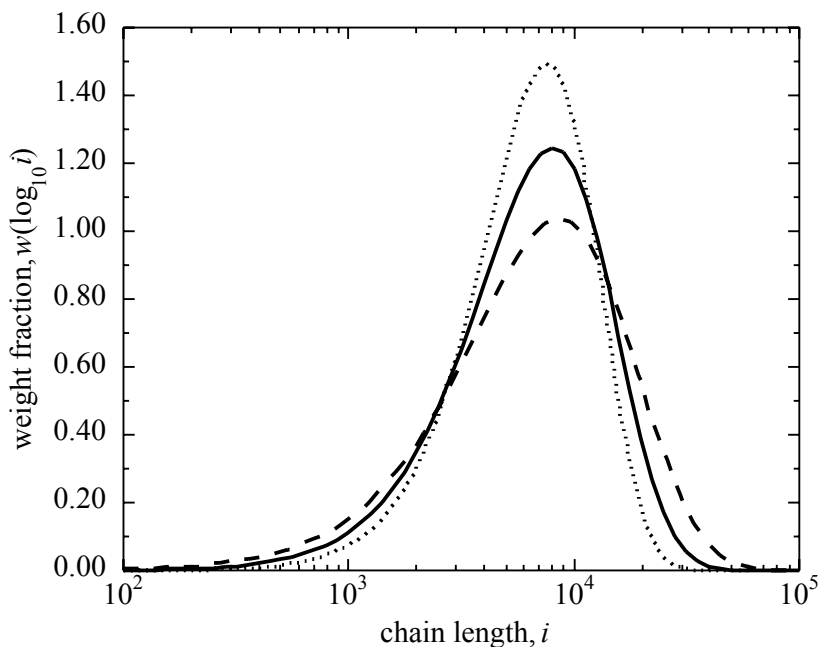


Figure 5. Chain-length distributions for transfer/disproportionation ( $F_w = 1$ ) with  $\nu = 4\,000$ . Middle (unbroken) line: direct results from Equation 3 ( $PDI = 2$ ); tallest (dotted) line: apparent results for  $a_{\text{sample}} = 0.5$ ,  $a_{\text{standard}} = 0.8$  ( $PDI = 1.60$ ); lowest (dashed) line: apparent results for  $a_{\text{sample}} = 0.8$ ,  $a_{\text{standard}} = 0.5$  ( $PDI = 2.83$ ).

Denoting the MHKS exponent as  $a$ , Figure 5 shows that  $a_{\text{sample}} > a_{\text{standard}}$  results in the apparent MWD being *broader* than the true MWD, while  $a_{\text{sample}} < a_{\text{standard}}$  gives a *narrower* apparent MWD. Further, by considering the relatively extreme case of having  $a$  of 0.5 and 0.8, Figure 5 shows that these effects can be very significant. This is especially so for LRP, where a synthesis often lives or dies according to the *PDI* it returns: a low apparent *PDI* (e.g. 1.3), suggesting a reasonably successful LRP, might actually result from a true *PDI* that would be judged a failure (e.g. 1.7); conversely, a high apparent *PDI* might be appraised a failure when in fact the true *PDI* is that of a living system (12).

There seems little doubt that this phenomenon must routinely contribute to misinterpretation of experimental results. As is clear, the way to avoid this issue is to use a standard that has approximately the same  $a$  value as the sample under investigation. Even if the  $a$  value of the sample is completely unknown, it is usually possible to estimate it by consulting the literature on polymers of a similar chemical nature.

Also coming under the broad umbrella of SEC calibration issues is branched polymers, which of course have lower hydrodynamic volume than equivalent linear polymers, as used for calibration. This topic has become of renewed focus with the advent of LRP, because it is finding much use for synthesis of a wide variety of non-linear architectures, including graft copolymers and star polymers. Readers will find this issue grappled with in a large body of literature – there is no easy, widely applicable solution. Worth specifically mentioning is a novel and elegant approach for SEC of star polymers that has been recently proposed and used by Vana et al. (13).

Of course calibration issues are not the only pitfalls with SEC. Baseline selection will be considered in the following subsection. Another issue of which users need to be aware is that refractive index (RI) is molecular-weight dependent at very low sizes. Thus there are serious limitations on the use of RI detectors for quantification of oligomers via SEC (14). In other words, standard RI detection – which assumes molecular-weight-independent RI – will not yield the true MWD at oligomeric sizes, something that is of genuine importance where polymers of very small  $DP_n$  are being prepared and analyzed (14).

## Baseline Selection in Size Exclusion Chromatography

When confronted by a SEC chromatogram, it is not clear to what extent the low-lying wings are polymer material and to what extent they are just baseline noise or artefacts. This is an issue because these regions contribute disproportionately to the *PDI* of the resulting MWD and modern SEC software enables them to be eliminated with the click of a mouse, thereby delivering a much reduced *PDI*. Many workers take this option, especially those with a background in organic chemistry, and therefore schooled in the micromolecular concept of chemically different molecules – such workers naturally tend to regard a continuous background signal as being noise. The result of this is to obtain an *apparent* MWD that is considerably narrower than the true MWD.

Some years ago the Moads carried out some simulations to investigate this (15). They showed that even just ignoring the bottom 1% of a classical transfer/disproportionation MWD could result in *PDI* decreasing from 2 to as little as 1.76, a result confirmed by calculations for the present work. So this effect can be very significant. Further, one can expect it to be even more important in LRP investigations, where there will be a Poisson-like central peak (see Figure 2) on top of a broad but low-level expanse of 'background' polymer. Writing off this background as baseline noise results in misleadingly low *PDI* being reported.

What can be done about this situation? Experimentally, correct baseline selection is a skill that comes with SEC experience. Theoretically, one should be on the lookout for unrealistically low *PDI*. For example, a LRP with  $DP_n = 20$  has a natural broadening of  $PDI = 1.05$ , and with SEC broadening operating on top of this one should expect a reported *PDI* of no less than 1.1.

### Signal Intensity in Time-of-Flight Mass Spectrometry

Without even noticing it, most polymer chemists have assumed that the signal intensity from TOF MS is proportional to the number of chains. A few years ago Schnöll-Bitai et al. drew attention to the fact that this is not the case (16), and in very recent work they have investigated this (17). The actual situation for TOF MS is that signal intensity is proportional to  $i^{0.5}n(i)$  (16,17). Figure 6 shows the implication of this for a transfer/disproportionation chain-length distribution (CLD) from classical RP (17). As can be seen, if one is unaware of this subtlety, then TOF MS will yield an apparent MWD that is narrower and considerably different to the true MWD.

In fact many reported TOF MS distributions from RP look remarkably like the apparent MWD in Figure 6, e.g. (18). In view of this it has been customary to say that TOF MS simply does not yield accurate  $n(i)$  at very low  $i$ . A large contributing factor to this situation may just be that signal intensities have not been correctly transformed into  $n(i)$ .

Similar can also be said of signal intensities from SEC with RI detection. For many years it was popularly taken that these intensities are the weight-CLD,  $w(i)$ , because RI detectors measure the weight of polymer. In fact the relationship is more complicated than this: to good approximation the actual situation is that signal intensity  $\sim i w(i) \sim i^2 n(i)$  (19,20). While modern SEC software carries out these transformations automatically for users, it is always to the advantage of workers to understand precisely what they are measuring, and therefore it is well to be familiar with the theory (19,20).

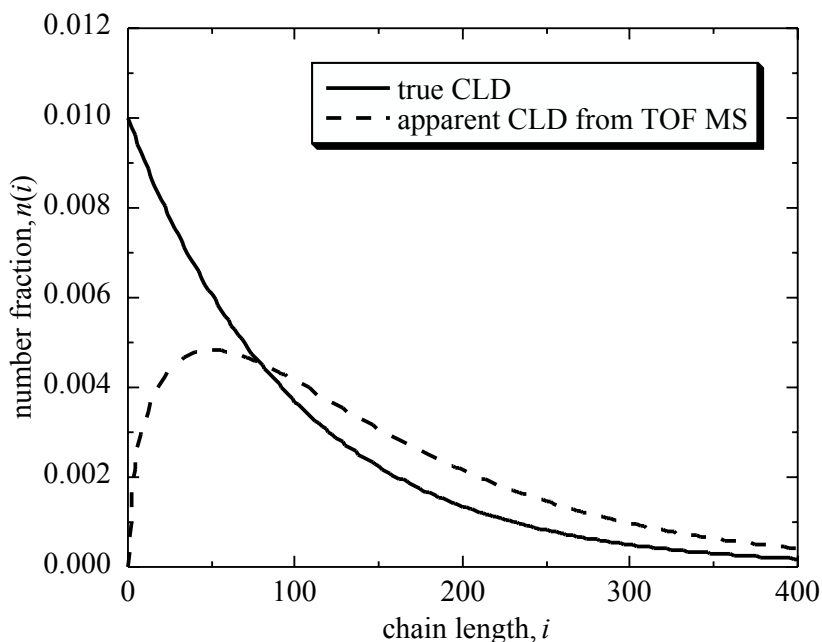


Figure 6. Unbroken line: Equation 3 with  $\nu = 100$  and  $F_w = 1$ ; dashed line: apparent MWD from TOF MS if it is assumed that signal intensity  $\sim n(i)$ .

## Real Sources of Polydispersity Perturbation

In this section I will summarize some *real* sources of polydispersity perturbation, i.e., factors that alter the true *PDI* of a MWD.

### Effect of Conversion

During a polymerization, all concentrations and some rate coefficients change in value. Thus the parameter  $\nu$  of Equation 4 is constantly changing in value, meaning that the *instantaneous* molecular weight distribution, Equation 3, is constantly changing. Of course what one determines from an experiment is the *cumulative* MWD, which is the sum of MWDs from each instant. The consequence of this is that the (cumulative) MWD is *broader* than each of the underlying instantaneous MWDs. To see that this is so, consider the simple example of summing two instantaneous exponential MWDs ( $F_w = 1$  in Equation 3 gives an exponential  $n(i)$ , e.g. see Figure 6). It is well known that the resulting cumulative MWD must have  $PDI > 2$ , and thus be broader than any exponential MWD ( $PDI = 2$ ).

Conversion-induced MWD broadening is a familiar (6) and much studied phenomenon. The main culprit in causing it is the rate coefficient for

termination,  $k_t$ , which sometimes decreases by many orders of magnitude during a polymerization (21). This is a consequence of termination being a diffusion-controlled reaction, which thus is sensitive to the large increases of viscosity that occur as polymer is produced. The archetypal monomer in this regard is methyl methacrylate, which shows large increases in  $DP_n$  (see Equations 4 and 6) and  $PDI$  as (bulk) polymerization proceeds. This is nicely presented and analyzed in (22), for example.

### Chain-Length-Dependent Termination

The defining assumption of the classical model of RP kinetics, Equation 3, is that of chain-length-independent reactivities: each reaction has a rate coefficient that is independent of chain length in value, as symbolized by the arrow sizes of Figure 3. This assumption is most gravely flawed for the reaction of termination, which, being diffusion controlled, results in small, mobile radicals reacting faster than large, ponderous radicals (21). This is the phenomenon of chain-length-dependent termination (CLDT).

The simplest realistic model of CLDT (23) is

$$k_t^{i,i} = k_t^{1,1} i^{-\alpha} \quad (8)$$

Here  $k_t^{i,i}$  is the rate coefficient for termination between radicals of chain length  $i$ , and  $\alpha$  is an exponent quantifying the strength of CLDT ( $\alpha = 0$  for chain-length-independent termination).

Of course Equation 8 specifies only *homotermination* rate coefficients; one requires also *cross-termination* rate coefficients. A simple model for these is that of the geometric mean:

$$k_t^{i,j} = (k_t^{i,i} k_t^{j,j})^{1/2} = k_t^{1,1} (ij)^{-\alpha/2} \quad (9)$$

There is no physical basis for Equation 9, but it is nevertheless useful because it is the only model for  $k_t^{ij}$  that yields closed expressions for polymerization quantities. In regrettably ignored work, Olaj et al. showed that the result for MWD in the absence of transfer is (24)

$$n(i) = F_n C i^{-0.5\alpha} \exp\left(-C' i^p\right) + (1 - F_n) A^2 p i^{1-\alpha} \exp\left(-A i^p\right) \quad (10)$$

Here  $C = (2R_i k_t^{1,1})^{0.5} / (k_p [M])$  is the inverse of the classical kinetic chain length (see Equation 4),  $p = 1 - (\alpha/2)$ ,  $C' = C/p$ ,  $A = 4C'/(4-\alpha)$  and  $F_n$  is as already defined (see below Equation 6). In analogy with the term ‘stretched exponential’ and its meaning, one might say that Equation 10 is a ‘stretched Flory-Schulz’ distribution. It has three parameters:  $F_n$  as before,  $C$  replacing  $\nu$ , and the new parameter  $\alpha$ .

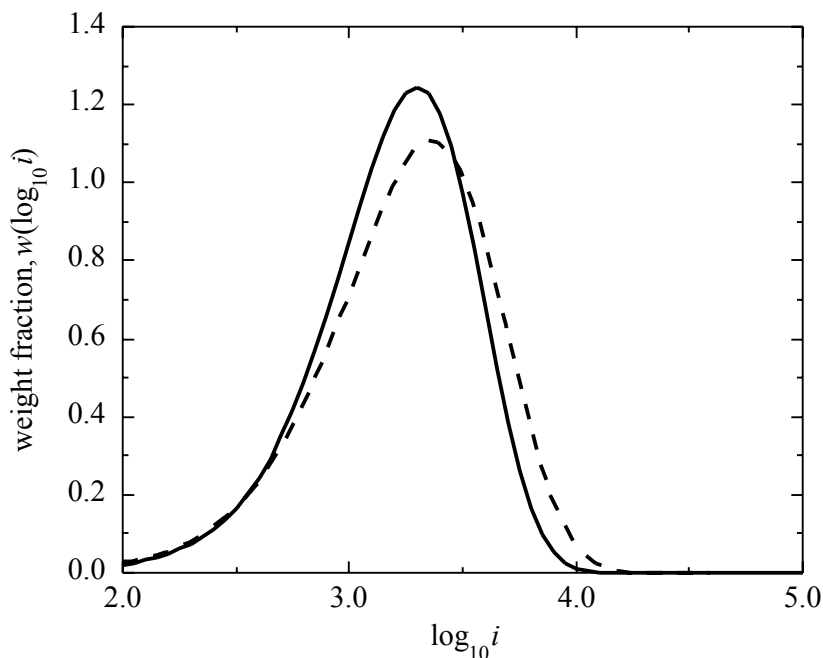


Figure 7. Chain-length distributions calculated using Equation 10 with  $F_n = 1$  (100% disproportionation). Full line:  $\alpha = 0$  (chain-length-independent termination); dashed line:  $\alpha = 0.3$  (CLDT). For both distributions  $DP_n = 1\,000$ .

Figure 7 presents calculations with Equation 10 that illustrate the effect of CLDT on MWD broadness.  $F_n = 1$  (100% disproportionation) was used, and for ease of comparison  $C$  was varied so as to give constant  $DP_n$ . It is clear that the effect of CLDT is to *broaden* MWDs.

What about combination? ( $F_n = 0$ ). Not surprisingly, Figure 8 shows that in this case CLDT has the same effect of broadening the MWD.

Figure 8 also shows results from low-conversion polymerization of styrene at 80 °C (25). Previously this data was fitted with Equation 3 ( $\alpha = 0$ ), yielding  $F_w = k_{td}/k_t = 0.25$  (7). This value is unrealistic, because it is well known that styrene terminates (almost) exclusively by combination (26). On the other hand, the new modeling of Figure 8, with  $F_w = 0$  and  $\alpha = 0.19$ , is highly satisfactory in that it is impeccable and in that it is well established that  $\alpha \approx 0.2$  for long-chain polystyrene (23). In fact the true value of  $\alpha$  from this data might be even closer to the theoretically expected value of 0.16 (23), because the modeling assumes that all broadening in the experimental data comes from CLDT, but in fact there will also be a small contribution from the SEC columns (see above).

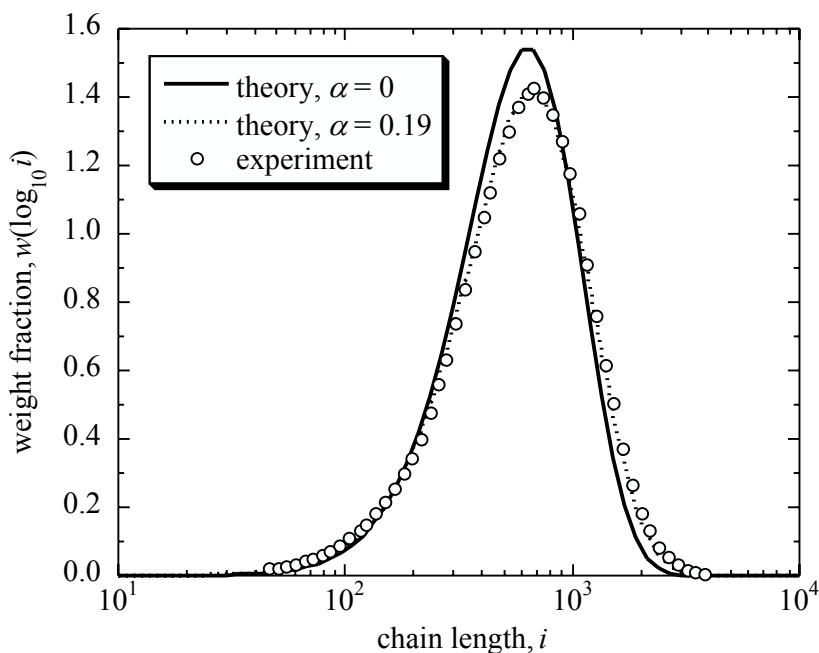


Figure 8. Lines: Equation 10 with  $F_n = 0$  (100% combination) and  $DP_n = 425$  for  $\alpha = 0$  (full) and  $\alpha = 0.19$  (dotted). Points: results for styrene at 80 °C (25).

In view of the success of the modeling of Figure 8, it may be useful to have a quick reference guide for the effect of CLDT on broadening. Such can be obtained from the following expression for  $PDI$  that can be derived for the model of Equation 9 (20,24):

$$PDI = \frac{1+\lambda}{2} \left\{ \frac{\Gamma\left(\frac{6-\alpha}{2-\alpha}\right)}{\left[\Gamma\left(\frac{4-\alpha}{2-\alpha}\right)\right]^2} + 1 - \lambda \right\} \quad (11)$$

Here  $\lambda = k_{id}/k_t$  ( $= F_w$  when  $k_{trX} = 0$  – see Equation 5) and  $\Gamma$  is the gamma function. Equation 11 is evaluated in Figure 9. If one knows the fraction of termination by disproportionation ( $\lambda$ ) and the strength of the CLDT ( $\alpha$ ), then one may use Figure 9 to look up the extent to which  $PDI$  is increased for a conventional radical polymerization. The figure makes clear that, as one would expect, stronger CLDT results in increased MWD broadness.

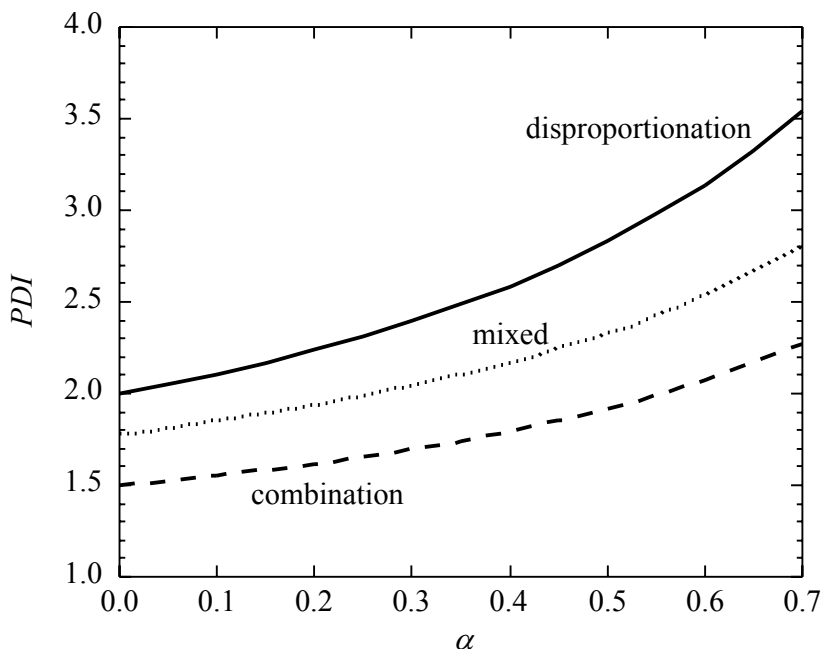


Figure 9. Polydispersity index,  $PDI$ , as a function of CLDT exponent  $\alpha$  for disproportionation, combination and  $\lambda = 0.333$  ("mixed"), as indicated.

In reality homotermination is usually more complicated than Equation 8 and cross-termination is different to Equation 9 (23). Remarkably, these details generally have no significant effect on MWDs (23), meaning that to all intents and purposes one can use the equations of this subsection for real systems.

Of course the quantitative results here do not apply for LRP. The 'background' polymer of such systems – i.e., the non-living polymer that mostly is not part of the central peak – is often largely formed by termination. What can be said from the work of this section is that this background portion of the MWD must become broader as a result of CLDT, which will cause  $k_t$  to decrease with time as the living chains become longer (see Equation 8). This in turn will result in the whole system – dormant and dead polymer – having increased  $PDI$ .

### Chain-Length Dependent Propagation

Olaj et al. (27) rekindled interest in the issue of chain-length-dependent propagation (CLDP), an issue that Heuts and coworkers have pursued most recently (28-31). CLDP results in very small radicals growing relatively quickly (28), and thus – opposite to CLDT – it causes *narrowing* of a MWD (29). The effect can be substantial, with  $PDI$  of 1.5 having been observed for transfer-controlled systems with  $DP_n \approx 15$  (30), as opposed to the classical kinetics value



of 2 for such systems (Equation 7 with  $F_w = 1$ ). Further, these experimental results have been well reproduced by modeling that incorporated CLDP (31). What emerged from this modeling is that CLDP can have an effect for  $DP_n$  of order 100 or less (28), which is well above the chain length for which  $k_p$  is actually elevated, but at the same time is well below what is observed in the majority of conventional RPs.

Turning briefly to LRP, such systems have  $DP_n$  that typically are smaller than in conventional RP. Also, CLDP will influence the central MWD peak of living polymer (cf. CLDT with LRP). Thus CLDP is more likely to be relevant than in conventional RP. Now the dominant framework is that of Equation 1 rather than Equation 3, although clearly the effect will still be one of narrowing. Matyjaszewski (32) has remarked that this may operate to counteract various broadening effects and keep LRP MWDs narrow; this remains to be properly investigated.

## Conclusion

A cynic may look at the figures of this paper and, in view of their sameness, remark that this work has been an exercise in making mountains out of molehills. Indeed, some may say this of kinetics in general. Be that as it may, the fact remains that an MWD does indeed look like a ‘mountain’, and the position (as commonly quantified by  $DP_n$ ) and broadness ( $PDI$ ) of the mountain are matters that remain of great scientific and technical importance. This is especially so in the era of LRP, a major *raison d’être* for which is lowering of  $PDI$ . Therefore it is of relevance to understand the broadness of molecular weight distributions in radical polymerization, as has been the subject of interest here. Although most illustrations have involved conventional RP, it has been made clear that the qualitative effects are the same in LRP. The overall moral to emerge from the deliberations here would have to be that potentially many factors contribute to MWD broadness, and thus one should beware simple descriptions that seek to ascribe  $PDI$  totally to one factor – life is rarely, if ever, that straightforward.

## Acknowledgements

Greg Smith, Kim van Berkel, Hans Heuts, Chris Barner-Kowollik and Bob Gilbert are all acknowledged for their contributions, great and small, to the author’s publications associated with this work. The author would also like to thank Irene Schnöll-Bitai, Yohann Guillaneuf and Patrice Castignolles for friendly discussions on the work of theirs that has been outlined here.

May the author also take this opportunity to pay his deep respects to the memory of Irene Schnöll-Bitai, recently deceased on 4 December 2008 – indeed, *Du hast den Berg erstiegen* (33).

## References

1. Young, R. J.; Lovell, P. A. *Introduction to Polymers*, 2nd ed.; Chapman & Hall: London, 1991.
2. Fischer, H. *J. Polym. Sci., Polym. Chem. Ed.* **1999**, *37*, 1885-1901.
3. Fischer, H. *Chem. Rev.* **2001**, *101*, 3581-3610.
4. Fukuda, T. *J. Polym. Sci., Polym. Chem. Ed.* **2004**, *42*, 4743-4755.
5. Goto, A.; Fukuda, T. *Prog. Polym. Sci.* **2004**, *29*, 329-385.
6. Rudin, A. *The Elements of Polymer Science and Engineering*, 1st ed.; Academic Press: Orlando and London, 1982.
7. Russell, G. T. *Aust. J. Chem.* **2002**, *55*, 399-414.
8. Baumgarten, J. L.; Busnel, J.-P.; Meira, G. R. *Journal of Liquid Chromatography & Related Technologies* **2002**, *25*, 1967-2001.
9. Buback, M.; Busch, M.; Lämmel, R. A. *Macromol. Theory Simul.*, **1996**, *5*, 845-861.
10. van Berkel, K. Y.; Russell, G. T.; Gilbert, R. G. *Macromolecules*, **2005**, *38*, 3214-3224.
11. Meira, G. R.; Netopilik, M.; Potschka, M.; Schnöll-Bitai, I.; Vega, J. *Macromol. Symp.* **2007**, *258*, 186-197.
12. Guillaneuf, Y.; Castignolles, P. *J. Polym. Sci., Polym. Chem. Ed.* **2008**, *46*, 897-911.
13. Boschmann, D.; Edam, R.; Schoenmakers, P. J.; Vana, P. *Polymer* **2008**, *49*, 5199-5208.
14. Gridnev, A. A.; Ittel, S. D.; Fryd, M. *J. Polym. Sci., Polym. Chem. Ed.* **1995**, *33*, 1185-1188.
15. Moad, G.; Moad, C. L. *Macromolecules* **1996**, *29*, 7727-7733.
16. Kornherr, A.; Olaj, O. F.; Schnöll-Bitai, I.; Zifferer, G. *Macromol. Theory Simul.* **2006**, *15*, 215-225.
17. Schnöll-Bitai, I.; Hrebicek, T.; Rizzi, A. *Macromol. Chem. Phys.* **2007**, *208*, 485-495.
18. Zammit, M. D.; Davis, T. P.; Haddleton, D. M.; Suddaby, K. G. *Macromolecules* **1997**, *30*, 1915-1920.
19. Shortt, D. W. *Journal of Liquid Chromatography & Related Technologies* **1993**, *16*, 3371-3391.
20. Clay, P. A.; Gilbert, R. G. *Macromolecules* **1995**, *28*, 552-569.
21. Buback, M.; Egorov, M.; Gilbert, R. G.; Kaminsky, V.; Olaj, O. F.; Russell, G. T.; Vana, P.; Zifferer, G. *Macromol. Chem. Phys.* **2002**, *203*, 2570-2582.
22. Cunningham, M. F.; Mahabadi, H. K. *Macromolecules* **1996**, *29*, 835-841.
23. Barner-Kowollik, C.; Russell, G. T. *Prog. Polym. Sci.* **2009**, in press ("Chain-length-dependent termination in radical polymerization: Subtle revolution in tackling a long-standing challenge").
24. Olaj, O. F.; Zifferer, G.; Gleixner, G. *Macromolecules* **1987**, *20*, 839-850.
25. Tefera, N.; Weickert, G.; Bloodworth, R.; Schweer, J. *Macromol. Chem. Phys.* **1994**, *195*, 3067-3085.
26. Moad, G.; Solomon, D. H. *The Chemistry of Radical Polymerization*, 2nd fully revised ed.; Elsevier: Oxford, UK, 2006.
27. Olaj, O. F.; Vana, P.; Zoder, M.; Kornherr, A.; Zifferer, G. *Macromol. Rapid Commun.* **2000**, *21*, 913-920.

28. Heuts, J. P. A.; Russell, G. T. *Eur. Polym. J.* **2006**, *42*, 3-20.
29. Heuts, J. P. A.; Russell, G. T.; Smith, G. B. *Aust. J. Chem.*, **2007**, *60*, 754-764.
30. Smith, G. B.; Russell, G. T.; Yin, M.; Heuts, J. P. A. *Eur. Polym. J.*, **2005**, *41*, 225--230.
31. Smith, G. B.; Heuts, J. P. A.; Russell, G. T. *Macromol. Symp.*, **2005**, *226*, 133-146.
32. Matyjaszewski, K.; private communication.
33. From a memorial verse by Irene.

## Chapter 3

# Molecular Design and Polymerization Behavior of Monomers Polymerizable via Radical Ring-opening

Takeshi Endo\* and Kazuhide Morino

Molecular Engineering Institute, Kinki University, 11-6 Kayanomori,  
Iizuka, 820-8555, Japan

Radical ring-opening polymerization (R-ROP) possesses the versatility of radical polymerization and the utility of ring-opening polymerization that functional groups can be introduced into the polymer backbone. Therefore, R-ROP is one of the most promising methods for the preparation of functional polymers. In this paper, we describe the molecular design and polymerization behavior of various cyclic molecules capable of undergoing R-ROP.

The history of ring-opening polymerization of cyclic monomers is not so long compared with vinyl polymerization and polycondensation. However, ring-opening polymerization has several characteristic features that vinyl polymerization and polycondensation do not have (1). Especially, the incorporation of various functional groups into polymer backbone is one of the most important and interesting benefits of ring-opening polymerization, which cannot be achieved by vinyl polymerization affording only polyethylene derivatives (Figure 1). Polycondensation can also provide polymers with functional groups in the main chain. However, more strict reaction conditions compared with ring-opening polymerization such as the requirement for exact stoichiometry or high conversion to reach high molecular weights are required for polycondensation. Furthermore, the small molecules generated as byproduct during polycondensation must be removed to obtain the polymer efficiently. Ring-opening polymerization commonly proceeds under mild conditions and does not generate small molecules as byproduct.

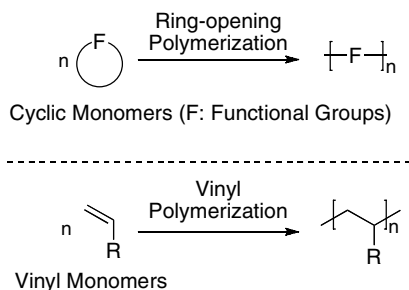


Figure 1. Schematic illustration of ring-opening and vinyl polymerization.

The small volume shrinkage of cyclic monomers in the course of polymerization is also interesting property of ring-opening polymerization (2). Generally, vinyl monomers exhibit volume shrinkage about two times larger than that of cyclic monomers with identical molecular weight. Some cyclic monomers such as spiro orthoesters (SOEs), bicyclo orthoesters (BOEs), and spiro orthocarbonates (SOCs) are also known to show volume expansion during polymerization. The volume shrinkage causes the various problems such as crack, bending, void, and lowering material properties in the field of filling, adhesive, and molding materials. These problems caused by volume shrinkage have not been completely solved yet, and therefore, cyclic monomers are expected to overcome these problems.

Ring-opening polymerization is classified into cationic, anionic, radical, metathesis, and coordination polymerization according to the propagating species. Many cyclic monomers undergo cationic, anionic, and coordination polymerization. On the other hand, there are several cyclic monomers that undergo radical ring-opening polymerization (R-ROP). Radical polymerization is preferred to ionic polymerization due to its tolerance of moisture and the lack of impurities in the obtained polymer such as metal salt residues used as initiator or catalyst. R-ROP possesses not only these advantages of radical polymerization but also the feature that the introduction of functional groups into the main chain of vinyl polymers is possible by the copolymerization of radically polymerizable cyclic monomers with vinyl monomers (Figure 2). Therefore, R-ROP is industrially promising method for the preparation of various functional polymers.

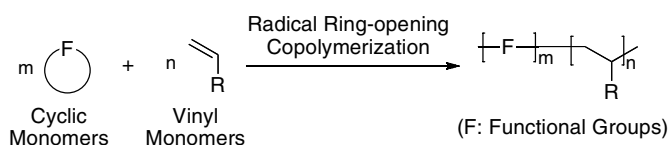


Figure 2. Schematic illustration of radical ring-opening copolymerization of cyclic monomers with vinyl monomers.

The monomers polymerizable via radical ring-opening are still rare, probably due to the difficulty in designing the molecular structure. Typical patterns of R-ROP of *exo*-methylene-substituted and vinyl-substituted cyclic monomers are shown in Figure 3 (3, 4). A double bond is necessary for monomers polymerizable via radical ring-opening, which can react with radical species. The radical species produced by the radical addition to the double bond cause ring-opening of cyclic structure, followed by the generation of propagating radical species. R-ROP is commonly accompanied by vinyl polymerization without ring-opening of the cyclic structure as side reaction. To avoid vinyl polymerization process and increase the selectivity of ring-opening process, the following three factors are important for the design of monomers polymerizable via radical ring-opening: (1) enough ring strain to cleave the X-Y bond, (2) formation of the thermodynamically stable functional group (C=X), and (3) substituent Z, which stabilizes the propagating radical end. To date, the design of radically polymerizable cyclic monomers has been carried out according to the above strategy and their synthesis and polymerization behavior have been positively examined. In this article, we describe the molecular design and radical polymerization behavior of various cyclic monomers that can undergo radical ring-opening polymerization.

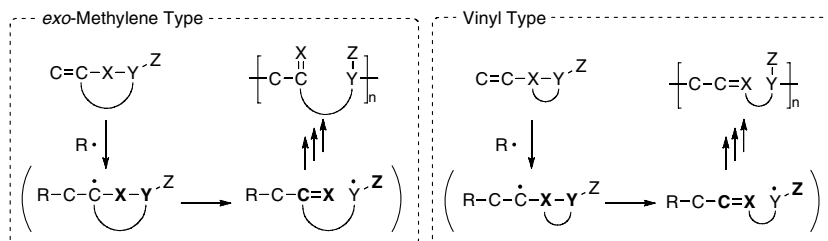


Figure 3. Typical patterns of radical ring-opening polymerization of *exo*-methylene-substituted and vinyl-substituted cyclic monomers.

## Vinylcyclopropane

Vinylcyclopropane derivatives are one of the most well-known monomers polymerizable via radical ring-opening and many papers for their polymerization behavior have been reported (3, 5). The R-ROP of vinylcyclopropane derivatives affords the corresponding polymers without vinyl polymerization (Figure 4). The release of cyclopropane ring strain is the driving force for the complete ring-opening of cyclopropane unit. The introduction of electron-withdrawing groups such as ester, chloro, and cyano stabilized the propagating radical species, resulting in the efficient ring-opening of the cyclopropane ring. The obtained polymer has double bonds in the polymer backbone, which can react with radical species during polymerization. Therefore, the units without double bond, probably cyclobutane structure generated by

intramolecular cyclization of the propagating radical end, are formed in the main chain (3). This side reaction can be suppressed by the introduction of bulky substituents such as a phenyl group into the  $\alpha$  position of vinyl groups (3). Recently, Feast et al. have reported that R-ROP of 1,1-difluoro-2-vinylcyclopropane mainly provided the polymers obtained by 1,4-ring-opening polymerization (6).

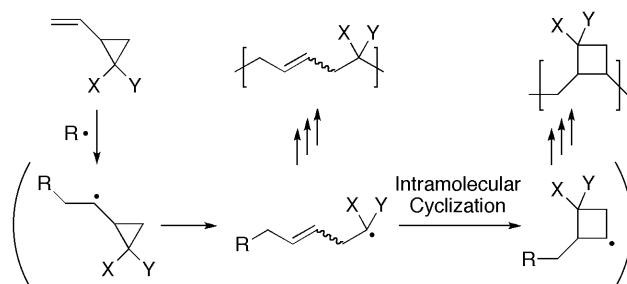


Figure 4. Radical ring-opening polymerization of vinylcyclopropane derivatives.

The volume change on R-ROP of vinylcyclopropane derivatives has been investigated. Most of vinylcyclopropane derivatives showed large volume shrinkage on R-ROP regardless of the large cyclopropane ring strain, probably due to the contribution of the formation of the cyclobutane-containing units. On the other hand, it has been reported that vinylcyclopropanes with phenoxy carbonyl (7) and adamantyloxycarbonyl (8) groups exhibit volume expansion during polymerization. This may be explained by the release of conformational restriction after polymerization, resulting in free-volume enlargement.

The radical copolymerization of 1,1-bis(ethoxycarbonyl)-2-vinylcyclopropane (ECVCP) with methyl methacrylate (MMA) gave the copolymer without double bond in the main chain (Figure 5) (3). Detailed structural analyses suggested that the obtained copolymer contained five-membered and/or six-membered rings formed by the reaction of the vinylcyclopropane propagating end with MMA followed by intramolecular cyclization. The copolymerization parameters were evaluated to be  $r_1 = 0.11$ ,  $r_2 = 21.51$  ( $M_1$ ; ECVCP,  $M_2$ ; MMA) by nonlinear least-square method. This difference in the monomer reactivity ratio might cause the unique radical ring-opening intramolecular cyclization copolymerization. It has been reported that similar polymerization behavior was also observed for the radical copolymerization of several vinylcyclopropanes with common vinyl monomers (3, 9).

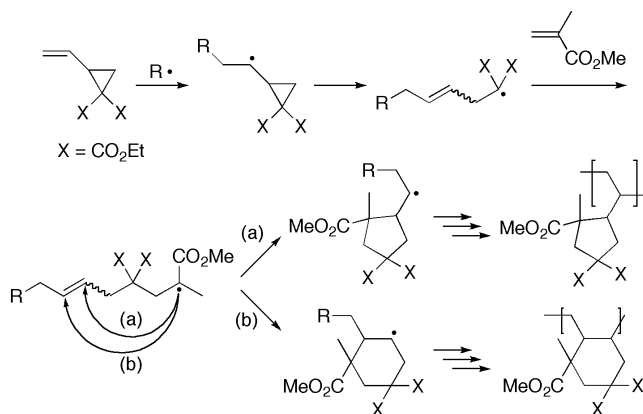


Figure 5. Radical ring-opening cyclization copolymerization of 1,1-bis(ethoxycarbonyl)-2-vinylcyclopropane with methyl methacrylate.

Emulsion polymerization possesses considerable processing advantages over bulk, suspension, and solution polymerization. We investigated the radical ring-opening emulsion polymerization behavior of ECVCP (3). ECVCP successfully underwent emulsion polymerization to give particle-shaped polymer with unimodal particle size distribution. This is the first example of radical ring-opening emulsion polymerization of vinylcyclopropane derivatives. Ritter and co-workers have recently reported the complexation of vinylcyclopropanes bearing hexyl, cyclohexyl, and (1H,1H,2H,2H)perfluorododecyl esters with methylated cyclodextrin and their radical polymerization behavior in aqueous media (10, 11).

The R-ROP of vinylcyclopropane derivatives has been applied to the preparation of functional polymers. For example, the R-ROP of 1,1-bis(hydroxymethylated)-2-vinylcyclopropane afforded the corresponding polymers bearing hydroxy groups in the side chain, which could be a good oxygen barrier material (3). Liquid-crystalline poly(vinylcyclopropane)s were also prepared by the R-ROP of vinylcyclopropanes bearing cholesterol moieties (12), chiral rod-like mesogenic groups (13), and perfluorinated chain segments (14). Vinylcyclopropanes with trimethylsiloxy groups provided poly(silyl enol ether)s through R-ROP, which could be regarded as versatile reactive polymers; the obtained poly(silyl enol ether)s could be hydrolyzed to afford polyketones and reacted with an electrophile such as benzaldehyde (Figure 6) (3). Polymeric allylsilane (3) and vinylsilane (3) obtained by the R-ROP of the corresponding trimethylsilyl-substituted vinylcyclopropanes also underwent the macromolecular reaction with acid and electrophiles.



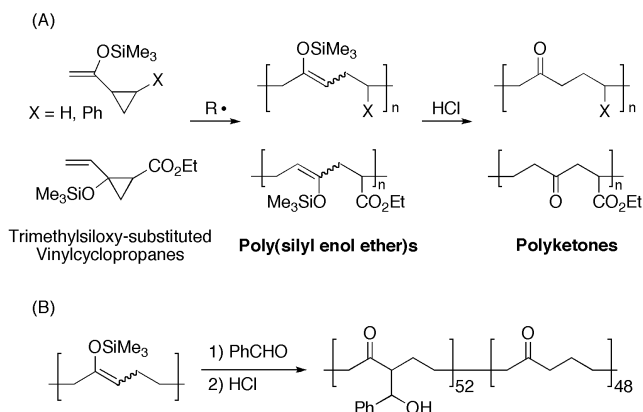


Figure 6. (A) Radical ring-opening polymerization of vinylcyclopropane with trimethylsilyloxy groups and acidic hydrolysis of the poly(silyl enol ether)s. (B) Macromolecular reaction of the poly(silyl enol ether) with electrophile.

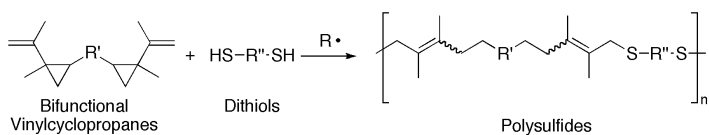


Figure 7. Radical ring-opening polyaddition of bifunctional vinylcyclopropanes with dithiols.

The complete ring-opening nature of the polymerization of a vinylcyclopropane stimulated us to apply it to radical ring-opening polyaddition (3). Bifunctional vinylcyclopropanes bearing spiroacetal, ester, and amide moieties underwent radical polyaddition with various dithiols successfully to generate the corresponding polysulfides bearing double bonds in the polymer backbone (Figure 7).

The R-ROP of 10-methylene-9,10-dihydroanthryl-9-spirocyclopropane (MDSC), which can be regarded as a vinylcyclopropane derivative, gave the interesting polymer with anthracene units in the main chain (Figure 8) (15). The formation of aromatic ring in addition to the release of the cyclopropane ring strain acts as the driving force of smooth ring-opening.

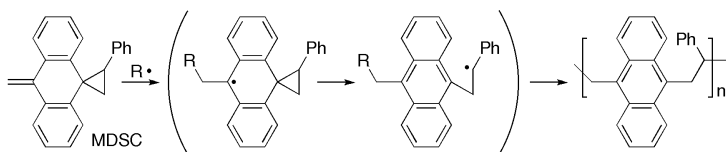


Figure 8. Radical ring-opening polymerization of 10-methylene-9,10-dihydroanthryl-9-spirocyclopropane (MDSC).

The recent great advance in living radical polymerization has made it possible to design and construct a wide variety of well-defined polymer architectures such as end-functionalized, block, graft, and star polymers (16-20). The living radical polymerization of monomers polymerizable via radical ring-opening has been also reported. Singha et al. reported that the controlled polymerization of ECVCP by copper-mediated atom transfer radical polymerization (ATRP) proceeded in selective 1,5-ring-opening manner to afford the corresponding polymer with narrow molecular weight distributions, which hardly contained cyclobutane units (21). We have demonstrated that the R-ROP of MDSC through reversible addition-fragmentation transfer (RAFT) process could afford the nonconjugated polymers having narrow molecular weight distribution with anthracene units in the main chain (22). The copolymerization of MDSC with styrene by RAFT process was also carried out to produce the copolymers having relatively high MDSC contents with low polydispersity (23).

A vinylcyclobutane has been also found to undergo R-ROP to afford a polymer with double bonds in the polymer backbone similarly to vinylcyclopropanes (3).

## Vinyloxirane

Vinyloxirane, an analog of vinylcyclopropane, can undergo R-ROP to afford the polymers with vinyl ether moieties in the main chain through the cleavage of carbon-carbon bond of the oxirane ring (Figure 9) (3). The R-ROP of 2-phenyl-3-vinyloxirane (X = H in Figure 9) gave the soluble polymer when the polymerization was performed in chlorobenzene. On the other hand, only gelled polymer was obtained by the bulk polymerization of 2-phenyl-3-vinyloxirane, probably due to crosslinking that occurred on the vinyl ether group of the resulting polymer (3). This problem was solved by the introduction of a methyl group into the  $\alpha$ -position of the vinyl group of 2-phenyl-3-vinyloxirane; the R-ROP of 2-methyl-3-phenyloxirane (X = Me in Figure 9) could afford the corresponding soluble polymers even when the polymerization was performed in bulk (3). Radical ring-opening polyaddition of bifunctional vinyloxiranes with various dithiols has been also found to afford poly(ether sulfide)s with double bonds in the main chain (Figure 10) (3).

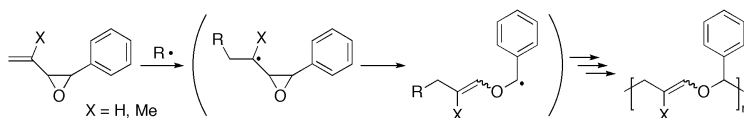
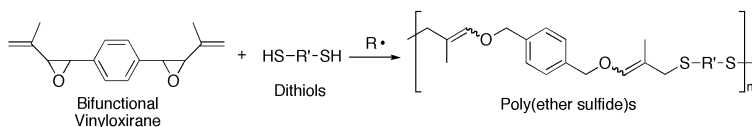


Figure 9. Radical ring-opening polymerization of vinyloxirane derivatives.



*Figure 10. Radical ring-opening polyaddition of bifunctional vinylloxirane with dithiols.*

The synthesis and radical polymerization of vinylthiiranes have been reported (3). However, the detailed polymerization behavior is not clear at present.

### 4-Methylene-1,3-dioxolane

4-Methylene-1,3-dioxolanes are known to show a characteristic radical polymerization behavior. The radical polymerization of 4-methylene-1,3-dioxolanes proceeds in the three modes: (1) vinyl polymerization, (2) ring-opening polymerization, and (3) ring-opening polymerization accompanied by the elimination of carbonyl compounds to produce a polyketone, which is one of the difficult polymers to be prepared by polycondensation and common ionic ring-opening polymerization (Figure 11) (3). The selectivity of the three polymerization modes is affected by the substituents; the elimination of a stable carbonyl compound accelerates the predominant ring-opening elimination polymerization. 2,2-Diphenyl-4-methylene-1,3-dioxolane (X = Y = Ph in Figure 11) selectively underwent R-ROP accompanied by the elimination of benzophenone to yield a polyketone (3). The polymerization rate was decreased as electron-withdrawing character of the substituents increased, whereas the polymer composition was independent of the substituents (3). The copolymerization of 2,2-diphenyl-4-methylene-1,3-dioxolane with various vinyl monomers such as *N*-vinyl-2-pyrrolidone, styrene, vinyl acetate, MMA, and acrylonitrile could provide the corresponding copolymers with ketone groups in the polymer backbone (3, 24). The copolymer with acrylonitrile showed good photodegradability (3).

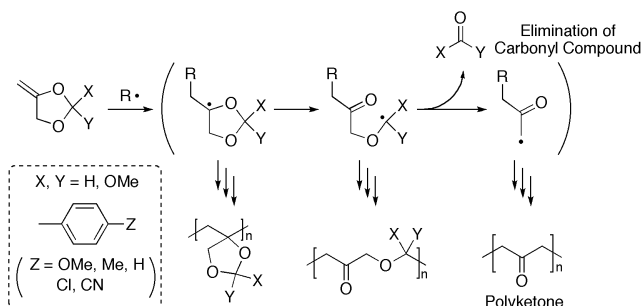


*Figure 11. Radical ring-opening polymerization of 4-methylene-1,3-dioxolane derivatives.*

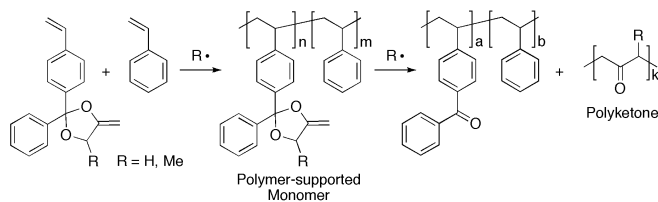


Figure 12. Template polymerization by radical ring-opening polymerization.

The radical ring-opening elimination polymerization of 4-methylene-1,3-dioxolane stimulated us to construct a novel template polymerization (3). The concept is that *polymers bear polymers*. Polymer-supported monomer, which had a structure of 2,2-diphenyl-4-methylene-1,3-dioxolane, reacted with radical species to afford polyketone and copolymer of styrene with vinylbenzophenone as newborn polymer and template, respectively (Figure 12). These polymers were easily separated by fractional precipitation without any particular chemical treatment after polymerization. On the other hand, common template polymerization requires annoying procedures for the separation of obtained polymers from template. On this point, our novel template polymerization system differs from conventional template polymerization.

## Cyclic Ketene Acetal

Cyclic ketene acetals can undergo R-ROP to afford the polymers having ester groups in the main chain (Figure 13). However, the degree of ring-opening of cyclic ketene acetal during R-ROP depends on the ring size and substituents. The R-ROP of seven-membered cyclic ketene acetal proceeds in complete ring-opening mode, whereas the R-ROP of five- and six-membered cyclic ketene acetals is accompanied by vinyl polymerization (3). The introduction of a radical-stabilizing group such as a phenyl group induced the complete R-ROP of five-membered cyclic ketene acetal. Gonsalves et al. reported that the polyesters obtained by the R-ROP of 2-methylene-1,3-dioxepane possessed branched structures due to the generation of radical species formed by the intramolecular hydrogen abstraction during polymerization (25).

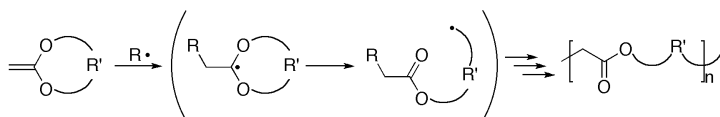


Figure 13. Radical ring-opening polymerization of cyclic ketene acetals.

The radical copolymerization of cyclic ketene acetal with various vinyl monomers such as styrene, MMA, vinyl acetate, and methyl vinyl ketone could afford the copolymers with ester groups in the main chain (26-28). These copolymers showed enzymatic degradability and photodegradability and are applicable as environmentally degradable materials.

The living R-ROP of cyclic ketene acetals was achieved with nitroso-mediated polymerization (NMP) (29), ATRP (30), and RAFT (31) methods to afford the polyesters with low polydispersities. Recently, it has been reported that the block and random copolymers with vinyl monomers showing low polydispersities could also be obtained by living radical ring-opening copolymerizations (32, 33).

The nitrogen analogs of cyclic ketene acetals also underwent R-ROP to produce polyamides (34). Radical copolymerization of the nitrogen analogs of cyclic ketene acetals with styrene gave the corresponding copolymers with amide groups in the main chain, which upon hydrolysis generated styrene oligomers with an amino group and a carboxylic acid group as the terminal groups (34).

8-Methylene-1,4-dioxaspiro-[4,5]deca-6,9-diene, another cyclic acetal, has been found to undergo the selective R-ROP to a polyarylene ether regardless of the small ring strain. This is due to the formation of a stable aromatic ring as the driving force (35).

## Benzocyclobutene

Benzocyclobutenes are the most convenient precursors of *o*-quinodimethanes, which are formed as reactive intermediates by isomerization upon heating. We have succeeded in the radical polymerization of *o*-quinodimethanes *in situ* produced through the thermal isomerization of the corresponding benzocyclobutenes (Figure 14) (3). The structures of obtained polymers, poly(*o*-xylylene)s, were identical with those formed by the C-C bond cleavage of cyclobutene ring, and therefore, the polymerization process can be regarded as R-ROP of benzocyclobutenes. Introduction of a substituent on the cyclobutene ring can lower the isomerization rate. In the presence of TEMPO, the formed polymer reinitiated the polymerization of styrene to afford the corresponding block copolymer (36).

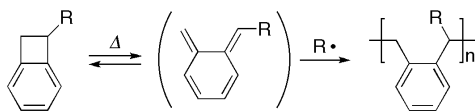


Figure 14. Radical ring-opening polymerization of benzocyclobutene derivatives.

A spiro cyclic hydrocarbon compound, *o*-xylylene dimer, could also undergo R-ROP to give poly(*o*-xylylene) due to the formation of a stable benzyl radical and an aromatic ring (37).

## Spiro Orthocarbonate (SOC)

As described above, SOCs are well known to exhibit volume expansion during cationic double ring-opening polymerization and have been examined as expandable curing materials that solve the various problems caused by volume shrinkage such as crack, bending, void, and lowering material properties in the field of filling, adhesive, and molding materials (2). Therefore, SOCs bearing *exo*-methylene groups were expected as monomers polymerizable via radical ring-opening showing volume expansion in the course of polymerization. The ideal R-ROP mechanism of SOCs is shown in Figure 15. However, five-membered SOCs bearing *exo*-methylene groups at the  $\alpha$ -position of the ether oxygen underwent only vinyl polymerization without ring-opening polymerization (3). The degree of ring-opening of a six-membered SOC bearing two *exo*-methylene groups at the  $\beta$ -position of the ether oxygen was quite low, where the main polymer unit was a vinyl polymerized one (3). The large volume shrinkage was also observed. For the purpose of the improvement of the predominant polymerization mode, we have readjusted the molecular structure of SOCs (3). As a result, unsymmetrical SOCs having one *exo*-methylene group at the  $\alpha$ - or  $\beta$ -position of the ether oxygen capable of generating benzyl radical as propagating end could undergo the R-ROP to afford the polymers with ring-opened and vinyl polymerized units. The degree of ring-opening depended on the ring size and steric hindrance of *exo*-methylene group.

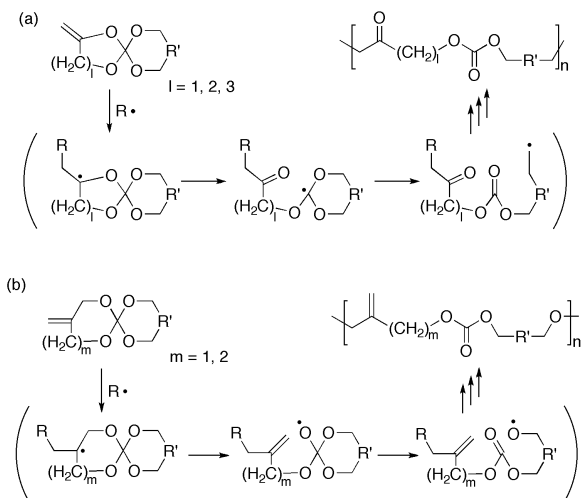


Figure 15. Radical ring-opening polymerization of spiro orthocarbonate derivatives bearing an *exo*-methylene group at  $\alpha$ - (a) and  $\beta$ -position (b) of the ether oxygen.

## Spiro Orthoester (SOE)

SOEs are also known as expandable monomers during cationic polymerization (2), and therefore, the R-ROP of *exo*-methylene-substituted SOE has been examined. Figure 16 shows the ideal R-ROP process of *exo*-methylene-substituted SOE. However, *exo*-methylene-substituted SOEs showed various polymerization modes depending on the molecular structures. The R-ROP of *exo*-methylene-substituted SOE showed a similar behavior to that of SOCs; the vinyl polymerization was accompanied by ring-opening polymerization (3). Pan et al. reported that SOEs with *exo*-methylene group attached to the cyclic ether underwent R-ROP to afford the polymers bearing single ring-opened and double ring-opened units with cyclic acetal and ester moieties, respectively (38). Furthermore, Pan and Bailey proposed that the polymer obtained by the R-ROP of 8,9-benzo-2-methylene-1,4,6-trioxaspiro[4,4]nonane (BMTN, R' = *o*-C<sub>6</sub>H<sub>4</sub> in Figure 16) consisted of ketone moieties generated by the ring-opening followed by the elimination of phthalide and vinyl polymerized units, which had no ester groups in the main chain (39). The R-ROP of BMTN in the presence of TEMPO proceeded in a living manner to afford polymers having double ring-opened units with ketone and ester groups (40). The polydispersity was significantly lower than that by the conventional radical polymerization.

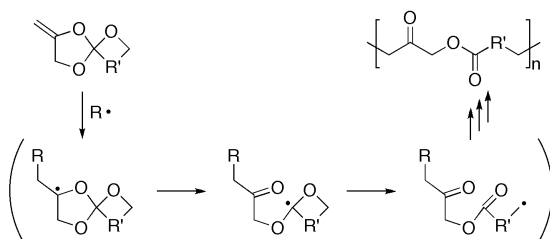


Figure 16. Radical ring-opening polymerization of spiro orthoester derivatives with *exo*-methylene group.

## Vinylcyclopropanone Cyclic Acetal

A vinylcyclopropanone cyclic acetal can be regarded as a hybrid monomer of vinylcyclopropane and cyclic ketene acetal, both of which are excellent monomers polymerizable via radical ring-opening showing complete ring-opening. Therefore, vinylcyclopropanone cyclic acetals are expected to exhibit double ring-opening polymerizability and some volume expansion during polymerization (Figure 17). However, the polymer structures obtained by R-ROP of vinylcyclopropanone cyclic acetals dramatically depended on the ring size of cyclic acetal moiety and substituent. Vinylcyclopropanone cyclic acetals with five- and six-membered cyclic acetal rings underwent single ring-opening polymerization of vinylcyclopropane moiety, resulting in the generation of the polymers bearing cyclic acetal moieties (3). On the other hand,

vinylcyclopropanone cyclic acetals with seven-membered cyclic acetal rings mainly underwent double ring-opening polymerization to afford the polymers with double bonds and ester groups in the main chain (3). The introduction of *exo*-methylene and phenyl groups increased the degree of double ring-opening (3). However, the units without double bonds such as cyclobutane and other unknown large cyclic units generated by the intramolecular reaction of double bonds with propagating radical species were also formed in the main chain (3). As a result, vinylcyclopropanone cyclic acetals showed small volume shrinkage.

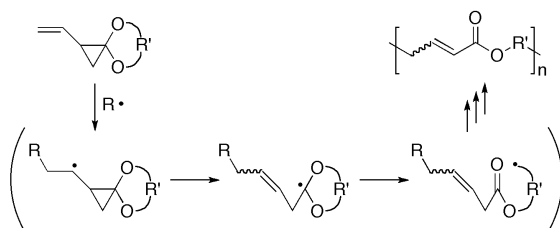


Figure 17. Radical ring-opening polymerization of vinylcyclopropanone cyclic acetal derivatives.

Vinylcyclopropanone cyclic dithioacetals can be regarded as analogues of vinylcyclopropanone cyclic acetals, and therefore, expected as double ring-opening polymerizable monomers. However, the R-ROP of vinylcyclopropanone cyclic dithioacetals selectively afforded the single ring-opened polymers regardless of the ring size of dithioacetal moiety (3). The refractive indices of the obtained polymers (1.655-1.665) were larger than those of the corresponding monomers (1.538-1.578).

## Other Monomers Polymerizable via Radical Ring-opening

Various monomers polymerizable via radical ring-opening other than those shown above have been also reported (Figure 18).

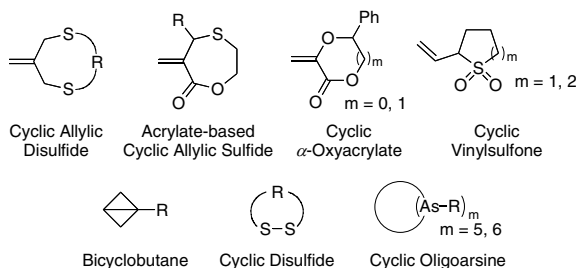


Figure 18. Structures of various monomers polymerizable via radical ring-opening.



Cyclic allylic disulfide readily underwent the R-ROP due to the facile cleavage of the bond between allylic carbon and sulfur atom, resulting in the production of polysulfides with *exo*-methylene groups (3, 41, 42). Acrylate-based cyclic allylic sulfide also showed a high radical polymerizability (3, 43). The copolymerization of acrylate-based cyclic allylic sulfide with MMA and styrene produced the corresponding copolymers bearing sulfide and ester moieties in the polymer backbone (43).

Cyclic  $\alpha$ -oxyacrylates can undergo the R-ROP due to the facile cleavage of the bond between benzyl carbon and ether oxygen atom as the driving force. The R-ROP of cyclic  $\alpha$ -oxyacrylates affords the poly( $\alpha$ -ketoester)s that are expected to be useful in biodegradable and photodegradable materials (3, 44). Matyjaszewski reported the synthesis of the copolymers of cyclic  $\alpha$ -oxyacrylates with MMA by ATRP method (45). The obtained copolymers had low polydispersities and showed photodegradability and hydrolytic degradability (i.e. biodegradability).

A five-membered cyclic vinylsulfone underwent the complete R-ROP to afford the polysulfone with double bonds in the main chain, whereas the R-ROP of a six-membered one was accompanied by vinyl polymerization (3, 46). A six-membered vinyldisulfone could undergo the R-ROP to afford the complete ring opened polymer (3, 47). A polysulfone with *exo*-methylene groups in the polymer backbone could be also prepared by the R-ROP of cyclic allylic disulfides followed by the oxidation (48).

Cyclic disulfides and bicyclobutanes are radically polymerizable exceptional monomers without a double bond. Cyclic disulfides underwent the R-ROP by UV irradiation to give polysulfides (3, 49). Lipoamide, which is a five-membered cyclic sulfide, could undergo the copolymerization with common vinyl monomers such as styrene, vinyl acetate, acrylonitrile and MMA, whereas the homopolymerization could not be achieved (3). The R-ROP of cyclic aromatic disulfide oligomers could also produce poly(phenylene sulfide) in combination with dihalogenated aromatic compounds (3, 50). Bicyclobutanes could undergo the R-ROP due to the release of the ring strain of cumulated cyclopropane rings to afford the polymers consisted of the rigid cyclopropane ring with high thermal stability (3, 51). ATRP of bicyclobutanes has been also found to produce the corresponding polymers with narrow molecular weight distribution (52).

Naka and Chujo reported that the radical copolymerization of acetylenic compounds with arsenic atomic biradical equivalent generated by the thermal- or photo-induced homolytic cleavage of cyclooligoarsines produced poly(vinylene-arsine)s (53). This polymerization was called "Ring-collapsed Radical Alternating Copolymerization", which may be regarded as the novel R-ROP. Cyclooligostibine (53) and cyclooligophosphine (53) could also undergo ring-collapsed radical alternating copolymerization with acetylenic compounds to afford poly(vinylene-stibine) and poly(vinylene-phosphine), respectively.

## Summary

In this article, we described the molecular design and polymerization behavior of monomers polymerizable via radical ring-opening. Although the number of monomers polymerizable via radical ring-opening reported so far is fewer than ionically and coordinatively polymerizable monomers, the field of R-ROP has steadily evolved under the stimulus of the development of living radical polymerization. R-ROP is a promising candidate for producing polymeric materials with various functions and environmental acceptability. We expect the further development of basic and applied researches for R-ROP toward practical application.

## References

- Ivin, K.; Saegusa, T. *Ring-Opening Polymerization*; Elsevier Applied Science: London, 1984.
- Takata, T.; Endo, T. In *Expanding Monomers: Synthesis, Characterization, and Application*; Sathir, R. K.; Luck, R. M., Eds.; CRC: Boca Raton, FL, 1992; Chapter 3.
- Sanda, F.; Endo, T. *J. Polym. Sci., Part A: Polym. Chem.* **2001**, *39*, 265-276.
- Colombani, D. *Prog. Polym. Sci.* **1999**, *24*, 425-480.
- Moszner, N.; Zeuner, F.; Völkel, T.; Rheinberger, V. *Macromol. Chem. Phys.* **1999**, *200*, 2173-2187.
- Feast, W. J.; Gimeno, M.; Kenwright, A. M. *Macromolecules* **2006**, *39*, 4076-4080.
- Sugiyama, J.; Ohashi, K.; Ueda, M. *Macromolecules* **1994**, *27*, 5543-5546.
- Sugiyama, J.; Kayamori, N.; Shimada, S. *Macromolecules* **1996**, *29*, 1943-1950.
- Takahashi, T. *J. Polym. Sci. Part A-1*: **1970**, *8*, 739-749.
- Alupej, V.; Ritter, H. *Macromol. Rapid. Commun.* **2001**, *22*, 1349-1353.
- Choi, S. W.; Kretschmann, O.; Ritter, H.; Ragnoli, M.; Galli, G. *Macromol. Chem. Phys.* **2003**, *204*, 1475-1479.
- Casper, P.; Ritter, H. *J. Macromol. Sci. Part A: Pure Appl. Chem.* **2003**, *40*, 107-113.
- Galli, G.; Baldini, A.; Chiellini, E.; Gallot, B. *Mol. Cryst. Liq. Cryst.* **2005**, *441*, 227-235.
- Galli, G.; Gasperetti, S.; Bertolucci, M.; Gallot, B.; Chiellini, F. *Macromol. Rapid. Commun.* **2002**, *23*, 814-818.
- Cho, I.; Song, K. Y. *J. Polym. Sci. Part A: Polym. Chem.* **1994**, *32*, 1789-1791.
- Hawker, C. J.; Bosman, A. W.; Harth, E. *Chem. Rev.* **2001**, *101*, 3661-3688.
- Braunecker, W. A.; Matyjaszewski, K. *Prog. Polym. Sci.* **2007**, *32*, 93-146.
- Moad, G.; Rizzardo, E.; Thang, S. H. *Polymer* **2008**, *49*, 1079-1131.
- Kamigaito, M.; Satoh, K. *Macromolecules* **2008**, *41*, 269-276.
- Ouchi, M.; Terashima, T.; Sawamoto, M. *Acc. Chem. Res.* **2008**, *41*, 1120-1132.

21. Singha, N. K.; Kavitha, A.; Sarker, P.; Rimmer, S. *Chem. Commun.* **2008**, 3049-3051.
22. Mori, H.; Masuda, S.; Endo, T. *Macromolecules* **2006**, *39*, 5976-5978.
23. Mori, H.; Masuda, S.; Endo, T. *Macromolecules* **2008**, *41*, 632-639.
24. Hiraguri, Y.; Endo, T. *J. Polym. Sci. Part C: Polym. Lett.* **1989**, *27*, 1-4.
25. Jin, S.; Gonsalves, K. E. *Macromolecules* **1997**, *30*, 3104-3106.
26. Bailey, W. J.; Kuruganti, V.K. *Polymeric. Mater. Sci. Eng.* **1990**, *62*, 971-975.
27. Hiraguri, Y.; Tokiwa, Y. *J. Polym. Sci. Part A: Polym. Chem.* **1993**, *31*, 3159-3163.
28. Hiraguri, Y.; Tokiwa, Y. *Macromolecules* **1997**, *30*, 3691-3693.
29. Wei, Y.; Connors, E. J.; Jia, X.; Wang, C. *J. Polym. Sci. Part A: Polym. Chem.* **1998**, *36*, 761-771.
30. Yuan, J. Y.; Pan, C. Y.; Tang, B. Z. *Macromolecules* **2001**, *34*, 211-214.
31. He, T.; Zou, Y. F.; Pan, C. Y. *Polym. J.* **2002**, *34*, 138-143.
32. Yuan, J. Y.; Pan, C. Y. *Eur. Polym. J.* **2002**, *38*, 1565-1571.
33. Yuan, J. Y.; Pan, C. Y. *Eur. Polym. J.* **2002**, *38*, 2069-2076.
34. Bailey, W. J. *Polym. J.* **1985**, *17*, 85-95.
35. Cho, I.; Song, K. Y. *Makromol. Chem. Rapid Commun.* **1993**, *14*, 377-381.
36. Chino, K.; Endo, T. *J. Polym. Sci. Part A: Polym. Chem.* **2000**, *38*, 3434-3429.
37. Errede, L. A. *J. Polym. Sci.* **1961**, *49*, 253-265.
38. Pan, C.-Y.; Wang, Y.; Bailey, W. J. *J. Polym. Sci. Part A: Polym. Chem.* **1988**, *26*, 2737-2747.
39. Pan, C.-Y.; Lu, S.-X.; Bailey, W. J. *Makromol. Chem.* **1987**, *188*, 1651-1658.
40. Jia, X.; Li, M.; Han, S.; Wang, C.; Wei, Y. *Mater. Lett.* **1997**, *31*, 137-139.
41. Evans, R.; Rizzardo, E. *J. Polym. Sci. Part A: Polym. Chem.* **2001**, *39*, 202-215.
42. Phelan, M.; Aldabbagh, F.; Zetterlund, P. B.; Yamada, B. *Macromolecules* **2005**, *38*, 2143-2147.
43. Phelan, M.; Aldabbagh, F.; Zetterlund, P. B.; Yamada, B. *Eur. Polym. J.* **2006**, *42*, 2475-2485.
44. Pinzhen, F. *Chin. J. Polym. Sci.* **1993**, *11*, 153-157.
45. Chung, I. S.; Matyjaszewski, K. *Macromolecules* **2003**, *36*, 2995-2998.
46. Cho, I.; Kim, S.-K.; Lee, M.-H. *J. Polym. Sci. Polym. Symp.* **1986**, *74*, 219-226.
47. Cho, I.; Choi, S. Y. *Makromol. Chem. Rapid Commun.* **1991**, *12*, 399-402.
48. Ochiai, B.; Kuwabara, K.; Nagai, D.; Miyagawa, T.; Endo, T. *Eur. Polym. J.* **2006**, *42*, 1934-1938.
49. Whiney, R. B.; Calvin, M. *J. Chem. Phys.* **1955**, *23*, 1750-1756.
50. Ding, Y.; Hay, A. S. *Macromolecules* **1997**, *30*, 2527-2531.
51. Drujon, X.; Riess, G.; Hall, H. K., Jr.; Padias, A. B. *Macromolecules* **1993**, *26*, 1199-1205.
52. Chen, X. P.; Padias, A. B.; Hall, H. K., Jr. *Macromolecules* **2001**, *34*, 3514-3516.
53. Naka, K. *Polym. J.* **2008**, *40*, 1031-1041.

## Chapter 4

# Electron Spin Resonance (ESR) Observation of Radical Migration Reactions in the Polymerization of Alkyl Acrylates

Atsushi Kajiwara

Nara University of Education Takabatake-cho, Nara 630-8528, JAPAN  
kajiwara@nara-edu.ac.jp

Electron Spin Resonance (ESR) spectroscopic studies directed at clarifying the fundamentals of radical polymerizations have been conducted. A combination of ESR and atom transfer radical polymerization (ATRP) provided significant new information on the reactivity and dynamics of propagating radicals in radical polymerizations. Moreover, chain lengths of the radicals can be differentiated by the combined method. Previously, it had been extremely difficult, even impossible, to obtain such information from ESR spectra during conventional radical polymerizations. To overcome this difficulty radical precursors of oligo- and poly(meth)acrylates were prepared by ATRP. The mechanisms of main chain transfer reactions have been investigated and the possibility of another chain transfer reaction, to ester side groups, was examined. Multi-step radical migration behavior in various alkyl acrylates was also investigated and experimental evidence for such chain transfer reactions will be shown in this paper.

## Introduction

Electron Spin Resonance (ESR) is the most powerful tool for investigation of radical species in radical polymerizations. When well-resolved spectra can be observed, the spectra provide information not only on the structure, properties, and concentration of radicals but also information on the initiating and

propagating (oligomeric and polymeric) radicals in radical polymerizations [1-15]. ESR spectroscopy was successfully applied to quantify radical concentration in the polymerizations [4, 8-11]. However, the direct detection method of ESR did not reveal information on many additional points that are very significant in radical polymerization chemistry so far. For example, the length of propagating chain is not known, direct observation of the penultimate unit effect is almost impossible, and detailed mechanisms of radical reactions remain extremely difficult to examine. These problems have not yet been fully resolved but the development of controlled radical polymerization techniques, especially atom transfer radical polymerization (ATRP), enables us to resolve some of these problems.

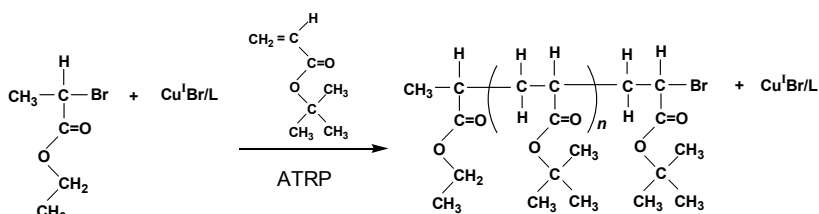


Figure 1 Atom transfer radical polymerization (ATRP) of tert-butyl acrylate for preparation of model radical precursors.

ATRP is one of the most widely applied polymerization techniques in the field of controlled/living radical polymerization. ATRP allows for preparation of a wide range of polymeric materials with controlled molecular weight and well-defined architecture [16-20]. The polymers formed in ATRP most frequently contain terminal carbon-halogen bonds. Giese *et al.* reported that these bonds can be homolytically cleaved by reaction with organotin compounds [21]. Accordingly, various radicals can be formed from the corresponding precursors prepared by atom transfer radical addition (ATRA) and ATRP (Fig. 1) and the generated radicals can be studied by ESR spectroscopy (Fig. 2). For example, polymeric (meth)acrylates with various chain lengths can be prepared as radical precursors by ATRP. Variation of the chain length of these polymeric radical precursors elucidates the effect of chain length of the formed radicals on the ESR spectra.

The investigations of radical reactions are difficult without using model reactions. The method using model radical have applied to investigate chain transfer reactions for propagating acrylate radicals.

Interpretation of ESR spectra observed in acrylate radical polymerizations has been very difficult [22-30]. However a clear interpretation of the ESR spectra of propagating and mid-chain radicals had been demonstrated with the aid of molecules prepared by ATRP[5,7]. A mechanism for the formation of mid-chain radicals was also clarified with the aid of uniform oligo model radicals generated from precursors prepared by ATRP[14,15]. Formation of a six-membered ring enables the radical to migrate to the monomer unit two units before the terminal unit. Since this shift needs at least three linked monomer units, it suggests that mid-chain radicals cannot be formed from a dimeric

radical. The ESR spectrum of the dimeric radical (H-ethyl acrylate (EA)-*tert*butyl acrylate (*t*BA)•) did not show any temperature dependent change in the range from -30°C to 150 °C.

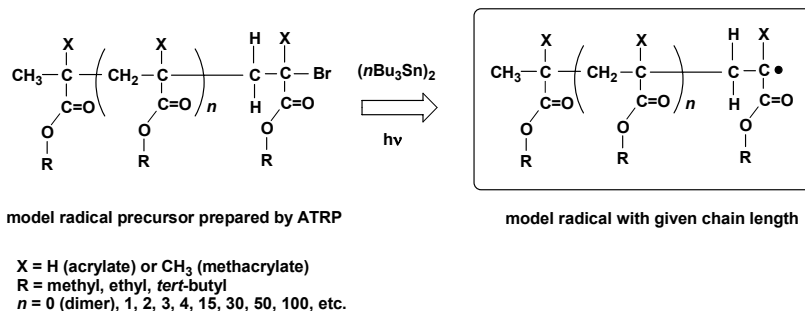


Figure 2 Radicals observed by ESR. Generation of model radicals from radical precursors prepared by ATRP

In the case of the model trimeric (H-EA-*t*BA-*t*BA•) and tetrameric radicals (H-EA-*t*BA-*t*BA-*t*BA•), their ESR spectra showed a clear temperature dependent change. The spectrum observed at -30 °C was very similar to that of the dimeric radical whereas the spectra observed at higher temperatures were totally different from that measured at lower temperatures. Interpretation of the higher temperature spectra suggested that a 1,5-hydrogen shift occurred in the uniform oligomeric model radicals. No other radicals except for the specific radicals at low and high temperatures were detected.

These findings strongly suggest that the mechanism of the chain transfer reaction in an acrylate radical polymerization is a 1,5-hydrogen shift that occurs through formation of a six-membered ring structure. The transfer is possible because formation of a six-membered ring is a kinetically favored process and the transfer occurred from a secondary radical to form a thermodynamically more stable tertiary radical. One further piece of information can be obtained from the result of the pentamer radical since the pentamer provides one more chance for the radical to migrate from a mid-chain radical to the other chain end. However, this migration was not observed for the pentameric model radical which has H-EA-*t*BA-*t*BA-*t*BA-*t*BA• structure. At that time, the reason for this was unresolved.

Although there may be some minor contribution of intermolecular chain transfer, these systematic studies have provided a clearer perspective of the mechanism of the intramolecular chain transfer reaction of propagating acrylate radicals. Nevertheless further investigation was required to provide decisive proof of the mechanism.

Two topics were examined in this research work: One is the possibility of 1,5-hydrogen shift reaction to form radicals on branched ester side groups; the other is a two-step radical migration reaction via sequential 1,5-hydrogen shift mechanism reactions. The results from these studies may be relevant to chain transfer reactions of alkyl radicals.

## Results and Discussion

### Possibility of radical migration to the side group of 2-ethylhexyl acrylate

In the investigation of *t*BA oligomers, 1,5-hydrogen shift reaction mechanism was explained by a combination of formation of a kinetically favorable six-membered ring structure and thermodynamically favorable transfer from secondary to tertiary radical (Fig. 3a) [15].

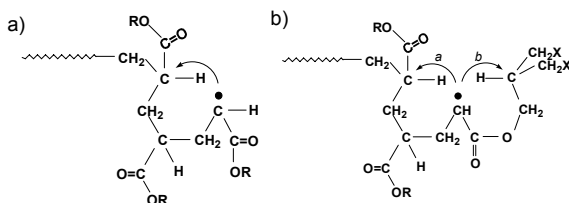


Figure 3 Schematic diagram of potential 1,5-hydrogen shift for propagating acrylate radicals (a) and potential 1,5-hydrogen shift for propagating radicals of acrylates with branched ester side groups (b).

This raises the possibility that we might observe a similar radical migration in any compound which has a chance to form a six-membered ring structure and form a tertiary radical from a secondary radical. Suitable compounds for investigation of another route for radical migration are *isobutyl acrylate* (*i*BA) and 2-ethylhexyl acrylate (2EHA). Both acrylates have branched ester side chains and they can form a six-membered ring structure with a propagating radical and a side branched methine proton as shown in Figure 3b. If the 1,5-hydrogen shift occurs, the resulting radicals should be a tertiary radicals, just as in the case of a 1,5-hydrogen shift to the main chain.

This question can be examined by ESR spectroscopy of dimeric model radicals of *i*BA or 2EHA. As mentioned above, dimeric model radical of acrylates do not undergo the 1,5-hydrogen shift reaction to the main chain. On the other hand, a radical generated from the precursor still has a possibility to migrate to the ester side group through formation of a six-membered ring structure.

A model dimeric radical precursor of 2EHA (H-EA-2EHA-Br) was prepared by ATRP. Initially a mixture of oligomers with dimeric, trimeric, tetrameric, and so on was obtained. The model dimeric radical precursor was separated and purified. ESR spectra of the radicals generated from the precursor at various temperatures were recorded. At 30 °C, the spectrum showed typical features associated with the propagating radical of acrylates. The spectra showed similar features as those measured at 30 °C (Fig. 4) even at higher temperatures of 90 and 120 °C, which indicates that no relocation of the initially formed radical center took place.

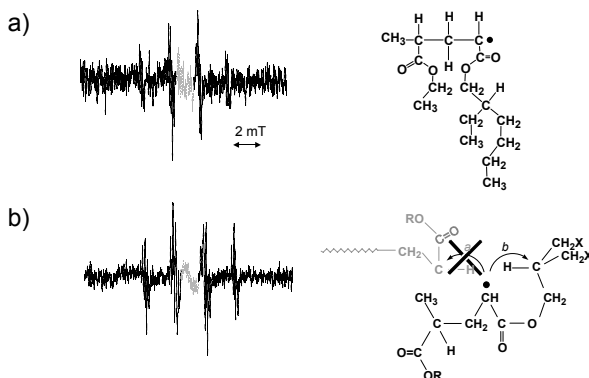
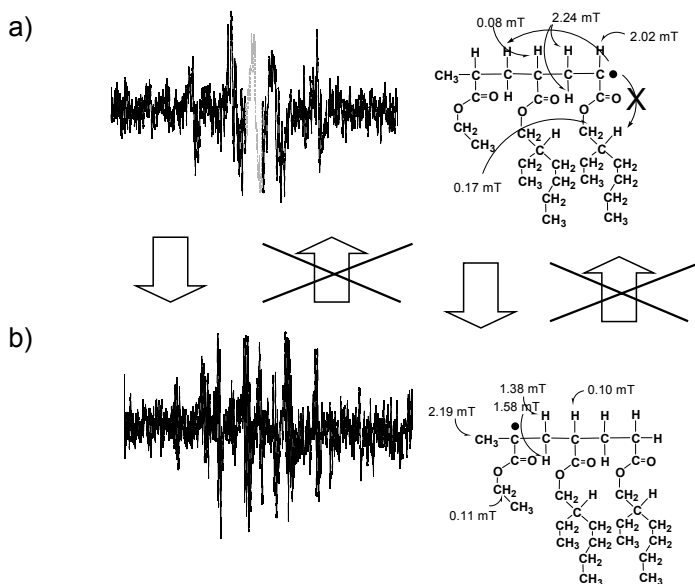


Figure 4 ESR spectra of dimeric model radical of 2EHA at  $-30\text{ }^{\circ}\text{C}$  in toluene and  $150\text{ }^{\circ}\text{C}$  in mesitylene (measurement condition; modulation: 100 kHz, 0.05 mT, time constant: 0.03 sec, sweep time: 15 mT/4 min). ESR spectra of radicals due to organo-tin compounds are shown in grey.

In the next step, ESR measurements were conducted for trimeric model radicals of 2EHA (H-EA-2EHA-2EHA•) as shown in Figure 5. Similar to the case of *t*BA [15], the ESR spectrum of this trimeric model radical showed that the radical migrated to the other end of the molecule at  $120\text{ }^{\circ}\text{C}$ . From these results, we can discard the possibility of radical migration to the ester side groups since no other kind of radicals were observed throughout the measurements. Lovell *et al.* reported that they observed no clear evidence for branching from side group of poly(2EHA) [31]. They investigated the structures of the resulting poly(2EHA) by  $^{13}\text{C}$  NMR spectroscopy. In that case, evidence for the presence of the radicals at the ester side groups was indistinct and some possibility for the migration of the radical center to the side groups remained in the NMR measurements. The present ESR results clearly show that the radical center did not migrate to the ester side group of poly(2EHA). Raise of the temperature caused remarkable spectroscopic change from  $-30\text{ }^{\circ}\text{C}$  to  $+120\text{ }^{\circ}\text{C}$ .

The ester side group of 2-ethylhexyl chain could be imagined to form a six-membered ring structure and the resulting radical should have a tertiary radical structure but the results indicate that the 1,5-hydrogen shift reaction did not occur indicating that there should be some electronic interactions for a formation of six-membered ring structure in polyacrylates or the stability of the resulting radical in “route a” and “route b” might be different. In “route a”, the resulting radical is located next to a carbonyl group and the presence of the carbonyl group would stabilize the radical to a greater degree than in the case of alkyl radical without a neighboring carbonyl group.





*Figure 5 Temperature dependent change in ESR spectra of trimeric model radical of 2EHA (measurement condition at -30 °C; solvent: toluene, modulation: 100 kHz, 0.1 mT, time constant: 0.03 sec, sweep time: 15 mT/4 min, at +120 °C; solvent: mesitylene, modulation: 100 kHz, 0.05 mT, time constant: 0.03 sec, sweep time: 15 mT/4 min).*

### Multi-step radical migration in propagating radicals of Octadecyl Acrylate

As mentioned above, in the previous study examining the pentameric oligomer of *t*BA a second radical migration step was not observed [15]. At that time, the reason was not clear. When model radicals, exemplary of radicals present in the polymerizations of various kinds of alkyl acrylates, were observed by ESR some alkyl acrylates showed faster radical migration to form mid-chain radicals even at low temperatures.

For example, a remarkable acceleration of the apparent rate of the radical migration was observed in the case of dodecyl- and 2-ethylhexyl-acrylates. These results suggested that acrylates with longer alkyl groups at their ester side groups showed faster radical migration than that observed with *t*BA radicals. Therefore the possibility of a second radical migration step was studied again using ethyl-, hexyl-, 2-ethylhexyl, dodecyl- and octadecyl-acrylates. Among these acrylates, octadecyl acrylate (OdA) demonstrated clear results.

Uniform dimeric, trimeric, tetrameric, and pentameric oligomeric model radical precursors of OdA were prepared by ATRP then separated and purified by repeated column chromatography.

In the case of the radical prepared from the pentamer there are two chances of 1,5-hydrogen shift reaction from the initially generated radical. The initial radical center migrated to form mid-chain radical through six-membered ring structure and then the mid-chain radical moved to form a radical located at the other end of the pentamer. Since expected spectroscopic features of radicals at

these specific sites are totally different, the resulting spectra can be differentiated by ESR, as shown in Figure 6.

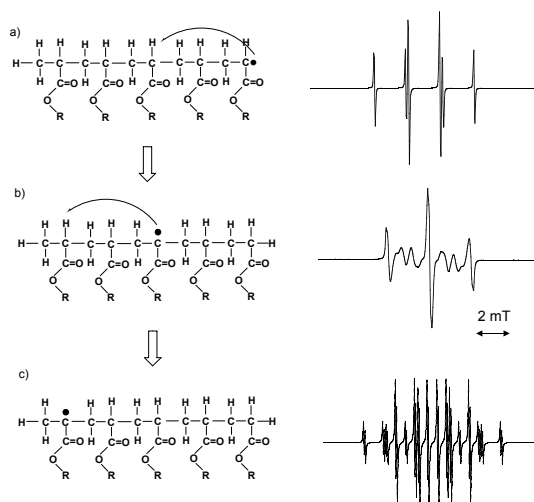


Figure 6 Expected ESR spectra for initially generated radical (a), mid-chain radical (b), and radical formed by two-step migration to locate at the other end (c) along with their expected structures.

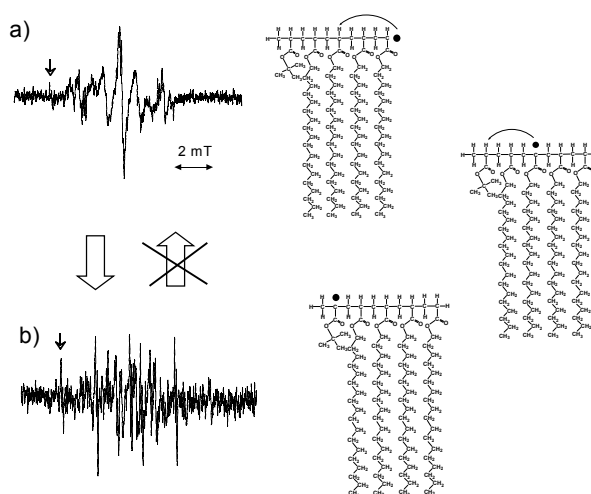


Figure 7 Temperature dependent spectroscopic change in ESR spectra of pentameric model radical of OdA. (measurement condition at 30 °C; solvent: hexane, modulation: 100 kHz, 0.1 mT, time constant: 0.03 sec, sweep time: 15 mT/4 min, at +120 °C; solvent: decane, modulation: 100 kHz, 0.05 mT, time constant: 0.03 sec, sweep time: 15 mT/4 min).

ESR spectra of the pentameric model radical of OdA observed at 30 (a) and 150 °C (b) are shown in Figure 7. At 30 °C, a complicated ESR spectrum was observed while at 150 °C an ESR spectrum due to the radical formed by two radical migrations-steps was exclusively observed. The spectrum is very similar to that observed in trimer model radical of various kinds of acrylates such as the spectrum of 2EHA shown in Figure 5b. In the ESR spectra observed at 30 °C, the spectra of three different radicals overlap. The observation of three different spectra indicates that radicals formed by two radical migration steps are detected. The reason for the observation of the second migration step can be considered to result from the formation of a helix structure for the propagating radicals (Fig. 8). The presence of the long alkyl ester groups may support the formation of the helix structure and facilitate the second migration step. ESR spectra for radicals formed from a uniform heptamer radical were also observed and the presence of a radical at the other chain end was observed. The successive radical migration reaction may be called as “multi-step” migration.

In the previous study, a second migration step was not observed for the model radical formed from the *t*BA pentamer. If it occurred at all, the second migration step was extremely slow. The reason for the retardation of the second migration step is still unresolved.

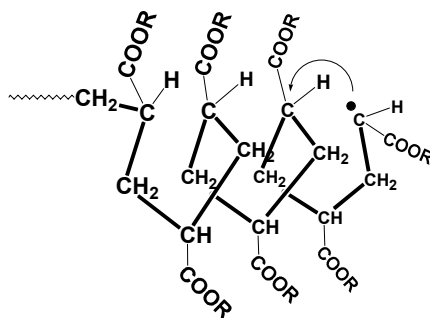


Figure 8 Potential helical structure of propagating radical of alkyl acrylates

### Evidence of intermolecular radical migration of alkyl radicals

There was no evidence in the ESR study of radicals formed from 2EHA precursors for the formation of tertiary alkyl radicals in the 2-ethylhexyl ester side group via a 1,5-hydrogen shift. On the other hand, 1,5-hydrogen shift reactions have been considered in the radical polymerizations of ethylene using various kinds of alkyl bromides as radical precursors to model propagating ethylene radicals of various chain lengths [32]. Model terminal propagating and mid-chain radicals can be generated using alkyl bromides that contain bromine atom at the chain end or mid-chain. The ESR spectra of the model propagating and mid-chain radicals are different and we can clearly differentiate one from the other. The ESR spectra of a butyl radical generated from butyl bromide can be observed. The butyl radical is a model of a dimeric ethylene radical and it does not show any trace of a 1,5-hydrogen shift reaction. The ESR spectrum of the butyl radical in benzene showed no change even at 80 °C. On the other hand,

the ESR spectrum of radicals formed at temperatures higher than 80 °C in decane indicate the presence of a mid-chain radical. These results suggest the occurrence of intermolecular chain transfer rather than intramolecular back-biting reaction in the case of alkyl radicals.

## Conclusions

The development of ATRP provides an opportunity to prepare precursor molecules that can be used to investigate reaction mechanism of radicals in radical polymerizations. Previous studies have clearly showed that radical migrations occur through a 1,5-hydrogen shift mechanism. Model radicals of oligo(OdA) and oligo(2EHA) clearly showed faster 1,5-hydrogen shift reaction through their main chains but the dimeric model 2EHA radical exhibited no evidence for a 1,5-hydrogen shift to its ester side group. On the other hand the model OdA pentamer radical clearly showed the results of two radical step migrations through the 1,5-hydrogen shift mechanism. A butyl radical, a model dimeric ethylene radical, demonstrated intermolecular chain transfer in decane solution. These results indicate that there should be some tendency for oligo- and poly-acrylates to form six-membered ring structures, like a helix structure through some kinds of internal electronic interactions.

## Experimental

Monomers, initiators, copper salts, and ligands were purified in the usual manner [33]. The presence of carbon-bromine terminal groups and the chain lengths of the radical precursors were checked by Electron Spray Ionization (ESI) mass spectra. Generation of model radicals from the model precursors was conducted by a reaction with an organotin compound under irradiation [21]. ESR spectra of radicals were recorded on a JEOL JES RE-2X spectrometer operating in the X-band, utilizing a 100 kHz field modulation, and a microwave power of 1 mW. A TE<sub>011</sub> mode universal cavity was used. Measurement temperature was controlled by JEOL DVT2 variable-temperature accessory. Spectroscopic simulations were carried out by JEOL IPRIT Data Analysis System. Molecular weights and molecular weight distributions were roughly estimated using a TOSOH CCP&8020 series GPC (SEC) system with TSK-gel columns. Polystyrene standards were used to calibrate the columns.

## Acknowledgements

The author is grateful to Professor Emeritus Mikiharu Kamachi, Osaka University, for his kind advice and discussions on ESR study of radical polymerizations. Sincere thanks are due to Professor Krzysztof Matyjaszewski, Carnegie Mellon University, for his kind suggestions and continuous encouragements. The author wishes to thank Professor Bernadette Charleux, Université Pierre et Marie Curie -Paris 6, for her suggestions for investigation of 2-ethylhexyl acrylate radicals.

## References

1. Fischer, H. *Adv. Polym. Sci.*, **1968**, 5, 463.
2. Kamachi, M. *Adv. Polym. Sci.* **1987**, 82, 207.
3. Yamada, B.; Westmoreland, D. G.; Kobatake, S.; Konosu, O. *Prog. Polym. Sci.*, **1999**, 24, 565.
4. Kamachi, M.; Kajiwar, A. *Macromol. Symp.* **2002**, 179, 53.
5. Kajiwar, A.; Matyjaszewski, K., "Advanced ESR Methods in Polymer Research" Wiley Interscience, NJ. 2006, Chapter 5, pp. 101-132.
6. Kajiwar, A.; Maeda, K.; Kubo, N.; Kamachi, M. *Macromolecules* **2003**, 36, 526.
7. Kajiwar, A.; Matyjaszewski, K.; Kamachi, M. "Controlled/Living Radical Polymerization", ACS Symposium Series 768, Matyjaszewski, K. ed., American Chemical Society, Washington, DC, 2000, p. 68.
8. Kamachi, M.; Kajiwar, A. *Macromolecules* **1996**, 29, 2378.
9. Kajiwar, A.; Kamachi, M. *Macromol. Chem. Phys.* **2000**, 201, 2160.
10. Kamachi, M.; Kajiwar, A. *Macromol. Chem. Phys.* **1997**, 198, 787.
11. Kamachi, M.; Kajiwar, A. *Macromol. Chem. Phys.* **2000**, 201, 2165.
12. Kajiwar, M. Kamachi, M. "Advances in Controlled/Living Radical Polymerization", ACS Symposium Series 854, Matyjaszewski, K. ed., American Chemical Society, Washington, DC, 2003, p. 86.
13. Kajiwar, A. *Kobunshi Ronbunshu*, **2004**, 61(4), 237.
14. Kajiwar, A. *Macromolecular Symposia* **2007**, 248, 50.
15. Kajiwar, A. "Controlled/Living Radical Polymerization" ACS Symposium Series 944; Matyjaszewski, K. ed., American Chemical Society, Washington, DC, 2006, p. 111.
16. "Controlled Radical Polymerization", ACS Symposium Series, 685, Matyjaszewski, K. ed., American Chemical Society, Washington, DC, 1998.
17. "Controlled/Living Radical Polymerization", ACS Symposium Series, 768, Matyjaszewski, K. ed., American Chemical Society, Washington, DC, 2000.
18. "Advances in Controlled/Living Radical Polymerization", ACS Symposium Series, 854, Matyjaszewski, K. ed., American Chemical Society, Washington, DC, 2003.
19. Wang, J. -S; Matyjaszewski, K. *J. Am. Chem. Soc.* **1995**, 117, 5614.
20. Wang, J. -S; Matyjaszewski, K. *Macromolecules* **1995**, 28, 7901.
21. Giese, B.; Damm, W.; Wetterich, F.; Zeitz, H. -G. *Tetrahedron Lett.* **1992**, 33, 1863.
22. Best, M. E.; Kasai, P. H. *Macromolecules* **1989**, 22, 2622.
23. Gilbert, B. G.; Lindsay Smith, J. R.; Milne, E. C.; Whitwood, A. C.; Taylor, P. *J. Chem. Soc., Perkin Trans. 2*, **1993**, 2025.
24. Doetschman, D. C.; Mehlenbacher, R. C.; Cywar, D. *Macromolecules* **1996**, 29, 1807.
25. Chang, H. R.; Lau, W.; Parker, H. -Y.; Westmoreland, D. G. *Macromol. Symp.* **1996**, 111, 253.
26. Sugiyama, Y. *Bull. Chem. Soc., Jpn.* **1997**, 70, 1827.
27. Azukizawa, M.; Yamada, B.; Hill, D. J. T.; Pomery, P. J. *Macromol. Chem. Phys.* **2000**, 201, 774.

28. Yamada, B.; Azukizawa, M.; Yamazoe, H.; Hill, D. J. T.; Pomery, P.J. *Polymer*, **2000**, *41*, 5611.
29. Willemse, R. X. E.; van Heck, A. M. ; Panchenko, E.; Junkers, T.; Buback, M. *Macromolecules* **2005**, *38*, 5098.
30. Buback, M.; Hesse, P.; Junkers, T.; Sergeeva, T.; Theis, T. *Macromolecules* **2008**, *41*, 288.
31. Heatley, F.; Lovell, P. A.; Yamashita, T. *Macromolecules*, **2001**, *34*, 7636.
32. Kajiwara, A. paper in preparation.
33. Armarego, W. L. F.; Perrin, D. D. “*Purification of Laboratory Chemicals*”, 4<sup>th</sup> ed. Butterworth-Heinemann, 1997.

## Chapter 5

# “Greening” of Copper Catalyzed Atom Transfer Radical Addition (ATRA) and Cyclization (ATRC) Reactions

Tomislav Pintauer<sup>1\*</sup>

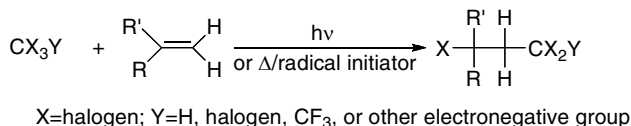
<sup>1</sup>Duquesne University, Department of Chemistry and Biochemistry, 600 Forbes Avenue, 308 Mellon Hall, Pittsburgh, PA 15282, USA

This article reports on recent advances in the area of catalyst regeneration in metal mediated atom transfer radical addition (ATRA) and cyclization (ATRC) reactions using environmentally benign reducing agents. The role of reducing agent in both processes is to continuously regenerate the activator (transition metal complex in the lower oxidation state) from the deactivator (transition metal complex in the higher oxidation state). As a result, single addition adducts in copper mediated ATRA and ATRC reactions can be synthesized using very low concentrations of copper catalysts (5-100 ppm). Previously, efficient catalysis for both processes required as much as several thousands ppm of copper. It is envisioned that the recent developments in this area could have profound industrial implications on the synthesis of small organic molecules, natural products and pharmaceutical drugs.

## Introduction and Background

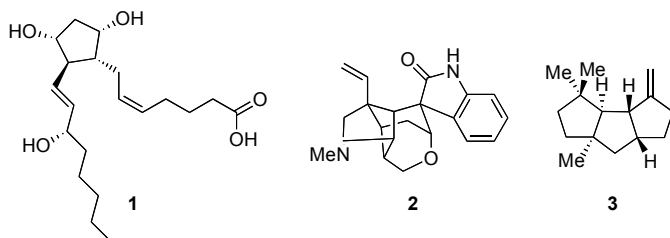
### Free Radical Reactions in Organic Synthesis

Radical chemistry has advanced tremendously since the discovery of triphenylmethyl radical in 1900 by Gomberg.<sup>1</sup> The early synthetic work started with Kharasch addition reaction (Scheme 1)<sup>2,3</sup> in which halogenated methanes were directly added to olefinic bonds in the presence of free radical initiators or light. However, it was not until early 1980s that the full potential of



*Scheme 1. Kharasch addition of polyhalogenated compounds to alkenes.*

radical chemistry as a tool for organic and natural product syntheses was realized due to a pioneering work of Giese (tin hydride mediated radical addition to olefins),<sup>4</sup> Barton (radical decarboxylation and deoxygenation)<sup>5,6</sup> and Curran (iodine atom transfer radical addition).<sup>7</sup> The first successful applications included key radical cyclization reactions which were later applied to the synthesis of numerous complex molecules including natural products such as prostaglandin,<sup>8</sup> alkaloid<sup>9</sup> and triquinane<sup>10</sup> (Scheme 2). Radical chemistry in natural product synthesis, like most of current methodologies, employs stepwise



*Scheme 2. Structures of prostaglandin F2a (1), gelsemine (2) and (-)- $\Delta^9(12)$ -capnellene (3) synthesized using radical means.*

formation of individual bonds in a target molecule using radical means. Increasingly common methodology also includes domino or tandem reactions which enable the synthesis of multiple carbon-carbon bonds in a single step.<sup>11,12</sup> Since 1980s, radical chemistry has come a long way due to its predictability, generality and variability. In other words, radical reactions can be conducted under mild conditions, are tolerant to many functional groups and solvents, and can be very stereoselective. As a result, radical carbon-carbon bond forming reactions are today routinely considered in strategic planning of complex molecules.<sup>13-16</sup>

Transition metal catalyzed atom transfer radical addition (ATRA) or Kharasch addition,<sup>2,3,17-21</sup> despite being discovered nearly 40 years before tin mediated radical addition to olefins and iodine atom transfer radical reaction, is still not fully utilized as a technique in free radical synthesis. The principal reason for small participation of ATRA in complex molecule and natural product syntheses is the large amount of transition metal catalysts needed to achieve high selectivity towards the desired target compound. This obstacle causes serious problems in product separation and catalyst regeneration, making the process environmentally unfriendly and expensive. The main focus of this article is to review recent advances in the area of catalyst regeneration in copper mediated atom transfer radical addition (ATRA) and cyclization (ATRC) reactions using environmentally benign reducing agents. This methodology

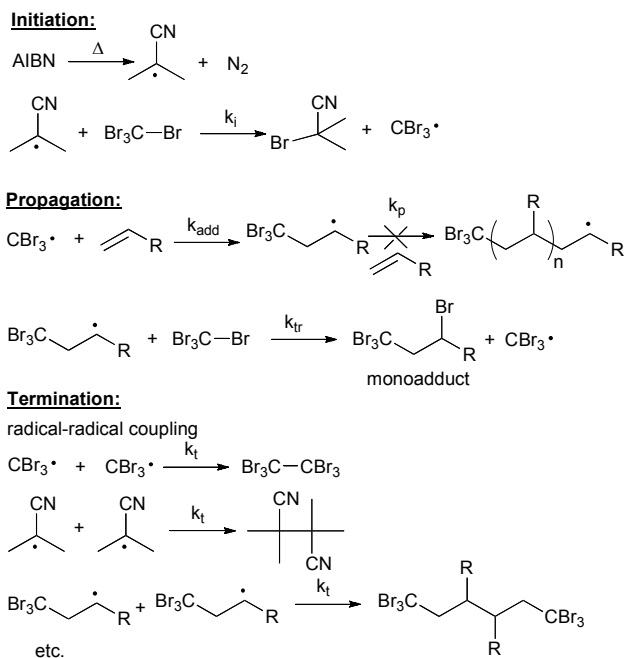


enables chemoselective formation of single addition adducts using very low concentrations of copper catalysts (5-100 ppm) and could have profound industrial implications on large scale preparation of small organic molecules, natural products and pharmaceutical drugs.

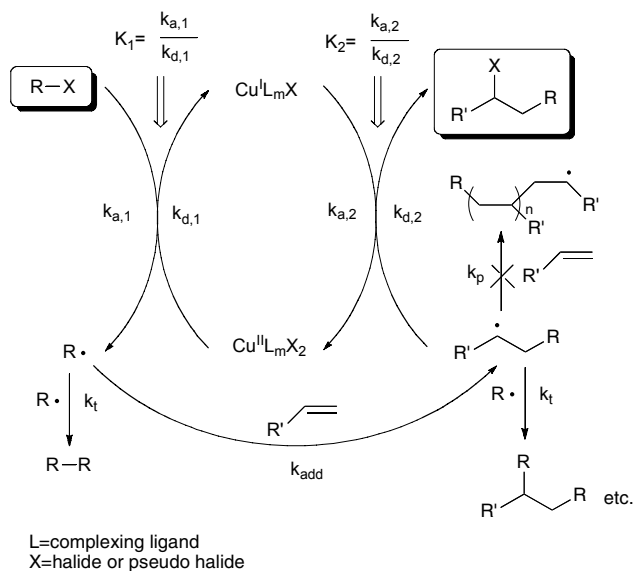
### **Fundamentals of Transition Metal Catalyzed ATRA**

The addition of halogenated compounds to alkenes or alkynes through a radical process is one of the fundamental reactions in organic chemistry.<sup>22,23</sup> It was first reported in the mid 1940s in which halogenated methanes were directly added to olefinic bonds in the presence of radical initiators or light.<sup>2,3</sup> The early work in this area mostly involved the ATRA of  $\text{CCl}_4$  and  $\text{CBr}_4$  to simple olefins in the presence of free radical azo and peroxide initiators. Very high yields of the monoadduct were obtained in the case of simple  $\alpha$ -olefins (1-hexene, 1-octene and 1-decene), but were significantly decreased for more reactive monomers such as styrene, methyl acrylate and methyl methacrylate. The principle reason for the decreased yield of the monoadduct was radical-radical coupling and repeating radical addition to alkene to generate oligomers and polymers. Although, radical-radical termination reactions by coupling and disproportionation could be suppressed by decreasing the radical concentration, telomerization reactions could not be avoided due to the low chain transfer constant ( $k_t/k_p$ , Scheme 3). The research was thus shifted in a direction of finding means to selectively control the product distribution. This was achieved in the early 1960s by recognizing that transition metal complexes are much more effective halogen transfer agents than alkyl halides. A number of species were found to be particularly active in ATRA process and they included the complexes of Cu, Fe, Ru and Ni.<sup>18-21,24,25</sup> Great progress has been made in not just controlling the product selectivity, but also in utilizing a variety of halogenated compounds (alkyl and aryl halides, *N*-chloroamines, alkylsulfonyl halides and polyhalogenated compounds). Furthermore, it was also demonstrated that a variety of alkenes (styrene, alkyl acrylates and acrylonitrile) could be used as the source of reactive unsaturation. Therefore, transition metal catalyzed (TMC) ATRA became broadly applicable synthetic tool.

Based on chemo-, regio-, and stereoselectivity, it is generally accepted that the mechanism of copper catalyzed ATRA involves free radical intermediates (Scheme 4).<sup>21,26,27</sup> Typically, copper(I) halide complexed by a suitable ligand undergoes an inner sphere oxidation through abstraction of a halogen atom from an alkyl halide. This reaction generates the corresponding copper(II) complex and an organic radical. The radical may terminate or add to an alkene in an inter- or intramolecular fashion. It can also abstract the halogen atom from the copper(II) complex and return back to the original dormant organic halide species or, if the abstraction of the halogen occurs after the addition to the alkene, the desired monoadduct will be formed. Abstraction of the halogen atom from the copper(II) complex generates the corresponding copper(I) complex, completing the catalytic cycle. Substrates for copper catalyzed ATRA are typically chosen such that if addition occurs, then the newly formed radical is much less stabilized than the initial radical and, will essentially react irreversibly with the copper(II) complex to form an inactive monoadduct. Therefore, in copper mediated ATRA, usually only one addition step occurs.



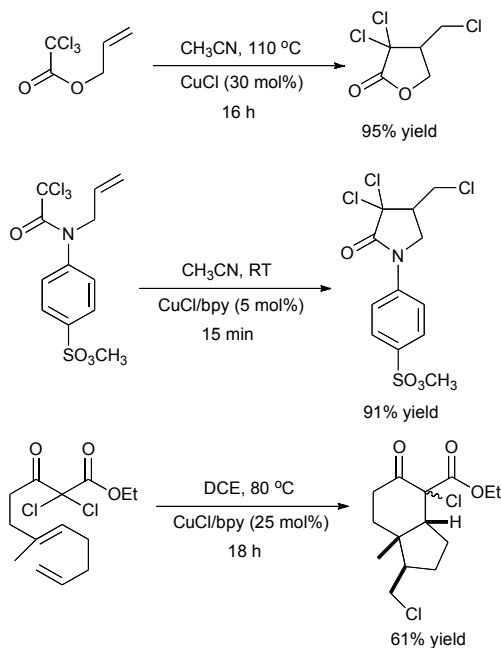
Scheme 3. Kharasch addition of  $\text{CBr}_4$  to alkene in the presence of AIBN.



Scheme 4. Proposed mechanism for copper catalyzed ATRA.

## Transition Metal Catalyzed ATRA in Organic Synthesis

Intramolecular copper mediated ATRA reactions are mechanistically similar to intermolecular reactions with the exception that the transferable halide atom and alkene are part of the same molecule.<sup>21</sup> It is also synthetically more attractive because it enables the synthesis of functionalized ring systems that can be used as starting materials in the synthesis of complex molecules. Furthermore, the halide functionality in the resulting product can be very beneficial because it can be easily reduced, eliminated, displaced, converted to a Grignard reagent, or can serve as a further radical precursor. The use of copper mediated ATRC in organic synthesis has been reviewed recently, however, we will concentrate on couple of elegant examples that have appeared in the literature over the past two decades (Scheme 5), in order to demonstrate its potential.<sup>21</sup> The first successful example of copper mediated ATRC reaction included the synthesis of trichlorinated  $\gamma$ -lactones from readily accessible alkenyl trichloroacetates.<sup>28</sup> The reaction was highly selective, but required elevated temperatures (110-130 °C) and large amounts of copper catalyst (20-30



Scheme 5. Successful examples of copper catalyzed ATRC reactions.

mol% relative to substrate). Some improvements have been achieved utilizing tetradentate nitrogen based ligands such as tris(2-pyridylmethyl)amine (TPMA) and tris[2-(N,N-dimethylamino)ethyl]amine (Me<sub>6</sub>TREN) (Scheme 6), resulting in a decrease in the amount of required catalyst (3-10 mol% relative to substrate) and reaction temperature (80 °C).<sup>29</sup> Copper mediated ATRC reactions have also been used to synthesize  $\gamma$ -lactams and similarly required relatively large amounts of copper catalysts (10-30 mol%).<sup>21</sup> Very recently, copper(I)

chloride, in conjunction with bipyridine or bis(oxazoline) ligand, was found to effectively catalyze ATRC reaction of unsaturated  $\alpha$ -chloro  $\beta$ -keto ester under mild reaction conditions, which was the first example of successful cascade or domino transition metal mediated ATRC.<sup>30</sup>

It is evident from the examples provided in Scheme 5, and many others in the literature, that copper catalyzed ATRC reactions can be utilized in the synthesis of various substrates that can be used as building blocks for the construction of complex molecules and natural products. However, as mentioned earlier, the principal drawback of this useful synthetic method until recently remained the large amount of catalyst required to achieve high selectivity towards the desired target product. Various methodologies have been developed to overcome this problem and they include: (a) the design of solid supported catalysts, (b) the use of biphasic systems containing fluoruous solvents, (c) the use of highly active copper(I) complexes based on ligand design and (d) catalyst regeneration in the presence of environmentally benign reducing agents. These methodologies are discussed in detail in the following sections.

## Development of Methodologies to Decrease the Amount of Copper Catalysts in ATRA and ATRC

### Solid Supported Catalysis

Solid supported catalysts have been utilized in ATRA and ATRC reactions in order to facilitate reaction work-up and enable catalyst recycling.<sup>21</sup> In one example, *N*-alkyl-2-pyridylmethanimines were immobilized on silica and in conjunction with  $\text{Cu}^{\text{I}}\text{Br}$  or  $\text{Cu}^{\text{I}}\text{Cl}$  utilized in ATRC reactions of trichloro-, dichloro- and monobromo-substrates.<sup>31</sup> Efficient *5-exo* and *5-endo* cyclizations could be mediated using this immobilized system, however, as commonly encountered, the solid supported catalyst was much less active than its homogeneous counterpart. The decrease in the catalytic activity was not induced by catalyst leaching, but rather accumulation of copper(II) deactivator. The accumulation of deactivator during ATRA or ATRC process was result of irreversible and often diffusion controlled radical-radical coupling reactions ( $k_r \approx 1.0 \times 10^9 \text{ M}^{-1} \text{ s}^{-1}$ ).

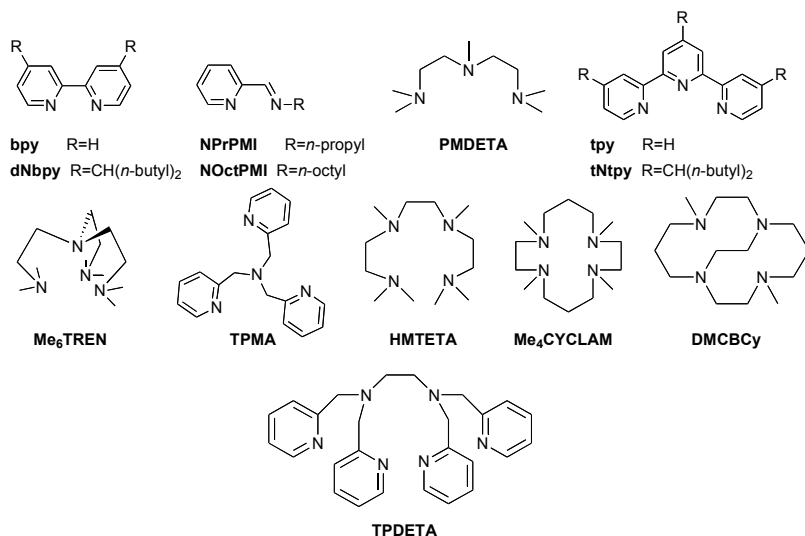
### Biphasic Systems

The use of biphasic systems utilizing perfluorous solvents containing the desired catalyst is widely used method in organic synthesis. Generally, the perfluorinated catalyst is confined to the perfluorous phase, while the organic reactants and products are contained in the organic phase. At elevated temperatures the two phases are miscible allowing homogeneous catalysis while at low (typically ambient temperatures) the phases are immiscible, enabling easy separation of products from the catalyst. The perfluorinated analogue of tris[2-(*N,N*-dimethylamino)ethyl]amine ( $\text{Me}_6\text{TREN}$ ) has been used in ATRC reactions of trichloroesters in perfluorocyclohexane.<sup>32</sup> The cyclization was found to proceed much slower than under homogeneous conditions, however, excellent yields of the desired cyclic product were obtained (97%). Furthermore, only slight decrease in the activity of the catalyst was observed after fourth recycling

and atomic absorption indicated that only 1-2% of copper leached into the organic phase. Similarly to solid supported catalyst, this promising system is also suffering from accumulation of the deactivator or copper(II) complex.

### Development of Highly Active Ligands in Copper Catalyzed ATRA

An alternative way to increase efficiency of copper catalysts in ATRA and ATRC reactions is to develop highly active catalysts that could be used in smaller concentrations. A significant amount of work in this area has been done for mechanistically similar atom transfer radical polymerization (ATRP),<sup>33-41</sup> which originated from ATRA. Both processes typically utilize bidentate, tridentate and tetradentate nitrogen based ligands which are depicted in Scheme 6. The complexing ligand, in conjunction with copper, is essential for both processes because it regulates the dynamic equilibrium for atom transfer ( $K_{ATRA/ATRP} = k_a/k_d$ , Scheme 4).<sup>35,42</sup> The activity of a certain ligand in ATRA/ATRP process is typically determined by measuring the activation ( $k_a$ ), deactivation ( $k_d$ ) and overall equilibrium constant for atom transfer ( $K_{ATRA/ATRP}$ ) (Scheme 4).<sup>37,38,41,43-46</sup> Also, for complexes that have similar "halidophilicities" or equilibrium constants for halide anion coordination to the copper(II) center, the redox potential can be used as a measure of catalyst activity.<sup>41,47</sup> Currently, the most active ligands in copper mediated ATRA/ATRP are tetradentate and multidentate nitrogen based ligands tris[2-(dimethylaminoethyl)amine (Me<sub>6</sub>TREN)<sup>48</sup>, tris[(2-pyridyl)methyl]amine (TPMA)<sup>29,32,49-52</sup>, 1,4,8,11-tetraaza-



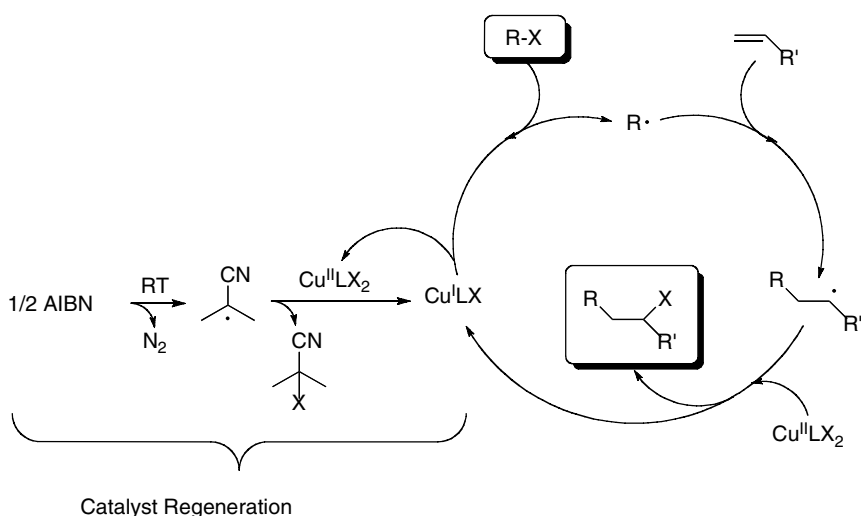
Scheme 6. Nitrogen based ligands commonly used in copper catalyzed ATRA and ATRP.

1,4,8,11-tetramethylcyclotetradecane (Me<sub>4</sub>CYCLAM)<sup>53</sup>, *N,N,N',N'*-tetrakis(2-pyridylmethyl)ethylenediamine (TPEDA)<sup>54</sup> and dimethylated 1,8-ethylene cross bridged 1,4,8,11-tetraazacyclotetradecane (DMCBcy)<sup>34</sup>.

## Highly Efficient Copper Catalyzed ATRA and ATRC Reactions in the Presence of Reducing Agents

### Regeneration of Catalyst in ATRA and ATRP

As aforementioned, the principle problem of copper catalyzed ATRA and ATRC reactions until recently remained the large amount of catalyst required to achieve high selectivity towards the desired product. The main reason was the accumulation of copper(II) complex as a result of unavoidable radical coupling reactions (Scheme 4). Originally, the solution to this problem has been found for copper catalyzed atom transfer radical polymerization (ATRP),<sup>33,55-59</sup> and was subsequently applied first to ruthenium<sup>60</sup> and then copper<sup>50,51</sup> catalyzed ATRA reactions. In all of these processes, the activator (transition metal complex in the lower oxidation state) is continuously regenerated from deactivator (transition metal complex in the higher oxidation state) in the presence of reducing agents such as phenols, glucose, ascorbic acid, hydrazine,



*Scheme 7. Proposed mechanism for copper(I) regeneration in the presence of AIBN as a reducing agent.*

tin(II) 2-ethylhexanoate, magnesium, and free radical initiators (Scheme 7).<sup>56</sup> As a result, a significant decrease in the catalyst concentration can be achieved. When applied to ATRA of  $\text{CCl}_4$  to alkenes catalyzed by  $\text{Cp}^*\text{RuIIICl}_2(\text{PPh}_3)$  complex in the presence of AIBN, TONs as high as 44500 were obtained.<sup>60</sup> Even more impressive TONs were achieved with  $\text{CBr}_4$  and  $[\text{CuII}(\text{TPMA})\text{Br}][\text{Br}]$  (TPMA=tris(2-pyridylmethyl)amine) complex (as high as 160000), enabling efficient ATRA reactions in the presence of as little as 5 ppm of copper.<sup>50</sup> Since the seminal reports by our<sup>51</sup> and the research group of Severin,<sup>60</sup> this method of catalyst regeneration in ATRA has attracted considerable academic interest,<sup>61-68</sup> and was even successfully applied to intramolecular ATRA or atom transfer radical cyclization (ATRC) reactions.<sup>67-69</sup> Detailed results are discussed below.

## Highly Efficient Copper Catalyzed ATRA in the Presence of AIBN as a Reducing Agent

In our seminal report,  $[\text{Cu}^{\text{II}}(\text{TPMA})\text{X}][\text{X}]$  (TPMA = tris(2-pyridylmethyl)amine), X= Br and Cl) complexes were found to be very active in ATRA reactions of polyhalogenated compounds to alkenes in the presence of reducing agent (AIBN).<sup>50,51</sup> Tetradentate nitrogen-based ligand TPMA was chosen for this study because its complexation to  $\text{Cu}^{\text{I}}\text{X}$  (X=Br or Cl) results in a formation of one of the most active catalysts in copper mediated ATRP (*vide supra*).<sup>54,70,71</sup> Despite the fact that  $\text{Cu}^{\text{I}}\text{Cl}/\text{TPMA}$  complex is highly active catalyst in ATRP, the conversion of only 2% was observed after 24 hours at 60 °C in ATRA of  $\text{CCl}_4$  to 1-hexene when the ratio of catalyst to olefin was 1:10000. This result was not surprising because the low catalyst/ $\text{CCl}_4$  ratio resulted in a complete deactivation of the catalyst. In other words, due to the irreversible radical coupling reactions (Scheme 4),  $\text{Cu}^{\text{I}}\text{Cl}/\text{TPMA}$  complex was converted to  $\text{Cu}^{\text{II}}\text{Cl}_2/\text{TPMA}$ . In the absence of  $\text{Cu}^{\text{I}}\text{Cl}/\text{TPMA}$ , 3-5% conversion of 1-hexene was observed resulting in the formation of monoadduct and oligomers/polymers. This situation was changed by the addition of external radical source such as AIBN. The slow decomposition of AIBN provided constant source of radicals, which continuously reduced  $\text{Cu}^{\text{II}}\text{Cl}_2/\text{TPMA}$  to  $\text{Cu}^{\text{I}}\text{Cl}/\text{TPMA}$  complex. Indeed, when the above reaction was conducted in the presence of 5.0 mol% AIBN (relative to the alkene), 88% conversion of 1-hexene was observed after 24 h with the main product being the desired monoadduct (yield=72 %, Table 1). Increasing the catalyst concentration, under the same reaction conditions, resulted in a complete conversion of 1-hexene and increase in the yield of monoadduct (98%). Similar results were also obtained with 1-octene. The TONs in these experiments ranged between 4900-7200 (1-hexene) and 4350-6700 (1-octene). Previously reported TONs for copper mediated ATRA ranged between 0.1 and 10.<sup>21,29,72-74</sup> The efficient regeneration of the copper(I) complex by AIBN suggested that ATRA reactions can also be conducted using air stable  $\text{Cu}^{\text{II}}\text{Cl}_2/\text{TPMA}$  complex, which was confirmed experimentally.

To test the applicability of this new methodology for copper(I) regeneration in ATRA, additional experiments were conducted using other alkenes as well as alkyl halides. Relatively high yields of monoadduct were obtained in ATRA of  $\text{CCl}_4$  to styrene and methyl acrylate, but with much higher catalyst loadings. For  $\text{Cu}^{\text{I}}\text{Cl}/\text{TPMA}$  to styrene ratio of 1:250, complete conversion of styrene was observed after 24 hours and monoadduct was obtained in 85% yield. Further increase in the ratio of styrene to catalyst still resulted in quantitative conversion of styrene, however, more pronounced decrease in the yield of monoadduct was observed. The decrease in the yield of monoadduct was mostly due to the formation of oligomers/polymers. Similar results were also obtained for methyl acrylate. The experiments with less active chloroform also worked reasonably well. Relatively high yields were obtained for all alkenes investigated at  $[\text{alkene}]_0:[\text{Cu}^{\text{I}}]_0$  ratios between 500 and 1000.

**Table 1. ATRA of polyhalogenated compounds to alkenes catalyzed by copper complexes with TPMA ligand in the presence of AIBN.<sup>a</sup>**

<i>Alkene</i>	<i>RX</i>	<i>[Alk]<sub>0</sub>: [Cu]<sub>0</sub></i>	<i>Yield (%)<sup>b</sup></i>	<i>TON</i>
$\text{Cu}^{\text{I}}(\text{TPMA})\text{Cl}$				
1-hexene	$\text{CCl}_4$	10000:1	72	7200
		5000:1	98	4900
1-octene	$\text{CHCl}_3$	1000:1	56	560
		$\text{CCl}_4$	10000:1	67
styrene	$\text{CHCl}_3$	5000:1	87	4350
		500:1	49	245
methyl acrylate	$\text{CCl}_4$	250:1	85	212
		1000:1	58	580
methyl acrylate	$\text{CHCl}_3$	1000:1	60	600
		1000:1	63	630
$[\text{Cu}^{\text{II}}(\text{TPMA})\text{Br}][\text{Br}]$				
methyl acrylate	$\text{CBr}_4$	/	32	/
		200000:1	81(76) <sup>c</sup>	$1.5 \times 10^5$
		100000:1	94	$9.4 \times 10^4$
		$\text{CHBr}_3$	1000:1	57
styrene	$\text{CBr}_4$	500:1	66	$3.3 \times 10^2$
		/	72	/
		200000:1	95(86) <sup>c</sup>	$1.9 \times 10^5$
	$\text{CHBr}_3$	100000:1	99	$9.9 \times 10^4$
		10000:1	70	$7.0 \times 10^3$
		5000:1	77	$3.9 \times 10^3$
1-hexene	$\text{CHBr}_3$	1000:1	92	$9.2 \times 10^2$
1-octene	$\text{CHBr}_3$	10000:1	61(59) <sup>c</sup>	$6.1 \times 10^3$
1-decene	$\text{CHBr}_3$	10000:1	69(54) <sup>c</sup>	$6.9 \times 10^3$
			63(64) <sup>c</sup>	$6.3 \times 10^3$

<sup>a</sup>All reactions were performed at 60 °C for 24 hours with  $[\text{RX}]_0: [\text{alkene}]_0: [\text{AIBN}]_0 = 4:1:0.05$  except reactions with  $\text{CBr}_4$  which were performed in  $\text{CH}_3\text{CN}$ . <sup>b</sup>The yield is based on the formation of monoadduct and was determined using  $^1\text{H}$  NMR spectroscopy. <sup>c</sup>Isolated yield after column chromatography.

Even more impressive results were obtained in the ATRA of polybrominated compounds to alkenes catalyzed by  $[\text{Cu}^{\text{II}}(\text{TPMA})\text{Br}][\text{Br}]$  complex and polybrominated compounds (Table 1).<sup>50</sup> For methyl acrylate, a significant improvement in the yield of the monoadduct was achieved using  $[\text{Cu}^{\text{II}}(\text{TPMA})\text{Br}][\text{Br}]$  to methyl acrylate ratios of 1:200000 (81%) and 1:100000 (94%). Furthermore, using identical reaction conditions, the complete conversion of styrene was also achieved with the main product being the desired monoadduct (95% and 99%, respectively). In the absence of catalyst, but in the presence of AIBN, moderate yields of the mono adduct were obtained for both monomers due to the fact that  $\text{CBr}_4$  is highly efficient chain transfer agent. The methodology for copper(I) regeneration in ATRA in the presence of reducing agent AIBN worked very well for less active bromoform. Relatively high yields



of monoadduct were obtained in ATRA of  $\text{CHBr}_3$  to methyl acrylate and styrene but with much higher catalyst loadings. Further decrease in the amount of catalyst for both monomers resulted in a decrease in the yield of the monoadduct. The decrease in the yield of monoadduct was mostly due to the formation of oligomers/polymers, which was explained by (a) insufficient trapping of radicals generated from AIBN by the copper(II) complex and (b) further activation of the monoadduct by the copper(I) complex (more pronounced in the case of methyl acrylate). In the ATRA of  $\text{CHBr}_3$  to 1-hexene, 1-octene and 1-decene, moderate yields of the monoadduct were attributed to incomplete alkene conversions.

The activity of  $[\text{Cu}^{\text{II}}(\text{TPMA})\text{Br}][\text{Br}]$  complex in ATRA of polybrominated compounds to alkenes in the presence of AIBN, based on catalyst loading, conversion of alkene and the yield of monoadduct, was approximately 10 times higher than the activity of previously reported  $[\text{Cu}^{\text{II}}(\text{TPMA})\text{Cl}][\text{Cl}]$  in the ATRA of polychlorinated compounds to alkenes.<sup>51</sup> Also, for comparable monomers and alkyl halides, its activity was very close to the activity of  $[\text{Cp}^*\text{Ru}^{\text{III}}\text{Cl}_2(\text{PPh}_3)]$  complex.<sup>60</sup>  $[\text{Cu}^{\text{II}}(\text{TPMA})\text{Br}][\text{Br}]$ , in conjunction with AIBN, effectively catalyzed ATRA reactions of polybrominated compounds to alkenes with concentrations between 5 and 100 ppm, which was by far the lowest number achieved in copper mediated ATRA.<sup>21,29,72-74</sup>

As evident from the results presented in Table 1, regeneration of activator ( $\text{Cu}^{\text{I}}(\text{TPMA})\text{X}$ ) in the presence of AIBN is very effective for monomers that are inactive in free radical polymerization such as simple  $\alpha$ -olefins. However, significant increase in the catalyst concentration for efficient ATRA is required for monomers with high propagation rate constants such as methyl acrylate and styrene. Potential solution to this problem is to utilize redox reducing agents that do not generate free radicals such as glucose,<sup>57</sup> ascorbic acid<sup>59</sup> or tin(II) 2-ethylhexanoate.<sup>57,58</sup> Also, on the other hand, metals such as magnesium<sup>67,68</sup> have been utilized. Detailed kinetic studies of copper catalyzed ATRA reactions in the presence of AIBN are discussed below.

## Kinetic Studies of Copper Catalyzed ATRA in the Presence of AIBN as a Reducing Agent

### *Effect of Deactivator Concentration on ATRA in the Presence of AIBN*

The main purpose of the reducing agent in transition metal catalyzed ATRA is to continuously regenerate the activator (transition metal complex in the lower oxidation state) which is needed to homolytically cleave the alkyl halide bond.<sup>50,51,55,56,60,67,75,76</sup> The effect of the concentration of  $[\text{Cu}^{\text{II}}(\text{TPMA})\text{Cl}][\text{Cl}]$  on alkene conversion and the yield of monoadduct for ATRA reactions in the presence of 5 mol% AIBN relative to alkene is shown in Table 2.<sup>77</sup> For simple  $\alpha$ -olefins such as 1-octene, the catalyst regeneration was efficient using alkene to copper(II) ratios as low as 10000:1. However, a more pronounced effect of the catalyst loading on alkene conversion and the yield of monoadduct was observed in the case of methyl acrylate and styrene. For styrene, a relatively high yield of the monoadduct was obtained at much higher catalyst loadings (100:1). A further increase in the ratio of styrene to copper(II) still resulted in

quantitative conversions, however, a more pronounced decrease in the yield of monoadduct was observed. The decrease in the yield of monoadduct was mostly due to the formation of polymers as a result of competing radical polymerization initiated by AIBN. This effect was even more pronounced in the case of methyl acrylate.

**Table 2. Effect of [Cu<sup>II</sup>(TPMACl)]Cl on ATRA of CCl<sub>4</sub> to Alkenes.<sup>a</sup>**

$[alkene]_0:[Cu^{II}]_0$	<i>l</i> -octene	Conversion(%) / Yield(%)	
		<i>styrene</i>	<i>methyl acrylate</i>
100:1	100/100	100/85	100/93
500:1	100/100	82/54	100/66
1000:1	100/99	65/38	100/47
2000:1	100/96	51/31	100/30
5000:1	100/94	47/29	100/16
7500:1	100/93	46/26	100/9
10000:1	99/90	40/25	100/7

<sup>a</sup> $[alkene]_0:[Cu^{II}]_0:[AIBN]_0=1:4:0.05$ ,  $[alkene]_0=0.95$  M, solvent=CH<sub>3</sub>CN. <sup>b</sup>The conversion of alkene and the yield of monoadduct were determined after 24h using <sup>1</sup>H NMR (relative errors are ±15%).

#### *Effect of AIBN and CCl<sub>4</sub> Concentrations on ATRA*

Similarly to the above, the concentration of AIBN (1-20 mol% relative to alkene) was found not to significantly affect the conversion and percent yield of the monoadduct in the case of *l*-octene (Table 3).<sup>77</sup> The optimum amount of AIBN in the ATRA of CCl<sub>4</sub> was found to be approximately 5 mol%.<sup>77</sup> Furthermore, the alkene conversion and the percent yield of monoadduct were relatively independent on AIBN concentration in the ATRA of CCl<sub>4</sub> to *styrene* and *methyl acrylate* when copper(II) loading was high (1 mol%). Further decrease in catalyst loading for both monomers resulted in quantitative conversions, but significantly lower yields.

**Table 3. Effect of AIBN Concentration on ATRA of CCl<sub>4</sub> to Alkenes.<sup>a</sup>**

$[alkene]_0:[AIBN]_0$	<i>l</i> -octene	Conversion(%) / Yield(%)	
		<i>styrene</i>	<i>methyl acrylate</i>
1:0.01	98/94	82/70	100/79
1:0.05	100/99	100/85	100/83
1:0.10	100/99	100/85	100/84
1:0.15	100/99	100/85	100/77
1:0.20	100/100	100/85	100/79

<sup>a</sup> $[alkene]_0:[CCl_4]_0:[Cu^{II}]_0=100:400:1$ ,  $[alkene]_0=0.95$  M, solvent=CH<sub>3</sub>CN. <sup>b</sup>The conversion of alkene and the yield of monoadduct were determined after 24h using <sup>1</sup>H NMR (relative errors are ±15%).

The efficiency of ATRA of CCl<sub>4</sub> to alkenes catalyzed by [Cu<sup>II</sup>(TPMA)Cl]Cl complex in the presence of AIBN as a reducing agent was

also found to depend on the concentration of alkyl halide.<sup>77</sup> For 1-octene, the optimum ratio of  $\text{CCl}_4$  to alkene was 1:2. This ratio also provided high conversion and percent yield of monoadduct for methyl acrylate and styrene, but at high catalyst loadings (1 mol% relative to alkene). Furthermore, the ratio of  $\text{CCl}_4$  to alkene as high as 6:1 was found not to have a significant effect on the ATRA of  $\text{CCl}_4$  to methyl acrylate and styrene when copper(II) concentrations were low (0.01-0.1 mol% relative to alkene). These results indicate that at low copper(II) concentrations, the percent yield of monoadduct is mostly governed by competing free radical polymerization initiated by AIBN and not further activation of the monoadduct by copper(I) complex. Additional factors such as Kharasch addition as a result of chlorine atom transfer from  $\text{CCl}_4$ <sup>78,79</sup> are currently being investigated in our laboratories.

### Reaction Kinetics

According to the proposed mechanism in Scheme 4, the rate of monomer consumption in copper catalyzed ATRA is given by the following expression:

$$-\frac{d[\text{alkene}]}{dt} = k_{\text{add}}[R^*][\text{alkene}]$$

Neglecting termination reactions due to persistent radical effect<sup>46,80-83</sup> and using a fast equilibrium approximation, the radical concentration ( $[R^*]$ ) in the system is given by:

$$[R^*] = \frac{k_{a,1}[\text{Cu}^I][\text{RX}]}{k_{d,1}[\text{Cu}^{II}]}$$

Combining these two expressions gives the following rate law for copper catalyzed ATRA:

$$-\frac{d[\text{alkene}]}{dt} = \frac{k_{a,1}k_{\text{add}}[\text{Cu}^I][\text{RX}][\text{alkene}]}{k_{d,1}[\text{Cu}^{II}]} = \frac{K_{\text{ATRA}}k_{\text{add}}[\text{Cu}^I][\text{RX}][\text{alkene}]}{[\text{Cu}^{II}]}$$

where  $K_{\text{ATRA}} = k_{a,1}/k_{d,1}$ . Therefore, the rate of alkene consumption in copper catalyzed ATRA depends on the equilibrium constant for atom transfer ( $K_{\text{ATRA}}$ ), concentrations of alkyl halide ( $[\text{RX}]$ ) and alkene, addition rate constant of alkene ( $k_{\text{add}}$ ), and the ratio of concentrations of activator ( $[\text{Cu}^I]$ ) and deactivator ( $[\text{Cu}^{II}]$ ). If the radical concentration in the system is constant, the plot of  $\ln([\text{alkene}]_0/[\text{alkene}]_t)$  vs.  $t$  should give a straight line with the slope being equal to the apparent equilibrium constant for atom transfer,  $K_{\text{ATRA}}^{\text{app}} = K_{\text{ATRA}}/[\text{Cu}^{II}]$ .

The reaction kinetics in the presence of free radical reducing agent such as AIBN appear to be rather complex. The principle reason is the incorporation of additional reaction steps that involve AIBN. These steps are: (a) decomposition of AIBN to generate free radicals, (b) reduction of copper(II) to copper(I) in the presence of AIBN and (c) free radical polymerization of alkene

initiated by AIBN. However, several empirical observations related to the overall rate law can be obtained through kinetic studies.

For alkenes that have low propagation rate constants in free radical polymerization, such as simple  $\alpha$ -olefins (1-hexene, 1-octene and 1-decene), high yields of monoadduct can be obtained using low copper(II) concentrations.<sup>50,51</sup> The catalytic activity for  $\alpha$ -olefins appears to be relatively independent on the concentration of AIBN. However, increase in the concentration of AIBN generally increases the reaction rate.<sup>77</sup> For ATRA of  $\text{CCl}_4$  to 1-octene catalyzed by  $[\text{Cu}^{\text{II}}(\text{TPMA})\text{Cl}][\text{Cl}]$ , the apparent reaction order was 0.36 with respect to AIBN, which is close to 0.5 typically observed in free radical polymerization. Similarly, the reaction order with respect to AIBN was found to be 0.49 in the case of styrene. Furthermore, for ATRA of  $\text{CCl}_4$  to 1-octene and styrene, the apparent rate constant of the reaction was found to generally increase as the concentration of copper(II) complex increased. The apparent reaction orders in copper(II) were non-integer numbers ranging from 0.2 (1-octene) to 0.7 (styrene). On the other hand, for methyl acrylate, a slight increase in the reaction rate was observed upon lowering the total copper(II) concentration from 1 ( $k_{\text{app}}=3.0\times 10^{-4} \text{ s}^{-1}$ ) to 0.1 ( $k_{\text{app}}=4.9\times 10^{-4} \text{ s}^{-1}$ ) mol% relative to alkene. For both methyl acrylate and styrene, decrease in the catalyst concentration resulted in dramatic decrease in the yield of monoadduct as a result of competing radical polymerization initiated by AIBN. This is illustrated in Figure 1a which shows the results of kinetic simulation of ATRA of  $\text{CCl}_4$  to methyl acrylate catalyzed by  $[\text{Cu}^{\text{II}}(\text{TPMA})\text{Cl}][\text{Cl}]$  in the presence of AIBN ( $[\text{MA}]_0:[\text{CCl}_4]_0:[\text{AIBN}]_0:[\text{Cu}^{\text{II}}]_0=500:2000:25:1$ ). As evident from Figure 1a, at the end of reaction approximately 70% of monoadduct was obtained, which is consistent with experimental data (Table 2). The remaining 30% percent can be attributed to polymers that were formed not by further activation of the monoadduct, but rather polymerization initiated by AIBN. More importantly, the results of simulation in Figure 1b clearly indicate constant concentrations of copper(I), copper(II) and radicals in the system. Therefore, ATRA quasi-equilibrium ( $k_a[\text{Cu}^{\text{I}}][\text{RX}]\approx k_d[\text{Cu}^{\text{II}}][\text{R}^*]$ ) is established almost immediately and operates during the entire time span of the reaction. Under these conditions, as pointed out in the case of ICAR ATRP of styrene,<sup>55</sup> the termination rate ( $R_t$ ) approaches the decomposition rate of AIBN ( $R_i$ ). The steady state radical concentration can be estimated by setting  $R_t=R_i$  or  $2k_{\text{dc}}[\text{AIBN}]=2k_t[\text{R}^*]^2$ , where  $k_{\text{dc}}$  is the decomposition rate constant for AIBN corrected by the initiation efficiency. Hence,

$$[\text{R}^*] = \sqrt{k_{\text{dc}}[\text{AIBN}]/k_t} \approx \sqrt{k_{\text{dc}}[\text{AIBN}]_0/k_t}$$

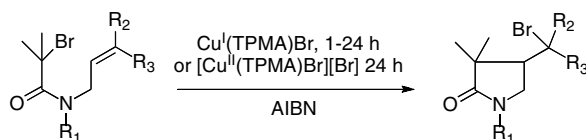
This equation shows that the radical concentration and consequently the rate of consumption of alkene in ATRA ( $k_{\text{add}}[\text{alkene}][\text{R}^*]$ , Scheme 4) under steady state conditions are dependent only on the AIBN concentration and its decomposition and termination rate constants. In other words, radical concentration in this system should not be governed by the choice of ATRA catalyst (which regulates the equilibrium constant for atom transfer,  $K_{\text{ATRA}}=k_a/k_d$ ) or the initial concentrations of copper(II) species. Indeed, these predictions have been shown to be in excellent agreement with experimental observations where apparent rates of polymerization in ICAR ATRP of styrene mediated by copper(II) bromide complexes with  $\text{Me}_6\text{TREN}$ , TPMA, PMDETA and  $\text{dNbpy}$

were very similar,<sup>55</sup> despite large differences in the equilibrium constants for atom transfer ( $K_{ATRP}$  (ethyl 2-bromoisobutyrate in  $\text{CH}_3\text{CN}$  at 35 °C)= $1.54\times 10^{-4}$ ,  $9.65\times 10^{-6}$ ,  $7.46\times 10^{-8}$  and  $3.93\times 10^{-9}$ , respectively).<sup>46</sup>

### Highly Efficient Copper Catalyzed ATRC in the Presence of Reducing Agents

In our recent study, intermolecular ATRA of polyhalogenated compounds to alkenes were successfully catalyzed using ppm amounts of copper(II) complexes with TPMA ligand in the presence of AIBN as a reducing agent.<sup>50,51,56,76</sup> The logical extension of this study is to conduct intramolecular ATRA or ATRC reactions which are synthetically more attractive because they enable the synthesis of functionalized ring systems that can be used as starting materials in the preparation of complex molecules.

**Table 4. ATRC of Bromoacetamides Catalyzed by Copper Complexes with TPMA Ligand in the Presence of AIBN.**



Temp (°C)	Solvent	R <sup>1</sup>	R <sup>2</sup>	R <sup>3</sup>	Cu Source	Yield (%)
50	$\text{CH}_2\text{Cl}_2$	Ts	H	H	CuBr	95
50	$\text{CH}_2\text{Cl}_2$	Ts	Me	H	CuBr	100
50	$\text{CH}_2\text{Cl}_2$	Ts	Ph	H	CuBr	99
50	$\text{CH}_2\text{Cl}_2$	Ts	Me	Me	CuBr	99
50	$\text{CH}_2\text{Cl}_2$	Bn	Me	Me	CuBr	14
110	Toluene	Bn	Me	Me	CuBr	80
50	$\text{CH}_2\text{Cl}_2$	Bn	Me	Me	$\text{CuBr}_2$	13
110	Toluene	Bn	Me	Me	$\text{CuBr}_2$	88

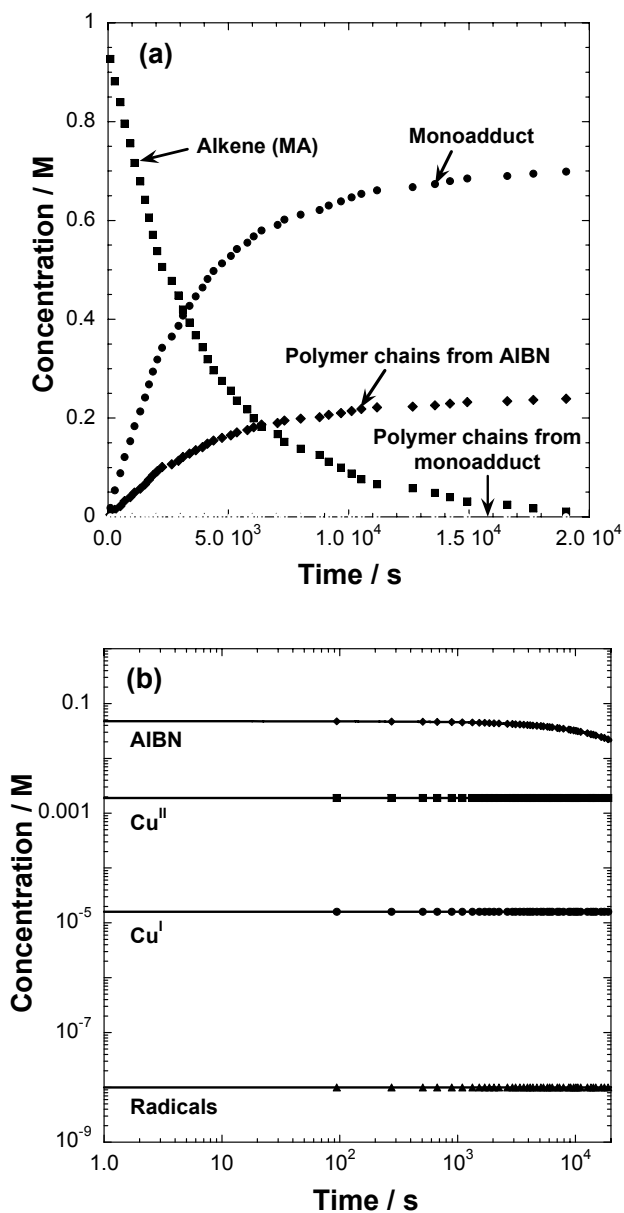
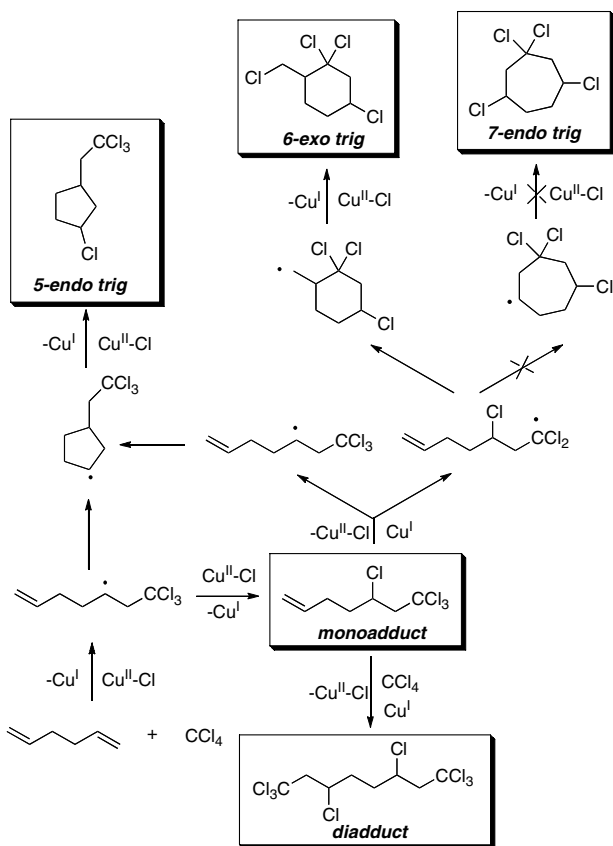


Figure 1. Simulation of kinetic plots for ATRA of  $\text{CCl}_4$  to methyl acrylate catalyzed by  $[\text{Cu}^{\text{II}}(\text{TPMA})\text{Cl}][\text{Cl}]$  in the presence of AIBN,  $[\text{MA}]_0: [\text{CCl}_4]_0: [\text{AIBN}]_0: [\text{Cu}^{\text{II}}]_0 = 500:2000:25:1$ .

The methodology used to regenerate activator in ATRA originally developed for Ru and Cu catalysts has been successfully utilized in a range of *5-exo trig* and *5-exo dig* ATRC reactions of bromoacetamides using 0.1-1 mol% of  $\text{Cu}^{\text{I}}(\text{TPMA})\text{Br}$  or  $[\text{Cu}^{\text{II}}(\text{TPMA})\text{Br}][\text{Br}]$  complexes (Table 4). The presence of AIBN as a reducing agent enabled a 30-300 fold reduction in the amount of catalyst.<sup>69</sup>

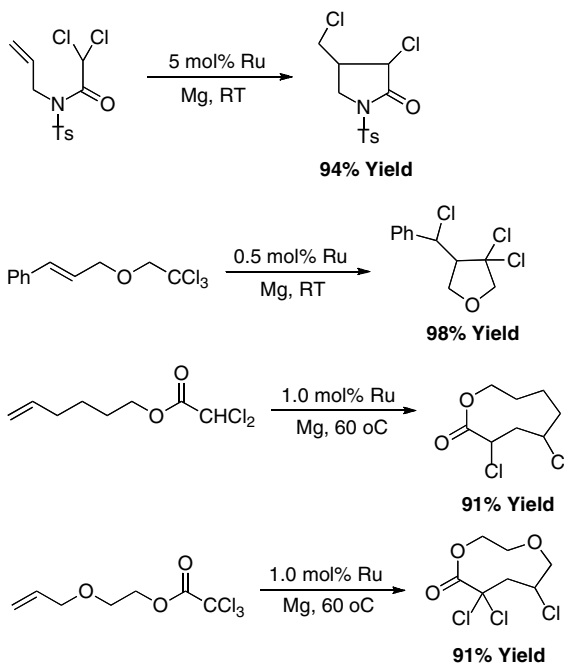
$[\text{Cu}^{\text{II}}(\text{TPMA})\text{Cl}][\text{Cl}]$  complex in the presence of AIBN as a reducing agent has also been shown to be a promising catalytic system for atom transfer radical addition of  $\text{CCl}_4$  to conjugated dienes.<sup>84</sup> In the case of the addition of  $\text{CCl}_4$  to 1,5-hexadiene several products can be obtained, the distribution of which is strongly dependent on reaction conditions (Scheme 8). With one equivalent of  $\text{CCl}_4$ , 10 mol% of AIBN and 0.01 mol% of  $[\text{Cu}^{\text{II}}(\text{TPMA})\text{Cl}][\text{Cl}]$  (all relative to 1,5-hexadiene), monoadduct and diadduct are formed in 85 and 15% yields, respectively. Further increase in the concentration of copper(II) complex affords *5-endo trig* and *6-exo trig* cyclic products. With 1 mol% of copper(II) complex, the yields of *5-endo trig* and *6-exo trig* products were determined to be 40 and 50%, respectively. *7-Endo trig* product was not observed under any reaction conditions. Furthermore, *5-endo trig* and *6-exo trig* products were not formed as a result of cascade reaction, but rather from activation of the of the monoadduct. The formation of five membered ring was quite surprising because *5-endo trig* cyclizations are disfavored according to Baldwin's rules.<sup>85-87</sup> Kinetic and mechanistic investigations of ATRA of polyhalogenated compounds to conjugated dienes in the presence of copper(II) catalysts and reducing agents are subject to further investigation in our laboratories.

Recently, ATRC reactions have also been conducted using  $\text{Cp}^*\text{Ru}^{\text{III}}\text{Cl}_2(\text{PPh}_3)$  complex in conjunction with magnesium as a reducing agent (Scheme 9).<sup>67,68</sup> For most substrates, very high yields of the desired product were obtained using relatively low catalyst concentrations (0.05-1 mol% relative to substrate). In this catalytic system, magnesium acts as a two-electron redox reducing agent, similarly to copper catalyzed ATRA and ATRC reactions in which reducing agents are free radical initiators such as AIBN.



Scheme 8. Observed Products in ATRC of  $\text{CCl}_4$  to 1,5-Hexadiene Catalyzed by  $[\text{Cu}^{\text{II}}(\text{TPMA})\text{Cl}][\text{Cl}]$  in the Presence of AIBN.





*Scheme 9. ATRC reactions catalyzed by  $Cp^*Ru^{III}Cl_2(PPh_3)$  in the presence of magnesium.*

## Conclusions and Future Outlook

In summary, recent advances in the area of catalyst regeneration in copper mediated atom transfer radical addition (ATRA) and cyclization (ATRC) reactions have been reviewed. Both processes utilize reducing agents such as free radical initiators (AIBN) that continuously regenerate the activator (transition metal complex in the lower oxidation state) from the deactivator (transition metal complex in the higher oxidation state). As a result, a significant decrease in the catalyst concentration can be achieved. Recent developments in this area could have profound industrial implications on the synthesis of small organic molecules, natural products and pharmaceutical drugs.

## References

- (1) Gomberg, M. *J. Am. Chem. Soc.* **1900**, *22*, 757-771.
- (2) Kharasch, M. S.; Jensen, E. V.; Urry, W. H. *Science* **1945**, *102*, 128-128.
- (3) Kharasch, M. S.; Jensen, E. V.; Urry, W. H. *J. Am. Chem. Soc.* **1945**, *67*, 1626-1626.
- (4) Giese, B. *Angew. Chem.* **1985**, *97*, 555-567.

- (5) Barton, D. H. R.; Crich, D.; Motherwell, W. B. *J. Chem. Soc. Chem. Comm.* **1983**, 17, 939-941.
- (6) Barton, D. H. R.; McCombie, S. W. *J. Chem. Soc. Perkin Trans. 1* **1975**, 1574-1585.
- (7) Curran, D. P.; Chen, M.-H.; Dooseop, K. *J. Am. Chem. Soc.* **1986**, 108, 2489-2490.
- (8) Stork, G.; Sher, P. M.; Chen, H.-L. *J. Am. Chem. Soc.* **1986**, 108, 6384-6385.
- (9) Hart, D. J. *Science* **1984**, 223, 883-887.
- (10) Curran, D. P.; Pakiewicz, D. M. *Tetrahedron* **1985**, 41, 3943-3958.
- (11) Tietze, L. F. *Chem. Rev.* **1996**, 96, 115-136.
- (12) Tietze, L. F.; Rackelmann, N. *Pure Appl. Chem.* **2004**, 76, 1967-1983.
- (13) Jasperse, C. P.; Curran, D. P.; Fevig, T. L. *Chem. Rev.* **1991**, 91, 1237-1286.
- (14) Koert, U. *Angew. Chem. Int. Ed. Eng.* **1996**, 35, 405-407.
- (15) Aldabbagh, F.; Bowman, W. R. *Contemp. Org. Synth.* **1997**, 261-280.
- (16) Renaud, P.; Sibi, M. P. *Radicals in Organic Synthesis*; Wiley-VCH: Weinheim, 2001; Vol. 2.
- (17) Curran, D. P. *Comprehensive Organic Synthesis*; Pergamon: New York, 1992.
- (18) Iqbal, J.; Bhatia, B.; Nayyar, N. K. *Chem. Rev.* **1994**, 94, 519-564.
- (19) Gossage, R. A.; Van De Kuil, L. A.; Van Koten, G. *Acc. Chem. Res.* **1998**, 31, 423-431.
- (20) Severin, K. *Curr. Org. Chem.* **2006**, 10, 217-224.
- (21) Clark, A. J. *Chem. Soc. Rev.* **2002**, 31, 1-11.
- (22) Curran, D. P. *Synthesis* **1988**, 6, 417-439.
- (23) Curran, D. P. *Synthesis* **1988**, 7, 489-513.
- (24) Nagashima, H. In *Ruthenium in Organic Synthesis*; Murahashi, S.-I., Ed.; Wiley-VCH: Weinheim, 2004, p 333-343.
- (25) Delaude, L.; Demonceau, A.; Noels, A. F. In *Topics in Organometallic Chemistry*; Bruneau, C., Dixneuf, P. H., Eds.; Springer: Berlin, 2004; Vol. 11, p 155-171.
- (26) Minisci, F. *Acc. Chem. Res.* **1975**, 8, 165-171.
- (27) Asscher, M.; Vofsi, D. *J. Chem. Soc.* **1961**, 2261-2264.
- (28) Nagashima, H.; Seki, K.; Ozaki, N.; Wakamatsku, H.; Itoh, K.; Tomo, Y.; Tsuyi, J. *J. Org. Chem.* **1990**, 55, 985-990.
- (29) De Campo, F.; Lastecoueres, D.; Verlhac, J.-B. *J. Chem. Soc., Perkin Trans. 1* **2000**, 575-580.
- (30) Yang, D.; Yan, Y.-L.; Zheng, B.-F.; Gao, Q.; Zhu, N.-Y. *Org. Lett.* **2006**, 8, 5757-5760.
- (31) Clark, A. J.; Filik, R. P.; Haddleton, D. M.; Radigue, A. P.; J., S. C.; Thomas, G. H.; E., S. M. *J. Org. Chem.* **1999**, 64, 8954-8957.
- (32) De Campo, F.; Lastecoueres, D.; Vincent, J.-M.; Verlhac, J.-B. *J. Org. Chem.* **1999**, 64, 4969.
- (33) Wang, J.-S.; Matyjaszewski, K. *J. Am. Chem. Soc.* **1995**, 117, 5614-5615.
- (34) Tsarevsky, N. V.; Braunecker, W. A.; Tang, W.; Brook, S. J.; Matyjaszewski, K.; Weismann, G. R. *J. Mol. Catal. A: Chem* **2006**, 257, 132-140.
- (35) Pintauer, T.; Matyjaszewski, K. *Coord. Chem. Rev.* **2005**, 249, 1155-1184.

- (36) Matyjaszewski, K.; Gnanou, Y.; Leibler, L. *Macromolecular Engineering-Precise Synthesis, Materials Properties, Applications*; Willey-VCH: Weinheim, 2007.
- (37) Matyjaszewski, K.; Gobelt, B.; Paik, H.-j.; Horwitz, C. P. *Macromolecules* **2001**, *34*, 430-440.
- (38) Matyjaszewski, K.; Paik, H.-j.; Zhou, P.; Diamanti, S. J. *Macromolecules* **2001**, *34*, 5125-5131.
- (39) Matyjaszewski, K.; Xia, J. *Chem. Rev.* **2001**, *101*, 2921-2990.
- (40) Lin, C. Y.; Coote, M. L.; Gennaro, A.; Matyjaszewski, K. *J. Am. Chem. Soc.* **2008**, *130*, 12762-12774.
- (41) Tang, W.; Kwak, Y.; Braunecker, W.; Tsarevsky, N. V.; Coote, M. L.; Matyjaszewski, K. *J. Am. Chem. Soc.* **2008**, *130*, 10702-10713.
- (42) Pintauer, T.; McKenzie, B.; Matyjaszewski, K. *ACS Symp. Ser.* **2003**, *854*, 130-147.
- (43) Matyjaszewski, K.; Nanda, A. K.; Tang, W. *Macromolecules* **2005**, *38*, 2015-2018.
- (44) Tang, W.; Matyjaszewski, K. *Macromolecules* **2006**, *39*, 4953-4959.
- (45) Tang, W.; Matyjaszewski, K. *Macromolecules* **2007**, *40*, 1858-1863.
- (46) Tang, W.; Tsarevsky, N. V.; Matyjaszewski, K. *J. Am. Chem. Soc.* **2006**, *128*, 1598-1604.
- (47) Qiu, J.; Matyjaszewski, K.; Thounin, L.; Amatore, C. *Macromol. Chem. Phys.* **2000**, *201*, 1625-1631.
- (48) Xia, J.; Gaynor, S. G.; Matyjaszewski, K. *Macromolecules* **1998**, *31*, 5958-5959.
- (49) Xia, J.; Zhang, X.; Matyjaszewski, K. *ACS Symposium Series* **2000**, *760*, 207-223.
- (50) Eckenhoff, W. T.; Garrity, S. T.; Pintauer, T. *Eur. J. Inorg. Chem.* **2008**, 563-571.
- (51) Eckenhoff, W. T.; Pintauer, T. *Inorg. Chem.* **2007**, *46*, 5844-5846.
- (52) Eckenhoff, W. T.; Pintauer, T. *Polym. Prepr. (Am. Chem. Soc. Div. Polym. Chem.)* **2008**, *49(2)*, 282-283.
- (53) Konak, C.; Ganchev, B.; Teodorescu, M.; Matyjaszewski, K.; Kopeckova, P.; Kopecek, J. *Polymer* **2002**, *43*, 3735-3741.
- (54) Tang, H.; Arulsamy, N.; Radosz, M.; Shen, Y.; Tsarevsky, N. V.; Braunecker, W. A.; Tang, W.; Matyjaszewski, K. *J. Am. Chem. Soc.* **2006**, *128*, 16277-16285.
- (55) Matyjaszewski, K.; Jakubowski, W.; Min, K.; Tang, W.; Huang, J.; Braunecker, W. A.; Tsarevsky, N. V. *Proc. Natl. Acad. Sci. U.S.A.* **2006**, *103*, 15309-15314.
- (56) Pintauer, T.; Matyjaszewski, K. *Chem. Soc. Rev.* **2008**, *37*, 1087-1097.
- (57) Jakubowski, W.; Matyjaszewski, K. *Angew. Chem. Int. Ed.* **2006**, *45*, 4482-4486.
- (58) Jakubowski, W.; Min, K.; Matyjaszewski, K. *Macromolecules* **2006**, *39*, 39-45.
- (59) Min, K.; Gao, H.; Matyjaszewski, K. *Macromolecules* **2007**, *40*, 1789-1791.
- (60) Quebatte, L.; Thommes, K.; Severin, K. *J. Am. Chem. Soc.* **2006**, *128*, 7440-7441.
- (61) Blackman, A. G. *Eur. J. Inorg. Chem.* **2008**, 2633-2647.

- (62) Diaz-Alvarez, A. E.; Crochet, P.; Zablocka, M.; Duhayon, C.; Cadierno, V.; Majoral, J. P. *Eur. J. Inorg. Chem.* **2008**, 786-794.
- (63) Iizuka, Y.; Li, Z. M.; Satoh, K.; Karnigaito, M.; Okamoto, Y.; Ito, J.; Nishiyama, H. *Eur. J. Org. Chem.* **2007**, 782-791.
- (64) Lundgren, R. J.; Rankin, M. A.; McDonald, R.; Stradiotto, M. *Organometallics* **2008**, *27*, 254-258.
- (65) Maiti, D.; Sarjeant, A. A. N.; Itoh, S.; Karlin, K. D. *J. Am. Chem. Soc.* **2008**, *130*, 5644-5645.
- (66) Oe, Y.; Uozumi, Y. *Adv. Synth. Catal.* **2008**, *350*, 1771-1775.
- (67) Thommes, K.; Icli, B.; Scopelliti, R.; Severin, K. *Chem. Eur. J.* **2007**, *13*, 6899-6907.
- (68) Wolf, J.; Thommes, K.; Brie, O.; Scopelliti, R.; Severin, K. *Organometallics* **2008**, *27*, 4464-4474.
- (69) Clark, A. J.; Wilson, P. *Tetrahedron Lett.* **2008**, *49*, 4848-4850.
- (70) Xia, J.; Gaynor, S. G.; Matyjaszewski, K. *Macromolecules* **1998**, *31*, 5958-5959.
- (71) Xia, J.; Matyjaszewski, K. *Macromolecules* **1999**, *32*, 2434-2437.
- (72) Quebatte, L.; Haas, M.; Solari, E.; Scopelliti, R.; Nguyen, Q. T.; Severin, K. *Angew. Chem., Int. Ed.* **2004**, *43*, 1520-1524.
- (73) Quebatte, L.; Haas, M.; Solari, E.; Scopelliti, R.; Nguyen, Q. T.; Severin, K. *Angew. Chem., Int. Ed.* **2005**, *44*, 1084-1088.
- (74) Quebatte, L.; Solari, E.; Scopelliti, R.; Severin, K. *Organometallics* **2005**, *24*, 1404-1406.
- (75) Eckenhoff, W. T.; Manor, B. C.; Pintauer, T. *Polym. Prepr. (Am. Chem. Soc. Div. Polym. Chem.)* **2008**, *49(2)*, 213-214.
- (76) Pintauer, T. *Polym. Prepr. (Am. Chem. Soc. Div. Polym. Chem.)* **2008**, *49(2)*, 12-13.
- (77) Balili, M. N.; Pintauer, T. *Polym. Prepr. (Am. Chem. Soc., Div. Polym. Chem.)* **2008**, *49(2)*, 161-162.
- (78) Brandrup, J.; Immergut, E. H.; Gulke, E. A. *Polymer Handbook*; Wiley-Interscience: New York, 1999.
- (79) Eastmond, G. C. In *Comprehensive Chemical Kinetics*; Bamford, C. H., Tipper, C. F. H., Eds.; American Elsevier: New York, 1976; Vol. 14A.
- (80) Fischer, H. *J. Am. Chem. Soc.* **1986**, *108*, 3925-3927.
- (81) Fischer, H. *J. Polym. Sci. Part A: Polym. Chem.* **1999**, *37*, 1885-1901.
- (82) Fischer, H. *Chem. Rev.* **2001**, *101*, 3581-3610.
- (83) Goto, A.; Fukuda, T. *Prog. Polym. Sci.* **2004**, *29*, 329-385.
- (84) Ricardo, C. L.; Pintauer, T. *Polym. Prepr. (Am. Chem. Soc. Div. Polym. Chem.)* **2008**, *49(2)*, 14-15.
- (85) Baldwin, J. E. *J. Chem. Soc., Chem. Comm.* **1976**, 734-736.
- (86) Baldwin, J. E. *J. Chem. Soc., Chem. Comm.* **1976**, 738-741.
- (87) Baldwin, J. E.; Cutting, J.; Dupont, W.; Kruse, L.; Silberman, L.; Thomas, R. C. *J. Chem. Soc., Chem. Comm.* **1976**.

## Chapter 6

# The Atom Transfer Radical Polymerization Equilibrium: Structural and Medium Effects

Nicolay V. Tsarevsky, Wade A. Braunecker, Wei Tang, and  
Krzysztof Matyjaszewski

Department of Chemistry, Carnegie Mellon University, 4400 Fifth Avenue,  
Pittsburgh, Pennsylvania 15213

The atom transfer radical equilibrium constant can be formally presented as the product of the equilibrium constant of C-X (X = Br, Cl) bond homolysis of the alkyl halide initiator and the catalyst halogenophilicity, which is the equilibrium constant of formation of Cu<sup>II</sup>-X bond from the corresponding Cu<sup>I</sup> complex and halogen atom. The latter can be further presented as the product of the equilibrium constants of halogen atom electron affinity, reduction of Cu<sup>II</sup>, and the formation constant (halidophilicity) of Cu<sup>II</sup> halide complex from the corresponding Cu<sup>II</sup> complex and a halide anion. This work illustrates how each of the equilibrium constants contributing to the overall ATRP equilibrium depends upon the nature of initiator, transferable halogen, ligand, and solvent. Such an understanding is important in the rational design and selection of catalysts for various monomer-solvent reaction systems.

### Introduction

The development of controlled radical polymerization (CRP) methods,(1,2) including atom transfer radical polymerization (ATRP),(3-6) nitroxide-mediated radical polymerization,(7) and reversible addition fragmentation chain transfer polymerization,(8,9) has led to the synthesis of an unprecedented number of novel, previously inaccessible polymeric materials. Well-defined polymers, i.e., polymers with predetermined molecular weight, narrow molecular weight distribution, and high degree of chain end functionalization, prepared by

controlled radical polymerization include segmented (block) and gradient copolymers,(10) and functionalized polymeric materials with various molecular architectures. In order to expand the range of reaction media, and monomers that can be successfully polymerized by ATRP, and to identify active catalysts that mediate well-controlled polymerization, preferably at low concentration, a deep understanding of the factors determining the catalyst performance is necessary.(11) This chapter describes the ATRP reaction from a thermodynamic point of view and provides insight on how the ATRP equilibrium can be tuned by proper selection of catalysts, initiators, and solvents. The kinetics of ATRP is equally important and has been dealt with in detail in other publications.(12)

## Thermodynamic Components of the ATRP Equilibrium

ATRP is the most versatile CRP technique and has already attracted considerable interest from industry.(13) It relies on establishing an equilibrium between an alkyl halide initiator (RX, X = Br, Cl) and a low oxidation state metal complex, generating a radical and a higher oxidation state complex with a coordinated halide ion. The atom transfer equilibrium is presented schematically on the left hand side of Figure 1.(14) The ATRP equilibrium constant, which is the ratio of the rate constants of RX activation and of radical deactivation, can be formally presented as a product of several contributing equilibrium constants shown in Figure 1 and eq. 1.

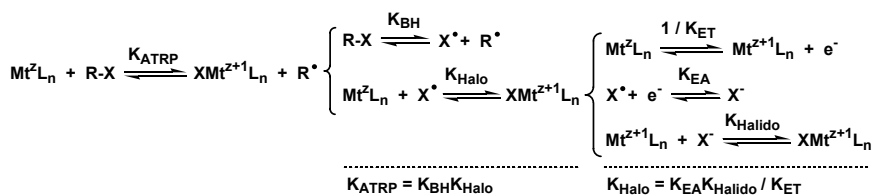


Figure 1. Atom transfer as a formal combination of a C-X bond homolysis of alkyl halide (RX), two redox processes, and coordination of a halide anion to a higher oxidation state ( $\text{M}^{\text{I}+\text{I}}$ ) complex. L represents a ligand.

$$K_{\text{ATRP}} \equiv \frac{k_{\text{act}}}{k_{\text{deact}}} = K_{\text{BH}}K_{\text{Halo}} = \frac{K_{\text{BH}}K_{\text{EA}}K_{\text{Halido}}}{K_{\text{ET}}} \quad (1)$$

The simplest way to formally “split”  $K_{\text{ATRP}}$  is to present it as the product of equilibrium constants of bond homolysis of the C-X bond ( $K_{\text{BH}}$ ), which is catalyst independent but depends on the nature of the propagating species ( $\text{R}^{\bullet}$ ) and transferable atom X, and the catalyst-related equilibrium constant of *halogenophilicity* ( $K_{\text{Halo}}$ ).  $K_{\text{Halo}}$  can further be broken down (Figure 1) and presented as the product of the formation constant  $K_{\text{Halido}}$  and two other equilibrium constants describing redox processes – the equilibrium constant of electron affinity of the halogen atom ( $K_{\text{EA}}$ ) and the equilibrium constant of electron transfer to and from the central metal atom ( $K_{\text{ET}}$ ), which characterizes

the ease with which the higher oxidation state metal complex  $Mt^{z+1}L_n$  (not the deactivator  $XMt^{z+1}L_n$ ) can be reduced. It is important to note the difference between the equilibrium constants termed *halogenophilicity* ( $K_{Halo}$ ) and *halidophilicity* ( $K_{Halido}$ ). The former defines the equilibrium between the higher oxidation state halide complex (deactivator) and the lower oxidation state complex (activator) plus a halogen atom and is therefore related to formation and homolytic cleavage of the  $Mt^{z+1}-X$  bond. The latter quantifies the affinity of the higher oxidation state complex  $Mt^{z+1}L_n$  to halide anions  $X^-$  to form the ATRP deactivator  $XMt^{z+1}L_n$  and is therefore a stability, complexation, constant. In other words,  $K_{Halo}$  is reciprocal to the  $Mt^{z+1}-X$  bond dissociation energy and unlike  $K_{Halido}$  is associated with a change in the oxidation state of the central metal atom. In some previous publications, these terms were not defined precisely, and one should be aware of the differences between the two equilibrium constants, halogeno- and halidophilicity.

In the following text, the central atom of the ATRP catalyst will be copper, which has been most extensively studied. Both the ATRP rate (eq. 2) and control over polymerization (related to the width of the molecular weight distribution, eq. 3) are catalyst-dependent and it is crucial to correlate the structure of the catalyst with its activity and performance. This should ultimately make possible the rational design of highly active catalysts that can be used at low concentration to mediate the controlled polymerization of various monomers in diverse reaction media.

$$R_p = k_p K_{ATRP} \frac{[RX][Cu^I L_n]}{[XCu^{II} L_n]} [M] \quad (2)$$

$$PDI = \frac{M_w}{M_n} = 1 + \frac{1}{DP_n} + \left( \frac{k_p [RX]_0}{k_{deact} [XCu^{II} L_n]} \right) \left( \frac{2}{conv} - 1 \right) \quad (3)$$

### Effect of the structure of propagating radicals on $K_{ATRP}$

The free energies of C-X bond homolysis for various alkyl halides have been calculated using DFT (15) and, more recently, high-level ab initio molecular orbital calculations, both in the gas phase and in solvents such as MeCN and DMF.(16) From these data, the equilibrium constants  $K_{BH}$  can be calculated as well as the relative values of  $K_{ATRP}$  for reactions where the catalyst is not changed. Knowing the propagation rate constants for monomers,(15,17) the relative rates of propagation become accessible (eq. 2). Figure 2 shows some calculated values for 5 alkyl bromides that resemble structurally the dormant chain ends in the ATRP of methyl acrylate (MA), methyl methacrylate (MMA), acrylonitrile (AN), styrene (Sty), and vinyl acetate (VAc). From the data in the figure, it can be concluded that if certain conversion of MA could be reached within 1 hour in an ATRP reaction mediated by a given catalyst, 5 hours would be required to reach the same conversion in the ATRP of MMA, only 19 seconds would be sufficient in the case of AN (although the control could be very poor for such a fast reaction), 50 hours for Sty, and as long as 94,000 hours

(about 11 years) for VAc. From these calculations it can be easily understood why no “universal” catalyst exists that can mediate the conventional ATRP of every monomer. It is therefore very important to understand the factors that determine catalytic activity in ATRP.

<b>Polymeric dormant state</b>					
<b>Model alkyl bromide</b>					
$\Delta G_{BH,298}$ [kcal mol <sup>-1</sup> ]	52.59	51.61	48.20	52.50	58.69
$K_{BH,298}$ [mol <sup>-1</sup> ]	$2.52 \times 10^{-39}$	$1.32 \times 10^{-38}$	$4.20 \times 10^{-36}$	$2.93 \times 10^{-39}$	$8.40 \times 10^{-44}$
$K_{ATRP,rel}$	1	5.2	$1.67 \times 10^3$	1.2	$3.33 \times 10^{-5}$
$k_p$ (90 °C) [M <sup>-1</sup> s <sup>-1</sup> ]	$4.7 \times 10^4$	$1.6 \times 10^3$	$5.4 \times 10^3$	844	$1.5 \times 10^4$
$R_{p,rel}$ (90 °C)	1	0.2	191.9	0.02	$1.06 \times 10^{-5}$
$t_{rel}$ [h]	1	5	0.0052	50	$9.4 \times 10^4$

Figure 2. Relative activities of alkyl bromide initiators in ATRP mediated by the same catalyst. The values for  $\Delta G_{BH,298}$  and  $K_{ATRP}$  are for MeCN as the solvent.

### Effect of the Transferable Halogen Atom on $K_{ATRP}$

Some comparisons between the values of  $K_{ATRP}$  for alkyl bromides and chlorides reacting with the same Cu-based catalyst in the same solvent (MeCN) are presented in Table 1. The alkyl bromides are characterized by larger values of the equilibrium constant than the corresponding alkyl chlorides. This is related to the higher bond dissociation energy or lower  $K_{BH}$  of the C-Cl bond (Figure 1 and eq. 1). However, C-Cl bonds are stronger than C-Br bonds by ca. 12-15 kcal mol<sup>-1</sup> and if the bond dissociation energy was the only factor determining the values of  $K_{ATRP}$ , those for alkyl bromides should be about 10 orders of magnitude larger than for the chlorides. According to Table I, the difference is less than one order of magnitude.  $K_{ATRP}$  is the ratio of the dissociation energies of the C-X and Cu<sup>II</sup>-X bonds (as mentioned above,  $K_{Halo} = 1 / K_{BH}(Cu^{II}-X)$ ). The lower than expected difference between  $K_{ATRP}(RCl)$  and  $K_{ATRP}(RBr)$ , based solely on the stability of C-X bonds, can also be attributed to the greater stability of the Cu<sup>II</sup>-Cl compared to Cu<sup>II</sup>-Br bond (higher chloro- than bromophilicity).<sup>(15)</sup> On the other hand, chlorine has a higher electron affinity compared to bromine (i.e., larger  $K_{EA}(Cl)$  in Figure 1 and eq. 1).<sup>(18-20)</sup>



**Table I.  $K_{ATRP}$  for several alkyl bromides and chlorides in a reaction with various  $Cu^I X$  ( $X = Br, Cl$ ) / TPMA catalysts in MeCN at  $22 \pm 2$  °C.**

<i>Initiator</i> <sup>a</sup>	$K_{ATRP}$ <sup>b</sup>	<i>Ref.</i>
1-PhEtBr	$4.58 \times 10^{-6}$	21
1-PhEtCl	$8.60 \times 10^{-7}$ (5.3)	21
MeBrPr	$3.25 \times 10^{-7}$	21
MeClPr	$4.1 \times 10^{-8}$ (7.9)	21
Allyl-Br	$1.72 \times 10^{-5}$	22
Allyl-Cl	$2.34 \times 10^{-6}$ (7.4)	22

<sup>a</sup> 1-PhEtX = 1-phenylethyl halide, MeXPr = methyl 2-halopropionate; <sup>b</sup> The value in parentheses is the ratio of  $K_{ATRP}$  of the alkyl bromide to its chloride analogue.

There is no available data for chlorophilicity and bromophilicity of  $Cu^I$  complexes but they can be calculated using eq. 1 and the data in Table I in conjunction with values of  $K_{BH}$  for alkyl halides. For instance,  $K_{BH}(MeBrPr) = 2.52 \times 10^{-39}$  M in MeCN (16) and using the value of  $K_{ATRP} = 3.25 \times 10^{-7}$  for a reaction catalyzed by the  $Cu^I Br$  complex of TPMA, (21) a value of  $K_{Bromo} = 1.3 \times 10^{32}$  M<sup>-1</sup> is obtained for the  $Cu^I$  / TPMA complex. Analogously, the chlorophilicity of the same complex is calculated from  $K_{BH}(MeClPr) = 2.1 \times 10^{-49}$  M (16) and  $K_{ATRP} = 4.1 \times 10^{-8}$  as  $K_{Chloro} = 2.0 \times 10^{41}$  M<sup>-1</sup>. The ratio of the chloro- to bromophilicity of  $Cu^I$  / TPMA is therefore  $1.5 \times 10^9$ . Again, this ratio compensates partially the higher bond dissociation energy of the C-Cl bond compared to C-Br leading to lower than expected ratio  $K_{ATRP}(RBr) / K_{ATRP}(RCl)$ .

Another component of the ATRP equilibrium constant, the halidophilicity, also depends upon the nature of the transferable atom (and the ligand). In systems where the halidophilicity is low, the  $XCu^II L_n$  complex can easily dissociate to halide ions and  $Cu^II L_n$  which cannot deactivate radicals, and the dissociative loss of deactivator ultimately leads to fast reactions (eq. 2) that are poorly controlled (eq. 3). It has been shown that halidophilicity is low in protic media, and it decreases significantly in mixed organic-aqueous solvents as the amount of water is increased.(23,24) The amount of deactivator present in the reaction system depends on the halidophilicity and on the total concentrations of  $Cu^II$  species and halide ions, according to eq. 4. Therefore, to minimize the dissociation of deactivator in systems where the halidophilicity is low, extra  $Cu^II$  complex and / or halide salts should be added. This has been shown to improve the polymerization control.(23,25,26) Halidophilicity is discussed in more detail in the following sections.

$$[XCu^II L_n] = \frac{F - \sqrt{F^2 - 4K_{Halido}^2 [Cu^II L_n]_{tot} [X^-]_{tot}}}{2K_{Halido}} \quad (4)$$

$$(F = 1 + K_{Halido} [Cu^II L_n]_{tot} + K_{Halido} [X^-]_{tot})$$

## Ligand Effect on the Activity of Cu-Based ATRP Catalysts

The values of  $K_{\text{ATRP}}$  for numerous alkyl halide – copper catalyst combinations have been determined (21,27) using modified kinetic equations describing the accumulation of the deactivator  $\text{XCu}^{\text{II}}\text{L}_n$  due to the persistent radical effect.(28) Figure 3 shows that the values of  $K_{\text{ATRP}}$  for the same alkyl halide (ethyl 2-bromoisobutyrate, EtBriB, which mimics the dormant chains of a polymethacrylate) vary by more than seven orders of magnitude as the N-based ligand is changed. Since the solvent and the alkyl halide used in all measurements were the same, the values of  $K_{\text{BH}}$  and  $K_{\text{EA}}$  (eq. 1) were constant and the variations in  $K_{\text{ATRP}}$  were caused by differences in the electron transfer equilibrium constant and the halidophilicity of the  $\text{Cu}^{\text{II}}$  complexes.

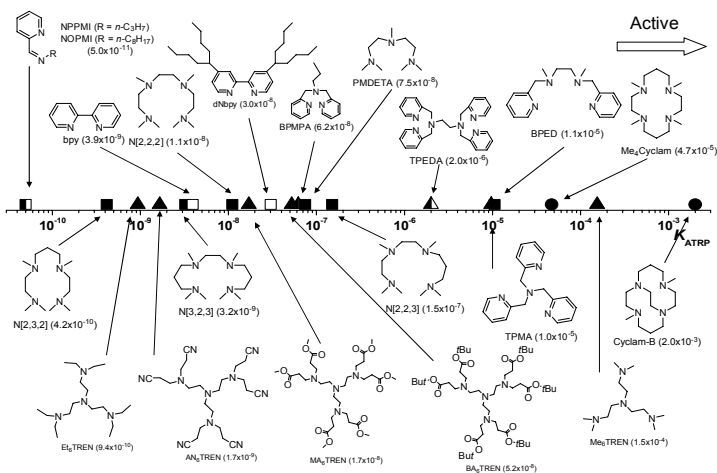


Figure 3.  $K_{\text{ATRP}}$  for the reaction of EtBriB with Cu complexes derived from various N-based ligands. Reactions were carried out in MeCN at  $22 \pm 2^\circ\text{C}$ . (Reprinted from ref. 27. Copyright ACS)

The activity of the ATRP catalyst is directly related to its reducing power, i.e., to the value of  $1 / K_{\text{ET}}$  or the redox potential of the couple  $\text{Cu}^{\text{II}}\text{L}_n / \text{Cu}^{\text{I}}\text{L}_n$ . The redox potential of the  $\text{Cu}^{\text{II}}\text{L}_n / \text{Cu}^{\text{I}}\text{L}_n$  couple is determined by the relative stabilization of the  $\text{Cu}^{\text{II}}$  vs. the  $\text{Cu}^{\text{I}}$  state by the ligand L. For ligands forming 1:1 complexes with copper ions,  $1 / K_{\text{ET}}$  is directly related to the ratio of the stability constants of the complexes in the two oxidation states ( $\beta^{\text{II}} / \beta^{\text{I}}$ ).<sup>(6,11,29)</sup>

$$E = E^0 + \frac{RT}{F} \left( \ln \frac{[\text{Cu}^{\text{II}}]_{\text{tot}}}{[\text{Cu}^{\text{I}}]_{\text{tot}}} - \ln \frac{1 + \beta^{\text{II}}[\text{L}]}{1 + \beta^{\text{I}}[\text{L}]} \right) \approx E^0 + \frac{RT}{F} \left( \ln \frac{[\text{Cu}^{\text{II}}]_{\text{tot}}}{[\text{Cu}^{\text{I}}]_{\text{tot}}} - \ln \frac{\beta^{\text{II}}}{\beta^{\text{I}}} \right) \quad (5)$$

In a detailed study,  $\text{Cu}^{\text{I}}\text{Cl}$  and  $\text{Cu}^{\text{I}}\text{Br}$  complexes of bpy, dNbpy, BPMPA, BPMODA, TPMA, PMDETA, and  $\text{Me}_6\text{TREN}$  were all characterized by cyclic voltammetry (CV) and the measured redox potentials were correlated with the activity of the complexes in the ATRP of MA initiated by ethyl 2-

bromopropionate.(30) The values of either  $k_{\text{act}}$  or  $K_{\text{ATRP}}$  and the redox potential of a series of copper complexes with tridentate N-based ligands (where the nitrogen atom was amine-, imine-, or pyridine-type) were well-correlated.(31) It should be noted that in order to predict the catalytic activity of a Cu complex in ATRP, the redox potential of the complex in the presence of halide ions should be determined, and not the potential of the catalyst with a non-coordinating counterion. The halidophilicity of the  $\text{Cu}^{\text{II}}\text{L}_n$  complex also contributes to the overall value of  $K_{\text{ATRP}}$  (eq. 1). Table II shows that an excellent correlation exists between the redox potentials (determined by CV) of Cu halides complexed with various N-based ligands and the value of  $K_{\text{ATRP}}$ . When the redox potentials of the corresponding trifluoromethanesulfonate complexes were determined and plotted against  $K_{\text{ATRP}}$ , the correlation was significantly poorer. The reason is that the value of the redox potential of the halide complexes is determined by both the value of  $K_{\text{ET}}$  and the relative halidophilicity of  $\text{Cu}^{\text{II}}\text{L}_n$  and  $\text{Cu}^{\text{I}}\text{L}_n$ . Since the values of  $K_{\text{Halido}}$  change as the N-based ligand is varied, deviations from linearity are observed in a plot of  $K_{\text{ATRP}}$  vs. the redox potential of trifluoromethanesulfonate complexes. When the differences in  $E_{1/2}$  of the  $\text{Cu}^{\text{II}}\text{Br}_2$  and  $\text{Cu}^{\text{II}}(\text{OTf})_2$  ( $\text{Tf} = -\text{SO}_2\text{CF}_3$ ) analogues are compared, the relative halidophilicity of  $\text{Cu}^{\text{II}}$  complexes can be estimated (assuming negligible halidophilicity of the  $\text{Cu}^{\text{I}}$  complexes). For example, for  $\text{Me}_6\text{TREN}$  and  $\text{bpy}$ , the differences are 230 and 160, respectively. Thus, the relative halidophilicities of the corresponding  $\text{Cu}^{\text{II}}$  complexes differ by approximately  $10^{3.9}$  and  $10^{2.7}$ . Using Table II and measuring the redox potential of a given  $\text{Cu}^{\text{II}}\text{X}_2$  complex, a reliable prediction can be made about its ATRP catalytic activity.

**Table II. Values of  $K_{\text{ATRP}}$  for the reaction of EtBr<sup>I</sup>B with  $\text{Cu}^{\text{I}}\text{Br}$  complexes of various ligands (L), and  $E_{1/2}$  for  $\text{Cu}^{\text{II}}\text{Br}_2$  and  $\text{Cu}^{\text{II}}(\text{OTf})_2$  complexes with the ligands in MeCN.(27)**

Ligand	$K_{\text{ATRP}}$	$E_{1/2}(\text{Cu}^{\text{II}}\text{Br}_2 / \text{L}) [V]$	$E_{1/2}(\text{Cu}^{\text{II}}(\text{OTf})_2 / \text{L}) [V]^a$
bpy	$3.9 \times 10^{-9}$	0.02	0.18
HMTETA	$1.1 \times 10^{-8}$	-0.02	0.10
PMDETA	$7.5 \times 10^{-8}$	-0.08	-0.04
TPMA	$9.6 \times 10^{-6}$	-0.24	0.02
$\text{Me}_6\text{TREN}$	$1.5 \times 10^{-4}$	-0.30	-0.07

<sup>a</sup> Unpublished data.

In order to check whether or not the assumption of low halidophilicity of the  $\text{Cu}^{\text{I}}$  complexes is correct, the halidophilicity of the  $\text{Cu}^{\text{II}}$  complexes can be calculated directly from eq. 1, provided that  $K_{\text{ATRP}}$ ,  $K_{\text{BH}}$ ,  $K_{\text{ET}}$ , and  $K_{\text{EA}}$  are known. For instance, the halidophilicity of the complex  $\text{Cu}^{\text{II}}(\text{bpy})_2^{2+}$  in MeCN can be estimated from a known value of  $K_{\text{ATRP}}$  for the reaction of  $\text{Cu}^{\text{I}}(\text{bpy})_2\text{Br}$  with 1-PhEtBr in MeCN ( $K_{\text{ATRP}} = 8.5 \times 10^{-10}$ ),(32) and  $K_{\text{BH}}$  for the same alkyl bromide ( $2.93 \times 10^{-39}$ ).(16) The value of  $K_{\text{EA}}$  for the bromine atom in MeCN can be calculated from the value of the redox potential for the couple  $\text{Br}^\bullet / \text{Br}^-$  in water (1.95 V vs. SHE) (33) and the Gibbs energy of transfer of  $\text{Br}^-$  from water

to MeCN ( $\Delta_{tr}G^0_{(Br^-,W \rightarrow MeCN)} = 31.3 \text{ kJ mol}^{-1}$ ) (34) according to eq. (6) as  $K_{EA,MeCN}(Br^\bullet) = 3.16 \times 10^{27}$ .

$$\begin{aligned} \ln K_{EA,MeCN}(Br^\bullet) &= -\frac{\Delta G^0_{(EA,MeCN)}}{RT} = -\frac{\Delta G^0_{(EA,W)} + \Delta_{tr}G^0_{(Br^-,W \rightarrow MeCN)}}{RT} = \\ &= \frac{FE^0_{X^+/X^-} - \Delta_{tr}G^0_{(Br^-,W \rightarrow MeCN)}}{RT} \end{aligned} \quad (6)$$

In a similar fashion to the way  $K_{EA}$  was calculated in MeCN vs. SHE,  $K_{ET}$  for the Cu catalyst can be calculated by measuring its redox potential ( $E_{1/2}$ ) vs. a reference electrode (0.01 M  $Ag^+/Ag$ ) in MeCN and calibrating this value vs. SHE knowing the free energy of transfer of  $Ag^+$  from water to MeCN ( $\Delta_{tr}G^0_{(Ag^+,W \rightarrow MeCN)} = -24.1 \text{ kJ mol}^{-1}$ ). (34) Finally, from a known redox potential of the  $Cu^{II}(bpy)_2^{2+} / Cu^I(bpy)_2^{2+}$  couple in MeCN, the value of  $K_{ET}$  can be calculated from eq. 7 as  $K_{ET} = 3.98 \times 10^4$ .

$$\begin{aligned} \ln K_{ET,MeCN} &= -\frac{\Delta G^0_{(ET,MeCN)}}{RT} = \\ &= \frac{FE^0_{Cu^{II}(bpy)_2^{2+}/Cu^I(bpy)_2^{2+}} - \Delta G_{(Ref,W)} + \Delta_{tr}G^0_{(Ag^+,W \rightarrow MeCN)}}{RT} \end{aligned} \quad (7)$$

Consequently, the bromidophilicity of  $Cu^{II}(bpy)_2^{2+}$  in MeCN is estimated as  $K_{Bromido} = 3.2 \times 10^6 \text{ M}^{-1}$ . It should be noted that the errors in the values of  $K_{BH}$  are of the order of about  $2 \text{ kcal mol}^{-1}$ , leading to uncertainty in the equilibrium constant by 1-2 orders of magnitude. In other words, the bromidophilicity of  $Cu^{II}(bpy)_2^{2+}$  can be estimated as  $10^4 - 10^8 \text{ M}^{-1}$ . On the other hand, halidophilicity of the  $Cu^{II}(bpy)_2^{2+}$  has been determined by means of electronic spectroscopy in various mixtures of MeCN and water. (24) From the published data, by extrapolation to zero water concentration, the bromidophilicity can be estimated as  $10^5 \text{ M}^{-1}$ , which is well within the estimated interval of  $10^4 - 10^8 \text{ M}^{-1}$ .

## Rational Selection of the ATRP catalyst

An “ideal” ATRP catalyst should be very stable and active (and if these requirements are met, it can be used at low concentration), but should also be an efficient deactivator (characterized by high  $k_{deact}$ ) to provide good polymerization control (eq. 4). Such catalysts are suitable for ARGET (35) and ICAR (36) ATRP, which are mediated by very low (ppm) amounts of Cu complexes. (Both techniques utilize reducing agents, which throughout the polymerization convert the deactivator accumulated in the system due to the persistent radical effect back to activator.) Figure 4 shows a “map” for catalyst selection, in which  $K_{ATRP}$  for various complexes is plotted against  $k_{deact}$ . The ligands are divided into four groups. Ligands in the lower right section of the map are typical ligands used in ATRP which give moderately fast polymerization with fairly large  $K_{ATRP}$  values (with the exception of the NPPMI complex) and also good control due to sufficiently large  $k_{deact}$  values. Most

“traditional” ATRP ligands belong to this group, such as bpy, dNbpy, PMDETA and HMTETA. The ligands in the upper right area are a new generation ligands which afford both fast polymerization (large  $K_{\text{ATRP}}$ ) and good control. These ligands were successfully used in new ATRP systems such as ICAR and ARGENT ATRP. Ligands in the lower left part of the map can form catalysts that mediate relatively slow polymerizations and do not provide good control. These are inefficient ligands for ATRP, therefore only a few of them are included in this report, such as N4[3,2,3] and N[2,3,2]. Although ligands in the top left area (e.g., Me<sub>4</sub>Cyclam) can form catalysts that afford very fast polymerization, the polymerization is uncontrolled due to too low deactivation rate constant. However, these ligands maybe potentially used for less reactive monomers, such as VAc.

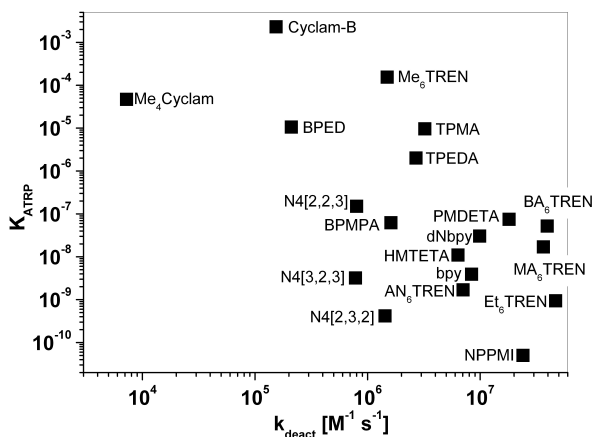


Figure 4. Map for selection of catalysts with best performance in ATRP. (Reprinted from ref. 27. Copyright ACS)

## Solvent Effects in ATRP

The solvent can have a marked effect on most of the equilibrium constants from Figure 1 and eq. 1 that contribute to  $K_{\text{ATRP}}$ . One potential exception is the equilibrium constant of C-X bond homolysis  $K_{\text{BH}}$ . Indeed, *ab initio* calculations of this constant in MeCN and DMF demonstrated that the values in these two solvents differ by less than 1 kcal mol<sup>-1</sup> for most alkyl halides, which corresponds to a difference in  $K_{\text{BH}}$  of less than one order of magnitude.<sup>(16)</sup> Reactions in which highly polar or charged species participate, are much more likely to be affected by the solvent properties such as solvation through donation of electron density, hydrogen bond-formation ability, polarity, etc. Therefore, the three components of  $K_{\text{Halo}}$ , namely  $K_{\text{EA}}$ ,  $K_{\text{ET}}$ , and  $K_{\text{Halido}}$  should change markedly with the solvent. The last constant was experimentally determined for Cu<sup>II</sup>(bpy)<sub>2</sub><sup>2+</sup> in methanol, acetone, and acetonitrile mixtures with water.<sup>(23,24)</sup> In pure methanol the bromidophilicity of the complex is  $4.7 \times 10^3$

$M^{-1}$ , whereas in MeCN it is estimated by extrapolation as  $10^5 M^{-1}$  and in acetone it is estimated as  $> 10^6 M^{-1}$ . Methanol solvates halide ions rather well via formation of hydrogen bonds and therefore facilitates the heterolytic dissociation of the  $Cu^{II}-X$  bonds, leading to low values of  $K_{Halido}$ . MeCN does not solvate well halide anions but may weakly coordinate to  $Cu^{II}$  species with an open coordination site, destabilizing the  $Cu^{II}$  halide complex but weaker compared to methanol. Lastly, acetone does not solvate well halide anions and has a lower affinity for  $Cu^{II}$  than MeCN and as a result, the halidophilicity in this solvent is the highest. The relative stabilization of  $Cu^I L_n$  and  $Cu^{II} L_n$  complexes by the solvent will cause changes in the redox potential and therefore in the values of  $K_{ET}$  of the couple  $Cu^{II} L_n / Cu^I L_n$ . Finally, the solvation of halide ions should markedly affect the values of  $K_{EA}$ , especially taking into account that the solvation of halogen atoms (neutral and symmetric species) is less likely to change with the solvent. The values of  $K_{EA}$  are accessible through measured values of transfer free energies of halide ions from water to organic solvents, as shown above (eq. 6). In many cases, the components of  $K_{ATRP}$  may change in different directions from one solvent to another and their changes may even compensate each other leading to similar  $K_{ATRP}$  values. As an example, Table III shows that the values of  $K_{ATRP}$  for the reaction of EtBriB in MeCN and MeOH are very close, although the bromidophilicity of  $Cu^{II}(bpy)_2^{2+}$  is higher in MeCN than in MeOH. This is compensated by the higher value of  $K_{EA}$  in MeOH.

**Table III.  $K_{ATRP}$  for the reaction of EtBriB with CuBr / bpy in MeCN and MeOH at  $22 \pm 2$  °C and values of contributing equilibrium constants.**

<i>Solvent</i>	$K_{ATRP}$	$K_{Bromido} [M^{-1}]$	$K_{EA}$
MeCN	$3.9 \times 10^{-9}$	$\sim 10^3$	$3.2 \times 10^{27}$
MeOH	$8.9 \times 10^{-10}$	$4.7 \times 10^3$	$1.0 \times 10^{31}$

To verify the model presented in this paper, it is interesting to calculate the values of  $K_{ATRP}$  and compare them with the experimental values. For instance, the values of the contributing equilibrium constants to the ATRP equilibrium between MeBriB and CuBr / bpy in a mixed solvent MeCN-H<sub>2</sub>O (9:1 v/v) are  $\log K_{BH} = -38.96$  (value in pure MeCN), (16)  $\log K_{Bromido} = 3.70$ , (24)  $\log K_{EA} = 28.8$  (from eq. 6), (37) and  $\log(1/K_{ET}) = -4.25$  (from eq. 7). (38) Therefore, the ATRP equilibrium constant can be calculated as  $\log K_{ATRP} = -9.6$ , which, taking into account the errors in all measured values, is in good agreement with the experimentally determined value (38) of  $\log K_{ATRP} = -8.1$ . Detailed studies on the effect of solvent on the values of  $K_{ATRP}$  and all contributing equilibrium constants are underway.

## Conclusions

A detailed model is provided and justified that represents the ATRP equilibrium constant as a combination of contributing equilibria: C-X bond homolysis, electron affinity of the halogen atom, reduction of  $Cu^{II}$ , and the

formation constant (halidophilicity) of  $\text{Cu}^{\text{II}}$  halide complex from the corresponding  $\text{Cu}^{\text{II}}$  complex and halide ions. The values of the ATRP equilibrium constant correlate well with the redox potentials of  $\text{Cu}^{\text{II}}$  halide complexes. The nature of the transferable group (bromine or chlorine) also affects the polymerization rate but the ATRP equilibrium constants of alkyl bromides are only about an order of magnitude higher than for structurally similar chlorides. This is attributed to the larger chloro- than bromophilicity of the  $\text{Cu}^{\text{I}}$  complexes.

**Acknowledgments.** The authors thank NSF (grant CHEM 07-15494) for funding.

## References

- (1) Matyjaszewski, K.; Davis, T. P., Eds. *Handbook of Radical Polymerization*; Wiley: Hoboken, 2002.
- (2) Braunecker, W. A.; Matyjaszewski, K. *Prog. Polym. Sci.* **2007**, *32*, 93.
- (3) Wang, J.-S.; Matyjaszewski, K. *J. Am. Chem. Soc.* **1995**, *117*, 5614.
- (4) Matyjaszewski, K.; Xia, J. *Chem. Rev.* **2001**, *101*, 2921.
- (5) Kamigaito, M.; Ando, T.; Sawamoto, M. *Chem. Rev.* **2001**, *101*, 3689.
- (6) Tsarevsky, N. V.; Matyjaszewski, K. *Chem. Rev.* **2007**, *107*, 2270.
- (7) Hawker, C. J.; Bosman, A. W.; Harth, E. *Chem. Rev.* **2001**, *101*, 3661.
- (8) Moad, G.; Rizzardo, E.; Thang, S. H. *Austral. J. Chem.* **2005**, *58*, 379.
- (9) Perrier, S.; Takolpuckdee, P. *J. Polym. Sci.: Part A: Polym. Chem.* **2005**, *43*, 5347.
- (10) Davis, K. A.; Matyjaszewski, K. *Adv. Polym. Sci.* **2002**, *159*, 1.
- (11) Tsarevsky, N. V.; Tang, W.; Brooks, S. J.; Matyjaszewski, K. *ACS Symp. Ser.* **2006**, *944*, 56.
- (12) Goto, A.; Fukuda, T. *Prog. Polym. Sci.* **2004**, *29*, 329.
- (13) Matyjaszewski, K.; Spanswick, J. *Mat. Today* **2005**, *8(3)*, 26.
- (14) Pintauer, T.; McKenzie, B.; Matyjaszewski, K. *ACS Symp. Ser.* **2003**, *854*, 130.
- (15) Gillies, M. B.; Matyjaszewski, K.; Norrby, P.-O.; Pintauer, T.; Poli, R.; Richard, P. *Macromolecules* **2003**, *36*, 8551.
- (16) Lin, C. Y.; Coote, M. L.; Gennaro, A.; Matyjaszewski, K. *J. Am. Chem. Soc.* **2008**, *130*, 12762.
- (17) Beuermann, S.; Buback, M. *Prog. Polym. Sci.* **2002**, *27*, 191.
- (18) Berry, R. S.; Reimann, C. W.; Spokes, G. N. *J. Chem. Phys.* **1962**, *37*, 2278.
- (19) Berry, R. S.; Reimann, C. W. *J. Chem. Phys.* **1963**, *38*, 1540.
- (20) Pandey, J. D.; Saxena, O. C. *J. Chem. Soc. (A)* **1969**, 397.
- (21) Tang, W.; Tsarevsky, N. V.; Matyjaszewski, K. *J. Am. Chem. Soc.* **2006**, *128*, 1598.
- (22) Jakubowski, W.; Tsarevsky, N. V.; Higashihara, T.; Faust, R.; Matyjaszewski, K. *Macromolecules* **2008**, *41*, 2318.
- (23) Tsarevsky, N. V.; Pintauer, T.; Matyjaszewski, K. *Macromolecules* **2004**, *37*, 9768.

- (24) Tsarevsky, N. V.; Braunecker, W. A.; Vacca, A.; Gans, P.; Matyjaszewski, K. *Macromol. Symp.* **2007**, *248*, 60.
- (25) Perrier, S.; Armes, S. P.; Wang, X. S.; Malet, F.; Haddleton, D. M. *J. Polym. Sci.: Part A: Polym. Chem.* **2001**, *39*, 1696.
- (26) Paneva, D.; Mespouille, L.; Manolova, N.; Degee, P.; Rashkov, I.; Dubois, P. *Macromol. Rapid Commun.* **2006**, *27*, 1489.
- (27) Tang, W.; Kwak, Y.; Braunecker, W.; Tsarevsky, N. V.; Coote, M. L.; Matyjaszewski, K. *J. Am. Chem. Soc.* **2008**, *130*, 10702.
- (28) Fischer, H. *J. Polym. Sci.: Part A: Polym. Chem.* **1999**, *37*, 1885.
- (29) Tsarevsky, N. V.; Braunecker, W. A.; Matyjaszewski, K. *J. Organomet. Chem.* **2007**, *692*, 3212.
- (30) Qiu, J.; Matyjaszewski, K.; Thouin, L.; Amatore, C. *Macromol. Chem. Phys.* **2000**, *201*, 1625.
- (31) Matyjaszewski, K.; Goebelt, B.; Paik, H.-j.; Horwitz, C. P. *Macromolecules* **2001**, *34*, 430.
- (32) Tsarevsky, N. V.; Braunecker, W. A.; Brooks, S. J.; Matyjaszewski, K. *Macromolecules* **2006**, *39*, 6817.
- (33) Saveant, J. M. *J. Phys. Chem.* **1994**, *98*, 3716.
- (34) Marcus, Y. *Pure Appl. Chem.* **1983**, *55*, 977.
- (35) Jakubowski, W.; Min, K.; Matyjaszewski, K. *Macromolecules* **2006**, *39*, 39.
- (36) Matyjaszewski, K.; Jakubowski, W.; Min, K.; Tang, W.; Huang, J.; Braunecker, W. A.; Tsarevsky, N. V. *Proc. Natl. Acad. Sci. USA* **2006**, *103*, 15309.
- (37) Gomaa, E. A. *Thermochim. Acta* **1989**, *152*, 371.
- (38) Tsarevsky, N. V.; Braunecker, W. A.; Matyjaszewski, K. *unpublished data*.



## Chapter 7

# ATRP of Methacrylates Catalysed by Homo- and Heterobimetallic Ruthenium Complexes

Yannick Borguet,<sup>a</sup> Xavier Sauvage,<sup>a</sup> Dario Bicchielli,<sup>a</sup> Sébastien Delfosse,<sup>a</sup> Lionel Delaude,<sup>a</sup> Albert Démonceau,<sup>a\*</sup> Laurianne Bareille,<sup>b</sup>

Pierre Le Gendre,<sup>b</sup> and Claude Moïse<sup>b</sup>

<sup>a</sup>Laboratory of Macromolecular Chemistry and Organic Catalysis  
University of Liège, Sart-Tilman (B.6a), B-4000 Liège, Belgium

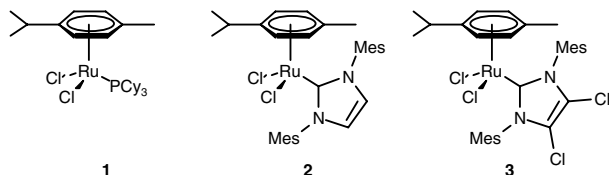
<sup>b</sup>ICMUB-UMR5260, Université de Bourgogne

Faculté des Sciences Mirande, 9 allée Alain Savary, 21000 Dijon, France

The catalytic activity of a series of ruthenium-based homo- and heterobimetallic complexes was determined by investigating the atom transfer radical polymerisation of methyl methacrylate. The complexes under investigation were [(arene)Ru( $\mu$ -Cl)<sub>3</sub>RuCl(C<sub>2</sub>H<sub>4</sub>)-(L)] (L = PCy<sub>3</sub> or a *N*-heterocyclic carbene ligand), [(*p*-cymene)-Ru( $\mu$ -Cl)<sub>3</sub>RuCl(=C=CHR)(PCy<sub>3</sub>)] (R = Ph or *t*-Bu), and [RuCl<sub>2</sub>(*p*-cymene){PCy<sub>2</sub>(CH<sub>2</sub>)<sub>2</sub>( $\eta^5$ -C<sub>5</sub>H<sub>4</sub>)TiX<sub>2</sub>( $\eta^5$ -C<sub>5</sub>H<sub>5</sub>)}] (X = Cl, F, and OBz). The catalytic activity of a variety of related [(*p*-cymene)-ClRu( $\mu$ -Cl)<sub>2</sub>Ru(O<sup>^</sup>N)(=CHPh)] complexes (O<sup>^</sup>N is a Schiff base ligand) is also reported. The results clearly demonstrate that the ligands strongly affect the ability of the resulting ruthenium complexes to favour the occurrence of a well-behaved ATRP.

Ruthenium-arene complexes are versatile and efficient catalyst precursors for various important organic transformations. This is due in part to the lability of the  $\eta^6$ -arene ligand that can be easily removed upon thermal or photochemical activation to release highly active, coordinatively unsaturated species. During the 1990s, we demonstrated that [RuCl<sub>2</sub>(*p*-cymene)(PR<sub>3</sub>)] complexes bearing basic and bulky phosphine ligands, such as

tricyclohexylphosphine ( $\text{PCy}_3$ , see structure **1**), were highly effective precatalysts for ring-opening metathesis polymerisation (ROMP) (1) and atom transfer radical polymerisation (ATRP) (2). The past decade also witnessed the experimental reality of stable nucleophilic *N*-heterocyclic carbenes (NHCs). These divalent carbon species are neutral, two-electron ligands with only little  $\pi$ -back-bonding tendency. They behave as phosphine mimics, yet they are better  $\sigma$ -donors and they form stronger bonds to metal centres than most phosphines.

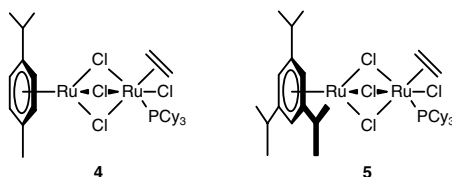


Scheme 1. Ruthenium-*p*-cymene complexes bearing a tricyclohexylphosphine or a NHC ligand

Their electronic and steric properties are liable to ample modification simply by varying the substituents on the heterocyclic ring. Therefore, NHCs have become ubiquitous ligands in organometallic chemistry and catalysis (3). In order to further expand the scope of ruthenium-arene catalyst precursors, we have adopted this class of ancillary ligands instead of phosphines to generate  $[\text{RuCl}_2(p\text{-cymene})(\text{NHC})]$  species, either preformed or *in situ* (4). Thus, complex **2** bearing the 1,3-dimesitylimidazolin-2-ylidene ligand displayed a remarkable activity for initiating ROMP of cyclooctene under visible light illumination (5), whereas complex **3** sporting a modified NHC ligand (4,5-dichloro-1,3-dimesitylimidazolin-2-ylidene) was an attractive challenger for promoting atom transfer radical addition (ATRA) (6) and polymerisation (7) processes.

## Homobimetallic Ruthenium- $\text{PCy}_3$ complexes

In 2005, Severin and co-workers investigated the reaction of  $[\text{RuCl}_2(p\text{-cymene})]_2$  with 1 equivalent of  $\text{PCy}_3$  under an ethylene atmosphere. Under these conditions, the ruthenium dimer afforded a new type of molecular scaffold (**4**), in which a  $\text{RuCl}-(\eta^2\text{-C}_2\text{H}_4)(\text{PCy}_3)$  fragment was connected *via* three  $\mu$ -chloro bridges to a ruthenium-*p*-cymene moiety. Complex **4** displayed an outstanding catalytic activity in ATRA reactions (8). By varying the nature of the arene ligand, the same group also synthesised the related homobimetallic complex **5** and successfully employed it as catalyst precursor for the ATRP of methacrylate monomers at a temperature of only 35 °C without the need of an additive such as  $\text{Al}(\text{O}i\text{-Pr})_3$  (9).



Scheme 2. Homobimetallic ruthenium–arene complexes bearing a tricyclohexylphosphine ligand

Thus, the polymerisation of methyl methacrylate in toluene was investigated using an initial catalyst/initiator/monomer molar ratio of 1:2:800 with ethyl 2-bromo-2-methyl-propionate as the initiator. Under these experimental conditions, all the criteria of living polymerisation were fulfilled. Indeed, the plot of  $\ln([M]_0/[M]_t)$  versus time followed a linear relationship, which is typical for a controlled polymerisation. Furthermore, a linear evolution

**Table 1. Polymerisation of Representative (Meth)Acrylates Catalysed by Ruthenium Complex 5**

Monomer	Yield (%)	$M_n$	$M_w/M_n$
MMA	95	38 500	1.14
EtMA	93	40 500	1.15
<i>i</i> -BMA	89	40 000	2.46
<i>t</i> -BuMA	88	47 000	1.14
<i>n</i> -BuA	2	§	§
<i>t</i> -BuA	12	§	§

of  $M_n$  as a function of monomer conversion was observed. The observed molecular weights agreed well with the calculated values and the polydispersities were very low. Unfortunately, longer reaction times led to a small amount of polymers with a higher molecular weight (less than 4%). If these polymers were included in the calculation, a final PDI of 1.68 was obtained. Focusing on the main polymer peak, however, a polydispersity of 1.14 was recorded (Table 1). A radical mechanism was supported by the tacticity of the polymer (rr:rm:mm = 64:29:7) and by the fact that the addition of 5 equivalents of galvinoxyl (relative to the initiator) blocked the reaction completely (9).

Other methacrylates such as ethyl methacrylate (EtMA), isobornyl methacrylate (*i*-BMA) and *t*-butyl methacrylate (*t*-BuMA) were successfully polymerised at 35 °C as well (Table 1). For PEtMA and P*t*-BuMA, very low polydispersities of 1.15 and 1.14 were obtained. For polymerisations of isobornyl methacrylate, on the other hand, a significantly broader molecular weight distribution of PDI = 2.46 was found. The two acrylates tested, *n*-butyl acrylate (*n*-BuA) and *t*-butyl acrylate (*t*-BuA), gave very low conversions (Table 1) (9).

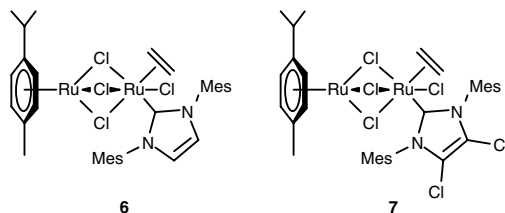
Complex 5 is remarkable, as it is efficient at room temperature. It should be noted, indeed, that ruthenium-catalysed polymerisations of methacrylates are generally performed at temperatures of around 80–85 °C and

that there are only a few Ru catalysts that allow one to work under milder conditions. The hydride complex  $[\text{RuH}_2(\text{PPh}_3)_4]$ , for example, was reported to catalyse the controlled polymerisation of MMA at 30 °C but significantly higher catalyst concentrations (MMA/Ru = 200:1) and reaction times (300 h) were required (10). Complex **5** thus ranges among the most active ruthenium catalysts for ATRP reactions described so far (9).

## Homobimetallic Ruthenium–*N*-Heterocyclic Carbene Complexes

In view of the enhancements brought by the replacement of phosphines by NHCs in monometallic ruthenium–arene catalyst precursors of type **1–3**, we decided to investigate the effect of similar modifications on the catalytic activity of complexes of type **4–5**. The preparation of complexes **6** and **7** was rather straightforward and could be achieved in a single step by heating the commercially available  $[\text{RuCl}_2(p\text{-cymene})]_2$  dimer with 1 equivalent of 1,3-dimesitylimidazol-2-ylidene and 4,5-dichloro-1,3-dimesitylimidazol-2-ylidene, respectively (11).

Having in hand the desired ruthenium–*N*-heterocyclic complexes **6** and **7**, we then investigated their catalytic activity in the ATRP of vinyl monomers (Table 2).



Scheme 3. Homobimetallic ruthenium–*p*-cymene complexes bearing a NHC ligand

**Table 2. Polymerisation of Methyl Methacrylate Initiated by Ethyl 2-Bromo-2-methylpropionate and Catalysed by Ruthenium Complexes 4, 6, and 7**

Complex	<b>4</b>	<b>6</b>	<b>7</b>
Yield (%)	78	81	47
$M_n$	36 500	40 000	19 000
$M_w/M_n$	1.05	1.25	1.10
$f$	0.85	0.8	1.0
$k_{app}$ ( $10^{-5} \text{ s}^{-1}$ )	2.11	2.81	0.93

First, methyl methacrylate was polymerised using ethyl 2-bromo-2-methylpropionate as initiator under standard conditions (2). The reactions were carried out in toluene under the exclusion of oxygen for 16 h at 85 °C with an initial monomer/initiator/catalyst molar ratio of 800:2:1. With both complexes **6** and **7**, the molecular weights increased linearly with conversion (Figure 1). The semilogarithmic plot of  $\ln([M]_0/[M]_t)$  versus time also followed a linear

relationship. These results strongly suggest that radical polymerisation took place in a controlled fashion with both catalysts. The nature of the ancillary ligand significantly influenced the rate of reaction. The 1,3-dimesitylimidazolin-2-ylidene ligand afforded a much more active catalyst (**6**) than its dichloro derivative (**7**). Indeed, the pseudo-first order rate constant ( $k_{app}$ ) computed for complex **6** was three times larger than for complex **7**. However, in terms of kinetics, complex **6** was only slightly superior to the tricyclohexylphosphine-based bimetallic species **4** (see Table 2 and Figure 1). When molecular weight distributions were examined, however, complex **4** took precedence over its NHC-containing congeners. Although the number-average molecular weight reached with this catalyst at 85 °C exceeded the value calculated from the initial monomer-to-initiator ratio (initiation efficiency,  $f$ , = 0.85), polydispersity remained as low as  $M_w/M_n = 1.05$ , whereas complexes **6** and **7** led to PDIs of 1.25 and 1.10, respectively, under the same experimental conditions. Moreover, the formation of small amounts of low molecular weight polymers that did not disappear over the course of the reaction was observed with the latter catalysts. Although minor (less than 1% of the total polymer mass), this phenomenon was not detected with catalyst **4**. It is attributed to the coupling or dismutation of oligomeric chains during the early stages of the polymerisation process ("persistent radical effect") (12).

When the polymerisation of MMA was carried out at 35 °C instead of 85 °C with complex **6**, the semilogarithmic plot of  $\ln([M]_0/[M]_t)$  versus time remained linear, but high molecular weight polymers were formed from the very beginning of the reaction and  $M_n$  as well as  $M_w/M_n$  remained almost constant ( $\approx 76 \text{ kg}\cdot\text{mol}^{-1}$  and 1.60, respectively) throughout the entire run. This behaviour sharply contrasts with the results reported for complex **5** at 35 °C that met all the criteria of controlled polymerisation (11). With the NHC-based complex **6**, the decrease of temperature most likely induced a switch of mechanism, from controlled ATRP to a redox-initiated free-radical process (7), although further investigations are needed to fully clarify this point.

Regarding the mechanism, it seems likely that, in a first step, the ethylene ligand in complexes **4–7** is cleaved off. The resulting coordinatively unsaturated ruthenium complex is then able to reversibly abstract a halogen atom from the initiator or subsequently from the growing polymer chain end. This mechanism is supported by the fact that the ethylene ligand in complex **4** can be replaced by a halogen atom as evidenced by the isolation of the mixed valence Ru(II)–Ru(III) complex  $[(p\text{-cymene})\text{Ru}(\mu\text{-Cl})_3\text{RuCl}_2(\text{PCy}_3)]$  (8).

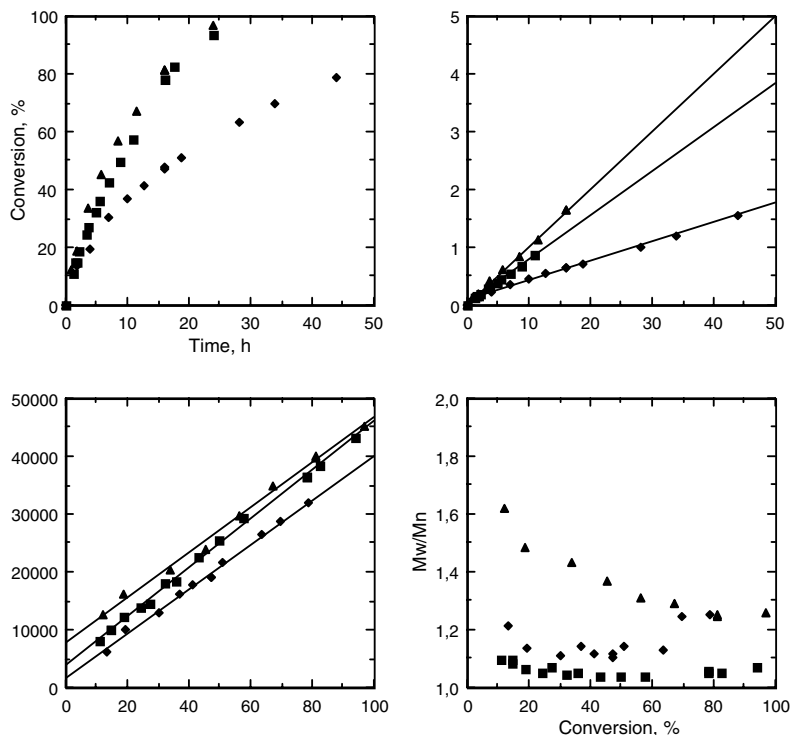


Figure 1. Experimental data for the polymerisation of MMA initiated by ethyl 2-bromo-2-methyl-propionate and catalysed by complexes **4** ( ), **6** ( ), and **7** ( ).

## Homobimetallic Ruthenium–Vinylidene Complexes

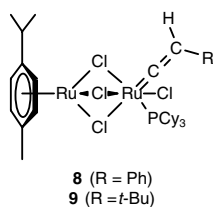
In order to further explore the reactivity of the homobimetallic ruthenium complexes, the reaction of **4** with terminal alkynes was investigated. Thus, when phenylacetylene or *tert*-butylacetylene was added to a solution of complex **4** in  $\text{CH}_2\text{Cl}_2$  or benzene, the rapid and quantitative formation of the corresponding ruthenium-vinylidene complexes, **8** and **9**, respectively, was observed (13). The formation of **8** and **9** can be rationalised by the displacement of the ethylene ligand by the respective acetylene followed by an alkyne-to-vinylidene transformation.

The activity of complexes **8** and **9** was then investigated for the ATRP of MMA using the standard experimental conditions (85 °C, with ethyl 2-bromo-2-methyl-propionate as the initiator). With both ruthenium-vinylidene complexes, the molecular weights increased linearly with conversion. Furthermore, the semilogarithmic plot of  $\ln([M]_0/[M]_t)$  versus time also followed a linear relationship. These results strongly suggest that the polymerisation took place in a controlled fashion. However, an induction period was clearly evidenced in the plots of conversion versus time and  $\ln([M]_0/[M]_t)$  versus time (Figure 2). Complexes **8** and **9**, however, differed from one another in the

polydispersity of the polymers thus obtained (Figure 2 and Table 3). With the phenyl-substituted vinylidene complex (**8**), the molecular weight distribution decreased with conversion, before to increase to some extent (up to 1.3) at the end of the polymerisation. Thus, the lowest polydispersity ( $M_w/M_n = 1.15$ ) was obtained after 40–60% conversion. When the *t*-butyl-substituted congener (**9**) was used,  $M_w/M_n$  was higher (1.6) and remained almost constant throughout the entire run.

The reasons why complexes **8** and **9** are active in ATRP are presently unclear. These complexes possess indeed two 18-electron ruthenium centres and, as such, should be unable to activate the carbon–halogen bond of the initiator or of the growing polymer chain end. On the other hand, the fact that an induction period was found for the ATRP of MMA indicates that the ruthenium–vinylidene complexes have to be activated prior to the ATRP process. There are in principle several plausible explanations for the formation of a coordinatively unsaturated 16-electron ruthenium species from the ruthenium–vinylidene complexes **8** or **9**: either the splitting of the bimetallic scaffold into two different unsaturated ruthenium intermediates (Path A, Scheme 5), the opening of a  $\mu$ -chloro bridge (Path B), or the release of the vinylidene ligand (Path C, Scheme 5).

Further investigations are needed to clarify this point. It should also be noted that when the homobimetallic ruthenium–ethylene complex **4** was treated with a stoichiometric amount of acetylene in THF, the  $\mu$ -carbide complex **11** was formed, presumably *via* the intermediate ruthenium–vinylidene complex **10** (Scheme 6) (13).



*Scheme 4. Homobimetallic ruthenium–p-cymene complexes bearing a vinylidene ligand*

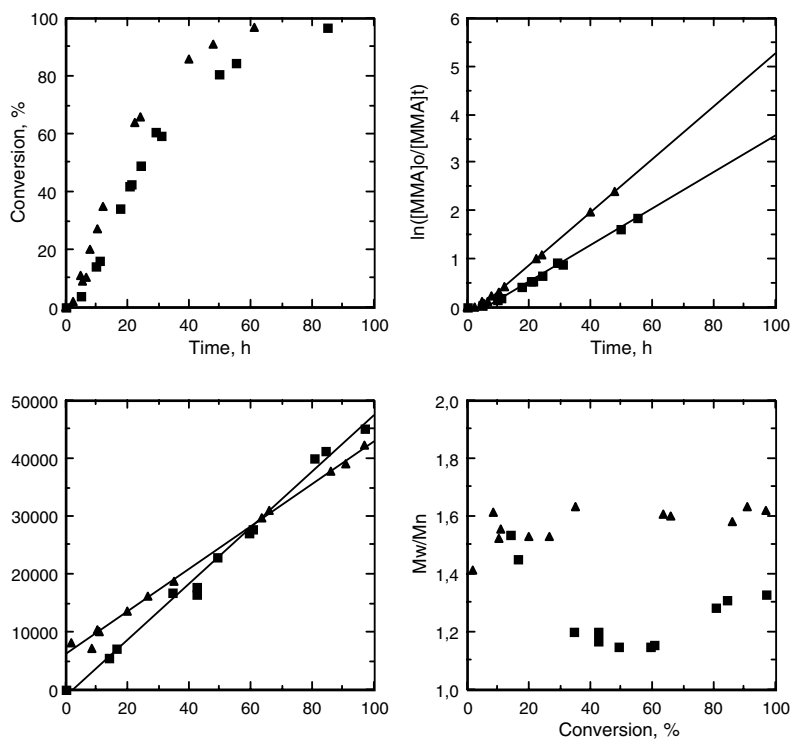
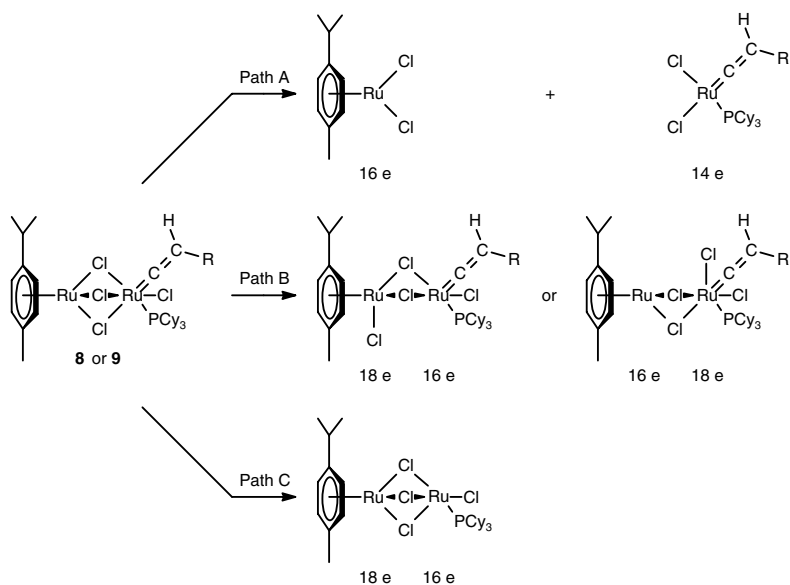


Figure 2. Experimental data for the polymerisation of MMA initiated by ethyl 2-bromo-2-methyl-propionate and catalysed by complexes **8** ( ) and **9** ( ).

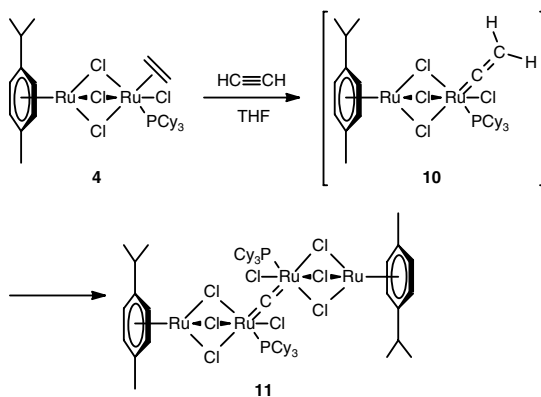
**Table 3. Polymerisation of Methyl Methacrylate Initiated by Ethyl 2-Bromo-2-methylpropionate and Catalysed by Ruthenium Complexes **8** and **9****

Complex	Yield (%)	$M_n$	$M_w/M_n$
<b>8</b>	49	23 000	1.15
<b>9</b>	66	31 000	1.6





*Scheme 5. Plausible explanations for the formation of coordinatively unsaturated 16-electron ruthenium species*

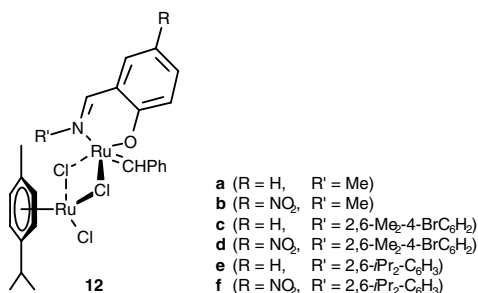


*Scheme 6. Formation of the ruthenium  $\mu$ -carbide complex 11*

## Homobimetallic Ruthenium–Benzylidene–Schiff Base Complexes

Recently, De Clercq and Verpoort reported the synthesis of a new class of homobimetallic ruthenium-benzylidene complexes bearing a Schiff base ligand (**12a–f**). These complexes proved to be highly efficient catalyst precursors in various olefin metathesis reactions (*14*) and atom transfer radical

addition of carbon tetrachloride across olefins (15). Their catalytic activity was also probed in ATRP reactions with methyl methacrylate, isobornyl methacrylate, methyl acrylate, *n*-butyl acrylate, and acrylonitrile. Unfortunately, none of the complexes **12a–f** was able to polymerise these monomers (15). However, when styrene was used as a monomer, complexes **12a–f** displayed a totally different behaviour (Table 4). Polymerisation took place and among the complexes investigated, **12c** was the most effective catalyst precursor, with a good yield of 71% after 17 h of reaction at 110 °C, a high initiation efficiency (*f*) of 0.87, and a polydispersity of 1.35. Furthermore, the relationship between molecular weight and monomer conversion was linear, as well as the semilogarithmic plot of  $\ln([M]_0/[M]_t)$  versus time, indicating thereby that the polymerisation proceeded in a controlled fashion.



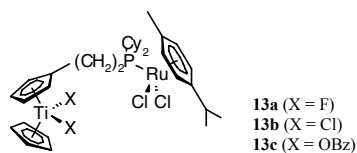
Scheme 7. Homobimetallic ruthenium–benzylidene complexes bearing a Schiff base ligand

Table 4. Polymerisation of Styrene  
Catalysed by Ruthenium Complexes 12a–f

Complex	Yield (%)	$M_n$	$M_w/M_n$	<i>f</i>
<b>12a</b>	11	Š	Š	Š
<b>12b</b>	0	Š	Š	Š
<b>12c</b>	71	34 000	1.35	0.87
<b>12d</b>	44	25 000	1.51	0.73
<b>12e</b>	63	31 000	1.42	0.85
<b>12f</b>	36	27 000	1.49	0.56

## Heterobimetallic Titanium–Ruthenium–*p*-Cymene Complexes

In recent years, we became interested in heterobimetallic titanium–ruthenium complexes. Complexes containing early as well as late transition metals are nowadays particularly attractive materials owing to their potential application in homogeneous catalysis. Indeed, the coordination of the substrate to one of the two metals may increase its reactivity towards the other. Such compounds, which often show a cooperative effect, may constitute a new class of catalysts that are able to improve the efficiency of known processes or to give new reactions. Nevertheless, probably because of their laborious access, only a few early–late bimetallic complexes have been tested in catalysis. The present strategy to construct such systems was to first synthesise a phosphine, in which a titanocene dihalide (difluoride or dichloride) or dibenzoate fragment is attached to PCy<sub>2</sub> *via* an ethylene spacer. In the next step, these early metal ligands were treated with [RuCl<sub>2</sub>(*p*-cymene)]<sub>2</sub> to provide a series of early–late Ti–Ru heterobimetallic complexes **13** (Scheme 8) (16).



Scheme 8. Heterobimetallic titanium–ruthenium–*p*-cymene complexes **13**

With these new complexes in hand, we next investigated their catalytic activity in the ATRP of MMA under the standard experimental conditions that were used above.

As shown in Table 5, the polymer yield strongly depends on the titanocene fragment. Thus, the difluorotitanocene-based complex (**13a**) exhibited the highest activity with 97% conversion after 16 h of reaction. Complexes **13b** (X = Cl) and **13c** (X = OBz) were less active with about 65% conversion. On the other hand, as indicated by the initiation efficiency, *f*, the number-averaged molecular weights correspond to the theoretical molecular weights calculated from the assumption that one polymer chain is generated from one initiator. Interestingly, the molecular weight distributions were also quite narrow ( $M_w/M_n = 1.2$ – $1.3$ ).

We next examined the living nature of the polymerisations. The results are summarised in Figure 3, which shows the plots of  $\ln([MMA]_0/[MMA]_t)$  against time, and of  $M_n$  and  $M_w/M_n$  against MMA conversion. When the polymerisation of MMA was carried out with the titanocene dihalide-based complexes **13a** (X = F) and **13b** (X = Cl), the semilogarithmic plot of  $\ln([MMA]_0/[MMA]_t)$  versus time was linear throughout the run. As expected from Table 5, complex **13a** ( $k_{app} = 5.40 \cdot 10^{-5} \text{ s}^{-1}$ ) was more active than complex **13b** ( $k_{app} = 1.72 \cdot 10^{-5} \text{ s}^{-1}$ ). However, the use of the titanocene dibenzoate congener led to a significant change of behaviour. Thus, at the very beginning of the polymerisation, the relationship between  $\ln([MMA]_0/[MMA]_t)$  and time was linear but, after a few hours of reaction, the rate of the MMA conversion decreased significantly and finally the polymerisation stopped. On the other hand, in all cases,  $M_n$  increased linearly

with conversion and high initiation efficiencies were obtained ( $f > 0.85$ ). Furthermore, the polydispersities decreased with conversion and reached the value of 1.2–1.3 at the end of the polymerizations.

**Table 5. Polymerisation of Methyl Methacrylate Initiated by Ethyl 2-Bromo-2-methylpropionate and Catalysed by Titanium/Ruthenium Complexes 13a–c**

Complex	13a	13b	13c
Yield (%)	97	63	66
$M_n$	45 000	26 000	27 000
$M_w/M_n$	1.20	1.25	1.30
$f$	0.85	0.95	1.0
$k_{app}$ ( $10^{-5} \text{ s}^{-1}$ )	5.4	1.72	5.41*

\*Initial apparent rate constant.

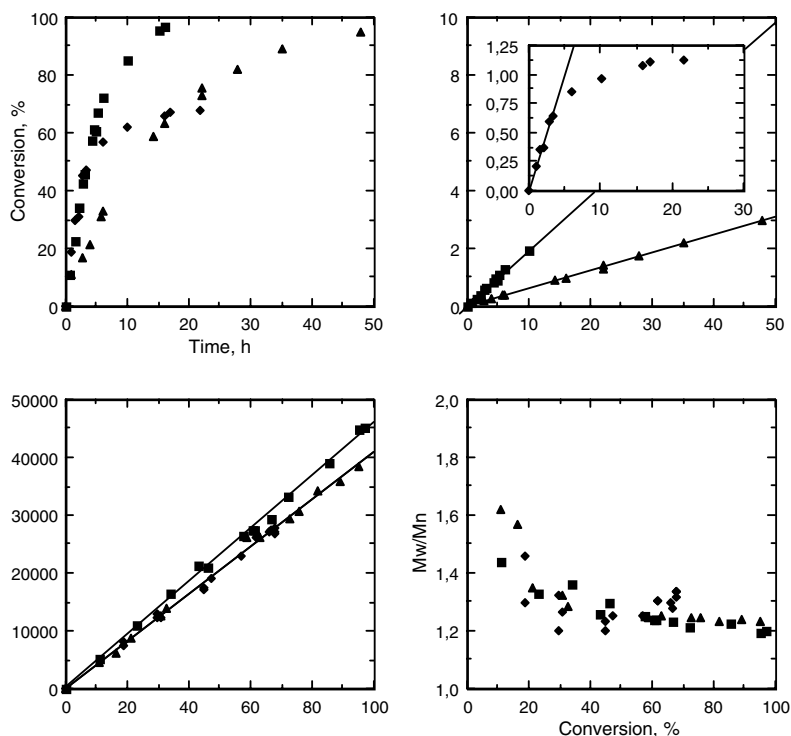
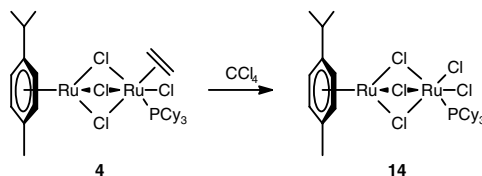


Figure 3. Experimental data for the polymerisation of MMA initiated by ethyl 2-bromo-2-methyl-propionate and catalysed by complexes 13a (■), 13b (◆), and 13c (▲).

## Bimetallic *versus* Monometallic Catalytic Species?

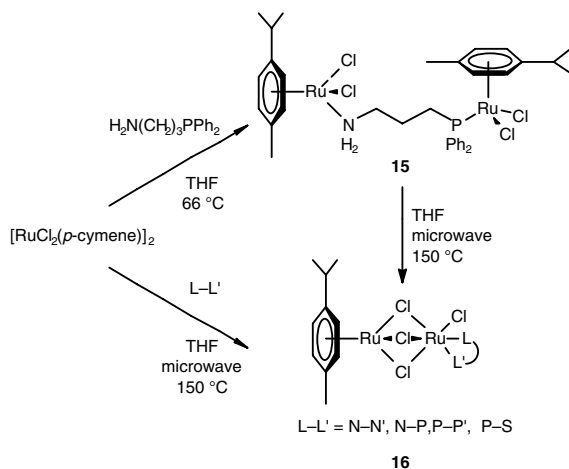
In the past decade, monometallic ruthenium catalysts have widely contributed to the development of ATRP (17, 18). With the advent of homobimetallic ruthenium complexes **4–9** and **12** as catalyst precursors, the following question arises: is the bimetallic scaffold intact throughout the polymerisation run? The answer is probably yes, although further investigations are needed to clarify this point. This answer is substantiated by a few observations:

(a) It has been shown that complex **4** is not only highly efficient in ATRP, but it also displays an exceptional catalytic activity in Kharasch chemistry (19). In particular, when a solution of complex **4** in toluene was heated to 40 °C in the presence of a large excess of  $\text{CCl}_4$ , the mixed valence  $\text{Ru}^{\text{II}}\text{–Ru}^{\text{III}}$  complex **14** (Scheme 9) was isolated and characterised by single crystal X-ray diffraction analysis. Noteworthingly, the structure demonstrates that both ruthenium fragments in complex **14** are connected *via* three chloro bridges, as in the parent compound **4** (19).

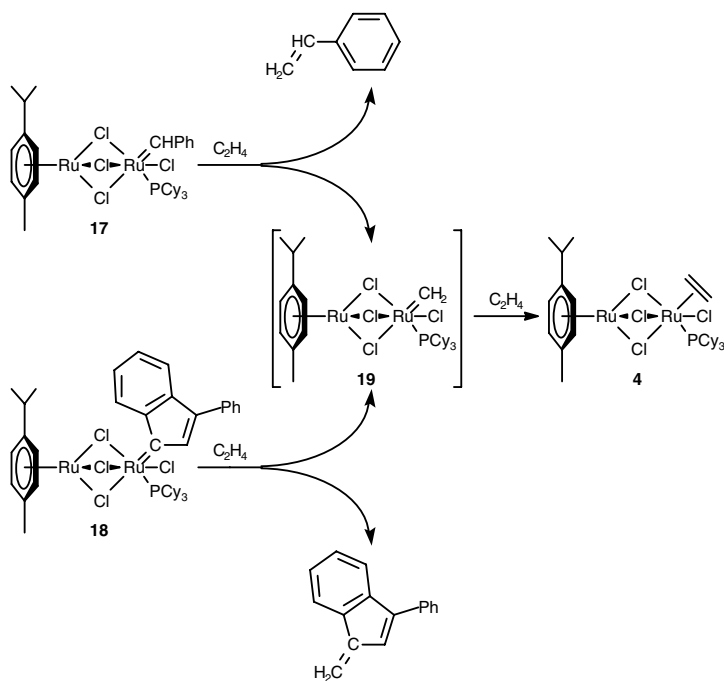


Scheme 9. Formation of the mixed valence  $\text{Ru}^{\text{II}}\text{–Ru}^{\text{III}}$  complex **14**

(b) It is also worth noting that homobimetallic ruthenium complexes **4** (bearing the  $\text{PCy}_3$  ligand), **6** and **7** (bearing a NHC ligand) are usually synthesised at a temperature ranging from 60 to 75 °C. An indication that the chloro bridges are viable at higher temperatures can be deduced from a recent paper of K. Severin and his co-workers (20). They found indeed that microwave heating at 130–150 °C can facilitate arene exchange in reactions of  $[\text{RuCl}_2(\text{arene})]_2$  complexes (arene = *p*-cymene or 1,3,5-triisopropyl-benzene) with neutral chelate ligands to afford the bimetallic complexes **16** (Scheme 10). The method was used for a variety of different ligands, such as diphosphines, a bulky  $\alpha$ -diimine, a chiral P–N-, and non-chiral P–N- and P–S-chelates. In an alternative route (Scheme 10), the dimer  $[\text{RuCl}_2(\textit{p}\text{-cymene})]_2$  was heated with 3-(diphenylphosphino)-1-propylamine in THF for 5 min without microwave heating to give the dinuclear complex **15**. After isolation and purification, complex **15** was subjected to microwave heating at 150 °C in THF for 4 h to give the corresponding homobimetallic ruthenium complex in 70% isolated yield (20).



*Scheme 10. Microwave-assisted direct synthesis of dinuclear ruthenium complexes containing N-N', N-P-, P-P', and P-S-chelate ligands*

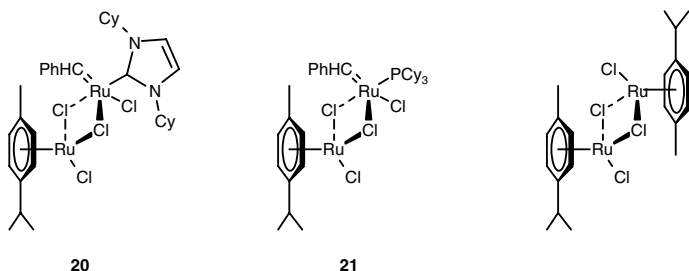


*Scheme 11. Reaction of homobimetallic ruthenium-benzylidene **17** and indenylidene **18** complexes with ethylene*

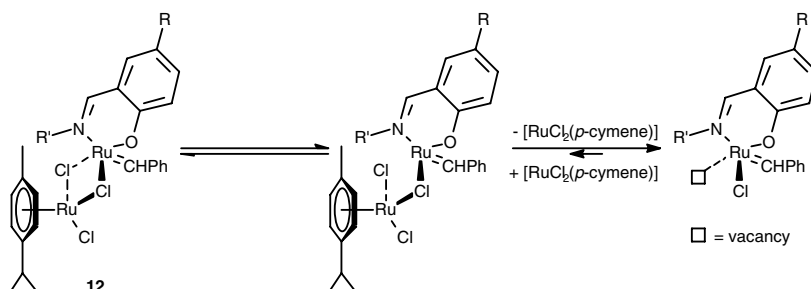
(c) On the other hand, some homobimetallic ruthenium complexes, such as **6** and **7**, are also highly active catalyst precursors in olefin metathesis (11). In

particular, when solutions of homobimetallic ruthenium-benzylidene (**17**) and ruthenium-indenylidene (**18**) complexes were placed under an ethylene atmosphere, styrene and 1-methylene-1*H*-indene were released from the benzylidene and indenylidene complexes, respectively, and the pure ruthenium-ethylene complex **4** was isolated (Scheme 11) (21). This transformation presumably occurred *via* a ruthenium-methylidene species **19** through a process that maintained the three chloro bridges. The situation seems to differ in the case of the dinuclear complexes **12**, in which both ruthenium centres are connected by only two  $\mu$ -chloro bridges. Dissociation of the complexes has been suggested (22), in agreement with the findings of Herrmann and co-workers (23) with similar dinuclear ruthenium complexes **20** (23) and **21** (24) (Scheme 12). A two-step dissociative mechanism involving a sequential heterolytic cleavage of the two chloro bridges in complexes **12** and liberation of the coordinatively labile ligand  $[\text{RuCl}_2(p\text{-cymene})]$  as the key step is highly probable (Scheme 13) (22).

It should also be emphasised that the presence of two chloro bridges in complexes **12**, **20**, and **21** has been suggested by comparison with the structure of the ruthenium dimer  $[\text{RuCl}_2(p\text{-cymene})]_2$ , whereas the three chloro bridges in complexes **4-9** have been evidenced by X-ray diffraction analysis. In solution, these bimetallic, bridged-chloride ruthenium complexes have been characterised by  $^1\text{H}$ ,  $^{13}\text{C}$ , and  $^{31}\text{P}$  NMR spectroscopy, but the exact number of chloro bridges is unknown. In the particular case of complexes **4-7**, since the alkene ligand is rather labile in solution, all NMR spectra were recorded in  $\text{CD}_2\text{Cl}_2$  saturated with ethylene. However, prolonged exposure to nitrogen or air led to progressive colour changes indicative of degradation.



Scheme 12. Structure of the dinuclear ruthenium complexes **20**, **21**, and  $[\text{RuCl}_2(p\text{-cymene})]_2$



Scheme 13. Proposed dissociative mechanism with complexes **12**

To conclude, it is likely that the bimetallic scaffold in ruthenium complexes **4–9** remains intact throughout the polymerisation runs. All the ATRP experiments discussed above were indeed performed under nitrogen or argon, using reagents and solvents dried, distilled, and stored under an inert atmosphere. Furthermore, the temperature at which the polymerisations were conducted (85 °C for MMA and 110 °C for styrene) are in the range of those used for the synthesis of these and related compounds. It should also be noted that the substrates and solvents used in ATRP are "weakly" interacting ligands that should probably not affect the dinuclear structure of the catalyst, contrary to strong donor ligands, such as CO, which might be responsible for the cleavage of the halogeno bridges (25). In case the bimetallic structural motif remains intact, cooperative effects between the two metal centres are expected, with one metal fragment playing the role of an electron reservoir for the catalytic site through the chloro bridges. This hypothesis has been notably substantiated by testing a library of 66 homo- and heterobimetallic catalyst precursors in Kharasch chemistry. Two chloro-bridged Rh–Ru complexes emerged from this screening, with an exceptionally high activity compared to all the other metal–ruthenium combinations under investigation (26).

## Conclusions

The catalytic activity of novel homo- (complexes **4–9** and **12**) and heterobimetallic ruthenium complexes (**13a–c**) was investigated in the ATRP of MMA. Complex **6** bearing the 1,3-dimesitylimidazolin-2-ylidene ligand displayed faster reaction rates than its 4,5-dichloro derivative (**7**) and the related phosphine-based complex **4**, although control was more effective with the latter catalyst. More importantly, the homobimetallic ruthenium complex **5** bearing the 1,3,5-triisopropylbenzene ligand instead of the commonly used *p*-cymene promoted a controlled ATRP of methacrylates at a temperature of only 35 °C, and the resulting polymers showed low polydispersities. Ruthenium-vinylidene complexes **8** and **9** also promoted controlled radical polymerisations, albeit a short induction period was observed. In addition, with complex **8** containing a phenyl-substituted vinylidene ligand, the polydispersity of PMMA (1.15–1.3) was lower than that monitored when the *t*-butyl analogue (**9**) was used ( $M_w/M_n \approx 1.6$ ). By contrast, the homobimetallic ruthenium-benzylidene complexes **12** containing a Schiff base ligand were devoid of catalytic activity toward ATRP of (meth)acrylates. On the other hand, heterobimetallic complexes bearing a dihalotitanocene fragment (**13a** and **13b**) were also highly efficient catalyst precursors, as they led to a well-behaved polymerisation process with a satisfactory control over the molecular weight distribution. On the contrary, with the dibenzoate analogue (**13c**), the polymerisation stopped after a few hours of reaction, affording nevertheless a polymer with a decent polydispersity. To sum up, the results clearly demonstrate that ancillary ligands exert a critical influence on the catalytic activity of homo- and heterobimetallic ruthenium complexes and, in addition, these bimetallic complexes significantly broaden the application field of their monometallic predecessors **1–3**. A cooperative effect between both metal fragments has been suggested.



## Experimental

The same protocol was followed for all the polymerisation tests of methyl methacrylate: ruthenium complex (0.0117 mmol) was placed in a glass tube containing a bar magnet and capped by a three-way stopcock. The reactor was purged of air (three vacuum–nitrogen cycles) before methyl methacrylate (1 mL, 9.35 mmol) and the initiator (ethyl 2-bromo-2-methylpropionate 0.1 M in toluene, 0.25 mL) were added ( $[MMA]_0/[initiator]_0/[Ru]_0 = 800:2:1$ ). The mixture was heated in a thermostated oil bath for 16 h at 85 °C and, after cooling, dissolved in THF and the product precipitated in heptane. The polymer was filtered off and dried overnight under vacuum.

$M_n$  and  $M_w/M_n$  were determined by size-exclusion chromatography with PMMA calibration.

Initiation efficiency,  $f = M_{n, \text{ theor.}}/M_{n, \text{ exp.}}$  with  $M_{n, \text{ theor.}} = ([MMA]_0/[initiator]_0) \times M_w(MMA) \times \text{conversion}$ .

## Acknowledgements

We are grateful to the ‘Fonds National de la Recherche Scientifique’ (F.N.R.S.), Brussels, for the purchase of major instrumentation, and the ‘Fonds pour la Formation à la Recherche dans l’Industrie et dans l’Agriculture’ (F.R.I.A.) for a fellowship to D.B. Financial support from the C.G.R.I. in the frame of the scientific cooperation between Wallonia-Brussels (Belgium) and France (Partenariat Hubert Currien) is also gratefully acknowledged.

## References

1. (a) Demonceau, A.; Stumpf, A. W.; Saive, E., Noels, A. F. *Macromolecules* **1997**, *30*, 3127. (b) Jan, D.; Delaude, L.; Simal, F.; Demonceau, A.; Noels, A. F. *J. Organomet. Chem.* **2000**, *606*, 55.
2. (a) Simal, F.; Demonceau, A.; Noels, A. F. *Angew. Chem. Int. Ed.* **1999**, *38*, 538. (b) Simal, F.; Sebillle, S.; Hallet, L.; Demonceau, A.; Noels, A. F. *Macromol. Symp.* **2000**, *161*, 73. (c) Simal, F.; Jan, D.; Delaude, L.; Demonceau, A.; Spirlet, M.-R.; Noels, A. F. *Can. J. Chem.* **2001**, *79*, 529.
3. For recent reviews, see: (a) Jafarpour, L.; Nolan, S. P. *Adv. Organomet. Chem.* **2001**, *46*, 181. (b) Herrmann, W. A.; Weskamp, T.; Böhm, V. P. W. *Adv. Organomet. Chem.* **2002**, *48*, 1. (c) Herrmann, W. A. *Angew. Chem. Int. Ed.* **2002**, *41*, 1290. (d) Dragutan, I.; Dragutan, V.; Delaude, L.; Demonceau, A. *Arkivoc* **2005**, (*x*), 206. (e) Dragutan, V.; Dragutan, I.; Delaude, L.; Demonceau, A. *Coord. Chem. Rev.* **2007**, *251*, 765.
4. Delaude, L.; Demonceau, A.; Noels, A. F. *Curr. Org. Chem.* **2006**, *10*, 203.
5. (a) Delaude, L.; Demonceau, A.; Noels, A. F. *Chem. Commun.* **2001**, 986. (b) Delaude, L.; Szypa, M.; Demonceau, A.; Noels, A. F. *Adv. Synth. Catal.* **2002**, *344*, 749. (c) Maj, A. M.; Delaude, L.; Demonceau, A.; Noels, A. F. *J. Organomet. Chem.* **2007**, *692*, 3048.

6. Richel, A.; Delfosse, S.; Cremasco, C.; Delaude, L.; Demonceau, A.; Noels, A. F. *Tetrahedron Lett.* **2003**, *44*, 6011.
7. Delaude, L.; Delfosse, S.; Richel, A.; Demonceau, A.; Noels, A. F. *Chem. Commun.* **2003**, 1526.
8. Quebatte, L.; Solari, E.; Scopelliti, R.; Severin, K. *Organometallics* **2005**, *24*, 1404.
9. Haas, M.; Solari, E.; Nguyen, Q. T.; Gautier, S.; Scopelliti, R.; Severin, K. *Adv. Synth. Catal.* **2006**, *348*, 439.
10. Takahashi, H.; Ando, T.; Kamigaito, M.; Sawamoto, M. *Macromolecules* **1999**, *32*, 6461.
11. Sauvage, X.; Borguet, Y.; Noels, A. F.; Delaude, L.; Demonceau, A. *Adv. Synth. Catal.* **2007**, *349*, 355.
12. Tang, W.; Tsarevsky, N. V.; Matyjaszewski, K. *J. Am. Chem. Soc.* **2006**, *128*, 1598.
13. Solari, E.; Antonijevic, S.; Gauthier, S.; Scopelliti, R.; Severin, K. *Eur. J. Inorg. Chem.* **2007**, 367.
14. De Clercq, B.; Verpoort, F. *Adv. Synth. Catal.* **2002**, *344*, 639.
15. De Clercq, B.; Verpoort, F. *Tetrahedron Lett.* **2002**, *43*, 4687.
16. Bareille, L.; Le Gendre, P.; Richard, P.; Moïse, C. *Eur. J. Inorg. Chem.* **2005**, 2451.
17. Kato, M.; Kamigaito, M.; Sawamoto, M.; Higashimura, M. *Macromolecules* **1995**, *28*, 1721.
18. (a) Ouchi, M.; Ito, M.; Kamemoto, S.; Sawamoto, M. *Chem. Asian J.* **2008**, *3*, 1358. (b) Ouchi, M.; Terashima, T.; Sawamoto, M. *Acc. Chem. Res.* **2008**, *41*, 1120.
19. Quebatte, L.; Solari, E.; Scopelliti, R.; Severin, K. *Organometallics* **2005**, *24*, 1404.
20. Albrecht, C.; Gauthier, S.; Wolf, J.; Scopelliti, R.; Severin, K. *Eur. J. Inorg. Chem.* **2009**, under press. doi: 10.1002/ejic.200801035
21. Sauvage, X.; Borguet, Y.; Zaragoza, G.; Demonceau, A.; Delaude, L. *Adv. Synth. Catal.* **2009**, *351*, under press. doi: 10.1002/adsc.200800664
22. Drozdak, R.; Allaert, B.; Ledoux, N.; Dragutan, I.; Dragutan, V.; Verpoort, F. *Coord. Chem. Rev.* **2005**, *249*, 3055.
23. Weskamp, T.; Kohl, F. J.; Hieringer, W.; Gleich, D.; Herrmann, W. A. *Angew. Chem. Int. Ed.* **1999**, *38*, 2416.
24. Dias, E. L.; Grubbs, R. H. *Organometallics* **1998**, *17*, 2758.
25. Gauthier, S.; Quebatte, L.; Scopelliti, R.; Severin, K. *Chem. Eur. J.* **2004**, *10*, 2811.
26. Quebatte, L.; Scopelliti, R.; Severin, K. *Angew. Chem. Int. Ed.* **2004**, *43*, 1520.

## Chapter 8

# Ruthenium Carborane Complexes in Atom Transfer Radical Polymerization

Dmitry F. Grishin, Ivan D. Grishin and Igor T. Chizhevsky

Research Institute of Chemistry, Nizhny Novgorod State University,  
Nizhny Novgorod, Russia

A. N. Nesmeyanov Institute of Organoelement Compounds, Russian  
Academy of Sciences, Moscow, Russia

Novel ruthenium complexes with carborane ligands were employed as efficient catalysts for controlled polymer synthesis via Atom Transfer Radical Polymerization (ATRP) mechanism. The ability of carborane ligands to stabilize high oxidation states of transition metals allows the proposed catalysts to be more active than their cyclopentadienyl counterparts. The proposed catalysts do not require additives such as aluminium alkoxides. It was shown that introduction of amine additives into the polymerization mixture leads to a dramatic increase of polymerization rate leaving polymerization controlled. The living nature of polymerization was proved via post-polymerization and synthesis of block copolymers.

### Introduction

Ruthenium complexes were among the first catalysts employed for controlled radical polymerization via ATRP mechanism (1, 2). On the one hand, this happened due to the fact that ATRP process originates from Kharash reaction of radical addition (3), which is catalyzed by complexes of this metal. On the other hand, this was associated with the unical properties of ruthenium atom, particularly the ability to assume different oxidation states and various coordination geometries (4-6).

Cyclopentadienyl derivatives of ruthenium were first complexes of this metal which were found to be able to catalyze ATRP (1, 7-10). Subsequently carborane (11-12) and alkylidene (13) ruthenium complexes were employed as ATRP catalysts.

In our work we proposed to use some novel *exo-nido*- (1, 3, 7) and *closo*-ruthenacarboranes (2, 4, 5, 6) as catalysts for atom transfer radical polymerization (Figure 1).

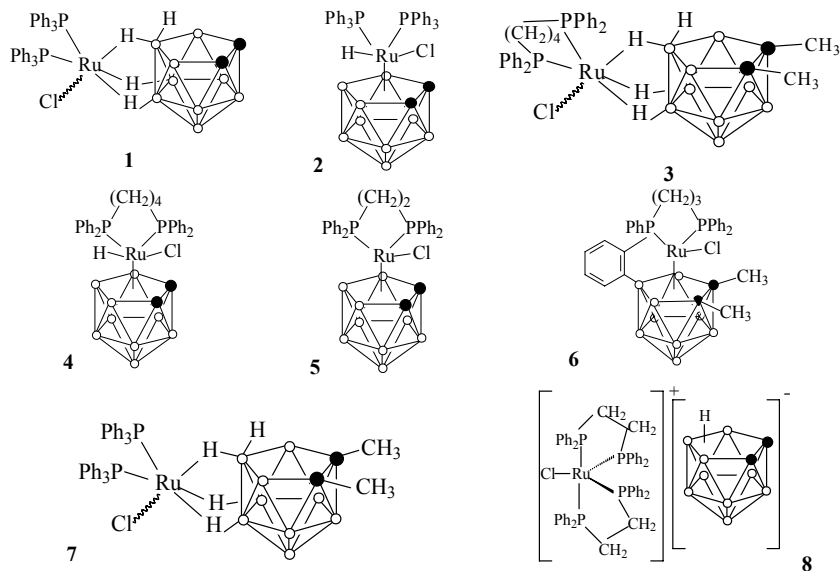


Figure 1. Structures of the examined ruthenium carborane complexes.

## Experimental

### Materials

Ruthenium carborane complexes 1-8, were synthesized under argon using anhydrous solvents, according to procedures described in the literature (14-16). Commercial phosphines and diphosphines (Strem Chemicals) were used. The obtained products were isolated and purified by column chromatography using silica gel Merck (230–400 mesh).

MMA and styrene were dried over calcium chloride and distilled under reduced pressure before use. Amines were dried and distilled over potassium hydroxide. Other solvents were purified using standard procedures (17).

## Polymerizations

Polymerizations were carried out in glass tubes under residual pressure of monomer (1.3 Pa). The monomer and exact portions of the initiator and the catalyst were placed in glass tubes, and degassed through three freeze–pump–thaw cycles in liquid nitrogen. The polymerization kinetics was monitored under isothermal conditions by the weighing method. The tube was placed in a thermostat for a strictly specified period of time. After that, the tube was taken out and frozen in liquid nitrogen to stop polymerization. The resulting polymer was dissolved into chloroform and precipitated into petroleum ether. Samples were twice reprecipitated to be cleaned of the residual monomer, initiator, and catalysts and dried in vacuum to a constant weight. After that the degree of conversion was calculated and MWDs were measured.

## Instrumentation

The MWDs of the obtained samples were determined by SEC on a Knauer setup with a linear column (Phenomenex, Linear 2). A RI Detector K-2301 differential refractometer and UV Detector K-2501 were used as the detectors for PMMA and polystyrene samples respectively. Chloroform was used as the eluent. The columns were calibrated using standard PMMA and polystyrene samples, obtained from Waters. The ChromGate software was implemented for interpretation of SEC data.

MALDI-TOF spectra of the samples were recorded via Bruker Microflex apparatus. Samples were prepared by mixing equal volumes of polymer solution in a concentration of 10g/l in THF and matrix DCTB in a concentration of 20g/l in acetone. LiTFA was added to the mixture. 1  $\mu$ l of the mixture was applied onto a stainless steel target plate.

## Results and Discussion

### Polymerization of Methyl Methacrylate and Styrene

Polymerization of methyl methacrylate (MMA) and styrene in bulk via ruthenacarboranes and carbon tetrachloride was investigated first. It was found that proposed ruthenium complexes were able to efficiently catalyze polymerization of MMA in conjunction with carbon tetrachloride as an initiator. Moreover, as follows from the data obtained (Table I), high conversion of the monomer is achieved in a number of cases. The structure of ruthenium carborane complexes (*closo* or *exo-nido*) has a substantial effect on the kinetic parameters of MMA and styrene polymerization, as well as on the molecular-weight characteristics of synthesized polymers.

**Table I. MMA and styrene polymerization in the presence of ruthenium carborane complexes (0.125 mol %) and carbon tetrachloride (0.25 mol %)**

Catalyst	MMA, $T=80^{\circ}\text{C}$				Styrene, $T=90^{\circ}\text{C}$			
	Time, h	conv, %	$M_n$	$M_w/M_n$	Time, h	conv, %	$M_n$	$M_w/M_n$
1	45	94	53500	1.6	200	98	34000	1.6
2	45	88	36000	1.6	100	89	32000	1.5
3	9	74	105000	2.7	120	99	31500	1.4
4	110	83	27000	1.2	70	89	21000	1.6
5	200	39	18000	1.2	70	91	20000	1.6
6	110	70	42000	1.4	200	68	17000	1.4
7	80	98	52000	1.9	100	88	44000	1.7
8	110	71	30000	1.5	100	96	40000	1.4

It should be mentioned that the highest conversions of MMA, namely 94 and 98% are observed for diamagnetic *exo-nido* complexes **1** and **7** with PPh<sub>3</sub> ligands at the metal center. In the presence of *exo-nido*-ruthenacarborane with the diphosphine ligand MMA conversion of 74% is reached after less than 9 h. It should also be noted that the polymers synthesized in the presence of *exo-nido* complexes have relatively high  $M_n$  and  $M_w$ , (Table I). For PMMA synthesis, the maximum molecular weights are observed in the presence of complex **3**. At the same time, the polydispersity of the samples obtained using the above complex is rather high (above 2.6). When *exo-nido* complexes **1** and **7** are employed, the polydispersity indexes are somewhat lower (Table I); however, they are rather high for polymerization processes proceeding in the living-chain mode. Thus, the obtained data suggests that the polymerization of methyl methacrylate in the presence of ruthenium *exo-nido* complexes is not controllable to a high extent.

The use of ruthenium *closo* complexes leads to polymers with markedly narrower MWDs (Table I). In particular, in the presence of ruthenium carborane complexes **4–6**, the  $M_w/M_n$  parameter does not exceed 1.4. In the case of compounds **4** and **5**, narrow-dispersed polymers are synthesized with  $M_w/M_n$  values of 1.23–1.25.

Note that MW of the samples synthesized using *closo* complexes, are noticeably lower as compared to the polymers obtained in the presence of either the *exo-nido* complexes or conventional radical initiators (such as AIBN and peroxides) where the molecular weights of polyacrylates range from several hundred thousands to several millions. Since ruthenacarboranes with the *closo* structure are more promising for the synthesis of narrow-dispersed polymers, we studied the kinetics of MMA polymerization in the presence of the above mentioned catalysts and analyzed the molecular-weight characteristics of the polymers in more detail, using complex **4** as an example.

The polymerization was found to proceed smoothly to high conversions. The time dependence of logarithmic initial-to-current monomer concentration ratio  $\ln(m_0/m)$  is linear (Figure 2, curve 1), thus indicating the absence of chain termination processes, as case inherent in polymerization proceeding in the living mode. MW of the obtained polymers increases linearly with the conversion (Figure 2). The polydispersity indexes somewhat decrease with the conversion, a fact that is also typical of controlled radical polymerization. GPC

traces of the obtained polymers are unimodal, and the peak gradually shifts toward higher molecular weights with conversion.

There is practically no difference in the polydispersity between PMMA samples prepared in the presence of the diamagnetic (18-electron) and paramagnetic (17-electron) *closo* complexes **4** and **5**, respectively. On the contrary, steric factors have a quite noticeable effect on the chain propagation step and the macromolecular characteristics of the samples. Thus, if the phosphine groups at the metal center are linked via methylene bridges (complexes **4** and **5**), favorable steric conditions for controlling the polymer chain growth probably occur that lead to the formation of polymers with MWDs much narrower than in the case of complex **2**.

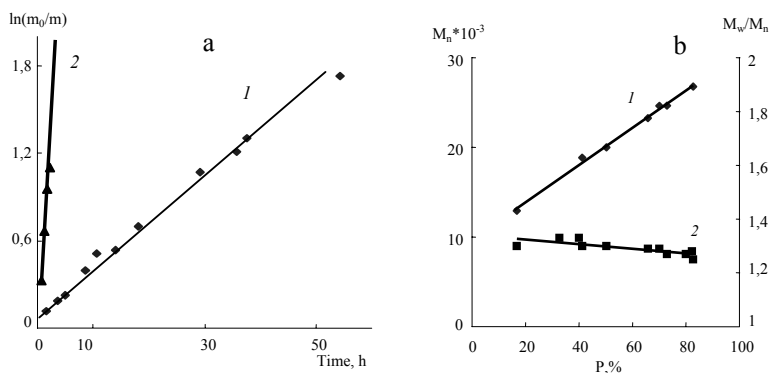


Figure 2. (a) Time dependence of  $\ln(m_0/m)$  for MMA polymerization without amine additive (1) and in the presence of *tert*-butylamine (2); (b) dependence of  $M_n$  (1) and the polydispersity index (2) on the conversion for polyMMA samples synthesized in the presence of complex **4** and  $\text{CCl}_4$  at 80 °C.

Fairly close polydispersity values of polymer samples prepared in the presence of complexes **1** and **2** having different structures may be explained by the transformation of *exo-nido* complex **1** into its *closo* isomer **2**, which is known to proceed in high yield at 80 °C (14). This transformation does not occur for the more sterically hindered C,C-dimethyl-substituted *exo-nido* complex **7**, and, in this case, a polymer with a higher polydispersity index ( $M_w/M_n = 1.93$ ) is formed. This finding indicates that the propagation step and the molecular-weight characteristics of PMMA are affected by both steric and structural features of the ruthenacarborane catalysts.

The stereoregularity of the obtained PMMA samples was investigated via NMR analysis. The obtained data showed that polymers are predominantly syndiotactic (rr:rm:mm=58:37:6), as in case of free radical polymerization of MMA initiated by AIBN (1).

The MALDI-TOF-MS analysis of the polyMMA, obtained in linear mode shows only one series of peaks, whose interval was regular, ca. 100, the molar mass of MMA unit. It indicates the absence of irreversible chain termination processes via recombination or disproportionation. According the proposed mechanism of polymerization the absolute masses of the peaks should be equal

the polyMMA with a  $\text{CCl}_3$  group at the  $\alpha$ -end, a chlorine atom at  $\omega$ -end and a lithium ion from salt used for MS analysis. So, for example for macromolecule of 84 monomer units it should be

$$35.5 \cdot 3 + 12 + 84 \cdot 100 + 35.5 + 7 = 8561$$

But the obtained data differ from calculated ones. The spectrum of the sample is shown on the Figure 3. There is only a peak with  $m/z=8517$ . The difference between predicted and obtained values is 44. This value is very close to 42.5, which equals the mass of  $\text{LiCl}$ . So the obtained data indicate that a halogen loss occurs during laser irradiation, as it is often observed for polymers, synthesized via ATRP (18). The presence of a  $\text{CCl}_3$  group at the  $\alpha$ -end allows to suppose that carbon tetrachloride acts as a monofunctional initiator when it is used for MMA polymerization.

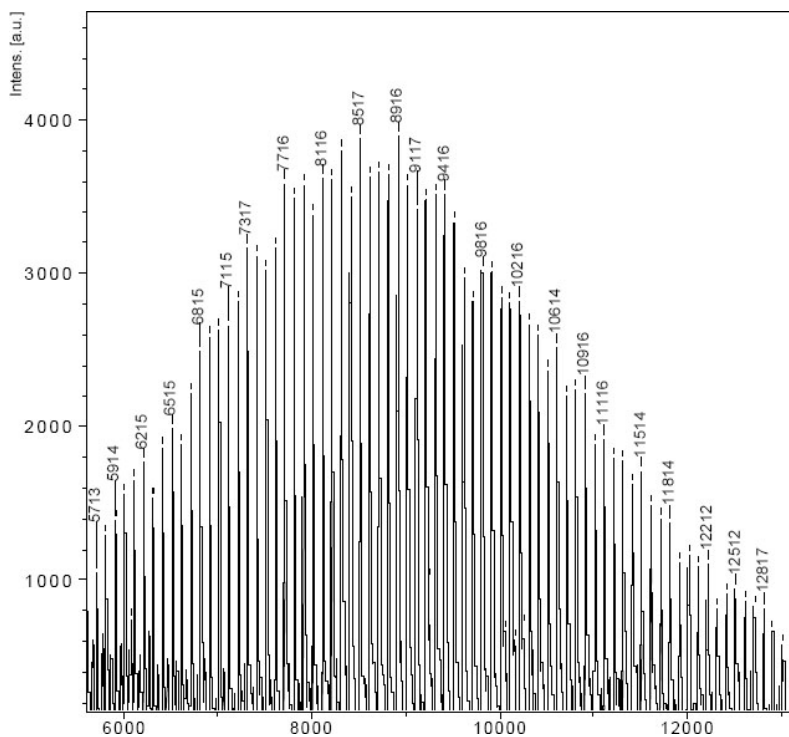


Figure 3. The MALDI-TOF mass spectrum of the obtained polyMMA

For styrene polymerization in the presence of all the complexes tested, the highest polymer molecular weights are observed in the case of *exo-nido*-ruthenacarboranes (Table I). The same compounds are more promising for the attainment of maximum monomer conversion. In the presence of compounds **1** and **3**, polymerization at 90 °C proceeds to a conversion close to 100% and the synthesized samples are characterized by lower polydispersity indexes (well below two) than, for instance, PMMA samples prepared in the presence of the same complexes.

Polystyrene samples synthesized in the presence of *closo* complexes **2** and **4-6** have somewhat higher polydispersity indexes (1.37-1.62) than the PMMA



samples synthesized via the same catalysts. However, the above values are lower than those observed in the presence of *closo*-ruthenacarboranes with phosphorus- or sulfur-containing cage substituents (11).

### Post-polymerization and block-copolymerization

One of the main inherent advantages of controlled radical polymerization is the possibility of obtaining block-copolymers. Our experiments showed that polymers obtained in the presence of ruthenacarborane **4** after purification from monomer, catalyst and initiator could be used as macroinitiator for the synthesis of block-copolymers. Figure 4 illustrates the shift of molecular weight distribution of the macroinitiator after addition of new portions of monomer and catalysts and reinitiation of polymerization. Virtually all of the chains were extended, corroborating that there is no significant amount of “dead” chains, incapable for propagation. MWD of the obtained PMMA-block-polystyrene is slightly broader than that of the initial macroinitiator. However, such situation usually exists in case of extending a living chain with another monomer.

Actually, when the same macroinitiator was used in post-polymerization of MMA, MWD of the obtained polymer became narrower than that of macroinitiator. (Figure 4). Shift of GPC trace into area of high molecular weights indicates the controlled character of polymerization of MMA in the presence of ruthenacarboranes.

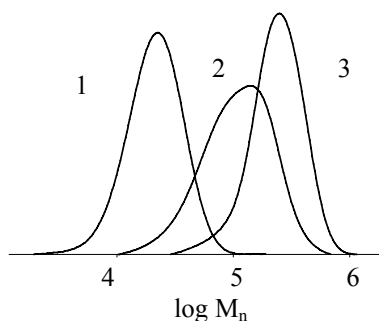
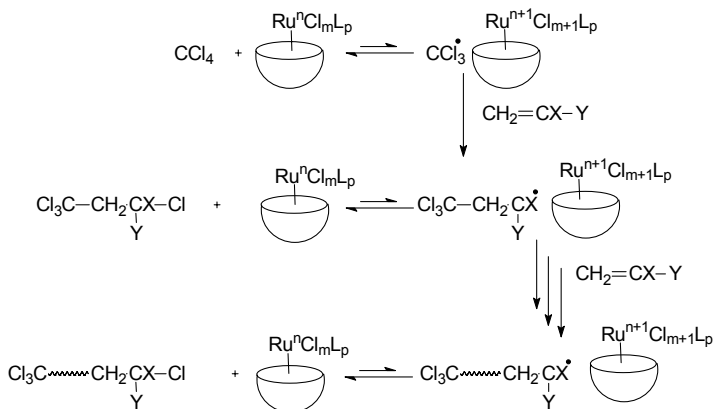



Figure 4. GPC traces of initial macroinitiator (1,  $M_n=18\ 200$ ,  $M_w/M_n=1.33$ ), PMMA-block-polystyrene (2,  $M_n=85\ 000$ ,  $M_w/M_n=1.57$ ) and post-PMMA, (3,  $M_n=207\ 000$ ,  $M_w/M_n=1.29$ )

According to our experimental data and recently published articles on living radical polymerization we propose the following mechanism for the polymerization of MMA and styrene in the presence of ruthenacarboranes:



where X – H, CH<sub>3</sub>; Y – Ph, COOCH<sub>3</sub>;

 -dicarbollide ligand;

 - propagating chain.

### Increase of polymerization rate caused by amine additives

The main disadvantage of controlled radical polymerization is its low rate, being at least two orders of magnitude lower than that of the conventional one. Recently it was shown that the rate of ATRP catalyzed by ruthenium cyclopentadienyl or alkylidene complexes may be increased by introduction of amines (19, 20).

Our investigations show that amine additives significantly accelerate controlled polymerization of MMA catalyzed by ruthenacarboranes. In particular, both *tert*-butylamine and triethylamine additions were found to result in dramatic (up to two orders of magnitude) rate increase of this process. The increase of the reaction rate was observed in case of both *closo* and *exo-nido* catalytic ruthenium systems. When *tert*-butylamine was used as an additive, MMA was smoothly polymerized up to 99% in less than 2.5 hours (Table II).

It was shown that the molecular weight of the polymer increased with monomer conversion (Figure 5), and the MWDs became narrower with the conversion. To prove the controlled nature of the polymerization of MMA in the presence of *tert*-butylamine, a post-polymerization was carried out. Fresh feeds of monomer, amine and ruthenium complex were added to the preliminary washed and dried polymer. A new portion of monomer polymerized smoothly in 5 hours.

Use of amine additives along with *exo-nido*-ruthenacarboranes resulted not only in increase of polymerization rate, but also led to narrowing of MWDs. Polymerization of MMA via complexes **3** and **7** as catalysts without amine

additives had poor control over molecular weights and produced the polymers with a broad polydispersity. Amine addition turned out as a way of improving control over polymerization process. Narrowing of MWDs was accompanied by the decrease of molecular weights. So, using amines in conjunction with *exo-nido*-ruthenacarboranes is a convenient way for increasing their regulating ability in ATRP.

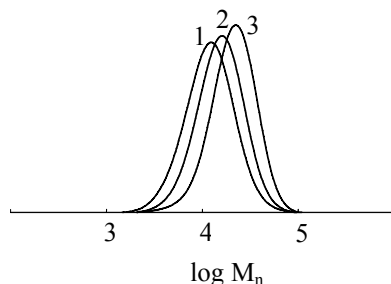


Figure 5. GPC traces of PMMA, synthesized in the presence of  $\text{CCl}_4$ , complex 4 and *tert*-butylamine. Conversion, %: 29 (1), 49 (2), 88 (3);  $M_n = 10100$  (1), 13100 (2), 18100 (3);  $M_w/M_n = 1.4$  (1), 1.4 (2), 1.3 (3).

Amines introduction into the polymerization mixture led also to a slight increase of polydispersity indexes, when *closo*-ruthenacarboranes were used as catalysts. Polydispersity of the formed polymers remained narrow (<1.5) in spite of little decrease of control over polymerization. The best control over polymerization was achieved in the presence of complexes 4 and 5, which are the most effective catalysts without additives.

**Table II. MMA polymerization in the presence of ruthenacarboranes (0.125 mol %), carbon tetrachloride (0.25 mol %) and amines (0.50 mol. %)**

Catalyst	In the presence of <i>tert</i> -butylamine				In the presence of triethylamine			
	Time, h	conv, %	$M_n$	$M_w/M_n$	Time, h	conv, %	$M_n$	$M_w/M_n$
2	2.5	97	40 500	1.7	6	87	35 000	1.6
3	2.5	99	38 000	1.5	6	91	39 000	1.6
4	2.5	97	19 000	1.3	14	97	26 500	1.4
5	2.5	95	18 000	1.3	6	91	25 000	1.3
6	6	99	36 000	1.5	6	69	30 000	1.5
7	2.5	99	37 000	1.6	2.5	89	30 000	1.5
8	2.5	99	41 000	1.6	2.5	99	40 000	1.7

Polymerization of MMA in the presence of paramagnetic ruthenium complexes is of special interest. Amine free polymerization proceeded slowly and stopped at low conversion. For example, maximum conversion of MMA catalyzed by 5 was nearly 40% in 200 hours. Introduction of *tert*-butylamine into the polymerization mixture led to fast polymerization (nearly 100% in two

hours). It is noteworthy that polydispersity index of the obtained polymers remained quite narrow ( $<1.3$ ).

The dependence of polymerization rates on the ratio of the catalyst to amine was investigated next. The obtained data show that varying this ratio from 1:1 to 1:4 has no influence on polymerization rate. Polydispersity indexes and MW do not depend on the concentration of amine. These results allow us to propose that amine does not participate in the chain transfer reactions, but interacts with ruthenium complex to generate in situ catalyst active for ATRP.

## Acknowledgments

The work was performed with the financial support of the Russian Foundation for Basic Research (project No 08-03-00100).

## References

1. Kato, M.; Kamigaito, M.; Sawamoto, M.; Higashimura, T. *Macromolecules* **1995**, *28*, 1721-1723.
2. Kamigaito, M.; Ando, T.; Sawamoto, M. *Chem. Rev.* **2001**, *101*, 3689-3745.
3. Kharash, M. S.; Jensen, E. V.; Urry, W. H. *Science* **1945**, *102*, 128-129.
4. Naota, T.; Takaya, H.; Murahashi, S-I. *Chem. Rev.* **1998**, *98*, 2599-2660.
5. Trost, B. M.; Toste, F. D.; Pinkerton, A. B. *Chem. Rev.* **2001**, *101*, 2067-2096.
6. Grishin, I. D.; Grishin, D. F. *Russ. Chem. Rev.* **2008**, *77*, 633-648.
7. Takahashi, H.; Ando, T.; Kamigaito, M.; Sawamoto, M. *Macromolecules* **1999**, *32*, 3820-3823
8. Ando, T.; Kamigaito, M.; Sawamoto, M. *Macromolecules* **2000**, *33*, 5825-5829
9. Watanabe, Y.; Ando, T.; Kamigaito, M.; Sawamoto, M. *Macromolecules* **2001**, *34*, 4370-4374
10. Kamigaito, M.; Watanabe, Y.; Ando, T.; Sawamoto, M. *J. Am. Chem. Soc.* **2002**, *124*, 9994-9995
11. Tutusaus, O.; Delfosse, S.; Simal, F.; Demonceau, A.; Noels A. F.; Nuñez, R.; Viñas, C.; Teixidor, F. *Inorg. Chem. Commun.* **2002**, *5*, 941-945.
12. Simal, F.; Sebillé, S.; Demonceau, A.; Noels, A. F.; Nuñez, R.; Abad, M.; Teixidor, F.; Viñas, C. *Tetrahedron Lett.* **2000**, *41*, 5347-5351.
13. Simal, F.; Demonceau, A. *Angew. Chem. Int. Ed.* **1999**, *38*, 538-540.
14. Chizhevsky, I. T.; Lobanova, I. A.; Bregadze, V. I.; Petrovskii, P. V.; Antonovich, V. A.; Polyakov, A. V.; Yanovsky, A. I.; Struchkov, Yu. T. *Mendeleev Commun.* **1991**, *1*, 47-49.
15. Cheredilin, D. N.; Balagurova, E. V.; Godovikov, I. A.; Solodovnikov, S. P.; Chizhevsky, I. T. *Russ. Chem. Bull.* **2005**, *54*, 2535-2539.
16. Grishin, I. D.; Kolyakina, E. V.; Cheredilin, D. N.; Chizhevsky, I. T.; Grishin, D. F. *Polymer Science, Ser. A.* **2007**, *49*, 1079-1085.

17. Weissberger, A.; Proskauer, E.; Riddick, J.; Toops, E. *Organic Solvents*; Interscience Publishers, INC, New York, 1955.
18. Nonaka, H.; Ouchi, M.; Kamigaito, M.; Sawamoto, M. *Macromolecules* **2001**, *34*, 2083-2088.
19. Hamasaki, S.; Kamigaito, M.; Sawamoto, M. *Macromolecules* **2002**, *35*, 2934-2940.
20. Opstal, T.; Verpoort, F. *Polym. Bull.* **2003**, *50*, 17-23.

## Chapter 9

# Controlling the Fast ATRP of N-Isopropylacrylamide in Water

Pierre-Eric Millard,<sup>1</sup> Nathalie C. Mougín,<sup>2</sup> Alexander Böker,<sup>2,§</sup>  
Axel H. E. Müller<sup>1,\*</sup>

<sup>1</sup>Makromolekulare Chemie II, <sup>2</sup>Physikalische Chemie II,  
Universität Bayreuth, D-95440 Bayreuth, Germany,  
e-mail: Axel.Mueller@uni-bayreuth.de

§Present address: Lehrstuhl für Makromolekulare Materialien und  
Oberflächen and DWI an der RWTH Aachen e.V., RWTH Aachen  
University, 52056 Aachen, Germany

The atom transfer radical polymerization (ATRP) of *N*-isopropylacrylamide (NIPAAm) conducted in pure water at low temperature (4 °C) proceeds in a controlled fashion ( $M_n/M_w \leq 1.2$ ) to near quantitative conversion. Different initiators, ligands, copper halides and ratios of copper (I) to copper (II) were investigated to enhance the control and reduce the termination. The reaction proceeds with a very fast kinetics and a high amount of Cu(II) is needed to slow down the polymerization. The generated polymers were successfully chain extended suggesting that well defined and complex architectures can be obtained.

Poly(*N*-isopropylacrylamide) (PNIPAAm) is a well-known thermo-responsive polymer and exhibits a lower critical solution temperature (LCST) of 32°C in water.<sup>1</sup> It assumes a random coil structure (hydrophilic state) below the LCST and a collapsed globular structure (hydrophobic state) above. Because of this sharp reversible transition, this polymer finds a vast array of applications, e.g., in the delivery of therapeutics, bioseparations and biosensors.<sup>2-4</sup> NIPAAm is generally polymerized via free radical polymerization. However, conventional free radical polymerization does not allow control of the molecular weight and to reach a narrow molecular weight distribution (MWD). For sophisticated

PNIPAAm-containing materials, defined molecular weight and end-group but also low polydispersity index are highly desirable.

Controlled free radical polymerization techniques have been intensively investigated during the past ten years. Nitroxide-mediated polymerization (NMP),<sup>5-7</sup> reversible addition fragmentation chain transfer (RAFT) polymerization<sup>8-10</sup> and atom transfer radical polymerization (ATRP)<sup>11, 12</sup> are the main radical polymerization techniques that allow the preparation of polymers with defined molecular weights and narrow polydispersities. Several teams have developed strategies to carry out NIPAAm polymerization with a good control. Schulte *et al.* performed this synthesis via NMP with a sterically hindered alkoxyamine and detailed mass spectrometry analysis.<sup>6</sup> In our laboratory we employed RAFT polymerization, in pure water, to obtain high molecular weight PNIPAAm with a very good control and without irreversible termination even at high conversion.<sup>13</sup>

Working in water is a great challenge and exhibits a high potential; it is an environmentally friendly solvent and also allows the presence of biological compounds like viruses, polypeptides or proteins in the polymerization process.<sup>14-17</sup> The synthesis of well-defined bioconjugates for biomedical applications has been an active area of research for many years. However before investigating the synthesis of biohybrids based on PNIPAAm, the homopolymerization in pure water has to be optimized to reach the best possible control. During the past few years, several studies have been realized in this field. Among them, Masci and co-workers were the first to report the successful ATRP of NIPAAm using a DMF/water mixture. However the experiment performed in pure water failed and a gel was formed immediately after the addition of the catalyst.<sup>18</sup> Because of the low solubility in water of usual ATRP initiators like methyl 2-bromopropionate or ethyl 2-bromoisobutyrate, a pure organic solvent or an aqueous mixture are commonly used yielding satisfactory results. Thus, Stöver and co-workers studied the influence of different alcohols and demonstrated good polymerization control especially in isopropanol by using CuCl/Me<sub>6</sub>TREN as catalyst system.<sup>19</sup> Nevertheless, to perform the polymerization in pure water another strategy used was to start from a macroinitiator, which is soluble in water. Kim *et al.* have succeeded to prepare linear PEG-*b*-PNIPAAm diblock copolymers and also hydrogel nanoparticles by ATRP of NIPAAm in water at 25 °C and 50 °C using a PEG macro-initiator.<sup>20</sup> Another example was recently described by Kizhakkedathu and co-workers. They synthesized mikto-arm star copolymers of poly(dimethylacrylamide) (PDMAAm) and PNIPAAm by sequential RAFT and ATRP from a multi-initiator-functionalized polyglycerol. The ATRP of NIPAAm was conducted after the RAFT polymerization of DMAAm in pure water in the presence of CuCl/Me<sub>6</sub>TREN. Monomodal and narrow MWD were achieved.<sup>21</sup> Additionally, several studies were performed to polymerize NIPAAm from surfaces, like gold, carbon black, polystyrene (PS) or dextran particles, directly in water.<sup>22-26</sup> Brooks and co-workers prepared PNIPAAm brushes by surface-initiated ATRP from polystyrene particles. High molecular weights (up to 800 kg/mol) and narrow MWD were obtained.<sup>27, 28</sup> However to the best of our knowledge, there is no report on the polymerization of NIPAAm via ATRP in pure water with low molecular weight water-soluble initiators.

Therefore, in the current study, we describe a novel strategy to obtain PNIPAAm via ATRP in pure water by using a fully soluble low molecular weight initiator. We detail the influence of the ratio CuBr/CuBr<sub>2</sub> or CuCl/CuCl<sub>2</sub> and of the choice of the ligand, to access this polymer with an excellent control, without irreversible termination even at high conversion and demonstrate the livingness of the process by a successful chain extension.

## Experimental

*Materials.* All chemicals and solvents were purchased from Sigma-Aldrich, Acros and Fluka at the highest available purity and used as received unless otherwise noted. NIPAAm (99%, Acros) was purified by two recrystallizations in a mixture of *n*-hexane and benzene (4:1 v:v). CuBr (98%, Aldrich) and CuCl (97%, Aldrich) were purified by stirring with acetic acid overnight. After filtration, they were washed with ethanol and ether and then dried in vacuum oven. N,N,N',N'',N'''-pentamethyldiethylenetriamine (PMDETA; 99%, Aldrich) and 1,1,4,7,10,10-hexamethyltriethylenetetramine (HMTETA; 97%, Aldrich) were distilled before use. Tris(2-dimethylaminoethyl)amine (Me<sub>6</sub>TREN) was prepared as described in the literature.<sup>29</sup> Water was obtained from a Milli-Q PLUS (Millipore) apparatus.

*Polymerization Procedure.* NIPAAm and 2-bromo-isobutyric acid (BIBA) were dissolved in 19 mL of pure water. Then CuBr/CuBr<sub>2</sub> or CuCl/CuCl<sub>2</sub>, respectively were added. Monomer concentrations and monomer/BIBA/Cu(I)/Cu(II)/Ligand ratios are given in Tables 1 and 2. The vial was capped with a rubber stopper to allow addition of the ligand and placed in an ice bath. In a second small flask, 2mL of aqueous ligand solution was prepared. Then both were deoxygenated by purging with nitrogen gas for 15 min. Afterwards 1mL of ligand solution was withdrawn with a degassed syringe and placed in the polymerization flask to start the reaction. The reaction was stopped after pre-selected time and quenched with air. PNIPAAm samples were purified by freeze-drying to remove the solvent. Then the solid was dissolved in dichloromethane and passed through a silica gel column to remove the ATRP catalyst. Finally PNIPAAm was precipitated from this solution into a 20-fold excess of diethyl ether before further analysis. The conversion of each sample was determined directly after freeze-drying by <sup>1</sup>H-NMR (in CDCl<sub>3</sub>) from the relative integration of peaks associated with the monomer in relation to those associated with the polymer. For NIPAAm, the monomer peak chosen as reference was its vinyl peak at  $\delta = 5.72\text{-}5.8$  ppm (dd,  $\text{CH}(\text{H})=$ ), which was compared to the proton peak of the isopropyl group at 4.1-3.8 ppm (m,  $\text{CH}(\text{CH}_3)_2$ ) of the polymer and monomer.

*Characterization.* Polymers were characterized by size exclusion chromatography (SEC) using a 0.05 M solution of LiBr in 2-*N*-methylpyrrolidone (NMP) as eluent. PSS GRAM columns (300 mm \* 8 mm, 7  $\mu\text{m}$ ): 10<sup>3</sup>, 10<sup>2</sup> Å (PSS, Mainz, Germany) were thermostated at 70 °C. A 0.4 wt % (20  $\mu\text{L}$ ) polymer solution was injected at an elution rate of 0.72 mL/min. RI and



UV ( $\lambda=270$  nm) were used for detection. Polystyrene standards were used to calibrate the columns, and methyl benzoate was used as an internal standard.  $^1\text{H-NMR}$  spectra were recorded on a Bruker AC-25 spectrometer in  $\text{CDCl}_3$  (reference peak  $\delta = 7.26$  ppm) at room temperature.

## Results and Discussion

### Homopolymerization of N-isopropylacrylamide

N-isopropylacrylamide (NIPAAm) was polymerized in the presence of 2-bromo-isobutyric acid (BIBA). This initiator was mainly chosen due to its high solubility in water. In addition, it has the advantage to introduce a carboxylic group to allow protein modification by active ester chemistry or post-polymerization modification.<sup>16</sup> Common ATRP initiators like methyl 2-bromopropionate and ethyl 2-bromoisobutyrate were also used but the resulting polymers always exhibited a high polydispersity index ( $\text{PDI} > 1.7$ ) and a multimodal distribution (results not shown). This absence of control can be explained by the very poor solubility of these initiators in water, which leads to a slow initiation. BIBA, as a weak acid, can partially protonate the tertiary amines used as ligands, which are weak bases<sup>30</sup> and thus destabilize a part of the copper complexes.<sup>31</sup> However the quantification of this phenomenon, which may affect the activation equilibrium of ATRP, is not investigated here due to the very efficient activity of the copper species involved in this polymerization. Another important parameter allowing for a successful polymerization is the reaction temperature. When polymerizations were carried out at room temperature with Cu(I) or with a high ratio Cu(I)/Cu(II), kinetics were extremely fast, typically less than a minute for full conversion. This very high rate of polymerization was also observed by Narumi et al. in DMF/water at 20°C. In this less polar solvent mixture, conversions of 98% were obtained after 30min only.<sup>32</sup> Moreover, due to the exothermic character of the propagation, the temperature in the medium increased drastically which accelerated the rate of polymerization but more importantly, the temperature raised at least above the LCST of PNIPAAm, leading to polymer collapse and a total loss of control. This increase in temperature during the polymerization of NIPAAm via ATRP was already described by Kuckling and co-workers for a DMF/water system. However for this solvent mixture, an increase of 5-10 K was observed which was not sufficient to observe the collapse of PNIPAAm.<sup>33</sup> To avoid this problem, a rather low monomer concentration, typically  $[\text{M}]_0 = 0.5$  M and an ice bath were used to control the heat evolution. Under these conditions all polymerizations were successfully achieved even in the absence of Cu(II).

A suitable choice of the ligand is crucial to reach a good control of NIPAAm polymerization.<sup>34</sup> Inspection of the data given in Table 1 clearly indicates that N,N,N',N'',N'''-pentamethyldiethylenetriamine (PMDETA) and 1,1,4,7,10,10-hexamethyltriethylenetetramine (HMTETA) are not the right choice to obtain a polymer with a low polydispersity when  $\text{CuCl}_2$  is not present in the media. The SEC profiles of the polymers made in the presence of PMDETA and HMTETA with CuCl only is strongly skewed towards low molecular weights, which might indicate a slow initiation step. Moreover, the

polymers have a higher molecular weight as compared to that made in presence of Me<sub>6</sub>TREN. A reasonable explanation is a low efficiency of this initiator in the presence of these two former ligands. This problem was already described in the case of BIBA.<sup>35</sup> By adding Cu(II) to the system, for PMDETA and HMTETA, kinetics slow down and the molecular weight distributions of the resulting polymers become sharper but still not below 1.2 (results not shown). Under these conditions, these two ligands do not seem to be suitable to obtain PNIPAAm with a good control. Me<sub>6</sub>TREN globally yields the best results for the different ratios of [CuCl]/[CuCl]<sub>2</sub> employed and was the ligand of choice for the continuation of the study. This ligand is known to be very active for ATRP compared to HMTETA and PMDETA.<sup>34</sup> Unfortunately it is also highly sensitive to oxygen which can drastically slow down the kinetics. Hence, kinetic reproducibility was difficult to achieve. However, the ATRP of NIPAAm in water did not exhibit any or less than few percents of termination even at full conversion. This property allowed us to solve the reproducibility problem. Therefore the reactions were always carried out at longer times than normally required to follow the kinetics, and then well defined polymers with narrow molecular weight distribution at full conversion were obtained. The complex of Cu(I) with Me<sub>6</sub>TREN is also known to disproportionate in aqueous media into Cu(0) and Cu(II).<sup>36</sup> This reaction generally leads to a loss of control of the overall process. In all our experiments with this ligand, we did not observe Cu(0) particles. Thus this reaction is possibly limited by two factors: (i) the general use of Cu(II) which displaces the equilibrium of disproportionation and (ii) by the presence of monomer and polymer which can coordinate to the complex and prevent this side-reaction.

**Table 1. Influence of the ligand on the ATRP of NIPAAm in water at 4 °C.<sup>a</sup>**

Ligand	Time min	$M_{n,exp}^b$ kg/mol	PDI <sup>b</sup>
PMDETA	95	32	1.79
HMTETA	130	29	1.94
Me <sub>6</sub> TREN	76	23	1.30

<sup>a</sup> [M]<sub>0</sub>=0.5 mol\*L<sup>-1</sup> with [M]<sub>0</sub>/[BIBA]<sub>0</sub>/[CuCl]<sub>0</sub>/[L]<sub>0</sub> = 100/1/1/1. Monomer conversion, determined by <sup>1</sup>H NMR in D<sub>2</sub>O > 99%. The theoretical-number-average molecular weight, evaluated according to the formula,  $M_n^{th}=M_M*conv*[M]_0/[BIBA]_0+M_{BIBA}$  = 11.5 kg/mol. <sup>b</sup> measured by size-exclusion chromatography (SEC) using polystyrene standards in 2-*N*-methylpyrrolidone (NMP) as eluent.

The influence of the catalyst system was also investigated by comparing CuCl- and CuBr-based systems at different ratios of [Cu(I)]/[Cu(II)]. The results are summarized in Table 2. In all cases CuBr provides a narrower molecular weight distribution of the resulting polymer than CuCl for the ATRP of NIPAAm in water, independent of the ratio [Cu(I)]/[Cu(II)] used. This effect is generally observed for acrylate polymerization. When CuCl is used the low rate of activation of the dormant species combined with the high reactivity of the secondary propagating radical lead to a lower control as compared to CuBr.<sup>37</sup>

Moreover, the deactivation rate constants for the CuBr<sub>2</sub> complexes are generally higher than for the chloride-based complexes.<sup>38</sup> As a result of the faster deactivation, better-defined polymers are obtained with the bromide system. In the case of the bromide system, already without addition of CuBr<sub>2</sub> to the reaction mixture, the polydispersity index is lower than 1.2. Here, already the addition of only a small amount of CuBr<sub>2</sub> leads to a drop in PDI around 1.1. This proves the excellent ability of this system to polymerize NIPAAm in a controlled fashion. For the chloride-based ATRP the MWD is broader but narrows by raising the amount of CuCl<sub>2</sub>. For both catalytic systems and for all the different ratios of [Cu(I)]/[Cu(II)], the SEC traces are monomodal and symmetrical. However, at full monomer conversion, especially for a low concentration of CuBr<sub>2</sub>, some SEC traces of CuBr mediated ATRP show a small amount of coupling which is the predominant termination reaction for acrylamide-based monomers. This termination was never detected even at full conversion in the case of CuCl mediated ATRP.

**Table 2. Influence of the ratio Cu(I)/Cu(II) on the ATRP of NIPAAm with Me<sub>6</sub>TREN as ligand in water at 4 °C<sup>a</sup>**

Catalyst	$\frac{[\text{BIBA}]_0/[\text{Cu(I)}]_0}{[\text{Cu(II)}]_0/[\text{L}]_0}$	$\frac{\text{Time}}{\text{min}}$	$\frac{M_{n,\text{exp}}^b}{\text{kg/mol}}$	PDI <sup>b</sup>
CuCl/CuCl <sub>2</sub>	1/1/0/1	76	23	1.30
CuCl/CuCl <sub>2</sub>	1/0.6/0.4/1	85	16	1.25
CuCl/CuCl <sub>2</sub>	1/0.5/0.5/1	90	16.5	1.20
CuBr/CuBr <sub>2</sub>	1/1/0/1	60	17	1.19
CuBr/CuBr <sub>2</sub>	1/0.85/0.15/1	100	18.5	1.08
CuBr/CuBr <sub>2</sub>	1/0.7/0.3/1	115	18	1.08
CuBr/CuBr <sub>2</sub>	1/0.6/0.4/1	130	19	1.09

<sup>a</sup>  $[\text{M}]_0 = 0.5 \text{ mol} \cdot \text{L}^{-1}$  and  $[\text{M}]_0/[\text{BIBA}]_0=100$ . Monomer conversion, determined by <sup>1</sup>H NMR in D<sub>2</sub>O > 99%. The theoretical-number-average molecular weight, evaluated according to the formula,  $M_n^{\text{th}}=M_M \cdot \text{conv} \cdot [\text{M}]_0/[\text{BIBA}]_0+M_{\text{BIBA}} = 11.5 \text{ kg/mol}$ . <sup>b</sup> measured by size-exclusion chromatography (SEC) using polystyrene standards in 2-*N*-methylpyrrolidone (NMP) as eluent.

Based on the above results, the CuBr-based catalyst with BIBA as initiator was chosen to study the kinetics due to its excellent ability to control the polymerization of NIPAAm in water at low temperature. The results are summarized in Figure 1. The polymerization was carried out in presence of Me<sub>6</sub>TREN and with a ratio  $[\text{CuBr}]/[\text{CuBr}_2] = 1/1$ . This relatively high amount of CuBr<sub>2</sub> is needed to slow down the kinetics which otherwise proceeds in less than a minute. This very fast ATRP in water was already observed for several types of monomers like poly(ethylene glycol) methacrylate, sodium 4-vinylbenzoate or dimethylacrylamide.<sup>39</sup> Tsarevsky *et al.* explained this phenomenon by some side reactions which occur during the ATRP in protic media, such as reversible dissociation and substitution (by a solvent or possibly by a polar monomer molecule) of the halide ligand from the deactivating Cu(II) complex. These

reactions lead to inefficient deactivation and therefore to faster polymerizations with unsatisfactory control.<sup>40</sup>

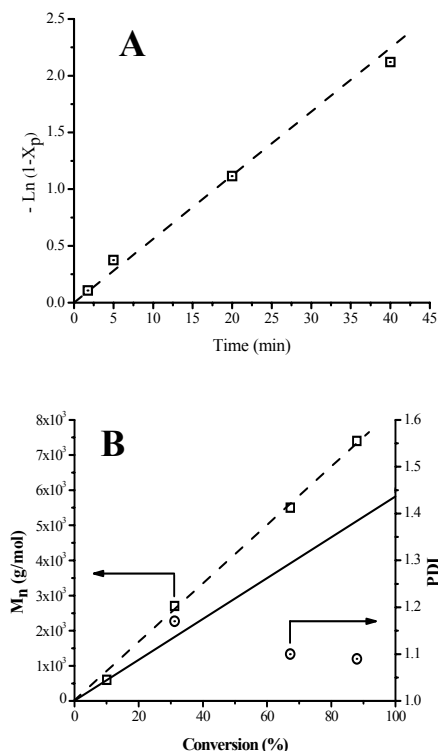


**Figure 1.** Kinetics of ATRP of NIPAAm (0.5 M) in water at 4 °C with  $[M]_0/[BIBA]_0/[CuBr]_0/[CuBr_2]_0/[Me_6TREN]_0 = 50/1/0.5/0.5/1$ . (A) First-order time-conversion plot. (B) Molecular weight and polydispersity index vs conversion. (—) theoretical number average molecular weight.

In our case the first-order time-conversion plot (Figure 1A) is linear at least up to 90% and an apparent first-order dependence on monomer concentration can be found during the major part of the polymerization. This tendency indicates the absence of side reactions. Figure 1B depicts the molecular weight and the polydispersity index evolution with the conversion. It is obvious that the molecular weight increases linearly with conversion demonstrating the controlled fashion of the process. The difference between the theoretical and the experimental molecular weight can be assigned to the calibration of the SEC on the basis of polystyrene standards. The resulting polydispersity indices are low (PDI < 1.2) and decrease with the conversion. Even at high conversions (close to 90%), the PDI is low (< 1.1). Moreover the SEC traces (not shown here) are always unimodal and symmetrical and do not show any trace of termination by recombination of growing radicals.

To prove the versatility of this process, different molecular weights of PNIPAAm were synthesized. Figure 2 indicates that an increase of the ratio of monomer/initiator leads (at a comparable conversion) to a linear increase of the molecular weight. The SEC traces display unimodal and narrow peaks. Moreover a large range of molecular weights from rather low (DP=30) to rather high (DP=400) were achieved. In all cases the PDI remains below 1.2 at full conversion, without any trace of termination. All these criteria indicate the controlled fashion of the ATRP of NIPAAm in water.

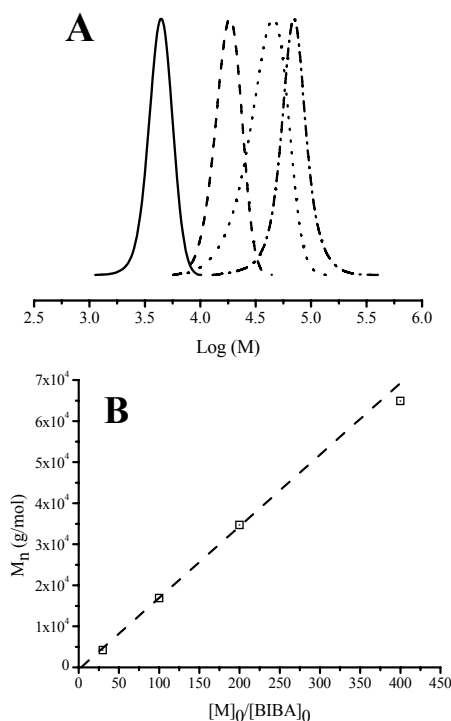


**Figure 2.** Influence of the ratio  $[monomer]/[initiator]$  for the ATRP of NIPAAm (0.5 M) in water at 4 °C with  $[BIBA]_0/[CuBr]_0/[CuBr_2]_0/[Me_6TREN]_0 = 1/0.7/0.3/1$ . (A) MWD at a ratio  $[M]_0/[BIBA]_0 =$  (—) 30, (---) 100, (•••) 200, (-•-) 400. (B) Dependence of  $M_n$  on the ratio  $[M]_0/[BIBA]_0$

### Chain Extension Experiments

To further demonstrate the livingness of the process a chain extension of PNIPAAm was carried out. The initial block was obtained by using a ratio  $[M]_0/[BIBA]_0/[CuCl]_0/[CuCl_2]_0/[Me_6TREN]_0$  of 120/1/1.6/0.4/2 with a NIPAAm concentration of 0.5 M. Then the block copolymer was synthesized by sequential addition after 38 min of a degassed aqueous solution of monomer (0.5 M) without purification of the macro-initiator. A CuCl-based catalyst was chosen to perform the reaction to avoid any termination. Indeed, in water, bromide-terminated polymers can be sensitive to halogen abstraction by nucleophilic substitution. Then with CuCl the resulting polymer-halide bound C-

Cl is much stronger and there is lower possibility of halogen abstraction. We also sometimes observed a tiny amount of termination by recombination of growing radical in the ATRP of NIPAAm with CuBr at full conversion. This termination was not really detected on any SEC traces in the case of CuCl catalyst. Because, for the chain extension, we used a strategy of direct addition of a second monomer solution, the first block has to be polymerized up to full conversion. Therefore to reduce these two different types of termination CuCl combined with Me<sub>6</sub>TREN was selected as catalyst system.

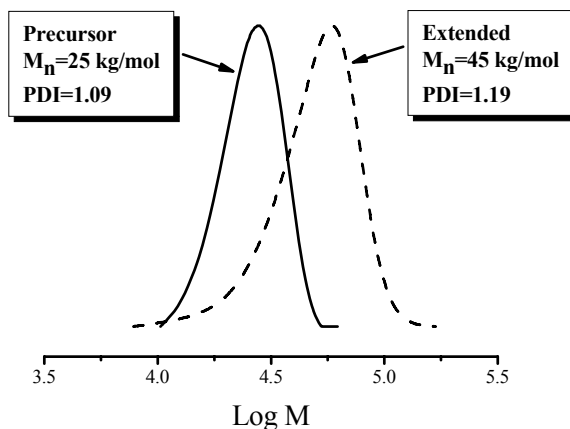


**Figure 3.** Molecular weight distribution for the chain extension of PNIPAAm by ATRP in water at 4°C.  $[M]_0=0.5\text{ M}$ ,  $[M]_0/[PNIPAAm_{120}\text{-Cl}]_0=300$ . (—) precursor, (---) extension after 40% conversion.

Figure 3 depicts the MWDs during the process. As for the homopolymerization, even for a full conversion of the first block, throughout chain extension, there is no appearance of a shoulder due to the termination by recombination. However a small tailing can be observed which might be due to a loss of terminal chloride of the precursor. Nevertheless, such evidence combined with a low PDI suggests that the large majority of the PNIPAAm precursor retained the functionality and was available for subsequent chain extension.

## Conclusions

We have demonstrated for the first time that ATRP of NIPAAm can be carried out in water at low temperature by using a low molecular weight water-soluble initiator. We also showed that by choosing an appropriate ligand and catalyst system a well-controlled polymerization can be achieved. Under these conditions, the controlled/living characteristics were proven when BIBA, CuBr/CuBr and Me<sub>6</sub>TREN were used for a large range of monomer/initiator ratios. Moreover, even at full conversion the polymerization control is maintained. The living character of the generated PNIPAAm was confirmed by subsequent chain extension directly by addition of a second portion of degassed

monomer solution. During chain extension, no side reactions were observed and the polydispersity remained low throughout the polymerization. Finally, due to the terminal carboxylic end group present on the polymer, post polymerization treatments like protein conjugation are possible. Given the environmental benefits associated with aqueous polymerizations at low temperature and the possibility to tailor a large variety of block lengths, we believe that the method reported in the present study represents a significant advance in the ability to prepare complex architectures based on this smart polymer. Results of the conjugation of PNIPAAm to proteins will be given in subsequent publications.

## Acknowledgements

This work was supported by the *Deutsche Forschungsgemeinschaft* (DFG), the Lichtenberg Program of the *VolkswagenStiftung* and by the European Union within the Marie Curie Research Training Networks “POLYAMPHI” and “BIOPOLYSURF” of the Sixth Framework Program.

## References

- 1 H. G. Schild, *Prog. Polym. Sci.* 1992, **17**, 163.
- 2 D. C. Coughlan and O. I. Corrigan, *Int J Pharm.* 2006, **313**, 163.
- 3 S. Kulkarni, C. Schilli, A. H. E. Müller, A. S. Hoffman, and P. S. Stayton, *Bioconj. Chem.* 2004, **15**, 747.
- 4 C.-C. Yang, Y. Tian, A. K. Y. Jen, and W.-C. Chen, *J. Polym. Sci., Part A: Polym. Chem.* 2006, **44**, 5495.
- 5 C. J. Hawker, A. W. Bosman, and E. Harth, *Chem. Rev.*, 2001, **101**, 3661.
- 6 T. Schulte, K. O. Siegenthaler, H. Luftmann, M. Letzel, and A. Studer, *Macromolecules*, 2005, **38**, 6833.
- 7 A. Studer and T. Schulte, *Chem. Record*, 2005, **5**, 27.
- 8 A. Favier and M.-T. Charreyre, *Macromol. Rapid Commun.*, 2006, **27**, 653.
- 9 G. Moad, Y. K. Chong, A. Postma, E. Rizzardo, and S. H. Thang, *Polymer*, 2005, **46**, 8458.
- 10 M. J. Monteiro, *J. Polym. Sci., Part A: Polym. Chem.* 2005, **43**, 3189.
- 11 K. Matyjaszewski, J. Xia, *Chem. Rev.*, 2001, **101**, 2921.
- 12 K. Matyjaszewski, J. Spanswick, B. S. Sumerlin, in *Living and Controlled Polymerization: Synthesis, Characterization and Properties of the Respective Polymers and Copolymers*. J. Jagur-Grodzinski, ed., Nova Science Publishers, New York, 2006, p. 1.
- 13 P.-E. Millard, L. Barner, M. H. Stenzel, T. P. Davis, C. Barner-Kowollik, and A. H. E. Müller, *Macromol. Rapid Commun.*, 2006, **27**, 821.
- 14 K. L. Heredia, D. Bontempo, T. Ly, J. T. Byers, S. Halstenberg, and H. D. Maynard, *J. Am. Chem. Soc.*, 2005, **127**, 16955.
- 15 X. Lou, C. Wang, and L. He, *Biomacromolecules*, 2007, **8**, 1385.
- 16 P.-E. Millard, N. C. Mougín, A. Böker, and A. H. E. Müller, *Polym. Prepr. (Am. Chem. Soc., Div. Polym. Chem.)* 2008, **49(2)**, 121.

- 17 N. C. Mougín, A. H. E. Müller, and A. Böker, *Polym. Mat. Sci. Eng.* 2008, **99**, 713.
- 18 G. Masci, L. Giacomelli, and V. Crescenzi, *Macromol. Rapid Commun.* 2004, **25**, 559.
- 19 Y. Xia, X. Yin, N. A. D. Burke, and H. D. H. Stöver, *Macromolecules*, 2005, **38**, 5937.
- 20 K. H. Kim, J. Kim, and W. H. Jo, *Polymer*, 2005, **46**, 2836.
- 21 K. Ranganathan, R. Deng, R. K. Kainthan, C. Wu, D. E. Brooks, and J. N. Kizhakkedathu, *Macromolecules*, 2008, **41**, 4226.
- 22 J. Cheng, L. Wang, J. Huo, H. Yu, Q. Yang, and L. Deng, *J. Polym. Sci., Part B: Polym. Phys.* 2008, **46**, 1529.
- 23 D. J. Kim, J.-y. Heo, K. S. Kim, and I. S. Choi, *Macromol. Rapid Commun.* 2003, **24**, 517.
- 24 D. J. Kim, S. M. Kang, B. Kong, W.-J. Kim, H.-j. Paik, H. Choi, and I. S. Choi, *Macromol. Chem. Phys.* 2005, **206**, 1941.
- 25 V. Mittal, N. B. Matsko, A. Butte, and M. Morbidelli, *Eur. Polym. J.* 2007, **43**, 4868.
- 26 A. Mizutani, A. Kikuchi, M. Yamato, H. Kanazawa, and T. Okano, *Biomaterials*, 2008, **29**, 2073.
- 27 J. N. Kizhakkedathu, K. R. Kumar, D. Goodman, and D. E. Brooks, *Polymer*, 2004, **45**, 7471.
- 28 J. N. Kizhakkedathu, R. Norris-Jones, and D. E. Brooks, *Macromolecules*, 2004, **37**, 734.
- 29 M. Ciampolini and N. Nardi, *Inorg. Chem.*, 1966, **5**, 41.
- 30 G. Golub, A. Lashaz, H. Cohen, P. Paoletti, B. Andrea, B. Valtancoli, D. Meyerstein, *Inorg. Chim. Acta*, 1997, **255**, 111.
- 31 N. V. Tsarevsky, W. A. Braunecker, A. Vacca, P. Gans, K. Matyjaszewski, *Macromol. Symp.*, 2007, **248**, 60.
- 32 A. Narumi, K. Fuchise, R. Kakuchi, A. Toda, T. Satoh, S. Kawaguchi, K. Sugiyama, A. Hirao, and T. Kakuchi, *Macromol. Rapid Commun.* 2008, **29**, 1126.
- 33 S. Mendrek, A. Mendrek, H.-J. Adler, W. Walach, A. Dworak, and D. Kuckling, *J. Polym. Sci., Part A: Polym. Chem.*, 2008, **46**, 2488.
- 34 W. Tang and K. Matyjaszewski, *Macromolecules*, 2006, **39**, 4953.
- 35 X. Zhang, J. Xia, S. G. Gaynor, and K. Matyjaszewski, *Polym. Mat. Sci. Eng.* 1998, **79**, 409.
- 36 N. V. Tsarevsky, K. Matyjaszewski, *Chem. Rev.*, 2007, **107**, 2270.
- 37 W. A. Braunecker and K. Matyjaszewski, *Prog. Polym. Sci.*, 2007, **32**, 93.
- 38 N. V. Tsarevsky, W. A. Braunecker, S. J. Brooks, K. Matyjaszewski, *Macromolecules*, 2006, **39**, 6817.
- 39 S. Perrier and D. M. Haddleton, *Macromol. Symp.* 2002, **182**, 261.
- 40 N. V. Tsarevsky, T. Pintauer, K. Matyjaszewski, *Macromolecules*, 2004, **37**, 9768.



## Chapter 10

# Controlled/“Living” Radical Polymerization of Vinyl Acetate

Huadong Tang, Maciej Radosz, Youqing Shen\*

Soft Materials Laboratory  
Department of Chemical & Petroleum Engineering  
University of Wyoming, Laramie, WY 82071  
E-mail: [sheny@uwyo.edu](mailto:sheny@uwyo.edu)

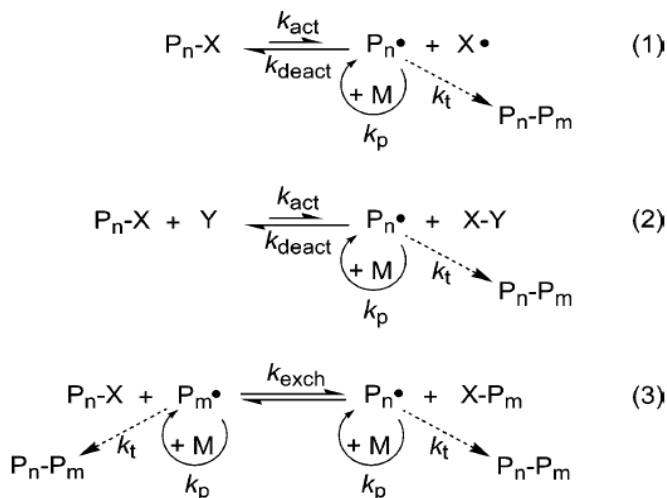
Controlled/“Living” radical polymerization (CRP) of vinyl acetate (VAc) via nitroxide-mediated polymerization (NMP), organocobalt-mediated polymerization, iodine degenerative transfer polymerization (DT), reversible radical addition-fragmentation chain transfer polymerization (RAFT), and atom transfer radical polymerization (ATRP) is summarized and compared with the ATRP of VAc catalyzed by copper halide/2,2':6',2''-terpyridine. The new copper catalyst provides the first example of ATRP of VAc with clear mechanism and the facile synthesis of poly(vinyl acetate) and its block copolymers.

## Introduction

Vinyl acetate (VAc) is one of the most important commercial vinyl monomers. The world capacity for VAc monomer was about  $4.3 \times 10^6$  tons in 1999 and  $5.0 \times 10^6$  tons in 2003, still increasing at about 100,000 tons/year.<sup>1</sup> VAc has been used as a basic chemical building block to prepare a wide variety of (co)polymers such as polyvinyl acetate (PVAc), polyvinyl alcohol (PVA), ethylene vinyl acetate copolymers, ethylene vinyl alcohol copolymers and polyvinyl acetals which have numerous applications in plastic, fiber, elastomer, coating, textile, adhesive, film, cosmetic, pharmaceutical, and photographic industries.<sup>2-4</sup> Therefore, great efforts have been made to explore the living radical polymerizations of VAc for making PVAc and PVA with controlled molecular weights and structures.

Unlike styrene, VAc is a less active monomer with the Alfrey-Price Q and e values of 0.026 and -0.22, respectively.<sup>5</sup> Its double bond is slightly electron rich and has little resonance interaction with the acetate group and thus its activity is close to ethylene or propylene other than styrene or butadiene. Consequently, VAc is easily polymerized by free radical polymerization but difficult to undergo anionic or cationic polymerization. Therefore, VAc has been polymerized with a wide range of conventional radical initiators such as azo, peroxide, hydroperoxide, redox initiator, photo initiation, and radiation initiation systems over past few decades.<sup>6</sup> Some unconventional organometallic initiators such as organoboron,<sup>7</sup> organomagnesium,<sup>8</sup> and organotitanium<sup>9</sup> have also been explored. Most of these reactions were based on a free-radical polymerization mechanism and thus the molecular weight, the molecular weight distribution, and the macromolecular architectures of the prepared PVAc were not controlled.

Recently, well-controlled narrow-dispersed PVAc has been prepared by employing controlled/"living" radical polymerization (CRP) techniques including stable free radical polymerization (SFRP), degenerative transfer polymerization (DT), reversible radical addition-fragmentation chain transfer polymerization (RAFT), and atom transfer radical polymerization (ATRP). Generally, these controlled/"living" methods include an activation step (with the rate constant  $k_{act}$ ) to generate growing radicals and a deactivation step (with the rate constant  $k_{deact}$ ) to deactivate the radicals and produce dormant species (Scheme 1 Eq. 1 and 2. The Eq. 3 represents DT and RAFT processes with the exchange rate constant  $k_{exch}$ ).<sup>10</sup> The fast reversible activation/deactivation process establishes a rapid dynamic equilibrium between the active radicals and the dormant species. Under appropriate conditions, the equilibrium substantially shifts to dormant species side with equilibrium constants  $K_{eq} = k_{act}/k_{deact}$  less than  $10^{-5}$ . Consequently, the growing radical concentration is held low and the radical termination reaction is suppressed. The terminated chains usually only contribute a few percents of total growing chains and thus can be negligible. Most of the radicals keep growing and alive, which makes these polymerizations behave like living systems. Unlike cationic and anionic living polymerizations, these controlled/"living" radical polymerizations tolerate many functional groups such as hydroxyl, carbonyl, amide, and amino groups, and can be carried out in a wide range of solvents including alcohols, water, ketones and hydrocarbons.



**Scheme 1.** General mechanisms of controlled/“living” radical polymerizations. (Reproduced with permission from American Chemical Society).<sup>10</sup>

#### CRP of VAc mediated by $\text{Al}(\text{iBu})_3/\text{Bpy}/\text{TEMPO}$

In 1994, Matyjaszewski group first reported the controlled/“living” radical polymerization of VAc initiated by the complex of  $\text{Al}(\text{iBu})_3/\text{Bpy}/\text{TEMPO}$  (Bpy = 2,2'-bipyridyl, TEMPO = 2,2,6,6-tetramethyl-1-piperidinyloxy).<sup>11</sup> In benzene at 60 °C, the semilogarithmic plots of  $\ln[\text{M}]\sim t$  were linear at different initiator concentrations (Figure 1), indicating the polymerization was first order with respect to monomer concentration and the concentration of growing radicals remained constant during the polymerization.

The molecular weight of prepared PVAc increased linearly with monomer conversion (Figure 2) and the molecular weight distribution ( $\text{PDI} = M_w/M_n$ ) was lower than 1.3, which suggested the radical termination in the polymerization was minimal and the polymerization was a controlled/ “living” process.

Many parameters affected the activity of  $\text{Al}(\text{iBu})_3/\text{Bpy}/\text{TEMPO}$ . For example, the initiator activity was dramatically changed when the  $[\text{TEMPO}]/[\text{Al}]$  ratio increased from 1 to 4. Aging of the initiation system also significantly influenced the polymerization kinetics and the system was very sensitive to moisture, oxygen and impurities.<sup>11</sup> Thus, the detailed polymerization mechanism of this system was not entirely clear.<sup>12</sup>

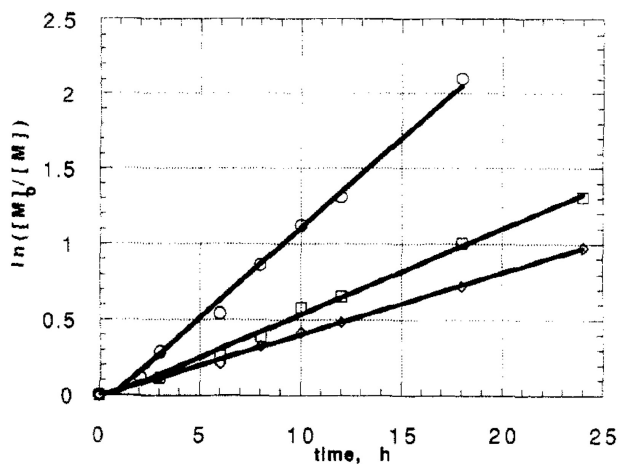


**Figure 1.** Kinetic plots for the polymerization of VAc initiated by  $Al(iBu)_3/Bpy/TEMPO$  (1:1:2) in benzene at 60 °C. Initiator concentration: 0.3 M ( $\square$ ) 0.05 M ( $\circ$ ); 0.01 M ( $\diamond$ ). (Reproduced with permission from American Chemical Society).<sup>11</sup>

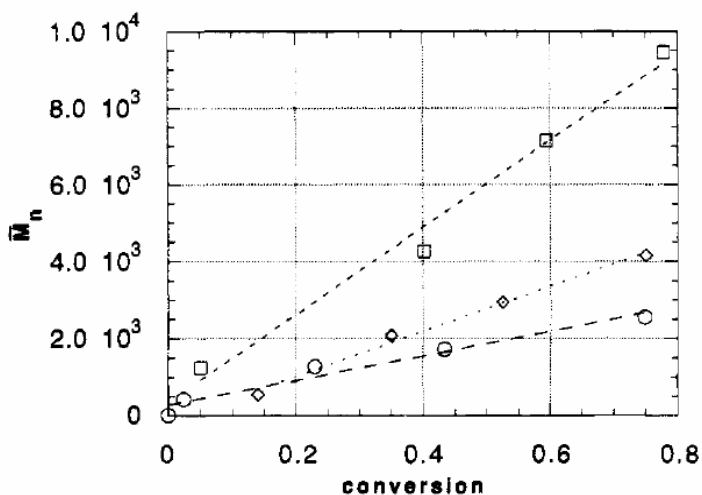
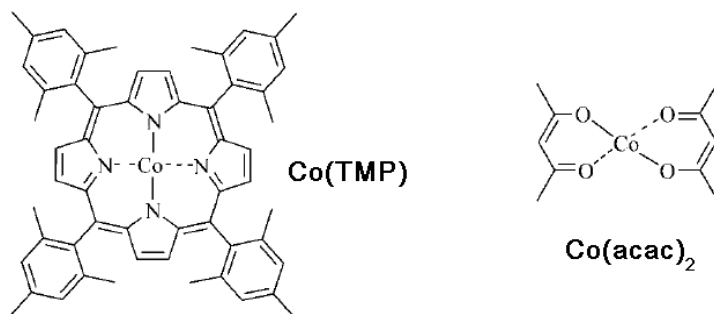


**Figure 2.** Molecular weight-conversion dependence for VAc polymerization initiated by  $Al(iBu)_3/Bpy/TEMPO$  (1:1:2). Initiator concentration  $[I]_0$ : 0.05 M, 60 °C ( $\square$ ); 0.05 M, 20 °C ( $\circ$ ); 0.3 M, 60 °C ( $\diamond$ ). (Reproduced with permission from American Chemical Society).<sup>11</sup>

## CRP of VAc mediated by organometallic compounds

### CRP of VAc mediated by organocobalt complexes

Certain organometallic compounds can be used to mediate controlled/"living" radical polymerization due to their liable and reversibly-cleavable metal-carbon bond. For example, organocobalt complex, such as tetramesitylporphyrinato Co(II) complex [Co(TMP)], has been used to mediate the CRP of acrylates.<sup>13</sup> The first successful cobalt-mediated CRP of VAc was reported by Debuigne and Jérôme et. al. using cobalt(II) acetylacetonate complex  $\text{Co}(\text{acac})_2$  (Scheme 2).<sup>14</sup>



**Scheme 2.**  $\text{Co}(\text{TMP})$  and  $\text{Co}(\text{acac})_2$

Figure 3 shows the molecular weight versus conversion plot for the polymerization of VAc mediated by  $\text{Co}(\text{acac})_2$ . The plot was linear and passed the origin, and the polydispersity of the prepared PVAc was lower than 1.3, indicative of "living" features of the polymerization. The "living" features were further confirmed by a chain extension experiment.<sup>14</sup>

The kinetic semilogarithmic plot for this polymerization was linear but didn't pass the origin (Figure 4). A significant induction time was observed in the polymerization of VAc by  $\text{Co}(\text{acac})_2$ . This induction time was attributed to the slow conversion of Co(II) to Co(III) complex by in situ generated radicals.<sup>14</sup> This group also conducted a successful suspension polymerization of VAc in water using  $\text{Co}(\text{acac})_2$  and prepared PVAc-PS and PVA-PS block copolymers by combination of the cobalt-mediated polymerization and ATRP.<sup>15, 16</sup>

Matyjaszewski et al. systematically investigated the effect of electron donors (ED), such as pyridine and triethylamine, on the CRP of VAc with  $\text{Co}(\text{acac})_2$ .<sup>17</sup> They proposed that the polymerization mechanism of VAc with  $\text{Co}(\text{acac})_2$  in the absence of electron donor was a degenerative transfer process as shown in scheme 3(a). The polymerization in the presence of electron donor was a stable free radical polymerization controlled by the reversible homolytic cleavage of cobalt(III) dormant species as shown in scheme 3 (b).<sup>17</sup>

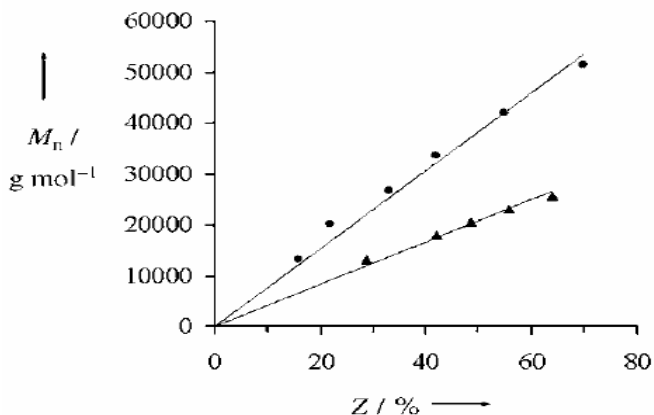


**Figure 3.** The dependence of PVAc molecular weight ( $M_n$ ) on monomer conversion ( $Z$ ) in the bulk polymerization of VAc at 30°C by  $\text{Co}(\text{acac})_2$ .  $[\text{VAc}]/[\text{Co}(\text{acac})_2] = 542$  (▲) and 813 (●). (Reproduced with permission from Wiley-VCH Verlag GmbH & Co.).<sup>14</sup>

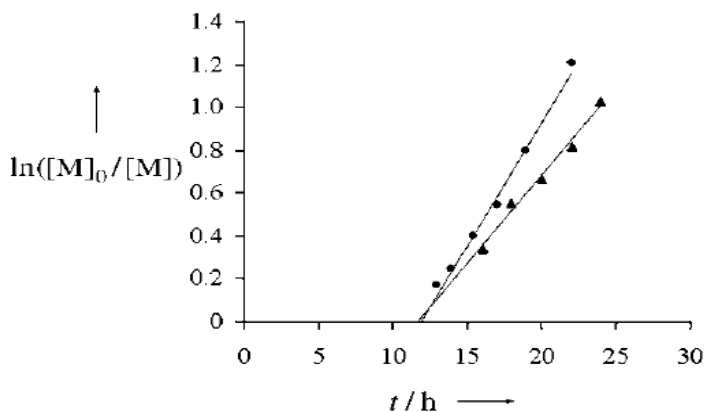
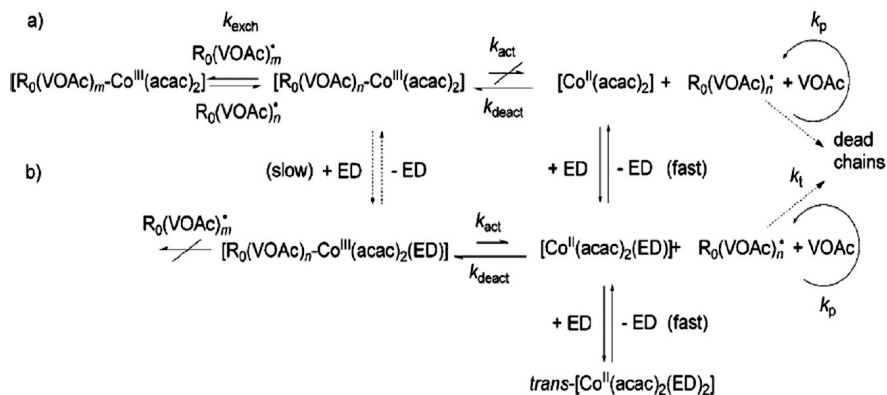


**Figure 4.** Kinetic plots for the bulk polymerization of VAc at 30°C by  $\text{Co}(\text{acac})_2$ .  $[\text{VAc}]/[\text{Co}(\text{acac})_2] = 542$  (▲) and 813 (●) (Reproduced with permission from Wiley-VCH Verlag GmbH & Co.).<sup>14</sup>



**Scheme 3.** Proposed mechanism for the CRP of VAc mediated by  $\text{Co}(\text{acac})_2$  in the (a) absence and (b) presence of electron donors. (Reproduced with permission from Wiley-VCH).<sup>17</sup>

Very recently, Wayland et al. found that the  $\text{Co}(\text{TMP})$  complex polymerized VAc in a controlled/“living” manner and the polymerization mechanism was a degenerative transfer process.<sup>18</sup> The authors subsequently investigated in detail the exchange of organic radicals between solution and organo-cobalt complexes. The interchange rate of organic radicals in solution with the latent radical in organo-cobalt complexes was determined to be  $7 \times 10^5 \text{ M}^{-1} \text{ s}^{-1}$ .<sup>19</sup> This fast radical exchange of organo-cobalt complexes with freely diffusing radicals in solution provided best support and explanation of the degenerative transfer mechanism in the polymerization of VAc mediated by the  $\text{Co}(\text{TMP})$  complex.

A well-defined PVAc-*b*-poly(acrylonitrile) block copolymer was prepared by Debuigne et al. using PVAc- $\text{Co}(\text{acac})_2$  as macroinitiator. The hydrolysis of this block copolymer produced the double hydrophilic pH- responsive poly(vinyl alcohol)-*b*-poly(acrylic acid) block copolymer.<sup>20</sup> The polymerization kinetics of acrylonitrile, the effects of reaction temperature and the solvent on the polymerization were subsequently examined.<sup>21</sup> In another study, the authors isolated two different cobalt species from the oligomeric PVAc- $\text{Co}(\text{acac})_2$  adducts and characterized their structures using many techniques.<sup>22</sup>

### CRP of VAc catalyzed by other organometallic compounds

Besides organocobalt complexes, organostibine has also been found to be able to mediate controlled/“living” polymerization of many vinyl monomers.<sup>23-26</sup> For example, Yamago et al reported that at 60 °C the polymerization of VAc mediated by  $\alpha$ -dimethylstibanyl ester reached 92% conversion in 5 h and produced narrowly dispersed PVAc (PDI = 1.26), but no detailed reaction kinetics was provided in their study.<sup>24</sup> Kamigaito et al. very recently found that a manganese carbonyl complex  $[\text{Mn}_2(\text{CO})_{10}]$  coupled with an alkyl iodide (R-I)

under visible light mediated a fast and controlled polymerization of VAc at 40 °C via a degenerative iodine transfer mechanism.<sup>27</sup>

### CRP of VAc via nitroxide mediated polymerization (NMP)

The polymerization of VAc by NMP was reported by Matyjaszewski group in 1996.<sup>28</sup> To reduce the bimolecular radical termination during the polymerization, the authors attached the stable nitroxyl radical (TEMPO: 2,2,6,6-tetramethylpiperidine-1-oxyl radical) to the interior of a dendrimer and used this modified TEMPO ([G-3]-TEMPO) as a scavenger combined with 2,2'-azobis(2-methyl-propionitrile) (AIBN) to polymerize VAc. Figure 5 shows the kinetic plot and the dependence of molecular weight on monomer conversion for the bulk polymerization of VAc at 80 °C in the presence of [G-3]-TEMPO/AIBN.

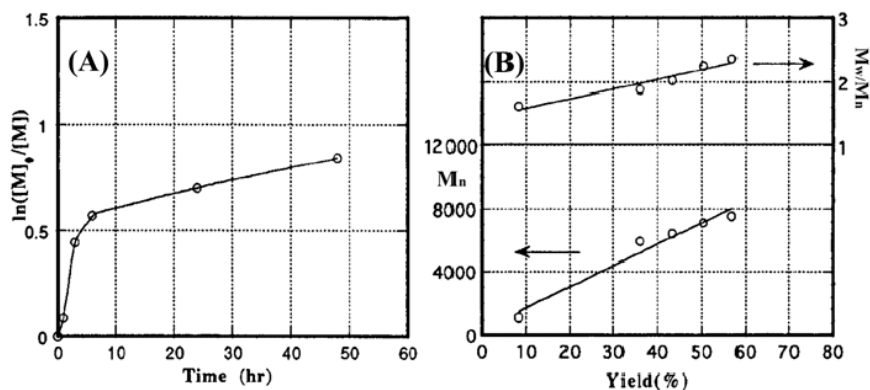


**Figure 5.** Bulk polymerization of VAc at 80 °C.  $[[G-3]-TEMPO/AIBN]_0 = 0.03$  M. (A) Kinetics. (B) Evolution of PVAc molecular weight and polydispersity with monomer conversion (Reproduced with permission from American Chemical Society).<sup>28</sup>

The linear increase of PVAc molecular weight with monomer conversion indicates that the polymerization was a controlled/“living” process. But the high polydispersity of PVAc and the nonlinearity of the semilogarithmic plot of  $\ln[M] \sim t$  suggests notable radical terminations due to the irreversible release of the growing radical chains from the cavity in the dendrimer.



*CRP of VAc by iodine-degenerative transfer polymerization (DT)*

Matyjaszewski group first succeeded in the DT of VAc using ethyl iodoacetate (EtIAc) or 2-iodopropionate as a transfer agent and AIBN or  $\alpha$ -cumyl peroxyneodecanoate as an initiator.<sup>29</sup> Typical kinetic and molecular weight versus conversion plots are shown in Figures 6 and 7. Apparently, the molecular weight increased linearly with monomer conversion and the polydispersity of the obtained PVAc was low ( $\sim 1.35$ ), suggesting the polymerization of VAc by the DT process was well controlled. End group analysis of the prepared PVAc revealed that the iodo-end group was not stable and decomposed during polymerization, resulting in aldehyde-ended polymers. In another study, VAc was polymerized by iodine transfer polymerization in fluoroalcohols to improve both molecular weight and tacticity controls.<sup>30</sup> VAc was also copolymerized with 1-alkenes by the DT process.<sup>31</sup>

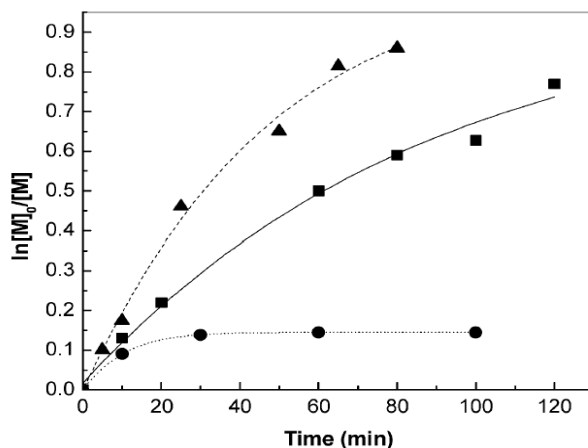


**Figure 6.** Kinetic plots for bulk polymerization of VAc with EtIAc as transfer agent and CPD as initiator (50 °C). (●)  $[VA]_0:[EtIAc]_0:[CPD]_0 = 500:1.0:0.15$ ; (■)  $[VA]_0:[EtIAc]_0:[CPD]_0 = 500:1.0:0.3$ ; (▲)  $[VA]_0:[EtIAc]_0:[CPD]_0 = 500:1.0:0.5$ . (Reproduced with permission from American Chemical Society).<sup>29</sup>

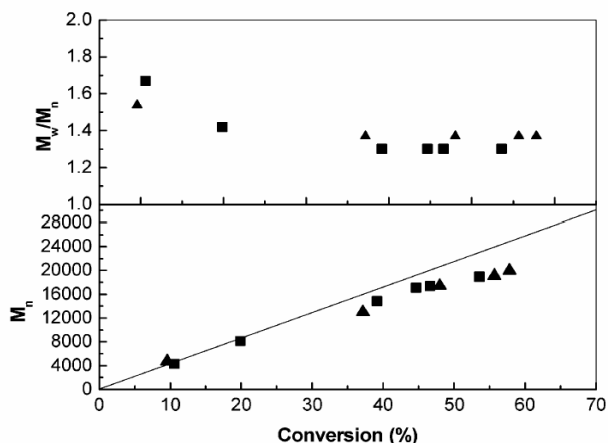
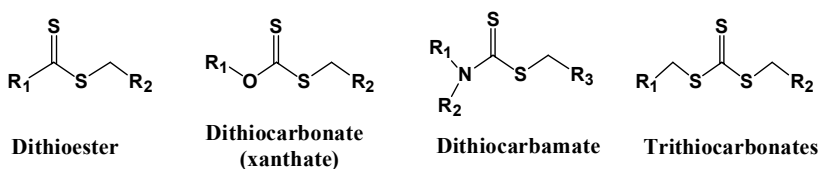


**Figure 7.** Dependence of molecular weight and polydispersity on monomer conversion for the bulk polymerization of VAc with EtIAC as transfer agent and CPD as initiator (50 °C). (■)  $[VA]_0: [EtIAC]_0: [CPD]_0 = 500:1.0:0.3$ ; (▲)  $[VA]_0: [EtIAC]_0: [CPD]_0 = 500:1.0:0.5$ . (Reproduced by the permission from American Chemical Society).<sup>29</sup>

#### CRP of VAc by reversible radical addition-fragmentation chain transfer

RAFT is a versatile controlled/"living" polymerization method and has been used for a wide range of monomers to prepare well-defined homo, block, graft, and more complexed polymer structures.<sup>32-34</sup> The detailed mechanism can be found elsewhere. The RAFT agent, a thiocarbonylthio compound, plays a major role in RAFT polymerization. To date, four types of thiocarbonylthio compounds (Scheme 4) including dithioester, dithiocarbonates (xanthates), dithiocarbamate, and trithiocarbonate have been explored as RAFT agents for the CRP of VAc.<sup>35-41</sup> Though dithioester is effective for polymerizations of styrenic and (meth)acrylic monomers, it was found to inhibit the polymerization of VAc.<sup>42</sup> Xanthates and dithiocarbamates have been successfully used to prepare well-defined PVAc. For example, Zard et al. reported dithiocarbamate as a universal RAFT agent for the polymerization of styrenic, (meth)acrylic and vinyl ester monomers.<sup>43</sup> Vana et al. polymerized VAc using methyl (ethyloxycarbonothioyl)-sulfanyl acetate (MESA) as RAFT agent and AIBN as initiator.<sup>44</sup> The polymerization was first order with respect to monomer concentration and the molecular weight of PVAc increased linearly with the monomer conversion (Figure 8), which suggested the xanthate/RAFT was an effective process for CPR of VAc.



**Scheme 4.** Thiocarbonylthio compounds explored as RAFT agents for VAc

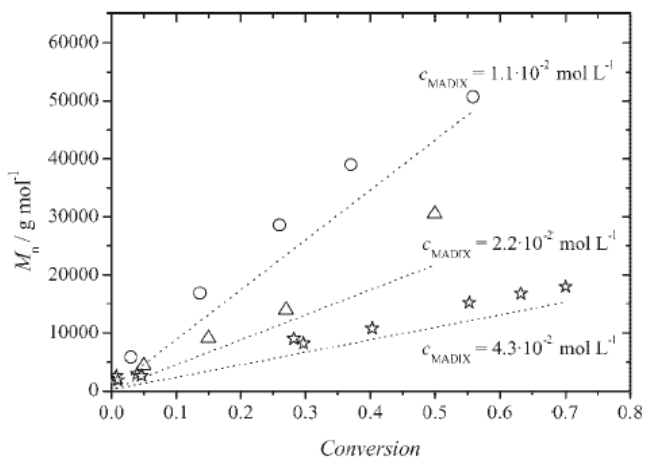
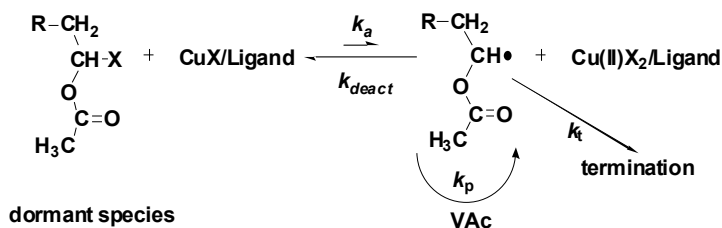


**Figure 8.** The dependence of molecular weight on monomer conversion in the bulk polymerization of VAc at 60 °C using AIBN as initiator and MESA as RAFT agent. RAFT agent concentration:  $C_{MADIX} = 1.1 \times 10^{-2}$  M ( $\circ$ );  $2.2 \times 10^{-2}$  M ( $\blacktriangle$ );  $4.3 \times 10^{-2}$  M ( $*$ ) (Reproduced with permission from WILEY-VCH Verlag GmbH & Co.)<sup>44</sup>

#### CRP of VAc by atom transfer radical polymerization (ATRP)

ATRP is one of the most powerful and versatile controlled/“living” radical polymerization techniques. A wide range of monomers including styrenic, acrylic, methacrylic and other vinyl monomers have been polymerized by ATRP to prepare well-defined homo, block, random, gradient, graft, branch, brush, star and more complex polymer structures.<sup>10, 45</sup> However, ATRP of VAc remained a challenge. In an ATRP process of VAc (Scheme 5), the carbon-halogen bond (C-Br or C-Cl) of the dormant PVAc chain is too strong to be homolytically activated for most ATRP catalysts.<sup>46</sup> Furthermore, the VAc double bond has no conjugated groups and thus the VAc propagating radical is not stabilized. The highly reactive radical easily reacts with the deactivation species such as Cu(II) complexes and thus is quickly deactivated. As a result, the VAc polymerization catalyzed by the most ATRP catalysts has low activation constants  $k_{act}$  but high deactivation constants  $k_{deact}$ , and therefore very low ATRP equilibrium constants ( $K_{eq} = k_{act}/k_{deact}$ ). Consequently, all the previous attempts to polymerize VAc by ATRP failed.

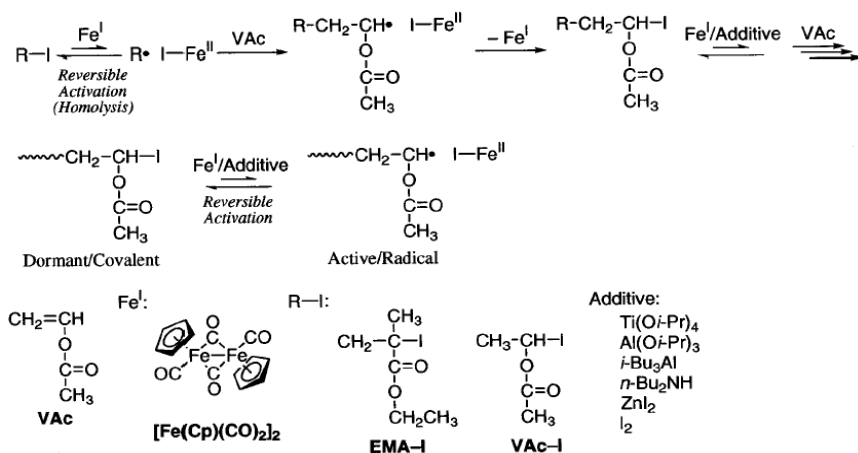


*Scheme 5. Mechanism of ATRP of VAc*

Sawamoto et al. reported in 2002 the polymerization of VAc mediated by dicarbonylcyclopentadienyliron dimer  $[\text{Fe}(\text{Cp})(\text{CO})_2]_2$  using iodide compounds as initiators and  $\text{Al}(\text{O-}i\text{-Pr})_3$  or  $\text{Ti}(\text{O-}i\text{-Pr})_4$  as an additive.<sup>47</sup> However, this catalyst system was found complicated in mechanism. The metal alkoxide additives and the iodide compounds played important roles in the polymerization of VAc. Without the additive or iodide compounds, the polymerization became extremely slow or even no polymerization occurred. Additionally, the iodine-degenerative transfer process could not be excluded in this polymerization because alkyl-iodides alone could mediate degenerative transfer polymerization of VAc, as discussed in the above section.<sup>29-31</sup> Thus, the mechanism of this polymerization system was proposed as shown in Scheme 6, but it was not verified and unclear.

We recently found a copper-based catalyst system,  $\text{CuBr}/2,2':6',2''\text{-terpyridine}$  (tPy) and  $\text{CuCl}/\text{tPy}$ , effective for the ATRP of VAc.<sup>48</sup> During our search for active catalysts for VAc, several previously reported highly active catalysts including  $\text{CuBr}/\text{Me}_6\text{TREN}$ ,<sup>49, 50</sup>  $\text{CuBr}/\text{TPEN}$ ,<sup>51, 52</sup> and  $\text{CuBr}/\text{Meco4-CYCLAM}$ <sup>53, 54</sup> were first tested for the ATRP of VAc (Table 1). These catalysts, however, either could not polymerize VAc or only polymerized VAc to very low conversions (< 10%).  $\text{CuBr}$  complexed with a cyclic ligand  $\text{Me}_4\text{CYCLAM}$  was reported to exhibit very high activity for acrylate, acrylamide and styrene monomers. The polymerization of VAc catalyzed by  $\text{CuBr}/\text{Meco}_4\text{CYCLAM}$  reached ~58% conversion in 12 h, but the produced PVAc had molecular weights unchanged with monomer conversions, indicating that the polymerization was not a controlled/“living” process but a conventional free radical polymerization.

On the contrary, we found  $\text{CuBr}$ (or  $\text{Cl}$ )/tPy was a good catalyst for the ATRP of VAc. As shown in Figure 9, the polymerizations by  $\text{CuBr}/\text{tPy}$  and  $\text{CuCl}/\text{tPy}$  proceeded smoothly and reached 70% and 80% conversion in 10 hours, substantially faster than the  $[\text{Fe}(\text{Cp})(\text{CO})_2]_2$ -catalyzed VAc polymerization (~60% conversion in 60 hours).<sup>47</sup> A slight “initial jumping” phenomenon was observed particularly for  $\text{CuBr}/\text{tPy}$  catalyzed polymerization. Both  $\ln([\text{M}]_0/[\text{M}])\text{-}t$  plots were linear, but didn't pass through the origin, indicating some radical terminations at early stages of reactions, but later the growing radical concentration basically remained constant.



**Scheme 6.** VAc polymerization mediated by  $[Fe(Cp)(CO)_2]_2$  (Reproduced with permission from American Chemical Society).<sup>47</sup>

**Table 1.** Bulk polymerizations of VAc at 70 °C by atom transfer radical polymerization using different copper catalysts\*

<i>catalyst</i>	<i>time (h)</i>	<i>conv (%)</i>	<i>M<sub>n,GPC</sub></i>	<i>PDI</i>
CuBr/HMTETA	10	no polym.	-	-
CuBr/TPMA	9	5	-	-
CuBr/Me <sub>6</sub> TREN	10	8	1500	1.85
CuBr/TPEN	8	6	1700	2.10
CuBr/Meco <sub>4</sub> CYCLAM	12	52	7700	1.82

\*[VAc] = 10.8 M, VAc/EBiB/catalyst = 150:1:1; EBiB: ethyl 2-bromoiso-butylate; HMTETA: 1,1,4,7,10,10-Hexamethyltriethylenetetramine; TPMA: tris[(2-pyridyl)methyl]amine; Me<sub>6</sub>TREN: tris[2-(dimethylamino)ethyl]amine; TPEN: *N,N,N',N'*-tetra[(2-pyridyl)methyl]ethylenediamine; Meco<sub>4</sub>CYCLAM: *N,N,N',N''*-tetra[(methoxycarbonyl)-ethyl]-1,4,8,11-tetraazacyclotetra-decane. (Adpated with permission from Wiley InterScience).

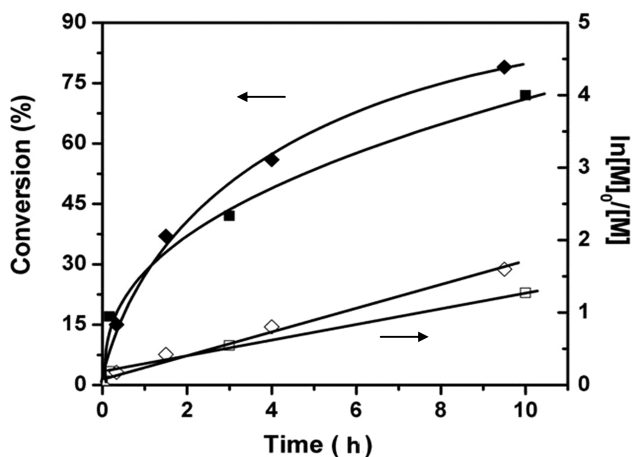


**Figure 9.** Kinetics of ATRP of VAc at 70 °C using EBiB as initiator and CuBr/tPy (■,□) or CuCl/tPy (◆,◇) as catalyst. Conditions: [VAc] = 10.8 M, [EBiB] = [CuBr/tPy] = [CuCl/tPy] = 72 mM. (Reproduced with permission from Wiley InterScience).<sup>48</sup>

Despite the fact that the molecular weight versus conversion plots didn't pass the origin (Figure 10), the molecular weight of the prepared PVAc increased linearly with monomer conversion, strongly indicative of that the copper-based catalyst indeed mediated a controlled/"living" polymerization of VAc, neither conventional free radical polymerizations nor redox-initiated radical telomerizations. The measured molecular weights of PVAc were higher than theoretical values with initiation efficiencies of about 0.75, consistent with the initial small fractions of radical terminations. The molecular weight distribution of the obtained PVAc was unimodal and the polydispersity was relatively narrow at low conversions ( $M_w/M_n \sim 1.4$  at 16% conversion) and broadened slightly at high conversions ( $M_w/M_n \sim 1.7$ , 80%). This polydispersity, however, is comparable to or even lower than that of PVAc prepared with  $[\text{Fe}(\text{Cp})(\text{CO})_2]_2$  catalyzt.<sup>47</sup>

Chain-extension polymerization of VAc was conducted to further prove the livingness of the ATRP of VAc. Figure 11 shows the GPC curves of the PVAc macroinitiator and the resulting polymer. The elution peak of the macroinitiator ( $M_n = 4500$ , PDI = 1.48) clearly shifted to the high molecular weight region ( $M_n = 10500$ , PDI = 1.64). There was a small portion of macroinitiator residue probably caused by the loss of bromine groups during the preparation or purification process of the macroinitiator. Nevertheless, this experiment again proved the living characters of the ATRP of VAc by CuBr/tPy. It also suggested a relatively high preservation of the end functionality of PVAc chains.

The terminal group of the prepared PVAc macroinitiator was analyzed by  $^1\text{H}$  NMR (Figure 12). Besides the strong peaks (peak f, d and e) from the repeat unit of VAc, small peaks (a, b, c) from initiator EBiB were also observed. The  $\omega$ -terminal methine proton (g) with a C-Br bond appeared at  $\sim 5.8$  ppm, indicating the preservation of end group in VAc polymerization. The primary C-

Br bond originated from the head-to-head chain propagation (i) was also found in the polymer. Based on the integration ratio of peak g and peak b, 89% of terminal bromide was found to be preserved. The number average molecular weight of PVAc was estimated to be 4230 from the integration of peak f and peak b, which is very close to the value (4500) measured by GPC. The presence of the terminal carbon-bromide group further proved that the VAc polymerization by the catalyst of CuBr/tPy was an ATRP process.

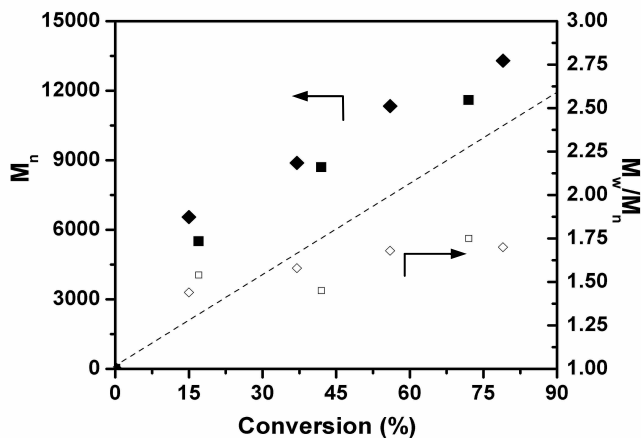


**Figure 10.** The molecular weight and polydispersity of PVAc as a function of monomer conversion for the ATRP of VAc using CuBr/tPy (■, □) and CuCl/tPy (◆, ◇) as catalysts. See Figure 9 for conditions. (Reproduced with permission from Wiley InterScience).<sup>48</sup>

Block copolymerization method was used to prepare polystyrene (PS)-b-PVAc block copolymer. A PS macroinitiator ( $M_n = 4200$ , PDI = 1.12) was synthesized by ATRP of styrene using CuBr/HMTETA as catalyst and EBiB as initiator. This macroinitiator initiated VAc in the presence of CuBr/tPy as catalyst, producing PS-b-PVAc block copolymer with slightly higher polydispersity (Figure 13). The elution peak of macroinitiator completely shifted to high molecular weight region ( $M_n = 7900$ ). No PS macroinitiators residue left, indicating complete formation of PS-b-PVAc block copolymer.

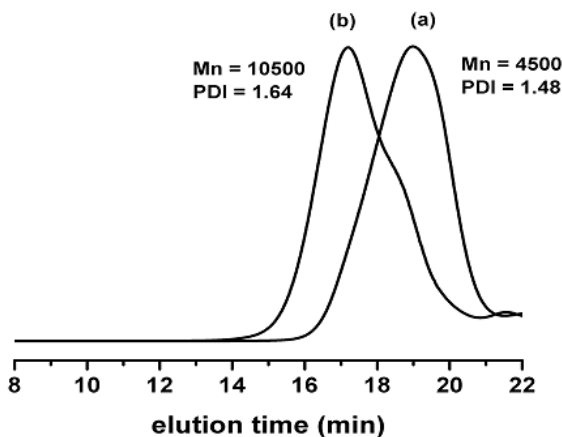


**Figure 11.** GPC curves of the PVAc macroinitiator (a) and the resulting PVAc polymer (b) in chain extension experiment. Experimental conditions: 70°C,  $[VAc] = 10.8\text{ M}$ ,  $[CuBr] = [tPy] = [PVAc_{macroini}] = 0.11\text{ M}$ . (Reproduced with permission from Wiley InterScience).<sup>48</sup>

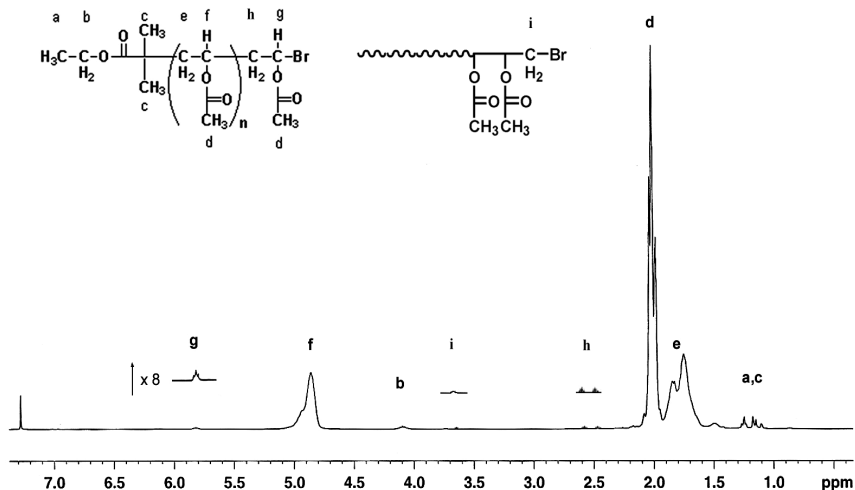


**Figure 12.**  $^1\text{H}$  NMR spectrum of PVAc prepared using CuBr/tPy as a catalyst and EBiB as an initiator. (Reproduced with permission from Wiley InterScience).<sup>48</sup>



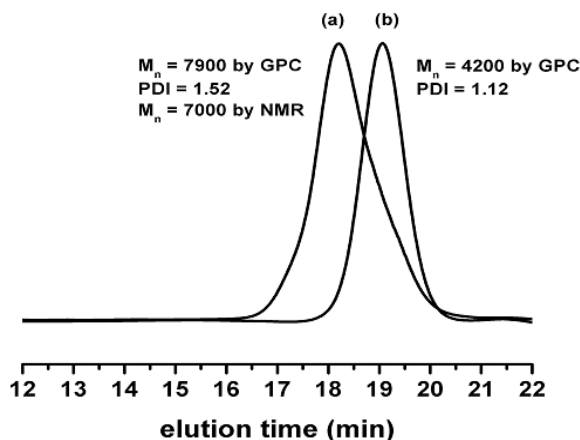


**Figure 13.** GPC curves of block copolymer PS-*b*-PVAc (a) and the corresponding PS macroinitiator (b). Conditions: 70°C, [VAc] = 10.8 M, [CuBr] = [tPy] = [PS<sub>macroini</sub>] = 0.14 M. (Reproduced with permission from Wiley InterScience).<sup>48</sup>

## Conclusion

VAc has been successfully polymerized via controlled/“living” radical polymerization techniques including nitroxide-mediated polymerization, organometallic-mediated polymerization, iodine-degenerative transfer polymerization, reversible radical addition-fragmentation chain transfer polymerization, and atom transfer radical polymerization. These methods can be used to prepare well-defined various polymer architectures based on PVAc and poly(vinyl alcohol). The copper halide/tPy is an active ATRP catalyst for VAc, providing a facile synthesis of PVAc and its block copolymers. Further developments of this catalyst will be the improvements of catalytic efficiency and polymerization control.

## References

1. Gustin, J.-L., *Chemical Health & Safety* **2005**, 36.
2. Cordeiro, C. F.; Petrocelli, F. P., *Vinyl acetate polymers*. John Wiley & Sons, Inc.: Hoboken, **2007**; Vol. 25.
3. Rhum, D., *Vinyl polymers. Poly(vinyl acetate)*. Interscience: New York, **1970**; Vol. 21.
4. Warson, H., *Vinyl acetate. 7. Applications*. Ernest Benn Ltd.: London, **1969**.
5. Young, L. J., *J. Polym. Sci.* **1951**, 54, 411.
6. Warson, H., *Vinyl acetate. 5. Polymerization*. Ernest Benn Ltd.: London, **1969**.

7. Furukawa, J.; Tsuruta, T.; Inoue, S., *J. Polym. Sci.* **1957**, 26, 234.
8. Belogorodskaya, K. V.; Nikolaev, A. F., Schibalovich, V. G., Pushkareva, L. I., *Vysokomol. Soedin. Ser. B.* **1980**, 22, 449.
9. Blandy, C.; Gervais, D.; Varion, J. P., *Eur. Polym. J.* **1984**, 20, 619.
10. Matyjaszewski, K.; Xia, J., *Chem. Rev.* **2001**, 101, 2921.
11. Mardare, D.; Matyjaszewski, K., *Macromolecules* **1994**, 27, 645.
12. Granel, C.; Jerome, R.; Teyssie, P.; Jasieczek, C. B.; Shooter, A. J.; Haddleton, D. M.; Hastings, J. J.; Gimes, D.; Grimaldi, S.; Tordo, P.; Greszta, D.; Matyjaszewski, K., *Macromolecules* **1998**, 31, 7133.
13. Wayland, B. B.; Poszmik, G.; Mukerjee, S. L.; Fryd, M., *J. Am. Chem. Soc.* **1994**, 116, 7943.
14. Debuigne, A.; Caille, J.-R.; Detrembleur, C.; Jerome, R., *Angew. Chem. Int. Ed.* **2005**, 44, 1101.
15. Debuigne, A.; Caille, J.-R.; Detrembleur, C.; Jerome, R., *Angew. Chem. Int. Ed.* **2005**, 44, 3439.
16. Debuigne, A.; Caille, J.-R.; Willet, N.; Jerome, R., *Macromolecules* **2005**, 38, 9488.
17. Maria, B.; Kaneyoshi, H.; Matyjaszewski, K.; Poli, R., *Chem.-Eur. J.* **2007**, 13, 2480.
18. Peng, C.-H.; Scricco, J.; Li, S.; Fryd, M.; Wayland, B. B., *Macromolecules* **2008**, 41, 2368.
19. Li, S.; Bruin, B. d.; Peng, C.-H.; Fryd, M.; Wayland, B. B., *J. Am. Chem. Soc.* **2008**, 130, 13373.
20. Debuigne, A.; Warnant, J.; Jérôme, R.; Voets, I.; Keizer, A. D.; Stuart, M. A. C.; Detrembleur, C., *Macromolecules* **2008**, 41, 2353.
21. Debuigne, A.; Michaux, C.; Jerome, C.; Jerome, R.; Poli, R.; Detrembleur, C., *Chem. Eur. J.* **2008**, 14, 7623.
22. Debuigne, A.; Champouret, Y.; Jerome, R.; Poli, R.; Detrembleur, C., *Chem. Eur. J.* **2008**, 14, 4046.
23. Yamago, S.; Iida, K.; Yoshida, J., *J. Am. Chem. Soc.* **2002**, 124, 2874.
24. Yamago, S.; Ray, B.; Iida, K.; Yoshida, J.; Tada, T.; Yoshizawa, K.; Kwak, Y.; Goto, A.; Fukuda, T., *J. Am. Chem. Soc.* **2004**, 126, 13908.
25. Yamago, S., *J. Polym. Sci., Part A: Polym. Chem.* **2006**, 44, 1.
26. Yamago, S.; Iida, K.; Nakajima, M.; Yoshida, J., *Macromolecules* **2003**, 36, 3793.
27. Koumura, K.; Satoh, K.; Kamigaito, M., *Macromolecules* **2008**, 41, 7359.
28. Matyjaszewski, K.; Shigemoto, T.; Frechet, J. M. J.; Leduc, M., *Macromolecules* **1996**, 29, 4167.
29. Iovu, M. C.; Matyjaszewski, K., *Macromolecules* **2003**, 36, 9346.
30. Koumura, K.; Satoh, K.; Kamigaito, M., *Macromolecules* **2006**, 39, 4054.
31. Borkar, S.; Sen, A., *J. Polym. Sci. Part A: Polym. Chem.* **2005**, 43, 3728.
32. Chiefari, J.; Chong, B.; Ercole, F.; Krstina, J.; Jeffery, J.; Le, T. P. T.; Mayadunne, R. T. A.; Meijs, G. F.; Moad, C. L.; Moad, G.; Rizzardo, E.; Thang, S. H., *Macromolecules* **1998**, 31, 5559.
33. Lowe, A. B.; McCormick, C. L., *Prog. Polym. Sci.* **2007**, 32, 283.
34. Goto, A. S. K.; Tsujii, Y.; Fukuda, T.; Moad, G.; Rizzardo, E.; Thang, S. H., *Macromolecules* **2001**, 34, 402.
35. Boschmann, D.; Vana, P., *Polym. Bull.* **2005**, 53, 231.

36. Stenzel, M. H.; Davis, T. P.; Barner-Kowollik, C., *Chem. Commun.* **2004**, 1546.
37. Russum, J. P.; Barbre, N. D.; Jones, C. W.; Schork, F. J., *J. Polym. Sci. Part A: Polym. Chem.* **2005**, 43, 2188.
38. Simms, R. W.; Davis, T. P.; Cunningham, M. F., *Macromol. Rapid Commun.* **2005**, 26, 592.
39. Bernard, J.; Favier, A.; Zhang, L.; Nilasaroya, A.; Davis, T. P.; Barner-Kowollik, C.; Stenzel, M. H., *Macromolecules* **2005**, 38, 5475.
40. Wood, M. R.; Duncalf, D. J.; Rannard, S. P.; Perrier, S. b., *Org. Lett.* **2006**, 8, 553.
41. Taton, D.; Wilczewska, A.-Z.; Destarac, M., *Macromol. Rapid Commun.* **2001**, 22, 1497.
42. Rizzardo, E.; Chiefari, J.; Mayadunne, R. T. A.; Moad, G.; Thang, S. H., *Controlled/Living Radical Polymerization: Progress in ATRP, NMP, and RAFT*. American Chem Society: Washington, **2000**.
43. Destarac, M.; Charlot, D.; Franck, X.; Zard, S. Z., *Macromol. Rapid Commun.* **2000**, 21, 1035.
44. Stenzel, M. H.; Cummins, L.; Roberts, G. E.; Davis, T. P.; Vana, P.; Barner-Kowollik, C., *Macromol. Chem. Phys.* **2003**, 204, 1160.
45. Kamigaito, M.; Ando, T.; Sawamoto, M., *Chem. Rev.* **2001**, 101, 3689.
46. Gillies, M. B.; Matyjaszewski, K.; Norrby, P.-O.; Pintauer, T.; Poli, R.; Richard, P., *Macromolecules* **2003**, 36, 8551.
47. Wakioka, M.; Baek, K. Y.; Ando, T.; Kamigaito, M.; Sawamoto, M., *Macromolecules* **2002**, 35, 330.
48. Tang, H.; Radosz, M.; Shen, Y., *AIChE J.* **2009**, DOI 10.1002/aic.11706.
49. Matyjaszewski, K.; Jakubowski, W.; Min, K.; Tang, W.; Huang, J.; Braunecker, W. A.; Tsarevsky, N. V., *Proc. Natl. Acad. Sci. U. S. A.* **2006**, 103, 15309.
50. Xia, J.; Matyjaszewski, K., *Macromolecules* **1998**, 31, 5958.
51. Tang, H.; Radosz, M.; Shen, H., *Macromol. Rapid Commun.* **2006**, 1127.
52. Tang, H.; Arulsamy, N.; Radosz, M.; Shen, Y.; Tsarevsky, N. V.; Braunecker, W. A.; Tang, W.; Matyjaszewski, K., *J. Am. Chem. Soc.* **2006**, 128, 16277.
53. Teodorescu, M.; Matyjaszewski, K., *Macromolecules* **1999**, 32, 4826.
54. Gromada, J.; Matyjaszewski, K., *Macromolecules* **2002**, 35, 6167.

## Chapter 11

# Reversible Chain Transfer Catalyzed Polymerization (RTCP) with Alcohol Catalysts

Atsushi Goto, Norihiro Hirai, Tsutomu Wakada, Koji Nagasawa,  
Yoshinobu Tsujii,\* and Takeshi Fukuda\*

Institute for Chemical Research, Kyoto University, Uji, Kyoto 611-0011,  
Japan

Alcohols (phenols, a vinyl alcohol, and an iodide derivative) worked as efficient catalysts for reversible chain transfer catalyzed polymerization (RTCP). Low-polydispersity ( $M_w/M_n \sim 1.2-1.3$ ) polystyrenes and poly(methyl methacrylate)s with predicted molecular weights were obtained with a fairly high conversion. Attractive features of the alcohol catalysts include their high reactivity (a small amount being required), low or no toxicity, and low cost (cheapness).

## Introduction

Living radical polymerization (LRP) has attracted growing attention as a powerful synthetic tool for well-defined polymers (1,2). The basic concept of LRP is the reversible activation of the dormant species Polymer-X to the propagating radical Polymer<sup>•</sup> (Scheme 1a) (1-3). A number of activation-deactivation cycles are requisite for good control of chain length distribution.

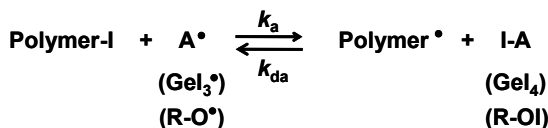
We recently developed a new family of LRP (Scheme 1b) (4-8), consisting of monomer, an alkyl iodide (dormant species: X = I), a conventional radical initiator (source of Polymer<sup>•</sup>), and a non-transition metal compound (germanium (Ge) (5,6), tin (Sn) (5,6), phosphorus (P) (6,7), or nitrogen (N) (8) compound), e.g., GeI<sub>4</sub>. GeI<sub>4</sub> works as a deactivator (I-A) of Polymer<sup>•</sup>, in situ producing GeI<sub>3</sub><sup>•</sup>. GeI<sub>3</sub><sup>•</sup> works as an activator (A<sup>•</sup>) of Polymer-I, producing Polymer<sup>•</sup> and GeI<sub>4</sub>. This cycle allows a frequent activation of Polymer-I. Mechanistically, this process is a *reversible chain transfer (RT)* with GeI<sub>4</sub> as a chain transfer agent, and Polymer-I is catalytically activated by an RT process. This is a new reversible activation mechanism, and we have proposed to term the related polymerization the RT-catalyzed polymerization (RTCP) (4,6). In this paper, the chain transfer agents (Sn, Ge, P, N, and oxygen (O) compounds (see below)) will be called RT catalysts or simply catalysts.

In RTCP, an effective activator radical (A<sup>•</sup>) undergoes no or little initiation (addition to monomer) but is still active enough to abstract iodine from Polymer-I. Phenoxy radicals (Ph-O<sup>•</sup>) are known not to initiate radical polymerization in most cases (2) and may be RTCP catalysts if they can activate Polymer-I. Based on this idea, we attempted to use phenol derivatives as catalysts, thus extending the element of the catalyst to O (Figure 1). Notably, the phenols include common antioxidants for foods and resins and natural compounds such as vitamins (Figure 1). Their commonness (hence cheapness) and environmental safety may be highly attractive for practical applications. In this paper, we will present the results of the styrene and methyl methacrylate (MMA) polymerizations, along with a mechanistic study.

### (a) Reversible activation (general scheme)



### (b) Reversible chain transfer (RT) with X = I



Scheme 1. Reversible Activation Processes. (a) General Scheme and (b) Reversible Chain Transfer.

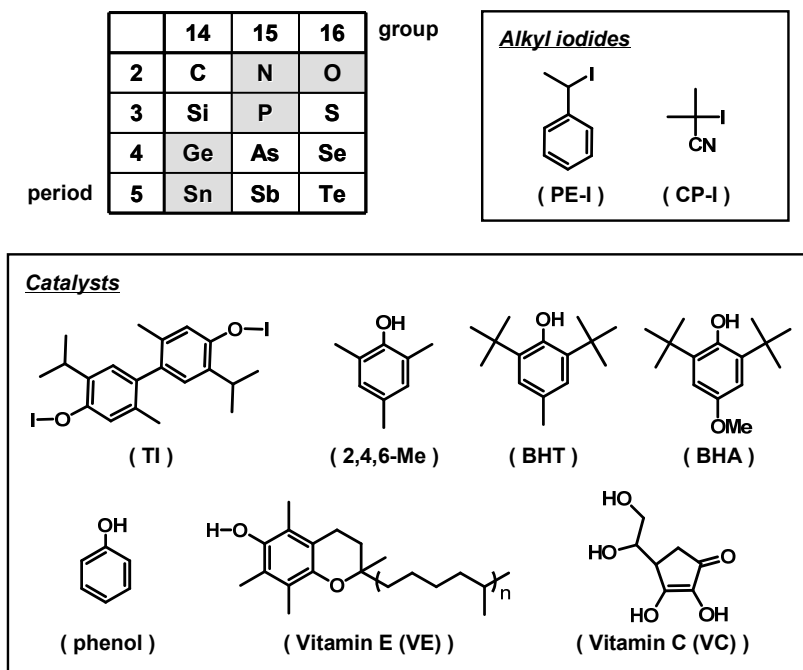


Figure 1. Table of elements and structures of catalysts and alkyl iodides.

## Experimental

### Materials

Styrene (99%, Nacalai Tesque, Japan), MMA (99%, Nacalai), and azobis(isobutyronitrile) (AIBN) (99%, Nacalai) were purified by distillation or recrystallization. 1-Phenylethyl iodide (PE-I) and 2-cyanopropyl iodide (CP-I) were prepared according to Matyjaszewski (9) and Balczewski (10), respectively. 2,2'-Azobis(2,4,4-trimethylpentane) (VR110) (99.9%, Wako Pure Chemical, Japan), *t*-butyl perbenzoate (BPB) (98%, Aldrich), di(4-*t*-butylcyclohexyl) peroxydicarbonate (PERKADOX16) (95%, Akzo), thymol iodide (TI) (95%, Wako), 2,4,6-trimethyl phenol (2,4,6-Me) (97%, Wako), 2,6-di-*t*-butyl-4-methyl phenol (3,5-di-*t*-butyl-4-hydroxy toluene (BHT)) (98%, Wako), 2,6-di-*t*-butyl-4-methoxy phenol (3,5-di-*t*-butyl-4-hydroxy anisole (BHA)) (97%, Aldrich), phenol (99%, Wako), vitamin E (VE) (99.5%, Wako), vitamin C (VC) (99%, Tokyo Kasei, Japan), and 2,2,6,6-tetramethylpiperidiny-1-oxy (TEMPO) (99%, Aldrich) were used as received.

## Gel Permeation Chromatography (GPC)

The GPC analysis was made on a Shodex GPC-101 liquid chromatograph (Tokyo, Japan) equipped with two Shodex KF-804L polystyrene (PSt) mixed gel columns (300 × 8.0 mm; bead size = 7 μm; pore size = 20–200 Å). Tetrahydrofuran (THF) was used as eluent with a flow rate of 0.8 mL/min (40 °C). Sample detection and quantification were made with a Shodex differential refractometer RI-101 calibrated with known concentrations of polymer in THF. The column system was calibrated with standard PSts and poly(methyl methacrylate)s.

## Polymerization

In a typical run, a mixture of styrene (3 mL), PE-I, VR110, and TI in a Schlenk flask was heated at 100 °C under argon atmosphere. After a prescribed time *t*, an aliquot (0.1 mL) of the solution was taken out by a syringe, quenched to room temperature, diluted by THF to a known concentration, and analyzed by GPC. The conversion was determined from the GPC peak area.

## Electron Spin Resonance (ESR) Study

In a typical run, a mixture of styrene, PE-I, BPP, and 2,4,6,-Me was degassed in an ESR tube, sealed off, and placed in the preheated ESR cavity. The spectrum was recorded at 100 °C on Bruker E500 with 100 kHz magnetic field modulation at microwave output of 5.0 mW. The system was calibrated with a degassed toluene solution of TEMPO at 100 °C. Calibration in the styrene solution is not recommendable due to the thermal initiation of styrene.

# Results and Discussion

## Thymol Iodide Catalyst

We first examined thymol iodide (TI) (Figure 1), a phenoxy iodide, as a catalyst (deactivator I-A). TI is commercially available and used as a medicine, and thymol (with an OH group instead of an OI group) is a scent component of thyme. We examined the polymerization of styrene at 100 °C, using PE-I (Figure 1) as a low-mass alkyl iodide (dormant species), VR110 as a conventional radical initiator (an azo initiator), and TI as a catalyst. In this polymerization (Scheme 1b), Polymer<sup>•</sup>, which is originally supplied by VR110, is supposed to react with TI (R-OI), in situ producing the activator radical, the thymoxy radical (R-O<sup>•</sup>) (and Polymer-I). If R-O<sup>•</sup> effectively abstracts I from PE-

I (or Polymer-I) to produce  $PE^*$  (or Polymer $^*$ ), cycles of activation and deactivation (RT) will be started. Table 1 (entry 1) and Figure 2 (filled circle) show the result. The number-average molecular weight  $M_n$  linearly increased with conversion and well agreed with the theoretical value  $M_{n,theo}$  (Figure 2). The polydispersity index (PDI or  $M_w/M_n$ , where  $M_w$  is the weight-average molecular weight) reached a low value of about 1.3 from an early stage of polymerization, indicating a high frequency of the activation-deactivation cycle. The small amount (5 mM (~500 ppm)) of TI required to control the polydispersity suggests a high reactivity of TI. This amount is as small as those of the previously studied catalysts (Sn, Ge, P, and N catalysts) (5 mM, typically). The system without TI (iodide-mediated polymerization) (Figure 2 (open circle)) gave much larger PDIs than that with TI (filled circles) (with other conditions set the same), demonstrating the effectiveness of TI.

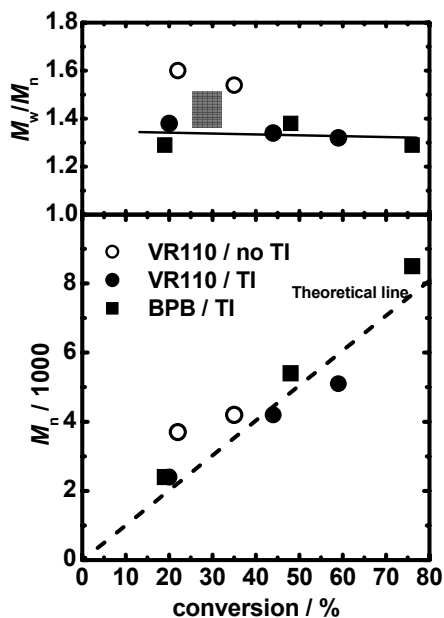


Figure 2. Plots of  $M_n$  and  $M_w/M_n$  vs conversion for the styrene polymerizations for entries 1 (●) and 2 (■) in Table 1 and for the system without TI (○) with other conditions set the same as that for entry 1.

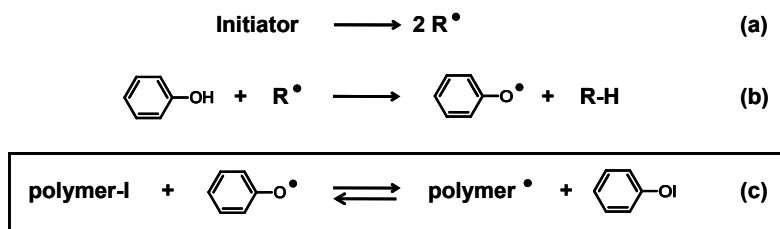


As a conventional radical initiator, the use of BPB, which decomposes faster than VR110, led to a faster polymerization (Figure 2 (filled square) and Table 1 (entry 2)). In the examined case, the conversion reached 76 % for 7 h, keeping a good polydispersity control.

**Table 1. Bulk Polymerizations of Styrene (8 M) (100 equiv to [PE-I]<sub>0</sub>) with PE-I, Conventional Radical Initiator (I), and Catalyst (100 °C).**

entry	Catalyst	I <sup>a</sup>	$\frac{[\text{PE-I}]_0/[\text{I}]_0}{[\text{Catalyst}]_0}$ (mM) <sub>b</sub>	t (h)	c <sup>c</sup> (%)	M <sub>n</sub> (M <sub>n,theo</sub> ) <sup>d</sup>	PDI
1	TI	VR110	80/80/5	24	59	5100 (5900)	1.32
2	TI	BPB	80/40/5	7	76	8500 (7600)	1.29
3	2,4,6-Me	VR110	80/80/5	24	50	4000 (5000)	1.17
4	BHT	VR110	80/80/5	24	51	4300 (5100)	1.23
5	Phenol	VR110	80/80/5	24	51	4100 (5100)	1.23
6	VE	VR110	80/80/5	24	50	4300 (5000)	1.23
7	VC	VR110	80/80/5	24	44	3500 (4400)	1.20
8	2,4,6-Me	BPB	80/40/5	7	65	6500 (6500)	1.15
9	BHT	BPB	80/40/5	7	70	6600 (7000)	1.36
10	Phenol	BPB	80/40/5	7	80	8100 (8000)	1.27
11	VE	BPB	80/40/5	7	81	8100 (8100)	1.20
12	VC	BPB	80/40/5	7	69	6500 (6900)	1.23

<sup>a</sup> VR110 = 2,2'-azobis(2,4,4-trimethylpentane) and BPB = *t*-butyl perbenzoate. <sup>b</sup>  $\frac{[\text{Styrene}]_0/[\text{PE-I}]_0/[\text{I}]_0/[\text{catalyst}]_0}{[\text{Styrene}]_0/[\text{PE-I}]_0/[\text{I}]_0/[\text{catalyst}]_0} = 100/1/1/0.0625$  for entry 1, for example. <sup>c</sup> Conversion. <sup>d</sup> Theoretical M<sub>n</sub> calculated with [styrene], [PE-I], and conversion.



*Scheme 2. Reaction scheme for precursor catalyst. The system includes initiator, phenol, and alkyl iodide (shown as polymer-I in this scheme).*

## Phenol Catalyst

For a catalyst, instead of using a deactivator (R-OI) (TI in the mentioned system), a precursor of a deactivator or an activator radical (R-O<sup>•</sup>), may be used as a starting compound. In this work, we used phenols R-OH as starting compounds (precursors), along with an alkyl iodide and a conventional radical

initiator (as in the TI system). The initiator gives a radical (Scheme 2a), which abstracts a hydrogen from R-OH to in situ produce an activator R-O $\cdot$  (Scheme 2b). The R-O $\cdot$  leads to the reversible activation (Scheme 2c).

We carried out the polymerization of styrene with PE-I, VR110, and 2,4,6-trimethyl phenol (2,4,6-Me) (Figure 1) at 100 °C (Figure 3 and Table 1 (entry 3)). With 5 mM of the phenol, small PDIs ( $\leq 1.2$ ) were achieved from an early stage to a later stage of polymerization. Thus, the precursor method was confirmed to be useful. Other phenols were also effective (Figure 3 and Table 1 (entries 4-7)). They include a common antioxidant BHT, phenol itself, a natural compound vitamin E (VE), and also a vinyl alcohol vitamin C (VC). The use of BPB (instead of VR110) led to a faster polymerization as in the TI system (Table 1 (entries 8-12)).

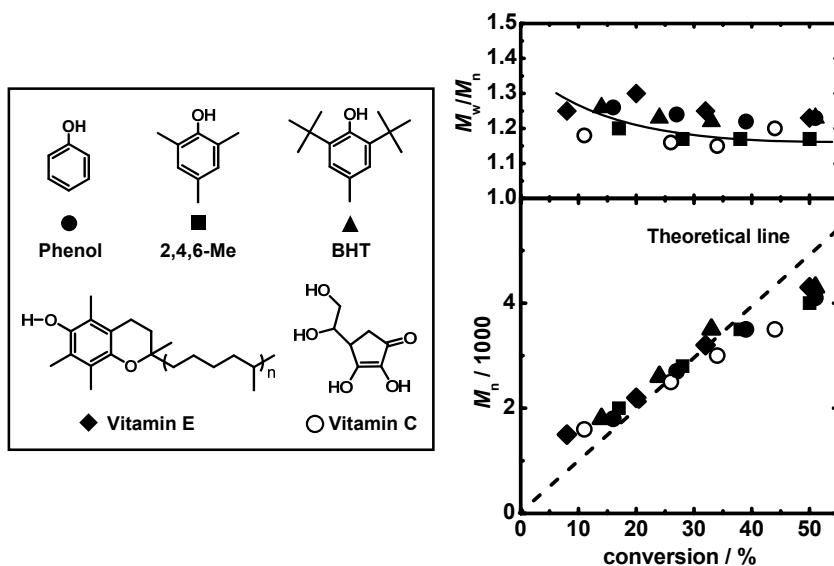


Figure 3. Plots of  $M_n$  and  $M_w/M_n$  vs conversion for the styrene polymerizations for entries 3-7.

The polymerization of MMA was also examined with the alcohols (precursors). To ensure a fast initiation from the alkyl iodide, we used a tertiary alkyl iodide, CP-I (Figure 1), instead of the secondary one, PE-I. All of the mentioned five alcohols and BHA (Figure 1) well controlled the MMA polymerization at 80 °C, as the examples in Table 2 illustrate. We are now systematically studying the relationship between the structure of alcohol and the polydispersity control, which will be reported elsewhere.

**Table 2. Bulk Polymerization of MMA (8 M) (100 or 200 equiv to [CP-I]<sub>0</sub>) with CP-I, Conventional Radical Initiator (I), and Catalyst (80 °C)**

<i>entry</i>	<i>Catalyst</i>	$[CP-I]_0/[I^a]_0/[catalyst]_0$ (mM) <sup>b</sup>	<i>t</i> (h)	<i>c</i> <sup>c</sup> (%)	<i>M<sub>n</sub></i> ( <i>M<sub>n,theo</sub></i> ) <sup>d</sup>	<i>PDI</i>
1	2,4,6-Me	80/80/10	0.5	79	6900 (7900)	1.30
2	BHA	80/80/10	1	80	7000 (8000)	1.23
3	VE	80/80/10	0.5	69	6500 (6900)	1.23
4	VE	40/40/5	1	72	12000 (14400)	1.35
5	VC	80/80/10	0.25	87	7200 (8700)	1.33

<sup>a</sup> I = PERKADOX16 (di(4-*t*-butylcyclohexyl) peroxydicarbonate). <sup>b</sup> [MMA]<sub>0</sub>/[CP-I]<sub>0</sub>/[I]<sub>0</sub>/[catalyst]<sub>0</sub> = 100/1/1/0.125 for entry 1, for example. <sup>c</sup> Conversion. <sup>d</sup> Theoretical *M<sub>n</sub>* calculated with [MMA], [PE-I], and conversion.

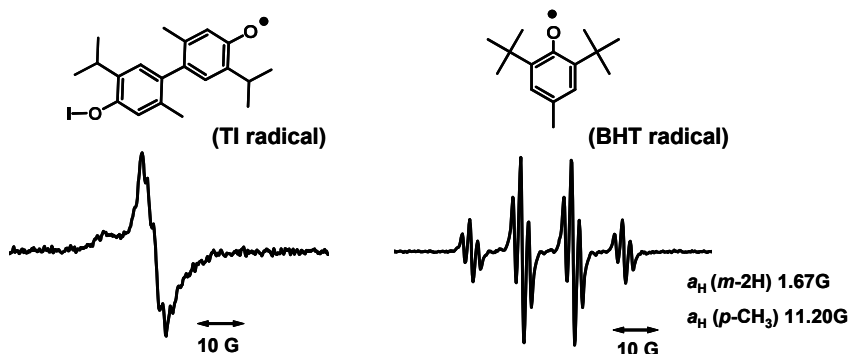


**Figure 4.** ESR spectra in the styrene polymerizations: (a) [PE-I]<sub>0</sub> = 400 mM; [AIBN]<sub>0</sub> = 200 mM; [TI]<sub>0</sub> = 150 mM (85 °C), and (b) [PE-I]<sub>0</sub> = 400 mM; [BPB]<sub>0</sub> = 200 mM; [BHT]<sub>0</sub> = 100 mM (100 °C).

### Experimental Proof for RT Process

As noted above, RTCP is supposed to involve the RT process. If RT exists, the catalyst radical (*A*<sup>•</sup> in Scheme 1b) is mediated and the propagating species is a free radical (Polymer<sup>•</sup> in Scheme 1b). Thus, we attempted to detect *A*<sup>•</sup> by ESR and confirm the free radical nature from the tacticity of the product polymer in the styrene polymerizations with TI (deactivator) and BHT (precursor).

*A*<sup>•</sup> was in fact observed in both systems (Figure 4). The spectrum for TI was broad probably due to the aggregation (association) of TI in the styrene medium, and that for BHT was clearly split into four peaks (1:3:3:1 ratio: hyperfine splitting constant *a<sub>H</sub>* = 11.20 G) by the methyl group at the para position and further split into three peaks (1:2:1 ratio: *a<sub>H</sub>* = 1.67 G) by the protons at the meta positions. In these experiments, we used a large amount (100–200 mM) of the catalyst to

facilitate the detection of  $A^{\bullet}$ . Nevertheless, the concentration of  $A^{\bullet}$  was low, on the order of  $10^{-6}$  M, in both cases, indicating that in a typical polymerization condition (with 5 mM of the catalyst), it is very low, on the order of  $10^{-8}$ – $10^{-7}$  M, and the activation (Scheme 1b) effectively occurs at such a low  $A^{\bullet}$  concentration. In Figure 4, Polymer $^{\bullet}$  (polystyrene radical) was not apparently detected due to its much lower concentration ( $10^{-8}$ – $10^{-7}$  M estimated from the polymerization rate) than that of  $A^{\bullet}$  ( $10^{-6}$  M).

The tacticity (pentad distribution) of the product polymer was analyzed by  $^{13}\text{C}$  NMR (data not shown). The tacticity was virtually the same with and without the catalyst (TI and 2,4,6-Me), meaning that the propagating species is a free radical. These results strongly indicate the existence of RT.

## Conclusions

Alcohols (phenols, a vinyl alcohol, and an iodide derivative (TI)) worked as effective catalysts for the RTCs of styrene and MMA. The existence of RT was strongly indicated by the two experiments. Attractive features of the alcohol catalysts include their high reactivity (a small amount being required), low or no toxicity, low cost (cheapness), insensitivity to air (robustness), and minor color and smell.

## Acknowledgements

This work was supported by Grants-in-Aid for Scientific Research, the Ministry of Education, Culture, Sports, Science and Technology, Japan (Grants-in-Aid 17002007 and 19750093), Industrial Technology Research Grant Program in 2007 from New Energy and Industrial Technology Development Organization (NEDO) of Japan, and Japan Science and Technology Agency (JST).

## References

1. For reviews: (a) *Handbook of Radical Polymerization*; Matyjaszewski, K.; Davis, T. P. Eds.; Wiley-Interscience: New York, **2002**. (b) Matyjaszewski, K. Ed. *ACS Symp. Ser.* **1998**, 685, **2000**, 768, **2003**, 854 & **2006**, 944. (c) Braunecker, W. A.; Matyjaszewski, K. *Prog. Polym. Sci.* **2007**, 32, 93-146.
2. *The Chemistry of Radical Polymerization*; Moad, G.; Solomon, D. H. Eds.; Elsevier, Amsterdam, **2006**.
3. For reviews on kinetics: (a) Fukuda, T. *J. Polym. Sci.: Part A: Polym. Chem.* **2004**, 42, 4743-4755. (b) Fischer, H. *Chem. Rev.* **2001**, 101, 3581-3618. (c) Goto, A.; Fukuda, T. *Prog. Polym. Sci.* **2004**, 29, 329-385.
4. Goto, A.; Tsujii, Y.; Fukuda, T. *Polymer* **2008**, 49, 5177-5185.

5. (a) Goto, A.; Zushi, H.; Kwak, Y.; Fukuda, T. *ACS Symp. Ser.* **2006**, *944*, 595-603. (b) Goto, A.; Zushi, H.; Hirai, N.; Wakada, T.; Kwak, Y.; Fukuda, T. *Macromol. Symp.* **2007**, *248*, 126-131.
6. Goto, A.; Zushi, H.; Hirai, N.; Wakada, T.; Tsujii, Y.; Fukuda, T. *J. Am. Chem. Soc.* **2007**, *129*, 13347-13354.
7. Goto, A.; Hirai, N.; Tsujii, Y.; Fukuda, T. *Macromol. Symp.* **2008**, *261*, 18-22.
8. Goto, A.; Hirai, N.; Wakada, T.; Nagasawa, K.; Tsujii, Y.; Fukuda, T. *Macromolecules* **2008**, *41*, 6261-6264.
9. Matyjaszewski, K.; Gaynor, S.; Wang, J. S. *Macromolecules* **1995**, *28*, 2093-2095.
10. Balczewski, P.; Mikołajczyk, M. *New J. Chem.* **2001**, *25*, 659-663.

## Chapter 12

# THE USE OF ATOM TRANSFER RADICAL COUPLING REACTIONS FOR THE SYNTHESIS OF VARIOUS MACROMOLECULAR STRUCTURES

Yasemin Yuksel Durmaz<sup>1</sup>, Binnur Aydogan<sup>1</sup>, Ioan Cianga<sup>1,2</sup>, Yusuf Yagci<sup>1</sup>

<sup>1</sup>Istanbul Technical University, Department of Chemistry, Maslak, Istanbul, 34469, Turkey

<sup>2</sup>Petru Poni Institute of Macromolecular Chemistry, Iasi, Romania

The use and limitations of Atom Transfer Radical Coupling (ATRC) reactions including polyrecombination reactions for the preparation of telechelic polymers, segmented block copolymers, and polycondensates are presented. Specifically, the preparation of telechelic polymers with hydroxyl, aldehyde, amino and carboxylic functionalities, poly(*p*-xylylene) and its block copolymers, and polyesters via ATRC process is described. The method pertains to the generation of biradicals at high concentration from polymers prepared by ATRP or specially designed bifunctional ATRP initiators. The possibility of using silane radical atom abstraction (SRAA) reactions, that can be performed photochemically in the absence of metal catalysts, as an alternative process to ATRC is also discussed.

In the past decade, the development of controlled/living radical polymerizations (CRP)<sup>1, 2</sup> has allowed the synthesis of (co)polymers not only with a predetermined degree of polymerization and narrow molecular weight distribution but also with high functionality and desired microstructure. Among the various controlled radical polymerization routes, atom transfer radical polymerization (ATRP) seemed to be the most versatile route because of its

simplicity and applicability to many vinyl monomers<sup>3-5</sup>. ATRP leads to the formation of halogen atoms at one or both chain ends due to the fast deactivation process. The coupling of bromine terminated polystyrenes was initially investigated by Fukuda *et al.*<sup>6</sup> Their synthetic utility was first recognized by us. We proposed a novel route for directly obtaining  $\alpha, \omega$ -telechelics by combining ATRP with atom transfer radical coupling (ATRC) processes<sup>7</sup>. We have also studied the combination of ATRP and atom transfer radical cross-coupling (ATRCC)<sup>8</sup>, and reverse ATRP and ATRC processes<sup>9</sup> as potential routes to prepare telechelic polymers. Following our work, other groups also reported successful synthesis of telechelics by ATRC of different halide-terminated polymers prepared by ATRP<sup>10-13</sup>. Recently, *p*-dibromo xylene, a typical ATRP bifunctional initiator, was polymerized in ATRC conditions, yielding poly(*p*-xylylene)<sup>14</sup>. Moreover, polyrecombination reactions were also shown to be a potential route for the synthesis of polymers that can not be prepared by free radical polymerization. By this way, certain condensation polymers and perfectly alternating copolymers can also be readily obtained from the structurally designed monomers.

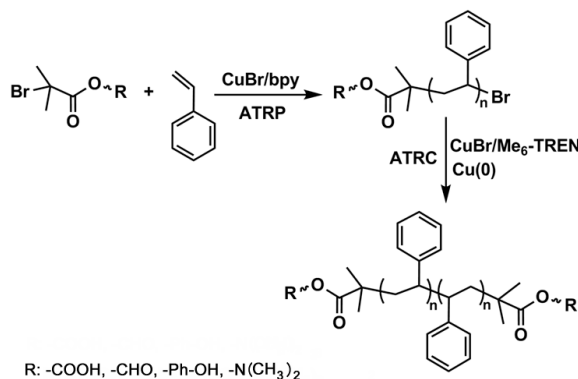
In this chapter, the use and limitations of ATRC reactions including polyrecombination reactions for the preparation of telechelic polymers, segmented block copolymers and polycondensates are discussed.

## Preparation of Telechelic Polymers

Telechelic polymers having a variety of functional groups are prepared by a wide range of polymerization methods, namely anionic<sup>15</sup>, cationic<sup>16</sup>, ring opening<sup>17,18</sup>, group transfer<sup>19,20</sup>, free radical<sup>21,22</sup>, metathesis<sup>23-30</sup> and step-growth<sup>31</sup> polymerization, and chain scission<sup>31</sup> processes. Among them living ionic polymerization methods are usually preferred since they allow the preparation of well-defined telechelics with better control of functionality, molecular weight and polydispersity. On the other hand, ionic techniques have serious limitations because of the requirement of high purity monomer and solvents, and monomer selectivity. Telechelics can also be prepared under classical free radical polymerization conditions by using a large amount of functional initiator<sup>32-37</sup> or performing the copolymerization of olefinic monomers with suitable heterocyclic monomers.<sup>38-40</sup> However, nonfunctionalized end group formation is unavoidable due to the mutual side reactions of the free radical process. Therefore, the overall structure of telechelics was not controlled or well-defined. Recent developments in CRP provide possibility to synthesize well-defined telechelic polymers also with radical routes. For example, the polymer produced by ATRP preserve the terminal halogen atom(s) and can be successfully converted into various end groups through appropriate transformation, especially nucleophilic substitution<sup>41</sup>, free radical reaction or electrophilic addition catalyzed by Lewis acids.

## Preparation of Telechelic Polymers by ATRC

Recently, an alternative route for obtaining directly  $\alpha,\omega$ -telechelics via combination of ATRP and ATRC processes have been proposed<sup>7</sup>. The ATRP initiators having aldehyde, tertiary amine, phenolic and carboxyl groups were used for the styrene polymerization to yield a polymer with the desired chain end at the  $\alpha$ -position. Then, bifunctional polystyrene telechelics, with double molecular weight of the starting materials, were prepared by coupling of mono-functional polymers in atom transfer radical generation conditions, in the absence of monomer, using CuBr as catalyst, tris[2-(dimethylamino)ethyl]amine (Me<sub>6</sub>TREN) as ligand, Cu(0) as reducing agent and toluene as solvent. The overall process is depicted in Scheme 1.



**Scheme 1.** Synthesis of  $\alpha,\omega$ -telechelics via combination of ATRP and ATRC processes.

ATRC, is based on the application of Cu(0) to an ATRP system, leading to the reduction of any Cu(II) in the reaction medium to form Cu(I). The increase of Cu(I) in the reaction medium dramatically shifts the equilibrium between active and dormant species to the side of the active radical species. So the high concentration of radicals presents in the system favor the recombination reactions between two macroradicals. This method was performed to obtain telechelic polymer from monotelechelic polystyrene and results showed that it is very effective way with high efficiency in a short reaction time. Figure 1 shows  $\alpha,\omega$ -telechelic polymer with double molecular weights as compared with the mono functional polystyrene obtained by ATRP using aldehyde functional initiator.



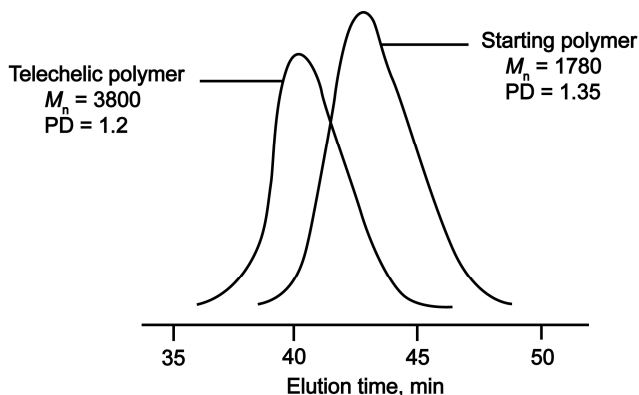
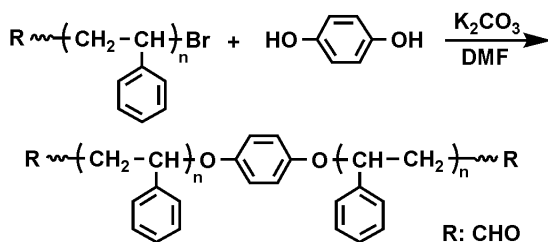


**Figure 1.** Gel Permeation Chromatography (GPC) traces of mono-aldehyde functional starting polymer and  $\alpha,\omega$ -telechelic polymer obtained by ATRC.

The direct coupling of monofunctional polymers prepared by ATRP can also be realized by etherification reaction with low-molar mass dialcohols. Typically, the preparation of aldehyde functional  $\alpha,\omega$ -telechelic polymers by classic etherification is demonstrated on the example hydroquinone as the coupling agent (Scheme 2).



**Scheme 2.** Synthesis of  $\alpha,\omega$ -telechelic polymer by etherification.

The comparison of coupling by ATRC and condensation processes are collected in Table 1. Although quantitative coupling efficiency was attained in both cases, ATRC is more convenient method for obtaining  $\alpha,\omega$ -telechelics, due to the shorter reaction time and easier reaction conditions. Moreover, the condensation coupling is more sensitive to the reaction stoichiometry which can be influenced by the experimental errors such as weighing, molecular weight determination, and transferring the components into a reaction vessel. In fact, these factors may be the reason for the relatively higher polydispersity observed in the condensation process.

**Table 1. Coupling of Mono-aldehyde Functional Polymer by ATRC and Classical Etherification.**

Run	Method	Polymer Conc. (mmol L <sup>-1</sup> )	Time (min)	$M_{n,NMR}^d$ (g mol <sup>-1</sup> )	$M_{n,GPC}^e$ (g mol <sup>-1</sup> )	$M_w/M_n^e$
1 <sup>a</sup>	ATRC <sup>c</sup>	15	1440	3750	3800	1.20
2 <sup>b</sup>	ATRC <sup>c</sup>	15	45	3900	4200	1.21
3 <sup>a</sup>	Etherification	305	4320	3770	3600	1.35

<sup>a</sup> Starting aldehyde functional polystyrene;  $M_{n,theo}$ :1740,  $M_{n,NMR}$ : 1830,  $M_{n,GPC}$ :1780,  $M_w/M_n$ :1.35.

<sup>b</sup> Starting aldehyde functional polystyrene:  $M_{n,theo}$ :2000,  $M_{n,NMR}$ : 2100,  $M_{n,GPC}$ :1970,  $M_w/M_n$ :1.38.

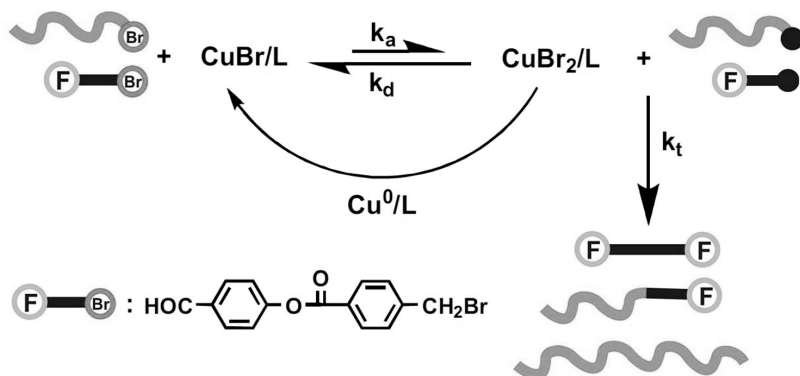
<sup>c</sup> Atom Transfer Radical Coupling Conditions: [Cu<sub>0</sub>]: 75 x 10<sup>-3</sup> M; [CuBr<sub>2</sub>]: 15 x 10<sup>-3</sup> M; [Me<sub>6</sub>TREN]: 30 x 10<sup>-3</sup> M; solvent: toluene; temperature: 110 °C.

<sup>d</sup> Determined by <sup>1</sup>H NMR spectra.

<sup>e</sup> Determined by GPC based on polystyrene standards.

### Preparation of Telechelic Polymers by ATRCC

Preparation of telechelic polymers by ATRCC was also demonstrated<sup>8</sup>. The concept is based on the activation of the dormant species at the chain ends of polystyrene (PS-Br) prepared by ATRP and also functional ATRP initiator (F-R-Br) in the absence of a monomer. Depending on the number of functionality of the polymer used in the system, ATRCC yields ω-polystyrene and α,ω-polystyrene telechelics. However, at least in principle, not only the desired functional polymers but also various side products may be formed due to the self coupling reactions of macroradicals generated from PS-Br, and low-molecular weight radicals from F-R-Br. The possible reactions of the model system are depicted in Scheme 3.



Scheme 3. General reactions of ATRCC process.

The chain end functionality was investigated by  $^1\text{H}$  NMR analysis. Figure 2 represents the  $^1\text{H}$  NMR spectra recorded for PS-Br prepared by ATRP and its coupling product in the presence of *F*-R-Br. The signal at 4.38 ppm was attributed for  $-\text{CH}(\text{Ph})\text{Br}$  (Figure 2a). When the spectrum of the coupling product was investigated (Figure 2b), the characteristic chemical shift for aldehyde proton was detected at 10.01 ppm. The aromatic protons of the initiator near the carbonyl groups appeared at 7.94 ppm. The other aromatic protons of the initiator were noted at around 7.34 ppm. It should be pointed out that the signal of the proton (r) located in the  $\alpha$ -position of the bromine end functionality disappeared after the reaction, confirming the efficient coupling reaction of PS-Br chains. However, the number of the styrene repeating units of the coupling product, which was estimated from the peak area integration of aromatic region (6.58 ppm), showed not only functional polymer formation (56 %) but also coupling of the macroradicals (44 %) occurred during ATRCC reaction. Protons originating from the self coupling reaction of PS-Br ( $-\text{CH}-\text{CH}-$ ) were located in 2–2.5 ppm region and overlapped with the other  $\text{CH}_2$  and  $\text{CH}$  protons of the polystyrene chains. Notably, low molar mass coupling products (*F*-R-*F*) were removed during the precipitation.

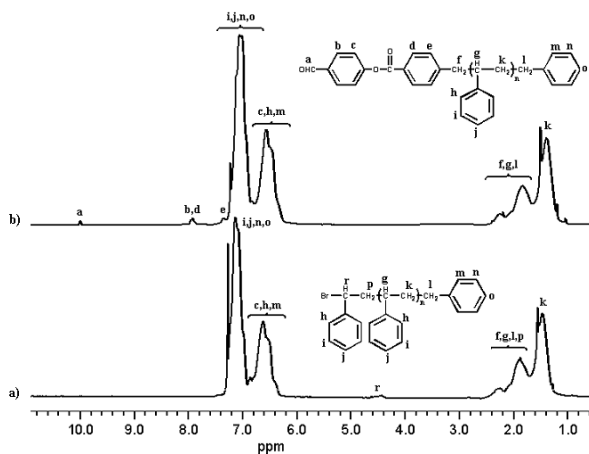


**Figure 2.**  $^1\text{H}$  NMR spectra of PS-Br ( $M_n$ : 2132,  $M_w/M_n$ : 1,2) (a) and its coupling product (b).

We have investigated the effect of various parameters such as catalyst concentration,  $[\text{PS-Br}]/[\text{F-R-Br}]$  ratio, PS-Br concentration, and time dependence on the ATRCC system. It has also been observed that under these experimental conditions the highest functionalization is achieved after 2h and then the composition of reaction mixture does not change significantly with time (Figure 3).

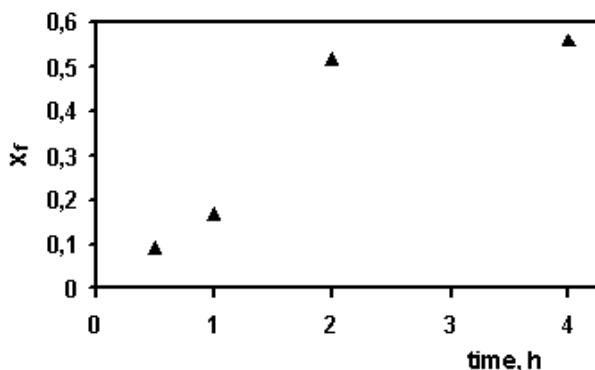


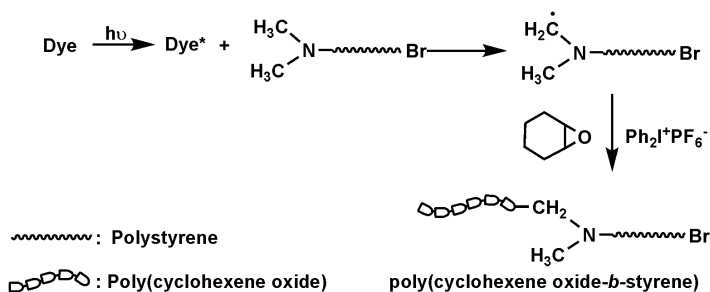
**Figure 3.** Variation of coupling efficiency in time for ATRCC using PMDETA as a ligand.  $[PS-Br]_0 / [F-R-Br]_0 / [Cu^0]_0 / [CuBr]_0 / [L]_0 : 1/15/15.6/3.1/22.5$ ,  $[PS-Br]_0 : 1.37 \text{ mmol L}^{-1}$ .

Further investigations regarding the effect of molecular structure of bromo end group on the coupling process were performed. In the system under consideration, PS-Br and F-R-Br possess structurally different end groups and consequently produce radicals with different stability and reactivity which may contribute to different equilibrium constants. In order to achieve similar reactivity between structurally different end groups Matyjaszewski proposed to introduce small amount of St in the ATRC<sup>13</sup>. Following the same strategy, styrene monomer was added to obtain structurally similar chain ends in ATRCC. As a result, styrene-terminated radicals are simultaneously formed from both this polymerization and initial PS-Br. This experiment was carried out in toluene at 110 °C with  $[PS-Br]_0 / [St] / [F-R-Br]_0 / [Cu]_0 / [CuBr]_0 / [L]_0 = 1/10/15/15.6/3.1/22.5$ . Under these conditions the highest functionalization (85 %) with  $M_n : 3039$  with 1.33 polydispersity was achieved. The increase of molecular weight of the resulting telechelic from the initial value ( $M_n : 2495$ ) is due to the addition of short styrene unit and also functional initiator.

Telechelic polymers can be used as cross-linkers, chain extenders, and precursors for preparation of condensation polymers, block and graft copolymers. Moreover, star and hyper-branched or dendric polymers are obtained by coupling reactions of monofunctional and multifunctional telechelics with appropriate reagents. Among them, the use of telechelics as the building blocks of polycondesates may be more common. For example, hydroxy-telechelic polymers are used for the preparation of polyurethanes or polyesters. Besides ATRC, these polymers can be synthesized by ATRP followed by end group transformation such as end-capping with allyl alcohol<sup>42</sup>. Also, the combination of ATRP and click chemistry is an interesting and promising strategy to synthesize various end functionalized polymers. Recently,  $\alpha,\omega$ -dihydroxy telechelic polystyrene was synthesized by combination of ATRP and subsequent modification via click reactions<sup>43</sup>. Furthermore, step-growth click coupling of telechelic polymers was performed by using  $\alpha$ -alkyne- $\omega$ -azido-terminated polystyrene and  $\alpha,\omega$ -diazido-terminated polystyrene was

polymerized with propargyl ether at room temperature to yield higher molecular weight polystyrene<sup>44</sup>.

Other important use of telechelic polymers is preparation of block copolymers. Depending on the type of telechelics (heterotelechelic or telechelic), AB and ABA type block copolymer can be obtained, respectively. Moreover, different polymerization modes can be easily combined by using telechelics<sup>45</sup>. Typically, appropriately functionalized telechelics can be used as initiators for photoinitiated free radical and cationic polymerizations. Scheme 4 depicts the general reactions for the combination of ATRP and photoinduced radical promoted cationic polymerization by using *N,N* dimethylaniline functional polystyrene. Macroradical generation in visible region was achieved via a visible light initiating system which involves a xanthene dye (erythrosin B), an aromatic *N,N*-dimethylamino group and diphenyliodonium hexafluorophosphate as the sensitizer, radical source and oxidant, respectively.



**Scheme 4.** Synthesis of block copolymer by combination of ATRP and Free Radical Promoted Cationic Polymerization.

## Preparation of Polycondansates

Since the radicals are generated from the initiator in the first step of ATRP reaction, it seemed appropriate to use any bifunctional ATRP initiator as a monomer in ATRC or even ATRP (without adding Cu(0)) conditions. In this way a large number of already reported or new compounds can be polymerized by polyrecombination reactions<sup>14</sup>. The fastest way to verify this assumption was, in a first stage, to polymerize a simple and traditional and commercially available ATRP bifunctional initiator, *p*-dibromoxylene, (Scheme 5).



**Scheme 5.** Synthesis of poly(*p*-xylylene) by polyrecombination in ATRC or ATRP conditions

Conditions and results of polyrecombination reaction of *p*-dibromoxylene in ATRC and ATRP conditions were collected in Table 2. First experiment was performed under typical ATRC condition at 110 °C for 20 h. Although the precipitate was extracted with toluene and THF, soluble polymer fraction or unreacted monomer could not be separated. At lower temperature and concentration, unreacted monomer was recuperated from the solution and the yield was calculated as 15%. Also, ATRP condition is efficient for this polyrecombination even at relatively low monomer and catalyst concentration.

**Table 2. Conditions of polyrecombination reaction of *p*-dibromoxylene in ATRC conditions**

Run	[M] (mol L <sup>-1</sup> )	[M]/[Cu <sup>0</sup> ]/ [CuBr]/[PMDETA]	Time (h)	Temperature (°C)	Yield <sup>d</sup> (%)
1	0.19	2/4/2/2	20	110	100
2	0.10	2/1/1/1	2	90	15
3	0.08	2/0/0.5/0.5 <sup>b</sup>	16	80	37
4	0.15	2/1/0.5/0.5 <sup>c</sup>	72	110	16.3 <sup>d</sup>

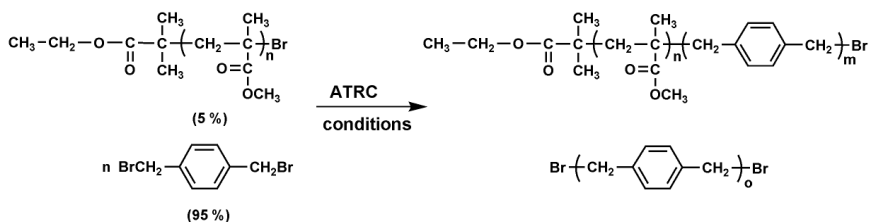
<sup>a</sup>Calculated gravimetrically from the unreacted monomer recuperated from reaction solution and extractions of insoluble part.

<sup>b</sup>ATRP conditions

<sup>c</sup>M is a mixture 95/5 *p*-dibromoxylene/PMMA-Br (molar ratio).

<sup>d</sup>In soluble fraction

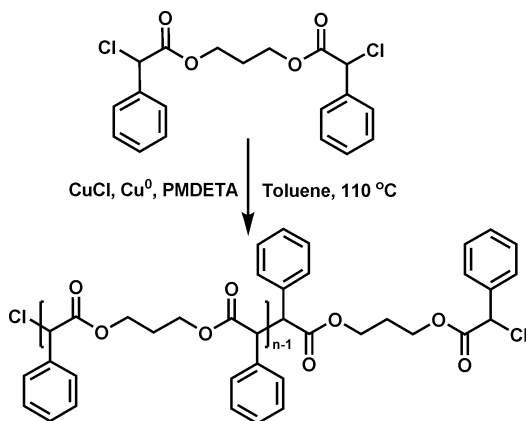
The polymers prepared, are insoluble in common organic solvents which therefore make them difficult to characterize using traditional NMR spectroscopic techniques. In order to obtain a more convenient material that can be analyzed, an experiment was performed in the presence of 5 mol % poly(methyl methacrylate) PMMA (Run 4 in Table 2). As the PMMA was obtained by ATRP, one end contains an activated Br atom. In this connection it should be pointed out that the polymeric halide end groups are structurally different than those of the benzylic halides of the monomer. The first reason of choosing PMMA as reaction partner for *p*-dibromoxylene is the copolymer <sup>1</sup>H NMR spectrum is free of signals in the regions where PPX should give peaks and the second is the experiment also tests the efficiency of other type of activated bromines that are usually used in initiating ATRP for such polyrecombination reactions. So, principally, it was expected that besides the homopolymer, poly(xylylene), a copolymer, PMMA-polyxylylene should be formed as depicted in Scheme 6. At the end of the reaction, insoluble homopolymer (16.3 %) was separated from the mixture.



*Scheme 6. Synthesis of poly(methyl methacrylate - b- p-xylylene) in ATRC conditions.*

This demonstrated not only the success of the synthesis of poly(p-xylylene), but also the activity of other type of activated bromine atoms in ATRC. In fact, the strategy described here opens a new pathway for the possibility for using of any potential ATRP bifunctional initiator as monomer, leading to new or already known polymers from very different classes.

Accordingly, new polyester was synthesized by using ATRC reaction (Scheme 7). For this purpose, a bifunctional ATRP initiator namely propane-1,3-diyl bis(2-chloro-2-phenylacetate) (PDBCP) was designed and synthesized as a monomer, and its polymerization was performed (Table 3). In this case, one mol of CuCl was introduced for every mol of monomer in order to facilitate successful coupling.



*Scheme 7. Polyrecombination of PDBCP in the ATRC conditions.*

Table 3 illustrates results of polyrecombination reaction of this monomer at fixed concentration of monomer and catalyst with different reaction times. As can be seen, although certain chain growth is achieved, the polydispersity of the resulting polymers is quite high. It is also noted that higher molecular weight polymers were formed at the early stages of the polymerization.

**Table 3. Synthesis of polyester by ATRC reactions.**

Run	Time (h)	Conversion (%)	$M_{n,NMR}^b$	$M_{n,GPC}^a$	$M_w/M_n^a$
1	24	30	6770	11440	3.29
2	48	33	4980	14210	2.65
3	96	35	4720	7840	2.80

Polymerization conditions;  $[M]_0 = 265$  mM,  $[M]_0 / [Cu^0]_0 / [CuCl]_0 / [L]_0 = 1/2/1/1$  in toluene at 110 °C. PMDETA used as a ligand.

<sup>a</sup> Determined by GPC based on polystyrene standards.

<sup>b</sup> Determined by <sup>1</sup>H NMR spectra.

The polymer formation was investigated by <sup>1</sup>H NMR analysis. Figure 4 represents the <sup>1</sup>H NMR spectra recorded for bifunctional monomer and its coupling product. The signal at 5.30 ppm was attributed for chloride end of monomer (Figure 4a). When the spectrum of the coupling product was investigated (Figure 4b), the characteristic chemical shift for chloride chain end of polymer was detected at 5.27 ppm and Ph-CH-CH-Ph protons (d) of the linkage appeared at 4.94 ppm. The aromatic protons of the polymer were noted between at 6.95-7.42 ppm. The aliphatic protons (b') of the polymer near the ester groups appeared at 3.51–4.28 ppm. The other aliphatic protons (c') of the polymer were noted between 1.07-1.84 ppm. The number average molecular weight ( $M_{n,NMR}$ ) were calculated using the values of the integrals of characteristic end peaks (a') for polymer in comparison with the integrals of aliphatic protons (b') of polymer.

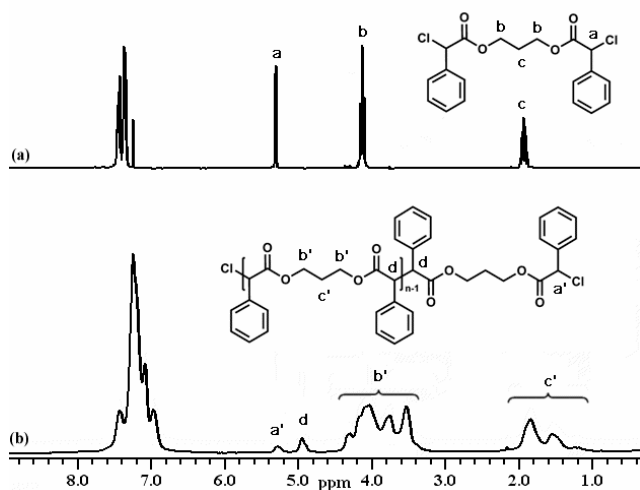


**Figure 4.** <sup>1</sup>H NMR spectrum of bifunctional monomer (a) and its coupling product (b).

The effect of catalyst concentration at constant monomer concentration was investigated. Figure 5 shows the GPC traces of the polymers obtained with



different catalyst concentration. As can be seen, the GPC curves shifted to a higher molecular weight and the peak areas of the lower molecular weight regions decreased as the catalyst concentration increased. Because, the higher catalyst concentration leads to increase in concentration of active radicals, this manifests itself in more coupling probability.

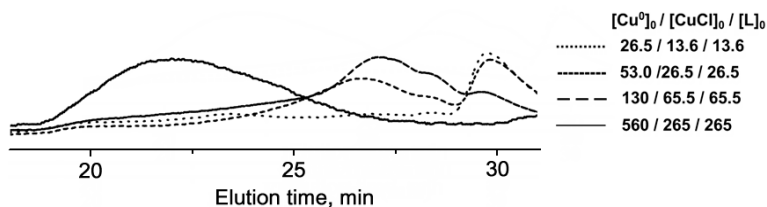
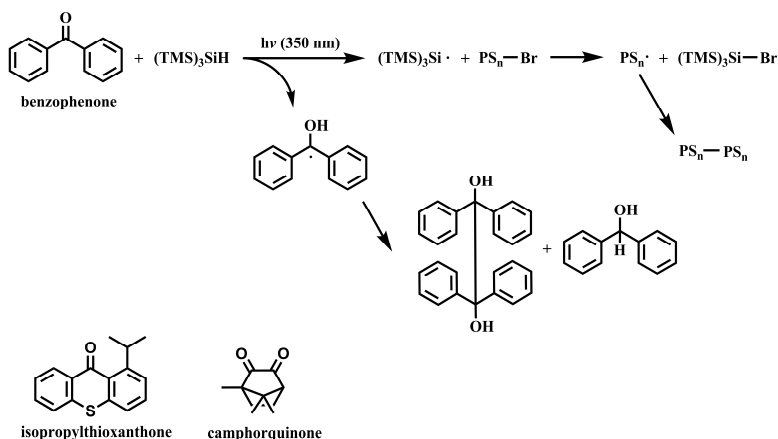


**Figure 5.** GPC traces of the polymers obtained at constant monomer concentration ( $[M]_0 = 265 \text{ mmol L}^{-1}$ ) with different catalyst concentration ( $\text{mmol L}^{-1}$ ).

Recently, a new methodology called as silane radical atom abstraction (SRAA) was introduced by Tillman and coworkers<sup>46-48</sup> as a metal-free alternative route for coupling of polymer radicals. They used the high bromophilicity of silane radicals in the generation of polymer radicals in the presence of a nitroxide trap<sup>49</sup>. It was independently demonstrated by Fouassier *et al*<sup>50</sup> that silane radicals can also be generated from the reactions of photoexcited Type II photoinitiators such as benzophenone, camphorquinone, Eosin and isopropylthioxantone. It seemed appropriate to combine the two processes for the coupling approach. Taking the advantage of high reactivity of triplet benzophenone, camphorquinone and isopropylthioxantone silane radicals were generated photochemically. The resulting radicals abstract bromine from the polymer chain ends to form macroradicals capable of undergoing coupling reactions in a usual manner. The overall process is presented in Scheme 8.



**Scheme 8.** Photoinduced coupling reaction of PS-Br in the presence of  $((\text{TMS})_3\text{Si-H})$ .

Experimentally, bromine terminated polystyrene (PS-Br) was irradiated at appropriate wavelengths depending on the absorption of the initiator in the presence of tris(trimethylsilyl)silane ((TMS)<sub>3</sub>Si-H) at room temperature and the results are summarized in Table 4. Although the highest coupling efficiency and a significant increase in the molecular weight (Figure 6) was observed with camphorquinone at visible region, it appears some side reactions are also occurring beside the coupling reaction.

**Table 4. Photoinduced coupling of polystyrene prepared by ATRP.**

Run	PS-Br (mol L <sup>-1</sup> )	Photoinitiator (mol L <sup>-1</sup> )	(TMS) <sub>3</sub> SiH (mol L <sup>-1</sup> )	Time (h)	λ (nm)	X <sub>c</sub>
1	0.083	BP (0.166)	0.498	2	350	0.14
2	0.042	ITX (0.083)	0.083	2	350	0.11
3	0.042	CQ (0.083)	0.083	1	430-490	0.57

Solvent: Benzene/Hexane (2/3)

BP: Benzophenone, ITX: Isopropylthioxanthone, CQ: Camphorquinone

(TMS)<sub>3</sub>SiH : Tris(trimethylsilyl)silane

λ is irradiation wavelength.

Coupling efficiencies (X<sub>c</sub>) were calculated from GPC.

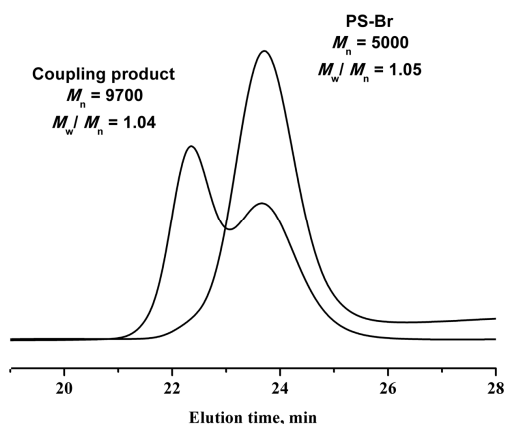
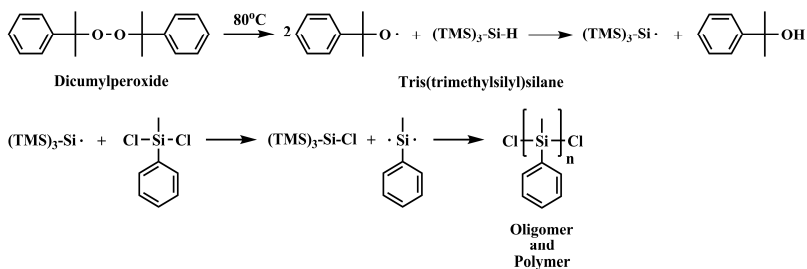


**Figure 6.** GPC overlays of PS-Br and Run 3.

We have also used SRAA reactions for the polymerization of bifunctional monomers such as propane-1,3-diyl bis(2-chloro-2-phenylacetate) (PDBCP) and dichloromethylphenylsilane (DCMPS). As mentioned above this approach was

previously attempted via ATRC for polyester synthesis. The overall reactions for the case of DCMPS are presented in Scheme 9.



**Scheme 9.** Polyrecombination of DCMPS under SRAA conditions.

Silane radicals were generated *in situ* using SRAA method in the presence of dicumyl peroxide and subsequent coupling reactions of PDBCP and DCMPS gave rise to not only oligomers but also high molecular weight polymers. As shown in Table 5, for both monomers limited conversions were observed due to rapid consumption of the radicals at the beginning of the reaction. In order to provide permanent radical generation by extending life time of dicumyl peroxide the temperature was decreased to 65 °C (Run 4 in Table 5). Expectedly, molecular weight increased by decreasing temperature.

At this point, further studies are necessary to optimize such coupling reactions.

**Table 5. Results of the coupling reactions of bifunctional monomers using SRAA in the presence of dicumyl peroxide.**

Run	Monomer	Temperature <sup>e</sup> (°C)	Time (h)	Conversion (%)	$M_{n, GPC}$ ( $g\ mol^{-1}$ )	$M_w/M_n$
1	PDBCP <sup>a</sup>	80	20	7.5	1650	4.48
2	PDBCP	80	2	4.2	4500	4.8
3	DCMPS	80	2	5	64370 1650	1.49 1.01
4	PDBCP	65	20	2.3	53500 6280	1.54 3.76

PDBCP: propane-1,3-diyl bis(2-chloro-2-phenylacetate)

DCMPS: dichloromethylphenylsilane

<sup>a</sup> *tert*-Butyl hyponitrite was used as a persistent radical source instead of dicumyl peroxide.

In conclusion, it has been demonstrated that ATRC reactions are useful for preparing various macromolecular structures such as telechelics and certain polycondensates. The method preserves to the generation of biradicals at high concentration from polymers prepared by ATRP or specially designed bifunctional ATRP initiators. The radical generation process is not limited to the metal catalyzed atom transfer reactions. Silane radical atom abstraction reactions can also be used for the formation of reactive radicals. Aromatic carbonyl assisted photoinduced reactions seemed to a promising alternative route for silane radical generation since it can be performed at room temperature and does not require metal catalysts.

Further studies in this line are now in progress.

## References

1. Kamigaito, M.; Ando, T.; Sawamoto, M. *Chem. Rev.* **2001**, 101, 3689.
2. Matyjaszewski, K.; Davis, T. P.; Eds. *Handbook of Radical Polymerization*; Wiley: Hoboken, NJ, **2002**.
3. Kato, M.; Kamigaito, M.; Sawamoto, M.; Higashimura, T. *Macromolecules* **1995**, 28, 1721.
4. Percec, V.; Barboiu, B. *Macromolecules* **1995**, 28, 7970.
5. Mishra, M. K.; Yagci, Y. in *Handbook of Radical Vinyl Polymerization*; Dekker, M., New York **1998**, p 233.
6. Yoshikawa, C.; Goto, A.; Fukuda, T. *e-Polymers* **2002**, no. 013.
7. Yurteri, S.; Cianga, I.; Yagci, Y. *Macromol. Chem. Phys.* **2003**, 204, 1771.
8. Durmaz, Y. Y.; Cianga, I.; Yagci, Y. *e-Polymers*, **2006**, 50.
9. Aydogan, B.; Yagci, Y.; **2007**, *Turk. J. Chem.*, 31, 1.
10. Otazaghine, B.; David, G.; Boutevin, B.; Robin, J. J.; Matyjaszewski, K. *Macromol. Chem. Phys.* **2004**, 205, 154.
11. Sarbu, T.; Lin, K. Y.; Ell, J.; Siegwart, D. J.; Spanswick, J.; Matyjaszewski, K. *Macromolecules* **2004**, 37, 3120.
12. Otazaghine, B.; Boutevin, B. *Macromol. Chem. Phys.* **2004**, 205, 2002.
13. Sarbu, T.; Lin, K. Y.; Spanswick, J.; Gil, R. R.; Siegwart, D. J.; Matyjaszewski, K. *Macromolecules* **2004**, 37, 9694.
14. Cianga, I.; Yagci, Y. *Designed Mon. & Polym.* **2007**, 10, 575.
15. Fontanille, M.; in: “*Comprehensive Polymer Science*”, Eds.: Allen, G.; Bevington, J. C.; Vol. 3, Pergamon Press, Oxford, **1989**, p. 425.
16. Kennedy, J. P.; Ivan, B.; “*Designed Polymers by Carbocationic Macromolecular Engineering: Theory and Practice*”, Hanser Verlag, München **1992**, p. 167.
17. Goethals, E. J.; *Makromol.Chem. Macromol. Symp.* **1986**, 6, 53.
18. Nakayama, Y.; Okuda, S.; Yasuda, H.; Shiono, T. *Reactive & Functional Polymers* **2007**, 67, 798.
19. Webster, O. W.; *Makromol.Chem. Macromol. Symp.* **1993**, 70, 75.
20. Webster, O. W.; *J. Polym. Sci., Polym. Chem. Ed.* **2000**, 38, 2855.

21. Brosse, J. C.; Depouet, D.; Epailard, F.; Soatif, J. C.; Legeay, G.; Dusek, K.; *Adv. Polym. Sci.* **1987**, 81, 167.
22. Onen, A.; Denizligil, S.; Yagci, Y. *Macromolecules* 1995, 28, 5375.
23. Hillmyer, M. A.; Grubbs, R. H. *Polym. Prepr. (Am. Chem. Soc. Div. Polym. Chem.)* **1993**, 34, 388.
24. Hillmyer, M. A.; Grubbs, R. H. *Macromolecules* **1993**, 26, 872.
25. Fraser, C.; Hillmyer, M.; Gutierrez, E.; Grubbs, R. H. *Macromolecules* **1995**, 28, 7256.
26. Hillmyer, M. A.; Nguyen, S. T.; Grubbs, R. H. *Macromolecules* **1997**, 30, 718.
27. Maughon, B. R.; Morita, T.; Bielawski, C. W.; Grubbs, R.H. *Macromolecules* **2000**, 33, 1929.
28. Morita, T.; Maughan, B. R.; Bielawski, C. W.; Grubbs, R. H. *Macromolecules* **2000**, 33, 6621.
29. Bielawski, C. W.; Scherman, O. A.; Grubbs, R. H. *Polymer* **2001**, 42, 4939.
30. Bielawski, C. W.; Jethmalani, J. M.; Grubbs, R. H. *Polymer* **2003**, 44, 3721.
31. Yagci, Y.; Nuyken, O.; Graubner, V.; in “*Encyclopedia of Polymer Science and Technology*”, Third Ed., Kroschwitz, J.I.; Ed. Wiley, New York, **2005**, Vol.12, pp 57-130.
32. Athey Jr. R. D. *Prog. Org. Coat.* **1979**, 7, 289.
33. Gobran, R. H.; Fettes, E. M.; eds., *High Polymers, Vol. XIX: Chemical Reactions of Polymers*, Wiley-Interscience, New York, **1964**, Chapt. 4.
34. French, D. M. *Rubber Chem. Technol.* **1969**, 42, 71.
35. Heitz, W. *Makromol. Chem., Macromol. Symp.* **1987**, 10/11, 297.
36. Starks, C. M. *Free Radical Telomerization*, Academic Press, New York, 1974.
37. Onen, A.; Denizligil, S.; Yagci, Y. *Macromolecules* **1995**, 28, 5375.
38. Bailey, W. J.; Chen, P. Y.; Chiao, W. B.; Endo, T.; Sidney, L.; Yamamoto, N.; Yonezawa, K.; in M. Shen, ed., *Contemporary Topics in Polymer Science*, Vol. 3, Plenum Press, New York, **1979**, p. 29.
39. Bailey, W. J.; Endo, T.; Gapud, B.; Lin, Y. N.; Ni, Z.; Pan, C. Y.; Shaffer, S. E.; Wu, S. R.; Yamazaki, N.; Yonezawa, K.; *J. Macromol. Sci.* **1984**, A 21, 979.
40. Bailey, W. J.; Gapud, B.; Lin, Y. N.; Ni, Z.; Wu, S. R. *ACS Symp. Ser.* **1985**, 282, 147.
41. Durmaz, Y. Y.; Yilmaz, G.; Yagci, Y.; *J. Polym. Sci., Polym. Chem. Ed.* 2007, 45, 423.
42. Keul, H.; Neumann, A.; Reining, B.; Hocker, H. *Macromol. Symp.* **2000**, 161, 63.
43. Gao, H.; Louche, G.; Sumerlin, B. S.; Jahed, N.; Golas, P.; Matyjaszewski, K. *Macromolecules* **2005**, 38, 8979.
44. Tsarevsky, N. V.; Sumerlin, B. S.; Matyjaszewski, K. *Macromolecules* **2005**, 38, 3558.
45. Muftuoglu, A. E.; Yurteri, S.; Cianga, I.; Yagci, Y. *J. Appl. Polym. Sci. Chem. Ed.* **2004**, 93, 387.

46. Thakur, S.; Tillman, E. S. *J. Polym. Sci. Part A: Polym. Chem.* **2007**, *45*, 3488.
47. Thakur, S.; Cohen, N. A.; Tillman, E. S. *Polymer* **2008**, *49*, 1483.
48. Thakur, S.; Smith, J. M.; Tillman, E. S.; Cohen, N. A.; Contrella N. D. *J. Polym. Sci. Part A: Polym. Chem.* **2008**, *46*, 6016.
49. Braslau, R.; Tsimelzon, A.; Gewandter, J. *Org. Lett.* **2004**, *6*, 2233.
50. Lalevee, J.; Dirani, A.; El-Roz, M.; Allonas, X.; Fouassier, J. P.; *Macromolecules* **2008**, *41*, 2003.

## Chapter 13

# Design of Thermoresponsive Materials by ATRP of Oligo(ethylene glycol)-based (Macro)monomers

Özgür Akdemir,<sup>1</sup> Nezha Badi,<sup>1</sup> Sebastian Pfeifer,<sup>1</sup> Zoya Zarafshani<sup>1</sup>  
André Laschewsky,<sup>2</sup> Erik Wischerhoff,<sup>1</sup> and Jean-François Lutz\*<sup>1</sup>

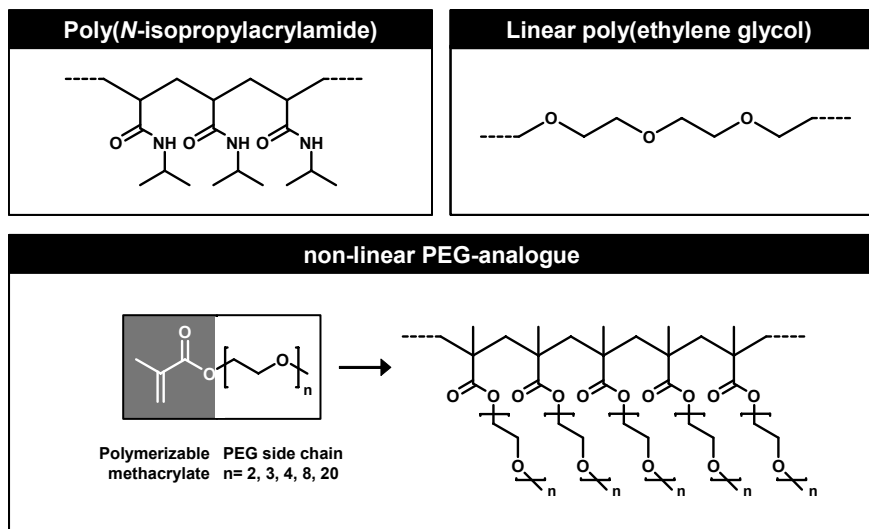
<sup>1</sup>Fraunhofer Institute for Applied Polymer Research  
Geiselbergstrasse 69, 14476 Potsdam-Golm, Germany. <sup>2</sup>University of  
Potsdam, Department of Chemistry.

\*Corresponding author: lutz@iap.fhg.de

It was recently demonstrated that synthetic polymers containing a hydrophobic backbone and short hydrophilic oligo(ethylene glycol) side-chains may exhibit a lower critical solution temperature (LCST) in aqueous medium. In particular, polymers constructed with oligo(ethylene glycol) acrylates or methacrylates seem particularly promising. Indeed, these oligo(ethylene glycol) (macro)monomers are often commercially available and can be easily polymerized by reversible addition-fragmentation transfer polymerization (RAFT) or atom transfer radical polymerization (ATRP). The latter technique is very versatile and allows the rational design of a wide variety of stimuli-responsive materials. For example, in the present chapter, some examples of thermoresponsive hydrogels, polymeric micelles and planar substrates are presented.

## Introduction

Synthetic macromolecules undergoing rapid conformational change in response to an external stimulus such as pH, temperature, ionic strength or irradiation became lately very important in applied materials science.<sup>1</sup> For example, thermoresponsive polymers exhibiting a lower critical solution temperature (LCST) in aqueous medium are very promising materials for bio-applications such as enzyme recycling, protein chromatography, controlled bio-adhesion, hyperthermia-induced drug delivery or tissue engineering.<sup>2</sup> Such polymers are soluble in water below the LCST but precipitate at temperatures above it. Hence, temperature can be used as a simple external trigger for controlling the hydrophilicity and therefore the structural shape of these macromolecules.



*Scheme 1. Molecular structure of various biorelevant polymers.*

Classic examples of synthetic polymers exhibiting an aqueous LCST include poly(*N,N'*-diethyl acrylamide), poly(dimethylaminoethyl methacrylate), poly(*N*-acryloylpyrrolidine), poly(2-isopropyl-2-oxazoline), elastin-like artificial polypeptides, poly(vinyl methyl ether) and poly(*N*-isopropylacrylamide) (PNIPAM, Scheme 1). The latter has been by far the most studied and applied thermoresponsive polymer and therefore can be considered as the “gold standard” in this field of research.<sup>3</sup> During the last decades, several thousands of research articles and patents described the synthesis, the properties and the applications of this fascinating macromolecule.

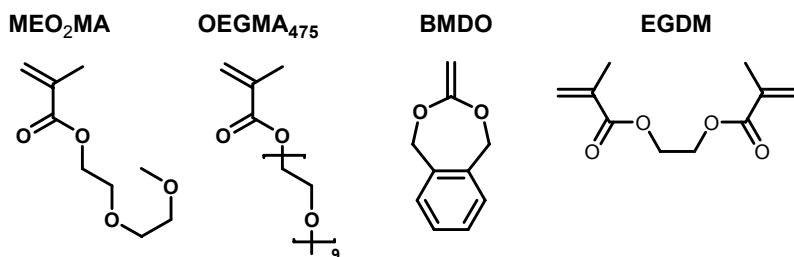


However, despite its widespread popularity in material science, PNIPAM has inherent disadvantages such as an irreversible phase transition and, for short polymers, a significant influence of end-groups on the thermal behavior.<sup>3</sup> Moreover, strictly speaking, PNIPAM is not a bio-inert polymer. Indeed, the presence of multiple secondary amide functions in the molecular structure of PNIPAM may lead to the formation of cooperative H-bonding interactions with other amide polymers, in particular with proteins. Thus, the design of new types of thermoresponsive polymers is a crucial topic in contemporary polymer chemistry.

In this context, graft (co)polymers with oligo(ethylene glycol) side-chains emerged lately as a promising new class of thermoresponsive polymers.<sup>4</sup> Indeed, these macromolecules exhibit, for the most, a defined LCST in aqueous or physiological medium.<sup>5-9</sup> This thermoresponsive behavior is believed to be related to the amphiphilic character of these polymers.<sup>10, 11</sup> Indeed, the hydrophilic oligo(ethylene glycol) side-chains form H-bonds with water, whereas the backbones, which are usually less polar in nature, lead to a competitive hydrophobic effect. For instance, oligo(ethylene glycol)-grafted polymers based on poly(vinyl ether)-,<sup>5</sup> poly(norbornene)-,<sup>12</sup> polyester-,<sup>13</sup> polystyrene-,<sup>14</sup> poly(acrylate)-,<sup>15, 16</sup> or poly(methacrylate)-<sup>17-21</sup> backbones were all reported to exhibit a LCST in water. Still, the latter category has been progressively more studied in recent years. Indeed, most of the oligo(ethylene glycol) methyl ether methacrylates are commercially available and moreover can be readily polymerized using versatile polymerization techniques such as atom transfer radical polymerization (ATRP) or reversible addition-fragmentation transfer polymerization (RAFT).<sup>22-25</sup> For example, we recently reported that the atom transfer radical copolymerization of two oligo(ethylene glycol) methacrylates of different chain-lengths, namely 2-(2-methoxyethoxy)ethyl methacrylate (MEO<sub>2</sub>MA, Scheme 2) and oligo(ethylene glycol) methyl ether methacrylate (OEGMA<sub>475</sub>,  $M_n = 475 \text{ g}\cdot\text{mol}^{-1}$ , Scheme 2), leads to the formation of thermoresponsive copolymers with a precisely tunable LCST in water.<sup>18</sup> The phase transitions measured for the copolymers P(MEO<sub>2</sub>MA-*co*-OEGMA) were found to be reversible and relatively insensitive to important parameters such as concentration of the copolymer in water, ionic strength and chain-length.<sup>17</sup> Moreover, the resulting polymers are certainly promising for bio-applications as they are principally composed of biocompatible oligo(ethylene glycol) segments. Indeed, PEG (Scheme 1) is an uncharged, water soluble, non-toxic, non-immunogenic, FDA-approved polymer, and thus is probably the most widely applied synthetic polymer in biotechnology and medicine in recent years. Hence, these novel polymers appear as promising candidates for building advanced stimuli-responsive materials. For example, the present chapter summarizes our recent efforts to prepare biorelevant materials such as hydrogel scaffolds, thermoresponsive polymeric micelles and switchable planar surfaces.

## Thermoresponsive Hydrogels

Thermoresponsive macroscopic copolymer hydrogels composed of MEO<sub>2</sub>MA and OEGMA<sub>475</sub> were prepared using ethylene glycol dimethacrylate (EGDM, Scheme 2) as a crosslinker.<sup>10</sup> Although such hydrogels can be easily synthesized by conventional radical polymerization, the ATRP method was selected to insure a homogeneous comonomer composition in each region of the macromolecular network. Indeed, in the ATRP process, all the chains constituting the network grow simultaneously and therefore consume homogeneously the comonomers. Such precaution would not be necessary if one is only interested in the swelling of the hydrogel at room temperature. However, if a thermoresponsive gel is targeted, a defined composition of the network is probably essential.



*Scheme 2. Molecular structure of the monomers used for preparing hydrogels.*

Two macroscopic gels with different MEO<sub>2</sub>MA/OEGMA<sub>475</sub> compositions were prepared: 90/10 and 80/20. The polymerizations were conducted in the presence of 1 molar equivalent of initiator and 1 molar equivalent of crosslinker. The hydrogels were molded into capillary tubes having an internal diameter of 4 mm. Figure 1 shows the swelling/deswelling behavior measured for these two samples. Dried hydrogel cylindrical monoliths with a length of 10 mm and an initial weight  $W_d$  of approximately 100 mg were placed in an excess of deionized water at room temperature. The weight of the swollen hydrogels  $W_s$  was then measured as a function of time. Prior to each measurement, the surfaces of the monoliths were shortly dried with a hygroscopic filter paper. The swelling ratio  $Q$  was then calculated according to equation 1.

$$Q = (W_s - W_d) / W_d \quad (1)$$

Both hydrogels exhibited a satisfying swelling capacity in pure water and appeared as homogeneous transparent materials in the swollen state. However, the swelling rates and the maximum swelling ratios were found to be proportional to the fraction of OEGMA<sub>475</sub> grafts in the network, which is a logical behavior previously observed for PEG grafted hydrogels.<sup>26</sup>

Moreover the hydrogels were found to be thermoresponsive. Their phase transitions were visually evaluated (i.e. the formation of a skin layer on the surface of the hydrogels was examined as a function of temperature) and found to be in the range 42-45°C for the gel with 10 mol% OEGMA<sub>475</sub> and 51-53°C for the gel with 20 mol% OEGMA<sub>475</sub>, which roughly correspond to the phase transitions previously observed for their single-chain counterparts.<sup>18</sup> Preliminary evaluation of the deswelling kinetics of these thermoresponsive hydrogels indicated that their thermally induced shrinkage is extremely fast (Figure 1). Such a behavior could be a consequence of the presence of the long OEGMA grafted chains, which can potentially act as water release channels within the network and therefore boost the deswelling kinetics.<sup>27</sup>

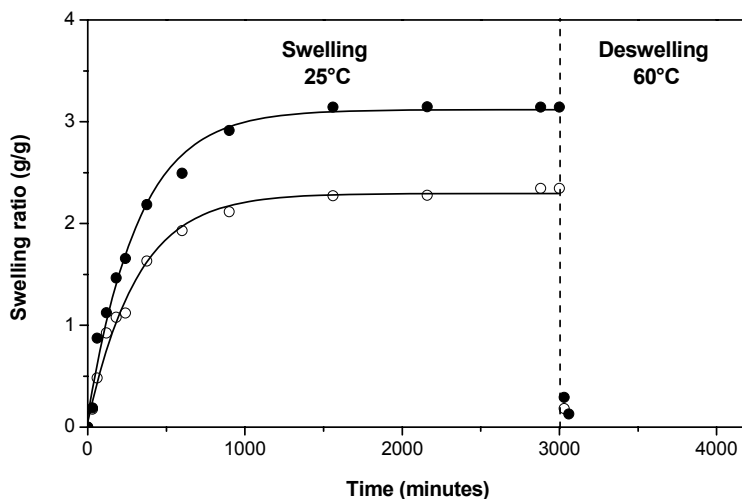


Figure 1. Evolution of the swelling ratio as a function of time for macroscopic hydrogels  $P(\text{MEO}_2\text{MA-co-OEGMA})$  containing either 10 mol% (empty symbols) or 20 mol% (full symbols) of OEGMA per chain. At  $t = 3000$  minutes, the temperature of the aqueous medium was quickly raised from 25°C to 60°C.

Additionally, degradable versions of these smart networks were also prepared. These degradable hydrogels were prepared via atom transfer radical tetrapolymerization of MEO<sub>2</sub>MA, OEGMA<sub>475</sub>, EGDM and 5,6-benzo-2-methylene-1,3-dioxepane (BMDO, Scheme 2). The latter monomer is a cyclic ketene acetal, which ring-opens in a radical process to form labile ester functions in the polymer main-chain.<sup>28</sup> The formed gels swelled in pure water (swelling trends were roughly comparable to those displayed on Figure 1), displayed a thermoresponsive behavior and furthermore were fully degradable. Indeed, the gels disintegrated completely after one day in KOH solution. However, these macroscopic objects could not be fully degraded in the presence of enzymes.

Besides covalently crosslinked hydrogels, we recently designed a series of thermoreversible physical hydrogels.<sup>29</sup> The building-blocks of these networks were synthesized by ATRP of MEO<sub>2</sub>MA and OEGMA<sub>475</sub> in the presence of either linear- or star-shaped PEG macroinitiators. The formed copolymers possess permanently hydrophilic PEG inner-blocks and thermoresponsive P(MEO<sub>2</sub>MA-*co*-OEGMA) outer-blocks. Below the LCST of the thermoresponsive segments, these (star)-block copolymers are double-hydrophilic (i.e. fully soluble in aqueous medium), whereas above LCST, P(MEO<sub>2</sub>MA-*co*-OEGMA) chains precipitate, thus resulting in the formation of a defined hydrogel network.<sup>29</sup>

## Thermoresponsive micelles

Macromolecular amphiphiles and their aggregates in water are an increasingly important aspect of modern colloidal science.<sup>30, 31</sup> Indeed, macromolecular surfactants such as amphiphilic block-copolymers or polysoaps spontaneously self-assemble in selective solvents into a variety of interesting and useful nanoscale morphologies. For example, amphiphilic diblock copolymers composed of distinct hydrophilic and hydrophobic segments self-organize in water into spherical micelles, cylindrical micelles or vesicles, depending on their hydrophilic-hydrophobic balance.<sup>32</sup> More complex morphologies (e.g. multicompartement micelles, toroids, crew-cut micelles, nanotubes, pearl-necklace structures) may be obtained by using surfactants with more elaborate molecular design (e.g. miktoarm stars or triblock copolymers) or by varying the experimental conditions for self-assembly (e.g. using co-solvents, cosolutes, temperature or pH variations).<sup>33</sup> Many of these polymeric micellar aggregates have been shown to be very promising for applications in cosmetics, food-industry, medicine and biotechnology.

In this context, we recently studied the synthesis and the aqueous self-organization of a new family of biocompatible surfactants composed of a cholesterol hydrophobic moiety and various poly(oligo(ethylene glycol) (meth)acrylate) hydrophilic segments.<sup>34</sup> The choice of cholesterol was motivated by the fact that this biological molecule and its esters are generally easily metabolized. Hence, cholesterol-based surfactants and their aggregates in water could be potentially used for drug-delivery or diagnostics applications. The cholesterol-based ATRP initiator cholesteryl-2-bromoisobutyrate (CBI) was synthesized by esterification of cholesterol in the presence of 2-bromoisobutyryl bromide and used for initiating the controlled radical polymerization of various monomers such as OEGMA<sub>475</sub>, MEO<sub>2</sub>MA, oligo(ethylene glycol) methyl ether acrylate (OEGA,  $M_n = 454 \text{ g}\cdot\text{mol}^{-1}$ ) and 2-(2-ethoxyethoxy)ethyl acrylate (EEO<sub>2</sub>A) (Table 1).

**Table 1. Molecular description of the surfactants prepared by ATRP.<sup>a</sup>**

	$M_1$	$M_2$	$M_1/M_2/CBI/Cu(I)/Bipy$	$t$ (h)	$conv.^b$	$M_n^c$	$M_w/M_n^c$
1	OEGMA	MEO <sub>2</sub> MA	3/17/1/1/2	17	0.99	8500	1.20
2	OEGMA	MEO <sub>2</sub> MA	6/34/1/1/2	14	0.98	10700	1.19
3	OEGMA	MEO <sub>2</sub> MA	4/16/1/1/2	14	0.97	8500	1.19
4	OEGMA	MEO <sub>2</sub> MA	8/32/1/1/2	14	0.99	12000	1.20
5	OEGA	-	40/-/1/1/2	3	0.29	4900	1.14
6	OEGA	-	40/-/1/1/2	1.5	0.21	3300	1.21
7	OEGA	EEO <sub>2</sub> A	8/32/1/1/2	3	0.46	4000	1.49

<sup>a</sup> Experimental conditions: copolymerization of methacrylates (Entries 1-4) 60°C, in ethanol solution (monomer/ethanol = 1:1.25 (v/v)) and in the presence of Cu(I)Cl ; homopolymerization and copolymerization of acrylates (Entries 5-7) 90°C, in bulk and in the presence of Cu(I)Br. <sup>b</sup> overall monomer conversion measured by <sup>1</sup>H NMR. <sup>c</sup> measured by SEC in THF.

The ATRP of the methacrylate monomers was performed at 60°C in ethanol solutions and in the presence of the catalyst copper(I) chloride/2,2' bipyridyl (Bipy) (Table 1, Entries 1-4).<sup>18</sup> Copolymers P(MEO<sub>2</sub>MA-*co*-OEGMA) of various chain-lengths and comonomer compositions were prepared and isolated in high yields. After purification, <sup>1</sup>H NMR analysis confirmed that the formed polymers exhibit a terminal cholesterol moiety. Additionally, as previously demonstrated, the molar fraction of OEGMA in the copolymers was found, in all cases, to be almost equal to the fraction of OEGMA in the initial comonomer feed.<sup>18</sup> Furthermore, SEC measurements in THF indicated that all the copolymers are rather well-defined (Table 1, Entries 1-4).

Oligo(ethylene glycol) acrylates generally polymerize rather slowly if the experimental conditions described above are used. Thus, as previously optimized, acrylate monomers were polymerized at 90°C, in bulk, and in the presence of a combination of copper(I) bromide and Bipy (Table 1, Entries 5-7).<sup>16</sup> Either homopolymers of OEGA (Table 1, Entries 5 and 6) or copolymers of OEGA and EEO<sub>2</sub>A (Table 1, Entry 7) could be successfully synthesized by ATRP using CBI as an initiator. After purification, <sup>1</sup>H NMR measurements in acetone-*d*<sub>6</sub> confirmed that all the formed (co)polymers contain an  $\alpha$ -terminal hydrophobic cholesterol moiety.

The aqueous self-organization of the formed macrosurfactants was studied by dynamic light scattering (DLS) and turbidimetry. Figure 2A shows typical size distributions measured by DLS for various acrylate-based surfactants (Table 1, Entries 5-7). The aggregation behavior of these surfactants in pure deionized water depends indeed on their hydrophilic-hydrophobic balance (i.e. on the volume fractions of the hydrophilic and hydrophobic segments).<sup>32</sup> For instance, cholesterol-*b*-POEGA macrosurfactants (Table 1, Entries 5 and 6) did not lead to the formation of large aggregates in pure water (Figure 2A). We previously reported that POEGA is a very hydrophilic homopolymer, which is soluble in pure water at any temperature up to 100°C.<sup>16</sup> Hence, POEGA segments, even with a theoretical degree of polymerization  $DP$  as short as 11 (Table 1, Entry 5) or 8 units (Table 1, Entry 6), probably lead to surfactants with a too high

hydrophilic volume fraction to observe aggregation. Therefore, the small objects (5-6 nm in diameters) observed by DLS for cholesterol-*b*-POEGA surfactants are most likely random coils (i.e. unimolecular micelles, in which the cholesterol hydrophobic moiety is protected from water by the POEGA coil).

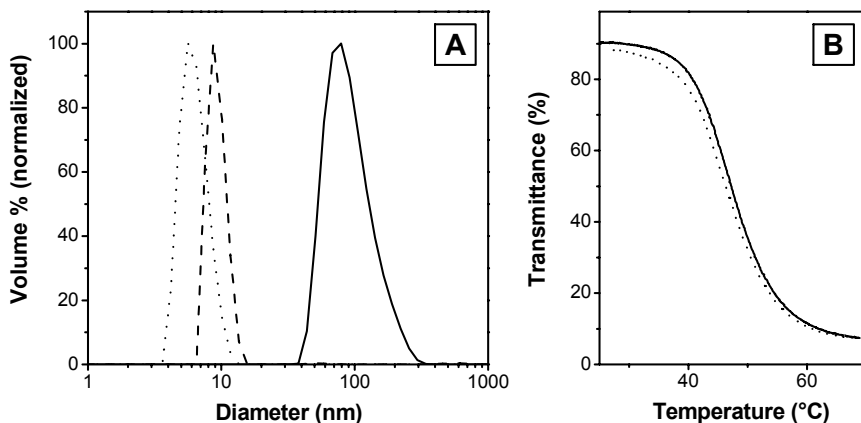


Figure 2. (A) Size distributions measured by dynamic light scattering at room temperature for individual solutions ( $10 \text{ mg}\cdot\text{mL}^{-1}$ ) of either cholesterol-*b*-POEGA samples (dashed line = Table 1, Entry 5; dotted line = Table 1, Entry 6) or cholesterol-*b*-P(EEO<sub>2</sub>A-co-OEGA) (full line = Table 1, Entry 7) in pure deionized water. (B) Plots of transmittance as a function of temperature measured for an aqueous solution ( $1 \text{ mg}\cdot\text{mL}^{-1}$ ) of cholesterol-*b*-P(EEO<sub>2</sub>A-co-OEGA) (Table 1, Entry 7). Solid line: heating, dotted line: cooling. Reproduced with permission from reference 34. Copyright Wiley-VCH Verlag GmbH & Co KGaA.

Random copolymers of EEO<sub>2</sub>A and OEGA are typically less hydrophilic than POEGA. Due to its short oligo(ethylene glycol) side-chain (i.e. only two EO units) and its terminal ethyl ether, the monomer EEO<sub>2</sub>A is less hydrophilic than OEGA. Thus, we previously demonstrated that well-defined copolymers P(EEO<sub>2</sub>A-co-OEGA) exhibit a LCST in water, which can be precisely adjusted by varying the comonomer composition.<sup>16</sup> For example, copolymers P(EEO<sub>2</sub>A-co-OEGA) containing 20 mol% of EEO<sub>2</sub>A exhibit a LCST in pure deionized water at approximately 40°C. Hence, the surfactant cholesterol-*b*-P(EEO<sub>2</sub>A-co-OEGA) (Table 1, Entry 7) is probably having a lower hydrophilic/hydrophobic balance than POEGA-based surfactants and therefore self-organized in pure water into rather monodisperse aggregates with an average hydrodynamic diameter  $D_h$  of approximately 100 nm (Figure 2A). <sup>1</sup>H NMR measurements in D<sub>2</sub>O confirmed the aggregation of the surfactants as the protons of cholesterol were undetectable in that solvent (data not shown). Moreover, as expected, these aggregates were found to be thermoresponsive and precipitated at higher temperatures. Turbidimetry measurements (Figure 2B) indicated that their LCST

is around 45°C, which is slightly higher than the value observed for the unbounded copolymer P(EEO<sub>2</sub>A-*co*-OEGA).<sup>16</sup> Other reports indicated that PEG-based thermoresponsive micelles can exhibit higher LCST than the corresponding hydrophilic segments.<sup>20, 35</sup> Moreover, the measured phase transition was relatively broad. This behavior is generally observed for thermoresponsive copolymers with a short *DP* (i.e. *DP* below 25 units) and is due to chain-to-chain deviations in comonomer composition.<sup>17</sup>

## Switchable bioactive surfaces

Surfaces coated with PEG or oligo(ethylene glycol) are generally regarded as materials of choice for preventing bioadhesion.<sup>36</sup> For instance, numerous publications described the protein-repellency of PEG-modified substrates.<sup>37</sup> Such anti-fouling behavior is mainly due to the steric repulsion between hydrated neutral PEG chains and proteins.<sup>38, 39</sup> Furthermore, as cell-adhesion mechanisms are generally protein-mediated, PEG-modified surfaces were also reported to be efficiently cell-repellent.<sup>40</sup> Thus, PEG-coated materials have been extensively studied in various bio-applications such as blood-compatible materials, implants and stealth carriers for either drug- or gene- delivery.

Yet, although very useful, bio-repellent PEG surfaces remain, on the whole, passive materials. Several emerging areas of biosciences and biotechnology certainly require “smarter” surfaces with more sophisticated properties. For instance, switchable surfaces capable of performing reversible bio-interactions are highly relevant for modern applications such as bioseparation, biosensors, bio-assays and cell engineering. Such smart surfaces can be, for example, constructed with stimuli-responsive polymers.<sup>41</sup> For instance, the thermoresponsive polymer PNIPAM and closely related polyacrylamides have been widely investigated for preparing biorelevant switchable surfaces.<sup>42-44</sup> Exhibiting a LCST at 32°C, PNIPAM is the currently most studied material for inducing surface changes between room- and body- temperature. However, as discussed in the introduction, PNIPAM is not a bio-inert polymer. This polymer may interact with biological objects such as proteins or cell. Thus, the development of efficient switchable surfaces based on polymers of other chemical nature is certainly a topical matter. For instance, surfaces exhibiting thermoresponsive properties comparable to those of PNIPAM and the bio-repellent behavior of hydrated PEG would be of high interest for numerous applications in modern biosciences.

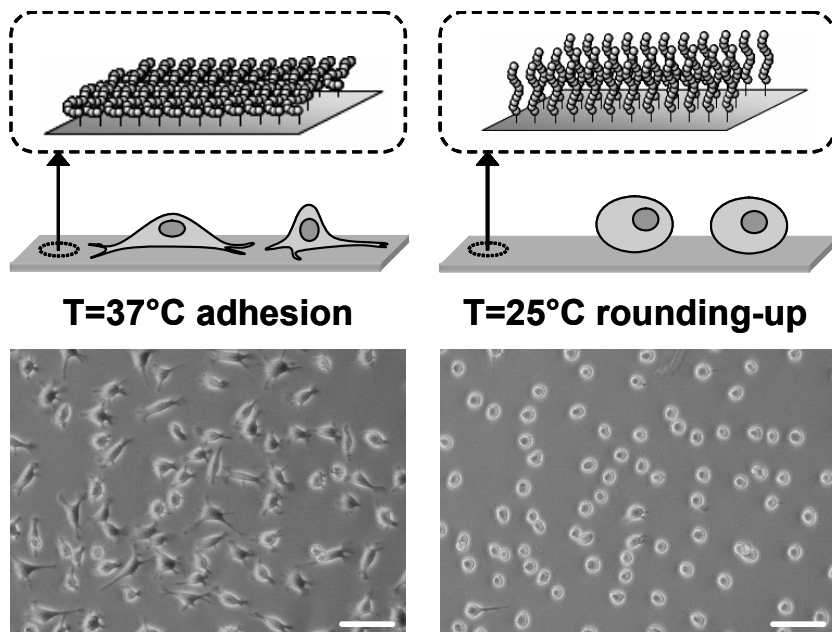


*Figure 3. Phase contrast microscopy images of L929 mouse fibroblasts on P(MEO<sub>2</sub>MA-co-OEGMA)-modified gold substrates after 44 hours of incubation at 37°C (left) and 30 minutes after cooling down the sample to 25°C (right). The surface presented in this figure was prepared using the macroinitiator “grafting-from” approach. Scale bars correspond to 100 μm. Cartoons (top panel) show a schematic view of the polymer coatings at 37 and 25°C. Reproduced with permission from reference 51. Copyright Wiley-VCH Verlag GmbH & Co KGaA.*

In this context, the P(MEO<sub>2</sub>MA-co-OEGMA) thermoresponsive polymers are particularly relevant. Indeed, polymer brushes of oligo(ethylene glycol) methacrylates can be easily prepared on flat substrates via either surface-initiated ATRP or surface adsorption of well-defined polymers with anchor moieties.<sup>45, 46</sup> Yet, brushes prepared with long PEG methacrylates (i.e. side-chains of 5 ethylene oxide units or longer) behave somewhat like standard biorepellent PEG coatings.<sup>47-49</sup> However, thermoresponsive polymers with shorter oligo(ethylene glycol) side-chains might behave differently. For instance, Huck and Jonas recently demonstrated that surface initiated P(MEO<sub>2</sub>MA-co-OEGMA<sub>475</sub>) brushes exhibit LCST values, which coincide with those observed for free copolymers in aqueous solution.<sup>50</sup> The partial dehydration and the change of conformation of these surface brushes above LCST may be of practical interest for tuning bio-adhesion.

In the present work, P(MEO<sub>2</sub>MA-co-OEGMA<sub>475</sub>)-modified gold surfaces were evaluated for their ability to control cell adhesion.<sup>51</sup> In such an application, temperature variations should be relatively mild as mammalian cells may be



damaged by extreme temperature fluctuations. Thus, the surfaces should ideally mediate cellular adhesion at physiological temperature and abandon it at room temperature. To attain such properties, a copolymer P(MEO<sub>2</sub>MA-*co*-OEGMA) containing in average 10 mol% of OEGMA<sub>475</sub> units per chain was selected. This copolymer exhibits a LCST of about 39°C in pure water,<sup>18</sup> whereas in phosphate buffer saline solution, due to a weak salting-out effect, the LCST is around 35°C, rendering it ideal for the present application.

To explore the potential of these thermoresponsive copolymers, three different strategies were investigated for modifying the surfaces. First, well-defined copolymers P(MEO<sub>2</sub>MA-*co*-OEGMA) were prepared by solution ATRP in the presence of a low molecular weight disulfide ATRP initiator, purified and subsequently adsorbed on clean gold substrates (“grafting-onto” approach).<sup>51</sup> Alternatively, the disulfide initiator was first adsorbed on gold surfaces, which were used to initiate the atom transfer radical copolymerization of OEGMA<sub>475</sub> and MEO<sub>2</sub>MA in ethanol/H<sub>2</sub>O mixtures (“grafting-from” approach). In the third strategy, pristine gold surfaces were first modified via layer-by-layer polyelectrolyte deposition and subsequently functionalized by a polyanionic ATRP macroinitiator (i.e. macroinitiator “grafting-from” approach).<sup>52, 53</sup> P(MEO<sub>2</sub>MA-*co*-OEGMA) brushes were then grown from the surfaces using either standard- or AGET- ATRP protocols.<sup>54</sup>

The three different types of P(MEO<sub>2</sub>MA-*co*-OEGMA)-modified gold surfaces were used for cultivating L929 mouse fibroblasts at 37 °C. The fibroblasts adhered efficiently and spread well on all types of substrates (Figure 3), indicating that the P(MEO<sub>2</sub>MA-*co*-OEGMA)-modified surfaces are bio-adherent at physiological temperature. The maximum of adhesion was typically observed after 40 h of cultivation. Such kinetics of adhesion are roughly comparable to those generally observed on PNIPAM-modified surfaces. However, when the temperature of the cultivation medium is decreased to 25 °C, a rapid cell rounding is observed within approximately 30 minutes (Figure 3), allowing their facile detachment and harvesting. No cell rounding of spread fibroblasts occurs on plain gold surfaces upon a temperature decrease from 37 °C to 25 °C. Thus, the P(MEO<sub>2</sub>MA-*co*-OEGMA)-modified gold substrates can be tuned from cell-attractive to cell-repellent (i.e. standard PEG repellency). Importantly, this behavior is reversible and successive cycles spreading/rounding can be triggered by temperature switches. Ultimately, the cells may be washed-off from the surface by gentle rinsing at room temperature.

## Conclusion

Thermoresponsive polymers based on oligo(ethylene glycol) acrylates or methacrylates can be easily prepared by atom transfer radical polymerization under straightforward experimental conditions (i.e. in bulk or in ethanol solution and in the presence of commercially available catalysts). Thus, these stimuli-responsive macromolecules can be exploited for preparing a wide range of smart advanced materials such as thermoreversible hydrogels, thermoresponsive block-copolymer micelles and switchable surfaces. Hence, some of the results

presented in this chapter are anticipated to be highly relevant for biotechnological applications such as protein chromatography, cell cultures, stem-cells differentiation, DNA bioseparation in PCR, tissue engineering, and implants.

## Acknowledgments

Fraunhofer society and Max-Planck society (joint project bioactive surfaces) and the Federal Ministry of Education and Research (BMBF programs NanoforLife and NanoChem) are acknowledged for financial support. Additionally, J.F.L. thanks Katja Uhlig, Dr. Andreas Lankenau and Dr. Claus Duschl (Fraunhofer IBMT, Potsdam) for the cell experiments.

## References

1. Gil, E. S.; Hudson, S. M. *Prog. Polym. Sci.* **2004**, 29, 1173-1222.
2. de las Heras Alarcón, C.; Pennadam, S.; Alexander, C. *Chem. Soc. Rev.* **2005**, 276-285.
3. Schild, H. G. *Prog. Polym. Sci.* **1992**, 17, 163-249.
4. Lutz, J.-F. *J. Polym. Sci. Part A: Polym. Chem.* **2008**, 46, 3459-3470.
5. Aoshima, S.; Sugihara, S. *J. Polym. Sci. A: Polym. Chem.* **2000**, 38, 3962-3965.
6. Han, S.; Hagiwara, M.; Ishizone, T. *Macromolecules* **2003**, 26, 8312-8319.
7. Ali, M. M.; Stöver, H. D. H. *Macromolecules* **2004**, 37, 5219-5227.
8. Kitano, H.; Hirabayashi, T.; Gemmei-Ide, M.; Kyogoku, M. *Macromol. Chem. Phys.* **2004**, 205, 1651-1659.
9. Sugihara, S.; Kanaoka, S.; Aoshima, S. *Macromolecules* **2005**, 38, 1919-1927.
10. Lutz, J.-F.; Weichenhan, K.; Akdemir, Ö.; Hoth, A. *Macromolecules* **2007**, 40, 2503-2508.
11. Maeda, Y.; Kubota, T.; Yamauchi, H.; Nakaji, T.; Kitano, H. *Langmuir* **2007**, 23, 11259-11265.
12. Cheng, G.; Hua, F.; Melnichenko, Y. B.; Hong, K.; Mays, J. W.; Hammouda, B.; Wignall, G. D. *Macromolecules* **2008**, 41, 4824-4827.
13. Jiang, X.; Smith, M. R.; Baker, G. L. *Macromolecules* **2008**, 41, 318-324.
14. Zhao, B.; Li, D.; Hua, F.; Green, D. R. *Macromolecules* **2005**, 38, 9509-9517.
15. Hua, F.; Jiang, X.; Li, D.; Zhao, B. *J. Polym. Sci. Part A: Polym. Chem.* **2006**, 44, 2454-2467.
16. Skrabania, K.; Kristen, J.; Laschewsky, A.; Akdemir, O.; Hoth, A.; Lutz, J.-F. *Langmuir* **2007**, 23, 84-93.
17. Lutz, J.-F.; Akdemir, O.; Hoth, A. *J. Am. Chem. Soc.* **2006**, 128, 13046-13047.
18. Lutz, J.-F.; Hoth, A. *Macromolecules* **2006**, 39, 893-896.
19. Becer, C. R.; Hahn, S.; Fijten, M. W. M.; Thijs, H. M. L.; Hoogenboom, R.; Schubert, U. S. *J. Polym. Sci. Part A: Polym. Chem.* **2008**, 46, 7138-7147.

20. Holder, S. J.; Durand, G. G.; Yeoh, C.-T.; Illi, E.; Hardy, N. J.; Richardson, T. H. *J. Polym. Sci. Part A: Polym. Chem.* **2008**, *46*, 7739-7756.
21. Yamamoto, S. i.; Pietrasik, J.; Matyjaszewski, K. *J. Polym. Sci. Part A: Polym. Chem.* **2008**, *46*, 194-202.
22. Matyjaszewski, K.; Xia, J. *Chem. Rev.* **2001**, *101*, 2921-2990.
23. Braunecker, W. A.; Matyjaszewski, K. *Progr. Polym. Sci.* **2007**, *32*, 93-146.
24. McCormick, C. L.; Sumerlin, B. S.; Lokitz, B. S.; Stempka, J. E. *Soft Matter* **2008**, *4*, 1760-1773.
25. Moad, G.; Rizzardo, E.; Thang, S. H. *Polymer* **2008**, *49*, 1079-1131.
26. Lee, W.-F.; Lin, Y.-H. *J. Appl. Polym. Sci.* **2003**, *90*, 1683-1691.
27. Kaneko, Y.; Nakamura, S.; Sakai, K.; Aoyagi, T.; Kikuchi, A.; Sakurai, Y.; Okano, T. *Macromolecules* **1998**, *31*, 6099-6105.
28. Lutz, J.-F.; Andrieu, J.; Üzgün, S.; Rudolph, C.; Agarwal, S. *Macromolecules* **2007**, *40*, 8540-8543.
29. Fechler, N.; Badi, N.; Schade, K.; Pfeifer, S.; Lutz, J.-F. *Macromolecules* **2009**, *42*, 33-36.
30. Rodriguez-Hernandez, J.; Chécot, F.; Gnanou, Y.; Lecommandoux, S. *Prog. Polym. Sci.* **2005**, *30*, 691-724.
31. Lutz, J.-F. *Polym. Int.* **2006**, *55*, 979-993.
32. Discher, D. E.; Eisenberg, A. *Science* **2002**, *297*, 967-973.
33. Gohy, J.-F. *Adv. Polym. Sci.* **2005**, *190*, 65-136.
34. Lutz, J.-F.; Pfeifer, S.; Zarafshani, Z. *QSAR Comb. Sci.* **2007**, *26*, 1151-1158.
35. Mertoglu, M.; Garnier, S.; Laschewsky, A.; Skrabania, K.; Storsberg, J. *Polymer* **2005**, *46*, 7726-7740.
36. Prime, K. L.; Whitesides, G. M. *Science* **1991**, *252*.
37. Gombotz, W. R.; Guanghai, W.; Horbett, T. A.; Hoffman, A. S. *J. Biomed. Mat. Res.* **1991**, *25*, 1547-1562.
38. Jeon, S. I.; Lee, J. H.; Andrade, J. D.; De Gennes, P. G. *J. Colloid Interface Sci.* **1991**, *142*, 149-158.
39. McPherson, T.; Kidane, A.; Szleifer, I.; Park, K. *Langmuir* **1998**, *14*, 176-186.
40. Desai, N. P.; Hubbell, J. A. *Biomaterials* **1991**, *12*, 144-153.
41. Nath, N.; Chilkoti, A. *Adv. Mater.* **2002**, *14*, 1243-1247.
42. Takezawa, T.; Mori, Y.; Yoshizato, K. *Bio/Technology* **1990**, *8*, 854-856.
43. Okano, T.; Yamada, N.; Okuhara, M.; Sakai, H.; Sakurai, Y. *Biomaterials* **1995**, *16*, 297-303.
44. Wischerhoff, E.; Zacher, T.; Laschewsky, A.; Rekaï, E. D. *Angew. Chem. Int. Ed.* **2000**, *39*, 4602-4604.
45. Pyun, J.; Kowalewski, T.; Matyjaszewski, K. *Macromol. Rapid Commun.* **2003**, *24*, 1043-1059.
46. Edmondson, S.; Osborne, V. L.; Huck, W. T. S. *Chem. Soc. Rev.* **2004**, *33*, 14-22.
47. Ma, H. W.; Hyun, J. H.; Stiller, P.; Chilkoti, A. *Adv. Mater.* **2004**, *16*, 338-341.
48. Popescu, D. C.; Lems, R.; Rossi, N. A. A.; Yeoh, C.-T.; Loos, J.; Holder, S. J.; Bouten, C. V. C.; Sommerdijk, N. A. J. M. *Adv. Mater.* **2005**, *17*, 2324-2329.

49. Tugulu, S.; Silacci, P.; Stergiopoulos, N.; Klok, H.-A. *Biomaterials* **2007**, *28*, 2536-2546.
50. Jonas, A. M.; Glinel, K.; Oren, R.; Nysten, B.; Huck, W. T. S. *Macromolecules* **2007**, *40*, 4403-4405.
51. Wischerhoff, E.; Uhlig, K.; Lankenau, A.; Börner, H. G.; Laschewsky, A.; Duschl, C.; Lutz, J.-F. *Angew. Chem. Int. Ed.* **2008**, *47*, 5666-5668.
52. Bertrand, P.; Jonas, A.; Laschewsky, A.; Legras, R. *Macromol. Rapid Commun.* **2000**, *21*, 319-348.
53. Edmondson, S.; Vo, C. D.; Armes, S. P.; Unali, G. F. *Macromolecules* **2007**, *40*, 5271-5278.
54. Jakubowski, W.; Matyjaszewski, K. *Angew. Chem. Int. Ed.* **2006**, *45*, 4482-4486.

## Chapter 14

# Gelation in Atom Transfer Radical Copolymerization with a Divinyl Cross-linker

Haifeng Gao, Wenwen Li, Ke Min and Krzysztof Matyjaszewski

Department of Chemistry, Carnegie Mellon University, 4400 Fifth Avenue,  
Pittsburgh, Pennsylvania 15213

ATRP was applied to the copolymerization of a monovinyl monomer and a divinyl cross-linker to study the experimental gelation behavior. The fundamental features of ATRP, including fast initiation and reversible deactivation reactions, resulted in a retarded gelation and the formation of a more homogeneous network in the ATRP process compared to gel formation in a conventional radical polymerization. The experimental gel point based on the monomer conversion in the ATRP reaction occurred later than the calculated value based on Flory-Stockmayer's mean-field theory, which was mainly ascribed to intramolecular cyclization reactions. The dependence of the experimental gel points on several parameters was systematically studied, including the ratio of cross-linker to initiator, the concentration of reagents, reactivity of vinyl groups, initiation efficiency of initiators, and polydispersity of primary chains.

### Introduction and Background

Radical copolymerization of monovinyl monomers with a small amount of divinyl cross-linkers produces soluble branched polymers and insoluble gels. The cross-linkage, provided by a cross-linker with both vinyl groups reacted, is formed in the polymer chains via reaction of pendant vinyl groups with the propagating chain-end radicals either intermolecularly or intramolecularly. The molecular weight and/or size of the branched polymers increase exponentially with the progress of intermolecular cross-linking reactions, and finally reach an

“infinite” value with the formation of a polymeric network (gel). The transition from sol to gel is defined as the “gel point”.<sup>1</sup>

Based on Flory-Stockmayer’s mean-field theory (F-S theory), the theoretical gel point in a system is reached when the weight-average number of cross-linking unit ( $\nu$ ) per primary chain equals unity:<sup>1,2</sup>

$$\nu_c = p\rho(DP_w - 1) = 1 \quad \text{Eq. 1}$$

where  $p$  is the conversion of double bonds,  $\rho$  is the fraction of all double bonds residing on divinyl molecules in the initial mixture, and  $DP_w$  is the weight-average degree of polymerization (DP) of the linear primary chains, which would be formed if all cross-linkages in the network at the gel point were cut. This calculation was established for an ideal polymer network with two basic assumptions: equal reactivity for all vinyl species and no occurrence of intramolecular cyclization reactions. When  $DP_w \gg 1$  and the polydispersity of primary chains ( $DP_w/DP_n$ ) are considered, Eq. 1 is expressed as:

$$\nu_c = p\rho DP_n \frac{DP_w}{DP_n} = p \left( \frac{2[X]_0}{[M]_0 + 2[X]_0} \right) \left[ p \left( \frac{[M]_0 + 2[X]_0}{[PC]_t} \right) \right] \frac{DP_w}{DP_n} = 1$$

which can be rewritten as:

$$\nu_c = p^2 \frac{2[X]_0}{[PC]_t} \frac{DP_w}{DP_n} = 1 \quad \text{Eq. 2}$$

where  $[M]_0$ ,  $[X]_0$  are the initial concentrations of monomer and divinyl cross-linker, respectively, and  $[PC]_t$  is the concentration of primary chains in the system at any time  $t$ . Therefore, the critical conversion of double bonds at the moment of gelation,  $p_c$  equals

$$p_c = \sqrt{\frac{[PC]_t}{2[X]_0} \frac{1}{DP_w/DP_n}} \quad \text{Eq. 3}$$

which indicates that the theoretical gel point based on the conversion of double bonds is determined by the initial amount of divinyl cross-linker, the instantaneous concentration of primary chains and the polydispersity.

## Different Gelation Processes Between Conventional RP and CRP

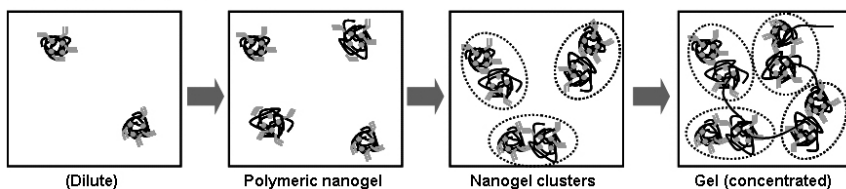
Highly branched polymers and/or gels with inhomogeneous structures are formed during most conventional radical polymerization (RP) reactions because of the intrinsic limitations of RP, including slow initiation, fast chain propagation, and unavoidable radical termination reactions.<sup>3-5</sup> Primary radicals are slowly but continuously generated in the system, resulting in a very dilute polymer solution at the beginning ( $\sim \mu\text{M}$ ). On the other hand, the generated primary radicals quickly propagate within a time scale of seconds before the occurrence of a termination reaction to permanently lose the chain-end functionality. Considering a typical value for the propagation rate constant ( $k_p \sim 10^3 \text{ s}^{-1}$ ), the  $DP_n$  of primary chains could exceed  $DP_n \sim 10^3$  at the beginning of polymerization. Therefore, based on Eq. 3, gelation in a conventional RP reaction should occur at very low conversion, e.g.,  $p_c = 0.16\%$ , under bulk conditions ( $[M]_0 = 10 \text{ M}$ ) with 1 mol% of cross-linker in the initial formula and

$DP_w/DP_n = 2$  for the primary chains. However, the measured experimental gel point based on monomer conversion is typically 1 or 2 orders of magnitude larger than the predicted value. This is mainly due to an excluded volume effect of polymer chains and a significant contribution of intramolecular cyclization reactions.<sup>3,5,6</sup> At the beginning of the copolymerization, the polymer chains formed in the reaction seldom overlap with each other because of the extremely low polymer concentration. Consequently, most of the pendant vinyl groups are consumed via intramolecular cyclization reactions, producing a less-swollen nanogel with a highly cross-linked nanodomain (Scheme 1A). As the reaction proceeds, the number of these nanogels increases and radicals generated later in the reaction connect these preformed overlapped nanogels into larger molecules and form a heterogeneous network.

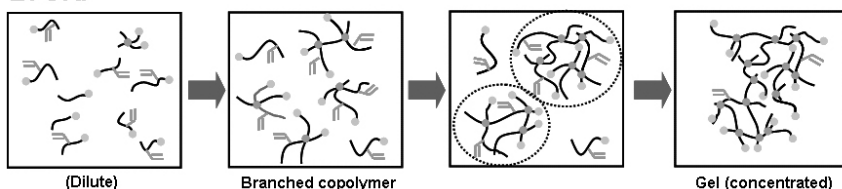
In contrast to conventional RP, recently developed controlled radical polymerization (CRP)<sup>7,8</sup> techniques have several advantages when targeting the preparation of more homogeneous polymer networks, due to fast initiation and quick reversible deactivation reactions. The fast initiation reactions, relative to propagation reactions, result in a rapid conversion of all initiators into primary chains and a nearly constant number of growing primary chains throughout the polymerization (Scheme 1B). Therefore, the concentration of primary chains in a well controlled CRP system is similar to the concentration of added initiators throughout the polymerization (e.g.,  $[PC]_t \sim [Initiator]_0 \sim \text{mM}$ ).<sup>8</sup> The fast initiation in CRPs implies that the theoretical gel point, based on Eq. 3, is now delayed to  $p_c = 5.0\%$  for a bulk system ( $[M]_0 = 10 \text{ M}$ , 1 mol% cross-linker,  $[Initiator]_0 = 1 \text{ mM}$ ) with  $DP_w/DP_n = 2$  for the primary chains. When the primary chain with a lower polydispersity ( $DP_w/DP_n = 1.1$ ) is considered, the value of  $p_c$  would be even higher,  $p_c = 6.7\%$ . This calculated result clearly explains the retarded gelation observed in CRP process due to the feature of fast initiation reactions.

Moreover, the dynamic equilibrium in a CRP system, established between a low concentration of active propagating chains and a large number of “dormant” chains, ensure that only a few monomer units are incorporated into the polymer chains in each activation/deactivation cycle. During the long “dormant” period, the polymer chains cannot propagate, but can diffuse and relax, which results in the probability of reaction of each vinyl species: monomer, cross-linker or pendant vinyl group, is statistically determined by their concentrations and reactivities. Thus, the application of CRP techniques results in a more homogeneous incorporation of branching points into the branched polymers and gels, as compared to the polymers synthesized by conventional RP methods under similar concentrations of comonomers.<sup>9-19</sup> Moreover, the chain-end functionalities are preserved in the branched polymers and/or gels synthesized by CRPs, which can be further used for chain-end modification and chain extension reactions.<sup>12,16,20-22</sup>

### A. Conventional RP



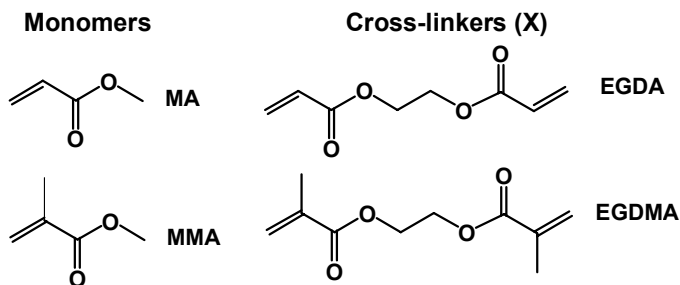
### B. CRP



**Scheme 1.** Comparison of different gelation behaviors in conventional RP and CRP processes.

## Determination of Experimental Gel Points in ATRP

Atom transfer radical polymerization (ATRP)<sup>23-26</sup> was selected as an exemplary CRP technique to systematically study the kinetics and gelation behavior during the concurrent copolymerization of monovinyl monomers and divinyl cross-linkers (Scheme 2). The effect of different parameters on the experimental gelation was studied, including the initial molar ratio of cross-linker to initiator, the concentrations of reagents, the reactivity of vinyl groups present in the cross-linker, the efficiency of initiation, and the polydispersity of primary chains. Experimental gel points based on the conversions of monomer and/or cross-linker at the moment of gelation, were determined and compared with each other in order to understand the influence of each parameter on the experimental gel points.



**Scheme 2.** Structures of monomers and divinyl cross-linkers used during the ATRP reactions



## Reactivity of Vinyl Groups during ATRcP of MA and EGDA

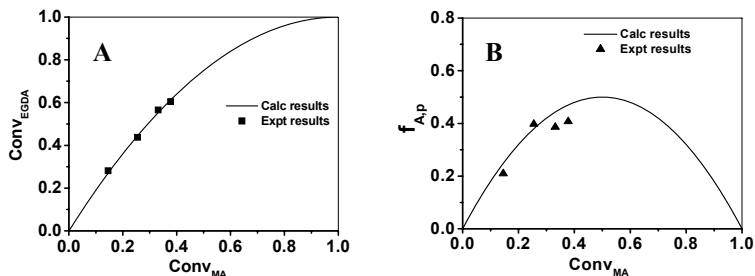


**Figure 1.** Comparison of calculated and experimental results of (A) conversions of MA and EGDA, and (B) fraction of pendant acrylate group ( $f_{A,p}$ ) during ATRcP of MA and EGDA with  $[MA]_0/[EGDA]_0/[EBrP]_0/[CuBr]_0/[CuBr_2]_0/[PMDETA]_0 = 50/10/1/0.45/0.05/0.5$ ,  $[MA]_0 = 6.0$  M, in DMF at 60 °C. The experimental conversions of MA and EGDA were determined by GC measurement. (Adapted with permission from reference 18. Copyright 2007 American Chemical Society.)

The atom transfer radical copolymerization (ATRcP) of methyl acrylate (MA) monomer and ethylene glycol diacrylate (EGDA) cross-linker (Scheme 2) was performed by using ethyl 2-bromopropionate (EBrP) as initiator,  $CuBr/N,N,N',N'',N''$ -pentamethyldiethylenetriamine (PMDETA) as catalyst and DMF as solvent. Moreover, 10 mol%  $CuBr_2$  of total copper species was pre-added to the reactions to minimize the initial nonstationary stage. Therefore, the ATRP of acrylate-based monomers under these conditions proceeds with fast initiation, high initiation efficiency and good control over the polydispersity of primary chains (low  $M_w/M_n$ ).

The reactivity of vinyl species from EGDA cross-linker and pendant vinyl group was comparable to that of MA monomer. If all acrylate double bonds have the same reactivity, at the conversion of MA monomer  $Conv_{MA}$ , the conversion of EGDA should be  $Conv_{EGDA} = 2Conv_{MA} - (Conv_{MA})^2$  and the fraction of cross-linkage versus the initially added cross-linker is  $f_{Cross-linkage} = 2(Conv_{MA})^2$ , because each cross-linker contains two vinyl bonds. Consequently, the fraction of pendant acrylate group should be  $f_{A,p} = Conv_{EGDA} - f_{Cross-linkage} = 2Conv_{MA} - 2(Conv_{MA})^2$ . In Figure 1A, the calculated results overlapped with the experimental conversions of MA and EGDA at different times before gelation, suggesting that the reactivity of each vinyl group in EGDA cross-linker is the same as that of free MA monomer. The experimental values of  $f_{A,p}$  were obtained by  $^1H$  NMR analysis of the polymer sols at different times after removal of the free MA and EGDA to determine the concentration of pendant acrylate groups. The experimental values of  $f_{A,p}$  were close to the lines based on the calculated results (Figure 1B), indicating that the reactivity of pendant acrylate group is similar to that of free MA monomer, at least at low conversion before gelation.

## Effect of Molar Ratios and Concentrations on Experimental Gel Points

The experimental gel points were significantly affected by the initial molar ratio of cross-linker to initiator. No gelation was observed when the initial molar ratio of EGDA cross-linker to EBrP initiator was less than unity, even under bulk conditions with complete conversion of vinyl species, when ATRP proceeded with high initiation efficiency and low polydispersity of primary chains. For comparison, the theoretical gel point based on F-S theory is reached at 71% monomer conversion for the equimolar ratio of cross-linkers to monodisperse primary chains. Since all vinyl groups show similar reactivities during the copolymerization of MA and EGDA (Figure 1), the delayed experimental gelation in the ATRcP processes was primarily attributed to the unavoidable intramolecular cyclization reactions. The cyclization reactions consume pendant vinyl groups but have no contribution to the increase of molecular weight of the branched polymers.

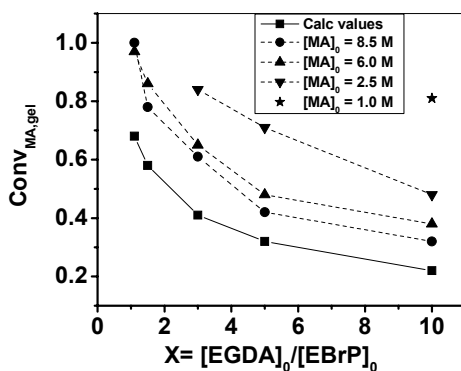


**Figure 2.** Comparison of calculated and experimental gel points at different concentrations of  $[MA]_0$  and molar ratios of  $X = [EGDA]_0/[EBrP]_0$ ; experimental conditions:  $[MA]_0/[EGDA]_0/[EBrP]_0/[CuBr]_0/[CuBr_2]_0/[PMDETA]_0 = 50/X/1/0.45/0.05/0.5$ , in DMF at  $60^\circ\text{C}$ . The experimental gel point was the moment when the reaction fluid lost its mobility at an upside down position for 10 seconds. (Adapted with permission from reference 24. Copyright 2008 American Chemical Society.)

The extent of cyclization reactions that occurred during the ATRcP reactions could be controlled by adjusting the initial concentration of reagents. For instance, by fixing the molar ratios of MA to EGDA and EBrP, a simple dilution of the ATRcP system via addition of more DMF solvent, dramatically postponed the experimental gelation to higher monomer conversion, i.e., longer reaction time, than the value obtained under concentrated conditions, or even prevented the gelation (Figure 2).<sup>27</sup> Since the experimental gel points under concentrated conditions was still higher than the F-S value, a reciprocal method could be applied to plot the experimental gel points based on monomer

conversions against  $1/[M]_0$ . Extrapolation to a zero value provides the imaginary experimental gel point at infinite concentration, which should represent a system with minimum intramolecular cyclizations (Figure 3). When the molar ratios of reagents were  $[MA]_0/[EGDA]_0/[EBrP]_0 = 50/10/1$ , the gel point at infinite concentration would occur at 26.0% of MA conversion, which was very close to the value of 22.3% of MA conversion based on the calculation provided by F-S theory.

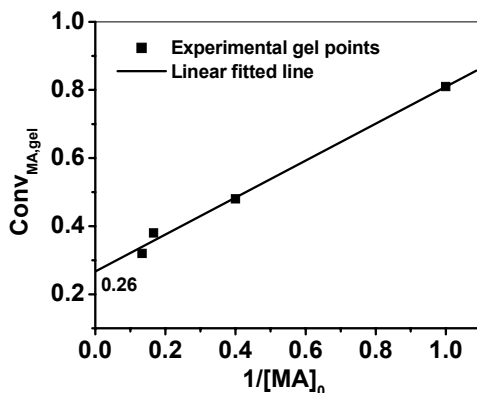


**Figure 3.** Reciprocal plot of experimental gel points based on MA conversions against  $1/[MA]_0$  during the ATRcP of MA and EGDA under different MA concentrations; experimental condition:  $[MA]_0/[EGDA]_0/[EBrP]_0/[CuBr]_0/[CuBr_2]_0/[PMDETA]_0 = 50/10/1/0.45/0.05/0.5$ , in DMF at 60 °C.

### Effect of Cross-linker Reactivity on Experimental Gel Points

In addition to the concentration effect, the reactivity of the vinyl groups in the cross-linker compared to monomer could also influence the experimental gel points during the ATRcP reactions. For instance, the ATRcP of MA and ethylene glycol dimethacrylate (EGDMA, Scheme 2) resulted in a different gelation behavior compared to the model copolymerization of MA and EGDA with equivalent reactivity for all acrylate groups.<sup>28</sup> The higher reactivity of methacrylate groups present in the EGDMA resulted in faster consumption of cross-linker and quicker generation of branching points into the copolymer chains, which represents an acceleration effect for experimental gelation. On the other hand, the branched polymer contained a gradient distribution of pendant methacrylate groups and branching points and resembled a star-like structure (Figure 4A). The pendant vinyl groups located in the more densely cross-linked core were isolated by the surrounded less cross-linked shell, which reduced the probability for intermolecular reactions and retarded gelation, a deceleration effect. These two effects inter-correlated with each other and significantly affected the experimental gel points of the poly(MA-co-EGDMA) system, depending on the amount of added EGDMA. The deceleration effect was dominant when the initial molar ratio of  $X = [EGDMA]_0/[R-Br]_0 < 2.3$ . While

the acceleration effect became dominant when higher amounts of EGDMA were used, leading to an experimental gelation at lower MA conversion compared to the ATRcP of MA and EGDA (Figure 4B).

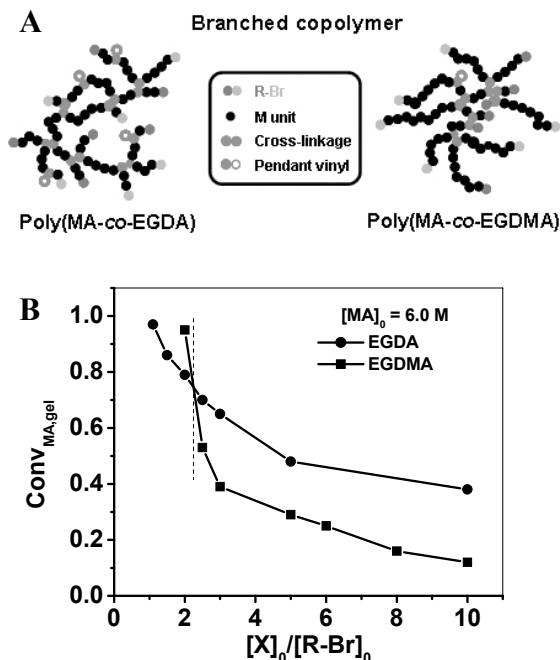


**Figure 4.** (A) Illustration of different structures of poly(MA-co-EGDA) and poly(MA-co-EGDMA) copolymers synthesized by ATRcP of MA with different cross-linkers, and (B) comparison of their experimental gel points based on MA conversions; experimental conditions:  $[MA]_0/[X]_0/[R-Br]_0/[CuBr]_0/[CuBr_2]_0/[PMDETA]_0 = 50/X/1/0.45/0.05/0.5$ ,  $[MA]_0 = 6.0$  M in DMF at 60 °C. (Adapted with permission from reference 25. Copyright 2008 American Chemical Society.)

### Effect of Initiation Efficiency and Polydispersity of Primary Chains on Experimental Gel Points

All of the systems discussed above employed an ATRP condition with high initiation efficiency ( $[PC]_t \sim [Initiator]_0$ ) and low polydispersity of primary chains ( $M_w/M_n \leq 1.1$ ). ATRP allows further control of the relative initiation rate of initiators and the polydispersity of primary chains via rationally adjusting the structure of initiators, the solubility of catalysts, and the concentration of deactivators. Based on Eq. 3., it is expected that by fixing the initial molar ratio of cross-linker to initiator and their concentrations, a reduced initiation efficiency and/or a broadening distribution of primary chains would decrease the onset of the experimental gel point based on monomer conversion and accelerate the gelation process.

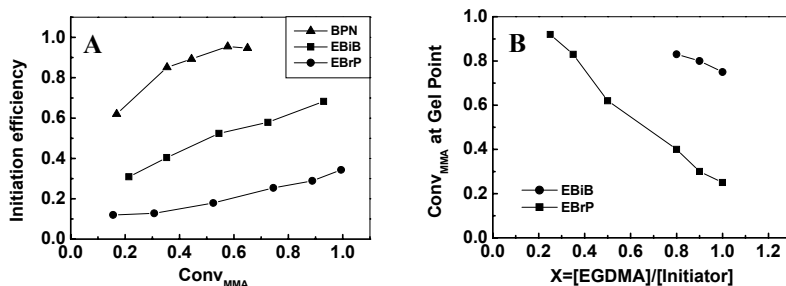


**Figure 5.** (A) Initiation efficiency of different ATRP initiators during the homopolymerization of MMA, and (B) comparison of experimental gel points during ATRcP of MMA and EGDMA by using different initiators with various ratios of  $X = [\text{EGDMA}]/[\text{Initiator}]$ ; experimental conditions:  $[\text{MMA}]_0/[\text{Initiator}]_0/[\text{CuBr}]_0/[\text{CuBr}_2]_0/[\text{bpy}]_0 = 50/1/0.4/0.1/1$  for ATRP, and  $[\text{MMA}]_0/[\text{EGDMA}]_0/[\text{Initiator}]_0/[\text{CuBr}]_0/[\text{CuBr}_2]_0/[\text{bpy}]_0 = 50/X/1/0.4/0.1/1$  for ATRcP,  $[\text{MMA}]_0 = 5.0 \text{ M}$  in acetone at  $50^\circ\text{C}$ ; linear polyMMA standards for THF GPC calibration.

When an initiator with slow initiation rate was employed, the added initiators were slowly but continuously transformed into primary chains, which are usually observed in GPC traces as a tailing toward the low molecular weight and a higher experimental molecular weight than the theoretical value. Some unreacted initiators could be still left in the system even after gelation, if the initiation rate is slow enough. Thus, the initiation rate directly affects the fraction of initiators transformed into polymer chains, i.e., the number of primary chains formed in the system. The influence of initiation efficiency on the experimental gel points was studied by using three initiators with progressively increased reactivities: EBrP, ethyl 2-bromoisobutyrate (EBiB) and 2-bromopropionitrile (BPN), for copolymerization of methyl methacrylate (MMA) and EGDMA under concentrated conditions. By using the least efficient EBrP as initiator, poly(MMA-*co*-EGDMA) based gels were obtained at 90% MMA conversion when the initial molar ratio of cross-linker to initiator was as low as 0.25 (Figure 5B), which was ascribed to the low initiation efficiency of EBrP (initiation efficiency =  $M_{n,\text{theor}}/M_{n,\text{GPC}}$ ). Increasing the initial molar ratio of  $X = [\text{EGDMA}]_0/[\text{EBrP}]_0$  to 1.0 resulted in an earlier gelation at 25% MMA conversion. With EBiB as the initiator, gels formed at 75% MMA conversion under similar polymerization conditions. In contrast, when the most efficient BPN initiator was used, no gel formed until the molar ratio of cross-linker to initiator exceeded unity.

The effect of polydispersity of primary chains on experimental gel points was also studied by using activators regenerated by electron transfer (ARGET)<sup>29,30</sup> ATRP for the copolymerization of MA and EGDA. Decreasing the copper concentration from tens of ppm to a few ppm increased the polydispersity of primary chains from  $M_w/M_n = 1.1$  to 2.0, which accelerated the experimental gel point during the copolymerization of monomer and cross-linker.

## Conclusions

The application of ATRP technique to copolymerization of monovinyl monomer and divinyl cross-linker retarded the experimental gelation, as compared to the conventional RP processes, due to the features of fast initiation and slow gradual chain growth in ATRP. The experimental gel point based on the monomer and/or cross-linker conversions were determined using a good ATRP system with fast initiation and low polydispersity of primary chains. All vinyl species were proved to have a similar reactivity during the ATRcP of MA and EGDA. However, the critical number of cross-linkage per primary chain required to reach the experimental gelation was twice higher than the value predicted from Flory-Stockmayer's theory, indicating that more than 50% of the cross-linker was consumed by intramolecular cyclization reactions even under bulk conditions. The experimental gel points determined during series of ATRcP reactions were significantly affected by several parameters. A higher molar ratio of cross-linker to initiator led to gelation at lower monomer conversions, while the experimental gelation was delayed or even prevented by simply diluting the system with solvent. When a divinyl cross-linker with higher reactivity than the vinyl group present in the monomer was used, experimental gelation was concurrently influenced by two effects: faster generation of cross-linkage and higher steric hindrance for intermolecular cross-linking, depending on the initial molar ratio of cross-linker to initiator. Decreasing the initiation efficiency of initiators and/or increasing the polydispersity of primary chains resulted in an earlier experimental gelation, at lower monomer conversion, or with substoichiometric amounts of cross-linker to initiator. All these results provided important guidelines for further exploration of the gelation processes during the ATRcP reactions under different experimental conditions.

## Acknowledgments

The authors are grateful to the members of the CRP Consortium at Carnegie Mellon University and NSF (Grant DMR 05-49353) for funding. W. Li acknowledges support from Bayer Fellowship.

## References

- (1) Flory, P. J. *Principles of Polymer Chemistry*; Cornell University Press: Ithaca, NY, 1953.
- (2) Stockmayer, W. H. *J. Chem. Phys.* **1944**, *12*, 125.
- (3) Matsumoto, A. *Adv. Polym. Sci.* **1995**, *123*, 41.
- (4) Funke, W.; Okay, O.; Joos-Muller, B. *Adv. Polym. Sci.* **1998**, *136*, 138.
- (5) Dusek, K.; Duskova-Smrckova, M. *Prog. Polym. Sci.* **2000**, *25*, 1215.
- (6) Gordon, M.; Roe, R.-J. *J. Polym. Sci.* **1956**, *21*, 75.
- (7) Matyjaszewski, K.; Davis, T. P., Eds. *Handbook of Radical Polymerization*; Wiley: Hoboken, 2002.

- (8) Braunecker, W. A.; Matyjaszewski, K. *Prog. Polym. Sci.* **2007**, *32*, 93.
- (9) Ide, N.; Fukuda, T. *Macromolecules* **1999**, *32*, 95.
- (10) Yu, Q.; Zeng, F.; Zhu, S. *Macromolecules* **2001**, *34*, 1612.
- (11) Isaure, F.; Cormack, P. A. G.; Graham, S.; Sherrington, D. C.; Armes, S. P.; Buetuen, V. *Chem. Commun.* **2004**, 1138.
- (12) Tsarevsky, N. V.; Matyjaszewski, K. *Macromolecules* **2005**, *38*, 3087.
- (13) Li, Y.; Armes, S. P. *Macromolecules* **2005**, *38*, 8155.
- (14) Liu, B.; Kazlauciuonas, A.; Guthrie, J. T.; Perrier, S. *Macromolecules* **2005**, *38*, 2131.
- (15) Wang, A. R.; Zhu, S. *Polym. Eng. Sci.* **2005**, *45*, 720.
- (16) Taton, D.; Baussard, J.-F.; Dupayage, L.; Poly, J.; Gnanou, Y.; Ponsinet, V.; Destarac, M.; Mignaud, C.; Pitois, C. *Chem. Commun.* **2006**, 1953.
- (17) Bannister, I.; Billingham, N. C.; Armes, S. P.; Rannard, S. P.; Findlay, P. *Macromolecules* **2006**, *39*, 7483.
- (18) Gao, H.; Min, K.; Matyjaszewski, K. *Macromolecules* **2007**, *40*, 7763.
- (19) Yu, Q.; Zhou, M.; Ding, Y.; Jiang, B.; Zhu, S. *Polymer* **2007**, *48*, 7058.
- (20) Siegwart, D. J.; Oh, J. K.; Gao, H.; Bencherif, S. A.; Perineau, F.; Bohaty, A. K.; Hollinger, J. O.; Matyjaszewski, K. *Macromol. Chem. Phys.* **2008**, *209*, 2179.
- (21) Oh, J. K.; Drumright, R.; Siegwart, D. J.; Matyjaszewski, K. *Prog. Polym. Sci.* **2008**, *33*, 448.
- (22) Coessens, V.; Pintauer, T.; Matyjaszewski, K. *Prog. Polym. Sci.* **2001**, *26*, 337.
- (23) Wang, J.-S.; Matyjaszewski, K. *J. Am. Chem. Soc.* **1995**, *117*, 5614.
- (24) Matyjaszewski, K.; Xia, J. H. *Chem. Rev.* **2001**, *101*, 2921.
- (25) Kamigaito, M.; Ando, T.; Sawamoto, M. *Chem. Rev.* **2001**, *101*, 3689.
- (26) Tsarevsky, N. V.; Matyjaszewski, K. *Chem. Rev.* **2007**, *107*, 2270.
- (27) Gao, H.; Li, W.; Matyjaszewski, K. *Macromolecules* **2008**, *41*, 2335.
- (28) Gao, H.; Miasnikova, A.; Matyjaszewski, K. *Macromolecules* **2008**, *41*, 7843.
- (29) Jakubowski, W.; Min, K.; Matyjaszewski, K. *Macromolecules* **2006**, *39*, 39.
- (30) Jakubowski, W.; Matyjaszewski, K. *Angew. Chem., Int. Ed.* **2006**, *45*, 4482.

## Chapter 15

# Segregated Polymer Brushes via “Grafting to” and ATRP “Grafting from” Chain Anchoring

Yong Liu, Viktor Klep and Igor Luzinov\*

School of Materials Science and Engineering, Clemson University,  
Clemson, SC 29634, USA

Synthesis of two-component heterogeneous segregated brushes utilizing the phase-separation phenomena in ultrathin polystyrene/poly(methyl methacrylate) films and the combination of “grafting-to” and “grafting-from” method of polymer anchoring is reported. First component PS brushes were prepared using the “grafting-to” approach; second component polyethylene glycol methyl ether methacrylate brushes were synthesized using a surface-initiated atom transfer radical polymerization. The segregated brushes demonstrated non-uniform surface response as evidenced by the study of the surfaces morphologies after being treated with selective solvents and by protein adsorption.

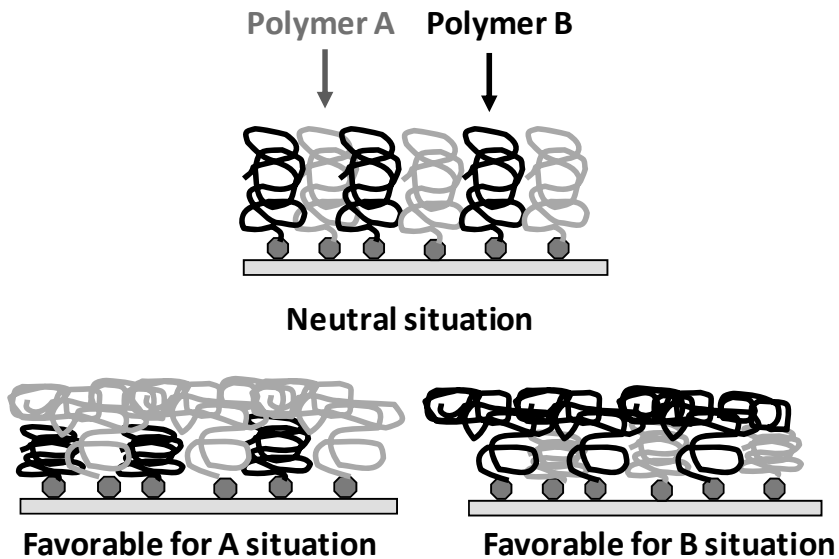
### Introduction

Ultrathin densely end-grafted polymer layers (polymer brushes) are well known to dramatically affect the surface properties of substrates, including adhesion, lubrication, wettability, friction, and biocompatibility (1). These layers are frequently used to modulate surface properties of various materials without altering their bulk performance. Perhaps one of the most exciting and promising areas for the development of polymer brush applications is that involving stimuli-responsive surfaces, which represent functional surfaces that can switch properties in response to external stimuli (2-34). A wide variety of properties can be targeted; the same surfaces can be hydrophobic or hydrophilic, sticky or non-adhesive, protein-repelling or adsorbing, positively or negatively charged, conductive or non-conductive. Various types of external stimuli including temperature, selective solvents, PH, ionic strength, electrical or



magnetic field and light irradiation were employed to initiate switching of these properties.

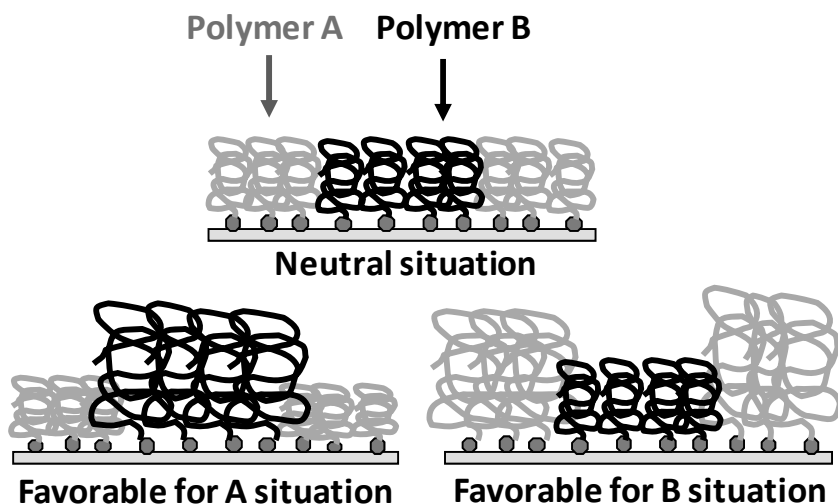
Stimuli-responsive surfaces were synthesized with block copolymer brushes (5), mixed binary polymer brushes (6,7), and Y-shape polymer brushes (8), all of which had been reported to demonstrate stimuli-responsive behavior. According to the literature, despite their nano-scale phase separated structures, these brushes displayed uniform surface response, where the entire brush layers changed surface properties on micro and nano scale. For example, the surface properties of the mixed brushes (consisting of two or more different polymers grafted to a surface) can be changed through treatment with a selective solvent for one grafted component (7,9,10). A nonpolar solvent can act as a selective solvent, swelling the hydrophobic polymer chains while collapsing the hydrophilic chains. If a solvent is favorable for the other component, it can bring the hydrophilic chains to surface, burying the hydrophobic chains underneath. This is illustrated in Scheme 1. In either situation, the surface



*Scheme 1. Uniform surface response of mixed polymer brushes.*

shows homogeneous properties or a uniform surface response.

To synthesize polymer brushes demonstrating non-uniform surface response on the micro and nano level, it is necessary to create segregated grafted layers possessing discrete areas to which dissimilar macromolecules are tethered. The size of these areas should be comparable to, or larger than, the end-to-end distance of the grafted macromolecules. These segregated brushes should then provide a non-uniform surface response, as shown in Scheme 2, due to their phase-segregated nature. In other words, different areas on the surface would respond differently to external stimuli. These segregated brushes have potential applications as sensors targeting multiple types of analytes, for the movement of micro/nano objects vertically on surfaces and as variable surface adsorption materials.



*Scheme 2. Non-uniform surface response of segregated polymer brushes.*

Fabrication of segregated binary polymer brushes, where two polymers are grafted to the same surface in a phase segregated pattern, has been reported (11-12 13 14). However, these preceding studies describe “forced” methods of patterning that employ lithographical methods. Our paper describes “non-forced” synthesis of segregated (patterned) polymer brushes utilizing phase-separation phenomena in ultrathin polystyrene/poly(methyl methacrylate) [PS/PMMA] polymer blend films. To synthesize the segregated brushes, PS brushes were first prepared using the “grafting-to” approach, where end-functionalized polymer molecules react with complementary functional groups located on the surface to form tethered chains (15). Second component poly(polyethylene glycol methyl ether methacrylate) [PolyPEGMA] brushes were synthesized using atom transfer radical polymerization [ATRP]. Specifically, a “grafting from” technique, which utilizes the polymerization initiated from the surface by attached (usually by covalent bonds) initiating groups, was employed (16). The non-uniform surface response of these brush surfaces was demonstrated by treating them with selective solvents, scanning probe microscopy imaging, and through protein adsorption.

## Experimental

Highly polished single-crystal silicon wafers of {100} orientation (Semiconductor Processing Co.) were used as a substrate. The wafers were first cleaned in an ultrasonic bath for 30 minutes, placed in a hot piranha solution (3:1 concentrated sulfuric acid/ 30% hydrogen peroxide) for one hour, and then rinsed several times with high purity water. Caution: Piranha solution is highly corrosive and extremely reactive with organic substances. Gloves, goggles, lab coat and face shields are needed for protection.

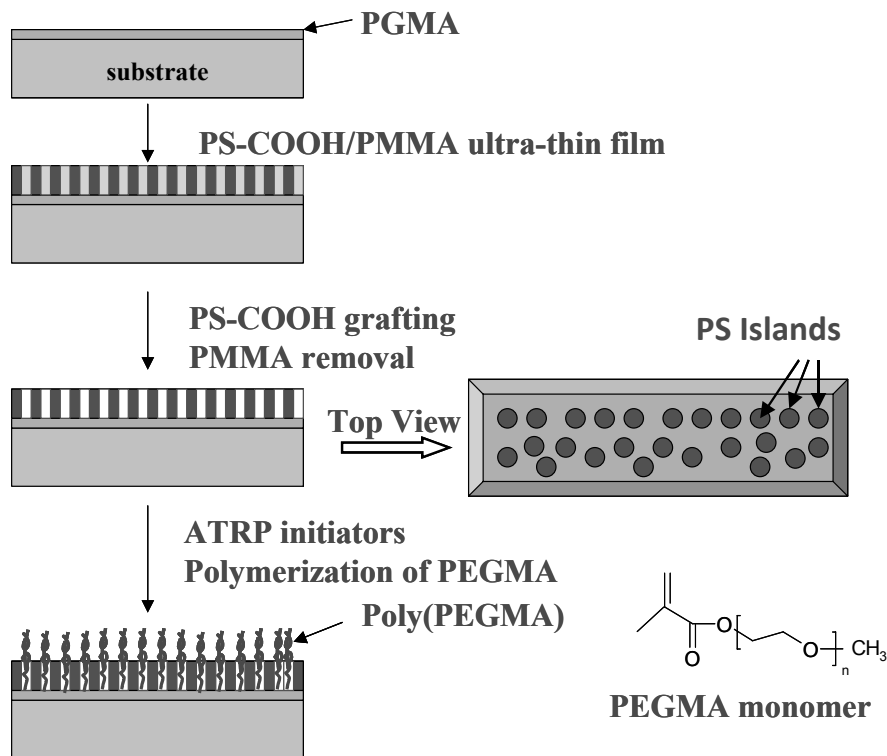
Glycidyl methacrylate (Aldrich) was polymerized via a free radical method to give PGMA,  $M_n=24,000$  g/mol,  $PDI=1.7$ . PS-COOH ( $M_n=45,900$  g/mol,  $PDI=1.05$ ) was purchased from Polymer Source Inc. PMMA ( $M_w=120,000$  g/mol), bipyridine and Polyethylene glycol methyl ether methacrylate (PEGMA,  $M_w=300$  g/mol) were used as received from Aldrich; Copper (I) bromide (CuBr), Copper (II) bromide (CuBr<sub>2</sub>) and 2-Bromo-2-methylpropionic acid (BPA) were used as received from Acros. Bovine serum fibrinogen was used as received from Sigma.

Scheme 3 shows the experimental steps for creating segregated polymer brushes. First, silicon wafer surfaces were modified with a thin poly(glycidyl methacrylate) (PGMA) layer. [Previous investigations have shown that PGMA is an effective anchoring layer for both “grafting to” and “grafting from” processes (15-1617181920).] A 15 nm ultrathin film consisting of carboxyl-terminated polystyrene and PMMA was introduced onto the PGMA modified surface by dip coating from PS-COOH/PMMA (30:70 weight ratio) Methyl Ethyl Ketone (MEK) solution. The samples were then annealed at 120 °C for 12 hours to allow PS-COOH grafting to PGMA modified surfaces. PMMA was subsequently removed by rinsing with solvent. As a result of the phase separation in the PS-COOH/PMMA ultrathin film, island-like structures of grafted PS brushes were created.

The samples were then exposed to 2-Bromo-2-methylpropionic acid (BPA) to form ATRP initiating sites (PGMA/BPA) for surface initiated polymerization [SIP] according to Ref.16. The reaction between epoxy functional groups of PGMA and BPA was conducted from the gaseous phase in argon atmosphere under reduced pressure (10 mmHg) at 30 °C for 12 hours. Unattached BPA was removed by multiple washing with MEK, including washing in an ultrasonic bath.

Finally, SIP of polyethylene glycol methyl ether methacrylate (PEGMA) was carried out, and PS/Poly(PEGMA) segregated binary brushes were prepared. SIP ATRP of PEGMA was carried out with maximum precaution to avoid oxygen. For this purpose, CuBr (80.3 mg, 0.56 mmol), CuBr<sub>2</sub> (50 mg, 0.22 mmol), bipyridine (0.245g, 1.56 mmol), PEGMA (16 ml, 56 mmol), 16 ml ethanol and 8 ml DI water were sealed in a flask and immediately exposed to several repeating freeze-pump cycles. The mixture was stirred at ambient temperature until complete dissolution of solids had occurred and a deep-brown homogeneous solution had formed. The final mixture was distributed between test tubes in a glove box (free O<sub>2</sub> content less than 5 ppm). The PS brushes/PGMA-BPA macroinitiator samples were immersed into each test tube in the glove box and sealed. For polymerization, the test tubes were immersed into a preheated water bath (30 °C) for assigned times. Ungrafted Poly(PEGMA) was removed from wafers by multiple washing with DI water, ethanol and MEK, followed by washing with MEK in an ultrasonic bath.

The thickness of the synthesized brushes was determined by means of ellipsometry performed on a COMPEL Automatic Ellipsometer (InOm Tech, Inc.) at a fixed 70° incidence angle. Refractive index for all polymers was assumed to be 1.5. Surface characterization was performed by Scanning Probe Microscopy (SPM) in tapping mode on a Dimension 3100 microscope (Digital Instruments, Veeco.). Static contact angle measurements were made using a



*Scheme 3. Fabrication of segregated binary brushes by combination of “grafting-to” and “grafting-from” methods.*

contact angle goniometer (Kruss, Model DSA10). Calculation of contact angle was made using the tangent method. Contact angle measurements were made with DI water (pH 7.0), and a static time of 60 seconds before the angle measurement.

## Results and Discussion

### Identification of Conditions for the Synthesis of the Segregated Brushes

Figures 1a and 1c show the structure of the phase-separated polymer blend films obtained by dip coating from a PS-COOH/PMMA (30:70 weight ratio) solution. The morphology of the as-deposited films of two different (15 and 30 nm) thicknesses agreed well with their PS content of 30%. Indeed, the minor PS phase was dispersed in the major PMMA phase. However, after the annealing and extraction of PMMA, the grafted PS layer demonstrated a rather different type of surface structures for the PS-COOH /PMMA films of different

thicknesses. The grafted PS layer displayed either a continuous phase (Figure 1b) or a disperse phase (Figure 1d) morphology, even though the content of PS-COOH remained constant in the PS-COOH/PMMA blend during the anchoring process. Thus, the morphology of the resulting PS brush was controlled by the thickness of the PS-COOH/PMMA film deposited.

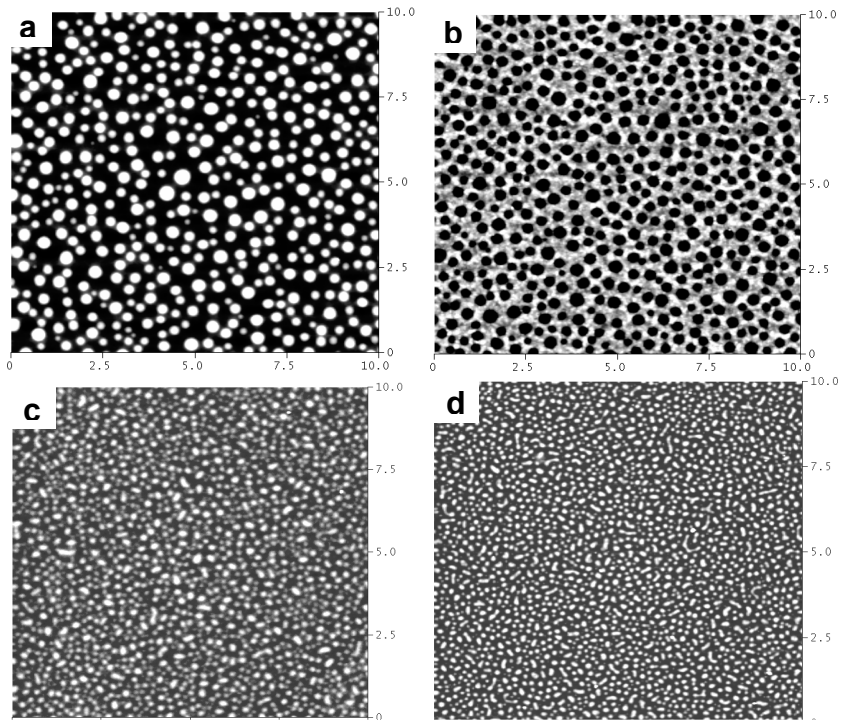


*Figure 1. Effect of PS-COOH/PMMA film thickness on grafted PS morphology: (a) 30 nm as-deposited PS-COOH/PMMA film; (b) 10 nm grafted PS after annealing and rinsing off PMMA, PS becoming continuous phase; (c) 15 nm as-deposited PS-COOH/PMMA film; (d) 7.5 nm grafted PS after annealing and rinsing off PMMA. (10x10  $\mu\text{m}$ )*

When an as-deposited film was thicker (30nm), there were enough reactive PS-COOH macromolecules to migrate to the PGMA/PMMA interface and graft to the PGMA layer under the PMMA phase. Accordingly, the resulting PS layer showed PS-matrix morphology, which was different from the morphology of the as-deposited film. In contrast, once the as-deposited film thickness decreased (15 nm), there was simply not an adequate amount of PS-COOH to support this “phase-inversion” process. Thus, this film demonstrated as-deposited morphology. The following experiments focused on the dispersed island-like grafted PS structures, and thus PS layer with thickness of 15 nm was used.

The thickness of the PGMA anchoring layer also played a pivotal role in the determination of the final structures of the segregated brushes. In fact, to obtain true segregated brushes, it was necessary to ensure that there were no Poly(PEGMA) chains growing at the same location where the PS-COOH macromolecules were already grafted. A combinatorial approach was employed to study the influence of the thickness of the PGMA anchoring layer on the grafting of PS-COOH and, later, on the SIP of PEGMA. For this purpose, samples having gradients in PGMA thickness were prepared according to the procedure described in Ref. 16. Next, the grafting of homogeneous PS-COOH layers was conducted using kinetics of the polymer anchoring to regulate the PS brush thickness. Samples with three grafted thicknesses (PS1, ~4nm; PS2, ~6nm; PS3, ~16nm) were obtained. As it was previously reported (15) thickness of the PGMA anchoring layer did not influence the thickness of the grafted PS brush significantly (Figure 2).

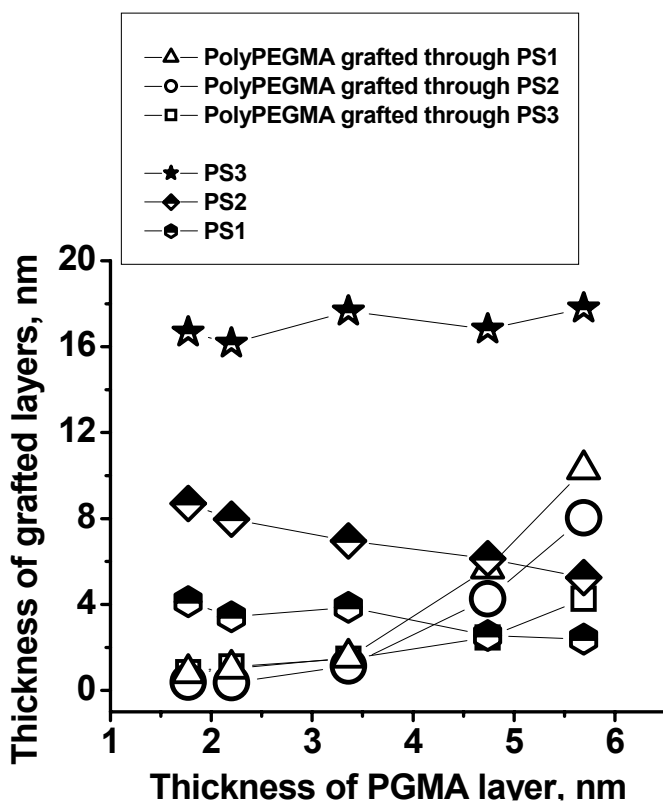


Figure 2. Effect of PGMA layer thickness on the grafting of PS-COOH and SIP of PEGMA on the surfaces covered with the grafted PS layer.

The samples were then exposed to BPA vapor to synthesize a surface attached ATRP initiator via the reaction between the carboxy functionality of

BPA and the epoxy groups of PGMA (16). Next, a SIP of PEGMA was conducted. Figure 2 shows that when the PGMA thickness was less than 2 nm, a negligible amount of Poly(PEGMA) was synthesized on the surface where PS was already grafted. Interestingly, the thickness of the PS grafted layer did not have a significant effect on the synthesis of Poly(PEGMA) for the thin PGMA anchoring layer. The obtained results indicated that most of epoxy groups in the PGMA layer were consumed during the attachment of PS-COOH by the grafting-to procedure. For the thicker PGMA layers the polymerization was observed indicating that the ATRP initiator was attached to the surface. However, when more PS was grafted during the first step, less Poly(PEGMA) grew during the second ATRP step. Indeed, in this case, fewer epoxy functionalities were available for BPA attachment as more were consumed by PS-COOH anchoring. Therefore, fewer initiating sites for SIP could be synthesized on the surface and consequently less Poly(PEGMA) chains could be grafted to the surface. In the subsequent experiments, PGMA thickness was kept at 1 nm to avoid grafting of Poly(PEGMA) onto the surface areas already grafted with PS brushes.

### Synthesis of the Segregated Brushes

For the procedure reported here, Si wafers modified with 1 nm thick PGMA film were annealed at 110 °C for 10 minutes to permanently attach PGMA to the wafer surfaces. The modified wafers were then dip-coated from a 0.5% g/ml PS-COOH/PMMA (30:70 weight ratio) MEK solution to obtain a 15 nm thick phase-separated ultrathin film. Next, the samples were annealed to allow for the grafting of PS-COOH to PGMA via reaction between carboxylic and epoxy functionalities.<sup>17</sup> During the annealing/grafting-to process, those areas covered by PMMA were protected so that PGMA could later react with BPA to provide a PGMA/BPA macroinitiator for SIP. After the extraction of PMMA, the effective thickness of the PS layers measured using an ellipsometer was  $7.5 \pm 0.5$  nm. Figure 3 shows the typical SPM image of the island-like morphology of the grafted PS brushes. The area covered with PS was  $35 \pm 5\%$ , which was in good agreement with the content of PS in the PS-COOH/PMMA blend (30%). The lateral size of the PS structural elements was on the order of 50-200 nm.

The SIP of PEGMA was carried out in an oxygen-free environment, using CuBr/Bipyridine as a catalyst in a water/ethanol mixture with PEGMA, Mw 300

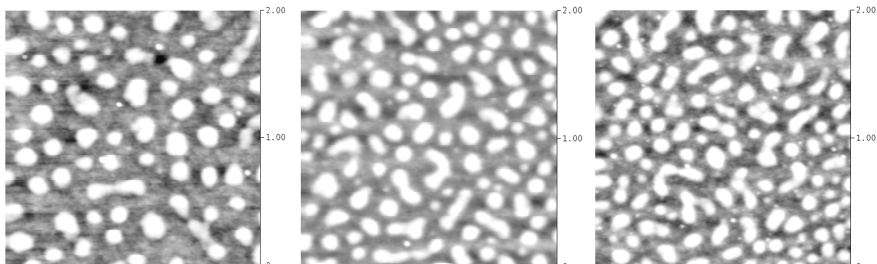


Figure 3. SPM topography images (2x2 microns) of three different island-like PS brushes prepared by “grafting-to” method, effective ellipsometric thickness of PS layer  $7.5 \pm 0.5$  nm.

as the monomer. Polymerization time varied from 1 to 24 hours; the second brushes of PolyPEGMA with a tunable thickness in the 1-65 nm range were synthesized, while keeping the first brush (PS) at a constant thickness ( $7.5 \pm 0.5$  nm). As a result, binary PS/Poly(PEGMA) brushes with a fixed PS thickness and a different thickness of a Poly(PEGMA) layer were obtained.

### **Wettability of the Segregated Brushes**

Water contact angle measurements were conducted to investigate the surface wettability of these surfaces when treated with different solvents. A selective solvent for PS was cyclohexane as it swelled the PS brushes while shrinking the PolyPEGMA chains. Ethanol was the selective solvent for PolyPEGMA brushes, while MEK was the nonselective solvent as it was a good solvent for both polymers. Treatment in the selective environments was achieved by immersing the sample into the designated solvent, then removing it from the solvent after 10 minutes and drying it under ambient conditions. After each measurement, the samples were refreshed with MEK and treated with the next selective solvent.

The water contact angle values for the brushes treated with the different solvents are shown in Figure 4. As could be expected, as the thickness of hydrophilic PEGMA brushes increased, the contact angle decreased. More importantly, however, the contact angle data shows that these surfaces did not exhibit switching in wettability after the treatment with the selective solvents. Therefore, PS chains and PolyPEGMA chains are located in their respective areas on the surface and do not overlap significantly to screen the dissimilar chains from water. The segregated brushes thus display a non-uniform surface response, as evidenced by the negligible change in the contact angle under different solvent treatments. This behavior clearly differentiates the segregated brushes from the conventional mixed brushes, demonstrating their switchable wettability when treated with selective solvents.

### **Morphology of the Segregated Brushes Treated with Different Solvents**

The non-uniform surface response of segregated PS/PolyPEGMA brushes was also studied by scanning with SPM. Figure 5 displays the different morphologies of the same segregated brushes treated under various conditions. For this sample, PS and PolyPEGMA brushes thickness were 7.5 nm and 1 nm, respectively. Figure 5a shows the image after the treatment of the brush with cyclohexane, Figure 5c after the ethanol exposure. In both images, the phase boundaries between the PS brushes and the PEGMA brushes are clearly observed. PS brushes after the cyclohexane treatment were more visible and extended, while after treatment with ethanol, PS shrunk inwardly and left an obvious phase boundary. The nonselective solvent, MEK (Figure 5b) resulted in no clear phase boundary and a morphology intermediate between the ones observed for the two selective solvents.



The different morphologies are demonstrated in Figure 6 when the PolyPEGMA thickness was increased to 21 nm. As these images show, the phase boundary is no longer evident, as the PEGMA chains tend to surround the PS islands and cover the PS. This phenomenon was the most obvious in the case of ethanol (Figure 6c). Treatment with cyclohexane swelled the PS, making it easily discernable, though fractional (Figure 6a). Once again, in the nonselective solvent (MEK), the morphology was intermediate between the other two (Figure 6b).

Figure 7 shows the different morphologies of the segregated brushes with comparable thicknesses of PolyPEGMA and PS (PS and PolyPEGMA, 7.5 nm and 5 nm, respectively). Figure 7a shows the image after treatment with cyclohexane; PS brushes were clearly visible and extended beyond the boundary. However, when the PolyPEGMA thickness increased from 1 to 5 nm, the clear corona seen in Figure 5a was not observed. Instead, a circle decorated

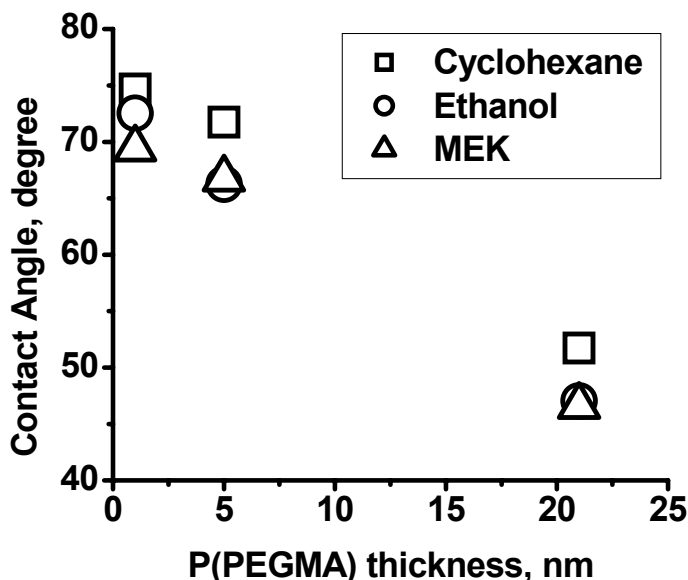
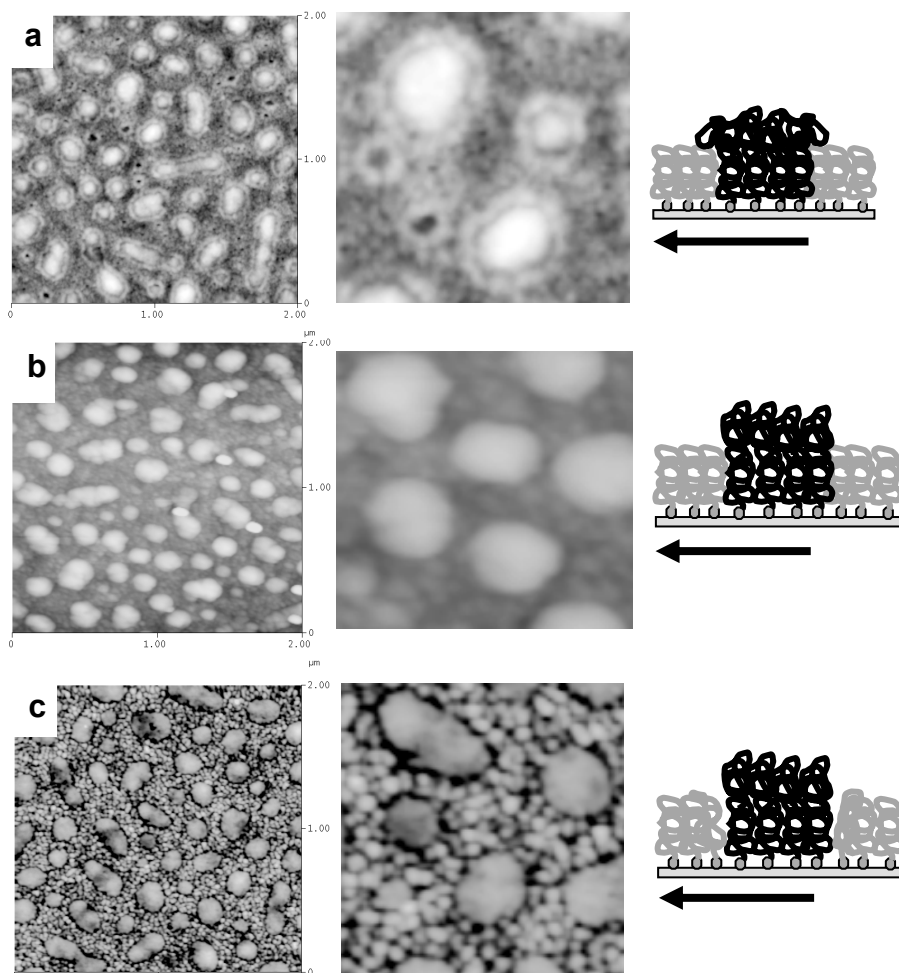


Figure 4. Water contact angle results for PS/Poly(PEGMA) segregated brushes influence of the solvent treatment.

with dotted lines was seen. Figure 7c indicates that, after the contact with ethanol, the phase boundaries between the PS brushes and the PEGMA brushes are clearly observed. In the nonselective solvent (Figure 7b), no clear phase boundary can be observed, and the morphology was intermediate between those observed for the two selective solvents.



*Figure 5. SPM topography images: (a) Segregated brushes of PS 7.5 nm and Poly(PEGMA) 1 nm after cyclohexane treatment; (b) The brushes after MEK treatment; (c) The brushes treated with ethanol. (Left-2x2 microns; Right-0.5x0.5 microns).*

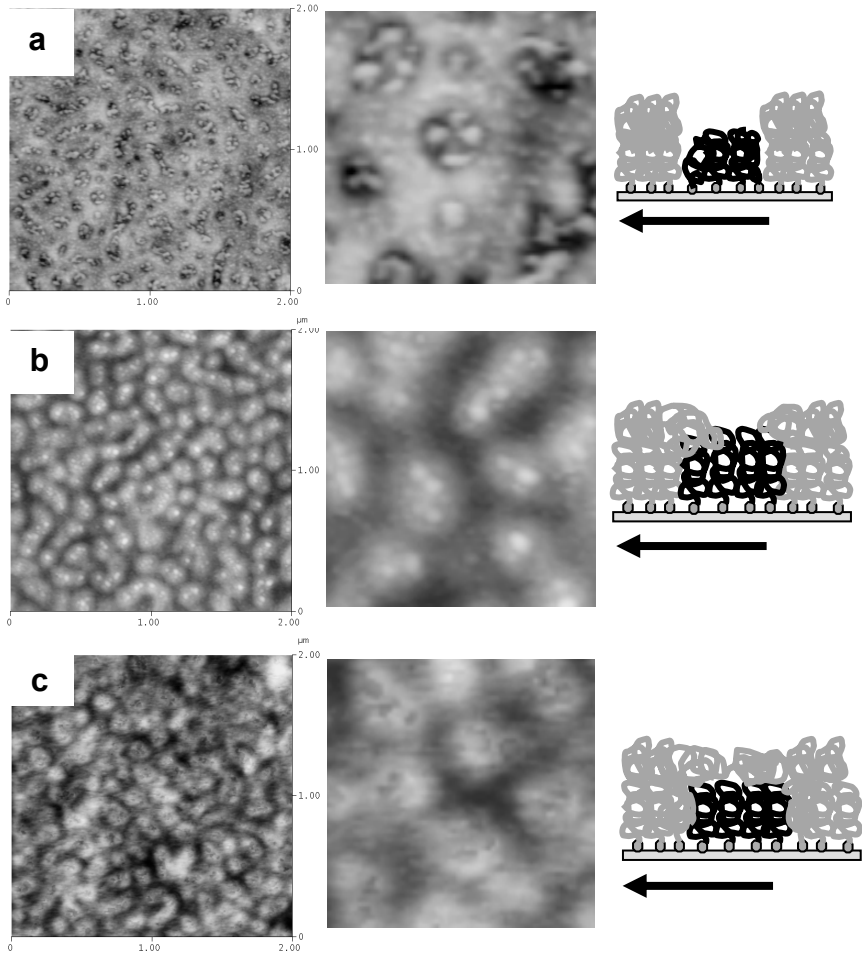
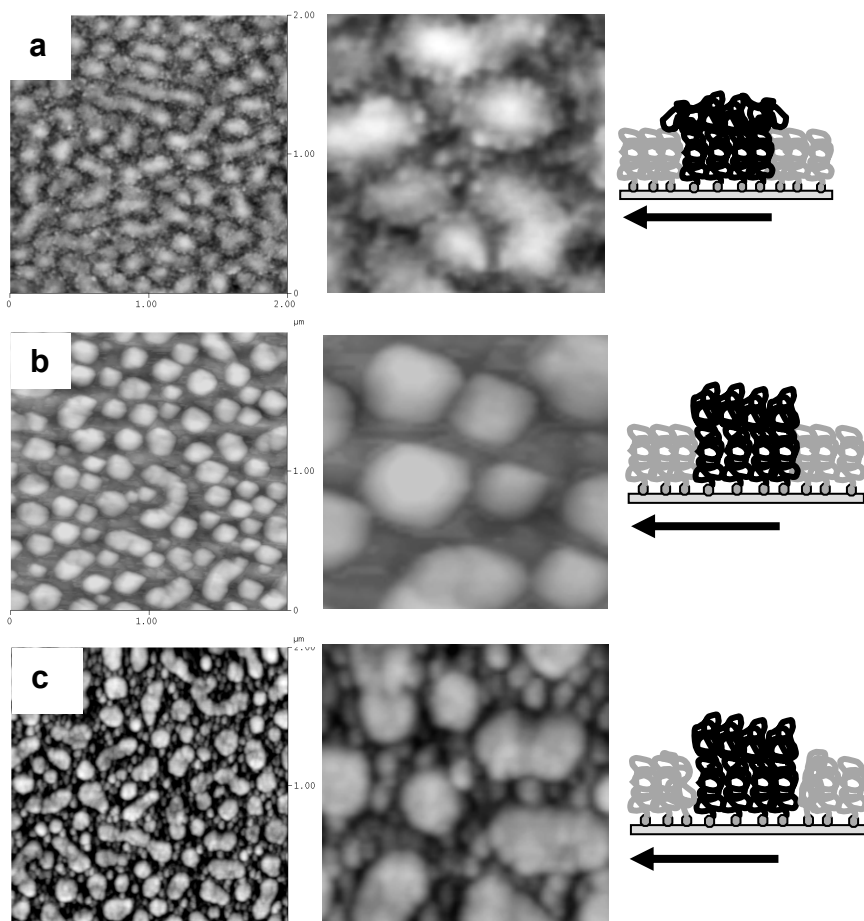


Figure 6. SPM topography images: (a) Segregated brushes of PS 7.5 nm and Poly(PEGMA) 21 nm after cyclohexane treatment; (b) The brushes after MEK treatment; (c) The brushes treated with ethanol. (Left-2x2 microns; Right-0.5x0.5 microns).



*Figure 7. SPM topography images: (a) Segregated brushes of PS 7.5 nm and Poly(PEGMA) 5 nm after cyclohexane treatment; (b) The brushes after MEK treatment; (c) The brushes treated with ethanol. (Left-2x2 microns; Right-0.5x0.5 microns).*

### *Protein adsorption on the surface of the segregated brushes*

PS is well-known for its protein absorption due to the high level of hydrophobic interactions, whereas PolyPEGMA brushes demonstrated an excellent non-fouling property (21). Therefore, it was interesting to study the protein adsorption onto the PS/Poly(PEGMA) segregated brushes. In this experiment the PS and PolyPEGMA brushes thicknesses were 7.5 nm and 21 nm respectively, and the sample was treated with MEK before the protein absorption. Adsorption of proteins was accomplished from 0.1 mg/ml buffer solution (phosphate buffer with PH=7.4) of bovine serum fibrinogen. The segregated brushes were kept in this fibrinogen solution for 24 hours, then rinsed with DI water, and dried in a clean room. Figure 8 shows the SPM image

of the segregated brushes after the fibrinogen adsorption. From visual inspection of the image it is clear that fibrinogen adsorbed on the brush surface. However, the fibrinogen adsorption occurred only at those places where PS brushes exist; at places where PolyPEGMA was grown, there was no fibrinogen adsorption.

When the PEGMA brush thickness was further increased to 65 nm, there

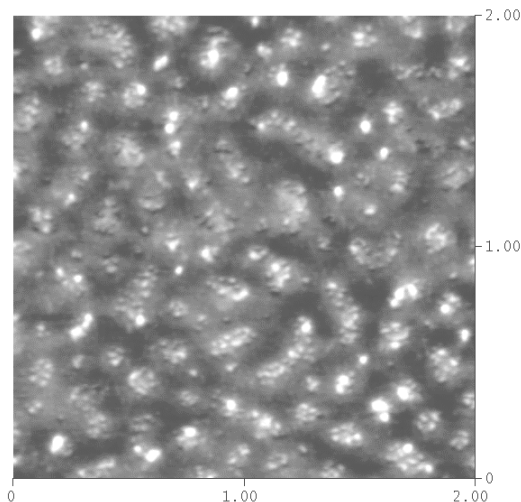


*Figure 8. Fibrinogen adsorption onto PS/Poly(PEGMA) segregated brushes. The PS and PolyPEGMA brushes thickness are 7.5 nm and 21 nm, respectively. SPM topography image 2x2 microns.*

was no protein adsorption no matter which selective solvent was used (Figure 9). The PEGMA was so thick that even though it could not screen PS chains from small water molecules in the wettability experiment, it screened the underneath PS chains from the contact with protein molecules.

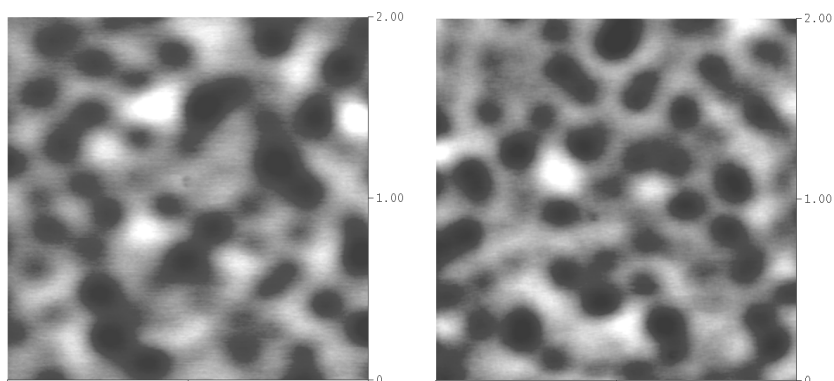


*Figure 9. SPM images (2x2 microns) representing topography before (left) and after (right) fibrinogen adsorption onto the segregated brushes of PS 7.5 nm and Poly(PEGMA) 65 nm after cyclohexane treatment. No protein adsorption observed.*

## Summary and Conclusions

Segregated polymer brushes were fabricated utilizing phase-separation phenomena in ultrathin polymer blend films (PS-COOH/PMMA) and the combination of “grafting-to” and “grafting-from” methods.

The first component PS brushes were prepared using the grafting-to approach; the second component PEGMA brushes were obtained through SIP. The thickness of the brushes obtained through SIP could be tuned in the 1-65 nm range.

The morphology of the grafted PS layer could be regulated by the thickness of the deposited PS-COOH/PMMA film. A thicker film led to continuous PS matrix grafted surface structures, while a thinner film resulted in a dispersed surface morphology.

The segregated brushes demonstrated a non-uniform surface response, as evidenced by the study of wettability and surfaces morphologies after being treated with selective solvents and protein adsorption. These segregated brushes surfaces have potential applications in bio-analytical devices and sensors.

## Acknowledgements

Authors acknowledge support by NSF grants DMR 0602528, CBET-0756457, and CMMI-0825773 and Department of Energy under award number DE-SC52-06NA27341.

## References

- 
1. Advincula, R. C.; Brittain, W. J.; Caster, K. C.; Ruhe, J. *Polymer Brushes*, Wiley-VCH Verlag GmbH & Co., Weinheim, 2004.
  2. Luzinov, I.; Minko, S.; Tsukruk, V.V. *Prog. Polym. Sci.* **2004**, *29*, 635.
  3. Minko, S. *Polymer Reviews* **2006**, *46*, 397.
  4. Luzinov, I.; Minko, S.; Tsukruk, V.V. *Soft Matter* **2008**, *4*, 714.
  5. Zhao, B.; Brittain, W. J.; Zhou, W.; Cheng, S. Z. D. *J. Am. Chem. Soc.* **2000**, *122*, 2407.
  6. Usov, D.; Gruzdev, V.; Nitschke, M.; Stamm, M.; Hoy, O.; Luzinov, I.; Tokarev, I.; Minko, S. *Macromolecules* **2007**, *40*, 8774.
  7. Minko, S.; Muller, M.; Motornov, M.; Nitschke, M.; Grundke, K.; Stamm, M. *J. Am. Chem. Soc.* **2003**, *125*, 3896.
  8. Julthongpiput, D.; Lin, Y.-H.; Teng, J.; Zubarev, E. R.; Tsukruk, V. V. *J. Am. Chem. Soc.* **2003**, *125*, 15912.
  9. Minko, S.; Patil, S.; Datsyuk, V.; Simon, F.; Eichhorn K.-J.; Motornov, M.; Usov, D.; Tokarev, I.; Stamm, M. *Langmuir* **2002**, *18*, 289.
  10. Draper, J.; Luzinov, I.; Minko, S.; Tokarev, I.; Stamm, M. *Langmuir* **2004**, *20*, 4064.

- 
11. Husemann, M.; Morrison, M.; Benoit, D.; Frommer, J.; Mate, C.M.; Hinsberg, W.D.; Hedrick, J.L.; Hawker, C.J. *J. Am. Chem. Soc.* **2000**, *122*, 1844.
  12. Zhou, F.; Jiang, L.; Liu, W.; Xue, Q. *Macromol. Rapid Commun.* **2004**, *25*, 1979.
  13. Liu, Y.; Klep, V.; Luzinov, I. *J. Am. Chem. Soc.* **128**, 8106.
  14. Synytska, A.; Stamm, M.; Diez, S.; Ionov, L. *Langmuir* **2007**, *23*, 5205.
  15. Iyer, K. S.; Luzinov, I. *Macromolecules* **37**, 9538.
  16. Liu, Y.; Klep, V.; Zdyrko, B.; Luzinov, I. *Langmuir* **2005**, *21*, 11806.
  17. Zdyrko B, Klep V, Luzinov I, *Langmuir* **2003**, *19*, 10179.
  18. Zdyrko B, Varshney SK, Luzinov I, *Langmuir* **2004**, *20*, 6727.
  19. K. S. Iyer, I. Luzinov, *Macromolecules* **2004**, *37*, 9538.
  20. Liu, Y.; Klep, V.; Zdyrko, B.; Luzinov, I. *Langmuir* **2004**, *20*, 6710.
  21. H. Ma, J. Hyun, P. Stiller, A. Chilkoti, *Adv. Mater.* **2004**, *16*, 338.

## Chapter 16

# Hybrid Block Copolymers Incorporating Oligosaccharides and D Synthetic Blocks Grown by Controlled Radical Polymerization

Jérôme Lohmann,<sup>1,2</sup> Clément Houga,<sup>1</sup> Hugues Driguez,<sup>\*2</sup> James Wilson,<sup>3</sup> Mathias Destarac,<sup>3</sup> Sébastien Fort,<sup>2</sup> Jean-François Le Meins,<sup>1</sup> Redouane Borsali,<sup>2</sup> Daniel Taton,<sup>\*1</sup> and Yves Gnanou<sup>\*1</sup>

<sup>1</sup> Laboratoire de Chimie des Polymères Organiques, Université Bordeaux 1-ENSCP - CNRS, 16 Avenue Pey Berland, 33607 Pessac cedex, France.

<sup>2</sup> CERMAV (UPR-CNRS 5301) Université Joseph Fourier and Institut de Chimie Moléculaire de Grenoble, BP 53. 38041 Grenoble Cedex 9, France

<sup>3</sup> Rhodia Recherches et Technologies, Centre de Recherches et Technologies d'Aubervilliers, 52 rue de la Haie Coq, 93308 Aubervilliers, France

Hybrid block copolymers incorporating a naturally occurring oligosaccharide and a vinylic block were synthesized by chemical modification of the anomeric chain-end of the oligosaccharide with a purposely designed coupling agent, followed by controlled radical polymerization (CRP). In this way, a series of dextran-*b*-polystyrene block copolymers were obtained using atom transfer radical polymerization (ATRP) as the CRP method. In this case, protection of the OH groups of dextran was required. The resulting diblocks were found to self-assemble into various morphologies (e.g. spherical micelles or vesicles) depending on the PS content. Secondly, xylo-oligosaccharides obtained by controlled enzymatic degradation of Tamarind kern powder were subsequently modified by a xanthate moiety without protection of the OH groups for further polymerization of acrylamide (Am) by MADIX. Well defined Xyloglucan-*b*-PAm block copolymers could be thus obtained.



## Introduction

Natural polysaccharides are abundant cheap and renewable materials that are the subject of an increasing interest, owing to their biodegradability, their molecular recognition by bioactive molecules, or their mucoadhesive properties.<sup>1, 2</sup> A convenient means to tailor the physicochemical properties of polysaccharides is to introduce functional groups along their backbone.<sup>3</sup> The (co)polymerization of mono- or disaccharides fitted with a polymerizable group is an alternate method often resorted to generate the so-called glycopolymers<sup>4, 5</sup> that combine the biological properties of saccharides and those of synthetic polymer chains. In contrast, the association of oligosaccharides in a block copolymer structure has not been studied in detail.<sup>6-10</sup> Synthesizing such hybrid block copolymers is motivated by the possibility to direct their self-assembly into nanoparticles, which could be subsequently used as active delivery systems or as novel macromolecular surfactants.

Here we describe the preparation of block copolymers containing either dextran or xyloglucan as the oligosaccharide, and either PS or PAm as the vinylic block. As depicted in Scheme 1 and Scheme 2, our synthetic strategy is based on the chemical modification (reductive amination or Huisgen 1,3-dipolar cycloaddition<sup>11</sup>) of the anomeric end group of the naturally occurring oligosaccharide, followed by either atom transfer radical polymerization (ATRP) or Macromolecular Design by Interchange of Xanthates (MADIX) of a vinylic monomer, as a means to grow the synthetic block. Investigation into the nanostructures formed by self-assembly in solution of the dextran-based diblock copolymers is also presented.

## Experimental

### Materials.

Dextran T10 (**1**) and tamarind kern powder were purchased from Amersham Bioscience and 3A Dainippon Pharmaceuticals, respectively. Cellulase 3042A was a gift from Genecor. Dimethylsulfoxide (DMSO), tetrahydrofuran (THF) and toluene (all from Baker) were distilled over CaH<sub>2</sub> prior to use. All other reagents were purchased from Aldrich. CH<sub>2</sub>Cl<sub>2</sub> and Et<sub>3</sub>N were dried over P<sub>2</sub>O<sub>5</sub> and distilled prior to use. Styrene (99%) was distilled over CaH<sub>2</sub> prior to use. 2,2'-Azobis(2-methylpropionitrile) (AIBN) and 4,4'-Azobis(4-cyanovaleric acid) (ACP) were recrystallized from ethanol and methanol, respectively.

### Instrumentation

<sup>1</sup>H NMR spectra were recorded on a Bruker AC 400 spectrometer. Apparent molar masses were determined by size exclusion chromatography (SEC) either in THF or H<sub>2</sub>O. For diblock copolymers soluble in THF, the device was equipped with a Jasco PU-980 pump, a PSS column (8\*300 mm,

5 $\mu$ m) calibrated using linear polystyrene standards and a refractive index detector (Varian RI-4) at a flow rate of 1 mL/min (25 °C). Water soluble polymers were characterized using a VARIAN 2510 SEC with TSKgel super AW columns (AW2500, AW4000 and AW5000 with pore sizes of 25, 450 and 1000 Å, respectively) calibrated using linear poly(ethylene glycol) standards and equipped with dual detector (RI and UV) using water with 8.5 g/L NaNO<sub>3</sub> as the eluent at 0.4 mL/min. Atomic Force Microscopy (AFM) images were recorded in air with a dimension microscope (Digital Instruments, Santa Barbara, CA), operated in tapping mode™. The probes were commercially available silicon tips with a spring constant of 40 N/m, a resonance frequency lying in the 270-320 kHz range and a radius of curvature in the 10-15 nm range. Dynamic Light Scattering (DLS) measurements were performed using an ALV laser goniometer, which consists of a 22 mW HeNe linear polarized laser operating at a wavelength of 632.8 nm and an ALV-5000/EPP multiple  $\tau$  digital correlator with 125 ns initial sampling time.

**Synthesis of bromoisobutyramide-ended dextran 1, silylated bromoisobutyramide-ended dextran 2.** These compounds were synthesized as described in reference 10.

**Synthesis of *N*-(2-azidoethyl)-2-bromopropanamide 6.** To a solution of *N*-(2-bromopropanoyl)succinimide 4<sup>12</sup> (669 mg; 2,7 mmol; 1eq.) in distilled CH<sub>2</sub>Cl<sub>2</sub> and kept in ice was added dropwise 2-azidoethanamine 6 (462 mg; 5,37 mol; 2eq.) and distilled triethylamine (1,12 mL; 8,07 mmol; 3eq.). The reaction was stirred at room temperature overnight and followed by TLC (8:2 Petroleum Ether-EtOAc). The solution was concentrated and purified by column chromatography (8:2 Petroleum Ether-EtOAc) to yield a solid (518,3mg, 88%). <sup>1</sup>H NMR (CDCl<sub>3</sub>):  $\delta_{\text{ppm}}$  7.24 (s, 1H, NH), 4.43 (q, 1H, CH), 3.46 (d, 4H, CH<sub>2</sub>-CH<sub>2</sub>), 1.84 (d, 3H, CH<sub>3</sub>).

**Synthesis of *S*-1-(2-azidoethylamino)-*O*-ethyl xanthate-ended xyloglucan 10.** Controlled enzymatic degradation of xyloglucan from tamarind kern powder by cellulase 3042A afforded a mixture of three xylo-oligosaccharides 7 with a degree of polymerization (DP): DP = 7, DP = 8 and DP = 9 with a mass proportion 15/35/50. This precursor was end-functionalized using propargylamine (in MeOH) followed by *N*-acetylation. "Click-chemistry" between 8 (50 mg, 40  $\mu$ mol) and 6 (12 mg, 60  $\mu$ mol, 1.5eq.) in a MeOH/H<sub>2</sub>O (1/1, v/v) solution (4 mL) was performed using an aqueous CuSO<sub>4</sub> solution (70  $\mu$ L, 8  $\mu$ mol, 0.2eq.)/sodium ascorbate (7 mg, 40  $\mu$ mol, 1eq.). The resulting product 9 (25 mg, 20  $\mu$ mol) reacted with potassium ethyl xanthogenate (21 mg, 130  $\mu$ mol, 8eq.) in DMF (2 mL), affording 10. Yield = 75 %.

**Synthesis of dextran-*b*-PS block copolymers 3.** Details of these syntheses can be found in reference 10. The molecular characteristics are summarized in Table 1.

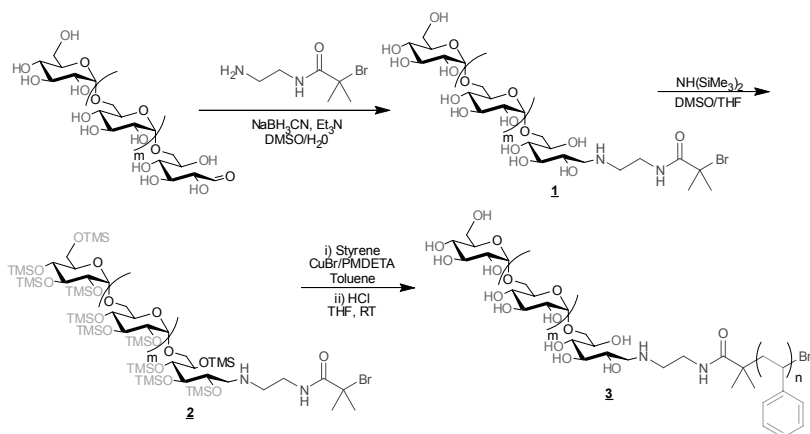
**Synthesis of XG-*b*-PAm block copolymers 11.** In a typical experiment, 10 (100 mg, 62  $\mu$ mol), ACP (3.5 mg, 12  $\mu$ mol,

0.2eq.), acrylamide (Am) (109.5 mg, 1.5 mmol, 25eq.) and 1.89 mL of deionized water were added into a Schlenk flask. The mixture was stirred for 5 minutes and degassed by three freeze-thaw cycles. The Schlenk flask was placed in a constant temperature oil bath at 70 °C for 24 h. The reaction was stopped by cooling the Schlenk flask with liquid nitrogen. The solution was dialyzed (molecular mass cut-offs of 2,000 Da) against distilled water before lyophilization. The polymer obtained was analyzed by aqueous SEC and  $^1\text{H}$  NMR.

## Results & Discussion

The key step in our synthesis of hybrid block copolymers is the chemical modification of the terminal anomeric aldehyde using a coupling agent possessing a functional group (bromoisobutyrate or dithiocarbonate for **2** and **10**, respectively) used to grow the synthetic block by ATRP or MADIX, respectively.

### Synthesis of dextran-*b*-PS block copolymers by ATRP.



Scheme 1. Synthetic strategy for Dex-*b*-PS block copolymers.

The synthesis of these block copolymers is based on the reductive amination of dextran using a bromoisobutyrate containing primary amine, followed by silylation of the oligosaccharide hydroxyls before polymerization of styrene by ATRP.<sup>10</sup> Three diblock copolymers were thus prepared with a DP of the PS block ranging from 5 to 775, that is from 7% to 92% w/w, using the same dextran-based precursor ( $M_n = 6600$  g/mol, PDI  $\sim 1.5$  corresponding to a DP = 40). Finally, these (silylated dextran)-*b*-PS block copolymers were readily

desilylated under acidic conditions (Scheme 1), affording the targeted amphiphilic Dex-*b*-PS block copolymers **3**.

**Table 1. Molecular characteristics of silylated dextran-*b*-PS copolymers.**

Run	Time (min) <sup>a</sup>	T (°C)	M <sub>n</sub> SEC <sup>b</sup>	DP <sub>n</sub> NMR <sup>c</sup>	PDI <sup>b</sup>	Φ <sub>PS</sub> (% w/w)
1	20	90	17500	5	1.4	7
2	40	100	82200	270	1.7	81
3	90	100	160000	775	1.9	92

<sup>a</sup>Conversions were around 50%. <sup>b</sup>By SEC in THF. <sup>c</sup>Composition of the vinylic block determined by <sup>1</sup>H NMR.

The structures formed by self-assembly in solution of these Dex-*b*-PS block copolymers were investigated as a function of their weight fraction in PS (from 7% to 92%).<sup>13</sup> Depending on the block copolymer composition, different modes of preparation were used to obtain nanoparticles in solution. While the self assembly could be brought about by direct dissolution in water for block copolymers with a low hydrophobic content (run 1, Table 1), a mixture of THF and DMSO was required for the samples with a higher content in PS, before totally removing the organic phase by dialysis and transferring the nanoparticles into pure water.

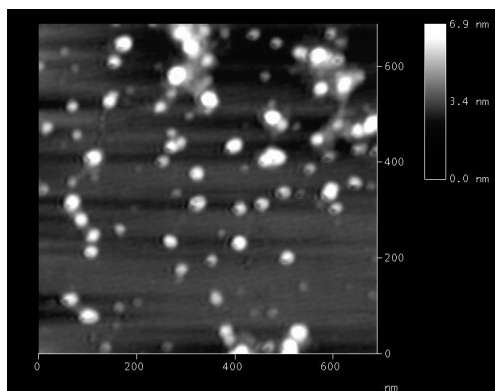


*Figure 1. AFM image obtained from a drop of a solution of Dex-*b*-PS<sub>5</sub> in water and evaporated on a mica surface.*

The self-assembly properties in water of Dex-*b*-PS<sub>5</sub> with a PS weight fraction of 7% was first investigated by DLS at 25°C at different angles. A main distribution was observed at 90° indicating a hydrodynamic radius of R<sub>H</sub> = 28 nm which is typically that of a micelle structure. Given the block copolymer composition, (~ 7% w/w PS) core-shell micellar structures with a dextran-based corona oriented towards the continuous aqueous phase are the expected morphology that should be at thermodynamic equilibrium. This was later

confirmed by AFM experiments carried out in a tapping mode (Figure 1): the measured diameter ( $\sim 40\text{nm}$ ) being in reasonable agreement with DLS findings.

Comparatively, block copolymers with a larger PS content ( $> 81\%$ ) gave rise to different morphologies depending on the region considered in the solvent mixture versus size. The solution properties of two block copolymers (Dex-*b*-PS<sub>270</sub> and Dex-*b*-PS<sub>775</sub>) are thus summarized in Figure 2.

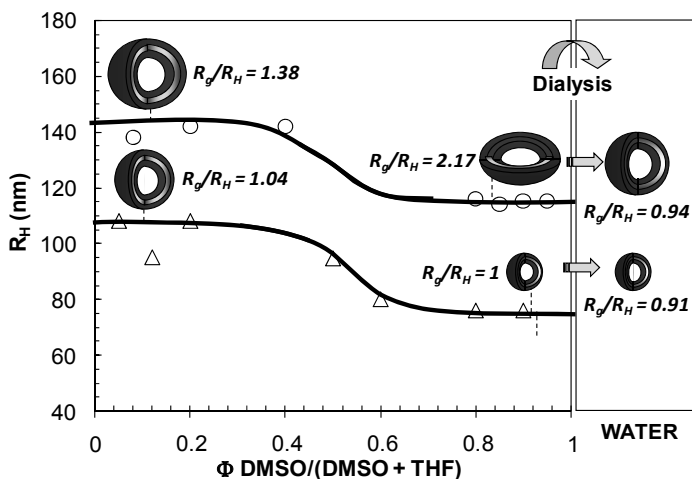


Figure 2. Evolution of hydrodynamic radius versus DMSO volumic fraction for different block-copolymers., O: Dex-block-PS<sub>270</sub>,  $\Delta$ : Dex-block-PS<sub>775</sub>. Dotted curve indicates the area where no scattered signal could be detected.

Schematical morphologies are inserted in the graph. Red colour illustrates dextran, blue colour polystyrene.

In the THF-rich region, the morphology obtained for both Dex-*b*-PS<sub>270</sub> and Dex-*b*-PS<sub>775</sub> block copolymers has been investigated by AFM, which revealed a donut-type structure indicative of the formation of vesicles. In the case of Dex-*b*-PS<sub>270</sub> (Figure 3-a), it appears that a large number of objects are in the range of  $\sim 100\text{-}400\text{ nm}$ , but in the case of Dex-*b*-PS<sub>775</sub> (Figure 3b) fewer objects are observed. The latter exhibit a characteristic size between  $300\text{ nm}$  and  $1\mu\text{m}$ , in relative good agreement with the  $R_H$  value obtained by DLS.

A transition region with no coherent scattering signal (dotted part in Figure 2) was found for each block copolymer solution. This region is characteristic of an efficient solvation of the copolymers which behave as unimers. These free chains subsequently self-assemble into reverse nanoparticles composed of a PS core and a dextran shell as the DMSO content increases. One can note that the characteristic sizes of these nanoparticles are lower compared to the ones measured in the THF region. When diluting the THF-rich solution with DMSO, the morphology of the Dex-*b*-PS<sub>270</sub> is modified, as indicated by the value of the  $R_g/R_H$  ratio stands higher than 2, which is characteristic of an anisotropic structure. In the case of Dex-*b*-PS<sub>775</sub>, a vesicular structure with a smaller size than in THF according to its  $R_g/R_H$  ratio is expected in DMSO but could not be

seen by an imaging technique. Indeed, evaporating DMSO under vacuum caused the disruption of the nanoparticles formed.

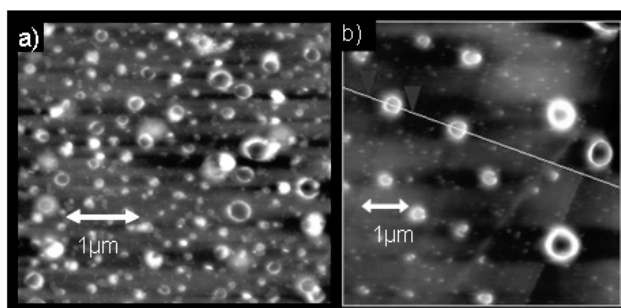


Figure 3. AFM images obtained in the THF region for a) *Dex-b-PS*<sub>270</sub> and b) *Dex-b-PS*<sub>775</sub> - bottom: Section profile of b).

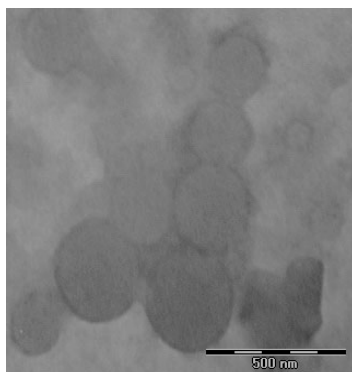
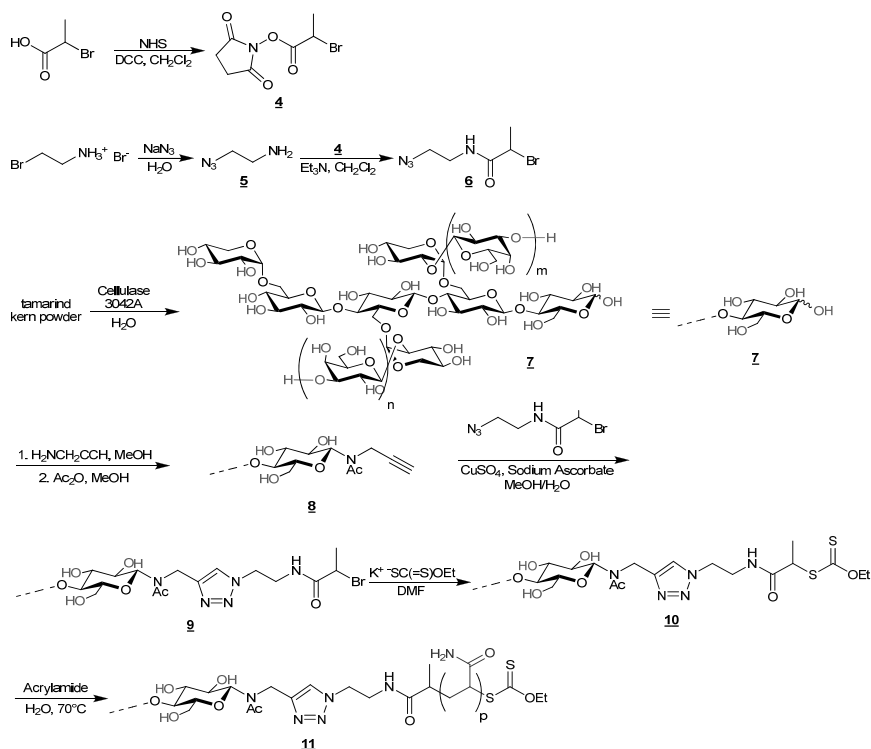


Figure 4. TEM image obtained for the *Dex-b-PS*<sub>270</sub> in water (0.1 mg/ml).

In order to account for the morphology, nanoparticles in DMSO were dialyzed against water. Hydrodynamic radii measured under these conditions remained unchanged upon addition of water onto DMSO solutions of *Dex-b-PS*<sub>775</sub>. In contrast, for *Dex-b-PS*<sub>270</sub>, the  $R_H$  value decreased from 115 nm to 64 nm. In water, the  $R_g/R_H$  ratio was close to one, irrespective of the block copolymer composition, suggesting a vesicular morphology and thus confirming the occurrence of a morphological change from an anisotropic structure to spherical vesicles for *Dex-b-PS*<sub>270</sub> from its initial DMSO-rich solution. Hollow spheres with low dispersity are clearly visible on TEM image (Figure 4), their characteristic sizes being in good agreement with those obtained by DLS.

## Synthesis of XG-*b*-PAm block copolymers by MADIX.



**Scheme 2.** Synthetic strategy of XG-*b*-PAm block copolymers.

Interestingly, the XG-based chain transfer agent (CTA) **10** was not subjected to the protection of its hydroxyl functions before being used as a macro CTA in aqueous media. The coupling reaction of alkyne-functionalized XG with *N*-(2-azidoethyl)-2-bromopropanamide by a copper(I)-catalyzed Huisgen 1,3 dipolar cycloaddition was carried out in a MeOH/H<sub>2</sub>O mixture. The xanthate function was introduced using an excess of potassium ethyl xanthogenate.

**Table 2.** Molecular characteristics of XG-*b*-PAm copolymers.

	Conv <sup>a</sup> (%)	M <sub>n</sub> SEC <sup>b</sup>	DP <sub>n</sub> NMR <sup>a</sup>	PDI <sup>b</sup>
<b>macro CTA</b>	-	1650	-	1.17
<b>XG-<i>b</i>-PAm<sub>25</sub></b>	96	9650	67	1.24
<b>XG-<i>b</i>-PAm<sub>50</sub></b>	96	20600	175	1.28
<b>XG-<i>b</i>-PAm<sub>100</sub></b>	99	35800	220	1.37

<sup>a</sup>Composition of the vinylic block determined by <sup>1</sup>H NMR. <sup>b</sup>By aqueous SEC.

Block copolymers with different length of PAm block were then directly grown from XG CTA by MADIX polymerization in water.<sup>14</sup> Table 2 shows an increase in molar mass with a polydispersity lower than 1.5 at complete conversion. However, the degree of polymerization determined by <sup>1</sup>H NMR is higher than expected, which can be explained by the peculiar behavior of the XG-CTA in aqueous solution. As shown in Figure 5 (black trace) XG-CTA has indeed a tendency to self-aggregate in water. Tamarind xyloglucan is water-soluble, but its individual macromolecules are not fully hydrated. Consequently, aggregated species exist in water even under dilute solutions. This is because the  $\beta$ -(1  $\rightarrow$  4) cellulose-like backbone promotes interchain interactions, therefore the oligosaccharide exhibit both hydrophobic and hydrophilic characters. Indeed, based on small-angle X-ray scattering (SAXS) and synchrotron radiation data<sup>15</sup> tamarind xyloglucan has been found to form multi-stranded aggregates in aqueous solution, with a high degree of particle stiffness and little homogeneity of the aggregation number.

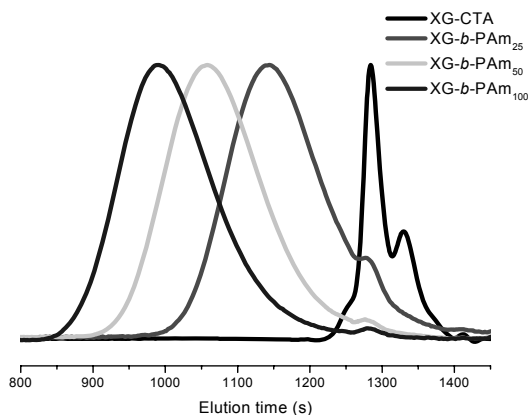


Figure 5. SEC traces in H<sub>2</sub>O of XG-CTA and XG-b-PAm block copolymers.

We thus speculate that polyacrylamide growing chains have a reduced accessibility to the terminal xanthate moiety. As a matter of fact, a mixture of XG-b-PAm diblock slightly contaminated by residual XG-CTA is obtained after MADIX polymerization. Almost complete elimination of the residual XG-CTA could be achieved, however, by dialysis against water, as illustrated in Figure 5.

## Conclusions

A series of well-defined hybrid block copolymers incorporating an oligosaccharide part (xyloglucan or dextran) as the natural building block and a synthetic polymer grown by ATRP (PS) or MADIX (PAm) were obtained, after covalent attachment of an ATRP initiating moiety or a MADIX entity, respectively, at the reducing end of the saccharidic block. The solution self-



assembly of the dextran based diblock copolymers gave rise to various stable spherical morphologies (core-shell micelles and vesicles) whose size varied with the overall composition of the copolymer. Following this approach, miscellaneous other hybrid block copolymers can be targeted which is currently under investigation in our group.

### Acknowledgment.

The authors are grateful to Rhodia for financial support and the permission to publish this work.

### References

1. Heinze, T., Polysaccharides I. In Heidelberg, S. B., Ed. *Advances in Polymer Science*, **2005**; Vol. 186, p 185.
2. Klemm, D., Polysaccharides II. In Heidelberg, S. B., Ed. *Advances in Polymer Science*, **2006**; Vol. 205, p 205.
3. Jenkins, D. W.; Hudson, S. M., *Chemical Reviews* **2001**, 101, 3245-3274.
4. Ladmiraal, V.; Melia, E.; Haddleton, D. M., *European Polymer Journal* **2004**, 40, 431-449.
5. Okada, M., *Progress in Polymer Science* **2001**, 26, 67-104.
6. Pfannemuller, B.; Schmidt, M.; Ziegast, G.; Matsuo, K., *Macromolecules* **1984**, 17, 710-716.
7. Bosker, W. T. E.; Agoston, K.; Cohen Stuart, M. A.; Norde, W.; Timmermans, J. W.; Slaghek, T. M., *Macromolecules* **2003**, 36, 1982-1987.
8. Akiyoshi, K.; Kohara, M.; Ito, K.; Kitamura, S.; Sunamoto, J., *Macromolecular Rapid Communications* **1999**, 20, 112-115.
9. Haddleton, D. M.; Ohno, K., *Biomacromolecules* **2000**, 1, 152-156.
10. Houga, C.; Meins, J. F. L.; Borsali, R.; Taton, D.; Gnanou, Y., *Chemical Communications* **2007**, 3063-3065.
11. Meldal, M.; Tomøe, C. W., *Chem. Rev.* **2008**, 108, 2952-3015.
12. Lecolley, F.; Tao, L.; Mantovani, G.; Durkin, I.; Lautru, S.; Haddleton, D. M., *Chemical Communications* **2004**, 2026-2027.
13. Houga, C.; Giermanska, J.; Lecommandoux, S.; Borsali, R.; Taton, D.; Gnanou, Y.; Le Meins, J.-F., *Biomacromolecules* **2009**, 10, 32-40.
14. Taton, D.; Destarac, M.; Zard, S. Z., *Macromolecular Design via the Interchange of Xanthates*. In *Handbook of RAFT Polymerization*, Wiley-VCH, Weinheim, **2008**; pp 373-422.
15. Lang, P.; Kajiwarra, K., *Journal of Biomaterials Science, Polymer Edition* **1993**, 4, 517-528.

## Chapter 17

# Controlled radical polymerizations as versatile synthetic routes for conjugated rod-coil block copolymers and their use as active polymer semiconducting materials in flexible organic electronic devices and systems

Cyril Brochon and Georges Hadziioannou

Laboratoire d'Ingénierie des Polymères pour les Hautes Technologies  
Université de Strasbourg  
Ecole Européenne de Chimie, Polymères et Matériaux (ECPM)  
25 rue Becquerel  
67087 Strasbourg, France

Controlled Radical Polymerization (CRP) such as Atom Transfer Radical Polymerization (ATRP) or Nitroxide Mediated Radical Polymerization (NMRP), can be used to obtain various well defined rod-coil conjugated diblock or triblock copolymers having well controlled opto-electronic properties. These copolymers are soluble in common organic solvents and can be self-organized giving rise at various nm length scale and thermodynamically stable structures. They show promising opto-electronic properties and fulfil the basic morphological requirements towards the fabrication of efficient flexible organic electronic devices.

### Introduction

Conjugated polymers are promising as functional polymer materials for the development of low cost flexible organic electronic devices and systems<sup>1</sup>. In this field, the processability (solubility) of the material, the control of their morphology and design and control of the optoelectronic functionality are of a

crucial importance. The design of semiconducting polymer materials for solution-processed photovoltaic devices has been extensively developed during the last years.<sup>2</sup> Relatively high energy conversion efficiencies (up to 5.2%)<sup>3</sup> were achieved with blends of poly-(3-alkyl) thiophenes (P3ATs) and fullerene derivatives as photoactive layer where electron-donating (donor) polymers and electron-accepting (acceptor) fullerenes form an interpenetrated network the so called donor-acceptor bulk heterojunction (BHJ) system. Device performances and stability strongly depend on the active layer morphology which can be dramatically affected by the process (spin coating, annealing, solvent quality ...).

Conjugated rod-coil block copolymers are constituted of a conjugated polymer (based on  $sp^2$  carbon), the "rod" block having semiconducting properties, and a classical polymer (based on  $sp^3$  carbon) "coil" block covalently bonded. Such materials are suitable to be used as active materials for flexible organic electronic devices and systems in particular in solar cells. Their suitability results from the fact that they can be designed so as to be soluble in common organic solvents and allow control of stable nm size structures as a consequence of their equilibrium mesomorphic phase separation. Moreover, by the judicious choice of the formation of carbon-carbon bonds in the polymerisation process involving  $sp^2$  and or  $sp^3$  carbons the optoelectronic properties of the rod-coil block copolymers can be designed/controlled adequately. Over the last decade, several groups have studied the self-organising properties and structure of this new class of rod-coil block copolymers in bulk and in thin film configurations.<sup>4,5</sup> The fact that the size, stability and structure of donor and acceptor phases is crucial in organic photovoltaic devices for their optimal performance, recently donor-acceptor block copolymers have been developed where each microphase has the required size and optoelectronic properties. These materials have been obtained from well-defined linear conjugated rod-coil block copolymers,<sup>6</sup> but also from grafted or comb-like rod-coil copolymers.<sup>7,8</sup> Also, block copolymers with architectures such as rod-rod conjugated donor-acceptor multiblock copolymers<sup>9</sup> or coil-coil diblock copolymers grafted with donor and acceptor side groups<sup>10</sup> have been developed. These novel materials can be used as active layer, to replace the P3AT/fullerene blends but also as surfactant/compatibilizer of the semiconducting polymer/fullerene blends. Indeed, block copolymers when used as surfactants/compatibilizers in blends reduce the interfacial tension and thus stabilise thermodynamically the phase separated materials.<sup>7</sup>

In this chapter, we will focus on the synthetic procedures of conjugated rod-coil block copolymers. These copolymers have semiconducting properties and have been subject of various experimental and theoretical studies regarding their phase separation properties. They can be obtained easily by controlled radical polymerization (CRP) or anionic polymerization. Anionic polymerization of the coil block allows the synthesis of such system in a very controlled way, either by using a conjugated macro-initiator<sup>11</sup> or by quenching the living polymer with an end functionalized conjugated block.<sup>12,13,14,15,16,17</sup> Rod-coil copolymers can be also obtained from a coil-coil copolymer by sequential anionic polymerization, where one of the two blocks is a precursor of a conjugated sequence.<sup>18</sup> However, CRP is a more suitable method for the synthesis of block copolymers with a

variety of structures, architectures and tolerant synthetic process conditions. Thus CRP offers an important advantage for the design of optoelectronic properties and the synthesis of functional polymer materials to be used in flexible organic electronic systems especially for solar cells. Indeed, in the later case the introduction of all functionalities on the block copolymer (for example electron-accepting and donating groups) requires functional monomer units in the coil and rod blocks respectively.

In the following sections, an overview of recent results regarding the synthesis by CRP of conjugated rod-coil suitable for flexible organic electronic systems, more specifically for photovoltaic devices, is presented. We will be particularly focusing on model semiconducting block copolymer materials and on small band gap copolymers.

## **Synthesis of well defined conjugated rod-coil block copolymers via controlled radical polymerization**

Well-defined rod-coil diblock or triblock copolymers can be obtained from conjugated macro-initiators by CRP. In each case the synthetic route requires the mono- (for diblock) or di-functionalization (triblock) of a previous conjugated polymer. For this purpose, this last one needs to be properly end capped with a high conversion and further transformed into a macro-initiator. Many examples can be found in the literature, such as poly(para phenylene vinylene) (PPV)<sup>6,19,20,21</sup>, Polythiophene<sup>22,23,24</sup>, Polyfluorene<sup>25,26</sup>, Poly(thienylene vinylene) (PTV)<sup>27</sup> or other designed oligomers.<sup>28</sup>

CRP allows the polymerization of functional monomers for the coil block which is suitable to tune the materials properties, for example it is possible to obtain amphiphilic conjugated triblocks copolymers with neutral<sup>25</sup> or ionic<sup>26</sup> blocks. The used CRP technique depends on the functionalization of the end-capping conjugated polymer, indeed conjugated macro-initiators can be tuned for Atom Transfer Radical Polymerization<sup>21,22,23,25,26,28</sup> (ATRP), Nitroxide Mediated Radical Polymerization<sup>6,19,20,23,24,27</sup> (NMRP) or Reversible Addition Fragmentation Transfer polymerization<sup>23</sup> (RAFT). Various coil blocks have been grown from these macro-initiators: polystyrene, polyacrylates and polymethacrylates derivatives, including functional monomers, and polyisoprene. ATRP seems to be a more versatile technique because it allows the polymerization of a wide range of functional monomers; however, considering the application in optoelectronic, the presence of residual catalyst could affect the material final properties. However, NMRP allows the synthesis of polymers without by-products and makes possible the incorporation of functional monomers, such as chloromethylstyrene, in the coil block.

### **Polyparaphenylenevinylene based block copolymers as model materials**

Polyparaphenylenevinylene based block copolymers are very interesting as model materials. Indeed poly((2,5-dialkyloxy)-1,4-phenylenevinylene) (DEH-PPV) can be obtained by Seigrist condensation<sup>29</sup> in order to obtain low polydispersity polymer with one aldehyde function. From this route, NMRP and

ATRP macro-initiators have been obtained easily from poly ((2,5-di(2'ethylhexyloxy)-1,4-phenylenevinylene) (DEH-PPV), a very soluble PPV derivative. The synthetic routes are schematically presented in Figure 1.

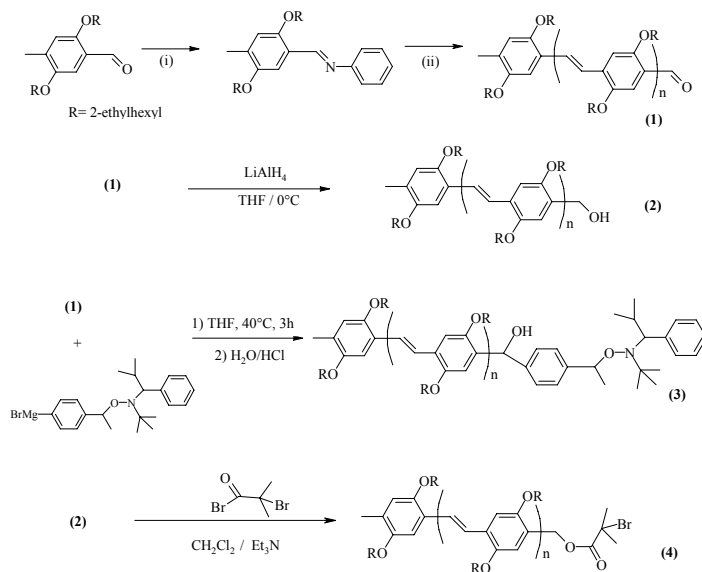


Figure 1. Syntheses of DEH-PPV macro-initiators for NMRP(3) and ATRP (4). (i) aniline, 60°C, 50 mmbar, 3 h (ii) tBuOK, DMF, 50°C, 1h then HCl/H<sub>2</sub>O

Aldehyde end-functionalized DEH-PPV **1** is obtained easily by Siegrist condensation with low polydispersity index (PDI<1.3). It can be converted into hydroxyl end-functionalized PPV **2** after reduction of the aldehyde moiety. PPV **1** is converted into NMRP macro-initiator **3** by reacting the Grignard reagent of the appropriated alkoxyamine.<sup>6</sup> ATRP macro-initiator **4** is obtained by a simple esterification on the hydroxyl end-functionalized PPV **2**.<sup>21</sup>

### NRMP synthesis

Polyparaphenylenevinylene based macro-initiator **2** was used for NMRP of various monomers (styrene, methyl acrylate, butyl acrylate).<sup>6,19,20</sup> From this compound various well defined rod-coil blocks copolymers with polystyrene and polyacrylate based coil blocks have been obtained. Furthermore, in each case, it is possible to random copolymerize a second monomer for instance chloromethylstyrene. The first monomer determines mechanical properties and phase transitions of the coil block, for example, butylacrylate based coils have low T<sub>g</sub> and can provide easy processability towards thin films. The second monomer (between 5% and 10% in molar ratio) provides the introduction of functional moieties which are necessary for a further modification in order to tune the electronic properties of the copolymer. NMRP from DEH-PPV macro-initiator **2** is schematically presented in Figure 2.

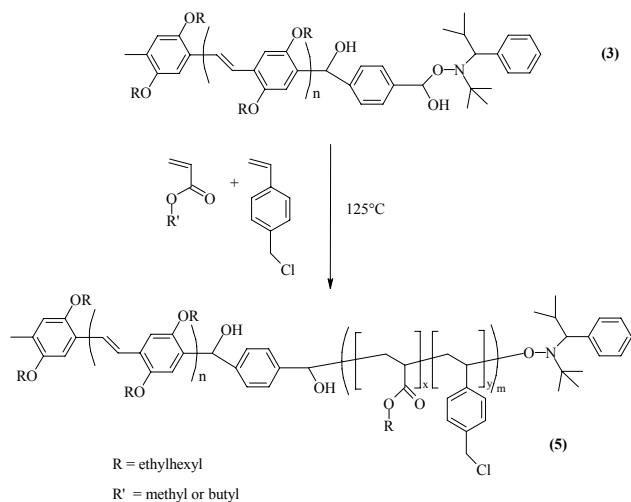


Figure 2. NMRP polymerization from DEH-PPV macro-initiator 2

Well defined block copolymer **5** has been obtained following the synthetic route described here. However, at high conversion, side reactions, radical addition on the PPV vinylene units can occur. For this reason, it is important to keep low conversion in order to avoid a loss of control.

#### ATRP synthesis

Another way to limit the side reactions on the PPV block consists of using ATRP polymerization. The polymerization occurs at lower temperature and well-defined block copolymers with polystyrene coil block (PPV-*b*-PS) have been obtained and characterised.<sup>21</sup> The synthesis is schematically represented in Figure 3.

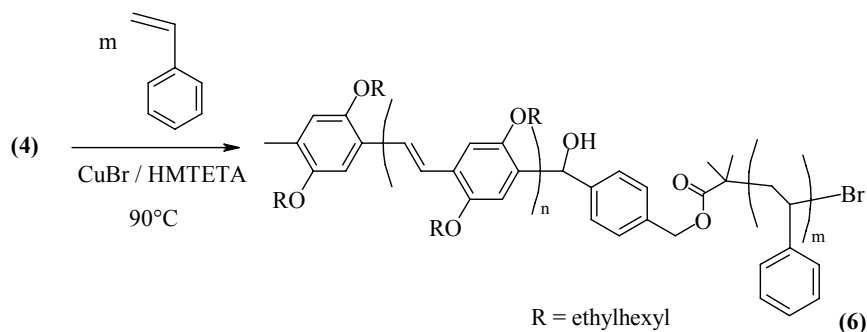
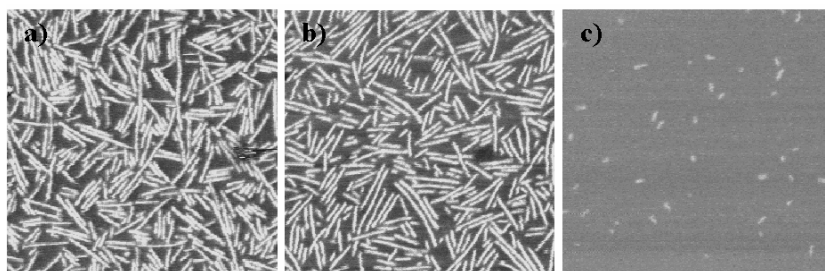


Figure 3. Synthesis of PPV-*b*-PS block copolymers by ATRP

Copolymers obtained by this method have low polydispersity indexes ( $PDI < 1.3$ ) with various coil length. Unfortunately, due the presence of residual copper in the materials, they have not been used for optoelectronic devices. However, these well-defined model copolymers have been used for the morphological studies.

#### *Morphology of PPV Based Model Copolymers*

Copolymers with poly(butylacrylate) coil present lamellar organization.<sup>20</sup> PPV lamellae have been observed with a wide range of coil fraction. Furthermore the distance between lamellae, increases when the coil volume fraction increases (Figure 4).



*Figure 4. tapping mode AFM images of (5) with different coil block fractions (0.42 ; 0.51 ; 0.85) a), b) and c) respectively.*

When coil block is made from polystyrene, lamellae where still observed, as shown on Figure 5),<sup>21</sup> but with a very narrow range of coil volume fraction: between 53% and 66%.

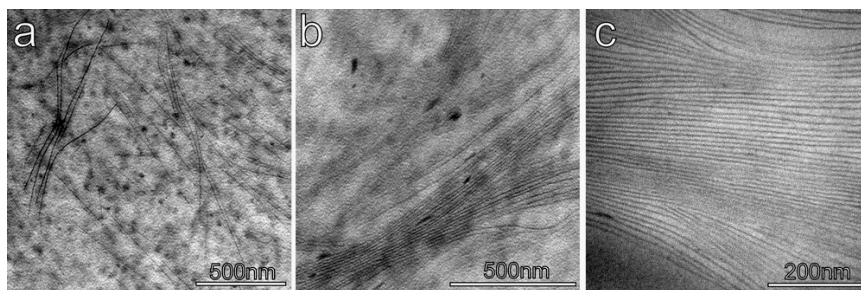


*Figure 5. TEM pictures of samples with overall molecular weight : a) 8000g/mol; b) 6400g/mol and c) 5800g/mol and the same rod block (2700 g/mo)l (from Journal of Applied Polymer Science, reference 21)*

Lowest molecular weight polymers, i.e. ones with the larger rod overall fraction, exhibit long range ordered lamellae, a slight increase in coil volume fraction induce a loss of long range order. When the coil size is further increased, a transition to an essentially isotropic phase is observed, without any evidence of a hexagonal or spherical intermediate phase.

In order to confirm these results, PPV-based copolymers with more controlled structures have been also synthesized by anionic polymerization with polystyrene (PS)<sup>15</sup> (copolymer **7**) and poly(4-vinyl pyridine) (P4VP)<sup>16</sup> (copolymer **8**) coils (as shown in Figure 6)

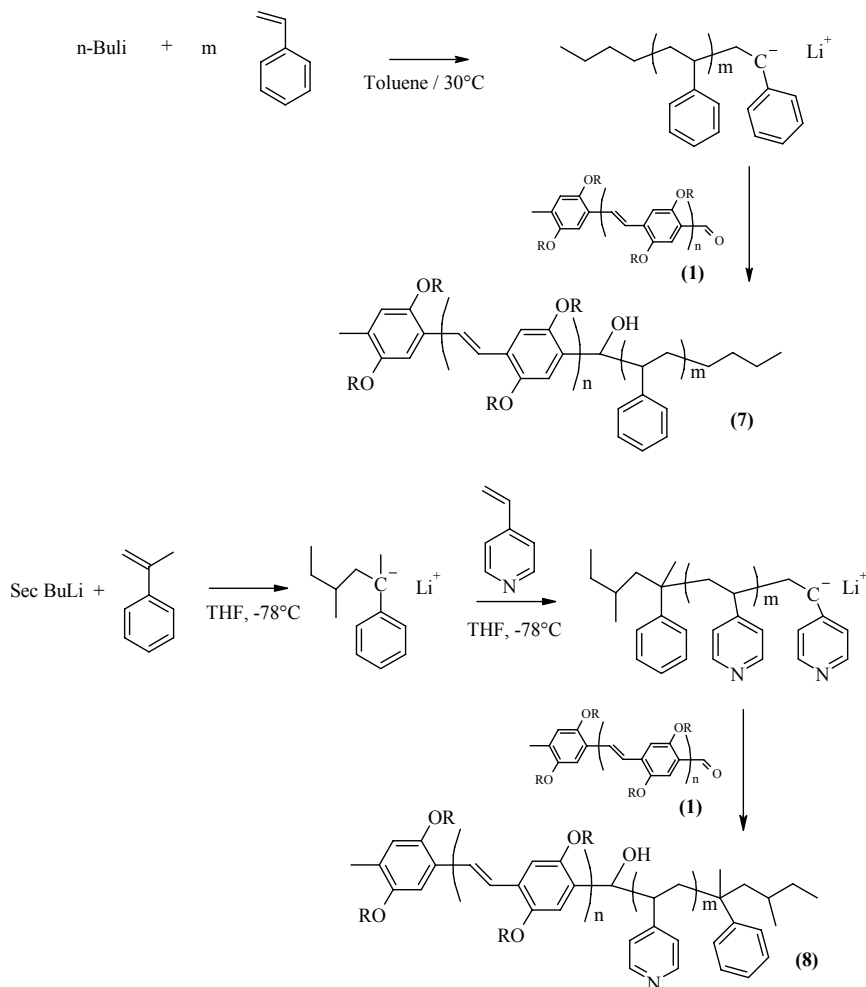


Figure 6. Synthesis of PPV-*b*-PS and PPV-*b*-P4VP block copolymers by anionic polymerization



PPV-b-PS made by anionic polymerization, exhibits the same lamellar morphology observed with copolymers made by ATRP.<sup>5,15</sup> This result confirms the good architecture control that CRP can provide for these copolymers. This study also confirms the unique transition between ordered lamellae and isotropic phase with the coil volume fraction. However, a transition between nematic and smetic C phases in the PPV lamellae has been also shown. This behavior is characteristic of a weakly segregated system.

For PPV-b-P4VP copolymers, depending on the coil fraction, various morphologies have been observed: cylindrical, spherical and lamellar (with or without liquid crystalline PPV phase).<sup>5,16</sup> This behavior is typical of a moderately segregated system which is due to the polar character of P4VP block.

### Poly(thienylene vinylene) based block copolymers as small band gap materials

A small band gap poly(thienylene vinylene) macro-initiator **9** has been synthesized by Horner-Wadsworth-Emmons condensation.<sup>27</sup> Rod-coil copolymers **10** have been obtained from it (Figure 7): they present red-shifted absorption spectra, which is very suitable for photovoltaic applications.

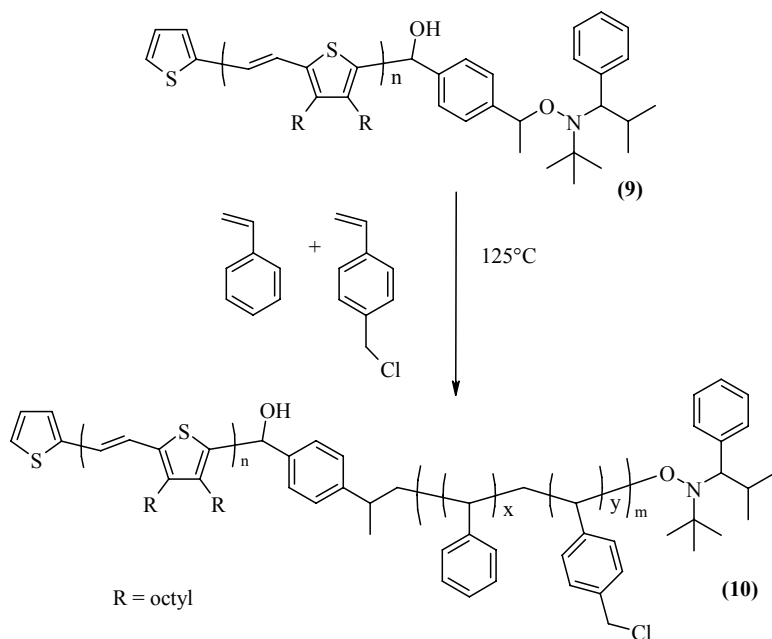


Figure 7. Synthesis of PTV-b-P(S-co-CMS) block copolymers by NMRP

The obtained copolymers exhibit a short range lamellar organization, with formation of PTV pellets with a width corresponding to a double layer of PTV.

### Poly(3-hexylthiophene)based block copolymers

Continuing to improve and tune optoelectronic properties, recently, block copolymers based on regioregular poly(3-hexylthiophene) (P3HT) have been synthesised by Mc Cullough *et al.*<sup>22,23</sup> with various coil blocks. Regioregular P3HT is well known for its strong  $\pi$ -stacking and its good electronic conduction properties. To adapt these materials for photovoltaic devices, another strategy has been proposed in order to graft fullerene moieties on the coil block.<sup>24</sup> For that purpose an “in situ” end-capping method has been developed. The synthetic route is schematically presented on Figure 8.

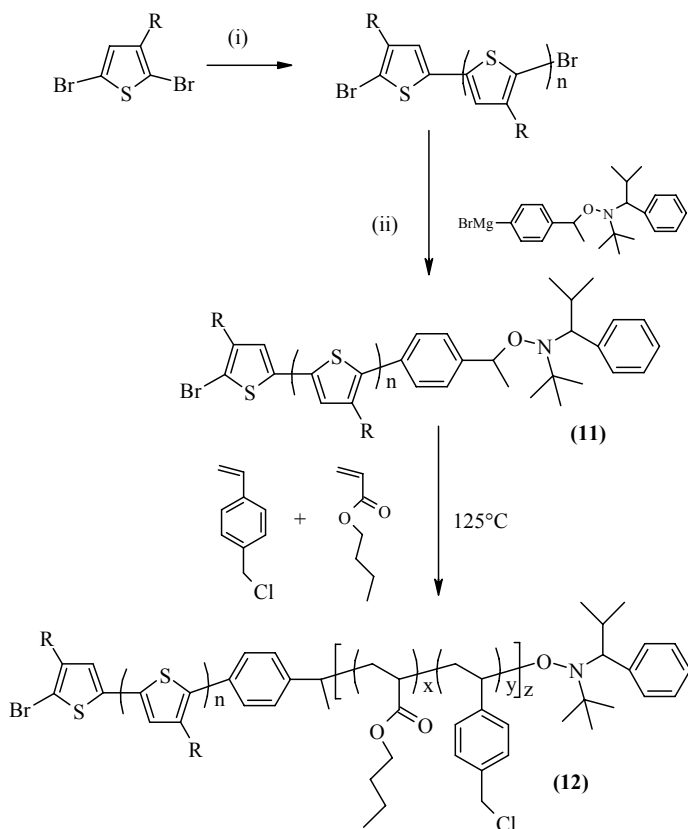


Figure 8. Overall scheme of P3HT-*b*-P(BA-co-CMS) synthesis (i) *tert*-butylmagnesium chloride, ether/THF, RT, then  $\text{Ni}(\text{dppp})\text{Cl}_2$ , ether/THF, RT; (ii) ether/THF, RT

The synthesis procedure of P3HT macro-initiator **11** was adapted from the Grignard Metathesis (GRIM) polymerization method as described by McCullough et al.<sup>30,31</sup> using 2,5-dibromo-3-hexylthiophene monomers. After reaction of the monomer with *tert*-butylmagnesium chloride, nickel catalyst is added and the polymerization takes place. The “living” character of this polymerization enables the introduction of a second Grignard reagent to end-functionalize the chain. In the present case the TIPNO based Grignard reagent is added, *in situ*, at the end of the polymerization, leading to the formation of the macro-initiator. To elucidate the structure of the end-terminated polymers, <sup>1</sup>H NMR spectroscopy was employed. Indeed the alkyl chain protons of the terminal thiophenes are shifted from 2.8ppm to 2.6ppm. Moreover, if both end-functions are equivalent the signal at 2.6ppm appears as a triplet while in the opposite case a multiplet is observed in which case trends to confirm the mono capping. P3HT macro-initiators characteristics are summarized in Table 1.

**Table 1. P3HT macro-initiators characteristics.**

	<i>t</i> (min)	<i>M<sub>n</sub></i> NMR (Kg/mol)	<i>M<sub>n</sub></i> GPC (Kg/mol)	PDI
<b>11b</b>	15	2.0	3.8	1.3
<b>11c</b>	30	1.3	1.9	1.8

Molecular weight values were obtained either by <sup>1</sup>H NMR (by comparison of the integrations of the chain end protons and polymer chain protons) or by GPC. In the last case, they are over-estimated because of the more rigid conformation of the molecules compared to standard polystyrene. Polydispersity indexes are low to moderate. By <sup>1</sup>H NMR it is possible to estimate the degree of regioregularity.<sup>32</sup> Using this feature the regioregularities of our P3HT macro-initiators have been estimated to be  $93 \pm 2.5\%$ . Rod-coil block copolymers (**4**) are obtained by NMRP using the P3HT as macro-initiator. The coil blocks are synthesized with various butylacrylate/chloromethylstyrene (BA/CMS) ratios and the results obtained with various polymerisation times are summarized in table 2. Molecular weights are estimated from GPC and from the <sup>1</sup>H NMR spectra by comparing the proton peaks of the P3HT aromatic cycle to BA *CH*<sub>2</sub> aliphatic chain peaks and CMS *CH*<sub>2</sub>*Cl* peaks.

**Table 2. P3HT based rod coil copolymers characteristics**

	$[M]_0/[3]_0$	$[BA]/[CMS]$ <i>In polymer</i>	<i>t</i> (h)	<i>M<sub>n</sub></i> NMR (Kg/mol)	<i>M<sub>n</sub></i> GPC (Kg/mol)	PDI
<b>12b</b> <sup>a</sup>	370	3.6	2	2.6	5.3	1.4
<b>12c</b> <sup>b</sup>	305	1.4	3	8.6	18.0	2.7
<b>12d</b> <sup>b</sup>	290	10.6	15	10.5	29.4	4.2

<sup>a</sup> From macroinitiator **11c**

<sup>b</sup> From macroinitiator **11b**

The coil block molecular weight increases with polymerization and conversion time. GPC traces of the macro-initiator **11b** and its copolymers **12c** and **12d** confirm that molecular weight increases with polymerization time and conversion which is characteristic of a controlled radical polymerization. The residual peak corresponding to the macro-initiator is small. It indicates a good ratio of re-initiating species which confirm the efficiency of the end capping reaction of P3HT. Furthermore, no bimodal distributions corresponding to the presence of tri-block copolymers are observable. This confirms that only one side of the chain is end-capped with the TIPNO. The same GPC traces are obtained with UV detector (450 nm) where only P3HT block absorbs photons, and confirm the efficient growth of the coil block onto the rod macro-initiator.

### Electron donor-acceptor rod-coil blocks copolymers.

In order to tune these materials for photovoltaic applications, it is possible to graft these CRP made well-defined rod-coil block copolymer with electron acceptor group. It has been achieved on PPV based<sup>6,19,20</sup> and on P3HT<sup>24</sup> based copolymers, by grafting C<sub>60</sub> molecules on the CMS moieties of the coil block. The same procedure was also used by others in order to put C<sub>60</sub> on a grafted comb-like P3HT-PS copolymer.<sup>8</sup> As an example, the procedure is schematically represented in Figure 9 for the P3HT based rod-coil copolymers.

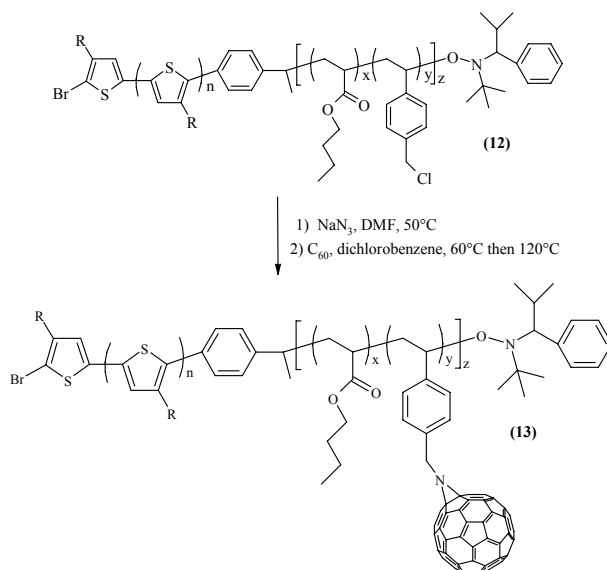


Figure 9. C<sub>60</sub> grafting on the P3HT rod-coil copolymer **12**

P3HT block copolymers are initially azidated and then C<sub>60</sub> grafted, using the same procedure used previously for PPV based copolymer. The resulting copolymers **13a** and **13b** contain respectively 37 and 28 weight percent ratio of C<sub>60</sub>. These copolymers present a good solubility in DCB, which indicates that no crosslinking reaction occurs during grafting as previously described. The photoluminescence (PL) spectra upon excitation at 355 nm of the copolymers, in solution and in thin films, as well as before and after the C<sub>60</sub> grafting, show a significant fluorescence quenching in the fullerene-grafted material. This suggests that efficient exciton dissociation takes place although the existence of a non-radiative recombination mechanism and/or energy transfer cannot be excluded.

## Conclusions

Versatile controlled radical polymerisation routes for the synthesis of conjugated rod-coil block copolymers towards photoactive polymer semiconducting materials have been developed. These synthetic routes allow control of the processability (solubility), the morphology, the optoelectronic functionality of these new functional polymer materials. These materials are very promising for photovoltaic application, since CRP allows the incorporation of functional monomers in the coil block. By adjusting the molecular architecture and composition of the rod coil block copolymers the active layer structure of the solar cell devices can be tuned in a predictable manner. Toward this goal, original donor-acceptor P3HT based diblock copolymers have been synthesised to improve the performance of organic photovoltaic devices based on fullerene derivatives and regioregular polythiophenes blends (PCBM/P3HT). These block copolymers have been used as surfactant in order to control the microstructure and thermodynamically stabilise the photoactive blend (P3HT/PCBM) material in the photovoltaic device. A preliminary result showed that the power conversion efficiency of the as cast P3HT/PCBM blends which was 1% increased by three and half fold to become 3,5% when an appropriate block copolymer was used as compatibilising agent for the P3HT/PCBM blend active photovoltaic material.

## Acknowledgements

We would like to acknowledge the fruitful discussions with Prof. Raffaele Menzenga and Nicolas Sary from Fribourg University (Switzerland). The contribution to this work from Prof. T. Heiser, N. Leclerc and P. Leveque from University of Strasbourg is greatly acknowledged.

We also thank the French National Agency for Research (ANR), the Region Alsace, for financial support through the NANORGYSOL and MONACOP programs.

## References

1. Heeger, A. J., *J. Phys. Chem. B*, **2001**, *105*, 8475.
2. Saraciftci, N. S.; Smilowitz, L.; Heeger, A. J.; Wudl, F. *Science*, **1992**, *258*, 1474.
3. Reyes-Reyes, M.; Kim, K.; Dewald, J.; Lopez-Sandoval, R.; Avadhanula, A.; Curran, S.; Carroll, D. L. *Org. Lett.* **2005**, *7*, 5749.
4. Olsen, B.; Segalman, R. *Materials Science and Engineering*, **2008**, *R62*, 37-66
5. Sary, N.; Brochon, C.; Hadziioannou, G.; Mezzenga, R. *Eur. Phys. J. E* **2007**, *24*, 379–384
6. (a) Stalmach, U.; de Boer, B.; Videlot, C.; van Hutten, P. F.; Hadziioannou, G.; *J. Am. Chem. Soc.*, **2000**, *122*, 5464-6472. (b) de Boer, B.; Stalmach, U.; van Hutten, P. F.; Melzer, C.; Krasnikov, V. V.; Hadziioannou, G. *Polymer*, **2001**, *42*, 9097-9109.
7. Sivula, K.; Ball, Z. T.; Watanabe, N.; Fréchet, J. M. *J. Adv. Mater.* **2006**, *18*, 206–210.
8. Chen, X.; Gholamkhash, B.; Han, X.; Vamvounis, G.; Holdcroft, S. *macromolecular rapid com.*, **2007**, *28*, 1792–1797.
9. Sun, S.-S. *Sol. Energy Mater. Sol. Cells* **2003**, *79*, 257.
10. (a) Lindner, S. M.; Thelakkat, M.; *Macromolecules*, **2004**, *37*, 8832-8835. (b) Lindner, S. M.; Hüttner, S.; Chiche, A.; Thelakkat, M.; Krausch, G.; *Angew. Chem. Int. Ed.*, **2006**, *45*, 3364–3368.
11. Marsitzky, D.; Klapper, M.; Mullen, K. *Macromolecules* **1999**, *32*, 8685-8688.
12. Li, W. J.; Wang, H. B.; Yu, L. P.; Morkved, T. L.; Jaeger, H. M. *Macromolecules* **1999**, *32*, 3034-3044.
13. Marsitzky, D.; Brand, T.; Geerts, Y.; Klapper, M.; Mullen, K. *Macromol. Rapid Commun.* **1998**, *19*, 385-389.
14. Tew, G. N.; Pralle, M. U.; Stupp, S. I. *J. Am. Chem. Soc.* **1999**, *121*, 9852-9866.
15. Sary, N.; Mezzenga, R.; Brochon, C.; Hadziioannou, G.; Ruokolainen, J. *Macromolecules* **2007**, *40* (9), 3277-3286.
16. Sary, N.; Rubatat, L.; Brochon, C.; Hadziioannou, G.; Ruokolainen, J.; Mezzenga, R.; *Macromol.*, **2007**, *40*, 6990-6997
17. Olsen, B. D.; Segalman, R., A.; *Macromol.*, **2007**, *40*, 6922-6929.
18. Leclere, P.; Parente, V.; Bredas, J. L.; Francois, B.; Lazzaroni, R. *Chem. Mat.* **1998**, *10*, 4010-4014.
19. van der Veen, M. H.; de Boer, B.; Stalmach, U.; van de Wetering, K. I.; Hadziioannou, G.; *Macromol.*, **2004**, *37*, 3673-3684.
20. Barrau, S.; Heiser, T.; Richard, F.; Brochon, C.; Ngov, C.; van de Wetering, K.; Hadziioannou, G.; Anokhin, D. V.; Ivanov, D. A.; *Macromol.*, **2008**, *41*, 2701-2710.
21. Brochon, C.; Sary, N.; Mezzenga, R.; Ngov, C.; Richard, F.; May, M.; Hadziioannou, G. *Journal of Applied Polymer Science*, **2008**, *110*, 3664-3670.

- 
22. (a) Liu, J. S.; Sheina, E.; Kowalewski T.; McCullough, R. D.; *Angew. Chem., Int. Ed.*, **2002**, *41*, 329 (b) M. C. Iovu, M. Jeffries-EL, E. E. Sheina, J. R. Cooper, R. D. McCullough, *Polymer* **2005**, *46*, 8582.
  23. Iovu, M.C.; Craley, C.R.; Jeffries-EL, M.; Krankowski, A.B.; Zhang, R.; Kowalewski, T.; McCullough, R.D.; *Macromol.*, **2007**, *40*(14), 4733-4735.
  24. Richard, F.; Brochon, C.; Leclerc, N.; Ekhardt, D.; Heiser, T.; Hadziioannou, G. *Macromol. Rapid Com*, **2008**, *29* (11), 885-891.
  25. Lu, S.; Fan, Q.L.; Liu, S.Y.; Chua, S.J. *Macromolecules*, **2002**, *35*, 9875-9881.
  26. Lu, S.; Fan, Q.L.; Chua, S.J. *Macromolecules*, **2003**, *36*, 304-310.
  27. Van de Wetering, K.; Brochon, C.; Ngov, C.; Hadziioannou, G. *Macromolecules* **2006**, *39* (13), 4289.
  28. Chochos, C.; Kallitsis, J.; Gregoriou, V. *J. Phys. Chem. B*, **2005**, *109*, 8755.
  29. Kretzschmann, H.; Meier, H. *Tet. Lett.*, **1991**, *38* (16) 5059-5062.
  30. Jeffries-EL, M.; Sauv e, G.; McCullough, R. D. *Macromolecules*, **2005**, *38* (25), 10346.
  31. Jeffries-EL, M.; Sauv e, G.; McCullough, R. D. *Adv. Mater.*, **2004**, *16* (12), 1017.
  32. Barbarella, G.; Bonglini, A.; Zambianchi, M. *Macromolecules*, **1994**, *27*, 3039.

## Chapter 18

# Linear Viscoelasticity of Polymer Tethered Highly Grafted Nanoparticles

Vivek Goel<sup>1</sup>, Joanna Pietrasik<sup>2,3</sup>, Krzysztof Matyjaszewski<sup>3</sup>, and Ramanan Krishnamoorti<sup>1</sup>

<sup>1</sup>Department of Chemical & Biomolecular Engineering, University of Houston, Houston, TX 77204.

<sup>2</sup>Department of Chemistry, Technical University of Lodz, Institute of Polymer and Dye Technology, 90924 Lodz, Poland.

<sup>3</sup>Department of Chemistry, Carnegie Mellon University, Pittsburgh, PA 15213.

The linear viscoelastic properties in the melt state of highly grafted polymers on spherical silica nanoparticles are probed using linear dynamic oscillatory measurements and linear stress relaxation measurements. While the pure silica tethered polymer nanocomposite exhibits solid-like response, the addition of a matched molecular weight free matrix homopolymer chains to this hybrid material, initially lowers the modulus and later changes the viscoelastic response to that of a liquid. These results are consistent with the breakdown of the ordered mesoscale structure, characteristic of the pure hybrid and the high hybrid concentration blends, by the addition of homopolymers with matched molecular weights.

### Introduction

Understanding the structure – processing – property correlations for polymers with dispersed nanoparticles remains a compelling area for research.<sup>1</sup> Model nanoparticle dispersions of polymer – grafted nanoparticles, either as pure hybrid materials or as mixtures with homopolymers that are chemically similar to the grafted chains, have become possible due to advances in living radical polymerization methods and provide a good framework for developing a



better understanding of the structure – processing – property correlations for polymer nanocomposites in general.<sup>2,3</sup>

Such hybrids, combining the behavior of linear polymer chains and hard-sphere character of nanoparticles, are capable of bridging much of our understanding of colloidal dispersions and that of star polymers.<sup>4,5</sup> When the grafting density of the polymer chains is high enough that the crowding caused by the grafting results in significantly altered conformations of the polymer, significant new issues arise and are captured by the developments in “polymer brushes”. In this work we have studied such hybrid materials where linear polymers are attached to spherical silica nanoparticles and the polymers are grafted such that they are in the brush regime. Specifically in this work we report on the linear rheological properties of such hybrid materials under conditions where the polymer by itself would be considered a liquid and with a relaxation time significantly smaller than 1 sec.

Previously, linear rheological measurements of other polymer hybrids (with no free polymer chains), including ones where the polymers have been attached to layered silicates, have indicated that with increased nanoparticle loading, at roughly the same grafting density, there is a transition from liquid-like to solid-like behavior.<sup>2,6</sup> This behavior has been attributed to the formation of a sample spanning percolative network that gets created with increased nanoparticle loading.<sup>7</sup> On the other hand, star polymers have shown extremely interesting behavior when high-functionality star polymers are studied either as pure melts or as dispersions in linear chains. For instance, upon addition of linear chains in the stars a re-entrant gelation transition is observed in those dispersions.<sup>8</sup> Interestingly, the hybrids studied here show some structural similarity with highly functional star polymers, most notably the formation of face centered cubic ordered crystalline order<sup>9</sup> that has been hinted previously in some studies of star polymers.

## Experimental

### Materials

The monomer n-butyl acrylate (BA, Acros, 99%) was purified by filtration through a basic alumina column to remove inhibitors before the synthesis. The procedure for the synthesis of 1-(chlorodimethylsilyl)propyl 2-bromoisobutyrate and the subsequent functionalization of the silica (30 % wt. silica in methyl isobutyl ketone, diameter  $D = 16.5$  nm, MIBK-ST, Nissan) was described previously.<sup>3</sup> Bis(2-pyridylmethyl)octadecylamine (BPMODA) was synthesized according to methods described previously.<sup>10</sup> CuBr (Aldrich, 99 %) was purified via several slurries in acetic acid followed by filtration and washing with methanol and ethyl ether, and stored under nitrogen before use. CuBr<sub>2</sub> (Aldrich, 99.999 %), polyoxyethylene (20) oleyl ether (Brij 98, Aldrich), hexadecane (Aldrich), L-ascorbic acid (AA, Aldrich, 99 %), dimethyl-2,6-dibromoheptanedioate (DMDBrHD, Aldrich, 97 %), N,N,N',N',N''-

pentamethyldiethylenetriamine (PMDETA, Aldrich, 99 %), anisole (Aldrich) and hydrofluoric acid (50 vol % HF, Acros) were used as received.

Poly(*n*-butyl acrylate) brushes were synthesized by activators generated by electron transfer (AGET) ATRP of BA from 2-bromoisobutyrate functionalized silica particles in miniemulsion under conditions similar to those reported previously, BA: SiO<sub>2</sub>-Br: CuBr<sub>2</sub>: BPMODA: ascorbic acid = 600: 1: 0.5: 0.5: 0.2, temperature 80°C, hexadecane 5 wt % based on monomer, Brij 98 - 14 wt % solid content.<sup>11</sup>

In a case of synthesis of PBA homopolymer, the polymerization was carried out at 70 °C. DMDBrHD (56.6 μL, 0.26 mmol), PMDETA (54.4 μL, 0.26 mmol), BA (11 mL, 78 mmol), and anisole (1.1 mL) were added to a 25-mL Schlenk flask equipped with a magnetic stir bar. The flask was sealed, and the resulting solution was subjected to three freeze-pump-thaw cycles. After equilibration at room temperature, CuBr (37.3 mg, 0.26 mmol) was added to the solution under nitrogen flow and the flask was placed in preheated oil bath. Aliquots were removed by syringe in order to monitor molecular weight evolution. After a predetermined time, the flask was removed from the oil bath and opened to expose the catalyst to air. The polymerization solution was diluted with CHCl<sub>3</sub> and passed over an alumina (activated neutral) column to remove the catalyst. Solvent was removed by rotary evaporation, and the polymer was isolated by precipitation into cold methanol.

## Characterization of Polymers

Molecular weight ( $M_n$ ) and molecular weight distribution ( $M_w/M_n$ ) were determined by GPC (Waters, 717 plus), with THF as eluent at 1 mL/min (Waters, 515) and four columns (guard, 10<sup>5</sup> Å, 10<sup>3</sup> Å, 100 Å; Polymer Standards Services) in series. Toluene was used as internal standard. Calculations of molar mass were determined using PSS software using a calibration based on linear polystyrene standards. Polymers were analyzed after etching silica with HF.

**Table 1. ATRP of *n*-butyl acrylate (BA) from functionalized silica particles or from small molecular weight initiator**

Sample	initiation	[BA]: [initiating site]	$M_{n, SEC}$ g/mol	$M_w/M_n$	# of tethered chains/particle
SiO <sub>2</sub> -PBA50K	AGET	600: 1	53,500 <sup>a</sup>	1.25	~ 600
PBA50K	Normal	300: 1	55,000	1.23	-

<sup>a</sup> Polymers were analyzed after etching silica with HF.

## Rheological Characterization

Rheological measurements were conducted using a TA Instruments ARES rheometer with a torque transducer with an operating torque range of 0.2 – 2000 g<sub>f</sub> cm and normal force range of 2 – 2000 g. Dynamic oscillatory shear measurements in the linear range were performed using a set of 25 mm diameter parallel plates. Frequency sweeps were performed using small amplitude oscillatory shear to investigate the linear viscoelastic properties, characterized by the storage and the loss moduli ( $G'$  and  $G''$  respectively). A sinusoidal strain of the form  $\gamma(t) = \gamma_0 \sin(\omega t)$  was applied, and the resultant shear stress  $\sigma(t)$  ( $= \gamma_0 (G' \sin(\omega t) + G'' \cos(\omega t))$ ) was monitored. The complex viscosity ( $\eta^*$ ) ( $= \frac{\sqrt{G''(\omega)^2 + G'(\omega)^2}}{\omega} = \frac{G^*}{\omega}$ ) is also reported, where  $G^*$  is the complex modulus.

Data was collected over a temperature range of 30 °C to 80 °C, and reduced to a master-curve via the principle of time-temperature superposition, at the reference temperature of 30°C.

Stress relaxation measurements were investigated at 30°C using a 25 mm diameter cone and plate geometry with a cone angle of 0.0998 rad. Specifically this cone and plate geometry was employed in order to produce a uniform shearing rate across the sample space as

$$\dot{\gamma} = \omega / \tan \alpha \quad (1)$$

where  $\dot{\gamma}$  is the shear rate ( $s^{-1}$ ),  $\omega$  is the cone angular velocity and  $\alpha$  is the cone angle. For stress relaxation, a step strain  $\gamma_0$  was applied at time  $t = 0$ , and the shear stress monitored as a function of time, with the modulus  $G(t)$  obtained as  $G(t) = \sigma(t) / \gamma_0$ .

## Results and Discussions

The linear viscoelastic behavior of the SiO<sub>2</sub> – PBA hybrid was examined using small amplitude oscillatory strain measurements. Typical linear dynamic viscoelastic data for the hybrid materials, with no free polymer chains, is shown in Figure 1. The presence of a frequency independent plateau in  $G'$ , with the value of  $G'$  exceeding that of  $G''$ , at low frequencies is observed in the time-temperature superposed mastercurves. We note that excellent time-temperature superposition is observed and that the temperature dependent frequency shift factors for the nanocomposites are virtually identical to that of the homopolymers of PBA. Corroboration of the long-time solid like response was also observed from stress relaxation measurements shown in Figure 2. In fact, using a two-point collocation method, the stress relaxation data were found to be in quantitative agreement with the linear dynamic moduli data.<sup>7</sup> We note that while the longest relaxation time for a free homopolymer chain of length

corresponding to that of a single grafted chain is  $\ll 1$  sec, the plateau observed at low frequencies persists for at least 100,000 seconds. Such solid-like rheological behavior is reminiscent of cross-linked elastomers, percolated and filler-dominated nano and macro-composites, and perhaps most relevantly to that of ordered block copolymers that form either body-centered cubic structures.<sup>12</sup> In fact, structural studies using small angle x-ray and neutron scattering along with electron microscopy of these hybrid materials indicate that the silica nanoparticles organize themselves in a face centered cubic lattice, and this arrangement might in fact be responsible for the observed solid-like character.

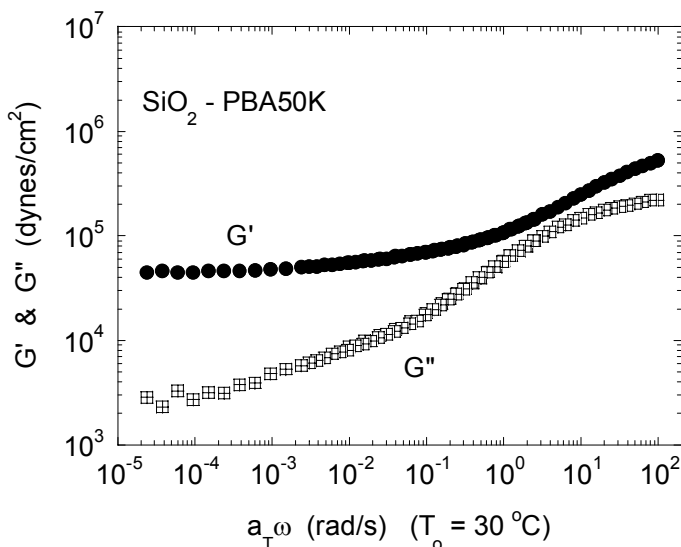


**Figure 1.** Linear dynamic oscillatory shear response of the 50K PBA based  $\text{SiO}_2$  hybrid sample. The data collected at temperatures between 30 and 80 °C were reduced to a single master curve using the principle of time-temperature superposition. The horizontal frequency shift factors ( $a_T$ ) were similar to that for the pure PBA homopolymer.

The polymer tethered silica hybrids were blended with a homopolymer with similar molecular weight to the one attached to the silica nanoparticles (Table 1). These mixtures of the grafted nanoparticles and their matched homopolymers were found to be homogenous using both electron microscopy and small angle x-ray scattering measurements. The linear viscoelastic properties of these blends were examined using melt rheological measurements and reported in Figure 3. We focus on the frequency dependence of the storage modulus ( $G'$ ) (Figure 3a), and the complex viscosity ( $\eta^*$ ) (Figure 3b) for this series of matched homopolymer – grafted nanoparticle blends. The blends, like the pure hybrids, exhibit thermo-rheological simplicity and further the shift factors are virtually identical in all cases.

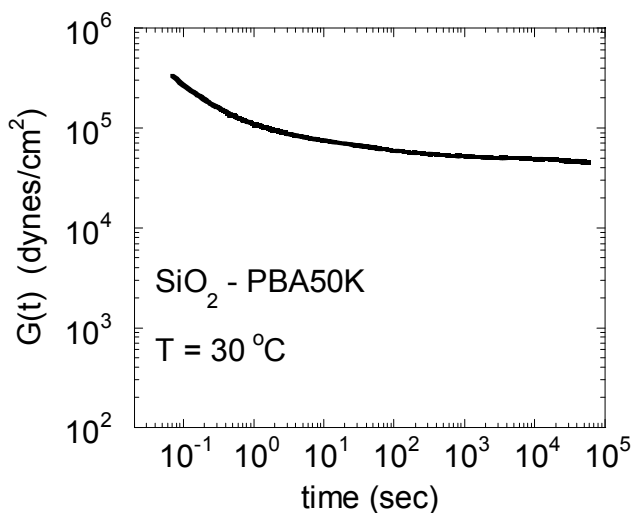


**Figure 2.** Time dependence of the linear stress relaxation modulus for the  $\text{SiO}_2$  – PBA50K hybrid at a strain of 0.02 is shown. The stress relaxation data for strain values below 0.04 were identical and exhibited solid-like behavior for  $\sim 80,000$  s after application of the step strain.

Blending of free homopolymer molecules to the polymer tethered silica hybrid systematically alters the viscoelastic response and most clearly observed in the low-frequency response of  $G'$  and  $\eta^*$ .<sup>2</sup> The low frequency plateau value of  $G'$  decreases with increasing homopolymer content and liquid-like behavior is observed for the blend with 20% silica hybrid material. This is also manifested as a low-frequency “Newtonian” type behavior for the complex viscosity,  $\eta^*$ , which becomes independent of frequency for the 20 % silica hybrid blend. On the other hand, the viscosity for the blends with higher hybrid concentration demonstrated a strong power-law behavior at low frequencies, consistent with the solid-like modulus behavior described in Figure 3a.

A convenient way to ascertain the transition from solid-like to liquid-like behavior is through a cross-plot of the complex modulus  $G^*$  versus the complex viscosity  $\eta^*$ , as shown in Figure 4. For the blend with 20 % silica hybrid, the behavior is similar to that of the pure homopolymer and demonstrates Newtonian behavior: the viscosity is well-behaved even at the lowest complex modulus values. On the other hand, the pure hybrid and the blends with high concentration of the silica hybrid, exhibit a diverging viscosity at finite values of the complex modulus, typical of materials with a finite yield stress. The value of the complex modulus at which  $\eta^*$  diverges is a measure of the yield stress.<sup>13</sup> As observed from Figure 4, the value of the yield stress decreases significantly with increasing homopolymer concentration in the blends.

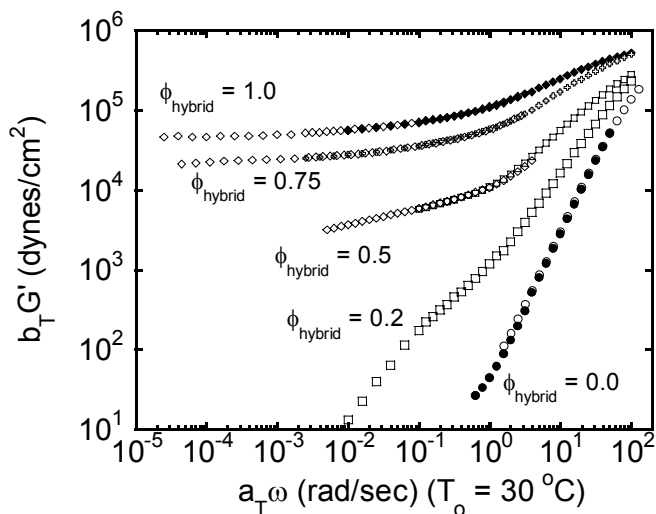


**Figure 3a.** Frequency dependence of the linear storage modulus ( $G'$ ) for the blends of  $\text{SiO}_2$ -PBA50K with a 50K PBA homopolymer are shown. Mastercurves were created by applying moduli shift factors ( $b_T$ ) and frequency shift factors ( $a_T$ ) to the data collected over a temperature range of 30 to 80 °C. The shift factors for the blends were found similar to those for the pure hybrid (Figure 1) and for pure PBA.

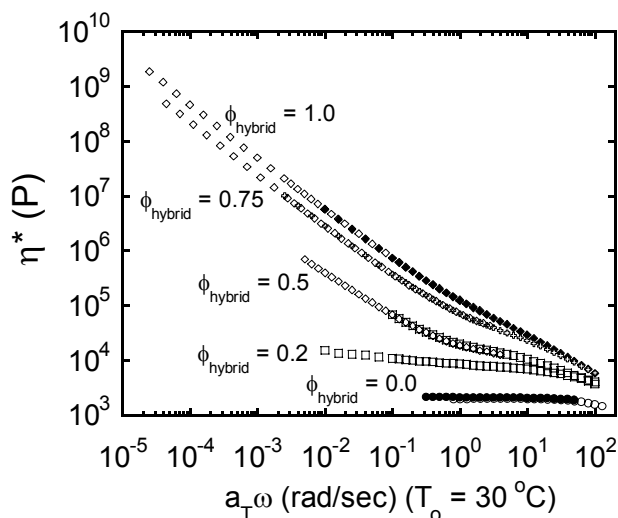


**Figure 3b.** Frequency dependence of the linear complex modulus ( $\eta^*$ ) for the blends of  $\text{SiO}_2$ -PBA50K with a 50K PBA homopolymer are shown. Data collected over a temperature range of 30 to 80 °C were superposed using the principle of time-temperature superpositioning to obtain the mastercurves shown here.

The yield stress and the low-frequency plateau storage modulus for the 50 % hybrid sample are ill-defined, because of the slight dependence of the modulus data with frequency over the entire low-frequency range. Therefore, we plot the storage modulus value as a function of hybrid concentration at a fixed frequency (in this case at  $\omega = 1$  rad/sec) in Figure 5. The modulus value at this single frequency changes dramatically across the blend composition and representative of the significant impact of tethering the polymer onto the surface of the nanoparticle and the ordering caused by such a physical coupling of the polymer and the nanoparticle, especially at high grafting densities. On the other hand, choosing a lower frequency to assess the composition dependence of the long-time (or low-frequency) plateau modulus for the high hybrid concentration blends, indicates a strong concentration dependence and captured as:

$$G'_{\text{low-}\omega \text{ plateau}}(\phi_{\text{hybrid}}) \propto (\phi_{\text{hybrid}})^{-4.1 \pm 0.5} \quad (2)$$

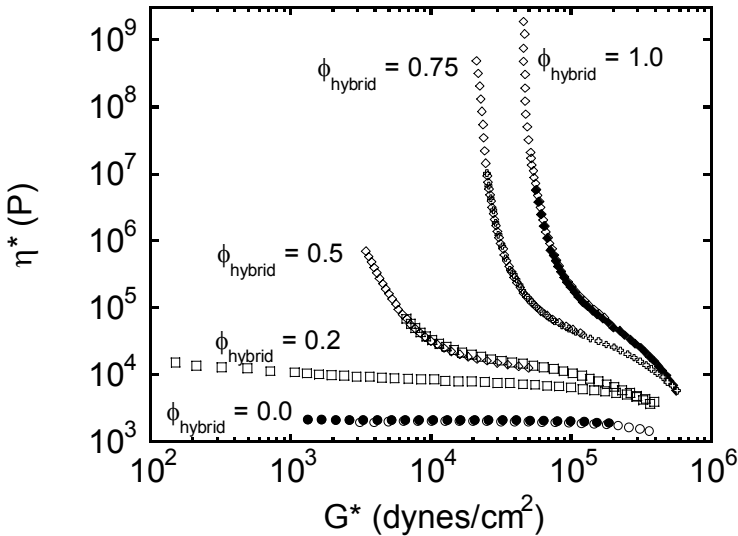


**Figure 4.** A cross-plot of the complex modulus ( $G^*$ ) and the complex viscosity ( $\eta^*$ ) from linear dynamic oscillatory measurements for the blends of the PBA50K homopolymer with the SiO<sub>2</sub>-PBA50K hybrid material. The samples with liquid like behavior (pure homopolymer and the blend with 20 % hybrid) demonstrate Newtonian behavior with the viscosity being well behaved down to the lowest value of the complex modulus. On the other hand, for the blends with higher levels of hybrid material, the viscosity diverges at significant values of the complex modulus, a feature characteristic of materials with a yield stress.

The scaling described in Equation 2 indicates that the modulus is a strong function of the hybrid loading and is consistent with the data obtained for other filled polymer systems as well as the scaling observed for block copolymers with spherical microdomains.<sup>5, 12, 14</sup>

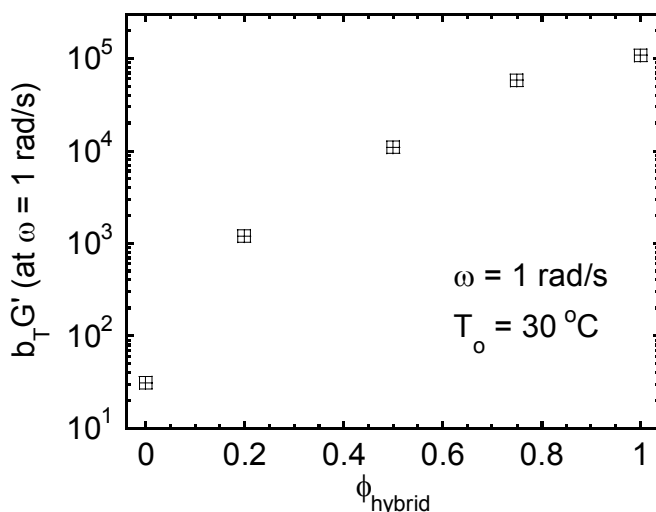


**Figure 5.** Blend composition dependence of the value of the storage modulus at a fixed frequency of 1 rad/s at a reference temperature of 30 °C. The frequency corresponds to a time scale significantly larger than the relaxation time of the polymer. The plateau at long times observed for the three highest hybrid concentration blends occur at frequencies lower than the frequency chosen here.

### Concluding Remarks

The development of hybrid nanocomposites with polymers tethered to nanoparticles provides a new paradigm of materials that can show self-assembly character and therefore quite interesting linear viscoelastic properties. Furthermore, due to their ability to form homogenous blends with a matched molecular weight polymer matrix that is unattached to the nanoparticles, a range of viscoelastic characteristics are observed. Starting at low concentrations of the added hybrid nanoparticles to the free homopolymer where Newtonian behavior is observed with a significantly enhanced viscosity, these blends rapidly become non-Newtonian with several rheological characteristics of a solid-like material i.e., the presence of a low-frequency (long time) plateau and the divergence of the low-frequency viscosity. While the modulus scaling appears to be similar to those observed for other filled systems as well as sphere forming block copolymers, it would be instructive and illustrative to compare these for different molecular weights of attached polymer, size of the nanoparticle, grafting density and chemically mismatched blends with varying degrees of attraction between matrix and tethered chains.

### Acknowledgements

VG and RK gratefully acknowledge the support of the National Science Foundation (CMMI-0708096). JP and KM thank the Kosciuszko Foundation and the National Science Foundation (DMR-05-49353) for their financial support.



## References

1. Krishnamoorti, R. *MRS Bulletin* **2007**, 32, (4), 341-347; Krishnamoorti, R.; Vaia, R. A. *J. Polym. Sci. Pt. B-Polym. Phys.* **2007**, 45, (24), 3252-3256; Winey, K. I.; Vaia, R. A. *MRS Bulletin* **2007**, 32, (4), 314-319.
2. Goel, V.; Chatterjee, T.; Bombalski, L.; Yurekli, K.; Matyjaszewski, K.; Krishnamoorti, R. *J. Polym. Sci. Pt. B-Polym. Phys.* **2006**, 44, (14), 2014-2023.
3. Pyun, J.; Kowalewski, T.; Matyjaszewski, K. *Macromol. Rapid Commun.* **2003**, 24, 1043-1059.
4. Likos, C. N.; Lowen, H.; Poppe, A.; Willner, L.; Roovers, J.; Cubitt, B.; Richter, D. *Phys. Rev. E* **1998**, 58, (5), 6299-6307; Likos, C. N.; Lowen, H.; Watzlawek, M.; Abbas, B.; Jucknischke, O.; Allgaier, J.; Richter, D. *Phys. Rev. Lett.* **1998**, 80, (20), 4450-4453; Vlassopoulos, D. *J. Polym. Sci. Pt. B-Polym. Phys.* **2004**, 42, 2931-2941.
5. Shih, W. H.; Shih, W. Y.; Kim, S. I.; Liu, J.; Aksay, I. A. *Phys. Rev. A* **1990**, 42, (8), 4772-4779.
6. Krishnamoorti, R.; Giannelis, E. P. *Macromolecules* **1997**, 30, 4097-4102.
7. Ren, J.; Silva, A. S.; Krishnamoorti, R. *Macromolecules* **2000**, 33, 3739-3746.
8. Stiakakis, E.; Vlassopoulos, D.; Likos, C. N.; Roovers, J.; Meier, G. *Phys. Rev. Lett.* **2002**, 89, (20), 208302-1-208302-4.
9. Chung, H.; Ohno, K.; Fukuda, T.; Composto, R. J. *Nano Letters* **2005**, 5, (10), 1878-1882; Morinaga, T.; Ohkura, M.; Ohno, K.; Tsujii, Y.; Fukuda, T. *Macromolecules* **2007**, 40, (4), 1159-1164; Morinaga, T.; Ohno, K.; Tsujii, Y.; Fukuda, T. *Eur. Polym. J.* **2007**, 43, (1), 243-248; Ohno, K.; Morinaga, T.; Koh, K.; Tsujii, Y.; Fukuda, T. *Macromolecules* **2005**, 38, (6), 2137-2142; Ohno, K.; Morinaga, T.; Takeno, S.; Tsujii, Y.; Fukuda, T. *Macromolecules* **2006**, 39, (3), 1245-1249; Ohno, K.; Morinaga, T.; Takeno, S.; Tsujii, Y.; Fukuda, T. *Macromolecules* **2007**, 40, (25), 9143-9150; Yamamoto, S.; Ejaz, M.; Tsujii, Y.; Fukuda, T. *Macromolecules* **2000**, 33, 5608-5612.
10. Xia, J.; Matyjaszewski, K. *Macromolecules* **1999**, 32, (8), 2434-2437; Tyeklar, Z.; Jacobson, R. R.; Wei, N.; Murthy, N. N.; Zubieta, J.; Karlin, K. D. *J. Am. Chem. Soc.* **1993**, 115, (7), 2677-2689; Pintauer, T.; Matyjaszewski, K. *Coord. Chem. Rev.* **2005**, 249, (11-12), 1155-1184.
11. Bombalski, L.; Min, K.; Dong, H.; Tang, C.; Matyjaszewski, K. *Macromolecules* **2007**, 40, (21), 7429-7432; Jakubowski, W.; Matyjaszewski, K. *Macromolecules* **2005**, 38, (10), 4139-4146; Min, K.; Gao, H. F.; Matyjaszewski, K. *J. Am. Chem. Soc.* **2005**, 127, (11), 3825-3830.
12. Sebastian, J. M.; Graessley, W. W.; Register, R. A. *J. Rheol.* **2002**, 46, (4), 863-879; Sebastian, J. M.; Lai, C.; Graessley, W. W.; Register, R. A. *Macromolecules* **2002**, 35, 2700-2706; Kossuth, M. B.; Morse, D. C.; Bates, F. S. *J. Rheol.* **1999**, 43, (1), 167-196; Rosedale, J. H.; Bates, F. S. *Macromolecules* **1990**, 23, (8), 2329-2338.

13. Mitchell, C. A.; Krishnamoorti, R. *J. Polym. Sci. Pt. B-Polym. Phys.* **2002**, 40, (14), 1434-1443; Mitchell, C. A.; Krishnamoorti, R. *Macromolecules* **2007**, 40, (5), 1538-1545.
14. Yurekli, K.; Krishnamoorti, R. *Macromolecules* **2002**, 35, (10), 4075-4083; Yurekli, K.; Krishnamoorti, R.; Tse, M. F.; Mcelrath, K. O.; Tsou, A. H.; Wang, H.-C. *J. Polym. Sci. Pt. B-Polym. Phys.* **2001**, 39, 256-275.

## Chapter 19

# Physical and mechanical properties of amphiphilic and adaptative polymer conetworks produced by Atom Transfer Radical Polymerization

Laetitia Mespouille<sup>1</sup>, Jean-Marie Raquez<sup>1</sup>, Curtis W. Frank<sup>2</sup>,  
Philippe Dubois<sup>1\*</sup>

<sup>1</sup>Center of Innovation and Research in Materials and Polymers (CIRMAP),  
Laboratory of Polymeric and Composite Materials, University of Mons-  
Hainaut, 20 Place du Parc, B-7000 Mons

<sup>2</sup>Department of Chemical engineering, Stanford University, Stanford,  
California 94305

Model amphiphilic polymer conetworks have been successfully produced by combination of ring-opening polymerization (ROP) of  $\epsilon$ -caprolactone and atom transfer radical polymerization (ATRP) of amino-functionalized methacrylate monomer. Their swelling properties have been investigated in Millipore<sup>®</sup> water as well as in toluene in order to demonstrate the amphiphilic nature of the gel. The control over the cross-linking degree and therefore the conetwork structure was highlighted by swelling experiments and confrontation of the results with the Flory-Rehner relationship. Environmental responsiveness towards pH and temperature was also demonstrated. The presence of the hydrophobic poly( $\epsilon$ -caprolactone) (PCL) cross-linkers was found to be beneficial for improving both stiffness and elongation at break of the resulting hydrogels but also for favouring their hydrolytic degradability. Moreover, tensile testing studies performed on two representative hydrogel samples produced by either ATRP or more conventional free-radical polymerization (FRP) allowed to reveal the strong impact of the polymerization mechanism over the mechanical

performances of the resulting conetworks. As a result, it came out that ATRP not only produces amphiphilic polymer conetworks with controlled architecture but allows also for significantly enhancing their physico-mechanical properties resulting in much less brittle materials.

Over the past decade, widespread attention has been paid to hydrogels owing to their high water content and their soft and rubbery consistency making them highly biocompatible, and resembling in their physical properties to some of the living tissues, more than other synthetic materials (1). Therefore, hydrogels were found very desirable for medical applications like, e.g., soft contact lenses (2), drug carriers (3), wound dressing systems (4), etc. More recently, a particular interest has been drawn by stimuli-responsive hydrogels, also called ‘intelligent’ or adaptative hydrogels because of their capability to undergo relatively large and abrupt transition in response to rather limited external stimuli in their environment (e.g., pH, temperature, ionic strength, osmotic pressure,...) (5-6). Inspired by a large array of reliable properties, adaptative hydrogels have found various applications into the biomedical field as switches (7), sensors (8), artificial muscles (9) and drug delivery systems (10). Regarding the scope of such high-tech applications, it appears of prime importance to understand the correlation between the intimate structure of the gels and their final properties. To date, thermo- or photo-initiated free-radical polymerization (FRP) has represented the most widespread used method to produce hydrogels due to its mild reaction conditions, high tolerance to protic impurities, as well as a wide range of monomers accessible (11-13). Unfortunately, traditional FRP proceeds in a non controlled fashion with large discrepancies to the mean-field theory of Flory and Stockmayer (14-18) leading to non-homogeneous and uncontrolled architectures with lots of non-idealities (e.g., as loops, dangling unreactive chain ends, clusters, additional cross-linking by entanglements, side reactions or physical interactions, no control over molecular weight and molecular weight distribution in between cross-linking points). As a consequence final properties cannot be predicted limiting their use in some specific applications.

To overcome those limitations, controlled/“living” radical polymerizations have been successfully employed for producing homogeneous polymer networks with a limited amount of defects. In this context, Ide and Fukuda (19) were the first to report the use of nitroxide-mediated polymerization (NMP) for the preparation of cross-linked polystyrene networks with a critical number density of cross-links varying only by a factor of 2 with respect to Flory’s theory. Masci et al. (20-22) evidenced both the impact of the polymerization mechanism over the final dynamic mechanical properties as well as over the structure of the gel by comparing samples produced either by reversible addition-fragmentation chain transfer polymerization (RAFT) or by FRP. Thereby, it was observed that hydrogel samples produced in a “living” way displayed higher degree of swelling than their homologues produced by FRP. Interestingly enough, Lu reported that RAFT polymerization allows the preparation of poly(N-

isopropylacrylamide) PNiPAAm-based hydrogels with accelerated shrinking kinetics and a high level of transparency owing to their homogeneous structure. Atom transfer radical polymerization (ATRP) has been also used to prepare linear polymer macromonomers or functional polymer precursors followed by a post-cross-linking step via free radical polymerization (23-24) or «Click» coupling reaction (25-26). More recently, the one-step gelation of various methacrylate derivatives has also been successfully reported by many groups (27-33). As a relevant illustration, Hunkeler et al. demonstrated a linear evolution of the N,N-dimethylamino-2-ethyl methacrylate (DMAEMA) monomer consumption *versus* time in agreement with a “living” process, as well as a number density of cross-links in accordance with Flory’s theory (27). Zhu et al. showed that the Cu-catalyzed ATRP of ethyleneglycol dimethacrylate (EGDMA) proceeds at a lower propagation rate as compared to FRP (28). The equilibrium between the dormant and the active propagating species induces a lower radical concentration, eliminating therefore the autoacceleration effect. However, it was also demonstrated that at high conversion, the mobility of the catalytic complex is altered, resulting in an increase of radicals and in Cu(II) deactivating agent into the network, leading to a diffusion controlled mechanism (31). Matyjaszewski described the preparation of nanogels by ATRP conducted in reverse mini-emulsion. Compared to FRP, nanogels are more stable and allow the controlled release of an encapsulated reagent (32). Recently, some of us reported the controlled preparation of amphiphilic hydrogels by ATRP as attested by the predetermined molecular weight and the narrower molecular weight distribution of the polymethacrylate backbone recovered after selective hydrolysis of the cross-linker. It was also demonstrated that the gels resulted from the slow and continuous addition of monomers onto the growing network instead of a more heterogeneous assembly of *in situ* generated microgels. Finally, SEM images confirmed clearly the impact of the polymerization mechanism employed over the gel structure (33).

In this chapter, we aim at presenting the physical properties of poly[2-(N,N-dimethylamino)ethyl methacrylate]-*l*-poly( $\epsilon$ -caprolactone) model amphiphilic polymer conetworks (APCNs) produced by ATRP in terms of swelling behavior, state of water molecules inside the gel, mechanical properties and degradability. The stimuli-responsive properties of the gels will be investigated by measuring their swelling behavior at various pH values and temperature. Most importantly, the controlled structure of the APCNs will be evaluated by measuring the swelling behavior at various cross-linking degrees. Last but not least, the impact of the polymerization mechanism over ultimate mechanical properties will be highlighted by tensile testing experiment directly performed on the water-swollen APCNs.

## Experimental section

### Material

$\epsilon$ -Caprolactone (CL) (Acros, 99%) was dried over calcium hydride at r.t. for 48h and then distilled under reduced pressure. 2-(N,N-dimethylamino)ethyl methacrylate (DMAEMA) (Aldrich, 98%) was deprived of its inhibitor by filtration through a basic alumina column, and depending on samples (see text) dried over calcium hydride at r.t. for 24h and then distilled under reduced pressure. Butane-1,4-diol (Acros, > 99%) was dried over calcium hydride for 48h at r.t. and distilled at 70°C under reduced pressure. Triethylamine (NEt<sub>3</sub>, Fluka, 99%) was dried over barium oxide for 48h at r.t. and distilled under reduced pressure. Copper bromide (CuBr, Fluka, 98%) was purified in acetic acid and recrystallized in ethanol under inert atmosphere until a white powder is obtained. Tin(II) bis-2-ethyl hexanoate (Sn(Oct)<sub>2</sub>, Aldrich, 95%), methacrylic anhydride (Aldrich, 94%), N,N-dimethylamino-4-pyridine (DMAP, Acros 99%), 1,1,4,7,10,10-hexamethyltriethylene tetramine (HMTETA, Aldrich, 97%), ethyl-2-bromoisobutyrate (E<sup>t</sup>BBr, Aldrich, 98%), N,N-dicyclohexylcarbodiimide (DCC, Acros, 99%), were used as received. Tetrahydrofuran (THF, Labscan, 99%) was dried over molecular sieves (4Å) and distilled over polystyryl lithium (PS<sup>-</sup>Li<sup>+</sup>) complex under reduced pressure just before use. Toluene (Labscan, 99%) was dried by refluxing over CaH<sub>2</sub>.

### Characterization

NMR spectra were recorded in various deuterated solvents (e.g., CDCl<sub>3</sub>, acetone-d<sub>6</sub>, D<sub>2</sub>O, THF-d<sub>8</sub>) at a concentration of 30 mg/0.6ml (<sup>1</sup>H NMR) or 60 mg/0.6 ml (<sup>13</sup>C NMR) using either a Bruker AMX300 or a Bruker AMX500. Size exclusion chromatography (SEC/GPC) was performed in THF or in THF + 2wt% NEt<sub>3</sub> (PDMAEMA-containing polymers) at 35°C using a Polymer Laboratories liquid chromatograph equipped with a PL-DG802 degasser, an isocratic HPLC pump LC 1120 (flow rate = 1ml/min), a Rheodin manual injection (loop volume = 200 μL, solution conc. = 2 mg/mL), a PL-DRI refractive index detector and four columns: a PL gel 10 μm guard column and three PL gel Mixed-B 10μm columns (linear columns for separation of M<sub>w</sub>PS ranging from 500 to 10<sup>6</sup> daltons). DSC measurements were performed under nitrogen flow using a DSC Q1000 from TA instruments (heating rate ranged from 1 to 10°C/min). Measurements of uniaxial extension were carried out using an Instron Model 5844 tensile testing apparatus. The hydrogel samples were cut into 0.7 × 3.0 cm long strips using parallel razor blades, and its thickness was measured with a calliper. The sample was then fixed by grips and kept moist with an ultrasonic air humidifier during the whole testing process. The initial grip distance was set to be 5.0 mm and a constant stretch rate of 0.01 mm/sec was applied to the sample until its failure (breakage). Testworks software recorded the load and extension data, which were used to calculate the true stress and strain, from which the average values for Young's modulus (E),

maximum strength, and elongation at break of water-saturated hydrogels could be determined. To determine the swelling behavior, dry hydrogel slabs were immersed in buffer solutions (pH = 2, 7, 10) or in Millipore® water or in toluene and withdrawn at determined time interval, blotted with tissue paper to absorb the excess of solvent on the surface and weighed. The swelling degree was determined as a function of time.

### Synthesis of the amphiphilic conetworks

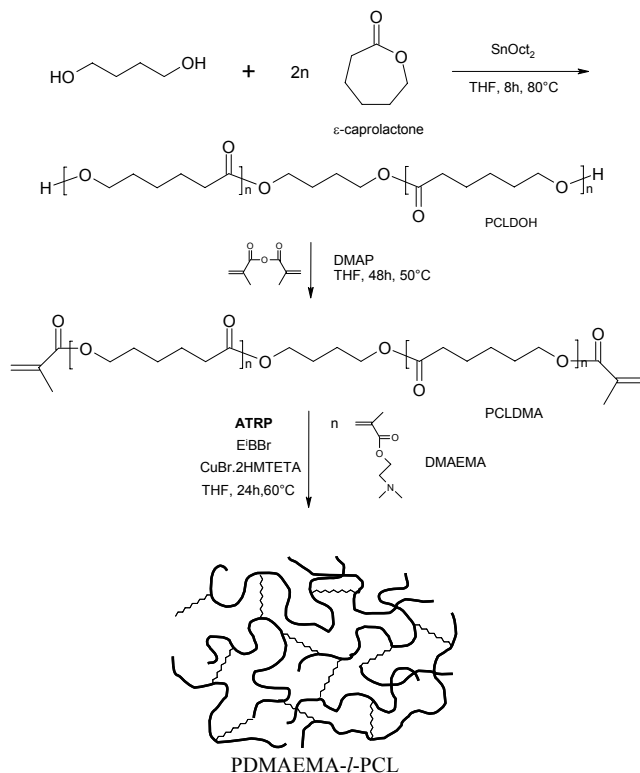
The overall synthesis of both PCL cross-linkers and poly[2-(N,N-dimethylamino)ethyl methacrylate-*linked*-poly( $\epsilon$ -caprolactone)] model amphiphilic conetworks PDMAEMA-*l*-PCL have been already reported in a separate contribution with all experimental conditions described in details (33).

## Results and discussion

According to our recently published study (33), poly[2-(N,N-dimethylamino)ethyl methacrylate-*linked*-poly( $\epsilon$ -caprolactone)] conetworks PDMAEMA-*l*-PCL were synthesized via a combination of controlled polymerization techniques, i.e., ring-opening polymerization (ROP) of  $\epsilon$ -caprolactone (CL) and atom transfer radical polymerization (ATRP) of 2-(N,N-dimethylamino)ethyl methacrylate (DMAEMA). The conetwork synthesis was built on a three-step strategy (see **Scheme 1**) where the first step relied upon the controlled ROP of CL initiated by 1,4-butanediol (Bu(OH)<sub>2</sub>) and catalyzed by tin(II) bis-2-ethyl hexanoate (Sn(Oct)<sub>2</sub>) in THF for 8h at 80°C to afford well-defined telechelic  $\alpha,\omega$ -hydroxy PCL (PCL(OH)<sub>2</sub>). In a second step,  $\alpha,\omega$ -hydroxy end-groups were esterified by methacrylic anhydride in the presence of DMAP catalyst in THF at 50°C allowing the quantitative preparation of  $\alpha,\omega$ -methacrylate PCL (PCLDMA). In a last step, PCLDMA was copolymerized with DMAEMA by ATRP in THF at 60°C using 2-ethyl bromoisobutyrate (E<sup>i</sup>BBr) and CuBr complexed by 1,1,4,7,10,10-hexamethyltriethylenetetramine (HMTETA) as initiator and catalytic complex, respectively. An initial [PCLDMA+DMAEMA]<sub>0</sub>/[E<sup>i</sup>BBr]<sub>0</sub>/[CuBr]<sub>0</sub>/[HMTETA]<sub>0</sub> molar ratio of 100/1/1/2 and an initial comonomer concentration of 4.8 mol.L<sup>-1</sup> were applied and PCLDMA macromonomers of various molecular weights (1800 ≤ M<sub>n</sub> ≤ 5200 g.mol<sup>-1</sup>) were employed for an initial molar fraction of 3%.

It is worth reminding that such a procedure allowed the preparation of homogeneous amphiphilic polymer conetworks PDMAEMA-*l*-PCL with very large gel fractions (F<sub>G</sub> usually higher than 90%) and a composition very close to the feed as attested for by N-elementary analysis (33). Most importantly and in opposition with the traditional free-radical polymerization (FRP), ATRP proved high efficiency to tailor the macromolecular parameters of the conetworks (e.g., number-average molecular weight of the polymethacrylic backbone closer to the predicted one and narrow polydispersity) largely influencing the final structure of the gel as evidenced by swelling testing and SEM analyses. The controlled

nature of the as-obtained hydrogels was further demonstrated by the lower deviation to Flory's theory in term of cross-linking density. Considering this precious observations, it was of interest to evaluate the physical and mechanical properties of the PDMAEMA-*l*-PCL conetworks in terms of swelling ability and related tensile strength, and to determine the structure-properties relationships by confronting the results with theory available for model networks. **Table 1** displays the main characteristic features of the investigated amphiphilic gels from the point of view of their chemical compositions, molecular weight between cross-linkers and ultimate gel fraction.



*Scheme 1: Three-step synthesis of poly[2-(N,N-dimethylamino)ethyl methacrylate-*l*-poly( $\epsilon$ -caprolactone)] conetworks (PDMAEMA-*l*-PCL)*



**Table I. Molecular parameters of PDMAEMA-*l*-PCL conetwork samples as obtained by ATRP in THF at 60°C, initiated by E<sup>i</sup>BBr and catalyzed by CuBr<sub>2</sub>HMTETA for an initial comonomer concentration of 4.8 mol.L<sup>-1</sup> and various degrees of cross-linking.**

Entry	$Mn_{PCLDMA}$ (g.mol <sup>-1</sup> ) <sup>a</sup>	$Fn_{PCLDMA}$ <sup>b</sup>	$Fw_{PCLDMA}$ (%) <sup>c</sup>	$F_G$ (%) <sup>d</sup>
1	3,100	3	37.9	94.0
2	1,700	2	31.1 <sup>e</sup>	87.5
3	1,700	3	31.1 <sup>e</sup>	95.6
4	1,700	4	31.1 <sup>e</sup>	91.0
5	4,300	3	41.5	> 99

<sup>a</sup> Number average molecular weight of PCLDMA as determined by <sup>1</sup>H NMR

<sup>b</sup> Initial molar fraction in PCL in the feed

<sup>c</sup> Initial weight fraction of PCL in the feed

<sup>d</sup>  $F_G$  = gel fraction obtained after elimination of residual catalyst, unreacted comonomers and any non cross-linked graft copolymers by using the following equation:  $F_G = w_g / w_p$  with  $w_g$  and  $w_p$ , the weight of the dried sol-free network sample after solvent evaporation under reduced pressure, and the total weight of comonomer introduced, respectively.

<sup>e</sup> Initial weight fraction of PCL (PCLDMA + PCLMA) in the feed

### Swelling behavior of PDMAEMA-*l*-PCL amphiphilic gels

Understanding of the swelling kinetics of cross-linked polymer networks is very important in the design and development of controlled drug release devices. The swelling behavior of any polymer network is a function of the nature of the polymer, the polymer-solvent compatibility and the degree of cross-linking. In the case of ionic networks, in addition to these factors, the ionization of fixed charges has to be taken into account as well.

Basically, a hydrogel swells until reaching an equilibrium, which, in the particular case of polyelectrolyte networks, is determined by a balance of three primary forces: (i) the elastic retractile response of the network, (ii) the net osmotic pressure within the network resulting from the mobile counterions surrounding the fixed charges, and (iii) the free energy of mixing of the network chains with the solvent.

In this section, we aim at determining the swelling properties of PDMAEMA-*l*-PCL polymer conetworks (produced in a controlled manner) in aqueous solution in order to highlight their amphiphilic and adaptative properties. To determine the swelling behavior of PDMAEMA-*l*-PCL amphiphilic polymer conetworks, dry hydrogel slabs of a representative sample (Entry 1, **Table I**) were immersed in Millipore<sup>®</sup> water and withdrawn at determined time interval, blotted with tissue paper to absorb the excess of water at surface and weighed. The swelling degree was determined as a function of time by using the following relationship:

$$S(\%) = (m_w - m_d) / m_d \quad (1)$$

with  $m_w$  and  $m_d$  the mass of the wet and dry gel, respectively. For a higher degree of accuracy, all swelling studies were conducted in triplicate at room temperature and standard deviations were calculated from the average values. **Figure 1** (cycle 1) depicts the average swelling profile of PDMAEMA-*l*-PCL in Millipore® water at r.t. As illustrated, the studied PDMAEMA-*l*-PCL conetwork is able to absorb a relatively large amount of water. The water uptake is relatively fast at the beginning but saturation (i.e., equilibrium) occurs only after 9h of soaking (at 47% swelling ratio specifically for this sample). The reproducibility of the swelling behavior was investigated by drying and swelling two times the same hydrogel slabs in Millipore® water at r.t. As evidenced in **Figure 1** (cycles 1 to 3), the swelling profile from each swelling cycle is very reproducible, demonstrating the high stability of the PDMAEMA-*l*-PCL hydrogels in the investigated conditions.

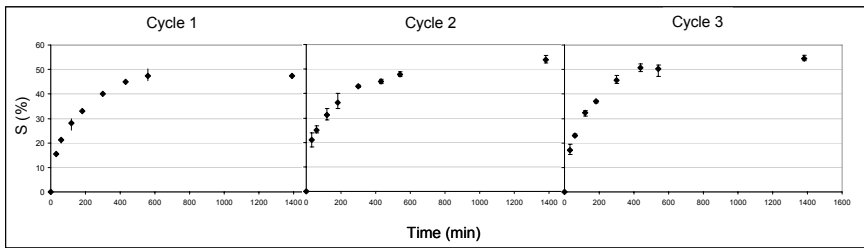


*Figure 1 : Reproducibility study of the swelling behavior of a representative PDMAEMA-*l*-PCL polymer network produced by ATRP (Entry 1, Table I) in Millipore® water at r.t.*

The extent of the reproducible character of swelling was further demonstrated by determining the diffusional constant  $n$  from the Fick equation (equation 2) for the first 60% water uptake.

$$M_t/M_\infty = Kt^n \quad (2)$$

where  $M_t$  is the mass of water absorbed at any time  $t$ ,  $M_\infty$  is the total mass of water absorbed at equilibrium and  $K$  and  $n$  are constant values. According to Fick theory, a value of  $n=0.5$  signifies a *Case I* or *Fickian* water diffusion mechanism (diffusion-controlled transport diffusion), while  $n=1$  indicates *Case II* diffusional or *anomalous* mechanism (relaxation-controlled transport diffusion). For  $0.5 \leq n \leq 1$ , the diffusional mechanism is not Fickian but both diffusion and polymer relaxation control the overall rate of water uptake. In the present work, diffusion constant values ( $n$ ) of 0.42, 0.34 and 0.43 were calculated from the slope of the plot of  $\log(M_t/M_\infty)$  versus  $\log t$  for swelling cycles 1, 2 and 3, respectively. Interestingly, and at the exception of the second cycle, the water uptake rates of each swelling measurements fit well and tends to indicate a Fickian diffusion ( $n \leq 0.5$ ) of water within the hydrogel. Even if this value is not strictly 0.5, it is important to point out here that we have an amphiphilic network

composed of polymers chains with opposite affinity for water, explaining probably the 20% difference between experimental and theoretical values.

The amphiphilic nature of the resulting conetwork was examined by swelling studies in toluene. As illustrated by **Figure 2** the studied gel is able to swell one order of magnitude more in toluene than in water. Such observation is likely explained by the high affinity of both PCL and PDMAEMA segments for toluene. Interestingly enough, the recorded swelling curve indicates again a Fickian-type diffusion ( $n \sim 0.5$ ) as in the case of aqueous swelling experiments. The effect of the cross-linking density over the swelling behaviour was evaluated by varying the relative content of PCLDMA cross-linkers in the conetwork from 2 to 4 mol% and the associate effect on the hydrogel swelling was investigated in Millipore<sup>®</sup> water at r.t.

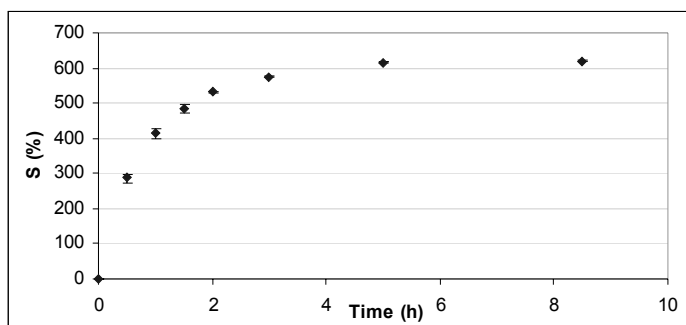
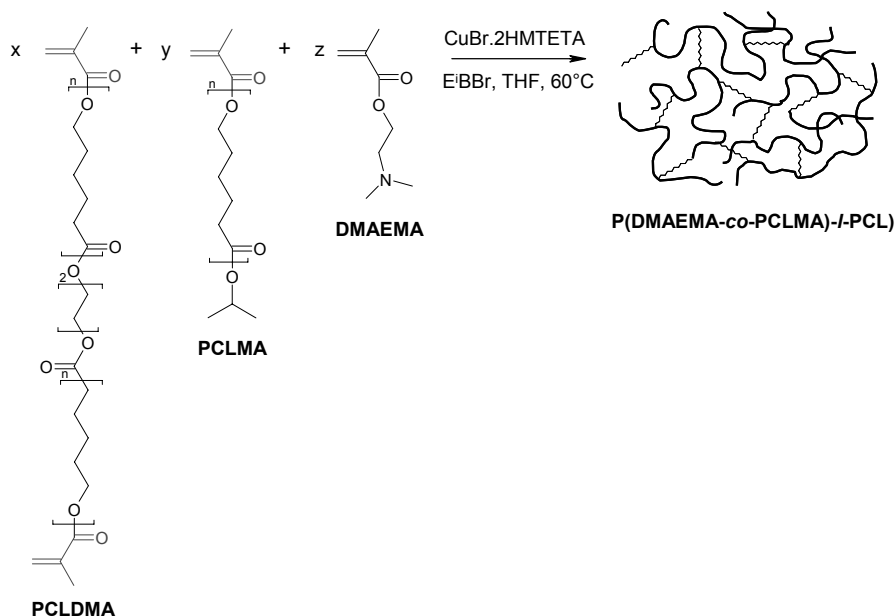


*Figure 2 : Swelling behavior of a representative PDMAEMA-l-PCL polymer conetwork (Entry 1, Table 1) in toluene at r.t.*

In order to maintain the PCL composition constant in the APCNs and therefore the hydrophilic-lipophilic balance (HLB) unchanged for the swelling studies while changing the PCLDMA cross-linking ratio, some polymer conetworks were produced by ATRP copolymerization of DMAEMA with  $\alpha,\omega$ -dimethacrylate poly( $\epsilon$ -caprolactone) (PCLDMA) cross-linker and  $\omega$ -methacrylate poly( $\epsilon$ -caprolactone) (PCLMA) macromonomer and adequate modulation of the initial  $[\text{PCLDMA}]_0/[\text{PCLMA}]_0$  ratio as depicted in **Scheme 2**. Practically, the copolymerizations have been initiated by 2-ethyl bromoisobutyrate (E<sup>i</sup>BBr) in THF at 60°C using CuBr<sub>2</sub>.2HMTETA as catalytic complex for an initial  $[\text{PCLDMA}+\text{PCLMA}+\text{DMAEMA}]_0/[\text{E}^i\text{BBr}]_0/[\text{CuBr}]_0/[\text{HMTETA}]_0$  molar ratio of 100/1/1/2 and an initial comonomer concentration of 4.8 mol.L<sup>-1</sup>. The PCLMA and the PCLDMA employed are characterized by an identical molecular weight of 1700 g.mol<sup>-1</sup> and polydispersity indices of 1.20 and 1.07, respectively.

**Table I** (entries 2-4) presents molar and weight compositions as well as the gel fraction ( $F_G$ ) of the polymer conetworks as recovered after 24h of reaction. Note also that  $F_G$  was determined from the following relationship:  $F_G = w_g / w_p$  (after extraction of the remaining soluble fraction) where  $w_g$  and  $w_p$  represent the weight of the final insoluble part and the initial weight of all introduced

comonomers, respectively. The swelling studies were performed in Millipore® water at r.t. in triplicate for each polymer conetwork and standard deviations were calculated (**Figure 3**). As expected, increasing the cross-linking degree of the conetwork lowers the swelling degree reached at equilibrium ( $S_{eq}$ ).



*Scheme 2: Synthesis of P(DMAEMA-co-PCLMA)-I-PCL conetworks with different degrees of cross-linking and constant PCL content by ATRP copolymerization between DMAEMA, PCLDMA cross-linker and PCLMA macromonomer.*

Indeed, according to the theory of Flory and Rehner (34), the swelling degree of polymer networks is governed by the thermodynamic compatibility of a polymer network with the solvent molecules and the elastic retractile forces of the polymer chains. The higher the degree of cross-linking in a hydrogel, the stronger associate elastic retractile forces will be, thus countering more effectively the thermodynamic swelling force.

Interestingly, it is predicted that the hydrogel swelling is inversely proportional to the degree of cross-linking in the network (34). Accordingly, the degree of swelling at equilibrium could be plotted against the inverse of the cross-linking molar fraction, as displayed in **Figure 4**. As predicted, the dependence of  $S_{eq}$  plotted against the inverse of cross-link molar fraction was found to be linear (with a linear regression coefficient ( $R^2$ ) > 0.99). It is worth pointing out that even if the number of gel samples was only limited to 3, the linear dependence between  $S_{eq}$  and the inverse of the cross-link molar fraction passes through the origin demonstrating the viability of such study. In accordance with Flory's theory, this linear dependence supports that the hydrogel swelling ability results from the balance between gel elasticity, which

is a function of the degree of cross-linking, and the thermodynamic compatibility existing between the polymer chains and solvent molecules.

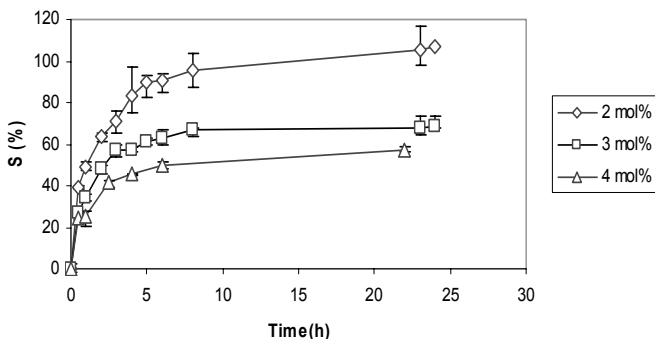


Figure 3: Swelling behavior of *P(DMAEMA-co-PCLMA)-l-PCL* polymer conetworks in Millipore® water at r.t. in function of the cross-linking degree:  $\diamond$ ) 2 mol%,  $\square$ ) 3 mol% and  $\triangle$ ) 4 mol% in dimacromonomer (see Table I, entries 2-4).

Moreover, such a linear relationship tends to demonstrate that the actual cross-linking degree of the APCNs is only dependent on the initial molar fraction in PCLDMA crosslinkers introduced in the polymerization medium and therefore attests for the absence of additional (physical) cross-links that could be due to polymer chain entanglements. Therefore and owing to the control over the molecular parameters of the APCNs, a correlation between gel structure and swelling behavior could be predicted from the Flory-Rehner relationship in the particular case of this study with a constant composition in PCL of about 30%.

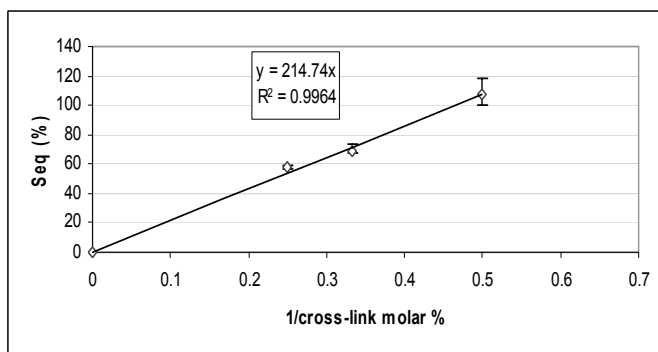
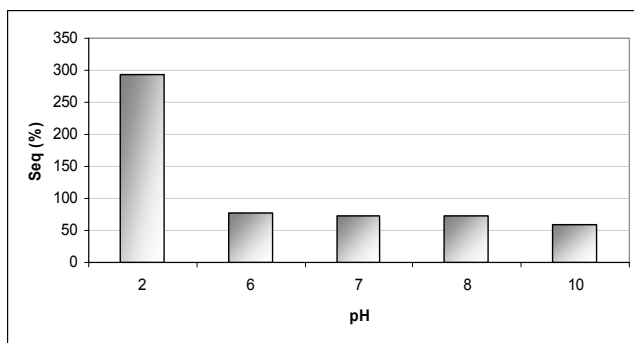


Figure 4: Inversely proportional dependence of the swelling degree at equilibrium in water with the cross-link molar fraction.

As already described in the literature, PDMAEMA polymer chains are pH-sensitive due to the presence of pendant tertiary amino functions characterized by a  $pK_a$  value of  $7.0 \pm 0.5$ . (35) PDMAEMA homopolymers are soluble in aqueous media at low pH as a weak cationic polyelectrolyte resulting from the protonation of the tertiary amine groups. At pH higher than 8, PDMAEMA homopolymer has a very low or zero charge density, and hydrogen bonding is the only responsible for its water solubility. As a result, PDMAEMA is characterized by a Lower Critical Solubility Temperature (LCST) above  $50^\circ\text{C}$  in basic aqueous solution (36). Owing to such remarkable physicochemical properties, the influence of external environmental conditions have been evaluated on PDMAEMA-*l*-PCL conetworks in aqueous conditions. A representative PDMAEMA-*l*-PCL conetwork as produced by ATRP (Entry 1, Table 1) has been swollen in aqueous solutions at different pH values ranging from 2 to 10. Aqueous solutions with low pH values were obtained by using HCl aqueous solutions of various concentrations while basic medium was obtained by using NaOH. In order to mitigate the confounding effect of osmotic pressure on pH, the swelling studies have been performed at a fixed ionic strength (IS :  $0.01 \text{ mol.L}^{-1}$ ) by adding NaCl salt. All swelling studies were performed at room temperature in triplicate. As illustrated by **Figure 5**, increasing the pH from 2 to 6 dramatically decreases the swelling degree reached at the equilibrium. Indeed, increasing the pH of the solution drastically reduces down the concentration of ionized groups in the polymer network. Hence the resulting electrostatic repulsion decreases, thereby reducing the swelling ability and the water uptake. It was also observed that in both basic and neutral conditions, the equilibrium was reached within 4 hours of swelling, although it took more than 24h in acidic conditions to reach the “equilibrium plateau” (**Figure 6**). Clearly it comes out that the swelling process and therefore the related water transport within the gel are affected by the pH.



*Figure 5: pH dependence of the swelling degree at equilibrium for a representative PDMAEMA-*l*-PCL conetwork (Entry 1, Table I).*

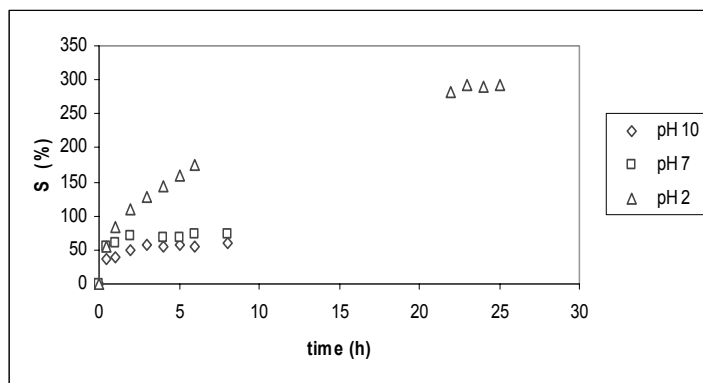


Figure 6: Swelling behavior of a representative PDMAEMA-I-PCL conetwork (Entry 1, Table I) at pH 2 ( $\Delta$ ), 7 ( $\square$ ) and 10 ( $\diamond$ ).

Temperature-sensitivity of PDMAEMA-I-PCL amphiphilic polymer conetworks (APCNs) has been also evidenced by measuring their swelling degree reached at equilibrium in Millipore<sup>®</sup> water at different temperatures ranging from 20 to 60°C. Practically a PDMAEMA-I-PCL conetwork (Entry 1, Table I) has been immersed in water at the desired temperature, removed from water and blotted with a tissue paper to remove the excess of water on the surface. The polymer sample was repeatedly weighed and re-immersed in water at a fixed temperature until the equilibrium of swelling was reached. As seen in **Figure 7**, increasing the temperature triggers a decrease of  $S_{eq}$ , reflecting the thermosensitivity of the PDMAEMA-based APCN. Upon increasing the temperature PDMAEMA polymer chains start to dehydrate and become less and less hydrophilic. As a result, coil-to-globule transition occurs involving a collapse of individual polymer chains and the expulsion of water out of the network. Besides the relationship between polymer chains and water molecules, the shrinkage of the polymer network can be explained by the appearance of intra- and intermolecular interactions. In the specific case of PDMAEMA, this intra- and intermolecular forces arise from hydrophobic interactions. From the sigmoid curve in the **Figure 7**, the volume phase transition of the PDMAEMA-I-PCL conetwork (Entry 1, Table I) was observed around 35°C. It was already reported (36) that with the formation of network, the LCST of cross-linked PDMAEMA chains was shifted from 50 down to 40°C, which is in quite good accordance with the measured value for our APCN sample (ca. 35°C). Moreover, it is well-known that by incorporating hydrophilic monomers, the LCST value tends to increase while an incorporation of hydrophobic monomers shifts the LCST value towards lower temperature. In the present study, this effect is not so significant regarding the relatively high amount of hydrophobic caprolactone subunits present in the conetwork ( $f_{CL} = 43.4 \pm 0.12\%$ ).

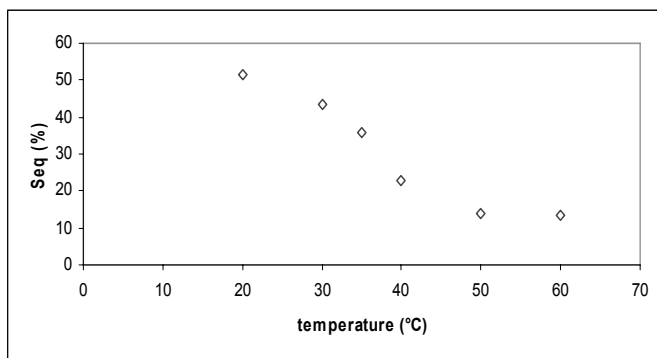


Figure 7: Temperature dependence of the swelling degree at equilibrium as recorded in water for a representative conetwork (Entry I, Table 1).

This unusual observation can be explained by the segmented nature of the polymer conetwork itself, which, in opposition to copolymer network usually built up on a rather statistical comonomer distribution, presents a lower alteration of intrinsic physicochemical properties of the PDMAEMA segments. Thermo-reversibility of hydrogels certainly represents another key feature for some applications such as sensors (37), thermo-responsive membranes (38-40) and drug delivery systems (41-43). Therefore, the reversibility of swelling-deswelling behavior has been investigated as a function of time in Millipore<sup>®</sup> water by varying the temperature below (20°C) and above (60°C) the LCST (thus recorded at ca. 35°C). Practically, hydrogels were successively immersed in water at 20°C or 60°C for 48h in order to reach the equilibrium and weighed before changing the temperature of the bath. **Figure 8** highlights the swelling-deswelling reversibility of the amphiphilic and adaptative PDMAEMA-*l*-PCL conetworks.

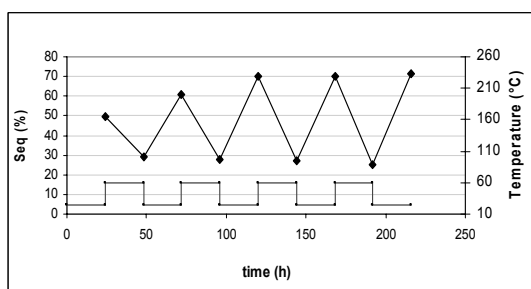


Figure 8: Reversibility of swelling-deswelling behavior as a function of time by varying the temperature between 20 and 60°C in Millipore<sup>®</sup> water at r.t. [PDMAEMA-*l*-PCL conetwork sample from Table I, Entry 1]



## Determination of the state of water molecules in PDMAEMA-*l*-PCL conetworks

Since polymer hydrogels comprise a significant proportion of water, the interaction of water molecules with the polymer network is important in determining properties of the swollen gel. The water content within a hydrogel swollen at the equilibrium is considered to contribute to the biocompatibility and low thrombogenicity of these materials (44). Additionally, water plays an important role in the function of a polymer biomaterial, for example, in facilitating the interaction of the polymer with blood (45) and in supporting the transport of pharmaceutical agents through the polymer matrix (46). While the presence of water is an important factor contributing to the biocompatibility of a hydrogel, the organization of water molecules within the hydrogel may provide a better understanding of the interactions that occur between the hydrogel and the biological system. A three-state model for water was first proposed by Jhon and Andrade (46) based on the observation of structured water near the water/solid interfaces in natural macromolecular gels. They suggested that water can behave dynamically and thermodynamically as part of the polymer chains when the water molecules interact strongly with such specific sites as the hydroxyl, amine or ester groups, and they classified this type of water as “bound” water. As the polar groups are hydrated, the network exposes the hydrophobic parts, which can interact with water. The water is preferentially structured around the polymer network leading to weak interactions, and the formation of “intermediate” water. Once ionic, polar and hydrophobic groups have interacted with water, the water fills the space between polymer chains that lead to the third classification of water: “free” or “bulk-like” water where the amount of interaction between water and polymer chains is insignificant. In the present work, the properties of the imbibed water were studied using Differential Scanning Calorimetry (DSC). Practically, 3 slabs of a representative PDMAEMA-*l*-PCL conetwork (Entry 1, Table I) were immersed in Millipore® water and allowed to swell until reaching different swelling levels, i.e., 32.3, 37.9 and 73.8%. The swollen polymer samples were introduced in aluminum pans, which were properly sealed. A ramp of 1°C/min increasing temperature rate was applied from -35°C to 10°C and the measurements were performed under nitrogen atmosphere.

**Figure 9** presents the thermograms of the samples swollen at (a) 0%, (b) 32.3 %, (c) 37.9 % and (d) 73.8 %. It was first observed that the total melting enthalpy was lower than that of pure water, suggesting significant polymer-water interactions and/or incomplete freezing of the imbibed water molecules. Actually this “non freezable” water is nothing but the aforementioned “bound” water. Secondly and as depicted by **Figure 9**, the shape of the melting curves exhibited two different peaks around 273 K for the swollen sample containing 32.3% water.

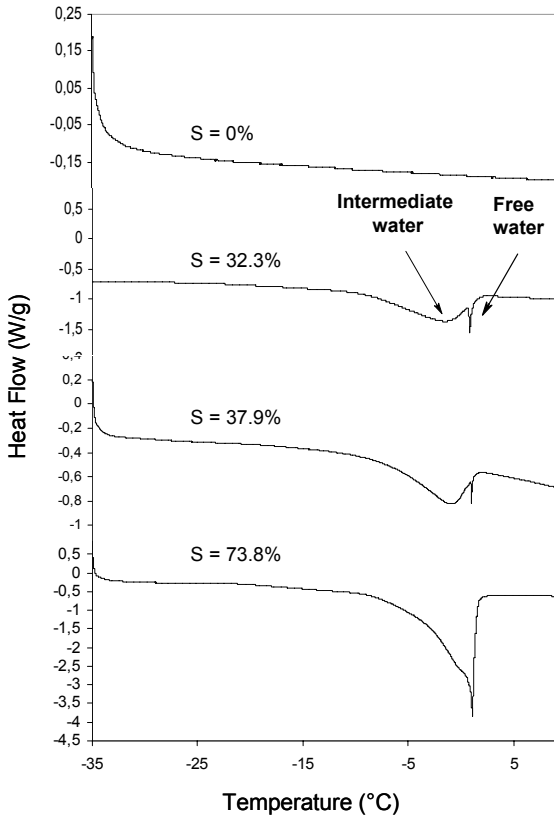


Figure 9: DSC melting endotherms of water for a representative PDMAEMA-*l*-PCL polymer network (Entry 1, Table I) swollen in Millipore® water and reaching a swelling degree (*S*) of 0, 32.3, 37.9 and 73.8%.

The water fraction that melts near 273 K was interpreted as “free” water, while the fraction with a slightly lower melting point was termed “intermediate” water. The amounts of bound, intermediate and “free/bulk-like” water was determined from the DSC thermogram (Table II) by using the following relationship :

$$F_{\text{bw}} (\%) = \frac{W_s}{W_{\text{H}_2\text{O}}} \times \frac{\Delta H_m}{\Delta H}$$

with  $W_s$  and  $W_{\text{H}_2\text{O}}$ , the weight of the swollen gel and imbibed water,  $\Delta H_m$  the latent heat of water ( $\Delta H_m = 334.52$  J/g) and  $\Delta H$  the melting enthalpy of water. This study revealed an increase in “bulk-like” water only after the bound and intermediate waters are saturated as clearly demonstrated by **Figure 10**.

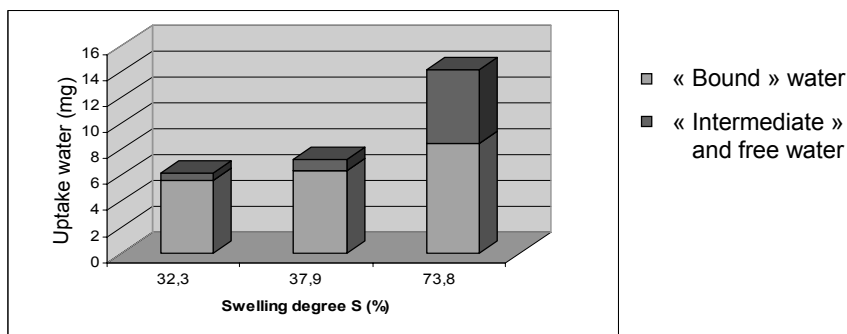


Figure 10: Relative proportion of “bound” and freezable (“intermediate” + free) water in a representative PDMAEMA-*l*-PCL (Entry 1, Table 1) as recorded at three different swelling degrees

**Table II. Fraction of “non freezable” (bound) water and “freezable” (intermediate + bulk-like) water in PDMAEMA-*l*-PCL conetwork (from Entry 1, Table 1) at three different swelling degrees.**

$S(\%)^a$	$\Delta H^b$ (j/g)	$F_{bw}^c$ (%)	$M_{bw}^d$ (mg)	$M_{(int+bulk)w}^e$ (mg)
32.3	7.13	91.3	5.66	0.54
37.9	11.29	87.7	6.38	0.90
73.8	55.37	59.6	8.45	5.73

<sup>a</sup> Swelling degree S(%) of hydrogel in Millipore<sup>®</sup> water at r.t. as determined from the following relationship:  $S(\%) = (m_w - m_d)/m_d$ ; with  $m_w$  and  $m_d$  the mass of the wet and dry gel, respectively.

<sup>b</sup> Melting enthalpy of water as obtained by DSC using a ramp of 1°C/min increasing temperature rate.

<sup>c</sup> Content in “bound” water in the gel as determined by the following relationship :

$$F_{bw} (\%) = \frac{W_s}{W_{H_2O}} \times \frac{\Delta H_m}{\Delta H}$$

with  $W_s$  and  $W_{H_2O}$ , the weight of the swollen gel and imbibed water,  $\Delta H_m$  the Latent heat of water ( $\Delta H_m = 334.52$  J/g) and  $\Delta H$  the melting enthalpy of water.

<sup>d</sup> Weight of “bound” water as determined by using the following relation :  $M_{bw} = F_{bw} \times W_{H_2O}$

<sup>e</sup> Weight of intermediate and “bulk-like” water as determined by using the following relation :  $M_{(int+bulk)w} = (1 - F_{bw}) \times W_{H_2O}$

Therefore and as previously developed by Sung *et al.* (47) and reported by other authors, a three-step imbibition process can be postulated. The hydrophilic sites within the PDMAEMA-*l*-PCL conetworks first attract and bind an amount of water, followed by the formation of a secondary hydration shell of water that is preferentially oriented around the bound water and the polymer network structure. Further absorbed water exists as “free” or “bulk-like” water.

### Evaluation of mechanical properties of PDMAEMA-*l*-PCL conetworks

Though hydrogels mechanical properties can be tuned on the basis of different chemistries, cross-linking density and water content, their mechanical strength are most of the time very low, limiting the practical application of hydrogels. However, many efforts to improved mechanical strength and ultimate strain have been achieved by focusing on copolymerization, alteration of cross-linking density, presence of crystalline domains, tuning of water content, etc. (46) Within the frame of this work, the strategy was to incorporate hydrophobic poly( $\epsilon$ -caprolactone) as cross-linker in the hydrogel architecture in order to level the water content and reinforce the mechanical strength. Major mechanical properties like tensile strength (TS), elongation at break (EB) and modulus (after 10% elongation) have been evaluated directly on swollen PDMAEMA-*l*-PCL conetworks by tensile testing measurements. Measurements were performed on rod-like networks specimen at r.t. with cross-head speed of 1 mm/min. Average values and the accompanied standard deviations were calculated, respectively, by measuring 3 samples per hydrogel.

In a first series of experiments, the positive impact of the incorporation of PCL segments on the mechanical properties of the PDMAEMA-*l*-PCL conetworks have been highlighted by comparing the resulting true strain-strain curve with that displayed by a PDMAEMA homopolymer network ( $[\text{DMAEMA}]_0/[\text{I}]_0 = 100$ ,  $F_{\text{N}_{\text{EGDMA}}} = 3\%$ ,  $F_{\text{G}} = 95.4\%$ ), both produced by ATRP in the same conditions. The PCLDMA cross-linker employed for this study was characterized by an average molecular weight of  $4300 \text{ g}\cdot\text{mol}^{-1}$  and a  $M_w/M_n$  of 1.2 (see Table I, entry 5).

Practically, tensile samples were allowed to swell in Millipore<sup>®</sup> water for 24h in order to reach the equilibrium prior mechanical testing. In such conditions, only strain due to mechanical deformation, and not to swelling process, was measured. **Figure 11** presents typical true stress-strain curves. It comes out that the introduction of PCL segments enhances the overall mechanical properties in comparison to the PDMAEMA hydrogel.

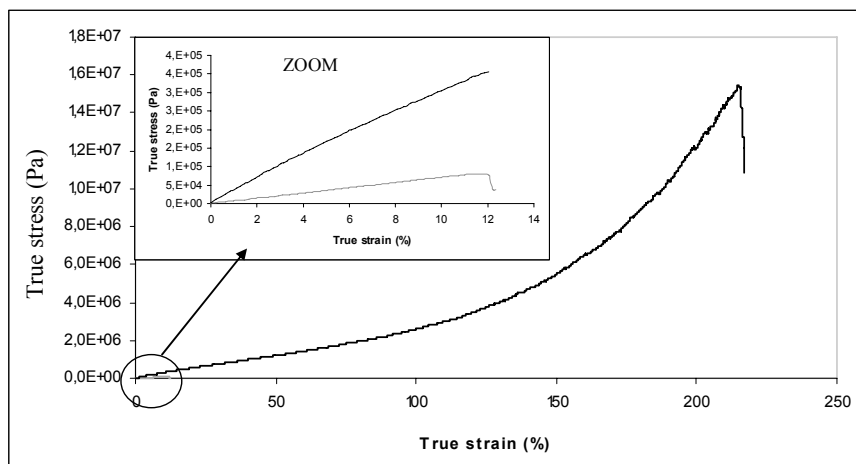


Figure 11: True stress-strain curves recorded by tensile testing for swollen PDMAEMA ( $S = 95.4\%$ , grey line) and PDMAEMA-*l*-PCL ( $S = 35.4\%$ , black line) hydrogels at r.t.

Indeed, the Young modulus, calculated from the slope of the curve within the region of 10% strain, increases from  $0.69 \pm 0.09$  to  $2.72 \pm 0.12$  MPa, confirming the formation of a stiffer material. This is further confirmed by an increase of the ultimate strength at break from 0.36 to 15.4 MPa. By the presence of the hydrophobic segments, the water content in the hydrogel decreases (from 180% in PDMAEMA hydrogel to 50% in PDMAEMA-*l*-PCL conetwork), enhancing stiffness but also strengthening polymer-polymer interactions and hydrophobic bonding within hydrogel. As a consequence, Young Modulus, tensile strength as well as energy to break increase significantly. Surprisingly, elongation at break was found to be extremely higher for the swollen PDMAEMA-*l*-PCL conetwork. Such an effect might be explained by the inability of PCL segment to crystallize in the polymer network (as attested for by DSC, not shown here) jointly to a low glass transition of PCL polymer chains ( $T_{gPCL} \sim -60^\circ\text{C}$ ). Therefore, PCL chains remain in a rubbery state with high possibility for molecular motion. It worth mentioning that these observations are consistent with the trends recently reported by Jones *et al.* for poly(hydroxyethyl methacrylate) (PHEMA) hydrogels when interpenetrated with PCL segments (48).

Young modulus, ultimate strength and percent elongation at break have been also determined experimentally for PDMAEMA-*l*-PCL conetworks with different contents in cross-linker ranging from 2 to 4 mol% but with a constant PCL weight fraction fixed at 31.1% (see **Table I, entries 2-4**). As a reminder, these APCNs were synthesized by ATRP copolymerization of DMAEMA with the suited amount of PCLDMA cross-linker ( $M_n = 1700 \text{ g}\cdot\text{mol}^{-1}$ ,  $M_w/M_n = 1.2$ ) and PCLMA macromonomer ( $M_n = 1700 \text{ g}\cdot\text{mol}^{-1}$ ,  $M_w/M_n = 1.07$ ) as illustrated by **Scheme 2**. As expected, an increase of the Young Modulus with the cross-linker content was observed (**Figure 12**).

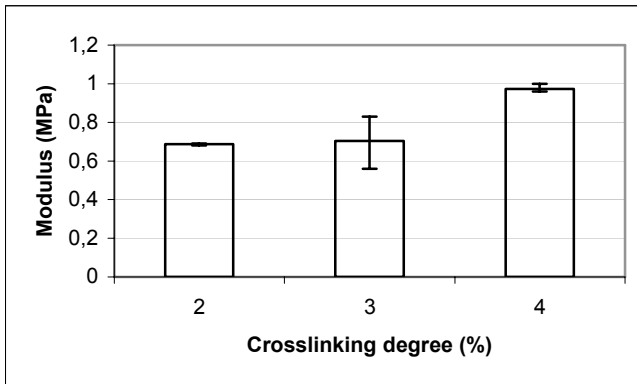


Figure 12 : Evolution of the Young modulus of PDMAEMA-*l*-PCL conetworks (Table I, Entries 2-4) with increasing cross-linker concentration from 2 to 4% (at constant hydrophobic PCL content : 31.1 wt%).

In a recent study, Jones *et al.* have demonstrated that the improvement of mechanical properties by interpenetration of PCL segments into a PHEMA network was also dependent on the molecular weight of the hydrophobic segments (48). Even if the introduction of PCL cross-linker in the gels proved efficient for largely enhancing the mechanical properties of PDMAEMA-*l*-PCL APCNs, it was also of interest to vary the length of PCL cross-linkers and to check possible effect on the Young modulus, ultimate strength and elongation at break. For this purpose, three PCLDMA cross-linkers characterized by average molecular weight of 1700, 4300 and 5800 g.mol<sup>-1</sup> were copolymerized to DMAEMA by ATRP to produce amphiphilic polymer conetworks with gel fraction ( $F_G$ ) ranging from 95 to 99 %. As shown in **Table III** and **Figure 13**, increasing the length of the PCL cross-linkers promotes some increase of the Young Modulus. The impact is more significant when passing from a PCLDMA molecular weight of 4300 to 5800 g.mol<sup>-1</sup>. In this latter case, the remarkably high stiffness value can be accounted for by the presence of crystalline PCL microdomains (in opposition to other studied polymer conetworks built on lower molecular weight PCL segments). These crystalline microdomains thus strengthen the polymer network but, since they are distributed within the amorphous PDMAEMA matrix, they also play as defects and reduce the ultimate elongation.

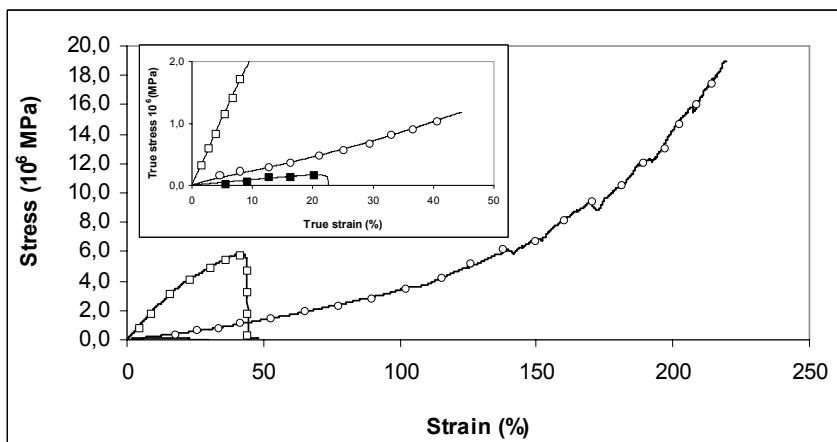


Figure 13 : True stress-strain curves recorded by tensile testing for the swollen PDMAEMA-*l*-PCL hydrogels at *r.t.* and containing PCLDMA cross-linker characterized by a  $M_n$  of 1700 (■), 4300 (○) and 5800  $g \cdot mol^{-1}$  (□).

**Table III. Molecular characteristics, gel fraction and mechanical properties of swollen PDMAEMA-*l*-PCL APCNs obtained by ATRP (with PCLDMA content of 3 mol.%).**

$M_n$ <sub>PCLDMA</sub> <sup>a</sup> ( $g \cdot mol^{-1}$ )	$f_{WPCL}$ <sup>b</sup> (%)	$F_G$ <sup>c</sup> (%)	Young Modulus <sup>d</sup> (MPa)	EB <sup>e</sup> (%)	TS <sup>e</sup> (MPa)	S <sup>f</sup> (%)
1700	25.1	95.2	$0.97 \pm 0.03$	$27.9 \pm 4.3$	$0.3 \pm 0.02$	57.5
4300	41.5	> 99	$2.72 \pm 0.12$	$257.1 \pm 3.5$	$35.0 \pm 0.94$	53.7
5800	53.3	> 99	$27.64 \pm 6.0$	$42.9 \pm 6.7$	$5.6 \pm 0.75$	21.0

<sup>a</sup> PCLDMA number-average molecular weight as determined by <sup>1</sup>H NMR spectroscopy in CDCl<sub>3</sub>

<sup>b</sup> Weight fraction of PCL in the feed

<sup>c</sup>  $F_G$  = gel fraction obtained after elimination of residual catalyst, unreacted comonomers and any non cross-linked graft copolymers (see text)

<sup>d</sup> Young modulus as determined from the slope of the true stress-strain curve (Figure 13) in the region of 10% strain

<sup>e</sup> Elongation at break (EB) and ultimate tensile strength (TS) as determined from the true stress-strain curve (Figure 13)

<sup>f</sup> Swelling degree at equilibrium

According to the aforementioned adaptative properties displayed by the PDMAEMA-*l*-PCL APCNs, the Young modulus has been also recorded as a function of the solution pH. For this purpose, specimens of a polymer conetwork (Entry 2, Table III) were allowed to swell until equilibrium in aqueous solution buffered at pH 4, 7 and 9, respectively, prior mechanical testing. It is worth mentioning that the ionic strength was maintained constant and fixed to 0.05 g.mol<sup>-1</sup>. **Figure 14** highlights the pH effect on the Young modulus values of the swollen polymer networks. The Young modulus increases from 1.33 to 4.12 MPa with increasing pH from 4 to 9. It is worth recalling that the swelling degree at equilibrium proved to be strongly pH dependent. In acidic conditions, pendant amino functions become protonated. As a consequence, the hydrogel absorbs a much larger quantity of water to lower the electrostatic repulsive forces within the polyelectrolyte conetwork, and displays a reduced stiffness. From a microstructural point of view, one would expect the stiffness of individual polymer chains to remain constant regardless of the degree of swelling. However, additional mechanic work is required to deform less swollen hydrogel where frictional and electrostatic effects are more pronounced.

Previous studies by some of us (33) have demonstrated the strong impact of the polymerization technique on the molecular parameters and the structure of the final polymer conetworks. As a consequence, it came out that uncontrolled free radical polymerization (FRP) reduced the swelling behavior of the network by a factor of 2 with respect to the value recorded for well tailored conetworks synthesized by ATRP. This difference was explained by the inhomogeneity of the resulting “uncontrolled” APCNs, i.e. presence of microclusters throughout the network structure as well as physical chain entanglements, which can contribute to additional cross-linking points. On this basis, it has been decided to check the influence of the polymerization mechanism (ATRP *vs.* FRP) on the mechanical properties of the resulting gels. For this purpose, two PDMAEMA-*l*-PCL APCNs, similar in terms of composition and cross-linking degree, were produced either by ATRP or by FRP. A PCLDMA cross-linker characterized by an average molecular weight of 1700 g.mol<sup>-1</sup> was employed for an initial molar fraction of 3%. Both copolymerization were conducted in THF at 60°C and initiated by 2-ethyl bromoisobutyrate and azobisisobutyronitrile (AIBN) for ATRP and FRP processes, respectively. The initial comonomer-to-initiator molar ratio was fixed to 100 and the initial [PCLDMA+DMAEMA]<sub>0</sub> to 4.8 mol.L<sup>-1</sup> (**Table IV**).



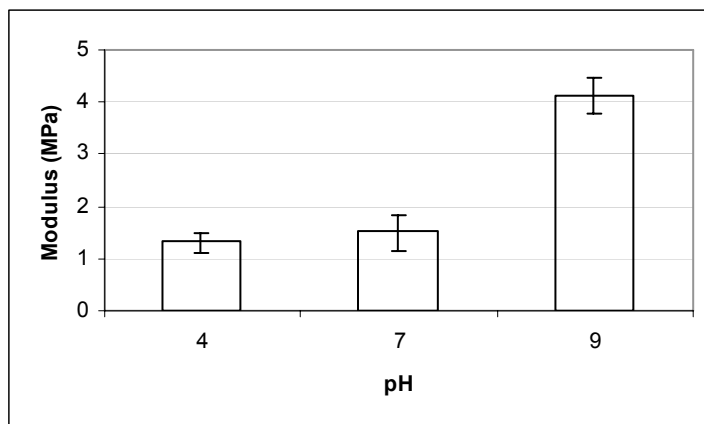


Figure 14 : Effect of pH on the Young modulus for a swollen representative PDMAEMA-*l*-PCL conetwork (Entry 2, Table 3) at r.t.

**Table IV. Gel fraction and mechanical properties of PDMAEMA-*l*-PCL APCNs obtained by ATRP or FRP in THF at 60°C using a PCLDMA cross-linker of 1700 g.mol<sup>-1</sup> (initial molar fraction : 3%).**

Sample	Mechanism	$F_G^a$ (%)	Young Modulus <sup>b</sup> (MPa)	$TS^c$ (MPa)	$EB^c$ (%)
1	ATRP	92.3	1.72 ± 0.49	0.37 ± 0.16	28.1 ± 7.64
2	FRP	99.5	3.49 ± 0.03	0.46 ± 0.13	14.7 ± 3.35

<sup>a</sup>  $F_G$  = gel fraction obtained after elimination of residual catalyst, unreacted comonomers and any non cross-linked graft copolymers (see text)

<sup>b</sup> Young modulus as determined from the slope of the true stress-strain curve (Figure 15) in the region of 10% strain

<sup>c</sup> Ultimate tensile strength and elongation at break as determined from the true stress-true strain curve (Figure 15)

**Figure 15** clearly shows the strong impact of the polymerization mechanism and the related control over the molecular parameters on the mechanical properties of the swollen conetworks. The hydrogel produced by FRP appears much stiffer as demonstrated by an increase of the Young modulus from 1.72 ± 0.49 (for the ATRP-synthesized APCN) to 3.49 ± 0.03 MPa (FRP-produced conetwork). Again, this higher stiffness might be related to a more densely cross-linked gel (physical entanglements and cluster inhomogeneity) characteristic of APCNs produced by FRP.

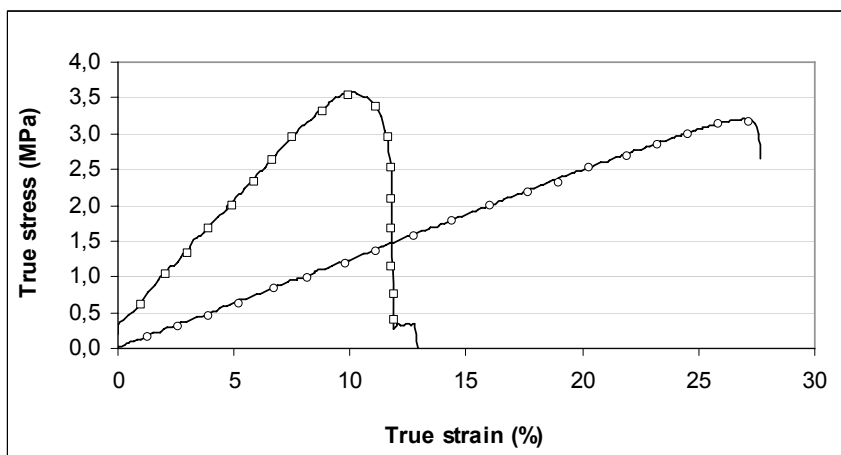


Figure 15 : True stress-strain curves recorded by tensile testing at r.t. on swollen PDMAEMA-*l*-PCL hydrogels as produced by ATRP (○) and FRP (□) (Table IV).

### Degradability study of PDMAEMA-*l*-PCL polymer conetworks

While hydrogels have amply demonstrated their potential in the biomedical field as biocompatible drug release systems or polymer scaffolds for tissue engineering, practical applications remain still limited. One of the most important reason is their non or low (bio)degradability, involving the removal of materials after use. Incorporation of biodegradable segments and/or cross-linkers could represent some interest for time-limited application materials. In the frame of this work, the degradable character of a representative PDMAEMA-*l*-PCL APCN (Entry 1, Table I) has been investigated in simulated body fluid (SBF, pH = 7.4,  $[Cl^-] = 147 \text{ mM}$ ,  $[HCO_3^-] = 4.2 \text{ mM}$ , (49)) at 37°C by measuring the evolution of the swelling degree at equilibrium as a function of time. For sake of comparison, the stability of a PDMAEMA homopolymer network similarly produced by ATRP was analyzed rigorously in the same conditions. The PDMAEMA homopolymer network was obtained by ATRP in THF at 60°C using 3 mol % of ethyleneglycol dimethacrylate (EGDMA) as cross-linker. The initial  $[DMAEMA+EGDMA]_0/[E^1BBr]_0/[CuBr]_0/[HMTETA]_0$  molar fraction was fixed to 100/1/1/2 and the comonomer concentration  $[DMAEMA+EGDMA]_0$  to  $4.8 \text{ mol.L}^{-1}$ . After 24h of copolymerization, and 48h of purification by immersion in a solvent mixture of Millipore® water/THF (1/1 by volume), a hydrogel characterized by a gel fraction of 95.4% was obtained. **Figure 16** presents the evolution of the swelling degree of the investigated PDMAEMA-*l*-PCL conetwork in SBF at 37°C as a function of degradation time.

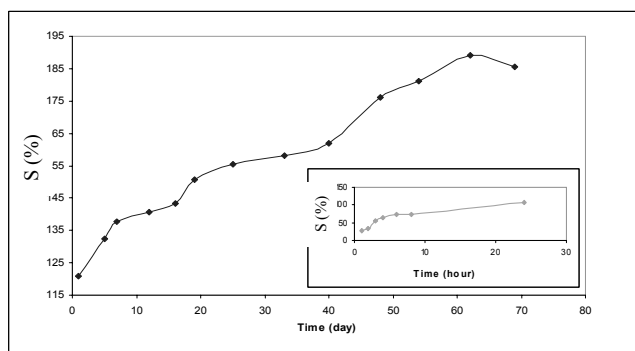


Figure 16 : Evolution of the swelling degree of a representative PDMAEMA-l-PCL conetwork in SBF at 37°C (inset : evolution over the first two days).

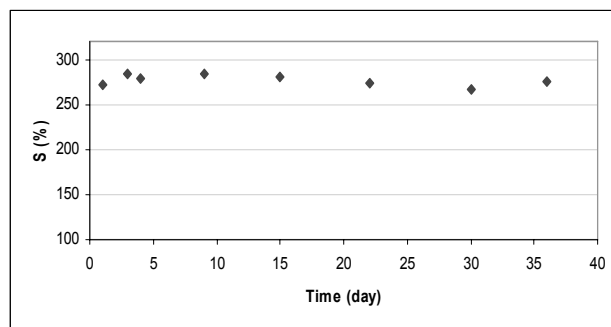


Figure 17 : Evolution of the swelling degree at equilibrium of a PDMAEMA homopolymer network (3% EGDMA,  $F_G = 95.4\%$ ) in SBF at 37°C.

Clearly, even though the swelling degree of the gel was kept almost constant over the first day (see inset, Figure 16), it then increased monotonously to reach about 190% after 60 days. Beyond two months in SBF, the gel started to disintegrate, with the impossibility to pursue the study. Therefore, the increase of the swelling ability has been attributed to the selective hydrolysis of ester bonds in the PCL cross-linkers. This was further confirmed by studying the evolution of the swelling degree at equilibrium for a PDMAEMA homopolymer network in the same medium at 37°C, and for which no increase of  $S_{eq}$  was observed over a period of time as long as 40 days (**Figure 17**). It can be concluded that incorporation of polyester cross-linker in the polymethacrylate network leads to the formation of degradable materials in near physiological conditions, likely making them suitable for tissue engineering applications as polymer scaffolds or drug release devices.

## Conclusions

The controlled radical copolymerization of PCL-based bismacromonomer (PCLDMA) with DMAEMA leads to the formation of amphiphilic gels able to swell both in water and in organic solvent like toluene. Moreover, the swelling behavior is perfectly reproducible demonstrating the high stability of these conetworks in Millipore® water at r.t. As expected, an increase of cross-linker density lowers the swelling degree reached at equilibrium. Interestingly enough,  $S_{eq}$  is inversely proportional to the cross-linker concentration supporting, according to Flory's theory, that gel swelling is only dependent on PCLDMA cross-linker introduced in the polymerization medium and underlines the absence of additional cross-links, e.g., via polymer chain entanglements.

PDMAEMA-*l*-PCL conetworks show a pH and thermal dependence with a LCST value of ca. 35°C. Differential scanning calorimetry demonstrates clearly the organization of water within the gel upon the swelling process with the formation of "bound" water at the early stage of swelling.

Interestingly, these hydrogels present a degradable character in SBF at 37°C increasing their interest, e.g., as scaffolds for tissue engineering. Moreover, the introduction of hydrophobic and hydrolyzable PCL segments in the network improves strongly the mechanical properties of the swollen conetworks in terms of stiffness, ultimate strength and elongation at break. The impact of the ATRP-polymerization mechanism has been also clearly highlighted, affording materials of mechanical performances by avoiding the formation of inhomogeneities throughout the conetwork structure as usually encountered with uncontrolled polymerization technique (FRP).

## Acknowledgments

CIRMAP is very grateful to "Région Wallonne" and European Union (FEDER, FSE) for general financial support in the frame of Objectif 1-Hainaut: Materia Nova, as well as to the Belgian Federal Government Office of Science Policy (SSTC-PAI 6/27). J-M.R. is *post-doctoral researcher* of the Belgian F.R.S.-F.N.R.S (*Fonds National de la Recherche Scientifique*).

## References

1. *Annals of Biomedical Engineering*; Hanson, S.R., Harker, L.A., Patner, B.D., Hoffman, A.S., Springer Netherlands, Vol 7, Number 3-4, May 1979
2. Wichterle, O.; Lim, D. *Nature*, **1960**, *185*, 117
3. Murthy, N.; Thng, Y.X.; Schuck, S.; Xu, M.C.; Fréchet, J.M.J. *J. Am. Chem. Soc.*, **2002**, *124*, 12398
4. Lutolf, M.; Pratt, A.B.; Vernon, B.; Elbert, D.L.; Tirelli, N.; Hubbell, J.A. *Trans. Soc. Biomater.*, **2000**, 651
5. Jeong, B.; Gutowska, A. *Trends Biotechnol.*, **2002**, *20*, 305

6. Kikuchi, A.; Okano, T. *Prog. Polym. Sci.*, **2002**, *27*, 1165
7. Iván, B.; Haraszti, M.; Erdödi, G.; Scherble, J.; Thomann, R.; Mülhaupt, R. *Macromol. Symp.*, **2005**, *227*, 265
8. Haraszti, M.; Tóth, E.; Iván, B. *Chem. Mater.*, **2006**, *18*, 4952
9. Iván, B.; Feldthusen, J.; Müller, A. H. E. *Macromol. Symp.*, **1996**, *102*, 81
10. Chang, D.P.; Dolbow, J.E.; Zauscher, S. *Langmuir*, **2007**, *23*, 250
11. Wang, C.; Yu, B.; Knudsen, B.; Harmon, J.; Moussy, F.; Moussy, Y. *Biomacromolecules*, **2008**, *9*, 561
12. Moschou, E.A.; Peteu, S.F.; Bachas, L.G.; Madou, M.J.; Daunert, S. *Chem. Mater.*, **2004**, *16*, 2499
13. *Biorelated Polymers and Gels: Controlled Release and Applications in Biomedical Engineering*; Okano T., Ed., Academic Press, Boston, 1998
14. Zhu, S.; Hamilec, A.E. *Macromolecules*, **1992**, *25*, 5457
15. Zhu, S.; Hamilec, A.E. *Macromolecules*, **1993**, *26*, 3131
16. Zhu, S. *Macromolecules*, **1996**, *29*, 456
17. Flory, P.J. *J. Am. Chem. Soc.*, **1941**, *63*, 3083
18. P.J. Flory, *J. Am. Chem. Soc.* **1941**, *63*, 3091
19. P.J. Flory, *J. Am. Chem. Soc.* **1941**, *63*, 3096
20. W.H. Stockmayer, *J. Chem. Phys.* **1943**, *11*, 45
21. W.H. Stockmayer, *J. Chem. Phys.* **1944**, *12*, 125
22. Ide, N; Fukuda, T. *Macromolecules*, **1999**, *32*, 95
23. Crescenzi, V.; Dentini, M.; Bontempo, D.; Masci, G. *Macromol. Chem. Phys.*, **2002**, *203*, 1285
24. Liu, Q; Zhang, P.; Lu, M. *J. Polym. Sci.: Part A, Polym. Chem.*, **2005**, *43*, 2615
25. Liu, Q.; Zhang, P.; Qing, A.; Lan, Y.; Shi, J.; Lu, M. *Polymer* **2006**, *47*, 6963
26. Matyjaszewski, K; Beers, K.L.; Kern, A.; Gaynor, S.G. *J. Polym. Sci.: Part A: Polym. Chem.*, **1998**, *36*, 823
27. Asgarzadeh, F.; Ourdouillie, P.; Beyou, E.; Chaumont, P. *Macromolecules*, **1999**, *32*, 6996
28. Johnson, J.A.; Lewis, D.R.; Diaz, D.D.; Finn, M.G.; Koberstein, J.T.; Turro, N.J. *J. Am. Chem. Soc.*, **2006**, *128*, 6564
29. Mespouille, L.; Coulembier, O.; Paneva, D.; Degée, P.; Rashkov, I.; Dubois, P. *J. Polym. Sci.: Part A: Polym. Chem.* **2008**, *46*, 4997
30. Jiang, C.; Shen, Y.; Zhu, S.; Hunkeler, D. *J. Polym. Sci.: Part A: Polym. Chem.* **2001**, *39*, 3780
31. Yu, Q.; Zeng, F.; Zhu, S. *Macromolecules* **2001**, *34*, 1612
32. Vargün, E.; Usanmaz, A. *J. Polym. Sci.: Part A: Polym. Chem.* **2005**, *43*, 3957
33. Kim, K.H.; Kim, J.; Jo, W.H. *Polymer*, **2005**, *46*, 2836
34. Wang, A.R.; Zhu, S. *Polym. Eng. Sci.* **2005**, *720*
35. Oh, J.K.; Tang, C.; Gao, H.; Tsarevsky, N.V.; Matyjaszewski, K. *J. Am. Chem. Soc.*, **2006**, *128*, 5578
36. Mespouille, L.; Coulembier, O.; Paneva, D.; Degée, P.; Rashkov, I.; Dubois, P., *Chem. Eur. J.*, **2008**, *14*, 6369
37. Flory, P.J.; Rehner, J. *J. Chem. Phys.*, **1943**, *11*, 521
38. Pradny, M.; Seveik, S. *Makromol. Chem.*, **1985**, *186*, 111

39. Cho, S.H.; Jhon, M.S. ; Yuk, S.H. *Eur. Polym. J.*, **1999**, 35, 1841
40. *Controlled Release and Applications in Biomedical Engineering, In Biorelated Polymers and Gels*; Okano T., Ed., Academic Press, Boston, 1998
41. Galaev, I.Y.; Mattiasson, B. *Trends Biotechnol.*, **1999**, 17, 335
42. Jeong, B.; Bae, Y.H.; Lee, D.S.; Kim, S.W. *Nature*, **1997**, 388, 860
43. Kurisava, M.; Terano, M.; Yui, N. *Macromol. Rapid Commun.*, **1995**, 16, 663
44. Peng, T.; Cheng, Y.L., *J. Appl. Polym. Sci.*, **1998**, 70, 2133
45. Shtanko, N.I.; Kabanov, V.Y. ; Apel, P.Y.; Yoshida, M.; Vilenskii, A.I. *J. Membrane Sci.*, **2000**, 179, 155
46. Omichi, H.; Yoshida, M.; Asano, M.; Nagaoka, N.; Kubota, H.; Katakai, R.; Spohr, R.; Reber, N.; Wolf, A.; Alder, G.M.; Ang, V., Bashford, C.L.; Pasternak, C.A. *Nucl. Instrum. Method B*, **1997**, 131, 350
47. Bruck, S.D. *J. Biomed. Mater. Res.*, **1973**, 7, 387
48. Jhon, M.S.; Andrade, J.D. *J. Biomed Mater. Res.*, **1973**, 7, 509
49. Andrade, J.D.; Lee, H.D.; Jhon, M.S.; Kim, S.W.; Hibbs, J.B.J. *Trans. Am. Soc. Artif. Intern. Organs* **1973**, 14, 1
50. Sung, Y.K.; Gregonis, D.E.; Jhon, M.S.; Andrade, J.D. *J. Appl. Polym Sci.*, **1981**, 26, 3719
51. Jones, D.S.; McLaughlin, D.W.J.; McCoy, C.P.; Gorman, S.P. *Biomaterials*, **2006**, 26, 1761
52. Kokubo, T.; Takodama, H. *Biomaterials*, **2006**, 27, 2907

## Chapter 20

# Acrylate Based Copolymers by ATRP: The Effect of Molecular Structure on Thermo-Mechanical Properties

Kaloian Koynov<sup>1</sup>, Azhar Juhari<sup>1</sup>, Tadeusz Pakula<sup>1+</sup>, and Krzysztof Matyjaszewski<sup>2</sup>

1) Max-Planck-Institute for Polymer Research, Ackermannweg 10, 55128 Mainz, Germany;

2) Department of Chemistry, Carnegie Mellon University, 4400 Fifth Avenue, Pittsburgh, Pennsylvania 15213

Acrylate copolymers with complex linear or star architectures were prepared and characterized. Precise control over the sequence distribution and overall composition of these materials was achieved by atom transfer radical polymerization. A strong correlation between the molecular structure and composition of the copolymers and their thermo-mechanical behavior was found. This provides a new way for creating advanced materials with tailored properties.

<sup>+</sup> deceased 06.07.2005

### Introduction

With the development of living anionic polymerization (1,2) and controlled/living radical polymerizations (CRPs) (3,4) the synthesis of copolymers, especially with complex architecture, has recently received

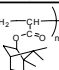
increased attention due to interests in both the academia and industry. Atom transfer radical polymerization (ATRP) (5–8) is one of the most common CRP methods and has been widely used for the synthesis of (co)polymers with predetermined degree of polymerization, narrow molecular weight distribution (9), high functionality (10) and desired microstructure (11–16). The preservation of an active chain end, most frequently a halogen group, enables synthesis of di-, tri- or multi-block copolymers with various architectures, such as stars (17–21) and brushes (22–25). The complex molecular structure has major effect on the thermo-mechanical behavior of these materials and allows tailoring of their properties.

In this contribution we show how to tune the thermo-mechanical properties of several acrylate based copolymers with complex architectures, synthesized via ATRP. First, we will discuss well-defined statistical, gradient and block copolymers consisting of isobornyl acrylate (IBA) and *n*-butyl acrylate (nBA). The thermo-mechanical properties of these materials were analyzed via differential scanning calorimetry (DSC), dynamic mechanical analyses (DMA), tensile tests and small-angle X-ray scattering (SAXS). The glass transition temperature ( $T_g$ ) of the statistical (P(IBA-co-nBA)) copolymers can be continuously tuned by changing the monomer feed. This way, it is possible to generate materials that can mimic thermal behavior of acrylate homopolymers but have significantly different mechanical properties. As a second example, the thermoplastic elastomer behaviour of tri-arm star block copolymers poly(*n*-butyl acrylate)-*b*-polyacrylonitrile (PBA-PAN) and poly(*n*-butylacrylate)-*b*-poly (methyl methacrylate) (PBA-PMMA) is presented. These materials retain phase separated morphology until very high temperature and their tensile properties can be easily tuned by adjusting the copolymers composition.

### **Linear copolymers of isobornyl acrylate and *n*-butyl acrylate**

The structure-property correlation of different copolymers with *n*-butyl acrylate and isobornyl acrylate units have been studied. The primary goal was to compare thermomechanical properties of block, gradient and statistical copolymers of nBA and IBA with various acrylate homopolymers (Scheme 1). The choice of nBA and IBA was dictated by very different thermal properties of the resulting homopolymers, glass transition temperature ( $T_g$ ) of PnBA is  $-54^\circ\text{C}$  while the  $T_g$  of PIBA is  $94^\circ\text{C}$ . Thus, their copolymerization with carefully selected ratios should result in polymers with thermal properties, i.e.,  $T_g$  similar to acrylate homopolymers: poly(*t*-butyl acrylate) (PtBA), poly(methyl acrylate) (PMA), poly(ethyl acrylate) (PEA) and poly(*n*-propyl acrylate) (PPA).



Polymer	Repeating unit	T <sub>g</sub> (°C)
n-butyl acrylate	$\left( \text{CH}_2 - \underset{\text{O}-\text{C}(=\text{O})}{\text{CH}} \right)_n$ CH <sub>2</sub> CH <sub>2</sub> CH <sub>2</sub>	-54
n-propyl acrylate	$\left( \text{CH}_2 - \underset{\text{O}-\text{C}(=\text{O})}{\text{CH}} \right)_n$ CH <sub>2</sub> CH <sub>2</sub> CH <sub>3</sub>	-40
ethyl acrylate	$\left( \text{CH}_2 - \underset{\text{O}-\text{C}(=\text{O})}{\text{CH}} \right)_n$ CH <sub>2</sub> CH <sub>3</sub>	-24
methyl acrylate	$\left( \text{CH}_2 - \underset{\text{O}-\text{C}(=\text{O})}{\text{CH}} \right)_n$ CH <sub>3</sub>	10
t-butyl acrylate	$\left( \text{CH}_2 - \underset{\text{O}-\text{C}(=\text{O})}{\text{CH}} \right)_n$ H <sub>3</sub> C-C(CH <sub>3</sub> ) <sub>2</sub>	43
isobornyl acrylate	$\left( \text{CH}_2 - \underset{\text{O}-\text{C}(=\text{O})}{\text{CH}} \right)_n$ 	94

various IBA/nBA ratio

random copolymers

block copolymers

gradient copolymers

}

compare to

PPA

PEA

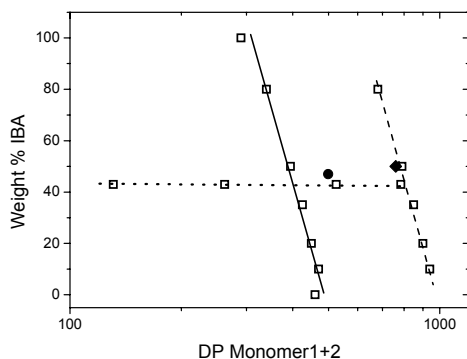
PMA

PrBA

**Scheme 1:** Copolymerization of isobornyl acrylate and n-butyl acrylate in different fashion and comparison of properties of resulting copolymers with acrylate based homopolymers such as PtBA, PMA, PEA and PPA.

Despite similar T<sub>g</sub> values, the mechanical properties of the copolymers and homopolymers can significantly differ, depending on the type of building units and their arrangement. In a similar way, one can copolymerize other monomers and affect not only physical properties of the final polymer materials, but also their degradation rates and toxicity, both of which are very important, for example, in biomedical applications.

**Statistical copolymers** of nBA and IBA with different molecular weights and compositions were synthesized under ATRP conditions, as described in detail earlier (26). In all ATRP reactions, a CuBr/PMDETA complex was used since it is commercially available and well mediates controlled polymerization of acrylate monomers. Polymerizations were performed at 50°C in acetone/anisole mixture using EtBrIB as the initiator. The schematic representation of all prepared materials is shown in Scheme 2. The solid line represents a series of polymers with similar DP but systematically increasing IBA content. Another such group of copolymers is indicated with a dashed line. Copolymers with similar IBA/nBA ratio but different degree of polymerization (DP), i.e., the dotted line, were also synthesized. When comparing the thermo-mechanical properties of acrylate homopolymers and P(IBA-co-nBA) copolymers, the first important question is whether the copolymer system is isotropic in the bulk state or rather exhibits a micro-phase separation. To answer this question, the DSC thermograms for all samples shown in Scheme 2 were measured.



**Scheme 2:** Schematic representation of prepared copolymer samples of  $P(\text{IBA-co-nBA})$  with different molecular weights, compositions and architectures: statistical (open squares), block (rhombi) and gradient (circles).

All statistical copolymers are completely amorphous and exhibit only a single glass transition at a temperature that increases with increasing IBA content. This indicates that there is no micro-phase separation in these materials, a finding further confirmed by DMA and SAXS experiments. The  $T_g$ 's of the statistical copolymers from the solid and dashed lines in Scheme 2 are plotted vs. their IBA content in Figure 1.

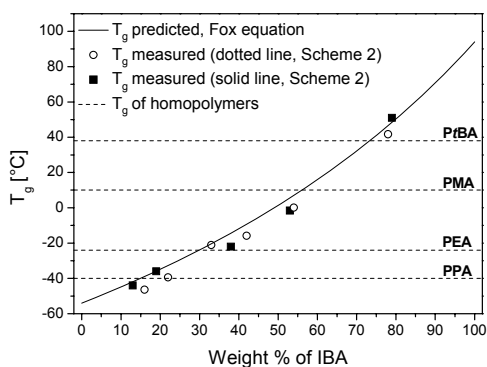


**Figure 1:** Tuning  $T_g$  in statistical copolymers of  $P(\text{IBA-co-nBA})$  with different IBA/nBA ratios and two different degrees of polymerization (Scheme 2, copolymers on solid and dotted lines).

The  $T_g$  varies continuously with composition in both low and high molecular weight samples. To describe such type of composition dependence of the  $T_g$  of copolymers or miscible polymer blends, the so-called Fox equation (27) is often used:

$$\frac{1}{T_g} = \frac{w_1}{T_{g1}} + \frac{w_2}{T_{g2}}$$

Here  $T_g$  is the glass transition temperature of the copolymer,  $T_{g1}$  and  $T_{g2}$  are the glass transition temperatures of the two homopolymers, and  $w_1$  and  $w_2$  are the weight fractions of the two repeat units in the copolymer. As can be seen in Figure 1, the experimentally measured  $T_g$  values closely follow the predictions of the Fox equation, which is represented by the solid line. Figure 1 demonstrates that it is possible to generate statistical P(IBA-co-nBA) copolymers that can mimic the thermal behavior of several homopolymers, such as PtBA, PMA, PEA, PPA. It is interesting to verify whether copolymers can mimic not only the  $T_g$ 's of the acrylate homopolymers, but also their mechanical properties. In order to do this, the dynamical mechanical analysis (DMA) was performed and the frequency dependencies of the storage ( $G'$ ) and the loss ( $G''$ ) parts of the shear modulus (master curves) of copolymer/homopolymer pairs with similar molecular weight and glass transition temperatures were compared. Typical results from such comparison between PEA homopolymer ( $T_g = -24^\circ\text{C}$ ,  $M_n = 96900$  g/mol) and IBA(33%)-nBA(67%) copolymer ( $T_g = -20^\circ\text{C}$ ,  $M_n = 107500$  g/mol) are shown in Figure 2.

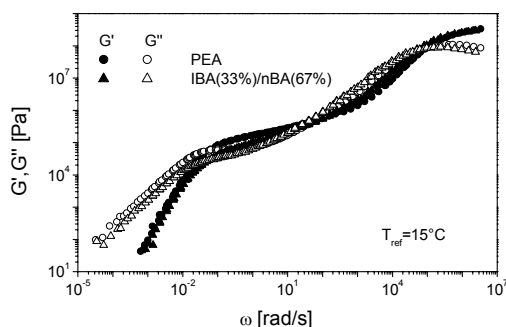


**Figure 2.** Comparison of the shear moduli spectra of PEA, ( $T_g = -24^\circ\text{C}$ ,  $M_n = 96900$  g/mol) and IBA(33%)-nBA(67%) copolymer ( $T_g = -20^\circ\text{C}$ ,  $M_n = 107500$  g/mol).

The two master curves overlap very well both in the high frequency region (due to the similar  $T_g$ 's) and in the low frequency region (due to the similar  $M_w$

values). Nevertheless, a closer look reveals that in the characteristic rubbery plateau region the storage modulus ( $G'$ ) of the P(IBA-co-nBA) copolymer is significantly lower than the corresponding value for the PEA homopolymer. This means that while mimicking perfectly the glass transition temperatures of the PEA, the P(IBA-co-nBA) copolymer is significantly softer than its homopolymer counterparts. The data for the  $G'$  in rubbery plateau region for all copolymer/homopolymer pairs studied are summarized in Table 1. For comparison the values for the PnBA and PIBA homopolymers are also shown. As can be seen from the table in all cases, the P(IBA-co-nBA) copolymers are significantly softer than the respective homopolymers having similar glass transition temperatures. The lower plateau modulus of the copolymers indicates that they should have higher entanglement  $M_w$  values. The effect is most likely related to the rather big and rigid side group of IBA, which prevents the copolymers chains from a denser packing and therefore results in a less dense and softer IBA containing copolymers. This conclusion is also confirmed by the very low plateau modulus of the IBA homopolymer itself. Further detailed studies are required, however, to get better inside on the observed trends in the plateau modulus dependence on copolymer composition.

**Table 1: Comparison of the glass transition temperature and the rubbery plateau storage modulus of acrylate co- and homopolymers**

<i>Polymer</i>	<i>T<sub>g</sub> [°C]</i>	<i>Plateau G' [kPa]</i>
PPA	-40	140
IBA(16%)-nBA(84%)	-39	95
PEA	-24	170
IBA(33%)-nBA(67%)	-20	70
PtBA	37	135
IBA(78%)-nBA(22%)	42	85
PnBA	-54	130
PIBA	105	80

**Gradient and block copolymers of nBA and IBA.** As discussed above, the statistical P(IBA-co-nBA) copolymers exhibit “homopolymer type” thermo-mechanical properties, with no evidence for a two phase behavior. However, the situation is remarkably different in the case of gradient and block copolymers (28-31). In order to illustrate this, the left panel of Figure 3 compares DSC and DMA spectra of a statistical and a gradient copolymer, with similar composition and molecular weight. The statistical copolymer shows a clear glass transition at a temperature between the  $T_g$ 's of the two homopolymers. The gradient copolymer, however, reveals a broad glass transition region with no obvious  $T_g$  and a very broad distribution of relaxation processes. The right panel of Figure 3, compares statistical and block copolymers. While, the statistical copolymer has a single glass transition, the block copolymer shows two glass transition temperatures corresponding to the  $T_g$ 's of each component indicating a micro-phase separation in the sample. With respect to the frequency dependence of  $G'$  and  $G''$  it is important to emphasize that in the case of the block copolymer,

merely an attempt for constructing a master curve is shown, as the temperature dependence of the shift factors does not conform to the WLF equation.

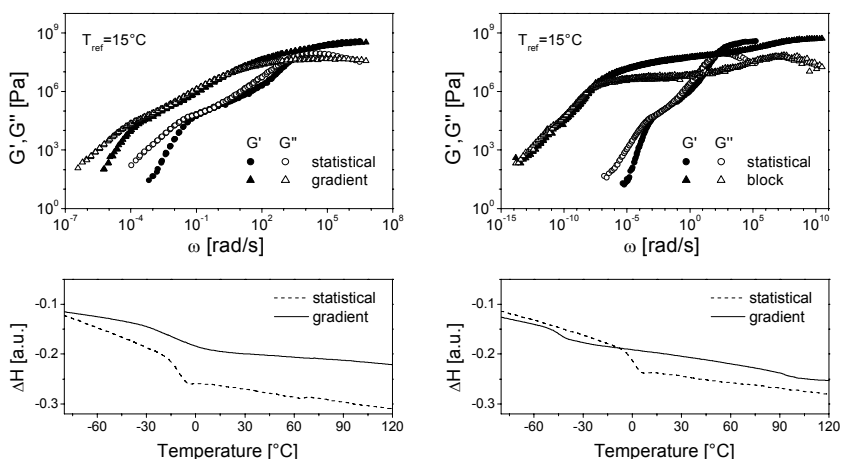


**Figure 3:** Comparisons between gradient IBA(47%)-nBA(53%),  $M_n = 74800$  g/mol and statistical IBA(44%)-nBA(56%),  $M_n = 53000$  g/mol copolymers (left panel) and block IBA(54%)-nBA(46%),  $M_n = 54600$  g/mol and statistical IBA(54%)-nBA(46%)  $M_n = 69000$  g/mol copolymers (right panel).

Nevertheless, this “master curve” provides additional evidences for the micro-phase separation in the sample. First of all the glass transitions of the two blocks are clearly distinguishable at low and high frequencies, respectively. Furthermore the behavior of the “master curve” in the very low frequency region, namely  $G'(\omega)$  overlapping with  $G''(\omega)$  and having a slope of  $\sim 0.5$  may indicate the formation of a lamella structure as theoretically predicted (32).

### Polar 3-arm Star Block Copolymer based on n-butyl acrylate

Thermoplastic elastomers (TPE) are an important class of materials combining elastomeric behavior with thermoplastic properties. Commonly these are ABA type triblock copolymers such as polystyrene-polyisoprene-polystyrene (SIS) or polystyrene-polybutadiene-polystyrene (SBS) that combine a soft central block with glassy end blocks. Although these materials have found wide spread commercial applications, the presence of unsaturated double bonds in the middle segments makes them susceptible to oxidation and eventually reduce the use lifetime (33). Different strategies, including change of outer and inner segments of ABA triblock copolymers (34) or design of materials bearing

novel architectures and topologies (35-37) have been used to address this issue and prepare TPE with tailored properties. For example, during the last several years, it was demonstrated that thermoplastic elastomers based on star block copolymers (35,38,39) may exhibit superior properties, as compared to the linear ABA triblock copolymer type TPEs. It was reported that multi-armed polystyrene-*b*-polyisobutylene (PS-*b*-PIB) star block copolymers have substantially better mechanical properties and much lower sensitivity to diblock contamination than their linear triblock counterparts (39). With this in mind, tri-arm star block copolymer thermoplastic elastomers were prepared, which comprise of poly(*n*-butyl acrylate)-*b*-polyacrylonitrile (PBA-*b*-PAN) or poly(*n*-butylacrylate)-*b*-poly (methyl methacrylate) (PBA-PMMA) arms. The incorporation of the polar hard segment of PAN and PMMA was possible with the aid of halogen exchange ATRP technique (40-43). The effect of molecular architecture and composition on the thermo mechanical properties of these star block copolymers is discussed below.

**3-arm star (PBA-*b*-PAN)** block copolymers with different molecular weights and compositions were synthesized by ATRP using halogen exchange strategy, as described in detail elsewhere (42). The composition of the copolymers was determined by <sup>1</sup>H NMR and is given in the Table 2. All copolymers had low polydispersities, as reported in Table 2.

**Table 2. Series of 3-arm Star PBA-PAN block copolymers**

<i>Sample</i>	<i>Arm composition</i>	$M_n$	<i>wt% PAN</i>	$M_w/M_n$
T-PBA304-PAN63	(BA <sub>304</sub> - <i>b</i> -AN <sub>63</sub> ) <sub>3</sub>	127000	8	1.14
T-PBA304-PAN109	(BA <sub>304</sub> - <i>b</i> -AN <sub>109</sub> ) <sub>3</sub>	134000	13	1.17
T-PBA304-PAN207	(BA <sub>304</sub> - <i>b</i> -AN <sub>207</sub> ) <sub>3</sub>	150000	22	1.17
T-PBA304-PAN331	(BA <sub>304</sub> - <i>b</i> -AN <sub>331</sub> ) <sub>3</sub>	169000	31	1.11
T-PBA388-PAN115	(BA <sub>388</sub> - <i>b</i> -AN <sub>115</sub> ) <sub>3</sub>	167000	11	1.07
T-PBA388-PAN165	(BA <sub>388</sub> - <i>b</i> -AN <sub>165</sub> ) <sub>3</sub>	175000	15	1.13
T-PBA388-PAN264	(BA <sub>388</sub> - <i>b</i> -AN <sub>264</sub> ) <sub>3</sub>	191000	22	1.15
T-PBA52-PAN26	(BA <sub>52</sub> - <i>b</i> -AN <sub>26</sub> ) <sub>3</sub>	24100	17	1.22
T-PBA547-PAN153	(BA <sub>547</sub> - <i>b</i> -AN <sub>153</sub> ) <sub>3</sub>	234000	10	1.16

Due to the strong incompatibility between the two phases, the PBA-PAN star copolymers are expected to show very strong phase separation. In an attempt to visualize this effect AFM imaging was performed on thin films prepared by spin-casting of polymer solutions in DMF onto silicon wafer substrates. Typical results are shown in Figure 4. The phase contrast AFM images of the films reveal the phase separated morphology of 3-arm star PBA-PAN block copolymers. Rigid PAN domains (brighter features in AFM images) are dispersed in the softer PBA matrix. The sample with lowest content of PAN (8wt%) shows round features, while the sample with 13wt% PAN displays a

mixture of round and elongated (cylindrical) features. As the round features may originate from either spheres or standing cylinders, other experimental techniques (e.g. SAXS as described below) are needed to unambiguously determine the film morphology. Finally the sample with highest PAN content (22wt%) displayed meandering curved features, characteristic for short-range ordered cylindrical structures or bicontinuous structures.

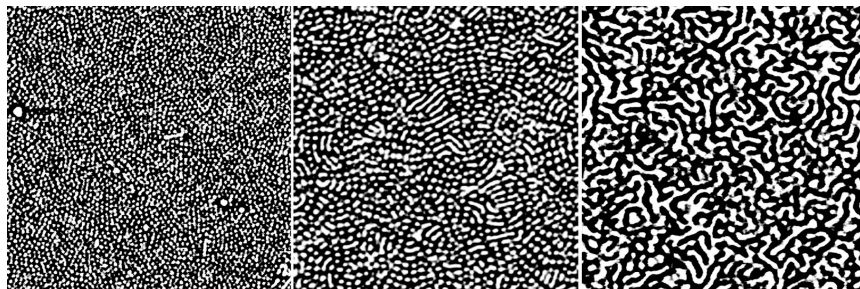


**Figure 4:** AFM phase images of 3-arm star PBA-PAN block copolymers: (left) T-PBA304-PAN63 (8wt% PAN); (middle) T-PBA304-PAN109 (13wt% PAN); and T-PBA304-PAN207 (22wt% PAN). Image size:  $2\ \mu\text{m} \times 2\ \mu\text{m}$ .

In order to get a better insight into the formed microstructures, SAXS analysis of thick films of all PBA-PAN copolymers listed in Table 2 was performed. Most of the materials revealed cylindrical morphologies and their different compositions affected the cylinders  $d$ -spacing in the micro-phase separated structures. Furthermore, the SAXS studies showed that annealing of the films for 2 hours at  $150^\circ\text{C}$  resulted in improved phase separation (42).

Dynamic mechanical properties of the PBA-PAN star copolymers were characterized through the temperature dependencies of the real ( $G'$ ) and imaginary ( $G''$ ) parts of the complex shear modulus. Some typical results for a series of copolymers with constant PBA content (DP equal to 304) and varying PAN fractions are shown in Figure 5 together with the respective DSC thermographs. In every case, 4 major transitions were observed. The first two correspond to the glass transitions of PBA ( $\sim -50^\circ\text{C}$ ) and PAN ( $\sim 105^\circ\text{C}$ ). The third transition, at temperatures around  $260^\circ\text{C}$ , manifests itself in a rather sharp drop in the storage modulus  $G'$ . Finally, at higher temperatures ( $280$ - $290^\circ\text{C}$ ) an exothermal process is observed in the DSC thermographs with intensity proportional to the content of PAN in the material.

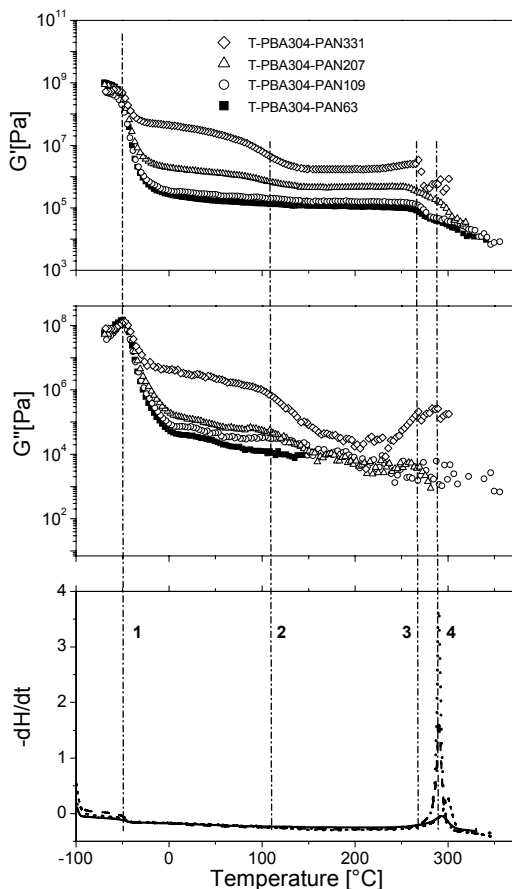


**Figure 5:** Thermomechanical and DSC analysis of 3-arm star PBA-*b*-PAN copolymers.

This process is related to chemical cross-linking of the PAN segments. As for the mechanical properties, the samples were glassy below the glass transition temperature of PBA, with storage modulus  $G' \sim 1$  GPa. Above this glass transition, the copolymers become elastic and show a  $G'$  plateau extending up to the softening temperature of PAN ( $\sim 100$  °C). The plateau value of  $G'$  depends strongly on the PAN content:  $\sim 0.1$  MPa for a pAN fraction  $< 0.1$  and  $\sim 100$  MPa for a PAN content of 0.3. In this elastic state the PAN blocks form the glassy domains connecting the flexible PBA blocks. This corresponds to a typical situation for a thermoplastic elastomer in which the hard phase elements (i.e. the glassy microdomains) act as physical crosslinks for the flexible component. Both storage and loss moduli decrease above the  $T_g$  of PAN but a second plateau with lower  $G'$  values (0.1 – 1 MPa) extends until temperatures of  $\sim 260$  °C. This indicates that the 3-arm star PBA-*b*-PAN copolymers maintain their microdomain morphology up to a very high ODT temperature of around 260°C, i.e., approximately 150°C above the glass transition of the PAN.



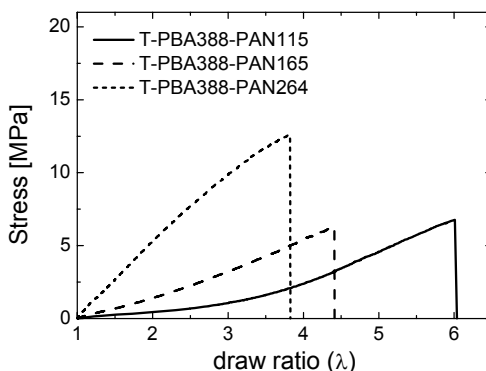


**Figure 6:** Stress - strain curves recorded for PBA-PAN star copolymers with varying content of PAN for same length of PBA.

Tensile mechanical properties of the PBA-PAN star copolymers were also investigated and some typical results are shown in Figure 6. The observed behavior is typical for elastomeric materials with elongations at break up to 600 %, and stress at break up to 13 MPa. As expected, the composition has a major effect on the tensile properties of the PBA-PAN star copolymers. The data showed that both the initial elastic modulus and the tensile strength increase strongly with PAN content, while the draw ratio at break seems to increase with the length of pBA segment and be reduced with increasing PAN content. This finding suggest an easy way for tuning the material properties by adjusting the copolymer composition.

**3-arm star (PBA-b-PMMA)** block copolymers have also been synthesized by ATRP (43). In order to study the effect of composition on the properties of the star PBA-PMMA block copolymers, 3 different samples with an increasing PMMA content were prepared. The precise compositions of these copolymers were determined by  $^1\text{H}$  NMR and are given Table 3. All materials exhibited good functionality and polydispersities below 1.3. As PBA and PMMA are strongly incompatible, the copolymers are expected to exhibit phase separated morphology. In order to study this effect in detail for a better understanding of the formed microstructures, SAXS analysis of thick films of the star copolymers listed in Table 3 was performed.

**Table 3. Series of 3-Arm Star PBA-PMMA block copolymers**

Sample	Arm composition	wt% of PMMA	$M_w/M_n$
T-PBA164-PMMA31	$((\text{BA})_{164}(\text{MMA})_{31})_3$	13	1.30
T-PBA164-PMMA76	$((\text{BA})_{164}(\text{MMA})_{76})_3$	26	1.29
T-PBA164-PMMA118	$((\text{BA})_{164}(\text{MMA})_{118})_3$	36	1.28

First, as-cast samples were studied and found that only the copolymer with highest PMMA content showed a well-ordered structure, consistent with hexagonally packed cylinders. The samples with lower PMMA content exhibited short-range ordering only. In order to examine the effect of thermal treatment on the copolymer films morphology, the SAXS experiments were

repeated after annealing the PBA-PMMA samples at 150°C. The results are presented in Figure 7.

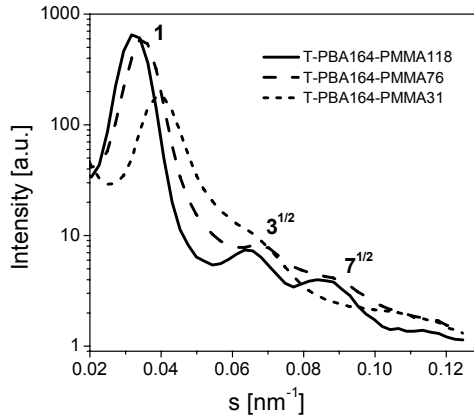


**Figure 7:** SAXS of 3-arm stars PBA-PMMA block copolymers after thermal annealing.

The annealed films exhibit good ordering, displaying at least three scattering peaks in each of the SAXS spectra. Furthermore, the ratios of the relative peak positions in all cases were  $s$ ,  $\sqrt{3}s$ ,  $\sqrt{7}s$ , i.e., again consistent with a hexagonal lattice. It is important to emphasize that, while all three PBA-PMMA copolymer studied exhibited similar cylindrical morphologies, their different compositions affect the cylinders  $d$ -spacing which increases with the increase of PMMA block length for the same length of the PBA segment.

Tensile behavior is of primary importance when considering the properties of a thermoplastic elastomer. The stress-strain dependencies for the 3-arm star PBA-PMMA block copolymers listed in Table 3 are shown in Figure 8. The data were recorded at room temperature and with drawing rate of 5 mm/min.

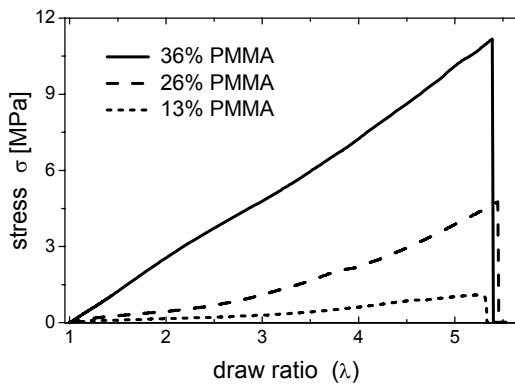


**Figure 8:** Stress-strain curves recorded for the 3-arm stars PBA-PMMA block copolymers.

The plots clearly indicate the elastomeric behavior of the star copolymers. The films of all three materials exhibited similar high elongation at break, about 500%, independent of the copolymer composition. As expected, the increase of the PMMA content in the copolymers resulted in an increase of the E modulus of the films from 1.02 to 4.76 and 11.18 MPa for samples with 13%, 26% and 36% PMMA respectively, suggesting a simple approach for tuning the tensile properties by adjusting the copolymers composition.

## Conclusions

Various acrylate copolymers with complex architectures have been synthesized via atom transfer radical polymerization. A strong correlation between the molecular structure and composition of the copolymers and their thermo-mechanical behavior have been found. This suggests a facile route for creating new advanced materials with tailored properties.

**Acknowledgments:** Financial support from NSF (DMR 05-49353), Universiti Teknologi MARA and the Ministry of Higher Education of Malaysia is gratefully acknowledged.

## References

- (1) Szwarc M. *Nature* **1956**, *178*, 1168.
- (2) Hadjichristidis, N.; Pitsikalis, M.; Pispas, S.; Iatrou, H. *Chem. Rev.* **2001**, *101*, 3747.
- (3) *Handbook of Radical Polymerization*, Matyjaszewski, K.; Davis, T. P. Eds., Wiley, New York 2002.
- (4) *Controlled/Living Radical Polymerization. From Synthesis to Materials*, ACS Symp. Ser. 944; Matyjaszewski, K. Ed., ACS, Washington, DC 2006.
- (5) Wang, J.-S.; Matyjaszewski, K. *J. Am. Chem. Soc.* **1995**, *117*, 5614.
- (6) Matyjaszewski, K.; Xia, J. *Chem. Rev.* **2001**, *101*, 2921.
- (7) Kamigaito, M.; Ando, T.; Sawamoto, M. *Chem. Rev.* **2001**, *101*, 3689.
- (8) Oh, J. K.; Drumright, R.; Siegwart, D. J.; Matyjaszewski, K. *Prog Polym Sci* **2008**, *33*, 448.
- (9) Patten, T. E.; Xia, J. H.; Abernathy, T.; Matyjaszewski, K. *Science* **1996**, *272*, 866.
- (10) Coessens, V.; Pintauer, T.; Matyjaszewski, K. *Prog. Polym. Sci.* **2001**, *26*, 337.
- (11) Davis, K. A.; Matyjaszewski, K. *Adv. Polym. Sci.* **2002**, *159*, 1.
- (12) Matyjaszewski, K.; Ziegler, M. J.; Arehart, S. V.; Greszta, D.; Pakula, T. *J. Phys. Org. Chem.* **2000**, *13*, 775.
- (13) Brouwer, H. De; Schellekens, M. A. J.; Klumperman, B.; Monteiro, M. J.; German, A. L. *J. Polym. Sci., Part A: Polym. Chem.* **2000**, *38*, 3596.
- (14) Kirci, B.; Lutz, J. F.; Matyjaszewski, K. *Macromolecules* **2002**, *35*, 2448.

- (15) Ray, B.; Isobe, Y.; Morioka, K.; Habaue, S.; Okamoto, Y.; Kamigaito, M.; Sawamoto, M. *Macromolecules* **2003**, *36*, 543.
- (16) Lutz, J. F.; Neugebauer, D.; Matyjaszewski, K. *J. Am. Chem. Soc.* **2003**, *125*, 6986.
- (17) Matyjaszewski, K.; Miller, P. J.; Pyun, J.; Kickelbick, G.; Diamanti, S.; *Macromolecules* **1999**, *32*, 6526.
- (18) Matyjaszewski, K. *Polym. Int.* **2003**, *52*, 1559.
- (19) Gao, H.; Tsarevsky, N. V.; Matyjaszewski, K. *Macromolecules* **2005**, *38*, 5995.
- (20) Gao, H.; Matyjaszewski, K. *Macromolecules* **2006**, *39*, 3154.
- (21) Gao, H.; Matyjaszewski, K. *Macromolecules* **2006**, *39*, 4960.
- (22) Beers, K. L.; Gaynor, S. G.; Matyjaszewski, K.; Sheiko, S. S.; Moller, M. *Macromolecules* **1998**, *31*, 9413.
- (23) Pyun, J.; Kowalewski, T.; Matyjaszewski, K. *Macromol. Rapid Commun.* **2003**, *24*, 1043.
- (24) Sheiko, S. S.; Sumerlin, B. S.; Matyjaszewski, K.; *Prog Polym Sci* **2008**, *33*, 759.
- (25) Tsarevsky, N. V.; Matyjaszewski, K. *Chemical Reviews* **2007**, *107*, 2270.
- (26) Jakubowski, W.; Juhari, A.; Best, A.; Koynov, K.; Pakula T.; Matyjaszewski, K. *Polymer* **2008**, *49*, 1567.
- (27) Fox, T. G.; *Bull. Am. Phys. Soc.* **1956**, *1*, 123.
- (28) Matyjaszewski, K.; Shipp, D. A.; McMurtry, G. P.; Gaynor, S. G.; Pakula, T. *J Polym Sci, Part A: Polym Chem* **2000**, *38*, 2023.
- (29) Matyjaszewski, K.; Ziegler, M. J.; Arehart, S. V.; Greszta, D.; Pakula, T. *J. Phys. Org. Chem.* **2000**, *13*, 775.
- (30) Kim, J.; Mok, M. M.; Sandoval, R. W.; Woo, D. J.; Torkelson, J. M. *Macromolecules* **2006**, *39*, 6152.
- (31) Mok, M.; Pujari, S.; Burghardt, W.; Dettmer, C.; Nguyen, S.; Ellison, C.; Torkelson J. *Macromolecules* **2008**, *41*, 5818.
- (32) Rubinstein, M.; Obukhov, S. P. *Macromolecules* **1993**, *26*, 1740.
- (33) Morton, M.; *Thermoplastic Elastomers*. In Holden, G.; Schroeder, H. E., Eds. Hanser: Munich, Germany, 1987; 67.
- (34) Yu, J. M.; Teyssie, P.; Jerome, R. *Macromolecules* **1996**, *29*, 8362.
- (35) Shim, J. S.; Asthana, S.; Omura, N.; Kennedy, J. P. *J Polym Sci, Part A: Polym Chem* **1998**, *36*, 2997.
- (36) Dair, B. J.; Honeker, C. C.; Alward, D. B.; Avgeropoulos, A.; Hadjichristidis, N.; Fetters, L. J.; Capel, M.; Thomas, E. L. *Macromolecules* **1999**, *32*, 8145.
- (37) Roos, S. G.; Mueller, A. H. E.; Matyjaszewski, K. *Macromolecules* **1999**, *32*, 8331.
- (38) Storey, R. F.; Shoemake, K. A. *J Polym Sci, Part A: Polym Chem* **1998**, *36*, 471.
- (39) Shim, J. S.; Kennedy, J. P. *J Polym Sci, Part A: Polym Chem* **1999**, *37*, 815.
- (40) Davis, K. A.; Matyjaszewski, K. *Chin J Polym Sci* **2004**, *22*, 195.
- (41) Matyjaszewski, K.; Shipp, D. A.; Wang, J.-L.; Grimaud, T.; Patten, T. E. *Macromolecules* **1998**, *31*, 6836.

- (42) Dufour, B.; Tang, C.; Koynov, K.; Pakula, T.; Matyjaszewski K. *Macromolecules*, **2008**, *41*, 2451.
- (43) Dufour, B.; Tang, C.; Koynov, K.; Pakula, T.; Matyjaszewski K. *Macr. Chem. Phys.* **2008**, *209*, 1686.

## Chapter 21

# Novel Baroplastic Materials

Sebnem Inceoglu and Metin H. Acar

Chemistry Department, Istanbul Technical University,  
Maslak 34469 Istanbul, Turkey

Tri- and star-block copolymers were investigated with respect to their “baroplastic” properties. A series of well-defined baroplastic materials containing immiscible low and high  $T_g$  segments were synthesized by atom transfer radical polymerization. The polymers with different topologies can be processed by applying pressure at room temperature. Processability and multiple recyclability were examined. The potential of baroplastic materials as processing aids in the processing of polystyrene at ambient temperature was also evaluated.

Today, the production of plastics is based on melt processing close to their melting temperature using different extrusion or molding equipment, which gives materials with desired shapes under applied pressure. Traditional melt processing consumes excess energy, and reduces the recyclability and performance of the products due to the degradation of polymers and additives.

Polymer miscibility has been the subject of numerous studies. Pressure is a thermodynamic parameter that can affect the phase behavior of polymer mixture and that can be used to enhance the miscibility of polymers. This property may have an important application in controlling microstructure. The phase behavior of blends and block copolymers under pressure has recently received significant attention (1-3).

Baroplastic di-block copolymers and core-shell polymer nanoparticles containing immiscible low and high  $T_g$  segments were processed under high pressure and at ambient temperature instead of moderate pressure at high temperature (4-10). In an attempt to understand the effect of structure on rheological flow, block copolymers with different topologies were obtained with the goal of expanding the range of existing baroplastics. The syntheses of baroplastic star-block copolymers may, in the future, address the problems encountered with core shell nanoparticles, whose processability are known to worsen the increase of the core size.

To extend the number of available baroplastic materials, a series of well-defined baroplastic tri-block, 3- and 4-arm star-block copolymers containing poly(2-ethylhexyl acrylate) (low  $T_g$  segment) and polystyrene (high  $T_g$  segment) were synthesized by atom transfer radical polymerization (ATRP) (11-16). The pressure induced processability and recyclability of the obtained polymers were investigated. Additionally, baroplastic materials (di-, tri-, and star-block copolymers) and polystyrene were mixed together at different compositions and pressed at room temperature in order to investigate the potential of the baroplastics as processing aids (17).

## Experimental

### Materials

Styrene (S, 99%, stabilized), 2-ethylhexylacrylate (EHA, 99+%, stabilized), copper(I) chloride (CuCl), copper(I) bromide (CuBr, 98%) and ethyl-2-bromopropionate (99%) were purchased from Acros. 2-Bromopropionyl bromide (97%), ethylene glycol (99%), 1,1,1-tris(hydroxymethyl)propane (97%), pentaerythritol (99%), 2,2'-bipyridine (bpyr, 99 +%) and N,N,N',N'',N''-pentamethyldiethylenetriamine (PMDETA, 99 %) were purchased from Aldrich. Tris(2-(dimethylamino)ethyl) amine (Me<sub>6</sub>-TREN) (18-19) and alkylated linear amine ligands (ALAL) (20-22) were synthesized according to literature procedures. All other solvents and chemicals were reagent grade, and were used as received.

### Synthesis of di-, tri- and tetra-functional initiators

Di-, tri- and tetra-functional ATRP initiators were prepared by esterification of 2-bromopropionylbromide with ethylene glycol, 1,1,1-tris(hydroxyl methyl) propane and pentaerythritol, respectively, according to the literature (23-25).

Required amounts of anhydrous dichloromethane solutions of hydroxy functional reagents and triethylamine were placed into a flask and cooled to 0 °C in an ice/water bath, and then a dichloromethane solution of 2-bromopropionyl bromide was added dropwise with stirring over a period of 1 hour. After required time, a white precipitate of triethylammonium bromide salt was removed by filtration and the mixture was extracted consecutively with distilled water, NaHCO<sub>3</sub> (aq), and distilled water. The organic phase was dried over Na<sub>2</sub>SO<sub>4</sub> (anhydrous) and filtered. After the solvent evaporation, initiators were isolated by purification.

### General procedure for homopolymer synthesis

A typical ATRP procedure was performed as follows; catalyst (CuCl or CuBr) was placed in a flask which was sealed with a Teflon stopper and contained a side arm with a Teflon valve (Chemglass). Then, the flask was deoxygenated by vacuum-thaw-nitrogen cycles. S or EHA, toluene and proper ligand (bpyr, PMDETA, Me<sub>6</sub>-TREN or ALAL) and finally, an appropriate mono-, di-, tri- or tetra-functional ATRP initiator were added. All liquid components were sparged with nitrogen prior to transferring them into the flask. The mixture was sparged with nitrogen for 10 min prior to placing it in a thermostatically controlled oil bath (at 100 °C for EHA or 110°C for S, 400 rpm

stirring rate). After the required time, the polymerization was terminated with methanol and diluted with THF, then passed through neutral alumina to remove the catalyst and precipitated into methanol. The product was dried in vacuum.

### General procedure for block copolymer synthesis

ATRP allows the synthesis of di-block copolymers by sequential (one-pot) or separated steps (two-pot) methods (26). To synthesize di-block, tri-block, 3- and 4-arm star-block copolymers by the two-pot method, a typical ATRP procedure was performed. First, a homopolymer was synthesized as mentioned above and then this was used as a macroinitiator. In addition to the two-pot procedure, one of the tri-block copolymers (P2 in Table I) was also synthesized by the one-pot ATRP procedure. Once first monomer polymerized to complete conversion, the second monomer was added to the flask under nitrogen to obtain the block copolymers. In both cases, the samples were taken periodically via a syringe to follow the molecular weight of the polymer by GPC and the conversion of polymerization by GC measurements.

### Instrumentations

<sup>1</sup>H-NMR spectra of the initiators and polymers were collected with a Bruker 250 MHz NMR instrument using CDCl<sub>3</sub> as the solvent. Molecular weights and polydispersities were measured by a gel permeation chromatography (GPC) system consisting of an Agilent 1100 series pump, four Waters Styragel HR columns (5E, 4, 3, 2) and an Agilent 1100 series RI detector with a THF flow rate of 0.3 mL/min; poly(methyl methacrylate) or polystyrene were used as calibration standards. Monomer conversions were determined either gravimetrically and/or with an ATI Unicam gas chromatograph (GC) with a FID detector and a J&W scientific 15 m DB WAX wideboard capillary column. Modulated differential scanning calorimetry (MDSC) measurements using Q200 (TA Instruments) were evaluated from the second heating run from -90 °C to 200 °C with a ramp rate of 10°C/min for both heating and cooling. Atomic force microscopy characterization was performed at 25 °C in air with a Nanoscope III Atomic Force Microscope (Veeco, Digital Instruments, Santa Barbara, CA USA) using tapping mode with single beam silicon cantilevers (spring constant: 44.13 N/m, drive frequency: 315 kHz, scan rate: 1 Hz). For processing, the obtained polymers in the powder form were introduced into the desired mold (piston diameter: 12 mm) and pressed by a Shimadzu hydraulic manual press providing up to 10 ton at 600 kg cm<sup>-2</sup>, for required times and pressures at room temperature. A mold for imprinting ITU (piston diameter: 10 mm, pressure: 300 kg cm<sup>-2</sup>) and an extruding mold (piston diameter: 12 mm, pressure: 400 kg cm<sup>-2</sup>, hole size: 1 mm x 8 mm) were used.

## Results and Discussion

In this study, well-defined PS-*b*-PEHA di-block, PS-*b*-PEHA-*b*-PS and PEHA-*b*-PS-*b*-PEHA tri-block, (PS-*b*-PEHA)<sup>3\*</sup> 3-arm star-block, (PEHA-*b*-PS)<sup>4\*</sup> and (PS-*b*-PEHA)<sup>4\*</sup> 4-arm star-block copolymers were synthesized via ATRP. In order to compare the effect of structures on the baroplastic behavior, some block copolymers were obtained with the replacement of inner/outer soft segments. Herein, some of the obtained block copolymers and their



characteristics are listed in Table I. Molecular weights and polydispersities of the block copolymers were traced by GPC as representatively shown in Figure 1 for tri-block copolymer (P4).

The block copolymer's composition was calculated using  $^1\text{H-NMR}$  measurements by integrating the characteristic peak of the PEHA segment ( $-\text{COOCH}_2-$ ) at 3.9 ppm versus the aromatic peaks of the PS segment at 6.34-7.06 ppm.  $^1\text{H-NMR}$  spectrum of 4-arm star-block copolymer (P7) is shown in Figure 2.

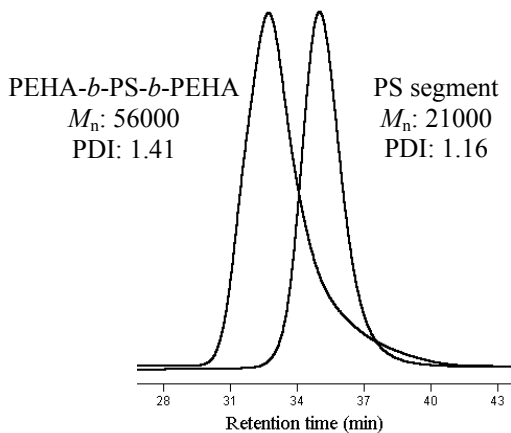


Figure 1: GPC traces of the PS segment and  $\text{PEHA}_{0.26}\text{-}b\text{-PS}_{0.48}\text{-}b\text{-PEHA}_{0.26}$  tri-block copolymer (P4).

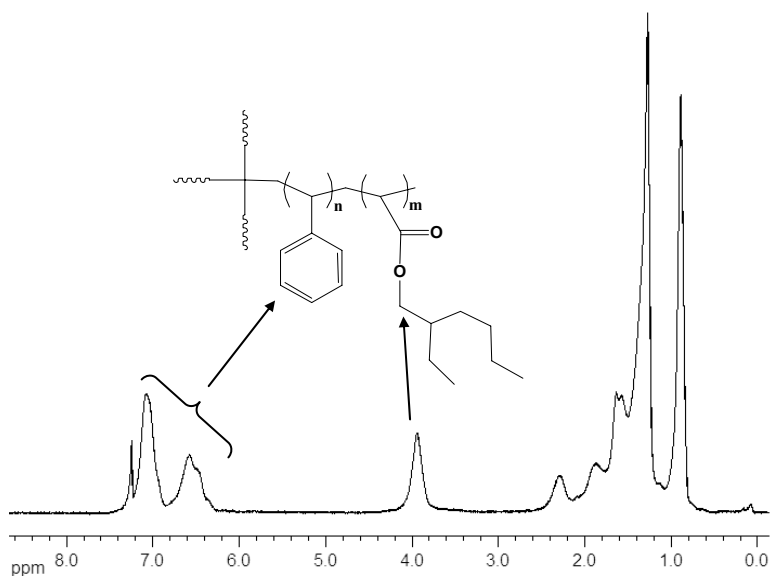




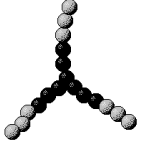
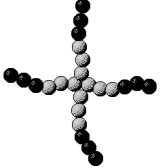
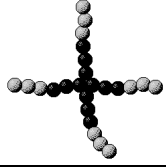
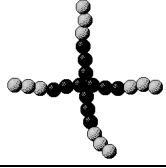


Figure 2:  $^1\text{H-NMR}$  spectrum of  $(\text{PS}_{0.48}\text{-}b\text{-PEHA}_{0.52})^{4*}$  4-arm star-block copolymer (P7) in  $\text{CDCl}_3$ .

**Table I. Baroplastic Materials  
Processing and Recycling of Baroplastic**

<i>Run</i>	<i>Block copolymer Structure</i>	<i>First segment <math>M_n</math> (PDI)</i>	<i>Block copolymer <math>M_n</math> (PDI)</i>	<i>PEHA, mol%</i>
P1	PS- <i>b</i> -PEHA 	32K (1.11)	53K (1.20)	39
P2	PS- <i>b</i> -PEHA- <i>b</i> -PS 	15K (1.25)	41K (1.38)	46
P3	PEHA- <i>b</i> -PS- <i>b</i> -PEHA 	16K (1.24)	32K (1.43)	50
P4		21K (1.16)	56K (1.41)	52
P5	(PS- <i>b</i> -PEHA) <sup>3*</sup> 	42K (1.21)	53K (1.31)	50
P6	(PEHA- <i>b</i> -PS) <sup>4*</sup> 	20K (1.61)	34K (1.71)	49
P7	(PS- <i>b</i> -PEHA) <sup>4*</sup> 	27K (1.14)	80K (1.38)	52
P8		41K (1.27)	98K (1.33)	50

The new plastics, called baroplastics, use molding equipment similar to that used for current commercial plastics but need little or no heating. Instead, these materials flow at ambient temperature when requisite pressures are applied, due to their specially designed nanophase structure which results from the phase separation of the soft and hard segments. The applied pressure simultaneously induces partial dissolution of the hard component in the soft component giving rise to decreased microphase separation.

The obtained block copolymers were processed using compression or piston molding to show their baroplastic behavior. Each of the samples was successfully molded at room temperature and maintained their shape with sufficient rigidity. After processing the starting 4-arm star-block copolymer (P6), a transparent object was obtained (Figure 3-a), which suggests a pressure-induced miscibility (baroplastic behavior). To optimize the processing condition, the effect of pressure and time were studied. The polymers in the powder form ( $\sim 0.1$  g) were introduced into the mold (piston diameter: 12 mm) and pressed at different pressures (50 to 500  $\text{kg cm}^{-2}$ ) and times (1 to 30 min). As shown in Figure 3-b, it was found that even 50  $\text{kg cm}^{-2}$  pressure for 1 min at room temperature is sufficient for a successful molding. This pressure is much lower than the pressure used in our previous study of baroplastic di-block copolymer and core-shell nanoparticles (4-8).

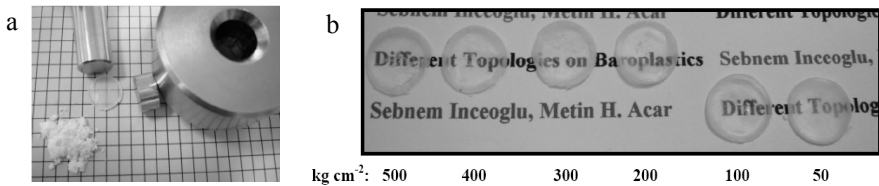


Figure 3. Images of a) the mold with starting and processed polymers, b) processed baroplastic( $\text{PEHA}_{0.49}\text{-}b\text{-PS}_{0.51}$ )<sup>4\*</sup> 4-arm star-block copolymer (P6), at different pressures for 1 min at room temperature.

The principle objective of the present work was to mold potential baroplastics with pressure at room temperature into well-defined shapes. As shown in Figure 4 and 5 a mold for imprinting ITU and an extruding mold to obtain rectangular shaped strip film of the obtained polymers, respectively, can be used successfully demonstrating the room temperature processability by pressure. The mechanical properties of the latter, if needed, can potentially be measured using this film with a dynamic mechanical analyzer (DMA).

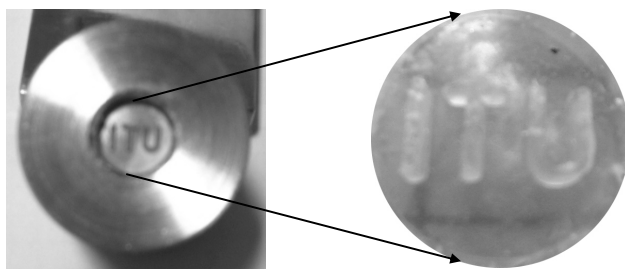


Figure 4. An Istanbul Technical University (ITU) imprinting mold from  $PS_{0.27}$ - $b$ - $PEHA_{0.46}$ - $b$ - $PS_{0.27}$  tri-block copolymer (P2).



Figure 5. Basic extrusion test of baroplastic  $PEHA_{0.26}$ - $b$ - $PS_{0.48}$ - $b$ - $PEHA_{0.26}$  tri-block copolymer (P4) via a custom-made "extruding mold".

Baroplastic systems containing nanophase structure of which one is a high  $T_g$  and the other is a low  $T_g$  domain can exhibit melt-like flow behavior under pressure at ambient temperature through an apparent semi-solid partial mixing mechanism that substantially preserves the high  $T_g$  phase. Evidence of the reduction of the microphase separation was demonstrated through differential scanning calorimetry (DSC). Figure 6 shows typical DSC curves of the starting, processed and 5 times recycled baroplastic tri-block copolymer (P2). Each of them shows two  $T_g$ 's corresponding to the PEHA and PS blocks. After applying pressure ( $400 \text{ kg cm}^{-2}$ , mold piston diameter: 12 mm), beside the already existing the two  $T_g$ 's, a new  $T_g$  appeared around  $47 \text{ }^\circ\text{C}$  that represents the mixed-phase of the immiscible segments.

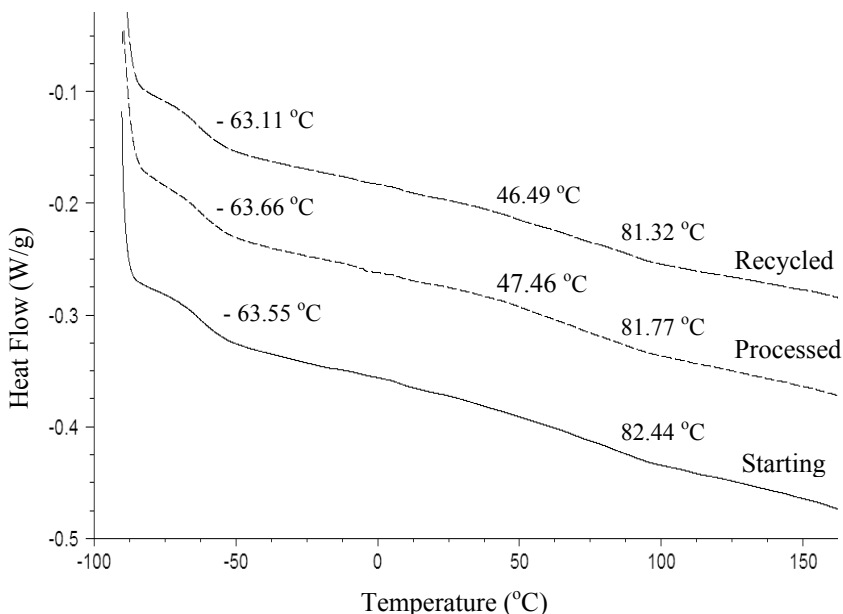


Figure 6: DSC curves of starting polymer, processed and 5 times recycled baroplastic  $PS_{0.27}$ - $b$ - $PEHA_{0.46}$ - $b$ - $PS_{0.27}$  tri-block copolymer (P2).

For AFM measurements, the block copolymer films were prepared by solution casting using dichloromethane on mica surface at room temperature. The solution concentration of block copolymers was adjusted around  $\sim 5\%$  (w/v). Three types of films were used in the measurements; solvent cast, annealed and pressure applied. In the latter two cases, to eliminate the thermal history and thus to reach the thermodynamic equilibrium, the block copolymer films were annealed overnight at  $110\text{ }^{\circ}\text{C}$  after solvent casting which is well above the glass transition temperatures of each polymer segment. The morphology of the solution casted films, annealed films and pressure applied films were investigated by Tapping Mode AFM. Since the AFM phase images of the annealed films showed more organized lamellar structure than the solution casted films, only annealed and pressured films phase images were compared. Representative AFM phase images of the baroplastic tri-block copolymers (P4) before (annealed) (Figure 7-a) and after applying pressure at  $300\text{ kg cm}^{-2}$  for 5 min (processed) (Figure 7-b) clearly demonstrate reduced microphase separation.

Before applying the pressure, annealed film displays a strong orientation of the lamellar structure for tri-block copolymer (P4). By applying pressure, this periodical distribution changes into a mixed morphology that represent the mixture of both ordered (phase-separated) and disordered (non-phase separated) structures (Figure 7-b). The formation of mixed morphology (reduction of phase

separation), supported by both AFM and DSC results, may suggest a rheological flow, which could be responsible for the baroplastic behavior.

The images were analyzed further to identify the soft and hard segments. In the literature, it was stated that for low- and high-density parts of a micro layered polyethylene sample and for a polydiethylsiloxane sample on Si, the phase angle shift is larger for hard segment and smaller for soft segment at moderate tapping regimes ( $r_{sp}=0.4-0.7$ ) (27). Although the tapping was performed at lighter regimes ( $r_{sp}=0.8-0.9$ ), according to the above literature, it is most probable that in our case, phase angle shift at around  $1$  to  $2^\circ$  for bright parts and  $-3$  to  $-4^\circ$  for dark parts which were measured along the two lines (upper left part in Figure 7-a) corresponds to lamellae of soft (PEHA) and hard (PS) segments, respectively.

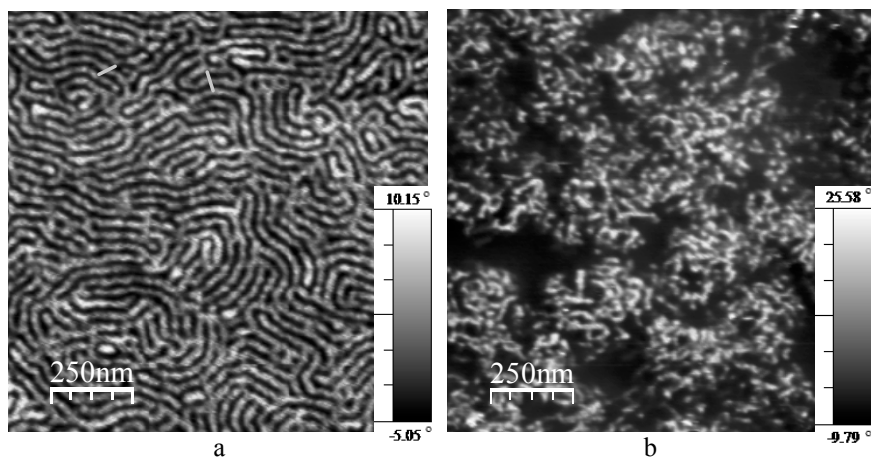
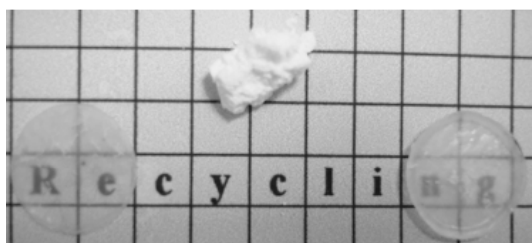


Figure 7: AFM phase images of  $PEHA_{0.26}\text{-}b\text{-}PS_{0.48}\text{-}b\text{-}PEHA_{0.26}$  tri-block copolymer (P4) a) before and b) after processing at  $300\text{ kg cm}^{-2}$  for 5 min.

Unlike inorganic glasses or metals, recycling of conventional polymers results in substantially lower grade materials, greatly limiting their reuse. A primary reason is the poor thermal stability that polymers exhibit at elevated temperatures necessary for reprocessing, which causes substantial discoloration and loss of mechanical performances. In contrary to conventional polymers, baroplastic materials can be remolded (recycled) many times at room temperature without losing the mechanical properties (4-9).

Herein, in addition to the existing baroplastics, we have shown that baroplastic tri- and star-block copolymers can be recycled multiple times. For example, recycling of P6 (Figure 8) was achieved by chopping and remolding at  $400\text{ kg cm}^{-2}$  for 30 min which was repeated five times. The fact that the resulting material is still remoldable is an indication of the recyclability of the material.

GPC measurements of the starting and the recycled baroplastic materials (P1 to P8) show no significant change in  $M_n$  and polydispersity indicating that the processing can be carried out without any degradation. The representative GPC traces can be seen in Figure 9 for tri-block copolymer (P2).



Recycled ←..... Polymer .....→ Processed

Figure 8: Images of starting polymer, processed and 5 times recycled ( $PEHA_{0.49}\text{-}b\text{-}PS_{0.51}$ )<sup>4\*</sup> 4-arm star-block copolymer (P6).

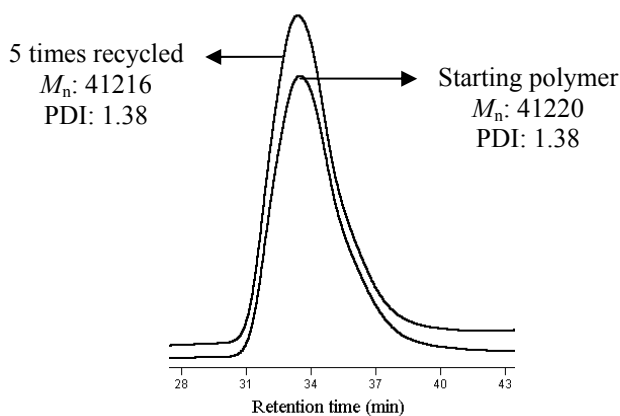


Figure 9: GPC traces of starting and 5 times recycled  $PS_{0.27}\text{-}b\text{-}PEHA_{0.46}\text{-}b\text{-}PS_{0.27}$  tri-block copolymers (P2).

As can be seen in Figure 6, DSC heat flow of the 5 times recycled material show both components'  $T_g$ 's and a mixed-phase  $T_g$  around 47 °C similar to the initial processed material. This observation also indicates that the recycled baroplastic materials maintain a mixed morphology (the mixture of ordered and disordered structure).

### Baroplastic as processing aid

It was also shown that baroplastic materials can be used as a processing aid to process high  $T_g$  homopolymer such as polystyrene (PS). To optimize the conditions, polystyrene and baroplastic materials in powder form were blended at different compositions and pressed using compression or extruding at room temperature. The results indicate that a room temperature moldable polystyrene/baroplastic blend can be obtained at 50 wt% baroplastic content with the di-block, tri-block and star-block copolymers. Figure 10 shows that the 50 wt% blend of PS (45K) and 4-arm star-block copolymer (98K, P8) can be processed in extruding mold at 400 kg cm<sup>-2</sup> pressure, 25 °C, yielding a rectangular shaped strip film.

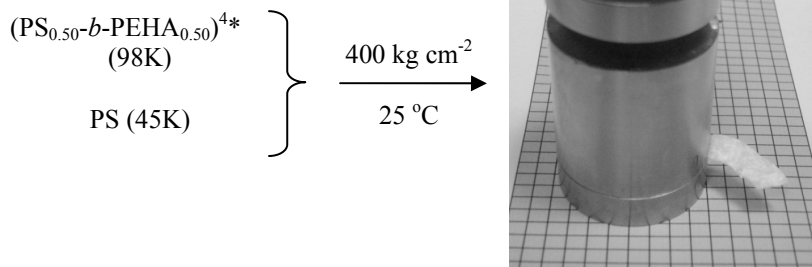


Figure 10. Images of processed PS homopolymer and baroplastic  $(\text{PS}_{0.50}\text{-}b\text{-PEHA}_{0.50})^{4*}$  4-arm star-block copolymer (P8) blend.

## Conclusions

Several di-, tri- and star-block copolymers with assorted compositions and molecular weights were synthesized by ATRP. The block copolymers obtained have shown baroplastic behavior by simple compression and/or extruding at room temperature.

It was shown that baroplastic materials can be recycled multiple times without degradation with properties equivalent to the virgin material. These results suggest a longer recycling life that could substantially reduce the amount of waste generation. Also, a material with this processing advantage would save energy and time since no heating and cooling are involved.

Baroplastic di-, tri- and star-block copolymers were shown to act as processing aids in the processing of homo-polystyrene. Detailed studies with different baroplastic materials as processing aids and the mechanical properties of the obtained materials are under investigation.

This work was supported by TUBITAK under Grant No. TMAG-107M323 and Istanbul Technical University Research foundation. The authors would like to thank Taner Aytun from Sabanci University for AFM measurements.

## References

1. Pollard, M.; Russell, T. P.; Ruzette, A. -V. G.; Mayes, A. M.; Gallot, Y. *Macromolecules* **1998**, *31*, 6493.
2. Mayes, A. M.; Ruzette, A. -V. G.; Russell, T. P.; Banerjee, P. A. *J. Chem. Phys.* **2001**, *114*, 8205.
3. Ruzette, A. -V. G.; Mayes, A. M.; Pollard, M.; Russell, T. P.; Hammouda, B. *Macromolecules* **2003**, *36*, 3351.
4. Gonzalez, J. A.; Acar, M. H.; Ryu, S-W.; Ruzette A. -V. G.; Mayes A. M. *Nature* **2003**, *426*, 424.



5. Acar, M. H.; Gonzalez, J. A.; Mayes, A. M. *Polym. Prep.* **2002**, 43(2), 55.
6. Acar, M. H.; Gonzalez, J. A.; Mayes, A. M. *Polym. Mat. Sci. Eng.* **2003**, 88, 159.
7. Ryu, S-W.; Gonzalez, J. A.; Acar, M. H.; Mayes, A. M. *Polym. Mater. Sci. Eng.* **2003**, 69, 770.
8. Structured baroplastic materials, Mayes A. M.; Ryu, S-W.; Gonzalez, J. A.; Acar, M. H. *World patent*, WO/2004/063271; *CA Patent*, 2005, 2512209; *European Patent*, 2005, EP1581592; *U.S. patent application*, 11/172,371.
9. Gonzalez, J. A.; Ryu, S-W.; Hewlett, S. A.; Ibrahim, S. H.; Mayes A. M. *Macromolecules* **2005**, 38, 8036.
10. Lee, D. H.; Kim, H. J.; Kim, J. K. *Macromol. Symp.* **2006**, 240, 123.
11. Wang, J. S.; Matyjaszewski, K. *Macromolecules* **1995**, 28, 7901.
12. Wang, J. S.; Matyjaszewski, K. *J. Am. Chem. Soc.* **1995**, 117, 5614.
13. Kato, M.; Kamigaito, M.; Sawamoto, M.; Higashimura, T. *Macromolecules* **1995**, 28, 1721.
14. Percec, V.; Barboiu, B. *Macromolecules* **1995**, 28, 7970.
15. Matyjaszewski, K.; Xia, J. *Chem. Rev.* **2001**, 101, 2921.
16. Kamigaito, M.; Ando, T.; Sawamoto, M. *Chem. Rev.* **2001**, 101, 3689.
17. Acar, M. H.; Inceoglu, S. *Abst. Pap. Am. Chem. Soc.* **2008**, 236, 270-Poly (2); *Polym. Prep.*, **2008**, 49(2), 30.
18. Queffelec, J.; Gaynor, S. G.; Matyjaszewski, K. *Macromolecules*. **2000**, 33, 8629.
19. Inceoglu, S.; Olugebefola, S. C.; Acar, M. H.; Mayes, A. M. *Des. Mon. Polym.* **2004**, 7, 18.
20. Acar, M. H.; Bicak, N. *J. Polym. Sci.-A-Polym. Chem.* **2003**, 41, 1677.
21. Acar, M. H.; Becer, C. R.; Ondur, H. A.; Inceoglu, S. *Abst. Pap. Am. Chem. Soc.* **2005**, 230, 242-Poly, U4109; *Polym. Preprint* **2005**, 46(2), 433.
22. Acar, M. H.; Becer, C. R.; Ondur, H. A.; Inceoglu, S. *In: Controlled/Living Radical Polymerization: From Synthesis to Materials*; ACS Symposium Series 994; Matyjaszewski, K. ed., American Chemical Society: Washington, DC, 2006; Chapter 8, pp 97-110.
23. Luan, B.; Pan, C-Y. *Eur. Polym. J.* **2006**, 42, 1467.
24. Matyjaszewski, K.; Miller, P. J.; Pyun, J.; Kickelbick, G.; Diamanti S. *Macromolecules* **1999**, 32, 6526.
25. Lecolley, F.; Waterson, C.; Carmichael, A. J.; Mantovani, G.; Harrisson, S.; Chappell, H.; Limer, A.; Williams, P.; Ohno, K.; Haddleton, D. M. *J. Mater. Chem.* **2003**, 13, 2689.
26. Muhlebach, A.; Gaynor, S. G.; Matyjaszewski, K. *Macromolecules* **1998**, 31, 6046.
27. Magonov, S. N.; Elings, V.; Whangbo, M. -H. *Surface Science* **1997**, 375 L385.

## Chapter 22

# Functionalisation of polyHIPE Materials by ATRP Surface Grafting

David M. Cummins<sup>1</sup> Pieter C. M. M. Magusin<sup>1</sup>, and Andreas Heise\*<sup>1,2</sup>

<sup>1</sup>Technische Universiteit Eindhoven, Den Dolech 2, P.O. Box 513,  
5600 MB, Eindhoven, The Netherlands

<sup>2</sup>Dublin City University, Glasnevin, Dublin 9, Ireland

Photopolymerization of a high internal phase emulsion (HIPE) containing a polymerizable ATRP initiator resulted in polyHIPE with ATRP initiator groups on the surface available for polymer grafting reactions. This was initially shown for the grafting of MMA. Further functionalization of the polyHIPE was obtained by the grafting of glycidyl methacrylate (GMA). The macroporous morphology and the up to 800 nm thick grafted pGMA layer was clearly visible in SEM micrographs. Epoxide ring-opening reactions of the epoxide groups with sodium azide yielded near quantitative azidation of the PGMA layer. Under optimized conditions, azide conversions of around 80 % were estimated from IR. Further modification was achieved by Huisgens-type 'click' chemistry with various alkynes, for example amino acids and a fluorescent alkyne. Moreover, amino functional silica microparticles were attached to the PGMA modified pHIPE.

## Introduction

Atom transfer radical polymerization (ATRP) is one of the most versatile methods for polymer grafting from solid supports (1-8) due to its tolerance towards many reaction conditions and the large array of monomers that can be used (9-11). We investigated ATRP for the surface modification of macroporous polymers obtained from high internal phase emulsions (HIPE). These HIPE materials are defined by an internal or droplet phase volume ratio of 0.74 or higher (i.e. the minimum volume of the emulsion comprised of droplets is 74%). Polymerization of a monomeric continuous phase of a HIPE leads to a highly porous cross-linked polymer material resulting in foams that have a well structured morphology, void size and interconnecting window size. Generally, the system is composed of an organic (continuous) phase containing a monomer such as styrene, a suitable emulsifier, an aqueous (dispersed) phase containing the radical initiator and a cross-linker, e.g. divinyl benzene. The addition of droplets of the aqueous phase into the organic phase during constant stirring results in a dilute reverse emulsion. Increasing the amount of water in the organic phase results in a concentrated emulsion with thin monomer films surrounding the water droplets (HIPE). Polymerization of HIPE was initially reported by Bartl and von Bonin (12, 13) and considerable advances in this technology were made by Hainey, Sherrington and Cameron (14, 15). A number of articles have discussed how structural features vary as a function of the synthetic conditions (16-20). The predominant work carried out in the synthesis of pHIPE involves thermal curing of styrenic systems (21). More recently, Pierre *et al.* have reported photopolymerization as a beneficial method for a faster and more benign polymerization (22).

Some investigated application areas for pHIPEs include ion-exchange resins (23), membrane filters for the removal of particulates from aerosol (24), solid phase peptide supports (25), supports for cells and enzymes (26, 27), and as materials for the removal of heavy metals (28, 29). All these applications require surface functionalization of the pHIPE, which can be achieved by the addition of a functional monomer to a HIPE formulation or by surface modification after cross-linking. While the first approach is limited by the stability of the HIPE (hydrophilic monomers destabilize the emulsion), the second approach has to rely on the chemistry possible with the pHIPE building blocks. Both approaches have also limitations in the density of functional groups which can be introduced.

The ability to conveniently modify pHIPE surfaces with a high density of functional groups is crucial to opening new application areas. An effective and versatile approach to this is surface grafting of polymer chains. Stable polymer brushes covalently attached to a surface possess excellent chemical and mechanical robustness as well as the flexibility to introduce a large variety of other functional monomers. Our strategy to highly functional pHIPE is shown in Figure 1. An ATRP initiator with polymerizable group (inimer) is added to the HIPE formulation. After UV-curing, ATRP is initiated from the pHIPE surface to obtain densely packed polymer brushes. By the right choice of functional monomers, further functionalization by a secondary reaction will be possible.

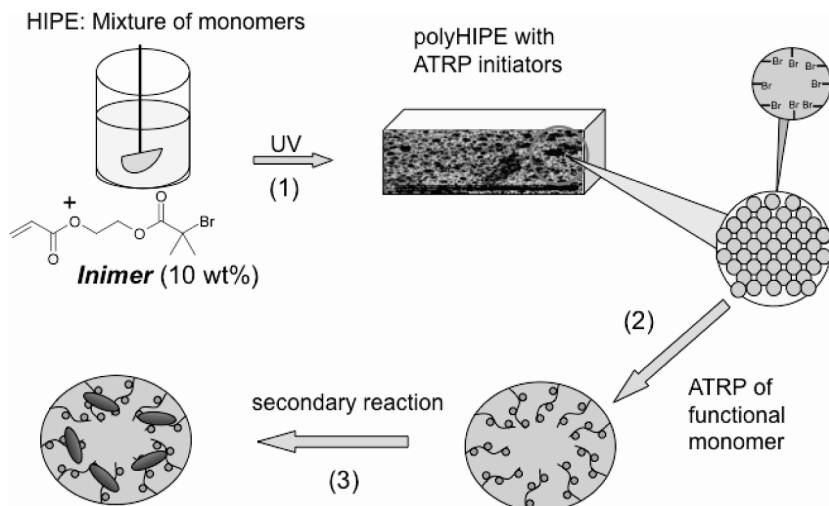


**Figure 1.** Synthesis of functional pHIPE in two steps: (1) formation of stable high internal phase emulsion (HIPE) in the presence of the inimer and UV curing to obtain pHIPE with ATRP initiator groups (I-pHIPE). (2) Grafting of MMA and GMA by ATRP from I-pHIPE surface. (3) Secondary reaction on the functional surface grafts.

## Experimental

The synthesis of the ATRP initiator functionalized pHIPE, the conditions for the ATRP grafting and the click reactions has been described previously (30, 31).

### *Modification of pHIPE-g-PGMA with silica microparticles*

Samples of control (non-functionalized) pHIPE and pHIPE-GMA were added to vials containing 15% w/w modified silica microparticles in methanol and THF. 10 drops of conc. HCl were added to each vial and the reactions were allowed to run for 16 hours. Two types of silica particles were used: (1) 3  $\mu\text{m}$  spherical Si-Amine ( $\text{Si}(\text{C}_3\text{H}_6)\text{NH}_2$ ), and (2) 3  $\mu\text{m}$  spherical Si-Thiol ( $\text{Si}(\text{C}_3\text{H}_6)\text{SH}$ ). After the reaction time the samples were placed in a sonicator for 1 h to remove any unbound Si particles.

## Results and Discussion

### Synthesis of polyHIPE materials with ATRP initiator

The pHIPE material used was prepared in a bulk amount by photo-polymerization of a HIPE containing the ATRP inimer (denoted I-pHIPE) (30). To enable comparison studies, a control pHIPE was also prepared which did not contain any ATRP initiator. This control was used in all experiments.

SEM images recorded after the polymerization of the HIPE (Figure 2) show the highly porous material (approximately 90% porosity based on the formulation). From these images, the average diameter of the pores was estimated to be approximately 25  $\mu\text{m}$ . Adjacent pores are interconnected by windows which were visually estimated to have an average diameter of 8  $\mu\text{m}$ . What is also apparent here is the presence of extremely small pores in an almost uniform pattern around the larger windows (white arrow in Figure 2). The reason for the formation of these pores is unknown yet but they are important for three reasons. Firstly, they give an indication of the thickness of the wall; secondly, they give an indication as to the strength of the wall as they are not consumed by the larger windows; and thirdly, due to the almost perfect alignment around the windows, they are most likely a result of the polymerization. Also observed is a divot like effect on the surface of the matrix walls which is a consistent character of the pHIPE samples prepared.

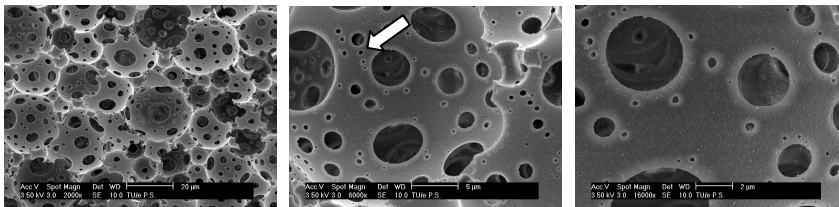


**Figure 2.** Scanning electron microscopy (SEM) images of I-pHIPE. Scale bar (left) = 20  $\mu\text{m}$ , (middle) = 5  $\mu\text{m}$ , (right) = 2  $\mu\text{m}$ .

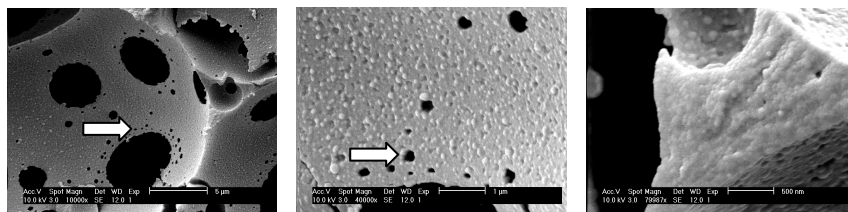


**Figure 3.** SEM images of *p*(HIPE-*g*-MMA); showing a distinct difference in the surface morphology of the matrix. Scale bar (left) = 5  $\mu\text{m}$ , (middle) = 1  $\mu\text{m}$ , (right) = 500 nm. (Reproduced from reference 30. Copyright 2007 American Chemical Society.)

### ATRP from pHIPE

Inspired by the work of Moine *et al.* who reported initial work on ATRP from thermally cured styrene based pHIPE (32), we investigated whether the advantages of fast acrylate UV-curing for pHIPE formation could be combined with ATRP surface grafting.

Efficient surface ATRP in polar solvents like methanol and water has been reported by Huck *et al.* (33, 34). They proposed that the activity of the catalyst is increased by the high dielectric constant of the solvent. The conditions allow for rapid polymerizations and lead to high layer thicknesses without the addition of sacrificial initiator (1). We adopted this method for our ATRP reactions from the I-pHIPE surfaces allowing us to maintain reaction control while rapidly grafting water insoluble polymers from the pHIPE. In order to exhibit the availability of the ATRP groups for grafting, we first used MMA as the monomer. Typically soft and rubbery I-pHIPE samples (0.5-1.0  $\text{cm}^3$ ) were added to the reaction mixture. Upon completion, the recovered pHIPE was brown in colour due to the absorption of the copper catalyst. Intensive washing with suitable solvents to remove ungrafted polymer and EDTA to remove all catalyst, yielded a white polymer functionalised pHIPE. The first indication of a successful modification is that the material had become more brittle. Characteristic signals of the PMMA could also be identified in the IR spectra of the obtained product (30).

SEM analysis provided stronger evidence for the grafting success. Figure 3 shows the images of the change in surface morphology due to the presence of polymer on the surface. When compared with the corresponding image in Figure 2, the overall porosity of the monolith has been preserved with little change between these samples and the precursors. This shows that the pHIPE can be washed thoroughly after grafting and that the monolith porosity remains intact. Notably, a change in surface roughness is observed and the divots present in the blank sample are now surrounded by smaller mounds. Also notable is that the small pores circling the windows are still visible. However, it is not possible from these images to determine the homogeneity and thickness of the grafted polymer layer.

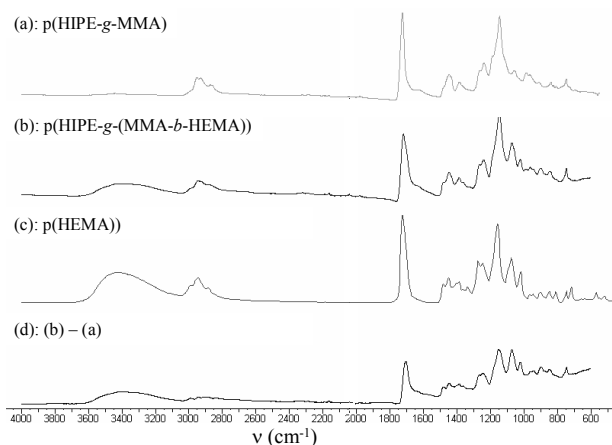


**Figure 4.** Infrared absorption spectra showing in descending order: (a) *p*(HIPE-*g*-MMA); (b) *p*(HIPE-*g*-MMA) after ATRP of HEMA (block copolymerization); (c) *p*(HEMA); and (d) spectrum resulting from the subtraction of (a) from (b). (Reproduced from reference 30. Copyright 2007 American Chemical Society.)

Further evidence for the grafting of the detected pMMA was provided by the fact that: **(i)** polymerization of MMA was not observed when I-pHIPE was used in the absence of ATRP catalysts; **(ii)** polymerization of MMA was not observed when the same reaction was carried out using control pHIPE without ATRP initiator, and **(iii)** when an ATRP reaction was conducted with free ATRP initiator in solution in the presence of a pHIPE, polymerization occurred in solution but not in the pHIPE. After polymerization of the MMA, the monolith went through the same washing procedure and although the reaction clearly produced PMMA, no corresponding signal was detected by IR for the pHIPE. This confirms the efficiency of the washing process and supports the conclusion that the PMMA is grafted from the pHIPE surface.

The ability to re-initiate further polymerization from the p(HIPE-*g*-MMA) was investigated with hydroxyethylmethacrylate (HEMA) to yield p(HIPE-*g*-(PMMA-*b*-PHEMA)). IR analysis revealed the presence of an O-H vibrational stretch at 3400 cm<sup>-1</sup> corresponding to the hydroxy group of the HEMA and confirming the presence of p(HEMA) on the surface (Figure 4). When compared to the precursor, changes in the fingerprint region of this sample provide further evidence for the grafting of the HEMA and compare well with results reported by Brantley (35).

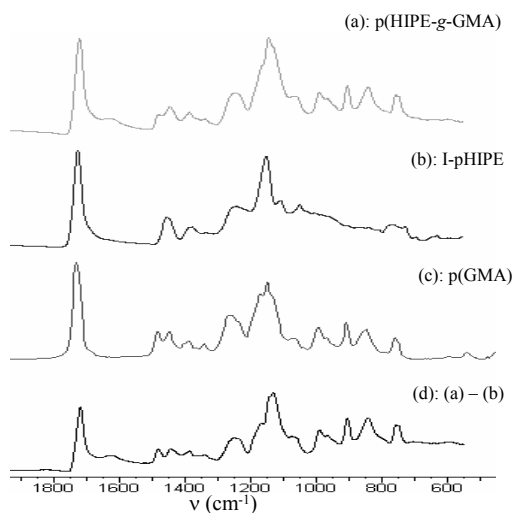


**Figure 5.** Infrared absorption spectra showing in descending order: (a) spectrum of pHIPE after GMA grafting; (b) I-pHIPE; (c) p(GMA) (from unbiased data base); and (d) spectrum resulting from the subtraction of (b) from (a). (Reproduced from reference 30. Copyright 2007 American Chemical Society.)

### Functionalization of pHIPE by ATRP grafting of glycidyl methacrylate (GMA)

A major benefit of the grafting of GMA from the pHIPE is the high density of reactive functionalities available for ring-opening of the epoxide group, e.g. carboxylic acids, alcohols, water or amines all yield a versatile platform for the further attachment of other functional materials. After the ATRP of GMA, the modified pHIPE became even more brittle than that with PMMA verifying that a reaction had occurred. IR analysis of the resulting p(HIPE-g-GMA) revealed the presence of the epoxide groups in the fingerprint region at around  $900\text{--}800\text{ cm}^{-1}$ . The presence of the band at  $904\text{ cm}^{-1}$  confirms that the epoxide rings remain closed confirming that they are unaffected by the reaction conditions used (Figure 5). As no free monomer or polymer existed in the network after the washing process, the change in the IR spectrum is attributed to the grafted pGMA polymer.



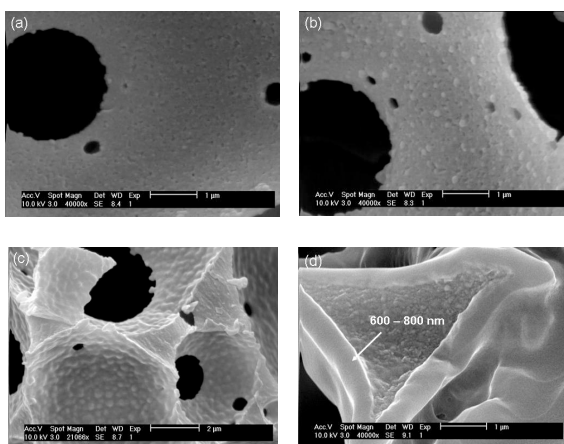


**Figure 6.** SEM images showing the polyGMA growth on the surface of pHIPE after (a) 3, (b) 5, (c) 16 and (d) 24 hours polymerization times.

In order to determine the change of surface morphology due to the GMA layer growth as a function of reaction time, samples were removed from the reaction after 1, 3 5, 16 and 24 hours. The samples were worked up in the standard manner and then examined using SEM (Figure 6). The results clearly show that up to the first three hours there is no evidence of polymer growth. However between three and five hours, small pockets of islands begin to appear. These islands suggest that the ATRP initiator is not uniformly distributed across the surface. After 16 hours the polymer layer has grown and is shown to cover the entire surface. The small windows that surrounded the larger windows before polymerization have now disappeared due to being covered and filled with PGMA. After 24 hours a 600 – 800 nm thick PGMA layer is clearly visible as a homogenous, uniform layer. The control pHIPE (without ATRP initiator) was added to a solution based ATRP reaction of GMA, under the same conditions as the functionalisations reaction but remained unmodified with polymerization of the GMA in solution only and not in the matrix. The rapid polymer growth of the GMA, in comparison to the MMA is in agreement with reports from Huck, who attributed this effect to the copper catalyst coordination with the epoxide group of the GMA, resulting in the displacement of the ligand and increasing the activity of the catalyst (1). While further functionalization experiments using the glycidyl groups confirm that they are fully intact after the polymerization, it cannot be excluded that partial cross-linking of the PGMA via the epoxy groups occurs in the graft layer.

### Secondary functionalization of p(HIPE-g-GMA) by ‘click’ reactions

Huisgen 1,3-dipolar cycloaddition (click reaction) between terminal alkynes and azides is a highly efficient approach for the post modification of polymers. This technique is tolerant to a wide range of reaction conditions and functional groups allowing fast coupling reactions under simple reaction conditions with

high yields and high selectivity (36-39). The use of Cu(I) catalysts further accelerates the process leading to quantitative coupling yields at 25 °C (40). These reactions have been highlighted in a number of material science applications recently (41, 42) e.g., the preparation of highly functionalized macromolecules (43 - 48) as well as in the surface immobilization of biomacromolecules (49 - 55). and the functionalization of self-assembled monolayers (SAMs) (56-60).

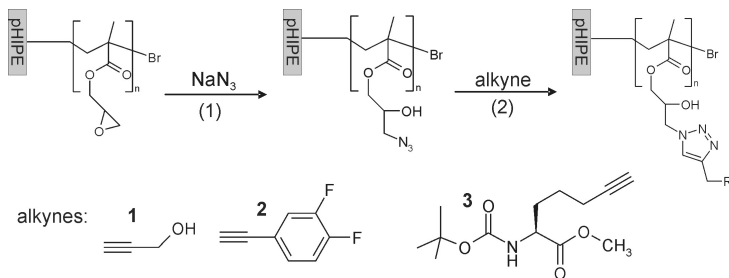


**Figure 7.** Schematic representation of the modification of macroporous pHIPE by click reactions; (1) formation of azide modified pHIPE by nucleophilic ring opening of epoxide groups on pGMA grafted pHIPE. (2) Click reactions with alkyne functional molecules. (Adapted from reference 31 by permission of The Royal Society of Chemistry.)

The azide functionalised pHIPE- $\text{N}_3$  was obtained by nucleophilic ring-opening of the epoxy-rings on the pHIPE by sodium azide (44). The appearance of a typical azide IR band at  $2100\text{ cm}^{-1}$  confirms the presence of the azide on the pHIPE. Click reactions were then conducted with different alkyne functionalized molecules (31). Special attention was given to assure that the reaction occurred throughout the three-dimensional morphology of the microporous substrates. Optimization of the reaction conditions for the ‘click’ reactions was performed using the small, non-bulky propargyl alcohol molecule **1** (Figure 7). The best results were obtained when the click reaction was carried out in the presence of Cu(I) at 55 °C in which case an almost equal reduction of the azide band of the internal and external pHIPE surface of 75 - 83 % was observed (with respect to carbonyl band). While the reaction also proceeds at room temperature, lower conversion and in the absence of Cu (I) even a distinct difference between the interior (33 %) and the exterior (67 %) of the pHIPE was observed. In the absence of propargyl alcohol, under otherwise identical conditions with pHIPE- $\text{N}_3$ , no reduction of the azide band was observed (31). The high conversions of the azide under optimized conditions suggest that functionalization must have occurred throughout the layer of the original pGMA surface layer on the pHIPE. It further shows that a homogeneous functionalization depends on geometry related parameters by its influence on mass transport through the macroporous material. This will be more significant for the functionalization of larger samples like monoliths for bioseparation.

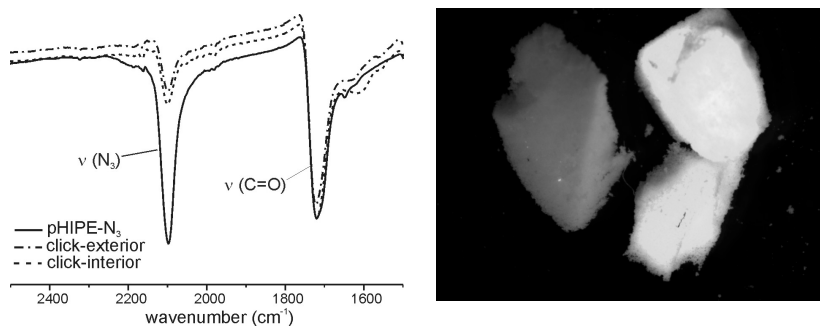


**Figure 8.** Left: ATR-FTIR transmittance spectra of pHIPE- $N_3$  before and after 'click' reaction with **1** (catalyst: Cu (I); 55 °C). Spectra show the reduction of the azide peak ( $\nu(N_3)$ ) in the exterior (click exterior) and the interior (click interior) of the pHIPE normalized against the polyacrylate of the pHIPE ( $\nu(C=O)$ ). Right: Fluorescent microscope image of control-pHIPE (left, no azide groups) and pHIPE- $N_3$  (right) after reaction with **2** and washing. The latter is cut in half showing the interior of the pHIPE. (Reproduced from reference 31 by permission of The Royal Society of Chemistry.)

The success of the click reaction was further visualized by attachment of 3,4-difluorophenylacetylene (DFA) **2** at 55°C. Fluorescent microscope pictures taken of the DFA modified pHIPE monolithic samples cut in half are shown in Figure 8 (right). The image clearly shows that the DFA modified material is highly fluorescent throughout the sample, while the control is not. This also confirms the efficiency of the washing procedure removing all unbound DFA. SEM analysis shows that the surface roughness of the samples has changed following the reaction (Figure 9).

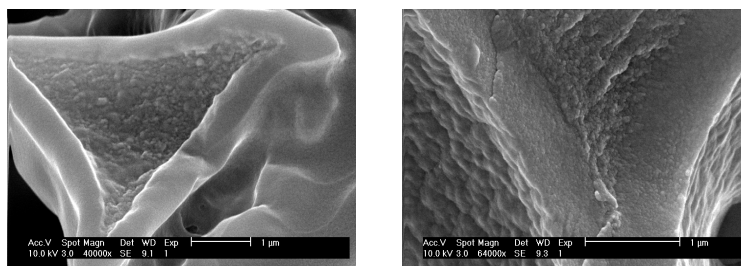


**Figure 9.** SEM images showing the surface morphology of pHIPE- $N_3$  before (left) and after (right) the 'click' reaction with **1**. (Reproduced from reference 31 by permission of The Royal Society of Chemistry.)

Moreover, we attached a number of amino acids via a pendant alkyne group. Commonly the attachment of amino acids to solid substrates is done via amide bond formation using the amino group of the amino acid. Since these amide bonds are highly susceptible to enzymatic degradation, a non-proteinogenic form of amino acids was prepared. Incorporation of an alkyne group enabled the reaction with an azide, effectively mimicking the amide bond (amide isostere) and forming a triazole ring. It has been shown that the biological activity of these amino acids, for example in glycopeptides, remained the same while the proteolytic degradation of the biological systems was inhibited (61). Using this method to successfully attach amino acids results in a biofunctional pHIPE with improved long term stability with both N- and C-terminus available for further modification or interaction.

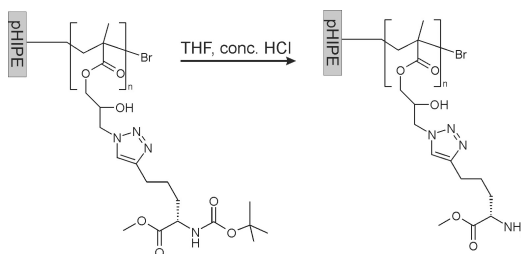


**Figure 10.** Deprotection of amino acid **3** attached to pHIPE. (Reproduced from reference 31 by permission of The Royal Society of Chemistry.)

As an example the attachment of **3** is shown. From IR analysis a 70 % azide conversion was estimated in the click reaction. Subsequently, the amino acid functionalized pHIPE sample was exposed to hydrochloric acid/THF, with the aim to selectively remove the N-terminal (BOC) protecting group (Figure 10). The success of the click reactions between the pHIPEs and the amino acids and the subsequent deprotection was monitored by  $^{13}\text{C}$  MAS NMR (31). Spectrum 1 in Figure 11 shows the  $^{13}\text{C}$  solid state NMR spectrum of a pHIPE- $\text{N}_3$ . Signals of the pHIPE acrylate matrix and the azide functional pGMA (b, c, d) can be assigned between 10 and 80 ppm and at 180 ppm. In the spectrum of the amino acid modified pHIPE, additional peaks can be identified (Figure 11, spectrum 2). After subtraction of the pHIPE- $\text{N}_3$  spectrum these signals can be assigned to the triazole ring formed upon click coupling and the deprotected amino acid (Figure 11, spectrum 3). For example, the olefinic carbon signals at 125 (e) and 148 ppm (f) are consistent with the triazole structure. Moreover, peaks g-k and m can be assigned to the amino acid attached to the pHIPE. Notably, the carboxy signal in the amino acid (m, 171 ppm) is slightly shifted upfield as compared to the carboxy signal of the polyacrylate matrix (a, 178 ppm), which indicates that the methyl ester protecting group has not been removed. In contrast, the fact that no  $-\text{NH}-\text{C}(\text{O})-\text{O}-$  signal at ca. 160 ppm, nor the quaternary  $^{13}\text{C}$  signal of the t-butoxy group expected around 80 ppm are observed in the spectrum, provides evidence that the BOC protection group has been removed in this reaction step.

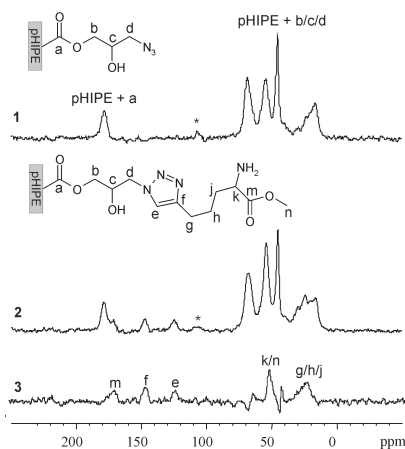


**Figure 11.** Solid-state CPMAS  $^{13}\text{C}$  NMR. 1: spectrum of pHIPE- $\text{N}_3$ ; 2: pHIPE modified with 6 after deprotection of amino acid (Scheme 2); 3: Difference spectrum. \*: spinning sideband. (Reproduced from reference 31 by permission of The Royal Society of Chemistry.)

While these results clearly show, that the triazole ring is formed upon click reaction and that it is stable under amino acid deprotection conditions, further measurements are necessary to quantify the yield of the deprotection reaction.

### Secondary functionalization of pHIPE-PGMA with silica microparticles

The increase in surface area of the pHIPE is important to open up new application areas. One approach is to attach spherical particles to the surface of the monolithic material. This has been, for example achieved by electrostatic interaction between charged latex nanoparticles and a monolithic surface (62). In preliminary experiments we investigated if functional silica microparticles could be covalently adsorbed to the p(HIPE-g-GMA) surface so as to produce stable, functional pHIPE with an increased surface area.

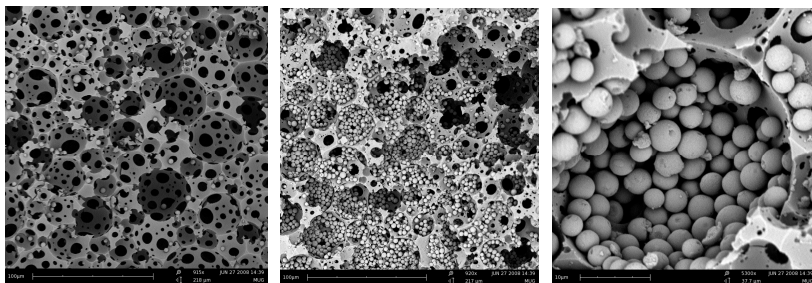


**Figure 12.** SEM images of pHIPE without PGMA graft layer (left: 100  $\mu\text{m}$ ) and p(HIPE-g-GMA) after reaction with amine functionalized Si particles (middle: scale bar 100  $\mu\text{m}$ ; right: scale bar 10  $\mu\text{m}$ ).

To achieve this, samples of unmodified pHIPE (without PGMA) and p(HIPE-g-GMA) were reacted with 3  $\mu\text{m}$  spherical Si-amine ( $\text{Si}(\text{C}_3\text{H}_6)\text{NH}_2$ ) functionalized particles. After the reaction, the samples were placed in a sonicator for 1 h to remove any unbound Si particles. SEM analysis of the Si-amine reaction clearly shows the difference between the control pHIPE and the p(HIPE-g-GMA) after the reaction. In the control almost all silica particles have been removed as they are not covalently bound to the surface (Figure 12). However in the functionalized pHIPE sample there is a high density of Si-Amine particles in the pores of the pHIPE which must be attached via the epoxy group. It should also be noted that the images have been made of the interior of the pHIPE samples after the reaction samples were sliced. This shows that the mass transport has occurred. The image on the right furthermore suggests that a monolayer of silica particles on the inside wall of the pore has been formed. Similar results were observed for the Si-thiol functionalized particles (not shown here). Currently measurements to determine the surface area are under way. While the modification with the functional particles needs to be further optimized, this approach has the advantage that not only the surface area of the pHIPE can be increased but at the same time highly useful functional groups ( $\text{NH}_2$  and  $\text{SH}$ ) are introduced.

## Conclusion

We have shown that an ATRP initiator group can be chemically incorporated into an acrylate based pHIPE formulation without compromising the emulsion stability. UV-curing of this formulation lead to pHIPE with ATRP initiator groups on the surface available for polymer grafting reactions. The latter was demonstrated by first grafting of pMMA and re-initiation of HEMA in a block copolymerization approach. Moreover, functionalized polyHIPE was obtained by the grafting of GMA. This resulted in a 600-800 nm smooth and homogeneous surface coverage of the pHIPE surface with a high density of reactive epoxy groups. These materials can be used as a platform for further functionalization as has been demonstrated by the attachment of alkynes via 'click' chemistry and amine functional silica microparticles.

## References

1. Jones, D. M.; Huck, W. T. S., *Adv. Mater.*, **2001**, 13, (16), 1256.
2. Matyjaszewski, K.; Dong, H.; Jakubowski, W.; Pietrasik, J.; Kusumo, A., *Langmuir*, **2007**, 23, 4528.
3. Huang, X.; Wirth, M. J., *Macromolecules*, **1999**, 32, 1694.
4. Matyjaszewski, K.; Miller, P. J.; Shukla, N.; Immaraporn, B.; Gelman, A.; Luokala, B. B.; Siclovan, T. M.; Kickelbick, G.; Vallant, T.; Hoffmann, H.; Pakula, T., *Macromolecules*, **1999**, 32, 8716.
5. Shah, R. R.; Mecerreyes, D.; Husemann, M.; Rees, I.; Abbott, N. L.; Hawker, C. J.; Hedrick, J. L., *Macromolecules*, **2000**, 33, 597.
6. Kim, J. B.; Bruening, M. L.; Baker, G. L., *J. Am. Chem. Soc.*, **2000**, 122, 7616.
7. Zhoa, B.; Brittain, W. J., *Macromolecules*, **2000**, 33, 8813.

8. Edmondson, S., Osborne, V.L., Huck, W.T.S., *Chem. Soc. Rev.*, **2004**, 33, 14.
9. Nicolas, J; Mantovani, G; Haddleton, D.M., *Macromol. Rapid Commun.*, **2007**, 28, 1083-1111.
10. Limer, A.; Haddleton, D.M., *Macromolecules*, **2006**, 39, 1353
11. Boyes, S.G., Brittain, W.J., Weng, X., Cheng, S.Z.D., *Macromolecules*, **2002**, 35, 4960.
12. Bartl, H.; von Bonin, W., *Makromol. Chem.*, **1962**, 57, 74.
13. Bartl, H.; von Bonin, W., *Makromol. Chem.*, **1963**, 66, 151.
14. Hainey, P.; Huxham, I. M.; Rowatt, B.; Sherrington, D. C., *Macromolecules*, **1991**, 24, 117.
15. Cameron, N. R.; Sherrington, D. C., *Adv. Polym. Sci.*, **1996**, 126, 163.
16. Willilams, J. M., *Langmuir*, **1988**, 4, 44.
17. Willilams, J. M.; Wroblewski, D. A., *Langmuir*, **1988**, 4, 656.
18. Kranjc, P.; Leber, N.; Brown, J. F.; Cameron, N. R., *React. Funct. Polym.*, **2006**, 66, 81.
19. Barbetta, A.; Cameron, N. R., *Macromolecules*, **2004**, 37, 3188.
20. Barbetta, A.; Cameron, N. R., *Macromolecules*, **2004**, 37, 3202.
21. Moine, L.; Deleuze, H.; Maillard, B., *Tetrahedron Letters*, **2003**, 44, 7813.
22. Pierre, S. J.; Thies, J. C.; Dureault, A.; Cameron, N. R.; Hest, J. C. M. v.; Carette, N.; Michon, T.; Weberskirch, R., *Adv. Mater.*, **2006**, 18, 1822.
23. Wakeman, R. J.; Bhungara, Z. G.; Akay, G., *Chem. Eng. J.*, **1998**, 70, 133.
24. Akay, G.; Bhungara, Z. G.; Wakeman, R. J., *Chem. Eng. Res. Des.*, **1995**, 73, 782.
25. Small, P. W.; Sherrington, D. C., *J. Chem. Soc. Chem. Commun.*, **1989**, 1589
26. Ruckenstein, E.; Wang, X.-B., *Biotech. Bioeng.*, **1994**, 44, 79.
27. Ruckenstein, E.; Wang, X., *Biotech. Bioeng.*, **1993**, 42, 821.
28. Benicewicz, B. C.; Jarvinen, G. D.; Kathios, D. J.; Jorgensen, B. S., *J. Radioanal. Nucl. Chem.*, **1998**, 235, 31.
29. Alexandratos, S. D.; Beauvais, R.; Duke, J. R.; Jorgensen, B. S., *J. Appl. Polym. Sci.*, **1998**, 68, 1911.
30. Cummins, D.; Wyman, P.; Duxbury, C. J.; Thies, J.; Koning, C. E.; Heise, A. *Chem. Mater.* **2007**, 19, 5285
31. Cummins, D.; Duxbury, C.J; Quaedflieg, P. J. L. M.; Magusin, P. C. M. M.; Koning, C. E.; Heise, A. *Soft Matter*, in press, DOI:10.1039/b810823d
32. Moine, L.; Deleuze, H.; Maillard, B., *Tetrahedron Letters*, **2003**, 44, 7813.
33. Edmondson, S.; Huck, W.T.S., *J. Mater. Chem.*, **2004**, 14, 730
34. Osborne, V.L.; Jones, D.M.; Huck, W.T.S., *Chem. Commun.*, **2002**, 1838.
35. Brantley, E.L.; Jennings, G.K., *Macromolecules*, **2004**, 37, 1476.
36. Kolb, H.C.; Finn, M.G.; Sharpless, K.B. *Angew. Chem. Int. Ed.* **2001**, 40, 2004.
37. Bock, V.D.; Hiemstra, H.; van Maarseveen, J.H. *Eur. J. Org. Chem.* **2006**, 51.
38. Huisgen, R. *1,3-Dipolar Cycloaddition Chemistry*, (Ed.: A. Padwa), Wiley, NY, 1984, pp. 1-176.
39. Hawker, C.J.; Wooley, K.L. *Science* **2005**, 309, 1200.

40. Tornøe, C.W.; Christensen, C.; Meldal, M. *J. Org. Chem.* **2002**, *67*, 3057.
41. Nandivada, H.; Jiang, X.; Lahann, J. *Adv. Mater.* **2007**, *19*, 2197.
42. O'Reilly, R.K.; Joralemon, M.J.; Wooley, K.L.; Hawker, C.J. *Chem. Mater.* **2005**, *17*, 5976.
43. Malkoch, M.; Schleicher, K.; Drockenmüller, E.; Hawker, C.J.; Russell, T.P.; Wu, W.; Fokin, J.J. *Macromolecules* **2005**, *38*, 3663.
44. Tsarevsky, N.V.; Bencherif, S.A.; Matyjaszewski, K. *Macromolecules* **2007**, *40*, 4439.
45. Lutz, J.-F.; Boerner, H.G.; Weichenhan, K. *Macromolecules* **2006**, *39*, 6376.
46. Geng, J.; Mantovani, G.; Tao, L.; Nicolas, J.; Chen, G.; Wallis, R.; Mitchell, D.A.; Johnson, B.R.G.; Evans, S.D.; Haddleton, D.M. *J. Am. Chem. Soc.* **2007**, *129*, 15156.
47. Srinivasachari, S.; Liu, Y.M.; Zhang, G.D.; Pevette, L.; Reineke, T.M. *J. Am. Chem. Soc.* **2006**, *128*, 8176.
48. Thibault, R.J.; Takizawa, K.; Lowenheilm, P.; Helms, B.; Mynar, J.L.; Frechet, J.M.J.; Hawker, C.J. *J. Am. Chem. Soc.* **2006**, *128*, 12084.
49. Seo, T.S.; Li, Z.; Ruparel, H.; Ju, J. *J. Org. Chem.* **2003**, *68*, 609.
50. Link, A.J.; Mock, M.L.; Tirell, D.A. *Curr. Opin. Biotechnol.* **2003**, *14*, 603.
51. Parrish, B.; Breitenkamp, R.B.; Emrick, T. *J. Am. Chem. Soc.* **2005**, *127*, 7404.
52. Whiting, M.; Muldoon, J.; Lin, Y.C.; Silverman, S.M.; Lindstrom, W.; Olson, A.J.; Kolb, H.C.; Finn, M.G.; Sharpless, K.B.; Elder, J.H.; Fokin, V.V. *Angew. Chem. Int. Ed.*, **2006**, *45*, 1435.
53. Slater, M.; Snauko, M.; Svec, F.; Frechet, J.M.J. *Anal. Chem.* **2006**, *78*, 4969.
54. Zhang, Y.; Luo, S.Z.; Tang, Y.J.; Yu, L.; Hou, K.Y.; Cheng, J.P.; Zeng, X.Q.; Wang, P.G. *Anal. Chem.* **2006**, *78*, 2001.
55. White, M.A.; Johnson, J.A.; Koberstein, J.T.; Turro, N.J. *J. Am. Chem. Soc.* **2006**, *128*, 11356.
56. Collman, J.P.; Devaraj, N.K.; Chidsey, C.E.D. *Langmuir* **2004**, *20*, 1051.
57. Devaraj, N.K.; Miller, G.P.; Ebina, W.; Kakaradov, B.; Collman, J.P.; Kool, E.T.; Chidsey, C.E.D. *J. Am. Chem. Soc.* **2005**, *127*, 8600.
58. Lee, J.K.; Chi, Y.S.; Choi, I.S. *Langmuir* **2004**, *20*, 3844.
59. Lummerstorfer, T.; Hoffmann, H. *J. Phys. Chem. B.* **2004**, *108*, 3963.
60. Sun, X.-L.; Stabler, C.L.; Cazalis, C.S.; Chaikof, E.L. *Bioconjugate Chem.* **2006**, *17*, 52.
61. B. H. M. Kuijpers, P. J. L. M. Quaedflieg; H. C. P. F. Roelen, R. W. Wiertz, R. H. Blaauw, F. P. J. T. Rutjes, *Synthesis* **2006**, *18*, 3146.
62. Hutchinson, Joseph P.; Hilder, Emily F.; Macka, Miroslav; Avdalovic, Nebojsa; Haddad, Paul R. *J. Chromatography A* **2006**, *1109*(1), 10-18.



## Chapter 23

# Systematic Polymeric Libraries via Atom Transfer Radical Polymerization

Wojciech Jakubowski, Nicolay V. Tsarevsky, and Patrick McCarthy

ATRP Solutions Inc., 166 N. Dithridge St. Suite G4, Pittsburgh PA 15213

The unique properties of block copolymers have attracted the interest of R&D scientists across broad market segments, and are expected to play a significant role in improving the performance of numerous commercial products. In order to introduce products based on block copolymers, one needs to establish a relationship between polymer structure and product performance. Easily accessible polymeric libraries will greatly accelerate this process. As an example, the straightforward synthesis of polystyrene-*b*-poly(*t*-butyl acrylate) (PSt-*b*-PtBA) copolymer library (5×5) is presented. ARGET/ICAR ATRP was designed for industrial level synthesis making the final library inexpensive and accessible for companies as well as for academic scientists. This library was then converted to polymeric surfactants polystyrene-*b*-poly(acrylic acid) (PSt-*b*-PAA). Stabilization of Fe<sub>2</sub>O<sub>3</sub> particles with PSt-*b*-PAA block copolymer surfactants was also investigated.

## Introduction

The early stages of the product development cycle require R&D scientists to screen many different polymer compositions for improvements in product performance. These experiments require generating libraries of polymers with varying structures and compositions. Libraries of block copolymers are especially in demand due to the current and potential future high-technology applications of block copolymers such as blend compatibilizers, surfactants, thermoplastic elastomers, drug delivery systems, etc. (1-3). Academic research reports often limited to a narrow range of polymeric samples for structure-property correlation. Tailor made polymeric libraries for product development have not been available until now. This is mostly due to challenging and time-consuming synthetic procedures or lack of full understanding of a particular polymerization technique. This is particularly true in the case of ionic polymerization methods in which preparation of block copolymers is very time consuming due to strict reaction condition requirements.

Controlled radical polymerization (CRP) (4, 5) techniques which were developed in the last decade are much more robust and therefore more suitable for facile synthesis of block copolymers. Atom transfer radical polymerization (ATRP) (6-9) is an especially powerful CRP technique which allows preparation of a wide range of well-defined block copolymers using mild conditions (10). An inherent feature but also a limitation of ATRP is the presence of a catalyst – a transition metal complex. The added expense associated with purifying any polymers generated during the ATRP process prevents this technique from being widely used in industry. Another problem with existing ATRP, as in any radical process, is that the reaction has to be carried out in rigorously deoxygenated systems to prevent trapping of propagating radicals by oxygen and hence waste of initiators and catalyst.

Recent research has resulted in the development of ATRP initiation systems that alleviates these problems. These new systems called ARGET (Activators ReGenerated by Electron Transfer) (11, 12) and ICAR (Initiators for Continuous Activator Regeneration) (13) ATRP allow a decrease in the amount of catalyst needed from 10,000 ppm to 10 ppm or less, where its removal or recycling would be unwarranted for most industrial applications (Figure 1a, 1b). Furthermore, ARGET/ICAR ATRP can be performed in the presence of limited amounts of air (14) and produce polymers with higher attainable molecular weight (15-17) and with higher chain end functionality (17) compared to the normal ATRP process. Moreover, it was demonstrated that the polydispersity of homopolymers as well as individual segments in block copolymers can be effectively controlled by adjusting the amount of catalyst in the ARGET/ICAR ATRP systems (18). Thus, these new techniques make the generation of block copolymer libraries much more feasible and inexpensive.

The main goal of this work was to synthesize a block copolymer library using the new ARGET/ICAR ATRP systems. As an example, a library of PSt-*b*-PtBA was selected covering a wide range of molecular weights and compositions (Figure 1c). This 5×5 library was transformed to PSt-*b*-PAA block copolymers which were extensively studied and widely used as polymeric surfactants (19). As an example, stabilization of Fe<sub>2</sub>O<sub>3</sub> particles with these block copolymer surfactants was investigated.

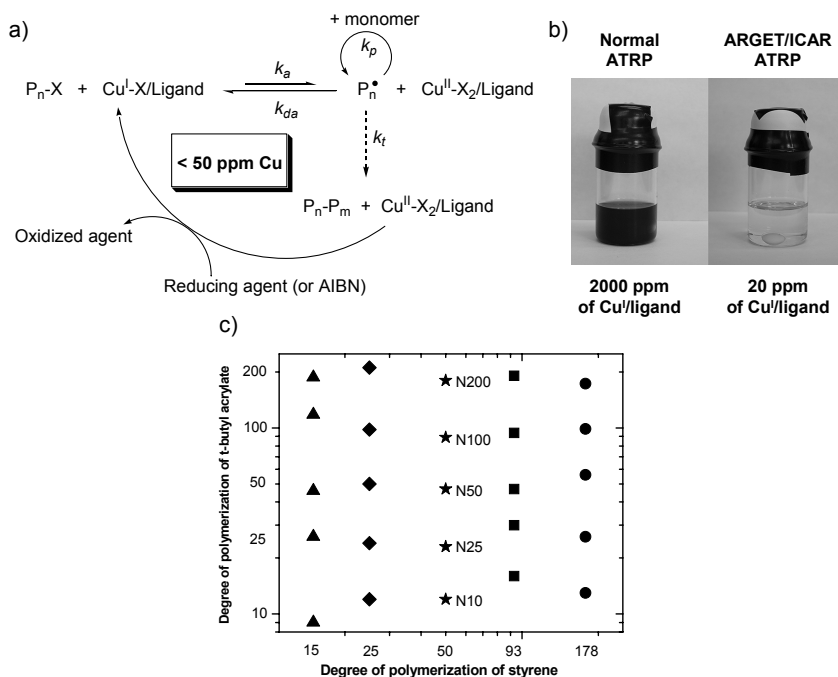


Figure 1. a) Mechanism for ARGET (and ICAR) ATRP where  $Cu^I$  activator is constantly regenerated by environmentally acceptable reducing agents (e.g. FDA approved compounds, sugars etc.) or organic radicals, b) appearance of reaction mixtures containing typical catalyst concentration used in normal and ICAR/ARGET ATRP and c) “map” of PSt-*b*-PtBA block copolymer library synthesized in this work.

## Results and Discussion

### Synthesis of Polystyrene (PSt) Macroinitiator via ICAR ATRP

A high proportion of living chains in the macroinitiator is required for the preparation of well-defined block copolymers. The synthesis of PSt macroinitiator with high chain-end functionality via normal ATRP is challenging due to side reactions such as  $\beta$ -H elimination (20). These side reactions are catalyzed by CuX/ligand complex and a significant reduction in terminal functionality for PSt can be observed, especially at high conversions (20, 21). The utilization of ICAR ATRP allows to decrease the amount of side reactions due to low Cu/ligand content and produce PSt macroinitiator with high chain-end functionality (17). Figure 2 presents the kinetic plot and evolution of molecular weights and polydispersities with conversion for polymerization of St with 50 ppm of  $CuBr_2/Me_6TREN$  catalyst in the presence of AIBN as reducing agent. Molecular weight control was excellent and followed theoretical values based on quantitative initiation. Due to high scale of synthesis (1 L), inhibitor was not removed from St monomer. This is the first example of successful ICAR ATRP of unpurified monomer.

Removal of the ATRP catalyst from the polymer is important for many commercial applications (8, 22). Thus, the polymerization solution with PSt macroinitiator was mixed with ATRP $_{\text{pure}}$  resin (10 wt % of resin vs. polymer) and stirred overnight in order to remove most of the residual amount of the catalyst. The copper catalyst was mostly removed from the polymer solutions using ATRP $_{\text{pure}}$  resin indicated by complete disappearance of a slightly greenish color from the  $\text{CuBr}_2/\text{Me}_6\text{TREN}$  complex. The solution was easily decanted from the resin and precipitated into hexane. The measurement by inductively coupled plasma mass spectroscopy (ICP-MS) revealed that after such a purification method, the concentration of Cu decreased one hundred times to only 0.5 ppm. A similar procedure was successfully applied in the synthesis of PSt with other degrees of polymerization ( $\text{DP}_n=10, 20, 100$  and  $200$ ) in order to generate a full polymeric library (Figure 1c). All of these results show industrial scalability of the ICAR ATRP process.

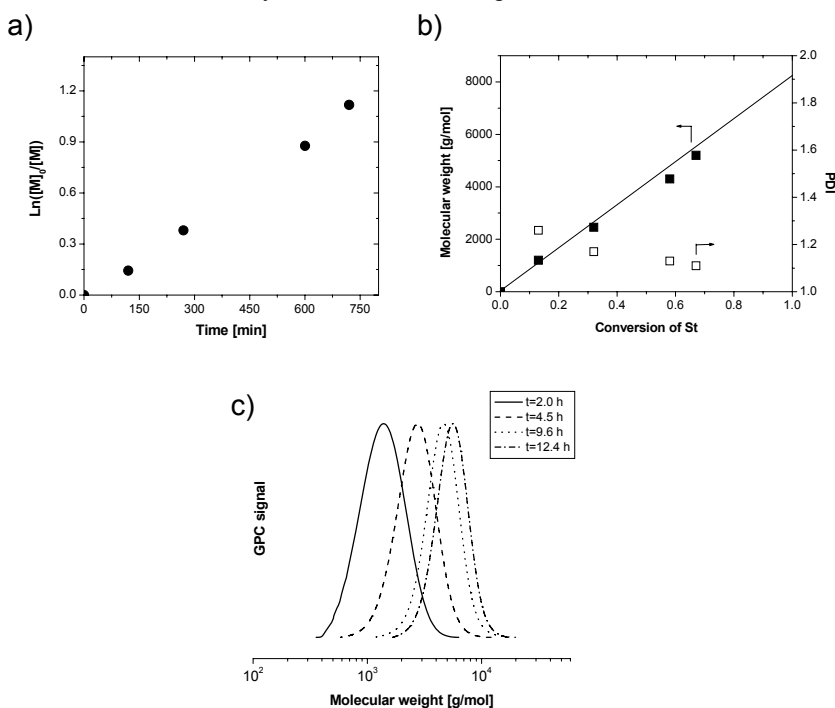


Figure 2. a) Kinetic plot, b) molecular weights and polydispersities as a function of conversion and c) evolution of GPC traces during ICAR ATRP of St.

Experimental conditions: St/DEBMM/ $\text{CuBr}_2/\text{Me}_6\text{TREN}/\text{AIBN} = 80/1/0.004/0.004/0.15$ , in bulk at  $70^\circ\text{C}$ .

### Synthesis of Polystyrene-*b*-Poly(*t*-Butyl Acrylate) (PSt-*b*-P*t*BA) via ARGET ATRP

The ARGET ATRP method was chosen for extension of PSt macroinitiator with *t*BA. This technique provides higher control over the polymerization of acrylates than ICAR ATRP (13, 23). It uses  $\text{Sn}(\text{EH})_2$  or other non-radical

reducing agents instead of AIBN. All of the polymerizations were carried out with low catalyst concentration ( $< 100$  ppm of Cu) and in the presence of  $\text{Sn}(\text{EH})_2$  as reducing agent. Figure 3 shows GPC traces of all synthesized copolymers from PSt macroinitiator with  $\text{DP}_n = 50$  (samples N on Figure 1c). In all cases, a smooth shift of the entire molecular weight distribution towards higher molecular weights was observed. These results prove that PSt synthesized by ICAR ATRP had high chain-end functionality. After the polymerizations were finished, block copolymers were purified with ATRPpure resin in order to remove residual copper catalyst. In each case the greenish color of the polymer solution disappeared after stirring overnight with the resin.

Table I presents properties of all synthesized copolymers from PSt macroinitiator with  $\text{DP}_n = 50$ . It can be seen that all copolymers have low molecular weight distribution and their molecular weights are close to the theoretical values. Degrees of polymerization calculated by nuclear magnetic resonance (NMR) were very close to those estimated from monomer conversion determined by gas chromatography. These results suggest that ARGET ATRP was controlled and is well suited for the synthesis of block copolymers. A similar approach was used to synthesize other PSt-*b*-PtBA for the 5×5 polymeric library presented on Figure 1c. Overall, 5 different PSt macroinitiators were prepared and next extended with PtBA with targeted  $\text{DP}_n = 10, 25, 50, 100$  and 200. In all cases polymers with narrow and monomodal molecular weight distribution were synthesized covering a wide range of molecular weights and compositions. Due to the straightforward synthesis and simple purification, it was possible to synthesize the polymeric library on a higher scale (100 g samples).

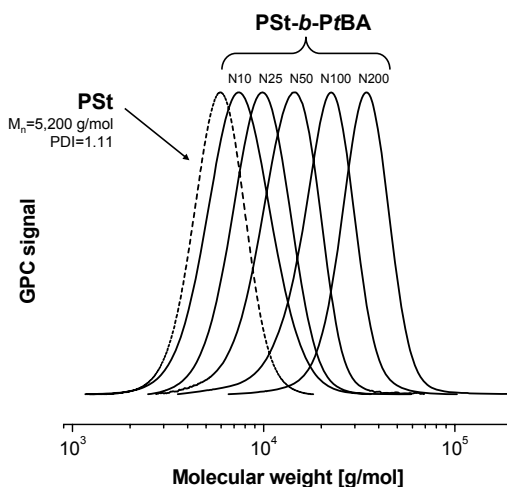


Figure 3. GPC traces of PSt and resulting PSt-*b*-PtBA block copolymers prepared by ARGET ATRP. General experimental conditions:  $t\text{BA}/\text{PSt}/\text{CuBr}_2/\text{TPMA}/\text{Sn}(\text{EH})_2 = 150/1/0.0075/0.05/0.05$ , in anisole (1.0 v/v vs. *t*BA) at 60 °C.

**Table I. Properties of PSt and PSt-*b*-PtBA Prepared by ARGET ATRP.**

Sample name	$M_n$ (Theor)	$M_n$ (GPC)	PDI	$DP_n$ PtBA <sup>b</sup>	$DP_n$ PtBA <sup>c</sup>	Wt% PtBA
PSt <sub>50</sub>	5,500	5,200	1.11	-	-	-
N10	6,700	6,800	1.16	12	12	23
N25	8,400	8,700	1.13	27	23	36
N50	11,300	11,800	1.14	51	47	54
N100	17,100	18,700	1.15	105	89	69
N200	28,100	30,200	1.12	195	180	82

<sup>a</sup>  $M_{n, \text{theor}} = M_{n, \text{PSt}} + ([t\text{BA}]_0 / [\text{DEBMM}]_0) \times \text{conversion} \times M_{\text{monomer}}$ ; <sup>b</sup> calculated with GPC results; <sup>c</sup> calculated with NMR results

### Synthesis of PSt-*b*-PtBA with Varying Molecular Weight Distribution

The influence of the polydispersity index (PDI) of a block copolymer (or one of its blocks) on its properties may be significant (24). The potential impact of polydispersity on block copolymer phase behavior was recognized early on and has been investigated by a variety of theoretical approaches (24-26). These predictions were confirmed experimentally only for bidisperse or multimodal distribution blends by mixing two or more nearly monodisperse copolymers usually prepared by ionic polymerizations (27-32). This is because, no simple polymerization technique allows for the control of polymer molecular weight while simultaneously allowing for variability of molecular weight distribution. Thus, analysis of block copolymers with different, yet continuous molecular weight distribution is of great interest.

ARGET/ICAR ATRP, for the first time, has made possible the simultaneous control of both molecular weight and PDI. It was shown that varying the amount of copper during ARGET ATRP of methyl methacrylate (11), *n*-butyl acrylate (11) and styrene (12) led to polymers that had controlled molecular weights and PDI's from 1.16 to > 2.0. This has opened the door to the synthesis of block copolymers having different PDI of each block (18). Figure 4 presents GPC traces of PSt macroinitiator with narrow molecular weight distribution and resulting PSt-*b*-PtBA block copolymers. The synthesis of these copolymers was performed using ARGET ATRP with different amounts of copper. Block copolymer synthesized with lower amount of Cu catalyst (3 ppm) has a clearly broader molecular weight distribution than copolymer synthesized with a higher amount of copper (50 ppm), PDI = 1.14 and 1.42 respectively. The PDI of the second block was estimated (33) as 1.25 when the catalyst amount was 50 ppm and 1.76 with 3 ppm. The properties of these materials are now under investigation.

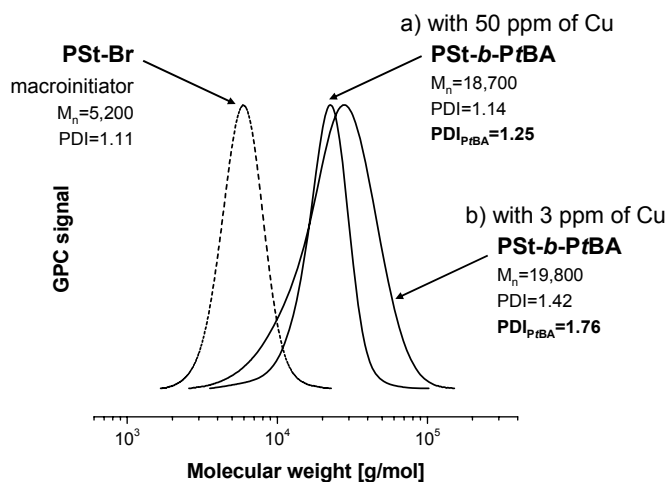


Figure 4. GPC traces after each step of synthesis of block copolymers *PSt-b-PtBA*. Experimental conditions for polymerization of *tBA* a) with 50 ppm of Cu catalyst:  $tBA/PSt/CuBr_2/TPMA/Sn(EH)_2 = 150/1/0.0075/0.05/0.05$  and b) with 3 ppm of Cu catalyst:  $tBA/PSt/CuBr_2/TPMA/Sn(EH)_2 = 150/1/0.0005/0.05/0.05$ , both in anisole (0.8 v/v vs. monomer) at 60 °C.

### Synthesis of Polystyrene-*b*-Poly(Acrylic Acid) (*PSt-b-PAA*)

All *PSt-b-PtBA* block copolymers were converted to *PSt-b-PAA* by deprotection of *tBu* groups (34). The reactions were performed in dichloromethane in the presence of trifluoroacetic acid (TFA) (5 mol eq. vs. *tBu* groups) at room temperature for 48 h. All transformations were quantitative as proved by NMR measurements. Figure 5 presents  $^1H$  NMR spectra before and after transformation. Disappearance of the signal from *tBu* groups at 1.38 ppm (A) was clearly observed in each case. *PSt-b-PAA* were then precipitated into acetonitrile and dried under vacuum.

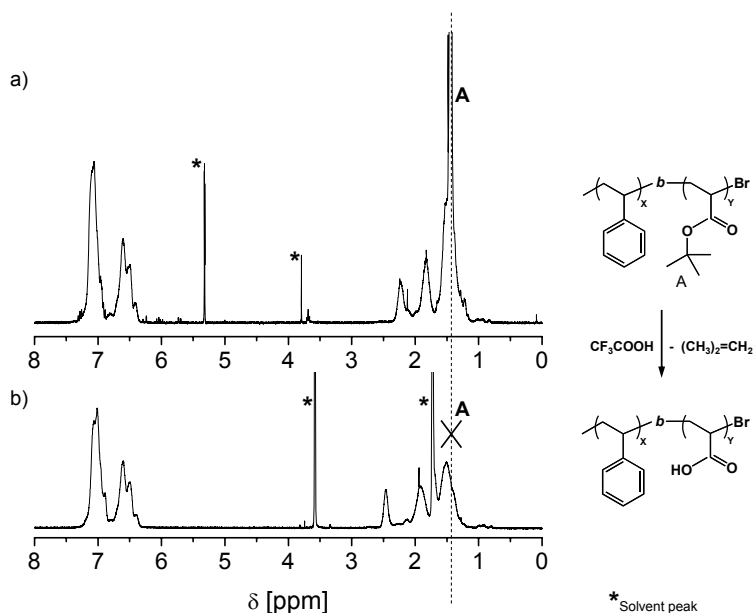


Figure 5.  $^1\text{H}$  NMR spectra of a) PSt-*b*-PtBA (sample N25 on Figure 1c and in Table I;  $X=50$  and  $Y=23$ ) in  $\text{CD}_2\text{Cl}_2$  and b) PSt-*b*-PAA in  $\text{THF-}d_8$  after transformation.

### Stabilization of $\text{Fe}_2\text{O}_3$ Particles with PSt-*b*-PAA Polymer Surfactants

PSt-*b*-PAA block copolymers are well studied in literature (19, 35-37) and extensively used as polymeric surfactants (34, 38-42). As an example, stabilization of  $\text{Fe}_2\text{O}_3$  particles with these block copolymer surfactants was investigated. The carboxylate groups from the PAA segment can coordinate to the metal centers on the surface of  $\text{Fe}_2\text{O}_3$  whereas the PSt segments form a hydrophobic shell around the particles. This can potentially stabilize suspensions of the particles in good solvents for PSt such as toluene. Figure 6a shows the evolution of the absorbance at 500 nm with time for suspensions of  $\text{Fe}_2\text{O}_3$  particles ( $< 50$  nm) in toluene in the absence of a stabilizing surfactant, and in the presence of two of the block copolymer surfactants from the library, namely one containing short PSt and PAA segments (PSt<sub>15</sub>-*b*-PAA<sub>9</sub>), and a surfactant with longer segments (PSt<sub>50</sub>-*b*-PAA<sub>47</sub>). In the absence of any surfactant, the oxide particles quickly precipitate and the absorbance (turbidity) was decreased to less than 1 within minutes.



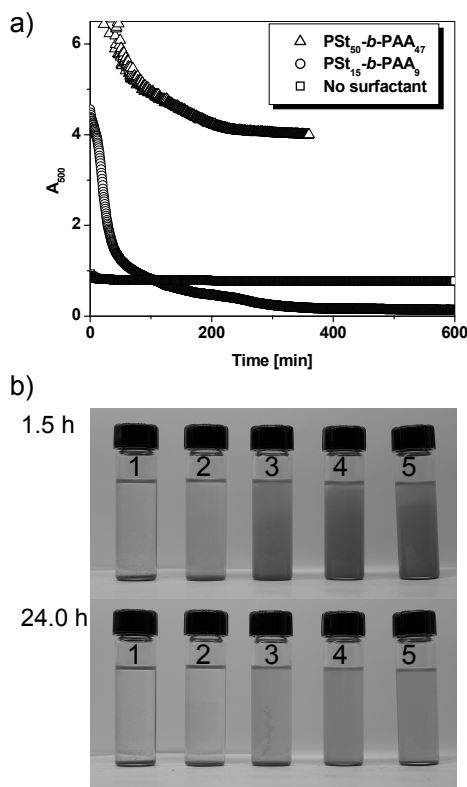


Figure 6. a) Evolution of absorbance at 500 nm with time for suspensions of  $Fe_2O_3$  in toluene prepared using no surfactant or stabilized with either  $PS_{15}-b-PAA_9$  or  $PS_{50}-b-PAA_{47}$ . b) Photographs of suspensions of  $Fe_2O_3$  in toluene in the absence of a surfactant (1) or stabilized with  $PS_{15}-b-PAA_9$  (2),  $PS_{50}-b-PAA_{47}$  (3),  $PS_{178}-b-PAA_{13}$  (4) and  $PS_{178}-b-PAA_{173}$  (5) after 1.5 and 24 hours.

The residual absorbance of about 0.7-0.8 was due to the presence of particles precipitating on the walls of the cuvette. When a surfactant with short hydrophobic and hydrophilic segments was used, the suspension was stable for longer time but within 1-2 hours the particles settled on the bottom of the cuvette. With the surfactant with longer segment sizes,  $PS_{50}-b-PAA_{47}$ , the suspension was stable for significantly longer time (note that the absorbance at 500 nm was stabilized at a value of around 4). The effect of surfactant composition on stabilization of the suspensions is also visualized in Figure 6b where photographs of suspensions are shown after 1.5 and 24 h. From Figure 6, it is clear that the surfactant composition plays a very important role, with surfactants containing longer PSt segments (up to  $DP_n = 178$ ) being better stabilizers. Importantly, the library allows for a full systematic study and identification of the best stabilizer for a particular combination of size of  $Fe_2O_3$  particles and solvent.

## Summary

The block copolymers prepared by the controlled radical polymerization techniques have a great potential to improve the performance of tomorrow's commercial products. In order to introduce products based on block copolymers, R&D scientists need to establish a relationship between polymer structure and product performance. Easily accessible polymeric libraries, which are now commercially available, will greatly accelerate this process. As an example, we presented a PSt-*b*-PtBA copolymer library (5×5) which covers wide range of molecular weights and compositions which are changed in a systematic way. A very straightforward synthesis of this library was achieved via ARGET/ICAR ATRP. These new techniques were designed for industrial level synthesis making the final library inexpensive and accessible for companies as well as for academic scientists. PSt-*b*-PtBA library was then converted to polymeric surfactants PSt-*b*-PAA. The stabilization of Fe<sub>2</sub>O<sub>3</sub> was greatly influenced by the molecular weight and composition of PSt-*b*-PAA copolymers. These results prove that polymeric libraries (several polymer samples with various molecular weights, compositions, architecture, etc. changed in systematic manner) will be required in finding optimal material for particular application.

## Experimental

### Materials

Styrene (St) (Aldrich, 99%) was used as received and *t*-butyl acrylate (*t*BA) (Aldrich, 99%) was passed through a column filled with basic alumina. Tris(2-dimethylaminoethyl)amine (Me<sub>6</sub>TREN, 99 %) and tris(2-pyridylmethyl)amine (TPMA, 99 %) are commercially available from ATRP Solutions Inc (www.atrpsolutions.com). ATRPpure resin (ATRP Solutions Inc.), diethyl 2-bromo-2-methylmalonate (DEBMM) (Aldrich, 98%), copper(II) bromide (Aldrich, 99%), tin(II) 2-ethylhexanoate (Sn(EH)<sub>2</sub>) (Aldrich, 95%), N,N-dimethylformamide (DMF) (Aldrich, 99%), methylene chloride (Fisher Scientific), trifluoroacetic acid (TFA) (Aldrich, 99%) and 2,2'-azobis(isobutyronitrile) (AIBN) (Aldrich, 99%) were used as received. Fe<sub>2</sub>O<sub>3</sub> particles (size < 50 nm) were purchased from Aldrich.

### Analysis

Molecular weight ( $M_n$ ) and polydispersity index (PDI) were determined by GPC, conducted with a Waters 515 pump and Waters 2414 differential refractometer using PSS columns (Styrogel 10<sup>5</sup>, 10<sup>3</sup>, 10<sup>2</sup> Å) in THF as an eluent at 35 °C and at a flow rate of 1 mL/min. Linear polystyrene standards were used for calibration. Conversion of monomers was determined using a Shimadzu GC 14-A gas chromatograph equipped with a FID detector using a J&W Scientific

30 m DB WAX Megabore column with anisole as an internal standard. Conversion was calculated by detecting the decrease of the monomer peak area relative to the peak areas of the standards. The  $^1\text{H}$  NMR spectra were recorded at 27 °C in  $\text{CD}_2\text{Cl}_2$  or  $\text{THF-}d_8$  on a Bruker Avance DMX300 NMR instrument operating at 300.13 MHz for  $^1\text{H}$ , and using the standard Bruker software. The kinetic studies of  $\text{Fe}_2\text{O}_3$  particle stabilization in toluene were carried out on a Cary5000 UV/Vis spectrometer by measuring the absorbance at 500 nm every 30 seconds for about 10 hours.

### Synthesis of Polystyrene (PSt) Macroinitiator via ICAR ATRP

A solution of catalyst was made by dissolving  $\text{CuBr}_2$  (77.9 mg, 0.35 mmol) and  $\text{Me}_6\text{TREN}$  (92.4  $\mu\text{L}$ , 0.35 mmol) in DMF (5 mL). This solution was added to a 1 L Ace Glass reactor together with St (800 mL, 6.98 mol), DEBMM (16.7 mL, 87.3 mmol) and AIBN (2.15 g, 13.1 mmol). The mixture was purge by nitrogen for 1 h and the reactor was placed in heating mantle at 70 °C. Samples were withdrawn at regular intervals and analyzed by GC and GPC to follow the progress of the reaction.

### Synthesis of Polystyrene-*b*-Poly(*t*-Butyl Acrylate) (PSt-*b*-PtBA) via ARGET ATRP

A solution of catalyst was made by dissolving  $\text{CuBr}_2$  (7.5 mg,  $3.4 \times 10^{-2}$  mmol) and TPMA (65.1 mg,  $22.4 \times 10^{-2}$  mmol) in DMF/anisole (1/10 mL). This solution was added to a 250 mL Schlenk flask together with PSt macroinitiator (23.3 g, 4.48 mmol), *t*BA (96.0 mL, 0.67 mol) and anisole (67 mL). The mixture was flushed with nitrogen for 0.7 h and the flask was placed in oil bath thermostated at 60 °C. An initial sample was taken before the reducing agent  $\text{Sn}(\text{EH})_2$  (72.7  $\mu\text{L}$ ,  $22.4 \times 10^{-2}$  mmol) was added. Samples were withdrawn at regular intervals and analyzed by GC and GPC to follow the progress of the reaction.

### Synthesis of Polystyrene-*b*-Poly(Acrylic Acid) (PSt-*b*-PAA)

A PSt-*b*-PtBA block copolymer (55.0 g, 7.97 mmol, N25 in Table I) was placed in 1.0 L round bottom flask equipped with magnetic stirring bar. The polymer was then dissolved in 330 ml of  $\text{CH}_2\text{Cl}_2$ . Next, trifluoroacetic acid (60.4 ml, 0.78 mol; 5 eq. vs. *t*Bu groups) was added to the polymer solution. The solution was stirred at room temperature for 48 h and then precipitated into acetonitrile. The polymer product (white powder) was filtered and dried under vacuum.

## Stabilization of Fe<sub>2</sub>O<sub>3</sub> with PSt-*b*-PAA Block Copolymers

For the spectral studies, a suspension of 1.0 mg of Fe<sub>2</sub>O<sub>3</sub> in 3 mL of toluene was prepared in a quartz cuvette. The suspension was sonicated for 1 min, and 0.15 mL solution of surfactant (40.0 mg in 2 mL of THF) or 0.15 mL of THF for the “blank” experiment was added. The mixture was then sonicated for 1 minute and the collection of absorbance data began another 1.5 minutes later. The samples for the pictures presented in Figure 6b were prepared in the same manner but using twice the amounts of all components, i.e., 2.0 mg of Fe<sub>2</sub>O<sub>3</sub>, 6 mL of toluene, and 0.3 mL of surfactant solution or THF.

## References

1. Hadjichristidis, N.; Pispas, S.; Floudas, G., *Block Copolymers: Synthetic Strategies, Physical Properties, and Applications*. John Wiley & Sons, Inc.: Hoboken, 2003.
2. Hamley, I. W., *Development in Block Copolymer Science and Technology*. Wiley: Chichester, UK, 2004; p 367 pp.
3. Matyjaszewski, K.; Gnanou, Y.; Leibler, L., *Macromolecular Engineering: From Precise Macromolecular Synthesis to Macroscopic Materials Properties and Applications*. Wiley-VCH: Weinheim, 2007.
4. Braunecker, W. A.; Matyjaszewski, K. *Progr. Polym. Sci.* **2007**, 32, 93.
5. Matyjaszewski, K.; Davis, T. P., *Handbook of Radical Polymerization*. Wiley Interscience: Hoboken, 2002.
6. Kamigaito, M.; Ando, T.; Sawamoto, M. *Chem. Rev.* **2001**, 101, 3689.
7. Matyjaszewski, K.; Xia, J. *Chem. Rev.* **2001**, 101, 2921.
8. Tsarevsky, N. V.; Matyjaszewski, K. *Chem. Rev.* **2007**, 107, 2270.
9. Wang, J.-S.; Matyjaszewski, K. *J. Am. Chem. Soc.* **1995**, 117, 5614.
10. Davis, K.; Matyjaszewski, K. *Adv. Polym. Sci.* **2002**, 159, 1.
11. Jakubowski, W.; Matyjaszewski, K. *Angew. Chem., Int. Ed.* **2006**, 45, 4482.
12. Jakubowski, W.; Min, K.; Matyjaszewski, K. *Macromolecules* **2006**, 39, 39.
13. Matyjaszewski, K.; Jakubowski, W.; Min, K.; Tang, W.; Huang, J.; Braunecker, W. A.; Tsarevsky, N. V. *Proc. Natl. Acad. Sci. USA* **2006**, 103, 15309.
14. Matyjaszewski, K.; Dong, H.; Jakubowski, W.; Pietrasik, J.; Kusumo, A. *Langmuir* **2007**, 23, 4528.
15. Dong, H.; Tang, W.; Matyjaszewski, K. *Macromolecules* **2007**, 40, 2974.
16. Pietrasik, J.; Dong, H.; Matyjaszewski, K. *Macromolecules* **2006**, 39, 6384.
17. Jakubowski, W.; Kirci-Denizli, B.; Gil, R. R.; Matyjaszewski, K. *Macromol. Chem. Phys.* **2008**, 209, 32.
18. Listak, J.; Jakubowski, W.; Mueller, L.; Plichta, A.; Matyjaszewski, K.; Bockstaller, M. R. *Macromolecules* **2008**, 41, 5919.
19. Gohy, J.-F. *Adv. Polym. Sci.* **2005**, 190, 65.
20. Lutz, J.-F.; Matyjaszewski, K. *J. Polym. Sci., Part A: Polym. Chem.* **2005**, 43, 897.
21. Lutz, J.-F.; Matyjaszewski, K. *Macromol. Chem. Phys.* **2002**, 203, 1385.

22. Tsarevsky, N. V.; Matyjaszewski, K. *J. Polym. Sci., Part A: Polym. Chem.* **2006**, *44*, 5098.
23. Mueller, L.; Jakubowski, W.; Tang, W.; Matyjaszewski, K. *Macromolecules* **2007**, *40*, 6464.
24. Leibler, L.; Benoit, H. *Polymer* **1981**, *22*, 195.
25. Matsen, M. W.; Bates, F. S. *Macromolecules* **1995**, *28*, 7298.
26. Sides, S. W.; Fredrickson, G. H. *J. Chem. Phys.* **2004**, *121*, 4974.
27. Court, F.; Yamaguchi, D.; Hashimoto, T. *Macromolecules* **2006**, *39*, 2596.
28. Hashimoto, T.; Yamaguchi, D.; Court, F. *Macromol. Symp.* **2003**, *195*, 191.
29. Mayes, A. M.; Russell, T. P.; Deline, V. R.; Satija, S. K.; Majkrzak, C. F. *Macromolecules* **1994**, *27*, 7447.
30. Noro, A.; Cho, D.; Takano, A.; Matsushita, Y. *Macromolecules* **2005**, *38*, 4371.
31. Vilesov, A. D.; Floudas, G.; Pakula, T.; Melenevskaya, E. Y.; Birshtein, T. M.; Lyatskaya, Y. V. *Macromol. Chem. Phys.* **1994**, *195*, 2317.
32. Yamaguchi, D.; Hashimoto, T. *Macromolecules* **2001**, *34*, 6495.
33. Fukuda, T. *J. Polym. Sci., Part A: Polym. Chem.* **2004**, *42*, 4743.
34. Burguiere, C.; Chassenieux, C.; Charleux, B. *Polymer* **2002**, *44*, 509.
35. Davis, K. A.; Charleux, B.; Matyjaszewski, K. *J. Polym. Sci., Part A: Polym. Chem.* **2000**, *38*, 2274.
36. Desjardins, A.; Eisenberg, A. *Macromolecules* **1991**, *24*, 5779.
37. Ramireddy, C.; Tuzar, Z.; Prochazka, K.; Webber, S. E.; Munk, P. *Macromolecules* **1992**, *25*, 2541.
38. Burguiere, C.; Pascual, S.; Bui, C.; Vairon, J.-P.; Charleux, B.; Davis, K. A.; Matyjaszewski, K.; Betremieux, I. *Macromolecules* **2001**, *34*, 4439.
39. Choucair, A.; Lavigneur, C.; Eisenberg, A. *Langmuir* **2004**, *20*, 3894.
40. Terreau, O.; Bartels, C.; Eisenberg, A. *Langmuir* **2004**, *20*, 637.
41. Zhang, L.; Eisenberg, A. *Science* **1995**, *268*, 1728.
42. Zhong, X. F.; Varshney, S. K.; Eisenberg, A. *Macromolecules* **1992**, *25*, 7160.

## Chapter 24

# Polypropylene-*graft*-poly(methyl methacrylate) Graft Copolymers: Synthesis and Compatibilization of Polypropylene/Poly lactide

Hideyuki Kaneko\*, Junji Saito, Nobuo Kawahara, Shingo Matsuo,  
Tomoaki Matsugi and Norio Kashiwa

Research Center, Mitsui Chemicals, Inc., 580-32 Nagaura, Sodegaura,  
Chiba 299-0265, Japan

Polypropylene-*graft*-poly(methyl methacrylate) (PP-*g*-PMMA) graft copolymers, possessing different compositions and branch lengths, were synthesized using 2-bromoisobutyrate group containing PP (PP-*g*-Br) as a macroinitiator for the metal-catalyzed living radical polymerization of MMA. The polypropylene/poly lactide (PP/PLA) binary blends and the PP/PLA/PP-*g*-PMMA ternary blends were prepared by melt-blending and compression molding. From the results of the tensile and flexural tests, the strength and modulus of the PP/PLA blends were significantly improved by addition of the PP-*g*-PMMA. On the other hand, the PP-*g*-PMMA was ineffective in improving the elongation at break and the Izod impact strength of these polymer blends. TEM observations suggested that the ternary blends had a well-dispersed morphology compared with the binary blends and the PP-*g*-PMMA worked as a compatibilizer for the PP/PLA blends.

### Introduction

Polymer blend technique is very important for the creation of novel polymeric materials combining different properties of polymers (*1*). In particular, the improvement of the mechanical properties using polymer blend technique

has been investigated for many years. In general, the mechanical properties of the polymer blends among two or more different polymers are directly associated with its morphology and the interfacial interaction between them. An immiscible polymer blend often causes an undesirable phase separation and significant decreases in its properties because of its weak interfacial interaction. To overcome these defects and achieve the desired and stabilized morphology of the immiscible polymer blend with sufficiently strong interfacial interaction, a utilization of an appropriate compatibilizer is one of the most effective ways. It is well known that block or graft copolymers consisting of different segments can act as a compatibilizer for such immiscible polymer blends and reduce the interfacial tension, resulting in a controlled morphology and some improved mechanical properties.

Polypropylene (PP) is one of the most widespread commodity plastics due to its outstanding combination of inexpensive production cost and excellent physical properties. However, because of the lack of polar functional groups on its polymer chain, PP usually suffers from poor adhesion to and incompatibility with other polymers or materials. This disadvantage has significantly limited many of its end uses. On the other hand, polylactide (PLA) is linear aliphatic polyester synthesized by ring-opening polymerization of lactide (2,3) and has high modulus and strength compared with PP. Since PLA is known for biocompatible and biodegradable polymers and is made from a renewable resource, it has recently attracted a lot of attention as a very important material for alleviating some problems with waste disposal and environmental burdens associated with traditional commodity plastics. Therefore, the introduction of PLA into PP is expected to achieve not only a differentiated product with improved mechanical properties but also an eco-friendly polymeric material with unique properties. However, the binary blends of PP and PLA are essentially immiscible due to differences in their chemical nature and thereby show macroscopically phase-separated morphology (4). To improve the phase-separated morphology, the addition of a compatibilizer is necessary but there are no appropriate compatibilizers for PP/PLA polymer blend thus far.

The recent synthesizing of polyolefin-based block and graft copolymers possessing some polar segments has achieved a well-defined polymer architecture with facile and precise control (5-8), resulting in improved and unique properties and new applications. For example, many kinds of polyolefin-based block or graft copolymers possessing poly(methyl methacrylate) (PMMA) (9-15), polystyrene (PS) (16-19), poly(ethylene glycol) (PEG) (20) and poly( $\epsilon$ -caprolactone) (PCL) (21,22) segments were successfully prepared by functionalization of polyolefin and subsequent post-polymerization processes, such as living anionic and controlled radical polymerizations, and confirmed to act as compatibilizers for polyolefin and polar polymer blends. The combination of polyolefin and hydrophilic segments, such as poly(ethylene glycol) (20), poly(*N*-isopropylacrylamide) (21), poly(acrylic acid) (22) and poly(2-hydroxyethyl methacrylate) (15), has enabled us to bring a hydrophilic nature to polyolefin. Furthermore, we previously reported on the mechanical properties of polypropylene-based graft copolymers, such as PP-*graft*-poly(methyl methacrylate) (PP-*g*-PMMA), PP-*graft*-polystyrene (PP-*g*-PS) and PP-*graft*-poly(*n*-butyl acrylate) (PP-*g*-PnBA) and discussed the performance

enhancements of these due to the introduction of each polar segment into the PP backbone (23).

In this article, we prepared PP-*g*-PMMA graft copolymers with different polymer structures through a controlled radical polymerization with a PP macroinitiator derived from the hydroxylated PP. In addition, we have confirmed that the thus-obtained graft copolymer worked as a compatibilizer for PP/PLA polymer blends and herein discuss the effect of PP-*g*-PMMA on the mechanical properties of the PP/PLA polymer blends.

## Experimental

### *General Procedures and Materials*

All manipulations of air- and water-sensitive materials were performed under dry N<sub>2</sub> atmosphere in a conventional N<sub>2</sub>-filled glove box. Dimethylsilylenebis(2-methyl-4-phenyl-1-indenyl)zirconium dichloride was prepared according with previous literature (24). Copper bromide (CuBr), copper chloride (CuCl), *N,N,N',N',N''*-pentamethyldiethylenetriamine (PMDETA), 2-bromoisobutryl bromide (BiBB), 10-undecen-1-ol, sodium methoxide in methanol (28 %) and methyl methacrylate (MMA) were purchased from Wako Pure Chemical Industries and used without further purification. Propylene was obtained from Mitsui Chemicals, Inc. Methylaluminoxane (MAO) was purchased from Albemarle as 1.2 M toluene solution with the remaining trimethylaluminum and evaporated in vacuo before use. Triisobutylaluminum was purchased from Tosoh-Finechem. Toluene, *o*-xylene and *n*-hexane used as a solvent were dried over Al<sub>2</sub>O<sub>3</sub> and degassed by bubbling with N<sub>2</sub> gas. Polypropylene and polylactide used in this study were Prime Polypro™ J713MB (Prime Polymer Co., Ltd.) and LACEA™ H-100 (Mitsui Chemicals, Inc.), respectively. The polymer pellets were used as provided.

### *Preparation of Hydroxylated PP (PP-*g*-OH)*

Toluene (800 mL) was introduced to a N<sub>2</sub>-purged 1-L glass reactor equipped with a mechanical stir bar, a temperature probe and a condenser and stirred vigorously. The reactor was kept at 45 °C with an oil bath and then the feeding of propylene gas (100 L/h) and hydrogen gas (5 L/h) was started. Subsequently, triisobutylaluminum (3.3 mmol) and 10-undecen-1-ol (3.0 mmol) were added. After 10 min, dimethylsilylenebis(2-methyl-4-phenyl-1-indenyl)zirconium dichloride (0.002 mmol) and 1.31 M toluene solution of MAO (1.0 mmol) were introduced into the reactor and then polymerization was immediately started. After 20 min, polymerization was quenched by injection of isobutyl alcohol. The polymerization mixture was poured into acidic methanol. The polymer was collected by filtration, washed with methanol and dried in vacuo at 80 °C for 10 h to give PP-*g*-OH (18.5 g; number-average molecular weight ( $M_n$ ) = 50,900, melting temperature ( $T_m$ ) = 151 °C, 0.14 mol% of



hydroxyl group according to  $^1\text{H}$  NMR measurements). By repeating this procedure, a sufficient amount of PP-g-OH for this study was obtained.

#### *Preparation of PP Macroinitiator (PP-g-Br)*

PP-g-OH (150 g), BiBB (10.9 mL) and *n*-hexane (1500 mL) were introduced into a  $\text{N}_2$ -purged 2-L glass reactor equipped with a mechanical stir bar and then were stirred vigorously at 60 °C for 3 h. The reaction mixture was cooled to 25 °C and poured into 2 L of acetone. The resulting polymer was collected by filtration, washed with acetone and dried in vacuo at 80 °C for 10 h.

#### *Radical Polymerization with PP Macroinitiator*

A typical polymerization process is as follows (for Run 3 in Table 1): PP-g-Br (15 g), MMA (25 mL) and *o*-xylene (275 mL) were placed in a 500-mL glass reactor equipped with a mechanical stir bar and then this slurry was stirred at ambient temperatures for 2 h under a nitrogen atmosphere. After adding a solution of CuCl/PMDETA in *o*-xylene (2.7 mmol as a copper atom and 2.7 mmol as PMDETA, pretreated for 5 min.), the mixture was heated to 80 °C to start the polymerization. Then, the reaction mixture was maintained at 80 °C for 30 min. under stirring. The reaction mixture was cooled to ambient temperatures under stirring and the obtained slurry was filtered and the obtained powder was washed with acetone and methanol. After filtration, the obtained white powder was dried in vacuo at 80 °C for 10 h.

#### *Cleavage of Graft Copolymers*

A typical cleavage process is as follows: The graft copolymer (1.0 g) was dissolved in *o*-xylene (120 mL) at 100 °C, and then methanol (100 mL) and 28 % sodium methoxide in methanol (9 mL) were added to the solution. The resulting mixture was stirred and refluxed for 9 h. The reaction mixture was cooled to 25 °C and poured into 800 mL of methanol. After filtration, the resulting polymer was extracted with chloroform and the cleaved PMMA branch was collected by evaporation of solvent from the filtrate. The GPC of the cleaved PMMA branch calibrated with PMMA were recorded by using a GL Sciences RI-504R differential refractometer with three Waters STYRAGEL columns (two sets of STYRAGEL HT 6E and STYRAGEL HR 5E) at 40 °C in chloroform.

#### *Polymer Characterization Methods*

$^1\text{H}$  NMR spectra were recorded on JEOL GSX-400 (400 MHz) spectrometers using 1,2-dichlorobenzene- $d_4$  as a solvent at 120 °C. The GPC calibrated with PP (for PP-g-OH) were recorded by using a Waters Alliance

GPC2000 equipped with four TSKgel columns (two sets of TSKgelGMH6-HT and two sets of TSKgelGMH6-HTL) and a refractive index detector at 140 °C in 1,2-dichlorobenzene and those calibrated with PS standard (for PP-g-PMMA) were recorded by using a CFC T-150A (Mitsubishi Kagaku Corp.) equipped with three columns (Shodex AT-806MS) and an IR spectrometer Miran 1ACVF at 140 °C in 1,2-dichlorobenzene.

### *Mechanical Property Tests*

50 g of each polymer was mixed to the required weight ratios (PP/PLA/PP-g-PMMA) as shown later in Table 1 and then kneaded by a labo plastomill at 200 °C. After 5 min of kneading, the specimens were prepared by compression molding at 200 °C for 10 min in a laboratory press. The tensile tests, the flexural tests and the Izod impact tests were performed at 23 °C according to JIS K7113, ASTM D 790 and ASTM D 256, respectively.

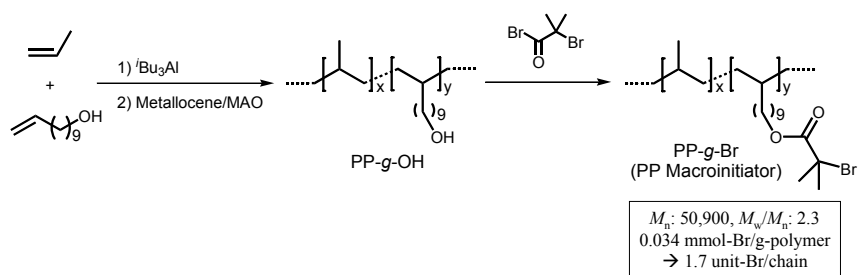
### *Transmission Electron Microscopy (TEM) Observations*

Ultrathin (*ca.* 100 nm) sections of the polymer, which had been pressed into a sheet, were cut on a Reica Ultracut Microtome equipped with a diamond knife at a low temperature and were then stained with RuO<sub>4</sub>. TEM observations were made with a Hitachi H-7000 transmission electron microscope at an acceleration voltage of 75 kV and at a magnification of 5,000.

## **Results and Discussion**

### *Preparation of PP-g-PMMA Graft Copolymer*

As reported previously (23), dimethylsilylenebis(2-methyl-4-phenyl-1-indenyl)zirconium dichloride is able to copolymerize propylene and 10-undecen-1-ol in the presence of triisobutylaluminum and activation with methylalminoxane (MAO) to give an isotactic polypropylene possessing hydroxyl groups at the side-chain ends (PP-g-OH). After conducting the copolymerization of propylene with 10-undecen-1-ol, the hydroxyl groups in the resulting copolymer were converted into 2-bromoisobutyrate groups by a reaction with excess amount of 2-bromoisobutyryl bromide in the presence of triethylamine, resulting in a 2-bromoisobutyrate group containing PP (PP-g-Br) as shown in the Scheme 1 below. From the content of the 2-bromoisobutyrate group and the number average molecular weight ( $M_n$ ) of the obtained PP-g-Br, the average number of the 2-bromoisobutyrate group in the PP-g-Br was estimated to be 1.7 units per chain. The thus-obtained PP-g-Br was used as a macroinitiator for the controlled radical polymerization.



*Scheme 1. Synthetic route for preparing PP-g-Br.*

The polymerization of MMA with a PP macroinitiator was carried out in an *o*-xylene using a copper-based catalyst system. To remove a homo-PMMA, the resulting polymers were purified by stirring and washing in acetone. Table 1 summarizes the results by altering polymerization conditions. Since the PP macroinitiator is not dissolved in *o*-xylene at 80 °C, the polymerization proceeded in heterogeneous conditions. To obtain variable copolymer compositions, several polymerizations with two types of catalysts, CuBr and CuCl, under a different monomer (MMA) concentration were conducted. The compositions of the copolymers, which were calculated from a polymer yield, were successfully controlled in the range of 21 – 69 wt% of MMA by the initial monomer concentration. Evolution of polymer yield versus initial monomer concentration for two types of catalysts is presented in Figure 1. Polymerization was faster with CuCl than with CuBr at the same initial monomer concentration. When CuCl was used as a catalyst with the PP macroinitiator, the PP-g-PMMA graft copolymers with higher MMA contents were obtained under the same polymerization condition compared with in the case of CuBr.

**Table 1. Summary of Polymerizations with PP-g-Br ( $T= 80\text{ }^{\circ}\text{C}$ ; PP-g-Br 15 g (0.51 mmol-Br); CuX 9.0 mmol; PMDETA 9.0 mmol)**

Run	CuX	MMA/ <i>o</i> -xylene (mL/mL)	Yield (g)	Composition (wt%)	
				Gravimetrically <sup>a</sup>	<sup>1</sup> H NMR <sup>b</sup>
1	CuBr	25/275	19.1	21.3	22.5
2	CuBr	50/250	22.1	32.3	32.5
3	CuCl	25/275	23.0	34.8	35.1
4	CuCl	50/250	28.2	46.7	48.5
5	CuCl	100/200	37.5	60.0	62.2
6	CuCl	200/100	48.6	69.1	68.8

<sup>a</sup> MMA content calculated from polymer yield.

<sup>b</sup> MMA content determined by <sup>1</sup>H NMR.

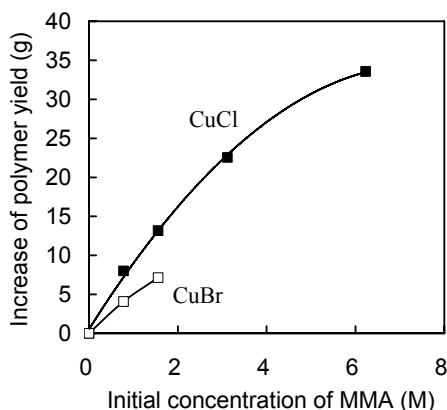


Figure 1. Evolution of increase of polymer yield versus initial monomer concentration for two types of catalysts.

The representative  $^1\text{H}$  NMR spectrum of PP-g-PMMA graft copolymer (Run 3 in Table 1) is shown in Figure 2. The signals assigned to PMMA ( $\delta$  3.5 and  $\delta$  1.0 – 2.2 ppm) were clearly observed and most of the methylene protons assigned to the 2-bromoisobutyrate group in the PP macroinitiator ( $\delta$  4.05 ppm) were slightly shifted to a higher magnetic field ( $\delta$  4.0 ppm), indicating the graft copolymerization was initiated at the 2-bromoisobutyrate group in the PP macroinitiator. From the integrated intensities of each unit, the compositions of these copolymers can be calculated as shown in Table 1. The compositions of the copolymers determined by  $^1\text{H}$  NMR were in good agreement with those calculated gravimetrically.

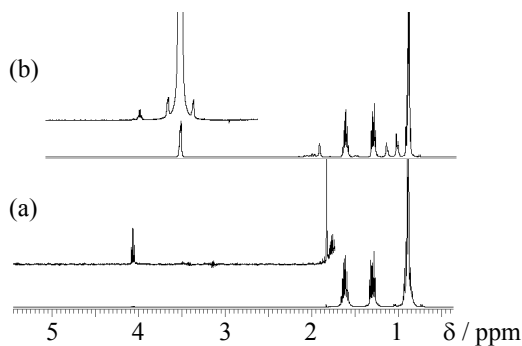


Figure 2.  $^1\text{H}$  NMR spectra of (a) PP-g-Br and (b) PP-g-PMMA (Run 3).

To determine an initiation efficiency of each polymerization condition, the PMMA branches were cleaved from the PP backbone and analyzed by GPC. As reported previously (12), PMMA branches were successfully detached from the PP backbone through an ester exchange reaction in a methanol/*o*-xylene mixed solvent in the presence of sodium methoxide. After the cleavage reaction, PMMA was easily extracted from the mixture by dissolution in chloroform.

GPC traces of the detached PMMA branches shifted with increasing the MMA contents to the higher molecular weight region (Figure 3). The molecular weight of the detached PMMA was higher than the theoretical value calculated from the number average molecular weight of the PP macroinitiator, the average number of the 2-bromoisobutyrate group in the PP macroinitiator and the MMA content of the resulting graft copolymer as shown in Table 2. In the case of the polymerization with CuBr (Run 1, 2), initiation efficiencies were relatively low (0.37 and 0.52, respectively). It is well known that halogen exchange technique provides a well-balanced combination between a faster initiation and a slower propagation to achieve a better control over metal-catalyzed living radical polymerization (25-27) and thereby this technique is useful for the preparation of block or graft copolymers with a well-controlled structure. In this study, the initiation efficiency for the polymerization with CuCl was higher than that with CuBr and was estimated to be 0.63 even at the lowest initial monomer concentration (Run 3), indicating that the actual average number of the PMMA branches in the resulting copolymer was 1.1 units per chain. In the case of the higher initial monomer concentration, the molecular weight of the PMMA branches got closer to the theoretical molecular weight. Consequently, the initiation efficiency increased and eventually reached 0.94. Such high initiation efficiency is the result of a faster initiation reaction between the 2-bromoisobutyrate group in the PP macroinitiator and CuCl.

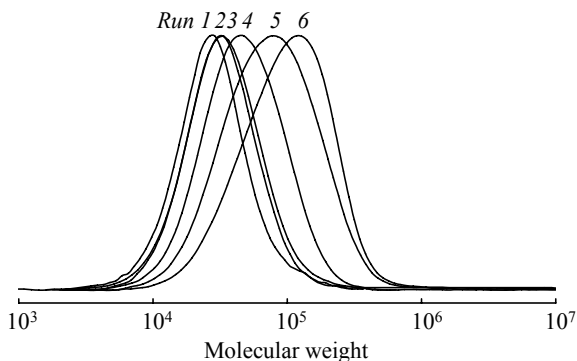


Figure 3. GPC traces of detached PMMA branches.

**Table 2. Molecular Weight and Initiation Efficiency of Detached PMMA**

Run	Detached PMMA branch		Initiation efficiency <sup>c</sup>
	$M_{n,theo}$ <sup>a</sup>	$M_{n,GPC}$ ( $M_w/M_n$ ) <sup>b</sup>	
1	8,100	23,300 (1.47)	0.37
2	14,300	27,600 (1.52)	0.52
3	16,000	25,900 (1.48)	0.63
4	26,200	36,800 (1.58)	0.77
5	45,000	54,600 (1.79)	0.90
6	67,000	71,000 (1.73)	0.94

<sup>a</sup>  $M_{n,theo} = [(M_n \text{ of PP-g-Br}) / (\text{weight fraction of PP in the PP-g-PMMA}) - (M_n \text{ of PP-g-Br})] / (\text{average number of 2-bromoisobutyrate in PP-g-Br})$ .

<sup>b</sup> Determined by GPC at 40 °C calibrated with PMMA standard.

<sup>c</sup> Initiation efficiency =  $M_{n,theo} / M_{n,GPC}$ .

On the other hand, the molecular weight distribution of the detached PMMA branches for the polymerization with CuCl was not narrower than those with CuBr unlike previously reported (25-26). These results might be attributed to the fact that the ratio of initiation to propagation rate did not increase enough to improve the control of polymerization because of the high concentration of propagating radicals. In fact, the polymerization rate did not decrease in spite of polymerization under a mixed halogen system. Table 3 shows the polymerization and the cleavage results under a reduced concentration of the catalyst. The molecular weight distribution of the detached PMMA branch became narrower along with reduced concentration of the catalyst, indicating lower concentration of the propagating radicals.

**Table 3. Summary of Polymerizations under the Reduced Concentrations of Catalyst ( $T= 80$  °C; PP-g-Br 15 g (0.51 mmol-Br); [CuCl]/[PMDETA]=1/1)**

Run	$[CuCl]_0$ (mM)	Composition <sup>a</sup> (wt%)	Detached PMMA branch		Initiation efficiency <sup>d</sup>
			$M_{n,theo}$ <sup>b</sup>	$M_{n,GPC}$ ( $M_w/M_n$ ) <sup>c</sup>	
1	9.0	34.8	16,000	25,900 (1.48)	0.62
7	6.0	35.3	16,300	28,100 (1.33)	0.58
8	3.0	27.6	11,400	23,300 (1.27)	0.49

<sup>a</sup> MMA content calculated from polymer yield..

<sup>b</sup>  $M_{n,theo} = [(M_n \text{ of PP-g-Br}) / (\text{weight fraction of PP in the PP-g-PMMA}) - (M_n \text{ of PP-g-Br})] / (\text{average number of 2-bromoisobutyrate in PP-g-Br})$ .

<sup>c</sup> Determined by GPC at 40 °C calibrated with PMMA standard.

<sup>d</sup> Initiation efficiency =  $M_{n,theo} / M_{n,GPC}$ .

The GPC traces of the PP macroinitiator and the graft copolymers are shown in Figure 4. The GPC curves slightly shifted to a higher weight region with the increase of MMA contents, indicating successful graft

copolymerization onto the PP macroinitiator. Although GPC traces of the graft copolymers were monomodal, their molecular weight distribution was broader than that of the PP macroinitiator. These facts might indicate that the resulting copolymers are a mixture of the graft copolymers with one or more PMMA branches and the PP macroinitiator without PMMA branches.

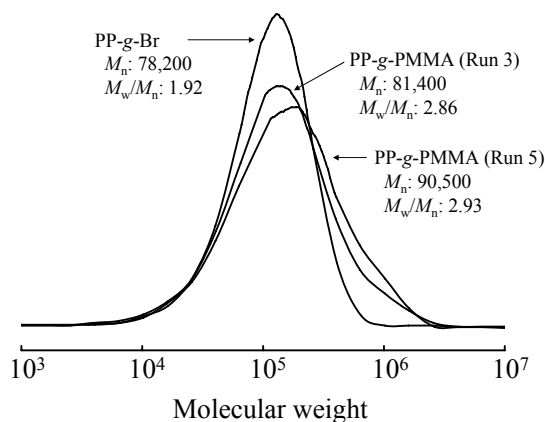


Figure 4. GPC traces of PP-g-Br before and after MMA polymerization.

#### Evaluation of PP-g-PMMA Graft Copolymer as a Compatibilizer

One of the applications of such graft copolymers is as a compatibilizer in polymer blends and composite materials. Since PMMA is miscible with PLA in a wide range of the blend compositions (28), the obtained PP-g-PMMA graft copolymers were expected to be useful as a compatibilizer for PP/PLA polymer blend. In this study, we selected the PP-g-PMMA graft copolymer (Run 3 in Table 1; MMA content = 35.1 wt%, average branch number = 1.1) as a compatibilizer, an injection-grade PLA and a PP impact copolymer, consisting of a high crystalline homo-PP phase and an amorphous ethylene-propylene random copolymer phase, as a base PP. The PP impact copolymer has an excellent stiffness/impact balance compared with the PP homopolymer. Melt-blending of the PP/PLA binary blends and PP/PLA/PP-g-PMMA ternary blends in the required weight ratios (PP/PLA/PP-g-PMMA) as shown in Table 4 were performed by labo plastomill at 200 °C for 5 min and then the specimens for mechanical tests and morphological studies were prepared by compression molding at 200 °C for 10 min. Mechanical properties of these samples are given in Table 4. In this study, a PLA exhibited high mechanical strength and modulus but very low elongation at break compared with a PP (Entry 1 and 9 in Table 4).

The tensile strength is plotted against the composition for all the blend samples in Figure 5(a). As seen from this figure, both PP and PLA had higher strength than the PP/PLA binary blends and the strength of the blends decreased with increasing concentration of the second blend component. The blend with around 50 wt% of PLA content had the lowest strength. These observations

agree with a previous report on the PLA/PP polyblend fiber.<sup>4</sup> On the other hand, in the case of PP/PLA/PP-g-PMMA ternary blend, the tensile strength gradually increased with increasing of PLA content in the polymer blend. For all of the blend compositions, the tensile strength with the graft copolymer was higher than that without it, indicating that the PP-g-PMMA worked as a compatibilizer and would reduce the interfacial tension between PP and PLA.

**Table 4. Tensile Properties of PP/PLA Polymer Blends**

Entry	PP/PLA/ PP-g-PMMA (weight ratio)	Tensile Strength (MPa)	Young's Modulus (MPa)	Elongation at Break (%)
1	100/ 0/ 0	25.1 ± 0.2	1280 ± 15	481 ± 69
2	80/ 20/ 0	20.6 ± 0.5	1080 ± 12	155 ± 41
3	80/ 20/ 5	27.6 ± 0.5	1510 ± 46	21.5 ± 6.1
4	60/ 40/ 0	16.2 ± 0.5	1440 ± 99	5.7 ± 0.2
5	60/ 40/ 5	28.0 ± 0.7	1650 ± 125	4.8 ± 0.6
6	40/ 60/ 0	18.7 ± 0.0	1450 ± 146	4.2 ± 0.7
7	40/ 60/ 5	39.5 ± 0.2	1910 ± 48	4.9 ± 2.5
8	20/ 80/ 5	48.4 ± 1.0	2230 ± 228	4.9 ± 2.0
9	0/100/ 0	65.8 ± 0.6	2340 ± 147	3.0 ± 1.1

Similar to the tensile strength, adding the graft copolymer was very effective to improve the Young's modulus of the PP/PLA blend samples for all of the blend compositions. This trend in the Young's modulus of each base polymer and blend samples is shown in Figure 5(b). In the PP/PLA/PP-g-PMMA ternary blend, the modulus almost linearly increased depending on the blend ratio of each pure polymer, suggesting that these polymer blends became compatible owing to the PP-g-PMMA graft copolymer. The flexural properties of these polymer blends also denoted the same tendency of the tensile properties as shown in Table 5.

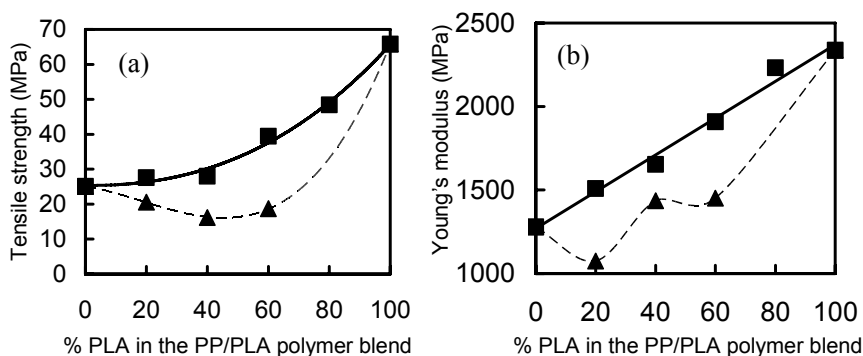


*Figure 5. Effect of the weight fraction of PLA on (a) the tensile strength and (b) the Young's modulus of the PP/PLA binary blend (triangles) and the PP/PLA/PP-g-PMMA ternary blend (squares).*



**Table 5. Flexural and Impact Properties of PP/PLA Polymer Blends**

Entry	PP/PLA/ PP-g-PMMA (weight ratio)	Flexural Strength (MPa)	Flexural Modulus (MPa)	Izod Impact Strength (J/m)
1	100/ 0/ 0	37.0 ± 0.4	1380 ± 33	161 ± 28
2	80/ 20/ 0	33.3 ± 0.6	1410 ± 105	33 ± 7.5
3	80/ 20/ 5	41.6 ± 1.9	1550 ± 14	43 ± 5.2
4	60/ 40/ 0	28.3 ± 0.2	1700 ± 118	24 ± 2.6
5	60/ 40/ 5	42.3 ± 0.7	1940 ± 23	22 ± 5.0
6	40/ 60/ 0	19.6 ± 1.0	1860 ± 182	- <sup>a)</sup>
7	40/ 60/ 5	34.0 ± 5.5	2260 ± 81	10 ± 0.0
8	20/ 80/ 5	31.4 ± 2.3	2740 ± 125	- <sup>a)</sup>
9	0/100/ 0	57.2 ± 4.4	2880 ± 210	30 ± 2.0

<sup>a</sup> Specimens could not be prepared by compression molding.

The elongation at break of the polymer blend showed considerable changes with the blend compositions as shown in Table 4. Addition of even 20 % of PLA into PP decreased the elongation by about 32 % compared to the PP and further addition of 5 % of PP-g-PMMA into this PP/PLA binary blend decreased the elongation by about 14 % compared to the binary blend. When the PLA content increased over 40 %, the elongation property of PP/PLA blend was thoroughly lost regardless of whether it was with or without the graft copolymer. Similarly, Izod impact strength of the polymer blends also decreased remarkably by adding even 20 % PLA.

#### *Morphology of PP/PLA Polymer Blends*

Figure 6 shows the TEM images of the PP-rich blend samples (PP/PLA = 80/20) before and after adding the PP-g-PMMA (Entry 2 and 3 in Table 4 and 5). Because of a poor miscibility between PP and PLA, the PLA domains (light-colored) in the PP matrix varied in size before adding the PP-g-PMMA (Figure 6(a)). After the PP-g-PMMA was added into the polymer blend, the PLA domains finely dispersed and their size became uniformly (Figure 6(b)), suggesting that the PP-g-PMMA evidently worked as a compatibilizer for PP/PLA polymer blend. On the other hand, the size of the darkly-colored domains assigned to ethylene-propylene copolymer (EP) phase seemed nearly constant and most EP domains remained in the homo-PP matrix before and after addition of the graft copolymer. This result indicates that this graft copolymer does not work as a compatibilizer for EP included in the base PP.

The morphologies of the PLA-rich blend samples (PP/PLA = 40/60) are shown in Figure 7 (Entry 6 and 7 in Table 4 and 5). Before adding the graft copolymer, both phases hardly dispersed from each other but separated to the size of over 500  $\mu\text{m}$  as shown in Figure 7(a) and 7(b). Introduction of the graft copolymer changed this dramatically. In the PLA-rich blend with the graft copolymer (Figure 7(c)), the spherical homo-PP domains of 1-6  $\mu\text{m}$  in diameter dispersed in the PLA matrix. The pronounced increases of the mechanical

properties after adding the graft copolymer might be related to this phase reversion. On the other hand, the elastomeric EP domains were confined to only the homo-PP phase because of their poor compatibility with the PLA phase. Therefore, one of the reasons for the significant decreases in the elongation and the impact strength in the PP/PLA blend is because the EP domains neither disperse in the PLA matrix nor act as a modifier.

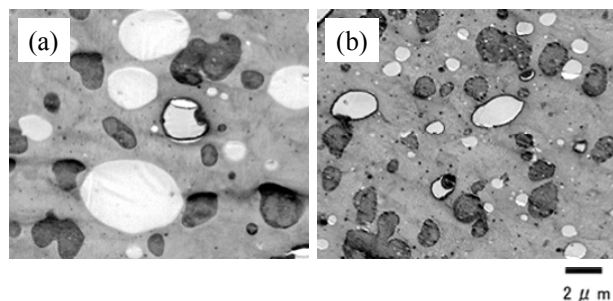


Figure 6. TEM images of (a) PP/PLA (80/20) and (b) PP/PLA/PP-g-PMMA (80/20/5) polymer blends.

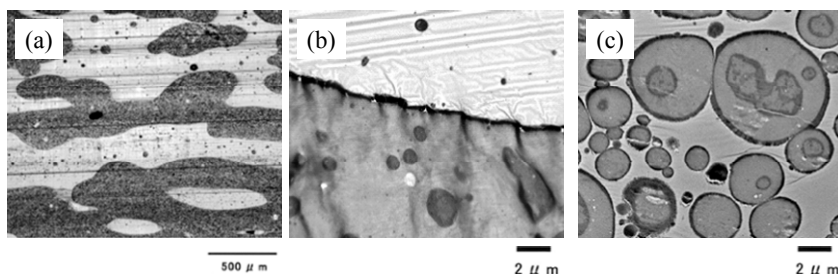


Figure 7. Morphologies of PP/PLA (40/60) polymer blend observed by (a) optical microscopy or (b) TEM and (c) PP/PLA/PP-g-PMMA (40/60/5) polymer blends observed by TEM.

## Conclusions

Polypropylene-*graft*-poly(methyl methacrylate) (PP-g-PMMA) graft copolymers with controlled compositions and branch lengths were prepared through metal-catalyzed living radical polymerization. The 2-bromoisobutyrate group containing PP (PP-g-Br), which was prepared by the metallocene-catalyzed copolymerization of propylene/10-undecen-1-ol and subsequent reaction with 2-bromoisobutyryl bromide, was used as a macroinitiator in the presence of CuCl or CuBr as a catalyst and PMDETA as a ligand. The compositions were controlled by the initial monomer concentration to afford different copolymer compositions in the range of 21 – 69 wt%. Polymerization was faster with CuCl than with CuBr under the same initial monomer concentration and the MMA contents of the resulting copolymers were varied

with the monomer concentration. The cleavage reaction between the PP backbone and PMMA branches was successfully carried out to give the detached PMMA branches. The molecular weight of the detached PMMA branch was higher than the theoretical value and the initiation efficiency of the macroinitiator was estimated to be in the wide range of 0.37 – 0.94. The thus-obtained PP-g-PMMA was evaluated as a compatibilizer for the PP/PLA polymer blends. The tensile strength and Young's modulus of the PP/PLA polymer blends with 5 wt% of PP-g-PMMA were remarkably higher than without PP-g-PMMA and in the case of the PP/PLA/PP-g-PMMA ternary blends the strength and modulus gradually increased with increasing the PLA composition. In addition, the flexural properties of these polymer blends also denoted the same tendency for the tensile properties. These results indicate that the PP-g-PMMA is a good compatibilizer for PP/PLA blends. On the other hand, the elongation at break and the Izod impact strength of the PP/PLA binary blends were much lower than those of the PP and the addition of the PP-g-PMMA was ineffective in improving these properties. TEM observations of these blend samples also demonstrated that the addition of the PP-g-PMMA promoted a fine dispersion between PP and PLA, resulting in an improvement in the mechanical properties of the polymer blends. However, the EP domains, which are expected to act as an impact modifier, interacted with not the PLA phase but only the PP phase in the polymer blends due to their poor compatibility in the PLA. Therefore, the significant decreases in the elongation and impact strength in the PP/PLA blends is caused by the localization of the EP domains in the PP phase.

## References

1. Koning, C.; Van Duin, M.; Pagnoulle, C.; Jerome, R. *Prog. Polym. Sci.* **1998**, *23*, 707-757.
2. Yin, M.; Baker, G. L. *Macromolecules* **1999**, *32*, 7711-7718.
3. Eguiburu, J. L.; Fernandez-Berridi, M. J.; Cossio, F. P.; San Roman, J. *Macromolecules* **1999**, *32*, 8252-8258.
4. Reddy, N.; Nama, D.; Yang, Y. *Polym. Degrad. Stab.* **2008**, *93*, 233-241.
5. Kawahara, N.; Saito, J.; Matsuo, S.; Kaneko, H.; Matsugi, T.; Kashiwa, N. *Adv. Polym. Sci.* **2008**, *217*, 79-119.
6. Lopez, R. G.; D'Agosto, F.; Boisson, C. *Prog. Polym. Sci.* **2007**, *32*, 419-454.
7. Chung, T. C. *Prog. Polym. Sci.* **2002**, *27*, 39-85.
8. Dong, J. -Y.; Hu, Y. *Coord. Chem. Rev.* **2006**, *250*, 47-65.
9. Caporaso, L.; Iudici, N.; Oliva, L. *Macromol. Symp.* **2006**, *234*, 42-50.
10. Liu, S.; Sen, A. *Macromolecules* **2001**, *34*, 1529-1532.
11. Matsugi, T.; Kojoh, S.; Kawahara, N.; Matsuo, S.; Kaneko, H.; Kashiwa, N. *J. Polym. Sci. Part A: Polym. Chem.* **2003**, *41*, 3965-3973.
12. Inoue, Y.; Matsugi, T.; Kashiwa, N.; Matyjaszewski, K. *Macromolecules* **2004**, *37*, 3651-3658.
13. Hwu, J. -M.; Chang, M. -J.; Lin, J. -C.; Cheng, H. -Y.; Jiang, G. -J. *J. Organomet. Chem.* **2005**, *690*, 6300-6308.

14. Chung, T. C.; Rhubright, D.; Jiang, G. J. *Macromolecules* **1993**, *26*, 3467-3471.
15. Kaneko, H.; Saito, J.; Kawahara, N.; Matsuo, S.; Matsugi, T.; Kashiwa, N. *Polymer* **2008**, *49*, 4576-4584.
16. Chung, T. C.; Lu, H. L.; Ding, R. D. *Macromolecules* **1997**, *30*, 1272-1278.
17. Dong, J. Y.; Hong, H.; Chung, T. C.; Wang, H. C.; Datta, S. *Macromolecules* **2003**, *36*, 6000-6009.
18. Caporaso, L.; Iudici, N.; Oliva, L. *Macromolecules* **2005**, *38*, 4894-4900.
19. Park, E. -S.; Jin, H. -J.; Lee, I. -M.; Kim, M. -N.; Lee, H. S.; Yoon, J. -S. *J. Appl. Polym. Sci.* **2002**, *83*, 1103-1111.
20. Lu, Y.; Hu, Y.; Wang, Z. M.; Manias, E.; Chung, T. C. *J. Polym. Sci. Part A: Polym. Chem.* **2002**, *40*, 3416-3425.
21. Chung, T. C.; Rhubright, D. *Macromolecules* **1994**, *27*, 1313-1319.
22. Lu, Y.; Hu, Y.; Chung, T. C. *Polymer* **2005**, *46*, 10585-10591.
23. Kaneko, H.; Matsuo, S.; Kawahara, N.; Saito, J.; Matsugi, T.; Kashiwa, N. *Macromol. Symp.* **2007**, *260*, 9-14.
24. Spaleck, W.; Kueber, F.; Winter, A.; Rohrmann, J.; Bachmann, B.; Antberg, M.; Dolle, V.; Paulus, E. F. *Organometallics* **1994**, *13*, 954-963.
25. Matyjaszewski, K.; Shipp, D. A.; Wang, J. -L.; Grimaud, T.; Patten, T. E. *Macromolecules* **1998**, *31*, 6836-6840.
26. Hong, S. C.; Pakula, T.; Matyjaszewski, K. *Macromol. Chem. Phys.* **2001**, *202*, 3392-3402.
27. Schellekens, M. A. J.; Klumperman, B.; van der Linde, R. *Macromol. Chem. Phys.* **2001**, *202*, 1595-1601.
28. Zhang, G.; Zhang, J.; Wang, S.; Shen, D. *J. Polym. Sci. Part B: Polym. Phys.* **2003**, *41*, 23-30.

## Chapter 25

# Novel Polyolefin Hybrids via Controlled/Living Radical Polymerization

**J. Saito, N. Kawahara, S. Matsuo, H. Kaneko,  
T. Matsugi, N. Kashiwa**

**Research Center, Mitsui Chemicals Inc., 580-32, Nagaura, Sodegaura,  
Chiba, 299-0265, Japan**

Polyolefin/non-polyolefin hybrid materials, named ‘Polyolefin Hybrids’, which are block, graft copolymers, have been synthesized via controlled/living radical polymerizations using a polyolefin macroinitiator. Polyolefin hybrids show a microphase separated morphology composed of polyolefin and non-polyolefin segments and display various enhanced physical properties by the selection of non-polyolefin segments. In addition, they exhibit a remarkable compatibility toward polyolefin and non-polyolefin blend polymers leading to the development of new polymer alloy materials. As an example of the polyolefin hybrids, the surface-polar-polymer-grafted polypropylene sheets that exhibit high hydrophilicity, electroconductivity, and antibacterial property is obtained. Thus, polyolefin hybrids are valuable value-added polyolefins.

Nowadays, various kinds of plastic products are used in our daily lives. In detail, polyolefins, represented by polyethylene and polypropylene, are modern indispensable materials because of their superb properties, namely, they are lightweight, inexpensive, possess good processability, chemical stability, high mechanical strength, etc. Therefore, their applications range over industrial materials, household products, and automobile parts to name just a few areas. The worldwide production of PE and PP went beyond 100,000,000 ton/year in 2005 and it is still increasing.

Recently, various approaches have been carried out to give polyolefins high functionality. Of these, the development for composite polyolefin materials has

been widely noted, for example, composites combined with polyolefin and organic materials such as polar polymers, carbon fiber or carbon nanotube, even inorganic materials such as metals, talc, clay, and silica<sup>1-4</sup>. However, polyolefins do not possess enough compatibility with other materials due to their poor polarity. Therefore, the development of these composite materials has focused on how both polyolefins and other materials make finely dispersed with each other. In this paper, we introduce the syntheses, structures and properties of new hybrid polymers consisting of polyolefin and polar polymers, named 'Polyolefin Hybrids'. Polyolefin hybrids are structurally well-defined hybrid polymers which have a chemical bond between polyolefin and non-polyolefin segments. The aim behind the development of polyolefin hybrids is to create novel value-added polyolefin materials which give polyolefins various new properties, such as improved mechanical strength, heat-resistance, compatibility, adhesion, hydrophilicity, electric conductivity, anti-bacterial properties, etc, derived from the non-polyolefin segments.

## **The Syntheses of Polyolefin Hybrids via Controlled/Living Radical Polymerization**

Generally, in order to introduce polar segments (functional groups or polar polymers) to polyolefins, it has been found necessary to utilize radical grafting methods harnessing either physical (corona, ultra-violet, electron beam, or plasma radiations) and/or chemical (peroxide, or AIBN, etc) techniques. However, it is difficult to control the grafted position and/or molecular weight of polar polymer segments precisely by these methods. In addition, undesirable side reactions such as the bond scission or cross-linkage of polyolefin segments can not be avoided. Therefore, structurally ill-defined functionalized polyolefins have been produced by conventional methods, thus far. In contrast, it has been reported that olefin polymerization using transition metal complex catalysts utilize methods for the syntheses of the functionalized polyolefins<sup>5-20</sup>. They are classified into three methods, an introduction of functional groups by copolymerization with olefin and polar monomers, an addition of functional groups to polymer chain-ends by the chain-transfer agents, and transformation to other functional groups by the chemical reaction with the obtained functionalized polyolefins. By using these methods, structurally well-defined functionalized polyolefins can be obtained. Recently, we have reported that various kinds of polyolefin hybrids have been synthesized from the thus obtained functional polyolefins using three methods, (1) polyolefin macroinitiator (PO-MI), (2) polyolefin macromonomer and (3) reactive polyolefin<sup>21-35</sup>. In this paper, we introduce the syntheses of polyolefin hybrids by the combination of PO-MI or chain transfer agent, and controlled/living radical polymerization (CRP) such as RAFT<sup>36,37</sup> or ATRP<sup>38-40</sup>, their properties and potential usages.

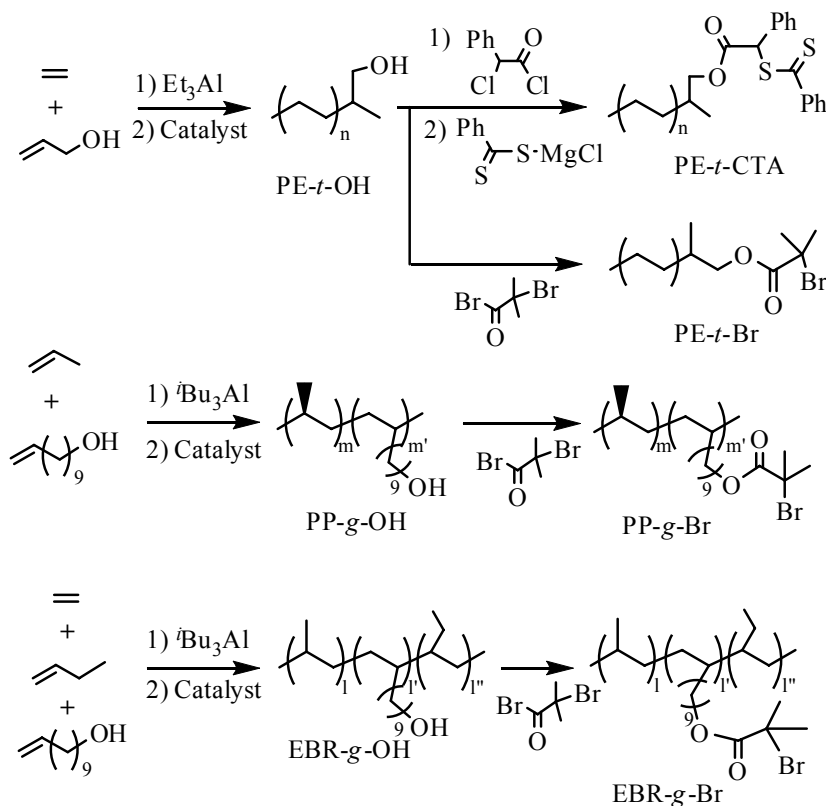


Figure 1. The Syntheses of Polyolefin Macroinitiators and a Chain Transfer Agent

PO-MIs or chain transfer agent were prepared by a reaction with the hydroxyl group containing polyolefins and a reagent that worked as an initiator or chain transfer agent for CRP. The molecular weight, comonomer ratio, position and amount of hydroxyl groups of the produced polyolefins were controlled by selecting appropriate copolymerization conditions, for example, kinds of catalysts, polymerization temperature, kinds of (co)monomers, and (co)monomer concentration (Figure 1).

For instance, terminal hydroxylated polyethylene (PE-*t*-OH) was prepared by the copolymerization of ethylene and allyl alcohol protected with triethylaluminum using a metallocene catalyst system<sup>20,21</sup>. The isotactic polypropylene having a grafted  $\text{C}_9\text{H}_{18}\text{OH}$  substituent (PP-*g*-OH) was obtained by the copolymerization of propylene and 10-undecen-1-ol protected with triisobutylaluminum using a metallocene catalyst system<sup>33</sup>. Poly(ethylene-*co*-1-butene) having a grafted  $\text{C}_9\text{H}_{18}\text{OH}$  substituent (EBR-*g*-OH) was also obtained in a similar way<sup>28</sup>. Chain transfer agent for RAFT polymerization was synthesized by the reaction of PE-*t*-OH and 2-chloro-2-phenylacetyl chloride, followed by the treatment with the dithiocarbonyl Grignard reagent. As a result,

polyethylene-carbonylphenylmethyl dithiobenzoate was obtained as a chain transfer agent (PE-*t*-CTA)<sup>30</sup>. Then, PO-MIs for ATRP were prepared by the reaction of hydroxylated POs (PE-*t*-OH, PP-*g*-OH and EBR-*g*-OH) and 2-bromoisobutyryl bromide to yield PE-*t*-Br, PP-*g*-Br and EBR-*g*-Br, respectively.

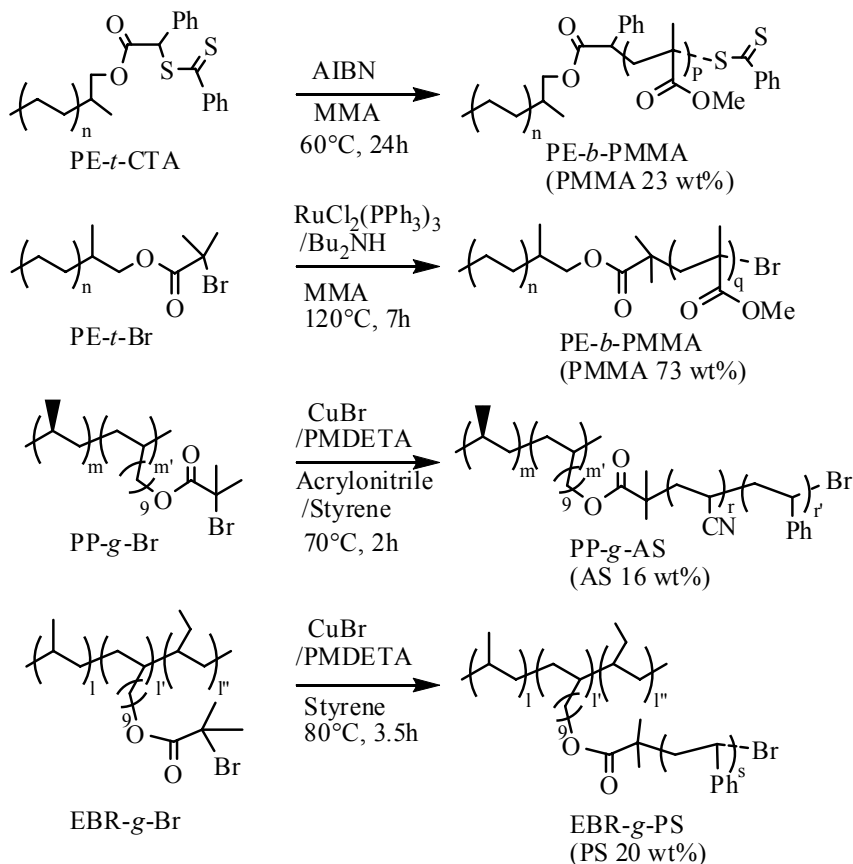


Figure 2. Some Synthetic Examples of Polyolefin Hybrids

Some synthetic examples of polyolefin hybrids are shown in Figure 2. RAFT polymerization of PE-*t*-CTA for MMA was initiated by AIBN in toluene at 60 °C. PE-*b*-PMMA (PMMA contents: 23 wt%) was successfully obtained<sup>30</sup>. PE-*b*-PMMA having the contents of PMMA (73 wt%) was yielded from PE-*g*-Br by ATRP for MMA with  $\text{RuCl}_2(\text{PPh}_3)_3/\text{Bu}_2\text{NH}$  as a catalyst<sup>21</sup>. ATRP for acrylonitrile/styrene using PP-*g*-Br as a PO-MI was carried out to produce PP-*g*-AS (poly(acrylonitrile-*co*-styrene)). Then, EBR-*g*-PS was obtained from EBR-*g*-Br as a PO-MI by ATRP for styrene<sup>28</sup>. By selecting the kinds of PO-MIs and polar monomers for CRP, various kinds of PO hybrids have been obtained.



## Structural Features of Polyolefin Hybrids

Polyolefin hybrids possess immiscible segments, polyolefins and non-polyolefins, linked by a chemical bond. Therefore, they display unique phase structures in which both polyolefin and polar polymer segments are finely dispersed at the nanometer level. In Figure 3, TEM micrographs of the blend polymer comprising PE and PMMA, and polyolefin hybrids, PE-*b*-PMMA, PP-*g*-AS, and EBR-*g*-PS are displayed. Although PE and PMMA blend polymer exhibited a macrophase separated morphology, PE-*b*-PMMA showed a microphase separated morphology between polyethylene and PMMA segments. Likewise, PP-*g*-AS, and EBR-*g*-PS also displayed microphase separated morphologies. Thus, polyolefin hybrids can control phase structures of the polymer consisting of polyolefin and polar polymer segments. These materials having such microphase separated morphologies are expected to give polyolefins with superior properties, such as high mechanical strength, hydrophilicity, adhesion, compatibility, electroconductivity, etc, derived from the polar polymer segments.

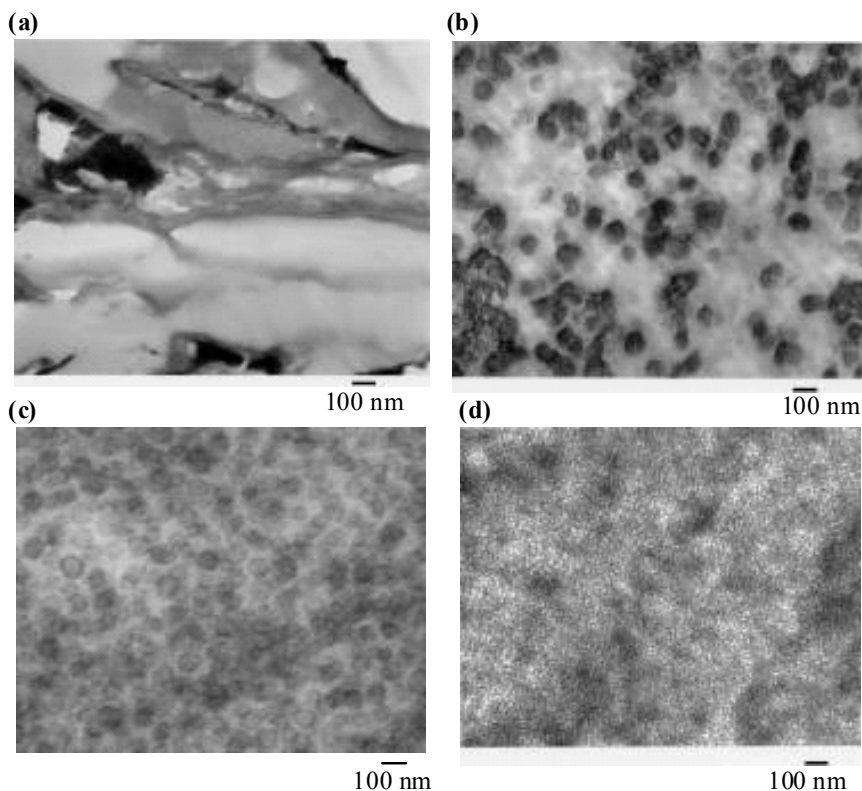


*Figure 3. TEM Micrographs of (a) PE and PMMA (25/75 wt%), (b) PE-*b*-PMMA (PMMA contents 75 wt%), (c) PP-*g*-AS (AS contents 16 wt%) and (d) EBR-*g*-PS (PS contents 20 wt%)*

In addition, by applying our synthetic techniques involving polyolefin hybrids applied to the surface modification of polypropylene films, surface polar polymer grafted polypropylene films can be synthesized. Namely, ATRP for MMA was carried out on the surface of a pressed PP films made by PP-MI. As a result, PP sheets having very thin and homogeneous PMMA layers were successfully obtained<sup>41</sup>. The thickness of the surface PMMA layer can be controlled in the range of 20-100 nm by the polymerization conditions. Moreover, the grafted PMMA density is achieved in a highly concentrated region of 0.19 -0.35 chain/nm<sup>2</sup> by altering the initiator concentration of the PP-MIs. Since polyolefins possess higher processability than other materials, we were able to be apply this knowledge to produce various kinds of molded materials based on polyolefins, such as sheets, fibers, particles, etc, which can be utilized as novel high performance materials (Figure 4).

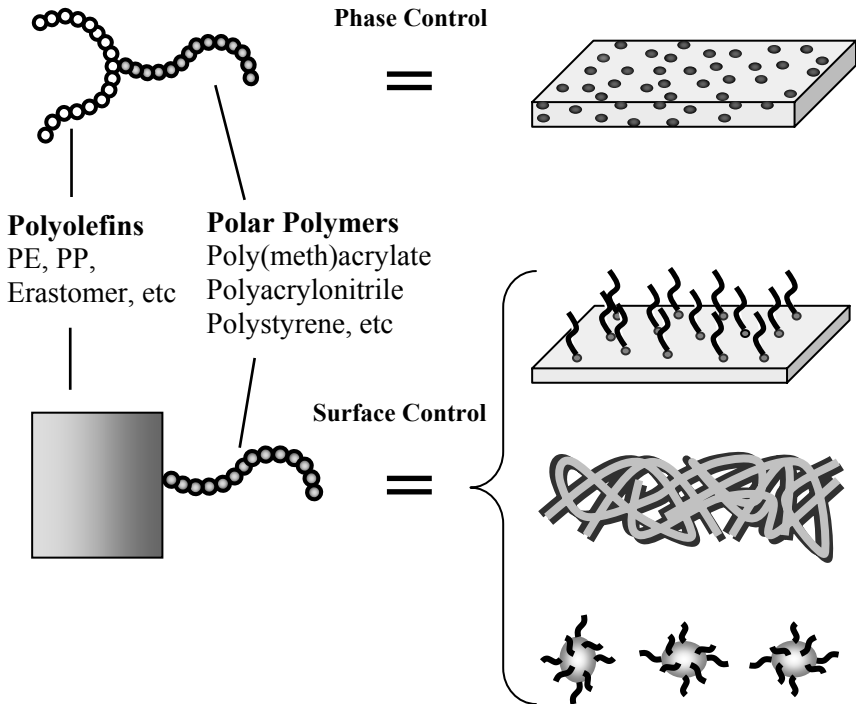


Figure 4. Phase and Surface Control by Polyolefin Hybrids

## Properties of Polyolefin Hybrids

Some physical properties of polyolefin hybrids are shown in Figure 5. Figure 5(A) displays a plot of polar polymer segments versus Flexural Modulus (FM) values of PP-g-PMMA and PP-g-AS. As the polar polymer (PMMA, or AS) contents increased from 0 wt% to 35 wt%, FM values of PP-g-PMMA and PP-g-AS increased from 1780 MPa of the precursor PP to 2240 MPa, 2400 MPa, respectively. In contrast, the FM value of the PP and PMMA blend (65/35 wt%) polymer was not changed (1800 MPa). Figure 5(B) shows the relationship between the contents of P<sup>n</sup>BuA (poly(n-butylacrylate)) and Izod impact strength values of PP-g-P<sup>n</sup>BuA. When P<sup>n</sup>BuA polymer contents were 33 wt%, Izod impact strength value was remarkably enhanced to 354 J/m. In Figure 5(C), the temperature dependence of the storage modulus of EBR-g-PS and the blend polymer of EBR/PS are displayed, so that, the stress-strain behavior of EBR-g-PS is shown in Figure 5(D). Figure 5(C) reveals that EBR-g-PS possessed higher heat-resistance than the blend polymer of EBR/PS. In addition, EBR-g-PS still retained enough elastic property although 20 wt% of hard PS segment was grafted to the soft EBR segment in Figure 5(D). These results clearly indicate that polyolefin hybrids are capable of increasing the physical properties compared to those of the precursor polyolefins.

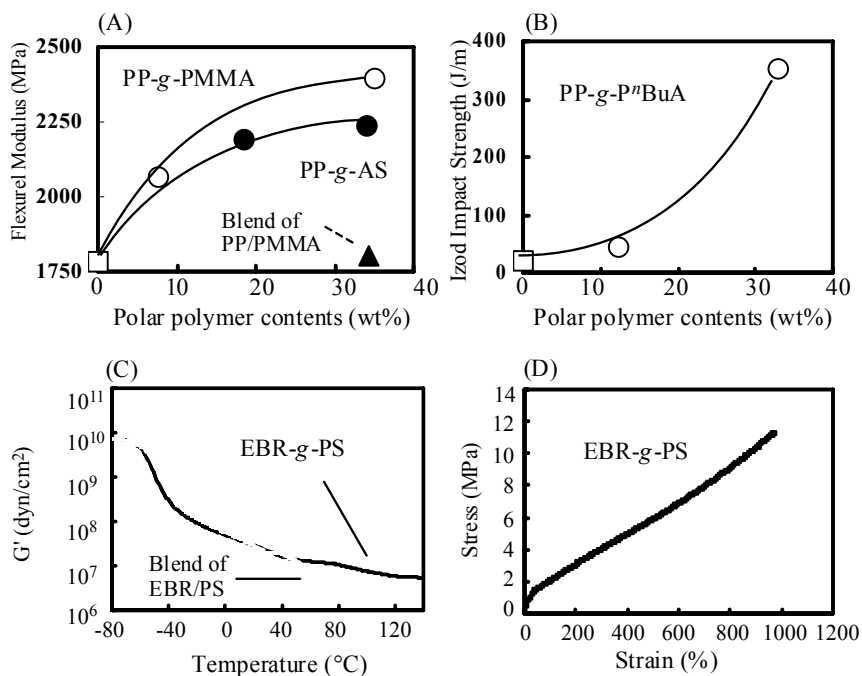


Figure 5. Physical Properties of Polyolefin Hybrids

On the other hand, polyolefin hybrids existing as hydrophilic polar polymer segments introduced to PP exhibited properties arising from hydrophilicity. The water contact angles on the surface of the film prepared by PP-g-P(PEGMA) (poly(polyethyleneglycol methacrylate)) is exhibited in Figure 6(A). As P(PEGMA) contents increased, the values of the contact angle were linearly decreased, meaning an increase in hydrophilicity on the surface. Figure 6(B) represents the plot of surface resistance values versus PMCC (poly(methacryloylcoline chloride)) contents on the surface of the film molded by PP-g-PMCC. Generally, the surface resistance value is correlated to the electroconductivity and polypropylene film surface showing low electroconductivity is displayed as  $1.0 \times 10^{17} \Omega$ . The surface resistance value of PP-g-PMCC (PMCC contents, 32 wt%) film is represented as a very low value of  $2.1 \times 10^7 \Omega$ , meaning that the obtained film had high electroconductivity as polypropylene film. Thus, polyolefin hybrids can increase not only mechanical strength but also hydrophilicity and electroconductivity.

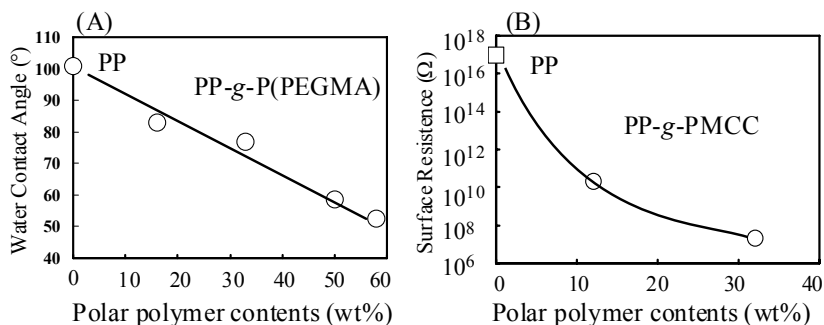
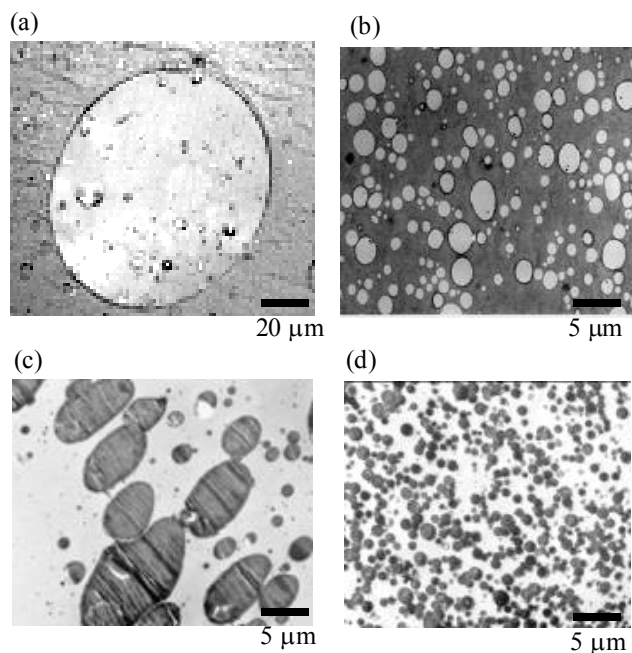


Figure 6. Water Contact Angles and Surface Resistance Values of Polyolefin Hybrid Films

One of the most promising applications of polyolefin hybrids is a compatibilizer for blend polymer for polyolefin and non-polyolefin. In Figure 7, TEM micrographs of PP/PMMA and EBR/poly(lactic acid) (PLA) blend polymers with and without polyolefin hybrids as a compatibilizer are displayed. Figure 7(a) represents the phase structure of a PP/PMMA (62/38 wt%) blend polymer. Since PP and PMMA are immiscible, huge PMMA domains ( $> 20 \mu\text{m}$ ) exist in the PP matrix. When 5 wt% of PP-g-PMMA (PMMA contents 38 wt%) was added to this blend polymer as a compatibilizer, PMMA domains were finely dispersed as is shown in Figure 7(b). As a result, the physical properties for both FM and FS were drastically enhanced from 35.3 MPa for FS and 1800 MPa for FM to 61.4 MPa for FS and 2200 MPa for FM, respectively.

Figure 7(c) shows the phase structure of the blend polymer composed of EBR/PLA (15/85 wt%). Macro-phase separated EBR domains in the PLA matrix were observed. By adding 5 wt% of PE-*b*-PMMA (PMMA contents; 75 wt%) to EBR/PLA (10/85 wt%) as a compatibilizer, finely dispersed EBR domains are observed in Figure 7(d). As a result, this polymer indicates very high Izod impact strength value (378 J/m) vis-à-vis the blend polymer's value

(72 J/m). From these results, it was confirmed that polyolefin hybrids possess high potential as a compatibilizer for a polyolefin/polar polymer alloy system.



*Figure 7. TEM Micrographs of (a) PP/PMMA (Weight ratio 68/32); (b) PP/PMMA/PP-g-PMMA (Weight ratio 68/32/5); (c) PLA/EBR (Weight ratio 85/15); (d) PLA/EBR/PE-b-PMMA (Weight ratio 85/15/5)*

A PP sheet having an initiator (PP-MI sheet) was prepared by the hot pressing of PP-g-Br. ATRP for MCC (methacryloylcoline chloride) having a hydrophilic ammonium cation moiety on the surface of a PP-MI sheet was carried out in ethanol with CuBr/PMDETA as a catalyst<sup>41</sup>. The formation of a very thin (50 nm) poly(methacryloylcoline chloride) layer was confirmed by a TEM micrograph (Figure 7). Figure 7(b) shows that ATRP occurs only on the surface of the PP-MI sheet. The water contact angle of the thus obtained PP hybrid sheet was very low (11°) compared to that of the PP-MI sheet (94°) in Figure 7(a). So that the surface resistance value of the obtained sheet was also a low value of  $4.9 \times 10^7 \Omega$ , meaning high electric conductivity.

In addition, thus obtained surface PMCC grafted PP sheet displayed not only hydrophilicity but also antibacterial property against coliform and staph aureus derived from the surface PMCC segment in Table 1.

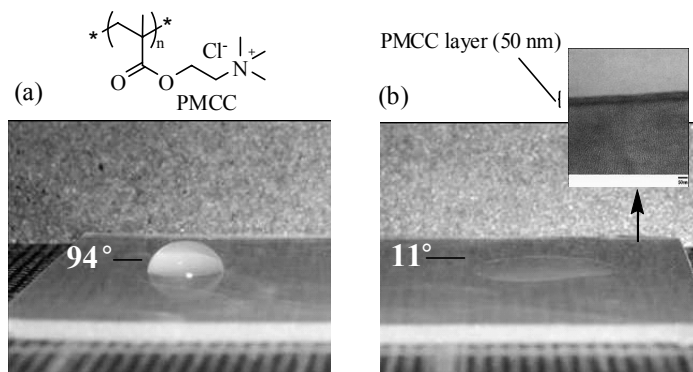


Figure 8. Water contact angle of (a) PP sheet and (b) surface PMCC grafted PP sheet and TEM micrograph of a cross-section of (b)

**Table 1. Antibacterial Properties of PMCC grafted PP sheet**

	<i>Coliform</i>	<i>Staph Aureus</i>
Inoculated Dose	$2.1 \times 10^5$	$2.2 \times 10^5$
Neat-PP sheet (after 24h)	$1.0 \times 10^7$	$1.2 \times 10^6$
PMCC grafted sheet (after 24h)	30	< 10

NOTE: The unit is the number of fungi per test piece

## Conclusion

The syntheses, properties and potential applications of polyolefin/non-polyolefin hybrid polymers, ‘Polyolefin Hybrids’, via controlled/living radical polymerization have herein been introduced. ‘Polyolefin Hybrids’ can control the phase structures, and the surface structures on molded polyolefin materials. ‘Polyolefin Hybrids’ can enhance the physical properties of polyolefins as well as add new properties such as hydrophilicity and antibacterial properties to them. Novel value-added polyolefin materials, “Polyolefin Hybrids”, have great potential as new value-added materials.

## Acknowledgment

We would like to thank Dr. R. Sugimoto, Dr. A. Todo and Mr. A. Valentine for fruitful discussions and suggestions.

## References

1. Kawasumi, M.; Hasegawa, N.; Kato, M.; Usuki, A.; Okada, A. *Macromolecules*, **1997**, *30*, 6333.
2. Kato, M.; Okamoto, H.; Hasegawa, N.; Tsukigase, A.; Usuki, A. *Polym. Eng. Sci.*, **2003**, *43*, 1312.
3. Kumar, S.; Doshi, H.; Srinivasaro, M.; Park, J. O.; Schiraldi, D. A. *Polymer*, **2002**, *43*, 1701.
4. Wiemann, K.; Kaminsky, W.; Gojny, F. H.; Shulte, K. *Macromol. Chem. Phys.* **2005**, *206*, 1472.
5. Mülhaupt, R.; Duschek, T.; Rieger, B. *Makromol. Chem. Makromol. Symp.*, **1991**, *48/49*, 317.
6. Chung, T. C. *Prog. Polym. Sci.*, **2002**, *27*, 39.
7. Yanjarappa, M. J.; Sivaram, S. *Prog. Polym. Sci.*, **2002**, *27*, 1347.
8. Dong, J-Y.; Hu, Y. *Coord. Chem. Rev.*, **2006**, *250*, 47.
9. Johnson, L. K.; Mecking, S.; Brookhart, M. *J. Am. Chem. Soc.*, **1996**, *118*, 267.
10. Mecking, S.; Johnson, L. K.; Wang, K.; Brookhart, M. *J. Am. Chem. Soc.*, **1998**, *120*, 888.
11. Younkin, T. R.; Connor, E. F.; Henderson, J. I.; Friedrich, S. K.; Grubbs, R. H.; Bansleben, D. A. *Science*, **2000**, *287*, 460.
12. Drent, E.; Dijk, R. van; Ginkel, R. van; Oort, B. van; Pugh, R. I. *Chem. Commun*, **2002**, 744.
13. Sujith, S.; Joe, D. J.; Na, S. J.; Park, Y.-W.; Choi, C. H.; Lee, B. Y. *Macromolecules*, **2005**, *38*, 10027.
14. Hearley, A. K.; Nowack, R. J.; Rieger, B. *Organometallics*, **2005**, *24*, 2755.
15. Luo, S.; Jordan, R. F. *J. Am. Chem. Soc.*, **2006**, *128*, 12072.
16. Liu, S.; Borkar, S.; Newsham, D.; Yennawar, H.; Sen, A. *Organometallics*, **2007**, *26*, 210.
17. Kochi, T.; Noda, S.; Yoshimura, K.; Nozaki, K. *J. Am. Chem. Soc.*, **2007**, *129*, 8948.
18. Aaltonen, P.; Lofgren, B. *Macromolecules*, **1995**, *28*, 5353.
19. Hagiwara, H.; Tsuchihara, K.; Sugiyama, J.; Takeuchi, K.; Shiono, T. *Macromolecules*, **2004**, *37*, 5145.
20. Imuta, J.; Kashiwa, N.; Toda, Y. *J. Am. Chem. Soc.*, **2002**, *124*, 1176.
21. Matsugi, T.; Kojoh, S.; Kawahara, N.; Matsuo, S.; Kaneko, H.; Kashiwa, N. *J. Polym. Sci. A*, **2003**, *41*, 3965.
22. Saito, J.; Kawahara, N.; Matsuo, S.; Kaneko, H.; Matsugi, T.; Kashiwa, N. *Koubunshi Ronbunshu*, **2007**, *64*, 897.
23. Kawahara, N.; Saito, J.; Matsuo, S.; Kaneko, H.; Matsugi, T.; Kashiwa, N. *Adv. Polym. Sci.*, **2008**, *217*, 79.
24. Kashiwa, N.; Matsugi, T.; Kojoh, S.; Kaneko, H.; Kawahara, N.; Matsuo, S.; Nobori, T.; Imuta, J. *J. Polym. Sci. A*, **2003**, *41*, 3657.
25. Inoue, Y.; Matsugi, T.; Kashiwa, N.; Matyjaszewski, K. *Macromolecules*, **2004**, *37*, 3651.
26. Kaneko H.; Kojoh, S.; Kawahara, N.; Matsuo, S.; Matsugi, T.; Kashiwa, N. *Macromol. Symp.*, **2004**, *213*, 335.

27. Kaneko, H.; Kojoh, S.; Kawahara, N.; Matsuo, S.; Matsugi, T.; Kashiwa, N. *J. Polym. Sci. A*, **2005**, *43*, 5103.
28. Matsugi, T.; Kojoh, S.; Kawahara, N.; Matsuo, S.; Kaneko, H.; Onogi, T.; Kashiwa, N. *Polymer Preprints*, **2005**, *46(2)*, 215.
29. Kaneko, H.; Matsugi, T.; Kawahara, N.; Matsuo, S.; Kojoh, S.; Kashiwa, N. *Kinetics and Catalysis*, **2006**, *47*, 227.
30. Kawahara, N.; Kojoh, S.; Matsuo, S.; Kaneko, H.; Matsugi, T.; Kashiwa, N. *Polym. Bull.*, **2006**, *57*, 805.
31. Matsuo, S.; Matsugi, T.; Saito, J.; Kawahara, N.; Kaneko, H.; Kashiwa, N. *Stud. Surf. Sci. and Cat.*, **2006**, *161*, 1.
32. Kawahara, N.; Saito, J.; Matsuo, S.; Kaneko, H.; Matsugi, T.; Kashiwa, N. *Polym. Bull.*, **2007**, *59*, 177.
33. Kaneko, H.; Matsuo, S.; Kawahara, N.; Saito, J.; Matsugi, T.; Kashiwa, N. *Macromol. Symp.*, **2007**, *260*, 9.
34. Kaneko, H.; Saito, J.; Kawahara, N.; Matsuo, S.; Matsugi, T.; Kashiwa, N. *Polymer*, **2008**, *49*, 4576.
35. Kaneko, H.; Saito, J.; Kawahara, N.; Matsuo, S.; Matsugi, T.; Kashiwa, N. *J. Polym. Sci. A*, **2009**, *47*, 812.
36. Moad, G.; Rizzardo, E.; Thang, S. H. *Aust. J. Chem.* **2006**, *59*, 669.
37. Chiefari, J.; Chong, Y. K.; Ercole, F.; Krstina, J.; Jeffery, J.; Le, T. P. T.; Mayadunne, R. T. A.; Meijs, G. F.; Moad, C. L.; Moad, G.; Rizzardo, E.; Thang, S. H. *Macromolecules* **1998**, *31*, 5559.
38. Matyjaszewski, K.; Xia, J. *Chem. Rev.*, **2001**, *101*, 2921.
39. Kamigaito, M.; Ando, T.; Sawamoto, M. *Chem. Rev.*, **2001**, *101*, 3689.
40. Hawker, C. J.; Bosman, A. W.; Harth, E. *Chem. Rev.*, **2001**, *101*, 3661.
41. Submitted for publication.



## Chapter 26

# Opportunities in Controlled Radical Polymerization

James Spanswick<sup>1</sup> and Bernard Pike<sup>2</sup>

<sup>1</sup>Bridges TIC 2365 Albright Lane, Wheaton, Illinois 60189

<sup>2</sup>Patent Attorney Troutman Sanders LLP, 1001 Haxall Point, Richmond, VA 23219

Controlled Radical Polymerization (CRP) is the most recently developed polymerization technology for the preparation of well defined functional materials. Three recently developed CRP processes are based upon forming a dynamic equilibrium between active and dormant species that provides a slower more controlled chain growth than conventional radical polymerization. Nitroxide Mediated Polymerization (NMP), Atom Transfer Radical Polymerization (ATRP) and Reversible Addition Fragmentation Transfer (RAFT) have been developed, and improved, over the past two decades, to provide control over radical polymerization processes. This chapter discusses the patents issued on ATRP initiation procedures, new functional materials prepared by CRP, and discusses recent improvements in all three CRP processes. However the ultimate measure of success for any CRP system is the preparation of commercially viable products using acceptable economical manufacturing procedures.

### Introduction and Background

Controlled Radical Polymerization (CRP) is the most recently developed polymerization technology that can be applied to the preparation of well defined (see below) functional materials. The most broadly utilized CRP processes are based on formation of an equilibrium between active and dormant species. This equilibrium provides a slower, more uniform chain growth than conventional

radical polymerization. Earlier developments on various aspects of “control” in radical polymerization processes, which started more than 40 years ago, are discussed by Matyjaszewski in chapter 8 of “The Handbook of Radical Polymerization” (1) including discussions on the contributions to the field by pioneering researchers such as Borsig, (2) Braun, (3) Kabanov, (4,5) Minoura, (6) and Otsu. (7)

Otsu coined the term “living” radical polymerization in 1982 to describe a polymerization conducted in the presence of dithiocarbamates. (7) However, as in conventional radical polymerization systems, polydispersities of the polymers formed in this process were generally high, molecular weight did not increase with conversion and initiation efficiencies were low. Another step toward development of CRP was disclosed in a patent application in 1984. (8,9) The patent describes the action of stable free radicals on the polymerization of acrylate based monomers. Chain end reactivation was demonstrated but the majority of the examples described the formation of low molecular weight products with terminal substituted alkoxyamine end groups. This concept of Stable Free Radical mediated Polymerization (SFRP) got a critical boost from Georges’ work at Xerox in 1993. (10,11) Goerges’ work describes a process for the preparation of higher molecular weight styrene-based polymers in the presence of a thermally labile terminal stable free radical, TEMPO, was described. Further development of SFRP involved use of more labile stable free radicals, and preformed alkoxyamines, (12) to provide more effective control over the dynamic equilibrium. Though considered a SFRP process these developments have progressed under the nomenclature of Nitroxide Mediated Polymerization. (13)

Atom Transfer Radical Polymerization (ATRP) was the second of the new CRP procedures to be disclosed (14,15) and has been successfully applied to copolymerization of a much wider spectrum of monomers than either of the existing SFRP processes. (16) Typically ATRP includes a transition metal catalyst to create a dynamic equilibrium with an initiator molecule comprising a radically transferable atom or group, often a halogen atom, causing reversible formation of a propagating radical by transferring the halogen back and forth between the catalyst and the dormant initiator/polymer chain end. ATRP was originally developed in 1994 and has been successfully used to prepare (*well defined*) polymers with predetermined molecular weights, low polydispersity, controlled composition, preselected topology and, most recently, tacticity. This chapter will discuss patents filed to protect various ATRP initiation procedures and preparation of novel functional materials using this procedure.

The other CRP process to be disclosed in the 1990’s relies on degenerative transfer of an atom or group and is best exemplified by the reversible addition-fragmentation transfer (RAFT) process that employs dithioesters as chain-transfer agents which was introduced in 1998. (17-19)

According to a SciFinder Scholar search, using various encompassing search terms#, for the different CRP processes, there are now more than 11,000 papers and published patents/application on CRP, with 7,000 publications on ATRP alone. Within the data set over 1500 patents use the abbreviations (CRP, ATRP, NMP and RAFT) for the different CRP processes.

<b>SciFinder Search Terms<sup>#</sup></b>	<b>No. of Patents Using the Term</b>
ATRP	1537*
CRP	1137
NMP	418
RAFT	196

<sup>#</sup>Terms used in SciFinder searches;

1. ATRP or atom transfer polymn or metal mediated radical or metal catalyzed radical
2. CRP or LRP or controlled radical polymn or living radical polymn
3. NMP or SFRP or nitroxide mediated polymn or stable free polymn
4. RAFT or reversible addition transfer or degenerative transfer or catalytic chain transfer

For all refine with RADICAL POLYMN

\*There are 24 corporations with more than ten patents.

A similar result can be obtained by a search of the issued and published patent applications available in the USPTO electronic database related to CRP, (results as of December 2008).

<b>US Patents Using Term(s)</b>	<b>Issued Patents</b>	<b>Published Applications</b>
ATRP	450	934
ATRP & Nitroxide	177	413
ATRP & RAFT	117	380
Nitroxide & RAFT	93	273

Use of multiple terms such as ATRP and Nitroxide or Nitroxide and RAFT in a patent/application may indicate that many researchers believe that more than one CRP procedure can be used to provide materials suitable for evaluation in their target application. With increasing frequency, a generic paragraph indicating suitable CRP procedures is included in the application rather than a commitment to one process. However, while the materials prepared by different CRP processes are structurally the same there can be subtle differences in the product based on the process chosen and reaction process conditions selected, as a result of different levels of control. This could indicate specific products have to be prepared by one specific procedure; but it is possible to play with the exchange process in ATRP and obtain exactly the same polymers as those prepared by RAFT or NMP, although with higher chain end functionality and without homopolymer impurities. Indeed it is possible to obtain the same end groups, if desired, by conducting simple high yield post-polymerization transformation reactions. (20-23)

## **Market Evaluation**

The composition, topology and functionality of materials prepared by CRP can be preselected to provide products with a wide spectrum of desirable properties and many corporations have prepared a number of materials by CRP for internal evaluation in their target markets. Target markets for these tailored

materials include paints, pigments and coatings, personal care and cosmetics, plastics, textiles, rubbers, biocompatible materials and ink jet media.

Robert Matheson of DuPont at The Knowledge Foundation meeting in Boston in 2000 estimated that the size of the market for materials prepared by CRP was in the range of \$20 Billion per year. The same estimate is reached by another more recent unpublished analysis of targeted applications for materials prepared by CRP, see Figure 1.

In this analysis, the size of the markets for any product listed in an issued US Patent including the term “ATRP” were obtained from published documents. The analysis used an anticipated percentage of this overall market considered to be addressable by the materials disclosed in the patent to determine the overall market for CRP materials.

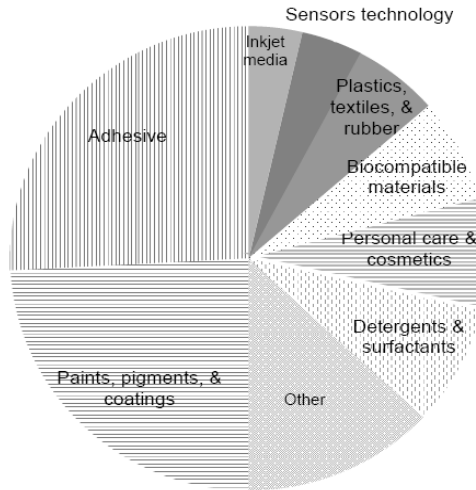


*Figure 1: Markets for products prepared by CRP*

<b>Markets</b>	<b>Market Size</b>	<b>Addressable Market</b>
Adhesives	\$21	\$0.7
Paints, pigments & coatings	\$83	\$8.3
Detergents & surfactants	\$14	\$0.2
Personal care & cosmetics	\$16	\$3.7
Biocompatible materials	\$14	\$2.6
Plastics, textiles & rubber	\$35	\$3.0
Sensor technology	\$2	\$0.1
Ink jet media	<u>\$15</u>	<u>\$1.5</u>
<b>Totals (all in \$billions)</b>	<b>\$200</b>	<b>\$20</b>

This analysis also generated a potential US market in the range of \$20 billion/year and a world market in excess of \$60 billion.

The size of the potential markets begs the question posed to one of the authors in 2004;

**“Why after 20 years of CRP has introduction of commercial products been so slow?”**

The reasons differ for each of the major CRP procedures, but as noted below, in 2004 each procedure still faced significant challenges.

- NMP
  - The Solomon patent (24) did not disclose a convenient broadly applicable technology and did not excite researchers
  - Georges work (10) produced higher MW polymers and triggered broad interest in CRP but the disclosed SFRP process was limited to monomers that undergo self initiation
  - There were limited commercially available initiators/control agents for polymerization of high molecular weight (meth)acrylates (25)
- ATRP
  - Alkyl halides, metal compounds and ligands are commercially available and it is the only catalytic CRP process, **BUT**
  - ATRP initially required high levels of catalyst thus requiring post-polymerization purification
  - Published procedures did not indicate existing equipment for bulk and emulsion free radical polymerization could be used
  - There was confusion over the definition of the term “ATRP” and its mechanism
- RAFT
  - There are no generic transfer agents and no specific transfer agents for selected monomers were commercially available
  - Odor and color of the product is a problem, particularly for low MW materials
  - Two large corporations owned patents covering RAFT agents
  - Final block copolymers contain some homopolymer.

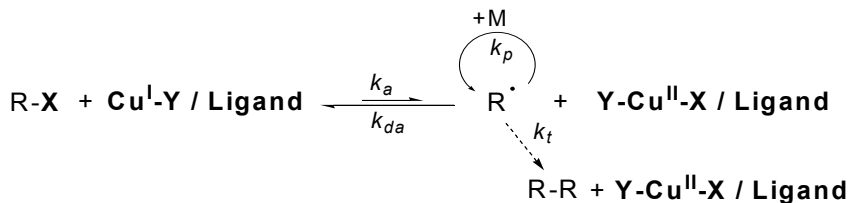
How these challenges have been overcome for NMP and RAFT will be summarized later but we would like to go into detail on the problems faced in commercialization of ATRP and hopefully clarify the intellectual property (IP) position, since both authors were involved in identifying and protecting the associated IP.

### **Development of ATRP**

First of all; “What is an ATRP?” It is a name given to a CRP process that displays similarities to the activation and deactivation steps occurring in catalytic “Atom Transfer Radical Addition” reactions. (14)

A typical simplified ATRP reaction scheme, *Scheme 1*, illustrates the four principle components of the reaction:

- 1) an initiator or dormant polymer chain comprising one or more radically transferable atoms or groups, R-X;
- 2) a transition metal capable of existing in two oxidation states, herein exemplified by copper, (Cu<sup>I</sup>-Y ↔ Y-Cu<sup>II</sup>-X);
- 3) a ligand to partially solubilize and adjust the reactivity of the formed transition metal complex (Ligand) and
- 4) one or more radically (co)polymerizable monomers, (M).



*Scheme 1: General scheme for transition metal catalyzed ATRP*

Generally ATRP reactions X and Y are the same radically transferable atom or group but as indicated in Scheme 1, for Cu mediated ATRP they might be different; Y can also be a non-transferable, non-coordinating counterion, such as a triflate.

Many authors have intermittently used other names/abbreviations for similar reactions utilizing the same components including: **Living (or controlled) Radical Polymerization Mediated by Transition Metal complexes (LRP-MTM)**, **Metal-Catalyzed Living Radical Polymerization (MC-LRP)**, **Copper Mediated Living Radical Polymerization (CM-LRP)**, **Transition Metal-Mediated Living Radical Polymerization (TMM-LRP)**, **Single-Electron Transfer Living Radical Polymerization (SET-LRP)** and recently **Outer Sphere Electron Transfer Metal-Catalyzed Polymerization (OSET-MCP)**.

Rather than looking at prior art to provide a historically relevant name (14) authors created many of these abbreviations to clarify their proposed mechanism. This may have created confusion as to the fundamental similarity of the reactions being discussed, and how to read and understand resulting IP.

In all of the above listed instances the disclosed process involves polymerization of radically (co)polymerizable monomers by a procedure requiring formation of a dynamic equilibrium requiring **Activation** of a dormant species (reaction of an alkyl (pseudo)halide initiator with a lower oxidation state transition metal complex comprising a ligand) and **Deactivation** of the growing polymer chain end (reaction of radical with transition metal complex in higher oxidation state comprising a radically transferable atom or group).

Names are not patentable. Mechanisms are not patentable. Composition of matter and processes are patentable.

Processes defined by what goes into a reactor and the process conditions are patentable, as are new products prepared by any polymerization procedure.

Carnegie Mellon University was the first to protect an ATRP in which the four components, shown in **Scheme 1**, are added to the reaction flask or are formed *in situ*. US Patent 5,763,548; (26) was filed on March 31, 1995 and issued on June 9, 1998 has been cited by 147 issued patents. This fundamental patent broadly defines suitable initiators, transition metals and ligands. Other

workers have examined and validated the disclosed processes. A second application describing improvements in the initial ATRP procedure, including a homogeneous aqueous polymerization system, was also filed in 1995. (27-30) Further as a consequence of the approximately 200 man years of work conducted in the laboratories of Carnegie Mellon University, CMU owns 28 issued US Patents on CRP with over 950 claims. More than 75 corresponding foreign patents are also included in the broad portfolio of CRP based intellectual property (IP) available for license to third parties who wish to practice ATRP and who are Members of the CRP Consortium when the license is signed.

[<http://www.chem.cmu.edu/groups/maty/crp/intprop.html>]

It appears that since ATRP is such a broadly applicable process, CMU's IP strategy was to initially patent ATRP processes and broadly/generically cover polymers with novel composition and site specific functionality. After the initial applications generically protecting novel polymer compositions were filed, the development of more specific compositions targeting specific commercial applications were to be left to industrial members of the ATRP Consortium in order to provide an incentive for technology transfer. After filing the initial four applications, (16,21,31,32) CMU's efforts focused on addressing solutions to problems slowing commercialization; development of more active catalysts; simplification of handling procedures; reduction of catalyst concentration, and expansion of the range of well controlled processes to include all dispersed media.

As a result of CMU's IP focus, 21 of the 28 issued US patents, plus several active applications, protect the fundamental ATRP process or improvements in the fundamental process, (26,27,30,33-48) while only five of the twenty eight address novel polymer compositions. (28,29,36,49,50) Nevertheless, these early material-focused patents disclose a number of materials that were not prepared by other CRP procedures until a later date. The difference in numbers is due to the fact that two issued patents are directed towards improvements in nitroxide mediated polymerization. (20,51) The first discloses an atom transfer radical addition reaction to form an alkoxyamine that has found use in ATRP kinetic studies, and the other focuses on rate enhancement of a NMP.

CMU's process based ATRP IP filed between 3/95 and 4/97 shows that the Matyjaszewski laboratories were the first to conduct an ATRP without an activator, first to add the transition metal in two oxidation states, first to conduct a homogeneous ATRP, first to use Mt(0) either alone or in conjunction with a metal in another oxidation state for a CRP, and the first to use a supported catalyst.

The early patents also disclose and protect a number of novel materials. Researchers at CMU were the first to prepare many gradient (52) and segmented copolymers by any CRP process, thereby exemplifying well defined copolymers with controllable monomer distributions unattainable by prior art procedures, and were the first to use a CRP initiator tethered to a solid.

The NMP patents and patents based on WO 98/40415 show CMU developed procedures for preparation of alkoxyamines and polymeric alkoxyamines from halogen containing precursors to exemplify ATRA using novel catalyst systems. (28,29) Indeed alkyl halides are frequently employed for preparation of nitroxides and RAFT agents.

CMU was very proactive in protecting ATRP initiation processes (i.e. what goes in the flask and what is formed in the flask). Variations on **SIX** different dominant initiation procedures were developed at CMU:

<b>Proposed Abbreviations</b>	<b>Components added to reaction</b>	<b>References</b>
<b>Normal ATRP:</b>	$Mt^n + L + R-X$	26
<b>Reverse ATRP:</b>	$X-Mt^{n+1} + L + FR$ initiators <sup>a</sup> or $Mt^0$	26 and 40
<b>SR&amp;NI ATRP:</b>	$X-Mt^{n+1} + L + R-X + FR$ initiators or $Mt^0$	35
<b>AGET ATRP:</b>	$X-M^{n+1} + L + R-X$ +organic or inorganic reducing agents	53
<b>ARGET ATRP:</b>	low amounts of $Mt^n$ or $X-Mt^{n+1} + L + R-X$ + organic or inorganic reducing agents	54
<b>ICAR ATRP:</b>	low amounts of $Mt^{n+1} + L + FR$ initiators	54

Note that the addition of a higher oxidation state transition metal and metal zero which acts to reduce the stable oxidation state transition metal complex was covered in an improvement to a “reverse ATRP” (26) in US Patent 6,541,580, (40) which is based on a provisional application filed 4/97. This application also discussed use of metal zero as the only source of the catalyst.

Recently, procedures disclosed under other abbreviations for different proposed mechanisms use/add/form *in situ* the same previously discussed components to the reaction flask and produce the same polymers (56) by essentially the same radical polymerization process. (56)

Several advances have been made to make ATRP more commercially attractive.

ARGET ATRP should allow direct preparation of block copolymers in existing large scale industrial equipment, publication No.: WO/2007/075817 (International Application No.: PCT/US2006/048656). Furthermore, it is envisioned that no catalyst removal step is required for many applications.

The use of existing industrial scale equipment is also possible for the recently developed *ab initio* emulsion polymerization process, publication No.: WO 2007025086 (International Application No.: PCT/US06/33152).

In the area of novel materials CMU protected (co)polymers prepared by ATRP: except with  $CCl_4$  initiator; and telechelic polymers prepared by CRP with  $MW > 20,000$ ; (49) copolymers with a true gradient segment; (30) polar ABA block copolymers, (30) and well defined graft copolymers and segmented copolymers with one or more CRP blocks where the macroinitiator had been prepared by another polymerization process. (36) In addition, the use of tethered initiators allowed synthesis of hybrid core/shell copolymers. Pending applications disclose other novel polymeric materials.

Commercial exploitation of this IP allows production of many high value added products. As noted above materials prepared by CRP find use in a number of high volume applications including:

- Solventless coatings
  - functional acrylics with  $f \geq 2$ , low  $\eta$ , uniform structure, gradients, blocks, amphiphiles with specific adhesion properties
- Surfactants, dispersants, encapsulants



- amphiphilic block copolymers: BA-VP, Sty-HEA, MMA-DMAEMA, BA-AA, St-AA, PEG-segmented copolymers
- control of topology & end groups possible
- Polar thermoplastic block copolymers
  - elastomers or adhesives, Sty-BA-Sty, MMA-BA-MMA
- Water soluble block copolymers
  - bio-mineralization
- Gels and hydrogels
- Various lubricants & additives
- Surface modifiers, bulk property modifiers
- New biomaterials & electronic materials
- Hybrids with natural & inorganic polymers

Returning to the question that was posed in 2004; “Why after 20 years of research on CRP has introduction of commercial products been so slow?”

We can now reply that after 20+ years of work, CRP is now ready for commercial exploitation:

- NMP
  - **Arkema** has BlocBuilder®, FlexiBloc™, Nanostrength® materials available (57) for commercial exploitation.
  - **Ciba** is utilizing internally developed control agents for synthesis of pigment dispersants, (58) as is
  - **IBM** for memory devices. (59,60)
- ATRP
  - **Dionex** (61) and **Kaneka** (62) have demonstrated the feasibility of developing products for targeted applications.
  - Several licenses have been signed and commercial evaluation has started in US, Japan and Europe.
  - Many other corporations are evaluating materials in a range of applications.
  - Ligands for active catalyst complexes are available and scalable systems using very low levels of catalysts have been demonstrated by **ATRP Solutions** while preparing their expansive catalogue. (63)
- RAFT
  - Synthesis of transfer agents have been simplified.
  - **CSIRO** has technology for license.
  - STREM** has research amounts of specific RAFT agents available. (64)
  - **Arkema** has commercial quantities of dibenzyltrithiocarbonate available. (57)

Therefore we strongly believe that in the near future an increasing number of new products prepared by CRP will be entering the marketplace. This belief is based on the fact that avenues that provide access to the technology are more clearly defined and the problems limiting industrial acceptability, noted just four years earlier, are being resolved.

## References

- (1) *Handbook of Radical Polymerization*; John Wiley and Sons Inc. Hoboken, **2002**.
- (2) Borsig, E.; Lazar, M.; Capla, M.; Florian, S. *Angew. Makromol. Chem.* **1969**, *9*, 89-95.
- (3) Braun, D. *Macromol. Symp.* **1996**, *111*, 63-71.
- (4) Garina, E. E.; Lagutkina, E. G.; Zubov, V. P.; Kabanov, V. A. *Vysokomol. Soedin., Ser. B.*, **1972**, *14*, 563-564.
- (5) Kabanov, V. A. *J. Polym. Sci., Polym. Symp.* **1975**, *50*, 71-94.
- (6) Lee, M.; Morigami, T.; Minoura, Y. *J. Chem. Soc., Faraday Trans. 1*, **1978**, *74*, 1738-1749.
- (7) Otsu, T.; Yoshida, M.; Tazaki, T. *Makromol. Chem., Rapid Commun.* **1982**, *3*, 133-140.
- (8) Solomon, D. H.; Rizzardo, E.; Cacioli, P. *Eur. Pat. Appl.*; (CSRIO). EP135280, **1985**.
- (9) Solomon, D. H. *Journal of Polymer Science, Part A: Polymer Chemistry* **2005**, *43*, 5748-5764.
- (10) Georges, M. K.; Veregin, R. P. N.; Kazmaier, P. M.; Hamer, G. K. *Macromolecules* **1993**, *26*, 2987-2988.
- (11) Georges, M. K.; Veregin, R. P. N.; Kazmaier, P. M.; Hamer, G. K.; *PCT Int. Appl.*; (Xerox Corp., USA). WO 9411412, **1994**.
- (12) Hawker, C. J.; *J. Am. Chem. Soc.* **1994**, *116*, 11185-11186.
- (13) Benoit, D.; Chaplinski, V.; Braslau, R.; Hawker, C. J.; *J. Am. Chem. Soc.* **1999**, *121*, 3904-3920.
- (14) Kato, M.; Kamigaito, M.; Sawamoto, M.; Higashimura, T.; *Macromolecules* **1995**, *28*, 1721-1723.
- (15) Wang, J.-S.; Matyjaszewski, K. *J. Am. Chem. Soc.* **1995**, *117*, 5614-5615.
- (16) Matyjaszewski, K.; Wang, J.-S.; *PCT Int. Appl.*; (Carnegie Mellon University, USA). WO 9630421, **1996**.
- (17) Le, T. P.; Moad, G.; Rizzardo, E.; Thang, S. H.; *PCT Int. Appl.*; (E.I. Du Pont De Nemours and Co., USA). WO 9801478, **1998**.
- (18) Rizzardo, E.; Thang, S. H.; Moad, G.; *PCT Int. Appl.*; (Commonwealth Scientific and Industrial Research Organisation; E.I. Du Pont De Nemours and Company). WO 99/05099, **1999**.
- (19) Destarac, M.; Charmot, D.; Zard, S. Z.; Franck, X.; *PCT Int. Appl.*; (Rhodia Chimie, Fr.). WO 0075207, **2000**.
- (20) Matyjaszewski, K.; Greszta, D. *USPTO*; (CMU) US5910549, 1999.
- (21) Matyjaszewski, K.; Gaynor, S. G.; Coca, S.; *PCT Int. Appl.*; (Carnegie Mellon University, USA). WO 9840415, **1998**.
- (22) Wager, C. M.; Haddleton, D. M.; Bon, S. A. F.; *European Polymer Journal* **2004**, *40*, 641-645.
- (23) Kwak, Y.; Nicolay, R.; Matyjaszewski, K.; *Macromolecules* **2008**, *41*, 6602-6604.
- (24) Solomon, D. H.; Rizzardo, E.; Cacioli, P. *USPTO*; US 4581429, **1986**.
- (25) Moad, G.; Rizzardo, E.; Thang, S. H. *Acc. Chem. Res.* **2008**, *41*, 1133-1142.
- (26) Matyjaszewski, K.; Wang, J.-S. *USPTO*; (CMU) US5763548, **1998**.

- (27) Matyjaszewski, K.; Coca, S.; Gaynor, S. G.; Greszta, D.; Patten, T. E.; Wang, J.-S.; Xia, J. *USPTO*; CMU: US5807937, **1998**.
- (28) Matyjaszewski, K.; Gaynor, S. G.; Coca, S. *USPTO*; CMU: US 6538091, **2003**.
- (29) Matyjaszewski, K.; Coca, S.; Gaynor, S. G.; Greszta, D.; Patten, T. E.; Wang, J.-S.; Xia, J. *USPTO*; CMU: US6887962, **2005**.
- (30) Matyjaszewski, K.; Gaynor, S. G.; Coca, S. *USPTO*; CMU: US 7125938, **2006**.
- (31) Matyjaszewski, K.; Coca, S.; Gaynor, S. G.; Greszta, D.; Patten, T. E.; Wang, J.-s.; Xia, J.; *PCT Int. Appl.*; (Carnegie Mellon University, USA). WO199718247, **1997**.
- (32) Matyjaszewski, K.; Coca, S.; Gaynor, S. G.; Nakagawa, Y.; Jo, S. M.; *PCT Int. Appl.*; (Carnegie-Mellon University). WO 9801480, **1998**.
- (33) Matyjaszewski, K.; Wang, J.-S. *USPTO*; CMU: US6624263, **2003**.
- (34) Matyjaszewski, K.; Coca, S.; Gaynor, S. G.; Nakagawa, Y.; Jo, S. M.: *USPTO*; CMU: US5789487, **1998**.
- (35) Matyjaszewski, K.; Coca, S.; Gaynor, S. G.; Nakagawa, Y.; Jo, S. M.: *USPTO*; CMU: US5945491, **1999**.
- (36) Matyjaszewski, K.; Coca, S.; Gaynor, S. G.; Nakagawa, Y.; Jo, S. M.: *USPTO*; CMU: US6162882, **2000**.
- (37) Senninger, T.; Sanchez, L.; Darcos, V.; Lastecoueres, D.; Verlhac, J.-B.; *USPTO*; Elf Atochem: US 5854364, **1998**.
- (38) Matyjaszewski, K.; Gaynor, S. G.; Qiu, J.; Teodorescu, M.; *USPTO*; (CMU). US6121371, **2000**.
- (39) Matyjaszewski, K.; Gaynor, S. G.; Coca, S.; *USPTO* (CMU). US 6512060 A, **2003**.
- (40) Matyjaszewski, K.; Gaynor, S. G.; Coca, S. *USPTO* (CMU). US6541580, **2003**; Cont.-in-part of U.S. 6407187.
- (41) Matyjaszewski, K.; Tsarevsky, N. *USPTO*; CMU: US6624262, **2003**.
- (42) Matyjaszewski, K.; Pyun, J. *USPTO*; CMU: US6627314, **2003**.
- (43) Matyjaszewski, K.; Gromada, J.; Li, M. *USPTO*; CMU: US6759491, **2004**.
- (44) Matyjaszewski, K.; Lutz, J.-F.; Shinoda, H.; *USPTO*; CMU: US7049373, **2006**.
- (45) Matyjaszewski, K.; Kowalewski, T.; Lambeth, D. N.; Spanswick, J.; Tsarevsky, N. V.; *USPTO*; CMU: US7056455, **2006**.
- (46) Matyjaszewski, K.; Kirci, B.; Lutz, J. F.; Pintauer, T.; *USPTO*; CMU: US7064166, **2006**.
- (47) Matyjaszewski, K.; Hong, S. C.; *USPTO*; CMU: US 7157530, **2007**.
- (48) Matyjaszewski, K.; Tsarevsky, N.; *USPTO*; CMU: US 7332550, **2008**.
- (49) Matyjaszewski, K.; Wang, J.-S.; *USPTO*; CMU: US6407187, **2002**.
- (50) Matyjaszewski, K.; Pakula, T.; *USPTO*; CMU: US7019082, **2006**.
- (51) Matyjaszewski, K.; Greszta, D.; *USPTO*; CMU: US6288186, **2001**.
- (52) Pakula, T. *Macromol. Theory and Simulations* **1996**, 5, 987-1006.
- (53) Matyjaszewski, K.; Bombalski, L.; Jakubowski, W.; Min, K.; Spanswick, J.; Tsarevsky, N.; *PCT Int. Appl.*; (CMU). WO 2005087819, **2005**.
- (54) Matyjaszewski, K.; Jakubowski, W.; Spanswick, J. *PCT Int. Appl.*; (CMU). WO2007025310, **2007**.

- (55) Singleton, D. A.; Nowlan, D. T., III; Jahed, N.; Matyjaszewski, K. *Macromolecules* **2003**, *36*, 8609-8616.
- (56) Haddleton, D. M.; Crossman, M. C.; Hunt, K. H.; Topping, C.; Waterson, C.; Suddaby, K. G. *Macromolecules* **1997**, *30*, 3992-3998.
- (57) <http://www.arkema-inc.com>.
- (58) Nesvadba, P. *Chimia* **2006**, *60*, 832-840.
- (59) [http://www.usatoday.com/tech/news/techinnovations/2007-05-03-ibm-chip\\_N.htm](http://www.usatoday.com/tech/news/techinnovations/2007-05-03-ibm-chip_N.htm).
- (60) Tang, C.; Lennon, E. M.; Fredrickson, G. H.; Kramer, E. J.; Hawker, C. J. *Science* **2008**, *322*, 429-432.
- (61) McCarthy, P.; Chattopadhyay, M.; Millhauser, G. L.; Tsarevsky, N. V.; Bombalski, L.; Matyjaszewski, K.; Shimmin, D.; Avdalovic, N.; Pohl, C. *Anal Biochem* **2007**, *366*, 1-8.
- (62) <http://www.kaneka.be>; <http://www.kanekatexas.com>.
- (63) <http://www.atrpsolutions.com>.
- (64) <http://www.strem.com/code/index.ghc>.

# Author Index

- Acar, M. H., 313–324  
Akdemir, Ö., 189–202  
Aydoğan, B., 171–187
- Badi, N., 189–202  
Bareille, L., 97–114  
Bicchielli, D., 97–114  
Böker, A., 127–137  
Borguet, Y., 97–114  
Borsali, R., 231–240  
Braunecker, W. A., 85–96  
Brochon, C., 243–256
- Chizhevsky, I. T., 115–125  
Cianga, I., 171–187  
Cummins, D. M., 327–341
- Delaude, L., 97–114  
Delfosse, S., 97–114  
Demonceau, A., 97–114  
Destarac, M., 231–240  
Driguez, H., 231–240  
Dubois, P., 269–296  
Durmaz, Y. Y., 171–187
- Endo, T., 33–48
- Fort, S., 231–240  
Frank, C. W., 269–296  
Fukuda, T., 159–168
- Gao, H., 203–213  
Gnanou, Y., 231–240  
Goel, V., 257–267  
Goto, A., 159–168  
Grishin, D. F., 115–125  
Grishin, I. D., 115–125
- Hadziioannou, G., 243–256  
Heise, A., 327–341  
Hirai, N., 159–168  
Houga, C., 231–240
- Inceoglu, S., 313–324
- Jakubowski, W., 343–355  
Juhari, A., 297–311
- Kajiwara, A., 49–59  
Kaneko, H., 357–371, 373–384  
Kashiwa, N., 357–371, 373–384  
Kawahara, N., 357–371, 373–384  
Klep, V., 215–230  
Koynov, K., 297–311  
Krishnamoorti, R., 257–267
- Laschewsky, A., 189–202  
Le Meins, J.-F., 231–240  
Li, W., 203–213  
Liu, Y., 215–230  
Lohmann, J., 231–240  
Lutz, J.-F., 189–202  
Luzinov, I., 215–230
- McCarthy, P., 343–355  
Magusin, P. C. M. M., 327–341  
Matsugi, T., 357–371, 373–384  
Matsuo, S., 357–371, 373–384  
Matyjaszewski, K., 3–13, 85–96,  
203–213, 257–267, 297–311  
Mespouille, L., 269–296  
Millard, P.-E., 127–137  
Min, K., 203–213  
Morino, K., 33–48  
Mougin, N. C., 127–137  
Müller, A. H. E., 127–137
- Nagasawa, K., 159–168
- Pakula, T., 297–311  
Pfeifer, S., 189–202  
Pietrasik, J., 257–267  
Pike, B., 385–396  
Pintauer, T., 63–84
- Radosz, M., 139–157  
Raquez, J.-M., 269–296  
Russell, G. T., 15–31

Saito, J., 357–371, 373–384

Sauvage, X., 97–114

Shen, Y., 139–157

Spanswick, J., 385–396

Tang, H., 139–157

Tang, W., 85–96

Taton, D., 231–240

Tsarevsky, N. V., 85–96, 343–355

Tsujii, Y., 159–168

Wakada, T., 159–168

Wilson, J., 231–240

Wischerhoff, E., 189–202

Yagci, Y., 171–187

Zarafshani, Z., 189–202

# Subject Index

## A

- Acrylate based copolymers
- 3-arm star (PBA-*b*-PMMA)
    - block copolymers, 307–309
  - 3-arm star poly(butyl acrylate)–poly(acrylonitrile) [PBA–PAN] block copolymers, 304–307
  - glass transition temperature (T<sub>g</sub>) of copolymer, 301
  - gradient and block copolymers of nBA and IBA, 302–303
  - linear, of isobornyl acrylate (IBA) and *n*-butyl acrylate (nBA), 298–303
  - mechanical properties of PBA–PAN star copolymers, 306–307
  - schematic of, of P(IBA-*co*-nBA), 300
  - shear moduli spectra of poly(ethyl acrylate) (PEA) and IBA–nBA copolymer, 301*f*
  - statistical copolymers of nBA and IBA, 299–302
  - stress-strain curves for 3-arm stars PBA–PMMA, 308–309
  - T<sub>g</sub> and rubbery plateau storage modulus of, 302*t*
  - T<sub>g</sub> in statistical P(IBA-*co*-nBA), 300*f*
- Activation, reversible processes, 160
- Activators regenerated by electron transfer (ARGET)
- atom transfer radical polymerization (ATRP), 6
  - mechanism for, ATRP, 344, 345*f*
  - polystyrene-*b*-poly(*t*-butyl acrylate) via, 346–347, 353
- Active ligands, catalysis for atom transfer radical addition (ATRA) and cyclization (ATRC), 69
- Alcohol catalysts. *See* Reversible chain transfer catalyzed polymerization (RTCP)
- Alkenes, addition of polyhalogenated compounds to, 71–73
- Alkyl iodides
- atom transfer radical polymerization (ATRP), 7
  - See also* Reversible chain transfer catalyzed polymerization (RTCP)
- Alkyl radicals, intermolecular radical migration, 56–57
- Amine additives, ruthenium-catalyzed atom transfer radical polymerization, 122–124
- Amphiphilic polymer conetworks (APCNs)
- characterization methods, 272–273
  - conetwork PDMAEMA-*l*-PCL ([poly[2-(*N,N*-dimethylamino)ethyl methacrylate-linked-poly(ε-caprolactone)]]), 271, 273–274
  - cross-links and Flory's theory, 271
  - degradability study of PDMAEMA-*l*-PCL, 292–293
  - determination of state of water molecules, 283–286
  - diffusion-controlled transport diffusion, 276
  - evolution of swelling degree, 292, 293*f*
  - experimental, 272–273
  - Fick equation for water uptake, 276
  - Flory–Rehner relationship and

- swelling behavior, 279
- fraction of non-freezable and freezable water in PDMAEMA-*l*-PCL, 284, 285*t*
- "free" or "bulk-like" water, 283–284
- gel fraction and mechanical properties of PDMAEMA-*l*-PCL, 291*t*
- hydrogel swelling and degree of crosslinking, 278–279
- mechanical properties of PDMAEMA-*l*-PCL, 286–291
- molecular characteristics, gel fraction and mechanical properties, 289*t*
- molecular parameters of PDMAEMA-*l*-PCL, 275*t*
- pH effect on Young modulus, 290, 291*f*
- pH-sensitivity of PDMAEMA polymer chains, 280
- polymerization mechanism and mechanical properties, 291, 292*f*
- proportion of bound and freezable water in PDMAEMA-*l*-PCL, 285*f*
- relaxation-controlled transport diffusion, 276
- reproducibility of swelling behavior, 276*f*
- reversibility of swelling-deswelling behavior vs. time, 282*f*
- stress-strain curves, 287*f*, 289*f*
- structure of final polymer, 290
- swelling behavior in toluene, 277
- swelling behavior of PDMAEMA-*l*-PCL gels, 275–282
- synthesis of P(DMAEMA-*co*-PCLMA)-*l*-PCL [ $\omega$ -methacrylate PCL = PCLMA], 277–278
- temperature-sensitivity of PDMAEMA-*l*-PCL, 281, 282*f*
- three-step synthesis of PDMAEMA-*l*-PCL, 274
- Young's modulus, 287, 288*f*, 290
- Anchoring. *See* Polymer brushes
- Anionic polymerization
  - polystyrene-*b*-poly(4-vinyl pyridine) based copolymers, 249–250
  - rod-coil copolymers, 244
- Architectures, block copolymers, 244
- Atom transfer radical addition (ATRA)
  - active ligand development, 69
  - AIBN and CCl<sub>4</sub> concentrations, 74–75
  - deactivator concentration, 73–74
  - efficient copper catalysis with AIBN, 71–73
  - fundamentals of transition metal catalyzed, 65
  - future outlook, 81
  - kinetic studies of copper catalyzed, 73–77
  - methodology for regenerating activator, 79
  - nitrogen based ligands, 69
  - organic synthesis, 67–68
  - polyhalogenated compounds to alkenes, 72*t*
  - proposed mechanism for copper catalyzed, 65, 66
  - reaction kinetics, 75–77
  - regeneration of catalysis in, 70
  - simulation of kinetic plots, 78*f*
  - transition metal catalyzed, 64
- Atom transfer radical copolymerization (ATRCp)
  - copolymerizing monovinyl monomer and divinyl cross-linker, 206, 212
  - cross-linker reactivity, 209–210
  - experimental gel points, 206–211
  - initiator efficiency, 210–211



- methyl acrylate (MA) and ethylene glycol diacrylate (EGDA), 206, 207
- molar ratios and concentrations, 208–209
- polydispersity of primary chains, 210–211
- structures of monomers and cross-linkers, 206
- Atom transfer radical cross-coupling (ATRCC)
- block copolymers, 178
- chain end functionality by  $^1\text{H}$  nuclear magnetic resonance (NMR), 176
- combination of ATRP and click chemistry, 177
- combining ATRP and, 172
- coupling efficiency, 177*f*
- general reactions, 175
- $^1\text{H}$  NMR spectra of polystyrene-Br and coupling product, 176*f*
- telechelic polymers by, 175–178
- uses of telechelic polymers, 177–178
- Atom transfer radical cyclization (ATRC)
- bromoacetamides catalyzed by copper complexes, 77*t*
- catalysis by  $\text{Cp}^*(*)\text{Ru}^{\text{III}}\text{Cl}_2(\text{PPh}_3)$  with magnesium, 79, 81
- copper mediated, 64
- efficient copper catalyzed, 77, 79
- future outlook, 81
- products in, of  $\text{CCl}_4$  to 1,5-hexadiene, 79, 80
- regeneration of catalysis in, 70
- successful copper catalyzed reactions, 67–68
- Atom transfer radical polymerization (ATRP)
- alkyl iodides, 7
- bifunctional initiator propane-1,3-diyl bis(2-chloro-2-phenylacetate) (PDBCP), 180
- block copolymerization of vinyl acetate (VAc) and styrene, 153, 155*f*
- bulk polymerization of VAc using copper catalysts, 151*t*
- chain-extension polymerization of VAc, 152, 154*f*
- commercial exploitation, 393
- controlled radical method, 5, 6*f*
- controlled radical polymerization method, 386
- development of, 389–393
- dimeric radical precursor of 2-ethylhexyl acrylate (2EHA), 52, 53*f*
- initiators, 6
- intermolecular radical migration of alkyl radicals, 56–57
- kinetics of, of VAc, 152*f*
- ligand and activity of Cu-based catalysts, 90–92
- map for catalyst selection, 93*f*
- mechanism, 8*f*
- mechanism for mid-chain radical formation, 50–51
- mechanism for VAc, 149, 150
- model trimeric, tetrameric, and pentameric radicals, 51
- multi-step radical migration in propagating radicals of octadecyl acrylate (Oda), 54–56
- nitrogen based ligands for copper catalysis, 69
- organometallic species, 7
- polymerizable monomers, 7–8
- possibility of radical migration to side group of 2EHA, 52–53
- potential 1,5-hydrogen shift for propagating acrylates, 52*f*
- potential structure of propagating radical of alkyl acrylates, 56*f*
- radicals by electron spin resonance (ESR), 51*f*
- regeneration of catalysis in, 70

Ru-benzylidene–Schiff base complexes, 105–106  
 solvent effects, 93–94  
*t*-butyl acrylate for model radical precursors, 50*f*  
 VAc by [Fe(Cp)(CO)<sub>2</sub>]<sub>2</sub>, 150, 151  
 vinyl acetate (VAc), 149–153  
*See also* Acrylate based copolymers; Amphiphilic polymer conetworks (APCNs); Atom transfer radical copolymerization (ATRCp); Electron spin resonance (ESR); Ruthenium carborane complexes; Ruthenium complexes; Systematic polymeric libraries; Vinyl acetate (VAc)

**Atom transfer radical polymerization (ATRP)**  
 equilibrium ( $K_{\text{ATRP}}$ )  
 alkyl bromides and chlorides in various catalysts, 89*t*  
 atom transfer equilibrium, 86*f*  
 equation, 86  
 equation for polydispersity index (PDI), 87  
 halidophilicity ( $K_{\text{Halido}}$ ), 87  
 halogenophilicity ( $K_{\text{Halo}}$ ), 86, 87  
 ligand effect on activity of Cu-based ATRP catalysts, 90–92  
 rational selection of ATRP catalyst, 92–93  
 reaction of EtBriB with CuBr/bpy, 94*t*  
 reaction of ethyl 2-bromoisobutyrate (EtBriB) with Cu complexes, 90*f*  
 selection of catalysts, 93*f*  
 solvent effects, 93–94  
 structure of propagating radicals and, 87–88  
 transferable halogen atom effect, 88–89  
 values for reaction of EtBriB with CuBr complexes, 91*t*

## B

**Baroplastic materials**  
 atomic force microscopy (AFM) images of tri-block copolymer before and after processing, 321*f*  
 basic extrusion test, 319*f*  
 block copolymers of polystyrene (PS) and poly(2-ethyl hexylacrylate) (PEHA), 315–316  
 block copolymer synthesis, 315  
 compression or piston molding, 318  
 core-shell polymer nanoparticles, 313  
 di-, tri-, and star-block copolymers, 315–316  
 diblock copolymers, 313  
 experimental, 314–315  
 formation of mixed morphology, 320–321  
 homopolymer synthesis, 314–315  
 images of mold, processed 4-arm star-block copolymer, 318*f*  
 instrumentation, 315  
 Istanbul Technical University (ITU) imprinting mold, 319*f*  
 molding equipment, 318  
 nanophase structure of high and low T<sub>g</sub>, 319, 320*f*  
 polymer miscibility, 313  
 processing aid, 322, 323*f*  
 processing and recycling of, 317*t*  
 recycling tri- and star-block copolymers, 319, 320*f*, 321, 322*f*  
 synthesis of di-, tri-, and tetra-functional initiators, 314  
**Baseline selection, size exclusion chromatography (SEC), 22–23**  
**Benzocyclobutene, radical ring-opening polymerization (R-ROP), 42**

- Bicyclobutanes, radical ring-opening polymerization (R-ROP), 45*f*, 46
- Bioconjugates, new, preparation, 8
- Bio-repellent, poly(ethylene glycol) (PEG), 197
- Biphasic systems, catalysis for atom transfer radical addition (ATRA) and cyclization (ATRC), 68
- 1,1-Bis(ethoxycarbonyl)-2-vinylcyclopropane (ECVCP), copolymerization with methyl methacrylate, 36, 37*f*
- 1,1-Bis(hydroxymethylates)-2-vinylcyclopropane, radical ring-opening polymerization, 37, 38*f*
- Blends. *See* Polypropylene-*g*-poly(methyl methacrylate) graft copolymers
- Block copolymers  
 combining ATRP and free radical cationic polymerization, 178  
 PMMA-*b*-styrene by Ru-carboranes, 121–122  
 PS-*b*-poly(acrylic acid), 349, 350*f*  
 PS-*b*-poly(acrylic acid) stabilizing Fe<sub>2</sub>O<sub>3</sub> particles, 350–351  
 styrene and vinyl acetate (VAc), 153, 155*f*  
 telechelic polymers for preparing, 178  
*See also* Baroplastic materials; Hybrid block copolymers; Rod-coil conjugated block copolymers; Systemic polymeric libraries
- Brushes. *See* Polymer brushes
- n*-Butyl acrylate. *See* Polymer-grafted nanoparticles
- C**
- Calibration, size exclusion chromatography without proper, 21–22
- Carboranes. *See* Ruthenium carborane complexes
- Carnegie Mellon University (CMU), development of atom transfer radical polymerization (ATRP), 390–392
- Catalysts, CuCl- and CuBr-based systems, 131–132
- Chain anchoring. *See* Polymer brushes
- Chain extension experiments  
 poly(*N*-isopropylacrylamide) (PNIPAAm), 134–135  
 vinyl acetate (VAc) polymerization, 152, 154*f*
- Chain-length-dependent propagation, polydispersity perturbation, 28–29
- Chain-length-dependent termination, polydispersity perturbation, 25–28
- Chain transfer agent  
 polyolefin hybrids, 374–375  
 xyloglucan based, 238–239
- "Click" chemistry  
 combining atom transfer radical polymerization and, 177  
 functional polymer method, 8  
 modification of macroporous poly(high internal phase emulsion) (pHIPE), 335*f*  
 secondary functionalization of grafted polymer, 334–338  
 spectra (infrared) of pHIPE-N<sub>3</sub> before and after, 336*f*  
 surface morphology of pHIPE-N<sub>3</sub> before and after, 336*f*
- Cobalt(II) acetylacetonate  
 structure, 143  
 vinyl acetate polymerization, 143, 144*f*, 145
- Column broadening, size exclusion chromatography, 20–21
- Commercial products, controlled radical polymerization, 11

- Compatibilizer, polypropylene-*g*-poly(methyl methacrylate) graft copolymer as, 366–368
- Computational modeling, controlled radical polymerization, 11
- Condensation. *See* Polycondensates
- Conetworks. *See* Amphiphilic polymer conetworks (APCNs)
- Conjugated polymers  
functional materials, 243–244  
*See also* Rod-coil conjugated block copolymers
- Controlled/living radical polymerization (CRP)  
approaches to intermittent activation, 5, 6*f*  
atom transfer radical polymerization (ATRP), 4, 6*f*, 7–8
- Carnegie Mellon University (CMU), 390–392
- challenges, 10–11
- commercial exploitation, 393
- computational modeling and simulation, 11
- controlled heterogeneity, 10
- cost-performance for commercial products, 11
- degenerative transfer (DT) mechanism, 6, 7, 8*f*
- development of ATRP, 389–393
- difference between conventional and, 5
- dynamic equilibrium of methods, 4–5
- energy and environment, 11
- functional groups for orthogonal chemistry, 11
- gelation processes, 204–205, 206
- key to attaining control, 5
- main methods, 5, 6*f*
- market evaluation, 387–389
- outlook, 8–11
- patents, 386, 387
- polyolefin hybrids, 374–376
- publications, 3–4, 386, 387
- rod-coil copolymers, 244–245
- SciFinder Scholar search results, 4*f*, 386, 387
- stable free radical polymerization (SFRP), 4, 6
- transition metal catalyzed ATRP, 390
- vinyl acetate (VAc), 141, 142*f*
- well-defined polymers, 85–86, 344  
*See also* Vinyl acetate (VAc)
- Conventional polymerization, chain-growth, 18–20
- Conventional radical polymerization, gelation processes, 204–205, 206
- Copolymers  
gel points, 204–205, 206  
graft, with oligo(ethylene glycol) side chains, 191  
random, of 2-(2-ethoxyethoxy)ethyl acrylate (EEO<sub>2</sub>A) and oligo(ethylene glycol) methyl ether acrylate (OEGA), 196–197  
thermoreponsive, for gold surface modification, 198–199  
*See also* Acrylate based copolymers; Atom transfer radical copolymerization (ATRCp); Block copolymers; Hybrid block copolymers; Polypropylene-*g*-poly(methyl methacrylate) graft copolymers; Rod-coil conjugated block copolymers
- Copper catalyzed reactions  
active ligand development, 69  
biphasic systems, 68–69  
ligand effect on activity of Cu-based ATRP catalysts, 90–92  
methodology development, 68–69  
polyhalogenated compounds to alkenes, 71–73  
solid supported catalysis, 68

*See also* Atom transfer radical addition (ATRA); Atom transfer radical cyclization (ATRC)

Core-shell polymer nanoparticles, baroplastic, 313

Cost performance, commercial products, 11

Coupling reactions  
 PS-Br using atom transfer radical cross-coupling, 176, 177*f*  
*See also* Atom transfer radical cross-coupling (ATRCC)

Cross-linker, divinyl  
 copolymerization of monovinyl monomers with, 203–204  
 reactivity of, and gel points, 209–210  
*See also* Atom transfer radical copolymerization (ATRCp)

Cyclic allylic disulfide, radical ring-opening polymerization, 45*f*, 46

Cyclic disulfides, radical ring-opening polymerization, 45*f*, 46

Cyclic ketene acetals, radical ring-opening polymerization, 41–42

Cyclic oligoarsines, radical ring-opening polymerization, 45*f*, 46

Cyclic  $\alpha$ -oxyacrylates, radical ring-opening polymerization, 45*f*, 46

Cyclic vinylsulfone, radical ring-opening polymerization, 45*f*, 46

Cyclization reactions  
 natural products, 64  
 transition metal catalyzed, 67–68

**D**

Degenerative transfer (DT)  
 controlled radical  
 polymerization method, 4, 5, 6*f*  
 mechanism, 8*f*

Degree of polymerization

conventional chain-growth polymerization, 19

ideal living polymerization, 16–17

Dextran  
 oligosaccharide, 232  
*See also* Hybrid block copolymers

Diblock copolymers, baroplastic, 313

*p*-Dibromoxylene,  
 polyrecombination reaction, 179

Divinyl cross-linkers  
 copolymerization of monovinyl monomers with, 203–204  
*See also* Atom transfer radical copolymerization (ATRCp)

**E**

Electron donor-acceptor, rod-coil block copolymers, 253–254

Electron spin resonance (ESR)  
 alkyl radicals, 56–57  
 dimeric radical precursor of 2-ethylhexyl acrylate (2EHA), 52, 53*f*  
 expected spectra for initial, mid-chain and final radicals with structures, 55*f*  
 experimental, 57  
 investigation of radical species, 49–50  
 mechanism for mid-chain radical formation, 50–51  
 model radical precursors, 50*f*  
 multi-step radical migration in propagating radicals, 54–56  
 styrene polymerization, 162, 166*f*  
 temperature dependent change in ESR spectra of model radicals, 54*f*, 55*f*  
 trimeric model radicals of 2EHA, 53

Emulsions. *See* Polymerization of high internal phase emulsions (pHIPE)

Energy, controlled radical polymerization, 11

Environment, controlled radical polymerization, 11

Equilibrium ( $K_{\text{ATRP}}$ ). *See* Atom transfer radical polymerization (ATRP) equilibrium ( $K_{\text{ATRP}}$ )

Etherification, synthesis of  $\alpha,\omega$ -telechelic polymer by, 174, 175*t*

2-(2-Ethoxyethoxy)ethyl acrylate monomer in surfactant preparation, 194–195

random copolymer with oligo(ethylene glycol) methyl ether acrylate, 196–197

*See also* Thermoresponsive materials

Ethyl 2-bromoisobutyrate (EtBriB), reaction with Cu complexes, 90–92

Ethylene glycol diacrylate (EGDA) atom transfer radical copolymerization (ATRP) of methyl acrylate with, 206, 207

reactivity and gel points, 209–210

*See also* Atom transfer radical copolymerization (ATRCp)

Ethyleneglycol dimethylacrylate (EGDMA), Cu-catalyzed ATRP, 271

2-Ethylhexyl acrylate (2EHA) dimeric radical precursor of 2EHA, 52, 53*f*

radical migration to side group of, 52–53

Ethyl iodoacetate (EtIAc), iodine-degenerative transfer polymerization of vinyl acetate (VAc), 147, 148*f*

Exo-methylene-substituted monomers, radical ring-opening polymerization, 35

Expandable monomers

spiro orthocarbonate (SOC), 43

spiro orthoester (SOE), 44

*See also* Radical ring-opening polymerization (R-ROP)

## F

Fibrinogen adsorption, surface of segregated brushes, 227–228

Flory–Schulz distribution, chain growth polymerization, 18, 19*f*

Flory's theory, cross-linked networks, 270, 271

Flory–Stockmayer's mean-field theory

crosslinking, 270

gel point, 204

Free radical reactions, organic synthesis, 63–65

Functional groups for orthogonal chemistry, controlled radical polymerization, 11

Functionalization. *See* Polymerization of high internal phase emulsions (pHIPE)

## G

Gelation

comparing convention and controlled radical processes, 204–205, 206

Flory–Stockmayer's mean-field theory, 204

*See also* Atom transfer radical copolymerization (ATRCp)

Glycidyl methacrylate (GMA). *See* Polymerization of high internal phase emulsions (pHIPE)

Graft copolymers. *See* Polypropylene-*g*-poly(methyl methacrylate) graft copolymers

Grafted nanoparticles. *See* Polymer-grafted nanoparticles

Grafting

atom transfer radical  
polymerization (ATRP), of  
glycidyl methacrylate  
(GMA), 333–334  
*See also* Polymer brushes;  
Polymerization of high  
internal phase emulsions  
(pHIPE)

## H

Halidophilicity, equilibrium  
constant, 87, 89  
Halogen atom, transferable, and  
ATRP equilibrium, 88–89  
Halogenophilicity, equilibrium  
constant, 86, 87  
Heterogeneity, controlling, 10  
High internal phase emulsions  
(HIPE)  
macroporous polymers from,  
328  
*See also* Polymerization of high  
internal phase emulsions  
(pHIPE)  
Hybrid block copolymers  
AFM (atomic force microscopy)  
of dextran-*b*-polystyrene  
(dex-*b*-PS<sub>5</sub>), 235*f*  
characteristics of silylated  
dextran-*b*-PS, 235*t*  
characteristics of xyloglucan-*b*-  
poly(acrylamide) (XG-*b*-  
PAm), 238*t*  
dex-*b*-PS synthesis by atom  
transfer radical  
polymerization (ATRP),  
234–237  
dex or XG as oligosaccharide,  
232  
experimental, 232–234  
hydrodynamic radius evolution  
vs. DMSO volume fraction,  
236*f*  
instrumentation, 232–233

morphology of dex-*b*-PS<sub>270</sub> and  
dex-*b*-PS<sub>775</sub> by AFM, 236–  
237  
PS or PAm as vinyl block, 232  
self-assembly of dex-*b*-PS<sub>5</sub> in  
water, 235–236  
strategy for dex-*b*-PS block, 234  
strategy for XG-*b*-PAm, 238  
synthesis of XG-*b*-PAm, by  
MADIX, 238–239  
transmission electron  
microscopy (TEM) for dex-*b*-  
PS<sub>270</sub>, 237*f*  
XG-based chain transfer agent,  
238, 239  
Hybridization (sp<sup>2</sup>), controlled  
radical polymerization, 9  
Hydrogels  
calculation of swelling ratio Q,  
192  
degradable versions, 193  
evolution of swelling ratio vs.  
time, 193*f*  
poly(*N*-isopropylacrylamide)  
(PNIPAAm), 270–271  
stimuli-responsive, 270  
structure of monomers for, 192  
thermoreponsive, 192–194

## I

Initiators for continuous activator  
regeneration (ICAR)  
atom transfer radical  
polymerization (ATRP), 344,  
345*f*  
CRP systems, 6, 7  
polystyrene macroinitiator  
synthesis, 345–346, 353  
*See also* Macroinitiators  
Iodine-degenerative transfer  
polymerization (DT)  
vinyl acetate (VAc), 147, 148*f*  
*See also* Vinyl acetate (VAc)  
Isobornyl acrylate (IBA)  
copolymers with *n*-butyl  
acrylate (nBA), 298–303

statistical copolymers of nBA and, 299–302  
*See also* Acrylate based copolymers

## K

### Kharasch addition

CBr<sub>4</sub> to alkene with AIBN, 66  
 polyhalogenated compounds to alkenes, 63–64

### Kinetics

chain-length-dependent termination, 25–28  
 controlled radical polymerization of vinyl acetate (VAc), 142*f*, 144*f*, 146*f*, 152*f*  
 Cu-based catalyst in polymerization of *N*-isopropylacrylamide (NIPAAm), 132–133  
 ruthenium complexes and amines in ATRP, 122–124

### Kinetic studies

AIBN and CCl<sub>4</sub> concentrations, 74–75  
 atom transfer radical addition (ATRA) reaction, 75–77  
 copper catalyzed atom transfer radical addition, 73–77  
 deactivator concentration, 73–74  
 simulation for ATRA of CCl<sub>4</sub> to methyl acrylate, 78*f*

## L

Libraries. *See* Systematic polymeric libraries

Ligands, activity of Cu-based ATRP catalysts, 90–92

### Living polymerization

ideal, 16–17  
 number-average degree of polymerization, 16

Poisson chain-length distributions, 17*f*  
 schematic of ideal, 16*f*

### Living radical polymerization (LRP)

term, 386  
 well-defined polymers, 160

Lower critical solution temperature (LCST), thermoresponsive polymers, 190

## M

### Macroinitiators

polyolefin hybrids, 374–375  
 synthesis to polypropylene-*g*-Br, 361, 362

*See also* Polypropylene-*g*-poly(methyl methacrylate) graft copolymers

### Macromolecular design by

interchange of xanthates (MADIX)  
 characteristics of xyloglucan-*b*-poly(acrylamide) (XG-*b*-PAm), 238*t*  
 degenerative transfer process, 6, 8  
 method for XG-*b*-PAm, 233–234  
 XG-based chain transfer agent (CTA), 238, 239  
 XG-*b*-PAm block copolymers, 238–239

Macrosurfactants, aqueous self-organization, 195–196

Market evaluation, controlled radical polymerization, 387–389

Mayo equation, fraction of dead chains, 19

### Mechanisms

atom transfer radical polymerization (ATRP) initiator systems, 344, 345*f*  
 copper(I) regeneration, 70



- proposed, for copper catalyzed atom transfer radical addition (ATRA), 65, 66
- proposed dissociative, with Ru complex, 111
- vinyl acetate polymerization by Co(II) acetylacetonate complex, 143, 145
- Methacrylates
  - polymer brushes of
    - oligo(ethylene glycol) methacrylates, 198
  - Ru-tricyclohexylphosphine complex, 99–100
- Methyl acrylate (MA)
  - atom transfer radical copolymerization (ATRP) with divinyl cross-linker, 206, 207
  - initiator efficiency and gel points for copolymer, 210–211
  - polydispersity of primary chains and gel points, 210–211
  - See also* Atom transfer radical copolymerization (ATRCp)
- 4-Methylene-1,3-dioxolanes, radical ring-opening polymerization, 40–41
- 10-Methylene-9,10-dihydroanthryl-9-spirocyclopropane, radical ring-opening polymerization, 38–39
- Methyl methacrylate (MMA)
  - copolymerization of 1,1-bis(ethoxycarbonyl)-2-vinylcyclopropane (ECVCP) with, 36, 37*f*
  - paramagnetic ruthenium complexes, 123–124
  - polymerization with Ru-carborane complexes, 117–121
  - reversible chain transfer catalyzed polymerization (RTCP), 165, 166
  - Ru-*N*-heterocyclic carbene complexes, 100–101, 102*f*
  - ruthenacarboranes and amines in ATRP of, 123*t*
  - Ru-tricyclohexylphosphine complex, 99–100
  - Ru-vinylidene complexes, 102–103, 104*f*
  - Ti-Ru-*p*-cymene complexes, 107–108
  - See also* Polycondensates; Polymerization of high internal phase emulsions (pHIPE); Reversible chain transfer catalyzed polymerization (RTCP); Ruthenium complexes
- Micelles, thermoresponsive, 194–197
- Microparticles of silica. *See* Polymerization of high internal phase emulsions (pHIPE)
- Miscibility, polymer, 313
- Molding equipment, baroplastic materials, 318, 319*f*
- Molecular weight
  - conversion dependence of, in vinyl acetate polymerization, 142*f*, 144*f*, 146*f*, 148*f*, 149*f*, 153*f*
  - poly(*N*-isopropylacrylamide) (PNIPAAm), 133
- Molecular weight distribution (MWD)
  - chain extension of poly(*N*-isopropylacrylamide) (PNIPAAm), 135
  - conversion-induced broadening, 24–25
  - polystyrene-*b*-poly(*t*-butyl acrylate) varying, 348, 349*f*
- Morphology
  - formation of mixed, in baroplastic systems, 320–321
  - polypropylene/poly lactide blends, 368–369
  - segregated polymer brushes, 223–224, 227–228
  - See also* Polymer brushes

## N

- Nanoparticles. *See* Baroplastic materials; Polymer-grafted nanoparticles
- Nanophase structure, baroplastic systems, 319, 320*f*
- N*-isopropylacrylamide (NIPAAm). *See* Poly(*N*-isopropylacrylamide) (PNIPAAm)
- Nitrogen based ligands, copper catalyzed atom transfer radical addition, 69
- Nitroxide mediated polymerization (NMP)  
commercial exploitation, 393  
controlled radical  
  polymerization (CRP) of vinyl acetate (VAc), 146–153  
kinetics of ATRP of VAc, 152*f*  
kinetics of bulk VAc  
  polymerization, 146*f*, 147*f*  
VAc by atom transfer radical polymerization (ATRP), 149–153  
VAc by iodine-degenerative transfer polymerization (DT), 147, 148*f*  
VAc by reversible radical addition-fragmentation chain transfer (RAFT), 148, 149  
*See also* Vinyl acetate (VAc)
- Non-uniform response, stimuli-responsive surfaces, 216–217

## O

- Octadecyl acrylate  
multi-step radical migration in propagating radicals, 54–56  
*See also* Electron spin resonance (ESR)
- Oligo(ethylene glycol), surface coating, 197
- Oligo(ethylene glycol) methyl ether acrylate (OEGA)

- monomer in surfactant preparation, 194–195  
random copolymer with 2-(2-ethoxyethoxy)ethyl acrylate, 196–197

*See also* Thermoresponsive materials

- Oligosaccharides. *See* Hybrid block copolymers

## Organic synthesis

- atom transfer radical addition (ATRA), 67–68  
free radical reactions, 63–65

## Organometallic compounds

- Co(II) acetylacetonate complex (Co(acac)<sub>2</sub>) and vinyl acetate (VAc) polymerization, 143, 144*f*, 145

- Co(II) tetramesitylporphyrinato complex, 143

- controlled radical polymerization, 7  
vinyl acetate (VAc)

- polymerization, 143–146  
*See also* Vinyl acetate (VAc)

## Organometallic radical

- polymerization (OMRP), 5, 6*f*, 7, 8*f*

- Orthogonal chemistry, controlled radical polymerization, 11

## P

- Patents, controlled radical polymerization, 386, 387

- Phase-separation phenomena  
segregated polymer brushes, 217, 229

*See also* Polymer brushes

- Phenol catalyst, reversible chain transfer catalyzed polymerization, 164–165, 166*f*
- Poisson chain-length distributions, ideal living polymerization, 17*f*
- Poly(acrylic acid) (PAA)  
polystyrene-*b*-PAA, 349, 350*f*

- PS-*b*-PAA stabilizing Fe<sub>2</sub>O<sub>3</sub> particles, 350–351
- Poly(acrylonitrile) (PAN). *See* Acrylate based copolymers
- Poly(*n*-butyl acrylate) (PBA). *See* Acrylate based copolymers; Polymer-grafted nanoparticles
- Poly( $\epsilon$ -caprolactone) (PCL). *See* Amphiphilic polymer conetworks (APCNs)
- Polycondensates
- bifunctional ATRP initiator propane-1,3-diyl bis(2-chloro-2-phenylacetate) (PDBCP), 180
  - bromine terminated polystyrene (PS-Br) in coupling reactions, 183
  - catalyst concentration at constant monomer concentration, 181–182
  - photoinduced coupling reaction of PS-Br, 182
  - PMMA (poly(methyl methacrylate)), 179
  - PMMA–polyxylylene, 179, 180
  - poly(*p*-xylylene) by polycombination in ATRC or ATRP, 178–179
  - polycombination of *p*-dibromoxylene, 179
  - polyrecombination of PDBCP in ATRC conditions, 180, 181*t*
  - silane radical atom abstraction (SRAA), 182, 183–184
  - silane radicals in situ, 184
  - SRAA for polymerizing bifunctional monomers, 183–184
- Polycondensation, functional polymers, 33
- Poly[2-(*N,N*-dimethylamino)ethyl methacrylate]-*l*-poly( $\epsilon$ -caprolactone) (PDMAEMA-*l*-PCL)
- controlled polymerization, 273–274
  - controlled structure, 271
  - degradability study, 292–293
  - determination of state of water molecules, 283–286
  - mechanical properties, 286–291
  - molecular parameters, 275*t*
  - pH sensitivity of PDMAEMA polymer chains, 280
  - reversibility of swelling-deswelling behavior, 282*f*
  - swelling behavior of, amphiphilic gels, 275–282
  - temperature sensitivity of, 281, 282*f*
  - three-step synthesis, 274
  - See also* Amphiphilic polymer conetworks (APCN)
- Polydispersity index (PDI)
- ATRP of *N*-isopropylacrylamide (NIPAAm), 133
  - ideal living polymerization, 17
  - poly(methyl methacrylate) (PMMA) by Ru-carboranes, 118–119
- Polydispersity perturbation
- baseline selection in size exclusion chromatography (SEC), 22–23
  - chain-length-dependent propagation, 28–29
  - chain-length-dependent termination, 25–28
  - column broadening in SEC, 20–21
  - effect of conversion, 24–25
  - real sources of, 24–29
  - SEC without proper calibration, 21–22
  - signal intensity in time-of-flight mass spectrometry (TOF MS), 23, 24*f*
- Poly(ethylene glycol) (PEG)
- structure, 190
  - surface coating, 197
- Poly(ethylene glycol methyl ether methacrylate) (PEGMA)
- "grafting-to" and "grafting-from" methods for segregated brushes, 219

- protein adsorption on
  - PS/polyPEGMA brushes, 227–228
- surface initiated polymerization (SIP), 218
- synthesis by SIP, 222–223
- wettability, 223, 224*f*
- See also* Polymer brushes
- Poly(2-ethyl hexylacrylate) (PEHA)
  - well-defined block copolymers with polystyrene, 315–316, 317*t*
  - See also* Baroplastic materials
- Poly(glycidyl methacrylate) (PGMA)
  - silicon wafer surfaces with, layer, 218
  - See also* Polymer brushes; Polymerization of high internal phase emulsions (pHIPE)
- Polyhalogenated compounds to alkenes, atom transfer radical additions, 71–73
- Poly(3-hexylthiophene) (P3HT)
  - block copolymers, 251–253
  - C<sub>60</sub> grafting on P3HT rod–coil copolymer, 253*f*
  - electron donor-acceptor, 253–254
  - rod-coil copolymers, 252*t*
- Poly(lactide) (PLA)
  - introduction into polypropylene (PP), 358
  - See also* Polypropylene-*g*-poly(methyl methacrylate) graft copolymers
- Polymer blends
  - techniques for immiscible, 357–358
  - See also* Polypropylene-*g*-poly(methyl methacrylate) graft copolymers
- Polymer brushes
  - dip coating from polystyrene-COOH/poly(methyl methacrylate) [PS-COOH/PMMA] solution, 219–220
  - experimental, 217–219
  - fabrication of segregated binary, 217
  - "grafting-to" and "grafting-from" methods for, 219
  - identification of synthetic conditions for segregated, 219–222
  - migration of PS-COOH macromolecules, 220
  - morphology of segregated, and solvent treatment, 223–224, 227–228
  - non-uniform surface response of segregated, 216–217
  - phase-separation phenomena, 217, 229
  - poly(glycidyl methacrylate) (PGMA) anchoring layer, 218, 221–222
  - protein adsorption on surface of segregated, 227–228
  - scanning probe microscopy (SPM) images, 218, 225*f*, 226*f*, 227*f*, 228*f*
  - stimuli-responsive surfaces, 216
  - surface initiated polymerization (SIP), 218
  - synthesis of segregated, 222–223
  - uniform surface response of mixed, 216
  - wettability of segregated, 223, 224*f*
  - See also* Polymerization of high internal phase emulsions (HIPE)
- Polymer conetworks. *See* Amphiphilic polymer conetworks (APCNs)
- Polymer-grafted nanoparticles
  - ATRP of *n*-butyl acrylate (BA) from functionalized silica particles, 259*t*

- blend composition dependence of storage modulus value, 265*f*
- characterization, 259
- complex modulus and complex viscosity of blends of homopolymer with, 264*f*
- experimental, 258–260
- frequency dependence of linear complex modulus, 263*f*
- frequency dependence of linear storage modulus, 263*f*
- linear dynamic oscillatory shear response of, 261*f*
- linear viscoelastic behavior, 260–261
- model nanoparticle dispersions, 257–258
- rheological characterization, 260
- SiO<sub>2</sub>-PBA hybrids blended with homopolymer, 261–262, 264
- time dependence of linear stress relaxation modulus for, 262*f*
- yield stress and low-frequency plateau storage modulus, 264
- Polymeric libraries. *See* Systematic polymeric libraries
- Polymerization of high internal phase emulsions (pHIPE)
  - atom transfer radical polymerization from, 331–332
  - azide functionalized, 335, 336*f*
  - deprotection of amino acid attached to, 337
  - evidence for grafting of poly(methyl methacrylate) (PMMA), 332
  - experimental, 329
  - functionalization by ATRP
    - grafting of glycidyl methacrylate (GMA), 333–334
  - modification of pHIPE-g-PGMA with silica microparticles, 329
  - polymer brushes, 328
  - scanning electron microscopy (SEM) images of p(HIPE-g-MMA), 331*f*
  - secondary functionalization of p(HIPE-g-GMA) by click reactions, 334–338
  - secondary functionalization of pHIPE-PGMA with silica microparticles, 338–339
  - SEM images of ATRP inimer (I-pHIPE), 330*f*
  - SEM images showing pGMA growth, 334*f*
  - surface functionalization, 328
  - surface grafting, 328
  - synthesis with ATRP initiator, 330
    - two-step synthesis, 329*f*
- Polymer miscibility, pressure, 313
- Poly(methyl methacrylate) (PMMA)
  - reaction partner for p-dibromoxylene, 179
  - See also* Acrylate based copolymers; Polycondensates; Polymerization of high internal phase emulsions (pHIPE); Polypropylene-g-poly(methyl methacrylate) graft copolymers
- Poly(*N*-isopropylacrylamide) (PNIPAAm)
  - catalyst system influence, 131–132
  - chain extension experiments, 134–135
  - challenge in water, 128
  - characterization methods, 129–130
  - controlled polymerization, 128
  - experimental, 129–130
  - homopolymerization, 130–134
  - influence of monomer/initiator ratio, 134*f*
  - kinetics of CuBr-based catalyst, 132–133
  - ligand choice, 130–131

- lower critical solution temperature (LCST), 197
- molecular weight and polydispersity index vs. conversion, 133*f*
- molecular weight distribution (MWD) for chain extension, 135*f*
- polymerization procedure, 129
- reversible addition-fragmentation chain transfer (RAFT) to, hydrogels, 270–271
- structure, 127, 190
- thermo-responsive, 127
- Polyolefin hybrids
  - antibacterial properties of poly(methacryloylcholine chloride) (PMCC) grafted polypropylene, 382*t*
  - approaches to give functionality, 373–374
  - macroinitiator and chain transfer agent syntheses, 375*f*
  - phase and surface control by, 378*f*
  - physical properties, 379*f*
  - properties of, 379–381
  - structural features of, 377–378
  - surface resistance values, 380*f*
  - synthesis via controlled/living radical polymerization, 374–376
  - synthetic examples, 376*f*
  - transmission electron micrographs, 377*f*, 381*f*
  - water contact angles, 380*f*, 382*f*
- Poly(paraphenylenevinylene) (PPV)
  - atom transfer radical polymerization (ATRP), 247–248
  - block copolymers as model materials, 245–250
  - morphology of PPV based model copolymers, 248–250
  - nitroxide mediated radical polymerization, 246–247
  - PPV-*b*-PS and PPV-*b*-poly(4-vinyl pyridine) by anionic polymerization, 249–250
  - PPV-*b*-PS copolymers by ATRP, 247*f*
- Polypropylene (PP)
  - antibacterial properties of poly(methacryloylcholine chloride) (PMCC) grafted PP, 382*t*
  - introduction of polylactide (PLA), 358
  - See also* Polyolefin hybrids
- Polypropylene-*g*-poly(methyl methacrylate) graft copolymers
  - cleavage of graft copolymers, 360
  - elongation at break of blends, 367*t*, 368
  - experimental, 359–361
  - flexural and impact properties of polypropylene/polylactide (PP/PLA) blends, 368*t*
  - gel permeation chromatography (GPC) of detached PMMA branches, 364*f*
  - GPC of PP-*g*-Br before and after MMA polymerization, 365–366
  - <sup>1</sup>H NMR spectra of PP-*g*-Br and PP-*g*-PMMA, 363*f*
  - initiator efficiency, 364, 365*t*
  - mechanical property tests, 361
  - molecular weight of detached PMMA, 365*t*
  - morphology of PP/PLA blends, 368–369
  - polymer characterization methods, 360–361
  - polymerizations with PP-*g*-Br, 362*t*
  - polymerizations with reduced catalyst, 365*t*
  - polymer yield vs. initial monomer concentration, 363*f*
  - PP-*g*-PMMA as compatibilizer for PP/polylactide blend, 366–368

- preparation of, 361–366
  - preparation of hydroxylated PP (PP-*g*-OH), 359–360
  - preparation of PP macroinitiator (PP-*g*-Br), 360
  - radical polymerization of PP macroinitiator, 360
  - synthetic route to PP-*g*-Br, 362
  - TEM (transmission electron microscopy) method, 361
  - TEM of PP/PLA and PP/PLA/PP-*g*-PMMA blends, 369*f*
  - tensile properties of PP/PLA blends, 367*t*
  - tensile strength of PP/PLA and PP/PLA/PP-*g*-PMMA blends, 367
  - Young's modulus of PP/PLA and PP/PLA/PP-*g*-PMMA blends, 367
  - Polyrecombination. *See* Polycondensates
  - Polysaccharides
    - natural, 232
    - See also* Hybrid block copolymers
  - Polystyrene (PS)
    - anionic polymerization of PS-based copolymers, 249–250
    - coupling PS-Br, 176, 177*f*
    - PS-*b*-poly(acrylic acid), 349, 350*f*
    - PS-*b*-poly(*t*-butyl acrylate), 346–347, 348*t*, 353
    - PS macroinitiator by initiators
      - for continuous activator regeneration (ICAR) ATRP, 345–346, 353
    - well-defined block copolymers
      - with poly(2-ethyl hexylacrylate) (PEHA), 315–316, 317*t*
      - See also* Baroplastic materials
  - Polystyrene/poly(methyl methacrylate) (PS/PMMA) blend films for segregated polymer brushes, 217
    - effect of PS-COOH/PMMA thickness on grafted PS, 220*f*
    - See also* Polymer brushes
  - Poly(thienylene vinylene) (PTV), block copolymers as small band gap materials, 250–251
  - Poly(vinyl acetate) (PVAc)
    - well-controlled narrow-dispersed, 140
    - See also* Vinyl acetate (VAc)
  - Poly(4-vinyl pyridine) (P4VP), poly(*p*-phenylenevinylene)-*b*-P4VP by anionic polymerization, 249–250
  - Poly(xylylene), homopolymer and copolymer with PMMA, 179–180
  - Post polymerization, post-poly(methyl methacrylate), 121
  - Pressure
    - polymer miscibility, 313
    - See also* Baroplastic materials
  - Processing aid, baroplastic as, 322, 323*f*
  - Product development. *See* Systematic polymeric libraries
  - Propagating radicals, effect on ATRP equilibrium, 87–88
  - Propagation, chain-length dependent, 28–29
  - Prostaglandin, structure, 64
  - Protein adsorption, surface of segregated brushes, 227–228
  - Publications, controlled radical polymerization, 3–4, 386, 387
- ## R
- Radical copolymerization, monovinyl monomers with divinyl cross-linkers, 203–204
  - Radical migration
    - intermolecular, of alkyl radicals, 56–57
    - multi-step, in propagating radicals, 54–56

- possibility of, to side group, 52–53
- Radical polymerization
  - background, 16–20
  - conventional chain-growth, 18–20
  - ideal living, 16–17
  - true monodispersity, 15–16
  - See also* Polydispersity
    - perturbation
- Radical ring-opening
  - polymerization (R-ROP)
    - acidic hydrolysis of poly(silyl enol ether)s, 37, 38*f*
    - benzocyclobutene, 42
    - bicyclobutanes, 45*f*, 46
    - bifunctional vinylcyclopropanes with dithiols, 38
    - 1,1-bis(hydroxymethylated)-2-vinylcyclopropane, 37
    - copolymerization of 1,1-bis(ethoxycarbonyl)-2-vinylcyclopropane (ECVCP) with methyl methacrylate (MMA), 36, 37*f*
    - cyclic allylic disulfide, 45*f*, 46
    - cyclic disulfides, 45*f*, 46
    - cyclic ketene acetal, 41–42
    - cyclic oligoarsines, 45*f*, 46
    - cyclic  $\alpha$ -oxyacrylates, 45*f*, 46
    - cyclic vinylsulfone, 45*f*, 46
    - emulsion polymerization of ECVCP, 37
    - exo-methylene- and vinyl-substituted cyclic monomers, 35*f*
    - illustration, 34*f*
    - 4-methylene-1,3-dioxolane, 40–41
    - 10-methylene-9,10-dihydroanthryl-9-spirocyclopropane (MDSC), 38
    - polymerizable monomers by, 35, 45–46
    - reaction of poly(silyl enol ether) with electrophile, 37, 38*f*
    - spiro orthocarbonate (SOC), 43
    - spiro orthoester (SOE), 44
    - template polymerization by, 41*f*
    - trimethylsiloxy groups, 37, 38*f*
    - vinylcyclopropane derivatives, 35–39
    - vinylcyclopropanone cyclic acetal, 44–45
    - vinylloxirane derivatives, 39–40
  - Radicals, structure of propagating, and ATRP equilibrium, 87–88
  - Recycling
    - baroplastic materials, 317*t*
    - tri- and star-block copolymers, 321, 322*f*
  - Reversible addition-fragmentation chain transfer (RAFT)
    - polymerization
      - commercial exploitation, 393
      - degenerative transfer process, 6, 8
      - thiocarbonylthio compounds, 149
      - vinyl acetate (VAc), 148, 149
      - See also* Vinyl acetate (VAc)
  - Reversible chain transfer (RT),
    - chain transfer agents, 160
  - Reversible chain transfer catalyzed polymerization (RTCP)
    - activation processes, 160
    - activator radical, 160
    - bulk polymerization of methyl methacrylate with 2-cyanopropyl iodide (CP-I), initiator and catalyst, 166*t*
    - bulk polymerization of styrene with 1-phenylethyl iodide (PE-I), initiator and catalyst, 164*t*
    - electron spin resonance (ESR), 162
    - elements and structures of catalysts and alkyl iodides, 161*f*
    - ESR spectra in styrene polymerization, 166*f*
    - experimental, 161–162
    - experimental proof for RT process, 166–167



- molecular weight vs. conversion
  - for styrene, 165*f*
- phenol catalyst, 164–165
- reaction for precursor catalyst, 164
- thymol iodide catalyst, 162–164
- Rheology. *See* Polymer-grafted nanoparticles
- Ring-opening polymerization (ROP)
  - classifications, 34
  - history, 33
  - illustration, 34*f*
  - See also* Radical ring-opening polymerization (R-ROP)
- Rod-coil conjugated block copolymers
  - architectures, 244
  - atom transfer radical polymerization (ATRP)
    - synthesis, 247–248
  - electron donor-acceptor, 253–254
  - morphology of
    - poly(paraphenylenevinylene) (PPV) based model copolymers, 248–250
  - nitroxide mediated radical polymerization (NMRP)
    - synthesis, 246–247
  - poly(3-hexylthiophene) based, 251–253
  - poly(thienylene vinylene) based,
    - as small band gap materials, 250–251
  - PPV based, 245–250
  - properties, 244–245
  - semiconducting, 244
  - synthesis of PPV-*b*-PS and PPV-*b*-P4VP by anionic polymerization, 249*f*
- Ruthenium carborane complexes
  - amine additives and
    - polymerization rate, 122–124
  - block copolymerization, 121–122
  - closo* and *exo-nido*, 117–119
  - experimental, 116–117
  - instrumentation, 117
  - mass spectrum of poly(methyl methacrylate) P(MMA), 120*f*
  - MMA polymerization, 117–120
  - MMA with ruthenacarboranes,
    - CCl<sub>4</sub> and amines, 123*t*
  - paramagnetic ruthenium complexes, 123–124
  - polydispersity indexes, 118–119
  - polymerization procedure, 117
  - post-polymerization, 121–122
  - structures, 116*f*
  - styrene polymerization, 120–121
  - See also* Ruthenium complexes
- Ruthenium complexes
  - atom transfer radical polymerization (ATRP), 97–98, 112
  - bimetallic vs. monometallic catalysts, 109–112
  - complexes with
    - tricyclohexylphosphine (PCy<sub>3</sub>) or *N*-heterocyclic carbenes (NHCs), 98
  - experimental, 113
  - formation of coordinatively unsaturated 16-electron, 103, 105
  - formation of mixed valence Ru<sup>II</sup>–Ru<sup>III</sup>, 109
  - formation of Ru  $\mu$ -carbide complex, 103, 105
  - heterobimetallic Ti–Ru-*p*-cymene complexes, 107–108
  - homobimetallic Ru-benzylidene–Schiff base complexes, 105–106
  - homobimetallic Ru–NHC, 100–101, 102*f*
  - homobimetallic Ru–PCy<sub>3</sub>, 98–100
  - homobimetallic Ru–vinylidene, 102–103, 104*f*
  - microwave-assisted direct synthesis of dinuclear, 110
  - organic transformations, 97–98
  - proposed dissociative mechanism with, 111

reaction of homobimetallic Ru-benzylidene and indenylidene, with ethylene, 110  
 structure of dinuclear, and  $[\text{Ru}(\text{Cl}_2(p\text{-cymene})_2)_2]$ , 111  
*See also* Methyl methacrylate (MMA); Ruthenium carborane complexes

## S

SciFinder Search terms, controlled radical polymerization, 4*f*, 386, 387

Secondary functionalization. *See* Polymerization of high internal phase emulsions (pHIPE)

Segregated polymer brushes  
 conditions for synthesis, 219–222  
 protein adsorption on surface of, 227–228  
 scanning probe microscopy (SPM) images, 225*f*, 226*f*, 227*f*, 228*f*  
 synthesis of, 222–223  
*See also* Polymer brushes

Self-assembly, dextran-*b*-polystyrene block copolymers, 235–236

Self-organization, aqueous, of macro surfactants, 195–196

Silane radical atom abstraction (SRAA)  
 coupling polymer radicals, 182  
 photoinduced coupling of PS-Br, 182, 183  
 polymerization of bifunctional monomers, 183–184

Silica microparticles  
 modification of poly(high internal phase emulsion)–poly(glycidyl methacrylate), 329  
 secondary functionalization of polymer with, 338–339

*See also* Polymerization of high internal phase emulsions (pHIPE)

Simulation, controlled radical polymerization, 11  
 Size exclusion chromatography (SEC)  
 baseline selection in, 22–23  
 chain-length distributions for transfer/disproportionation, 21*f*  
 column broadening in, 20–21  
 signal intensity in time-of-flight mass spectrometry (TOF MS), 23, 24*f*  
 without proper calibration, 21–22

Solid supported catalysis, atom transfer radical addition (ATRA) and cyclization (ATRC), 68

Solvent effects, atom transfer radical polymerization (ATRP), 93–94

Solvents, challenge of water, 128

Spiro orthocarbonate (SOC), radical ring-opening polymerization, 43

Spiro orthoester (SOE), radical ring-opening polymerization, 44

Stable free radical polymerization (SFRP)  
 concept, 386  
 CRP method, 4, 5, 6*f*, 7  
 mechanism, 8*f*  
 organometallic species, 7

Star-block copolymer  
 3-arm (PBA-*b*-poly(methyl methacrylate)) (PBA-*b*-PMMA), 307–309  
 3-arm, poly(*n*-butyl acrylate)–poly(acrylonitrile) (PBA–PAN), 304–307  
 polar 3-arm, based on nBA, 303–309

*See also* Acrylate based copolymers; Baroplastic materials

Stimuli-responsive surfaces

- block copolymer brushes, 216
  - hydrogels, 270
  - non-uniform response, 216–217
  - polymer brush applications, 215–216
  - uniform response, 216
  - See also* Polymer brushes
  - Structure of polymers
    - controlled radical polymerizations, 85–86
    - polyolefin hybrids, 377–378
  - Styrene
    - block copolymerization by Ru-carboranes, 121–122
    - block copolymerization of vinyl acetate (VAc) and, 153, 155*f*
    - polymerization with Ru-carborane complexes, 120–121
    - reversible chain transfer catalyzed polymerization (RTCP), 162–164, 165
    - Ru-benzylidene–Schiff base complexes, 106
    - See also* Reversible chain transfer catalyzed polymerization (RTCP)
  - Surface grafting. *See* Polymerization of high internal phase emulsions (HIPE)
  - Surface initiated polymerization (SIP), poly(ethylene glycol methyl ether methacrylate) (PEGMA), 218
  - Surface resistance, polypropylene (PP) and poly(methacryloylcholine chloride)-grafted PP, 380*f*
  - Switchable bioactive surfaces
    - biosciences and biotechnology, 197
    - potential, 199
    - thermoreponsive copolymer modified gold surfaces, 198–199
    - See also* Thermoresponsive materials
  - Systemic polymeric libraries
    - activators regenerated by electron transfer (ARGET), 344, 345*f*
    - analytical methods, 352–353
    - atom transfer radical polymerization (ATRP) initiator systems, 344, 345*f*
    - experimental, 352–354
    - initiators for continuous activator regeneration (ICAR), 344, 345*f*
    - polystyrene (PSt) macroinitiator via ICAR ATRP, 345–346, 353
    - PSt-*b*-PAA surfactants stabilizing Fe<sub>2</sub>O<sub>3</sub> particles, 350–351, 354
    - PSt-*b*-poly(acrylic acid) (PSt-*b*-PAA), 349, 350*f*, 353
    - PSt-*b*-poly(*t*-butyl acrylate) (PSt-*b*-PtBA) via ARGET ATRP, 346–347, 348*t*, 353
    - synthesis of PSt-*b*-PtBA with varying molecular weight distribution, 348, 349*f*
- ## T
- Telechelic polymers
    - atom transfer radical coupling (ATRC), 173–174
    - block copolymers by, 178
    - coupling mono-aldehyde polymer by ATRC and etherification, 175*t*
    - mono-aldehyde starting polymer and  $\alpha,\omega$ - by ATRC, 174*f*
    - preparation by ATR cross coupling (ATRCC), 175–178
    - preparation methods, 172
    - $\alpha,\omega$ -telechelic polymer by etherification, 174
    - See also* Atom transfer radical cross-coupling (ATRCC)
  - Template polymerization, radical ring-opening polymerization, 41

- TEMPO (2,2,6,6-tetramethylpiperidine-1-oxyl) radical, nitroxide mediated polymerization, 146
- Terminated chains, controlled radical polymerization, 9
- Termination, chain-length dependent, 25–28
- Thermodynamics. *See* Atom transfer radical polymerization (ATRP) equilibrium ( $K_{\text{ATRP}}$ )
- Thermoresponsive materials
- aqueous self-organization of macro surfactants, 195–196
  - calculation of swelling ratio  $Q$ , 192
  - degradable versions of smart networks, 193
  - evolution of  $Q$  vs. time for macroscopic hydrogels, 193*f*
  - graft copolymers with oligo(ethylene glycol) side chains, 191
  - hydrogels, 192–194
  - lower critical solution temperature (LCST), 190
  - micelles, 194–197
  - molecular structures, 190
  - polymerization techniques, 191
  - random copolymers of 2-(2-ethoxyethoxy)ethyl acrylate (EEO<sub>2</sub>A) and oligo(ethylene glycol) methyl ether acrylate (OEGA), 196–197
  - structures of monomers for preparing hydrogels, 192
  - surfactants by atom transfer radical polymerization (ATRP), 195*t*
  - switchable bioactive surfaces, 197–199
  - synthetic polymer examples, 190
- Thiocarbonylthio compounds, reversible addition-fragmentation polymerization (RAFT) agents, 149
- Thymol iodide, reversible chain transfer catalyzed polymerization (RTCP), 162–164
- Time-of-flight mass spectrometry (TOF MS), signal intensity in, 23, 24*f*
- Titanium-ruthenium-*p*-cymene, heterobimetallic, complexes, 107–108
- Transition metal catalysis
- atom transfer radical addition (ATRA), 64
  - fundamentals of ATRA, 65
- U**
- Uniform response, stimuli-responsive surfaces, 216
- V**
- Vinyl acetate (VAc)
- block copolymerization of styrene and, 153, 155*f*
  - chain extension experiments, 152, 154*f*
- Co(TMP)
- [tetrakis(ethylporphyrinato)Co(II) complex], 143
- cobalt(II) acetylacetonate complex (Co(acac)<sub>2</sub>), 143
- commercial monomer, 140
- controlled radical polymerization (CRP) techniques, 140, 141
- copper catalysts in ATRP, 151*t*
- CRP by  $\alpha$ -dimethylstibanyl ester, 145
- CRP by atom transfer radical polymerization (ATRP), 149–153
- CRP by iodine-degenerative transfer polymerization (DT), 147, 148*f*

CRP by organocobalt complexes, 143, 144*f*, 145

CRP by organometallic compounds, 143–146

CRP by reversible radical addition-fragmentation chain transfer (RAFT), 148, 149

CRP mediated by Al(*i*Bu)<sub>3</sub>/Bpy/TEMPO, 141, 142*f*

CRP via nitroxide mediated polymerization (NMP), 146–153

electron rich double bond, 140

ethyl iodoacetate (EtIAC) as transfer agent, 147, 148*f*

kinetic plots for polymerization, 142*f*, 144*f*, 146*f*, 152*f*

manganese carbonyl complex, 145–145

mechanism for CRP by Co(acac)<sub>2</sub>, 143, 145

mechanism of ATRP of, 149, 150

mechanisms of CRP, 141

molecular weight-conversion dependence, 142*f*, 144*f*, 146*f*, 148*f*, 149*f*, 153*f*

nitroxyl radical TEMPO (2,2,6,6-tetramethylpiperidine-1-oxyl), 146

polymerization by Fe(Cp)(CO)<sub>2</sub>, 150, 151

thiocarbonylthio compounds as RAFT agents, 149

Vinylcyclopropane derivatives, radical ring-opening polymerization, 35–39

Vinylcyclopropanone cyclic acetal,

radical ring-opening polymerization, 44–45

Vinyloxirane, radical ring-opening polymerization, 39–40

Vinyl polymerization, illustration, 34*f*

Vinyl-substituted monomers, radical ring-opening polymerization, 35

Viscoelasticity. *See* Polymer-grafted nanoparticles

## W

Water

challenge as solvent, 128

*See also* Poly(*N*-isopropylacrylamide) (PNIPAAm)

Water contact angle, segregated brushes, 223, 224*f*

Water contact angles polypropylene (PP) and poly(methacryloylcholine chloride)-grafted PP, 382*f*

PP and poly(polyethylene glycol methacrylate)-grafted PP, 380*f*

Wettability, segregated polymer brushes, 223, 224*f*

## X

Xyloglucan (XG) oligosaccharide, 232

*See also* Hybrid block copolymers